TARGETING THE MICROENVIRONMENT NICHE IN SOLID TUMORS

EDITED BY: Cirino Botta, Marco Rossi, Niels Weinhold and Niccolò Bolli
PUBLISHED IN: Frontiers in Oncology

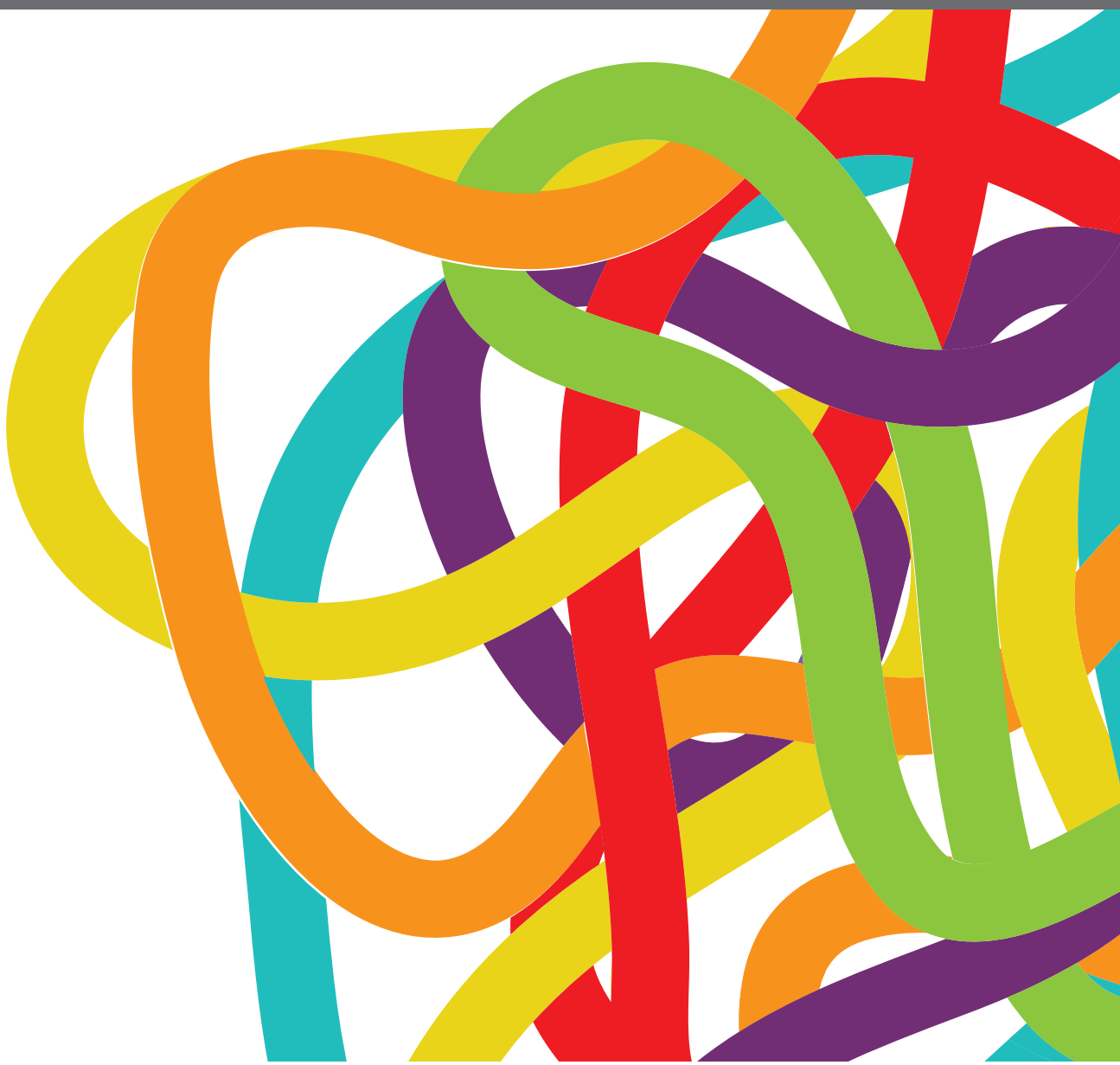

frontiers Research Topics

frontiers

ISSN 1664-8714
ISBN 978-2-88974-772-6
DOI 10.3389/978-2-88974-772-6

About Frontiers

Frontiers is more than just an open-access publisher of scholarly articles: it is a pioneering approach to the world of academia, radically improving the way scholarly research is managed. The grand vision of Frontiers is a world where all people have an equal opportunity to seek, share and generate knowledge. Frontiers provides immediate and permanent online open access to all its publications, but this alone is not enough to realize our grand goals.

Frontiers Journal Series

The Frontiers Journal Series is a multi-tier and interdisciplinary set of open-access, online journals, promising a paradigm shift from the current review, selection and dissemination processes in academic publishing. All Frontiers journals are driven by researchers for researchers; therefore, they constitute a service to the scholarly community. At the same time, the Frontiers Journal Series operates on a revolutionary invention, the tiered publishing system, initially addressing specific communities of scholars, and gradually climbing up to broader public understanding, thus serving the interests of the lay society, too.

Dedication to Quality

Each Frontiers article is a landmark of the highest quality, thanks to genuinely collaborative interactions between authors and review editors, who include some of the world's best academicians. Research must be certified by peers before entering a stream of knowledge that may eventually reach the public - and shape society; therefore, Frontiers only applies the most rigorous and unbiased reviews.
Frontiers revolutionizes research publishing by freely delivering the most outstanding research, evaluated with no bias from both the academic and social point of view. By applying the most advanced information technologies, Frontiers is catapulting scholarly publishing into a new generation.

What are Frontiers Research Topics?

Frontiers Research Topics are very popular trademarks of the Frontiers Journals Series: they are collections of at least ten articles, all centered on a particular subject. With their unique mix of varied contributions from Original Research to Review Articles, Frontiers Research Topics unify the most influential researchers, the latest key findings and historical advances in a hot research area! Find out more on how to host your own Frontiers Research Topic or contribute to one as an author by contacting the Frontiers Editorial Office: frontiersin.org/about/contact

TARGETING THE MICROENVIRONMENT NICHE IN SOLID TUMORS

Topic Editors:
Cirino Botta, University of Palermo, Italy
Marco Rossi, Magna Græcia University, Italy
Niels Weinhold, Heidelberg University, Germany
Niccolò Bolli, University of Milan, Italy

Citation: Botta, C., Rossi, M., Weinhold, N., Bolli, N., eds. (2022). Targeting the Microenvironment Niche in Solid Tumors. Lausanne: Frontiers Media SA.
doi: 10.3389/978-2-88974-772-6

Table of Contents

frontiers in Oncology

ORIGINAL RESEARCH
published: 10 March 2020
doi: 10.3389/fonc.2020.00259

Regulatory Mechanism of ITGBL1 in the Metastasis of Colorectal Cancer

Lu Qi[1,2,3]*, *Fuyao Song*[1,2,3] *and Yanqing Ding*[1,2,3]*

[1] Department of Pathology, Nanfang Hospital, Southern Medical University, Guangzhou, China, [2] Department of Pathology, School of Basic Medical Sciences, Southern Medical University, Guangzhou, China, [3] Guangdong Provincial Key Laboratory of Molecular Oncologic Pathology, Guangzhou, China

Integrin, beta-like 1 (ITGBL1) protein is located in the extracellular matrix (ECM) and involved in the development and metastasis of many tumors. However, the regulatory mechanism of ITGBL1 in colorectal cancer (CRC) remains unclear. This study was to analyze the expression profile of CRC and to identify the expression change of *ITGBL1* gene at different stages of CRC. Survival analysis showed that *ITGBL1* was related to the metastasis of CRC, and CRC patients with a high expression of *ITGBL1* had earlier metastasis. Gene Set Enrichment Analysis (GSEA) indicated the relationship between *ITGBL1* expression and molecular events of CRC. The results indicated that a high expression of *ITGBL1* was linked to Wnt signaling pathway, cell polarity, and tissue development, while a low expression of *ITGBL1* was related to cellular respiration, electron transfer chain, and oxidative phosphorylation. With the expression profiles from interstitial and parenchyma CRC tissues, a comparison was made to determine the difference between high/low expression of *ITGBL1* and Wnt signaling pathway, respectively, and further confirmed the close relation between *ITGBL1* and Wnt signaling pathway. To determine the relation, an interaction network of ITGBL1 and Wnt signaling proteins was constructed. It was found that β-catenin interacted with multiple extracellular Wnt signals and could bind to ITGBL1. As a result, the regulatory mechanism of ITGBL1 in CRC is related to extracellular Wnt signals and may affect extracellular Wnt signals via β-catenin.

Keywords: colorectal cancer, integrin, beta-like 1 (ITGBL1), Wnt signaling pathway, tumor microenvironment

OPEN ACCESS

Edited by:
Cirino Botta,
Cosenza Hospital, Italy

Reviewed by:
Daniele Caracciolo,
University Magna Graecia of Catanzaro, Italy
Juan José Garcés,
University Clinic of Navarra, Spain

***Correspondence:**
Lu Qi
kuuga888@qq.com
Yanqing Ding
dyq@fimmu.com

Specialty section:
This article was submitted to Cancer Molecular Targets and Therapeutics, a section of the journal Frontiers in Oncology

Received: *16 October 2019*
Accepted: *14 February 2020*
Published: *10 March 2020*

Citation:
Qi L, Song F and Ding Y (2020) Regulatory Mechanism of ITGBL1 in the Metastasis of Colorectal Cancer. Front. Oncol. 10:259. doi: 10.3389/fonc.2020.00259

INTRODUCTION

Integrin, beta-like 1 (ITGBL1) is a β-integrin-related extracellular matrix (ECM) protein. Recently, studies on ITGBL1 have been increasing, and it was reported that *ITGBL1* could promote bone metastasis of breast cancer through transforming growth factor (TGF)-β signaling pathway (1). Studies showed that ITGBL1 could promote the invasion of ovarian cancer cell through Wnt/planar cell polarity (PCP) signaling and focal adhesion kinase (FAK)/Src pathway (2), and high expression of ITGBL1 was related to the poor prognosis and drug resistance of ovarian cancer (3). In gastric cancer, ITGBL1 was linked to epithelial–mesenchymal transition (EMT) phenotype and poor prognosis (4). Studies reported that hypermethylation of *ITGBL1* was correlated with poor prognosis of acute myeloid leukemia (5). Furthermore, studies also revealed that ITGBL1 could activate nuclear factor (NF)-κB signaling pathway and promote the EMT, invasion, and migration of prostatic cancer (6). The abovementioned studies revealed that ITGBL1 was associated with the invasion and metastasis of tumors. It was reported that *ITGBL1* was significantly upregulated in CRC, and its high expression was related to shortened survival of CRC patients. Additionally, knockdown of *ITGBL1* suppressed CRC cell proliferation, migration, and invasion (7). Another

study showed that *ITGBL1* was associated with the overall survival rate (OSR) and relapse-free survival (RFS) of CRC patients, and subgroup validation demonstrated that a high *ITGBL1* expression was correlated with shorter RFS in stage II patients, which suggested that *ITGBL1* was a promising candidate biomarker for predicting the relapse of CRC (8). In the earlier study, a comparison of CRC expression data from normal to distant organ metastasis (normal, stage I, II, III, IV, liver, and lung metastasis) was made. There was screening of 39 genes with continuously increasing expression which contained *ITGBL1* (9). These studies showed that ITGBL1 played a vital role in the development of CRC. ITGBL1 was involved in the formation of tumor microenvironment, but the molecular mechanism of ITGBL1 in CRC remained unclear. Therefore, this study aims to analyze the molecular mechanism of ITGBL1 in CRC and determine the regulatory mechanism of ITGBL1 in the metastasis of CRC.

MATERIALS AND METHODS

ITGBL1 Expression Analysis in Colorectal Cancer

It was found previously that the expression of *ITGBL1* was continually increasing in CRC. In this study, CRC expression profiles GSE41258 (54 normal cases, 28 stage I cases, 50 stage II cases, 49 stage III cases, 58 stage IV cases, 47 liver metastasis cases, and 20 lung metastasis cases) from the Gene Expression Omnibus (GEO) database (10) which showed the expression of *ITGBL1* at different stages of CRC were analyzed. Additionally, we confirmed the expression of *ITGBL1* through expression profile GSE49355 and RNA-sequencing GSE50760. GSE49355 included 18 normal cases and 20 CRC cases with primary focus and 19 CRC cases with liver metastasis. GSE50760 included 18 normal cases, 18 CRC cases with primary focus, and 18 CRC cases with liver metastasis. *ITGBL1* gene expression in that data was obtained and divided into different groups according to tumor progression. The comparison of the difference in each group was performed by one-way ANOVA test, and *P*-value was calculated by Kruskal–Wallis test.

Survival Analysis of *ITGBL1* in Colorectal Cancer

ITGBL1 gene expression was continuously increasing in CRC, and many studies reported that ITGBL1 was associated with tumor metastasis. Therefore, a survival analysis of *ITGBL1* gene expression and CRC metastasis was conducted by using expression profile GSE28722 from the GEO database. GSE28722 included 125 CRC cases with data of survival times and metastasis. *ITGBL1* gene expression in those data was obtained and divided into the high *ITGBL1* expression group ($n = 62$) and the low *ITGBL1* expression group ($n = 62$) according to a median value (deleting median). Kaplan–Meier curve (11) was used to depict the survival curve of the two groups, and log rank test (12) was performed to analyze the statistical difference between the two groups with the *P*-value calculated. Considering the American Joint Committee on Cancer (AJCC) staging and the effect of patients' age (taking 60-year-olds as the dividing point) on metastasis, and Cox proportional-hazards regression was performed to further determine the effect of *ITGBL1* on metastasis.

Molecular Mechanism Analysis of ITGBL1 in Colorectal Cancer

To clarify the molecular mechanism of ITGBL1 in CRC, an analysis of the dataset GSE39582 from the GEO database was carried out. GSE39582 included 566 CRC cases, which were divided into the high *ITGBL1* expression group ($n = 283$) and the low *ITGBL1* expression group ($n = 283$) according to the median value of *ITGBL1* expression (probe ID: 205422_s_at) based on the Gene Ontology (including biological process, molecular function, and cellular component) and signaling pathway (including KEGG pathway and REACTOME pathway). Enrichment analysis was performed on the high *ITGBL1* expression group and the low *ITGBL1* expression group by using Gene Set Enrichment Analysis (GSEA) [false discovery rate (FDR) $< 25\%$, nominal $p < 1\%$], with the version of gene set as V7.0 (13). ITGBL1 was mainly located in the ECM and related to the tumor microenvironment, so GSE35602 was used to screen the *ITGBL1*-related differentially expressed gene (DEG) in the parenchyma and interstitial of CRC. GSE35602 included 12 cases with CRC parenchymal tissue data and 12 cases with CRC interstitial tissue data. According to the median value of *ITGBL1* expression (probe ID: A_23_P408363), *ITGBL1* expression data from CRC parenchymal tissue and interstitial tissue were divided in the high *ITGBL1* expression group ($n = 6$) and the low *ITGBL1* expression group ($n = 6$), respectively. GEO2R (14) was used to screen DEG in the high *ITGBL1* expression group and the low *ITGBL1* expression group with the *P*-value limited <0.01 and the fold change as 4. Based on the DEG, ITGBL1-related molecular events in parenchymal and interstitial tissues were examined to elicit the differences between them.

RESULTS

ITGBL1 Expression Change in Colorectal Cancer

GSE41258, GSE49355, and GSE50760 showed the expression change of *ITGBL1* during the progression of CRC. The results showed a significant difference of *ITGBL1* expression at different stages of CRC ($P < 0.0001$, $P = 0.0003$, and $P < 0.0001$). *ITGBL1* expression was continuously increasing with the development of CRC (**Figures 1A–C**), suggesting that *ITGBL1* played an important role in the development and metastasis of CRC.

Survival Analysis of *ITGBL1* in Colorectal Cancer

The analysis on the association between *ITGBL1* expression and the metastasis of CRC patients through dataset GSE28722 showed that *ITGBL1* expression was correlated with the metastasis of CRC (log rank $P = 0.0103$) [hazard ratio (HR) $= 0.3924$ (95% CI: 0.1982–0.7772)] (**Figure 1D**). *ITGBL1* expression was negatively related to the metastasis-free survival,

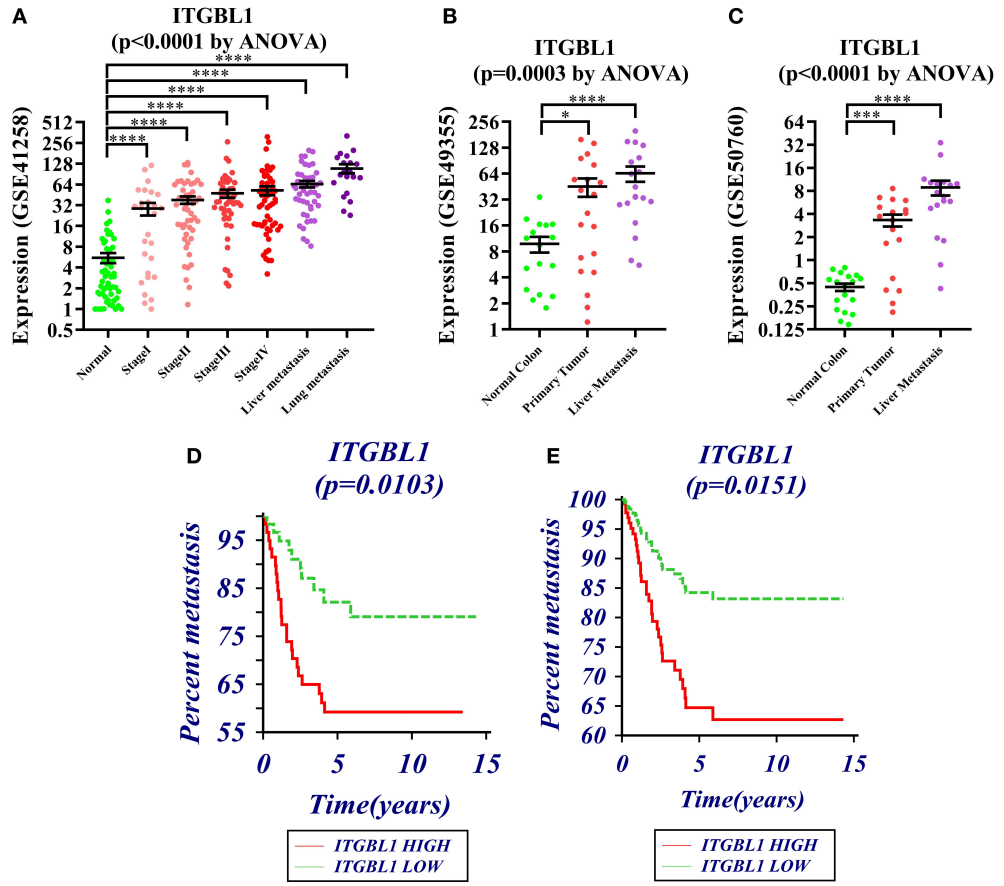

FIGURE 1 | (A–C) Expression changes of *ITGBL1* in the development and metastasis of colorectal cancer (CRC) (*$P < 0.05$, **$P < 0.01$, ***$P < 0.001$, ****$P < 0.0001$). **(D)** Survival curve of *ITGBL1* and the metastasis time of CRC patients (Kaplan–Meier survival estimate and univariable survival analysis model). **(E)** Survival curve of *ITGBL1* and the metastasis time of CRC patients (Cox proportional hazards regression model and multivariate analysis model, excluding the influence of tumor stages and ages on metastasis time).

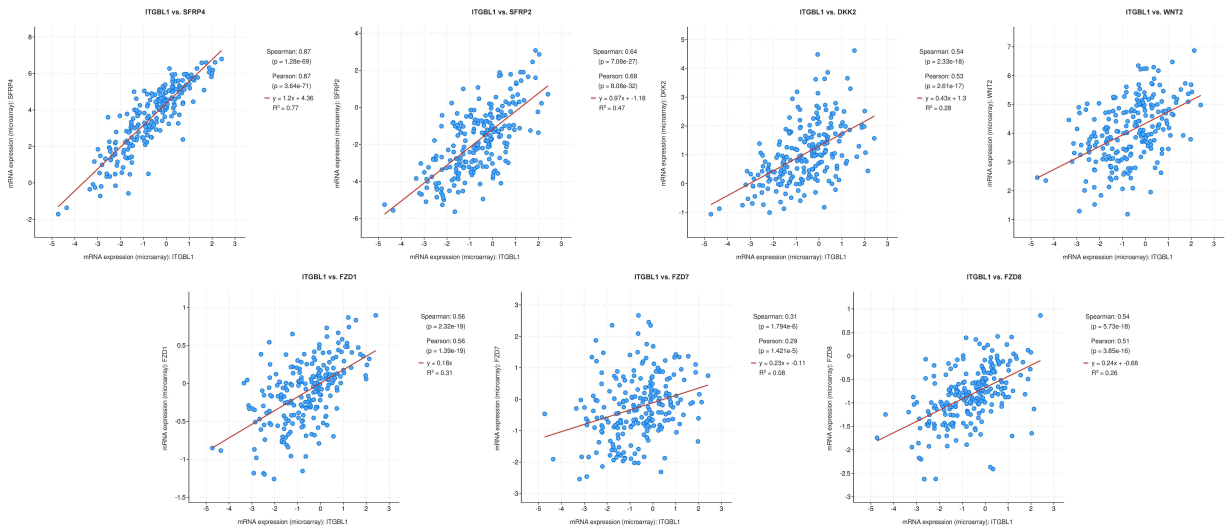

FIGURE 2 | Co-expression relationship of *ITGBL1* and seven extracellular Wnt signals. Y axis in this figure represented mRNA relative expressions of these seven extracellular Wnt signals, and X axis represented mRNA relative expressions of ITGBL1. The red line indicated regression line.

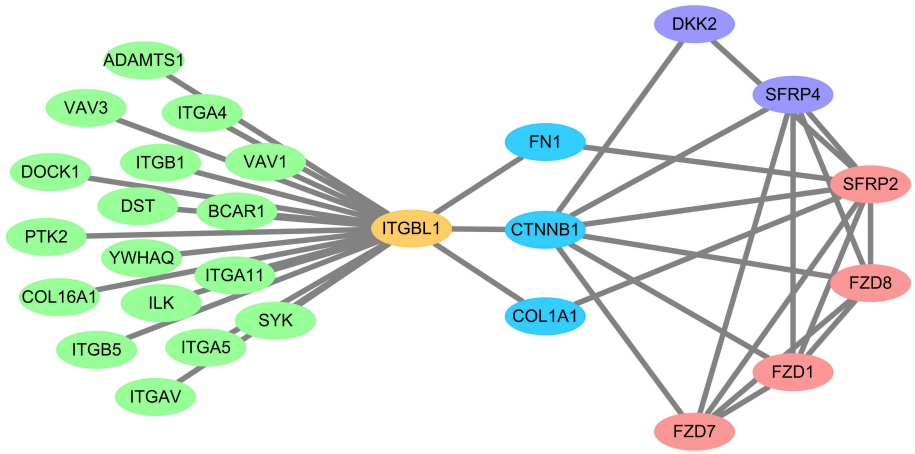

FIGURE 3 | Interaction network of ITGBL1 and extracellular Wnt signal. The red nodes (SFRP2, FZD1, FZD7, FZD8) were extracellular Wnt signals that were upregulated in the stroma. The purple nodes (SFRP4, DKK2) were extracellular Wnt signals that were upregulated in both the stroma and parenchyma. The blue nodes (FN1, CTNNB1, COL1A1) were all ITGBL1 binding proteins, and they also bound to extracellular Wnt signal. The green nodes were ITGBL1 binding proteins. The yellow node was the ITGBL1 protein.

and a high expression of *ITGBL1* could promote the metastasis of CRC. Cox proportional-hazards regression showed that *ITGBL1* was an independent factor of CRC metastasis ($P = 0.0151$). Patients in the high *ITGBL1* expression group had a higher risk of metastasis than that of the low *ITGBL1* expression group [HR = 2.5345 (95% CI: 1.2012–5.3477)] (**Figure 1E**).

Molecular Mechanism of ITGBL1 in Colorectal Cancer

GSEA was performed on the high *ITGBL1* expression group and the low *ITGBL1* expression group based on the GSE39582 dataset. It was found that in the high *ITGBL1* expression group, top 20 of biological process in enrichment were mainly related to Wnt signaling pathway, cell polarity, tissue development, axon, and morphogenesis. Cellular component was mainly associated with cell matrix junction, cytoskeleton, and cell membrane. Molecular function was related to ECM binding, adhesion molecule binding, integrin binding, and FRIZZLED protein binding. Signaling pathway related to high *ITGBL1* expression was mainly linked to cytoskeleton, Wnt signaling pathway, pathway in cancer, and pathway related to tumor development. In the low *ITGBL1* expression group, top 20 of biological process in enrichment were mainly related to cellular respiration, electron transfer chain, and oxidative phosphorylation (see **Supplementary Material**). Those results demonstrated that *ITGBL1* was involved in various molecular events in the progression of CRC and was mainly related to cell adhesion. Enrichment analysis showed that Wnt signaling pathway in the high *ITGBL1* expression group occurred frequently in the biological process, which suggested that *ITGBL1* might be closely related to Wnt signaling pathway.

DEG screening was performed on CRC parenchymal tissue and interstitial tissue based on the dataset GSE35602. In parenchymal tissue, resulting in 137 upregulated genes (*SERP4* had the highest significant difference) and 17 downregulated genes in the high *ITGBL1* expression group. In interstitial tissue, there were 343 upregulated genes (*SERP2* and *SERP4* had the highest significant difference) and 38 downregulated genes in the high *ITGBL1* expression group. GSEA was used to analyze 12 cases with CRC interstitial tissue data, and the results were similar to GSE39582 analysis. This further confirmed the accuracy of the enrichment analysis. In enrichment result of molecular function, Wnt protein binding ranked first in the high *ITGBL1* expression group, which proved the close association between *ITGBL1* expression and Wnt signaling pathway in the interstitial tissue of CRC. Based on the GSEA analysis of GSE39582, 31 genes with enrichment function in KEGG_WNT_SIGNALING_PATHWAY were obtained. Intersection was performed between those 31 genes and upregulated genes in the high *ITGBL1* expression group in CRC parenchymal tissue and interstitial tissue, respectively. In interstitial tissue, seven intersected genes (*SFRP2*, *WNT2*, *FZD1*, *FZD7*, *FZD8*, *SFRP4*, and *DKK2*) were attained. In parenchymal tissue, two intersected genes (*SFRP4* and *DKK2*) were obtained. So, *SFRP4* and *DKK2* were significantly expressed in both parenchymal tissue and interstitial tissue. The encoded proteins of those genes were mainly located in the cell membrane or ECM as the extracellular signal protein of Wnt signaling pathway. Co-expression analysis was performed between the above seven genes and *ITGBL1* using 222 microarray data of CRC obtained in The Cancer Genome Atlas (TCGA) (15) by using cBioPorta (16). It was observed that *SFRP4* was the most relevant gene with *ITGBL1* expression, and other genes were also correlated with *ITGBL1* in varying degrees (**Figure 2**). PrePPI was performed to analyze the interaction relationship between ITGBL1 and the seven proteins. Cytoscape (17) was applied to construct protein–protein interaction network by selecting proteins with combining probability more than 0.8. It is found that six out of seven of those genes (proteins) could be bound to ITGBL1 indirectly, and

CTNNB1 (β-catenin) was the key protein (**Figure 3**). Hence, those six Wnt-related genes were upregulated in the high *ITGBL1* expression group and had co-expression relationship with *ITGBL1*. The encoded proteins of those six genes could bind to CTNNB1, and CTNNB1 could bind to ITGBL1, which suggested that CTNNB1 played an important role in the regulatory mechanism of ITGBL1 in the metastasis of CRC. According to the GSEA analysis of GSE39582, REACTOME_BETA_CATENIN_INDEPENDENT_WNT_ SIGNALING ranked first in the enrichment of REACTOME, which also suggested the important role of CTNNB1 in the relationship of ITGBL1 and Wnt signaling pathway.

DISCUSSION

ECM is closely related to the invasion and metastasis of tumors and involved in the formation of the tumor microenvironment. ITGBL1 is located in the ECM and related to the tumor microenvironment. This study analyzed the expression change of *ITGBL1* at different stages of CRC and determined that *ITGBL1* expression was associated with the metastasis of CRC. By analyzing the expression profile of CRC, it was discovered that *ITGBL1* was closely related to extracellular Wnt signals (*SFRP2*, *WNT2*, *FZD1*, *FZD7*, *FZD8*, *SFRP4*, and *DKK2*) *via CTNNB1*. CTNNB1 (β-catenin) is a key protein of Wnt signals and linked to the development of tumor (18). As reported, CTNNB1 could affect autophagy in glioblastoma, and cell autophagy was related to the tumor microenvironment (19) and was also involved in adrenocortical carcinomas (20). Molecular mechanism related in CRC was correlated with CTNNB1; for instance, genetic variations of the CTNNB1 were related to the progression of CRC (21). SNX3 could inhibit the metastasis of CRC via downregulating β-catenin (22), miR-150 could suppress the metastatization process of CRC by inhibiting β-catenin (23). FOXM1 could promote the growth and metastatization process of CRC by activating β-catenin (24). In the serum of patients with CRC, the expression of β-catenin was higher than that in normal people (25). In addition to CTNNB1, this study also found that extracellular Wnt signals (*SFRP2*, *WNT2*, *FZD1*, *FZD7*, *FZD8*, *SFRP4*, and *DKK2*) were correlated with *ITGBL1* expression. Those proteins and ITGBL1 were cell membrane or extracellular proteins and had higher relation with *ITGBL1* in the interstitial tissue of CRC. Those proteins were closely related to the development of CRC. For instance, methylation could inhibit gene expression and hypermethylation of *SERP2* and was negatively associated with the invasion of CRC (26). Depletion of WNT2 could inhibit CRC (27), while cancer-associated fibroblasts (CAFs)-derived WNT2 could promote the progression of CRC. Moreover, FZD8 might be a WNT2 receptor (28, 29), while miR-375 could suppress human CRC metastasis by inhibiting FZD8 (30). FZD1 is a Wnt responsive gene in colon-derived tissues which were expressed in CRC, and paracancerous normal mucosa was involved in Wnt signaling within the tumor microenvironment (31). RNA interference-mediated silencing of *FZD7* inhibited invasion in CRC, and its expression was associated with the activation of Wnt signaling (32). High expression of SFRP4 was correlated with advanced CRC (33), and CRC patients with overexpressed SFRP4 had lower overall survival (34). DKK2 expression accelerates aerobic glycolysis and promotes angiogenesis in CRC (35). Therefore, those extracellular Wnt signals were related to activation of Wnt signaling pathway and the metastatization of CRC. The study established that the regulatory mechanism of ITGBL1 in the development and metastatization of CRC might be closely related to those proteins. Hence, ITGBL1 is closely associated with the metastatization of CRC and involved in the tumor microenvironment.

DATA AVAILABILITY STATEMENT

All datasets generated for this study are included in the article/**Supplementary Material**.

AUTHOR CONTRIBUTIONS

LQ designed and performed the study, analyzed the data, and wrote the manuscript. FS collected the data and literature. YD revised and approved the final manuscript.

FUNDING

This work was supported by the National Key Basic Research Program of China (973 program, 2015CB554002), the National Natural Science Foundation of China (81972754, 81773101), and the Scientific Research Starting Foundation of Southern Medical University (PY2018N003).

SUPPLEMENTARY MATERIAL

The Supplementary Material for this article can be found online at: https://www.frontiersin.org/articles/10.3389/fonc.2020.00259/full#supplementary-material

Table S1 | GSEA enrichment analysis of the high ITGBL1 expression group and the low ITGBL1 expression group. Screening results of ITGBL1-related differentially expressed genes (DEGs) in parenchyma and interstitial of CRC.

REFERENCES

1. Li XQ, Du X, Li DM, Kong PZ, Sun Y, Liu PF, et al. ITGBL1 Is a Runx2 transcriptional target and promotes breast cancer bone metastasis by activating the TGFbeta signaling pathway. *Cancer Res.* (2015) 75:3302–13. doi: 10.1158/0008-5472.CAN-15-0240
2. Sun L, Wang D, Li X, Zhang L, Zhang H, Zhang Y. Extracellular matrix protein ITGBL1 promotes ovarian cancer cell migration and adhesion through Wnt/PCP signaling and FAK/SRC pathway. *Biomed Pharmacother.* (2016) 81:145–51. doi: 10.1016/j.biopha.2016.03.053
3. Song J, Yang P, Lu J. Upregulation of ITGBL1 predicts poor prognosis and promotes chemoresistance in ovarian cancer. *Cancer Biomark.* (2019) 27:51–61. doi: 10.3233/CBM-190460

4. Li R, Zhuang C, Jiang S, Du N, Zhao W, Tu L, et al. ITGBL1 predicts a poor prognosis and correlates EMT phenotype in gastric cancer. *J Cancer*. (2017) 8:3764–73. doi: 10.7150/jca.20900
5. Lian XY, Ma JC, Zhou JD, Zhang TJ, Wu DH, Deng ZQ, et al. Hypermethylation of ITGBL1 is associated with poor prognosis in acute myeloid leukemia. *J Cell Physiol*. (2019) 234:9438–46. doi: 10.1002/jcp.27629
6. Li W, Li S, Yang J, Cui C, Yu M, Zhang Y. ITGBL1 promotes EMT, invasion and migration by activating NF-kappaB signaling pathway in prostate cancer. *Onco Targets Ther*. (2019) 12:3753–63. doi: 10.2147/OTT.S200082
7. Qiu X, Feng JR, Qiu J, Liu L, Xie Y, Zhang YP, et al. ITGBL1 promotes migration, invasion and predicts a poor prognosis in colorectal cancer. *Biomed Pharmacother*. (2018) 104:172–80. doi: 10.1016/j.biopha.2018.05.033
8. Matsuyama T, Ishikawa T, Takahashi N, Yamada Y, Yasuno M, Kawano T, et al. Transcriptomic expression profiling identifies ITGBL1, an epithelial to mesenchymal transition (EMT)-associated gene, is a promising recurrence prediction biomarker in colorectal cancer. *Mol Cancer*. (2019) 18:19. doi: 10.1186/s12943-019-0945-y
9. Qi L, Ding Y. Construction of key signal regulatory network in metastatic colorectal cancer. *Oncotarget*. (2018) 9:6086–94. doi: 10.18632/oncotarget.23710
10. Clough E, Barrett T. The gene expression omnibus database. *Methods Mol Biol*. (2016) 1418:93–110. doi: 10.1007/978-1-4939-3578-9_5
11. Stel VS, Dekker FW, Tripepi G, Zoccali C, Jager KJ. Survival analysis I: the Kaplan-Meier method. *Nephron Clin Pract*. (2011) 119:c83–8. doi: 10.1159/000324758
12. Koletsi D, Pandis N. Survival analysis, part 2: Kaplan-Meier method and the log-rank test. *Am J Orthod Dentofacial Orthop*. (2017) 152:569–71. doi: 10.1016/j.ajodo.2017.07.008
13. Subramanian A, Kuehn H, Gould J, Tamayo P, Mesirov JP. GSEA-P: a desktop application for gene set enrichment analysis. *Bioinformatics*. (2007) 23:3251–3. doi: 10.1093/bioinformatics/btm369
14. Barrett T, Wilhite SE, Ledoux P, Evangelista C, Kim IF, Tomashevsky M, et al. NCBI GEO: archive for functional genomics data sets–update. *Nucleic Acids Res*. (2013) 41:D991–5. doi: 10.1093/nar/gks1193
15. Zhu Y, Qiu P, Ji Y. TCGA-assembler: open-source software for retrieving and processing TCGA data. *Nat Methods*. (2014) 11:599–600. doi: 10.1038/nmeth.2956
16. Gao J, Aksoy BA, Dogrusoz U, Dresdner G, Gross B, Sumer SO, et al. Integrative analysis of complex cancer genomics and clinical profiles using the cBioPortal. *Sci Signal*. (2013) 6:l1. doi: 10.1126/scisignal.2004088
17. Shannon P, Markiel A, Ozier O, Baliga NS, Wang JT, Ramage D, et al. Cytoscape: a software environment for integrated models of biomolecular interaction networks. *Genome Res*. (2003) 13:2498–504. doi: 10.1101/gr.1239303
18. Gao C, Wang Y, Broaddus R, Sun L, Xue F, Zhang W. Exon 3 mutations of CTNNB1 drive tumorigenesis: a review. *Oncotarget*. (2018) 9:5492–508. doi: 10.18632/oncotarget.23695
19. Nàger M, Sallán MC, Visa A, Pushparaj C, Santacana M, Macià A, et al. Inhibition of WNT-CTNNB1 signaling upregulates SQSTM1 and sensitizes glioblastoma cells to autophagy blockers. *Autophagy*. (2018) 14:619–36. doi: 10.1080/15548627.2017.1423439
20. Maharjan R, Backman S, Åkerström T, Hellman P, Björklund P. Comprehensive analysis of CTNNB1 in adrenocortical carcinomas: identification of novel mutations and correlation to survival. *Sci Rep*. (2018) 8:8610. doi: 10.1038/s41598-018-26799-2
21. Sygut A, Przybyłowska K, Ferenc T, Dziki Ł, Spychalski M, Mik M, et al. Genetic variations of the CTNNA1 and the CTNNB1 genes in sporadic colorectal cancer in Polish population. *Pol Przegl Chir*. (2012) 84:560–4. doi: 10.2478/v10035-012-0093-1
22. Pan B, Zhang T, Yang W, Liu Y, Chen Y, Zhou Z, et al. SNX3 suppresses the migration and invasion of colorectal cancer cells by reversing epithelial-to-mesenchymal transition via the beta-catenin pathway. *Oncol Lett*. (2019) 18:5332–40. doi: 10.3892/ol.2019.10860
23. He Z, Dang J, Song A, Cui X, Ma Z, Zhang Y. The involvement of miR-150/beta-catenin axis in colorectal cancer progression. *Biomed Pharmacother*. (2020) 121:109495. doi: 10.1016/j.biopha.2019.109495
24. Yang K, Jiang B, Lu Y, Shu Q, Zhai P, Zhi Q, et al. FOXM1 promotes the growth and metastasis of colorectal cancer via activation of beta-catenin signaling pathway. *Cancer Manag Res*. (2019) 11:3779–90. doi: 10.2147/CMAR.S185438
25. Li S, Huang M, Liu Q, Wang D, Wu R, Zhang X, et al. Serum expression of beta-catenin is a potential detection marker in patients with colorectal cancer. *Dis Markers*. (2019) 2019:5070524. doi: 10.1155/2019/5070524
26. Yang Q, Huang T, Ye G, Wang B, Zhang X. Methylation of SFRP2 gene as a promising noninvasive biomarker using feces in colorectal cancer diagnosis: a systematic meta-analysis. *Sci Rep*. (2016) 6:33339. doi: 10.1038/srep 33339
27. Jung YS, Jun S, Lee SH, Sharma A, Park JI. Wnt2 complements Wnt/beta-catenin signaling in colorectal cancer. *Oncotarget*. (2015) 6:37257–68. doi: 10.18632/oncotarget.6133
28. Kramer N, Schmöllerl J, Unger C, Nivarthi H, Rudisch A, Unterleuthner D, et al. Autocrine WNT2 signaling in fibroblasts promotes colorectal cancer progression. *Oncogene*. (2017) 36:5460–72. doi: 10.1038/onc.2017.144
29. Aizawa T, Karasawa H, Funayama R, Shirota M, Suzuki T, Maeda S, et al. Cancer-associated fibroblasts secrete Wnt2 to promote cancer progression in colorectal cancer. *Cancer Med*. (2019) 8:6370–82. doi: 10.1002/cam4.2523
30. Xu L, Wen T, Liu Z, Xu F, Yang L, Liu J, et al. MicroRNA-375 suppresses human colorectal cancer metastasis by targeting Frizzled 8. *Oncotarget*. (2016) 7:40644–56. doi: 10.18632/oncotarget.9811
31. Planutis K, Planutiene M, Nguyen AV, Moyer MP, Holcombe RF. Invasive colon cancer, but not non-invasive adenomas induce a gradient effect of Wnt pathway receptor frizzled 1 (Fz1) expression in the tumor microenvironment. *J Transl Med*. (2013) 11:50. doi: 10.1186/1479-5876-11-50
32. Ueno K, Hiura M, Suehiro Y, Hazama S, Hirata H, Oka M, et al. Frizzled-7 as a potential therapeutic target in colorectal cancer. *Neoplasia*. (2008) 10:697–705. doi: 10.1593/neo.08320
33. Kamposioras K, Konstantara A, Kotoula V, Lakis S, Kouvatseas G, Akriviadis E, et al. The prognostic significance of WNT pathway in surgically-treated colorectal cancer: beta-catenin expression predicts for disease-free survival. *Anticancer Res*. (2013) 33:4573–84.
34. Nfonsam LE, Jandova J, Jecius HC, Omesiete PN, Nfonsam VN. SFRP4 expression correlates with epithelial mesenchymal transition-linked genes and poor overall survival in colon cancer patients. *World J Gastrointest Oncol*. (2019) 11:589–98. doi: 10.4251/wjgo.v11.i8.589
35. Deng F, Zhou R, Lin C, Yang S, Wang H, Li W, et al. Tumor-secreted dickkopf2 accelerates aerobic glycolysis and promotes angiogenesis in colorectal cancer. *Theranostics*. (2019) 9:1001–14. doi: 10.7150/thno. 30056

Conflict of Interest: The authors declare that the research was conducted in the absence of any commercial or financial relationships that could be construed as a potential conflict of interest.

frontiers in Oncology

ORIGINAL RESEARCH
published: 16 June 2020
doi: 10.3389/fonc.2020.00968

Akt Inhibition Is Associated With Favorable Immune Profile Changes Within the Tumor Microenvironment of Hormone Receptor Positive, HER2 Negative Breast Cancer

Douglas K. Marks[1], Robyn D. Gartrell[2], Margueritta El Asmar[3], Shuobo Boboila[4], Thomas Hart[5], Yan Lu[4], Qingfei Pan[6], Jiyang Yu[6], Hanina Hibshoosh[4,7], Hua Guo[8], Eleni Andreopoulou[9], Lisa Wiechmann[10], Katherine Crew[4,11,12], Joseph Sparano[13], Dawn Hershman[4,11,12], Eileen Connolly[13†], Yvonne Saenger[4,11†] and Kevin Kalinsky[4,11*†]*

[1] Perlmutter Cancer Center, NYU Langone Health, New York, NY, United States, [2] Department of Pediatrics, Pediatric Hematology/Oncology and Medicine, Hematology/Oncology, Columbia University Irving Medical Center, New York, NY, United States, [3] Bloomberg-Kimmel Institute for Cancer Immunotherapy, Johns Hopkins University School of Medicine, Baltimore, MD, United States, [4] Herbert Irving Comprehensive Cancer Center, Columbia University, New York, NY, United States, [5] College of Physicians and Surgeons, Columbia University Irving Medical Center, New York, NY, United States, [6] Department of Computational Biology, St. Jude Children's Research Hospital, Memphis, TN, United States, [7] Department of Pathology and Cell Biology, College of Physicians and Surgeons, Columbia University, New York, NY, United States, [8] Weill Cornell Medicine, New York Presbyterian Hospital, New York, NY, United States, [9] Department of Surgery, College of Physicians and Surgeons, Columbia University Irving Medical Center, New York, NY, United States, [10] Department of Medicine, College of Physicians and Surgeons, Columbia University Irving Medical Center, New York, NY, United States, [11] Department of Medicine, Albert Einstein College of Medicine, Montefiore Medical Center, Bronx, NY, United States, [12] Department of Biostatistics, Mailman School of Public Health, Columbia University, New York, NY, United States, [13] Division of Radiation Oncology, Columbia University Irving Medical Center, New York, NY, United States

Background: The PI3K/Akt/mTOR pathway in part impacts tumorigenesis through modulation of host immune activity. To assess the effects of Akt inhibition on the tumor micro-environment (TME), we analyzed tumor tissue from patients with operable hormone receptor positive, HER2 negative breast cancer (BC) treated on a presurgical trial with the Akt inhibitor MK-2206.

Methods: Quantitative multiplex immunofluorescence (qmIF) was performed using CD3, CD8, CD4, FOXP3, CD68, and pancytokeratin on biopsy and surgical specimens of MK-2206 and untreated, control patients. nanoString was performed on surgical specimens to assess mRNA expression from MK-2206-treated vs. control patients.

Results: Increased CD3+CD8+ density was observed in post vs. pre-treatment tissue in the MK-2206-treated vs. control patients (87 vs. 0.2%, $p < 0.05$). MK-2206 was associated with greater expression of interferon signaling genes (e.g., *IFI6*, $p < 0.05$) and lower expression of myeloid genes (*CD163*, $p < 0.05$) on differential expression and gene set enrichment analyses. Greater expression of pro-apoptotic genes (e.g., *BAD*) were associated with MK-2206 treatment ($p < 0.05$).

Conclusion: Akt inhibition in operable BC was associated with a favorable immune profile in the TME, including increased CD3+CD8+ density and greater expression of interferon genes. Additional studies are warranted, as this may provide rationale for combining Akt inhibition with immunotherapy.

Keywords: breast cancer, tumor microenvironment, MK-2206, AKT inhibitor, quantitative multiplex immunofluorescence, tumor immunobiology, pre-surgical

OPEN ACCESS

Edited by:
Cirino Botta, Unit of Clinical Hematology, Cosenza Hospital, Italy

Reviewed by:
Maria Cucè, University of Catanzaro, Italy
Flavia Biamonte, Magna Graecia University of Catanzaro, Italy

***Correspondence:**
Yvonne Saenger
yms4@cumc.columbia.edu
Kevin Kalinsky
kk2693@cumc.columbia.edu

† These authors have contributed equally to this work and share senior authorship

Specialty section:
This article was submitted to Cancer Molecular Targets and Therapeutics, a section of the journal Frontiers in Oncology

Received: *11 March 2020*
Accepted: *15 May 2020*
Published: *16 June 2020*

Citation:
Marks DK, Gartrell RD, El Asmar M, Boboila S, Hart T, Lu Y, Pan Q, Yu J, Hibshoosh H, Guo H, Andreopoulou E, Wiechmann L, Crew K, Sparano J, Hershman D, Connolly E, Saenger Y and Kalinsky K (2020) Akt Inhibition Is Associated With Favorable Immune Profile Changes Within the Tumor Microenvironment of Hormone Receptor Positive, HER2 Negative Breast Cancer. Front. Oncol. 10:968. doi: 10.3389/fonc.2020.00968

INTRODUCTION

Targeted therapies have changed the treatment landscape of breast cancer (BC); however, until recently, BC was generally considered a minimally "immunogenic" malignancy and less likely to benefit from novel immunotherapeutic agents. While it has been established that lymphocyte rich tumors demonstrate increased chemosensitivity across BC subtypes, tumor infiltrating lymphocytes (TILs) have recently been identified as a candidate biomarker for efficacy of checkpoint inhibition (1–4). Of the BC subtypes, triple negative breast cancer (TNBC) has demonstrated an impressive response rate to immune checkpoint blockade combined with chemotherapy (2). By contrast, hormone receptor positive (HR+)/HER2− BC is frequently referred to as immunologically "cold" as these tumors have both lower TIL densities and response rates to immunotherapy as compared with TNBC (3, 5). There remains a significant need to identify effective strategies for augmenting the immunologic response in HR+/HER2− breast tumors, potentially including combination approaches (6–8).

The phosphatidylinositol 3 kinase (PI3K)/Akt murine thymoma viral oncogene (AKT)/mammalian target of rapamycin inhibitor (mTOR) pathway drives anti-apoptotic signaling and cell division in BC through activating point mutations, somatic copy number abnormalities, and increased gene expression (9). In addition to direct anti-neoplastic activity, there is growing evidence that agents targeting the PI3K/Akt/mTOR pathway have indirect anti-tumor activity mediated through the host immune response (10). While the PI3K/Akt/mTOR pathway is essential to immune cell maturation, the pathway also regulates expression of cytokines associated with recruitment of myeloid derived suppressor cells (MDSC) and regulatory T-cells as well as expression of PD-L1 on tumor cells (11). Specifically, treatment with the allosteric AKT inhibitor MK-2206 has previously demonstrated the capacity to downregulate PD-L1 at the transcriptional level in TNBC cell lines as well as augment the effect of a tumor specific vaccine in murine models (12, 13).

In this study, we define the impact of Akt inhibition on the tumor microenvironment (TME) in a series of patients with HR+/HER2− BC treated on a pre-surgical trial with MK-2206 (9). We performed *in situ* analysis with quantitative multiplex immunofluorescence (qmIF), on the pre-treatment core biopsies and post-treatment surgical specimens from patients treated with MK-2206 and evaluated differences in the TME compared to prospectively enrolled untreated controls. In addition, we performed transcriptomic expression analysis on the surgical specimens with nanoString to assess the effects of MK-2206 on the transcription of PI3K/Akt/mTOR pathway target genes as well as a broad panel of immune related genes.

METHODS

Patient Samples

Archival tissue was collected from an open-label, single arm, presurgical trial with MK-2206 (NCT013195390). Patients were enrolled between October 2011 and March 2013 and received two weekly oral doses of MK-2206 prior to surgery: first dose at day−9 (+/− 1 day) and second dose at day−2 (+/− 1 day) from the date of surgery (9). Untreated control patients were prospectively accrued, and their tumor tissue was collected with the same methodology.

qmIF

Four micrometer slides were stained using Opal^{TM} (Perkin Elmer, Hopkinton, MA) multiplex 6-plex kits for DAPI, CD3 (T-cells, LN10, Leica, 1:200), CD8 [Cytotoxic T-cells, 4B11, Leica, Ready to use (RTU)], CD68 (macrophages, KP1, 155 Biogenex, RTU), pancytokeratin (Tumor, PCK-26, Biocare, 1:200), CD4 (T helper cells, EPR6855, Abcam, 1:2000), and FOXP3 (T regulatory cells, 236A/E7, Abcam, 1:300). QmIF was performed on diagnostic core biopsies and surgical specimens by the recommended staining protocol including single stain controls and unstained controls. Five representative areas were selected to include three areas with tumor and up to 50% stroma and two areas with at least 90% tumor (**Supplementary Figure 1**). These images were factored equally into the analysis for each patient. For samples of small size, a minimum of two areas meeting the above criteria were required for inclusion. All images were confirmed as representative tumor areas by breast pathology (HH).

Images were captured using the Mantra^{TM} pathology workstation (PerkinElmer). Images were analyzed using inForm ^{TM} software (PerkinElmer) for tissue segmentation, cell segmentation, phenotyping, and scoring per previously published methods (**Supplementary Figure 1B**) (14). Cells were phenotyped for tumor, T-cells, macrophages, and other (negative for pancytokeratin, CD3, and CD68), then scored for concatenating variables CD4, CD8, and FOXP3. Subsequently, data obtained from all representative images were compiled to yield density values for each patient. Nearest neighbor analysis to assess for differences in spatial distribution of immune cell subsets following MK-2206 was performed by previously described methods (14). Image data was exported from inForm^{TM} version 2.2.1 (PerkinElmer). The inForm data from all images for each patient were processed in separate proprietary software designed in R Studio (version 0.99.896, Boston, MA). In this software, images were combined and analyzed to concatenate variables (i.e., CD3+CD4+FOXP3+) and determine density and distances of distinct phenotypes.

NanoString

mRNA was manually extracted from FFPE slides of representative surgical specimens of patients who received MK-2206 ($n = 5$) or control ($n = 5$). Bioanalyzer calculations were performed to determine the quantity of mRNA (ng) to satisfy the quality requirements of nanoString platform. Subsequently, the PI3K (180 genes) and IO360 (770 genes) were run on these surgical specimens (15).

Statistical Methods

For qmIF analysis, statistical analysis was performed using Mann-Whitney *U*-test. For nanoString analysis, data quality assessment, differential expression, and statistical

comparison was performed by the systems biology data-driven network-based Bayesian inference of drivers (NetBID, https://github.com/jyyulab/NetBID) (16). Gene Set Enrichment Analysis (GSEA) was performed using MSigDB (v6.1) and "fgsea" package in R, with default parameters. Multiple comparison analysis was performed using Benjamini-Hochberg method.

Ethics

Patient provided written consent to participate in the presurgical study which was approved by the Columbia University Irving Medical Center and Albert Einstein Cancer Center institutional review boards.

RESULTS

Patient Population

Between September 2011 and July 2014, 12 patients with newly diagnosed invasive BC were prospectively enrolled to receive MK-2206 (9). In addition, tissue from diagnostic core biopsies and surgical specimens were prospectively collected on 6 untreated controls (9). For this analysis, seven patients treated with MK-2206 and one control patient were excluded for insufficient tissue. One MK-2206-treated patient was excluded from qmIF analysis due to poor tissue quality. In total, 9 patients with paired biopsy and surgical specimens (5 MK-2206 and 4 control) had evaluable tissue for qmIF analysis. 10 surgical specimens (5 MK-2206 and 5 control) were evaluable for nanoString.

All patients included in our analyses had HR+/HER2− tumors with invasive ductal histology. Of the MK-2206-treated patients included in this study, one patient received the 200 mg dose, one patient 135 mg, and the remaining three with 90 mg (**Supplementary Table 1** for clinicopathologic features).

Treatment With MK-2206 Increases CD3+CD8+ Cytotoxic T-Cell (CTL) Density

The density of each immune subset was measured by qMIF analysis at the time of biopsy and in the surgical specimen (**Figures 1A,B**). As frequently seen in HR+/HER2− BC, the baseline immune infiltrate was observed to be modest in the biopsy specimens from the MK-2206 and control groups, with lymphocytes representing the majority of the immune infiltrate in this cohort (17). Patients treated with MK-2206 exhibited a significant increase in median cytotoxic T-cells (CD3+CD8+) density, as compared to untreated control patients for whom no change was observed (87 vs. 0.2%, $p = 0.03$, **Figure 1C**, **Supplementary Figures 2–3**). No change was detected in the macrophage (CD68), T helper (CD4) T reg (CD4+FOXP3+) density following MK-2206 treatment as compared to paired pathology specimens from controls. A numerical increase in the CD8/FOXP3 ratio was observed in MK-2206-treated patients, which demonstrated a higher mean CD8/FOXP3 ratio in post treatment specimens as compared to control patients (19.4 vs. 4.6), although this finding did not reach statistical significance ($p = 0.32$).

Using nearest neighbor analysis, we observed a numerical reduction in median pixel distance (−12.5%) between CTL cells and tumor cells following treatment, suggesting that the increased density of effector T-cells is not relegated to the periphery. This observation was not seen in the control group when comparing the baseline biopsy to surgical excision specimen.

MK-2206 Associated With Gene Expression Change in Downstream Targets of PI3K/Akt/mTOR Pathway

mRNA expression analysis confirms the *in-vivo* inhibitory activity of MK-2206 on PI3K/AKT/mTOR pathway. MK-2206 was associated with lower mean expression levels of genes associated with cell cycle progression including *CTNNB1* (raw

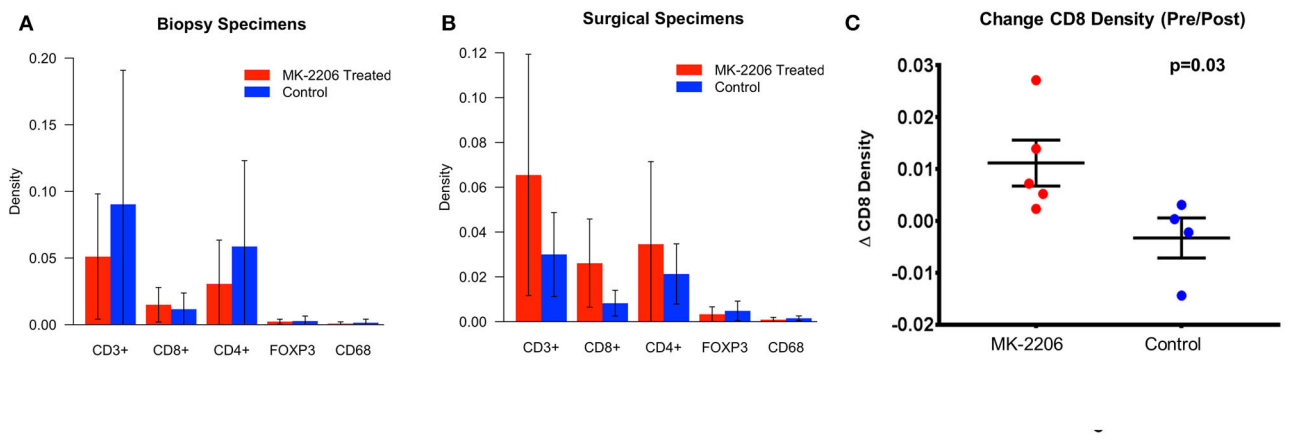

FIGURE 1 | qMIF Analysis of biopsy and surgical specimens from a pre-surgical trial with MK-2206. **(A)** Mean density by immune cell subtype in biopsy specimens of MK-2206 (red) vs. control (blue). **(B)** Mean density by immune cell subtype in surgical specimens of MK-2206 (red) vs. control (blue). **(C)** Change in CD8 density between baseline biopsy and surgical specimen of MK-2206-treated (red) and control (blue) patients.

$p = 0.01$) and *CCND2* (raw $p = 0.02$) in comparing post-surgical specimens from MK-2206-treated patients to control. Additionally, greater expression of pro-apoptotic gene products *BAD* (raw $p < 0.01$) *DDIT* (raw $p = 0.03$) was observed in surgical specimens after MK-2206 vs control. Consistent, with these findings, a trend toward greater *CASP9* expression was also found (raw $p = 0.067$). No significant difference in expression of *BAX* was observed between the two groups.

Following MK-2206, mean *IGF-1R* expression was greater in MK-2206-treated patients as compared to untreated controls (472.4 vs. 226.0 copies, raw $p = 0.01$) (**Figure 2**). We also observed greater expression of *HER3* with double the mean mRNA copy number for *HER3*; although, the difference did not reach statistical significance (1060.6 vs. 577.4 copies, raw $p = 0.14$).

Transcriptomic Analysis Highlights Greater Expression of Interferon Related Gene Expression and Lower Expression of Myeloid Related Genes in MK-2206-Treated Patients

Using the nanoString 770 gene IO-360 panel, differential expression (DE) between surgical specimens from patients treated with MK-2206 vs. untreated controls identified 31 genes with 1.5-fold higher/lower expression (**Figure 3**) (15). Mean expression levels of myeloid related genes, including *CD163* (raw $p = 0.03$), *CSF1R* (raw $p < 0.01$), *HLA-DR* (raw $p = 0.05$), *P2RY13* (raw $p = 0.02$), *ITGAM* (raw $p = 0.03$), *MS4A6A* (raw $p = 0.04$), were lower in the surgical specimens from patients treated with MK-2206 compared to control.

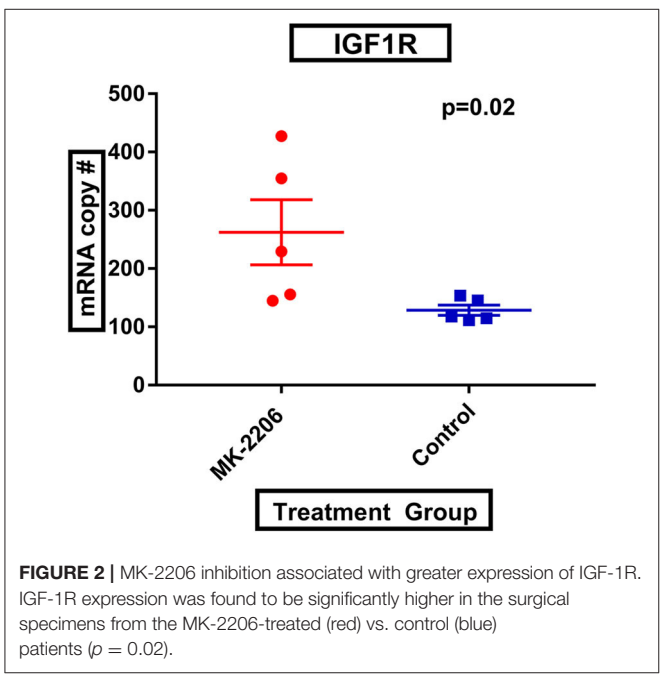

FIGURE 2 | MK-2206 inhibition associated with greater expression of IGF-1R. IGF-1R expression was found to be significantly higher in the surgical specimens from the MK-2206-treated (red) vs. control (blue) patients ($p = 0.02$).

By contrast, of the immune genes with greater expression in the MK-2206 patients, the majority were related to interferon related signaling and included *IFI6* ($p = 0.02$), *IFIT1* ($p = 0.01$), *ISG15* ($p = 0.02$), *OAS1* ($p = 0.02$), *IRF9* ($p = 0.01$), and *OAS2* ($p = 0.01$) (**Figure 3**).

GSEA was performed in surgical samples with the untreated group considered the reference baseline, and 23 pathways were found to be enriched, with 10 pathways increased and 13 pathways decreased. Three distinct canonical gene sets ascribed to interferon signaling, *GO, HALLMARK and REACTOME* were observed to be statistically increased in the MK-2206-treated

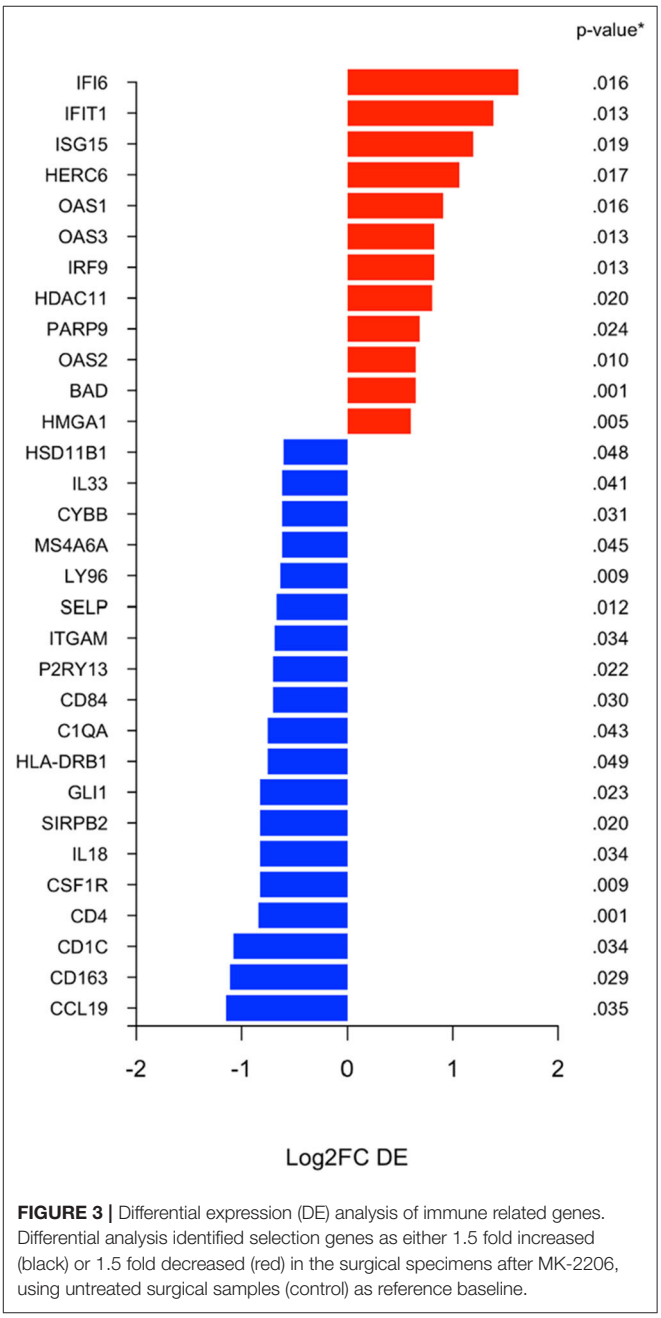

FIGURE 3 | Differential expression (DE) analysis of immune related genes. Differential analysis identified selection genes as either 1.5 fold increased (black) or 1.5 fold decreased (red) in the surgical specimens after MK-2206, using untreated surgical samples (control) as reference baseline.

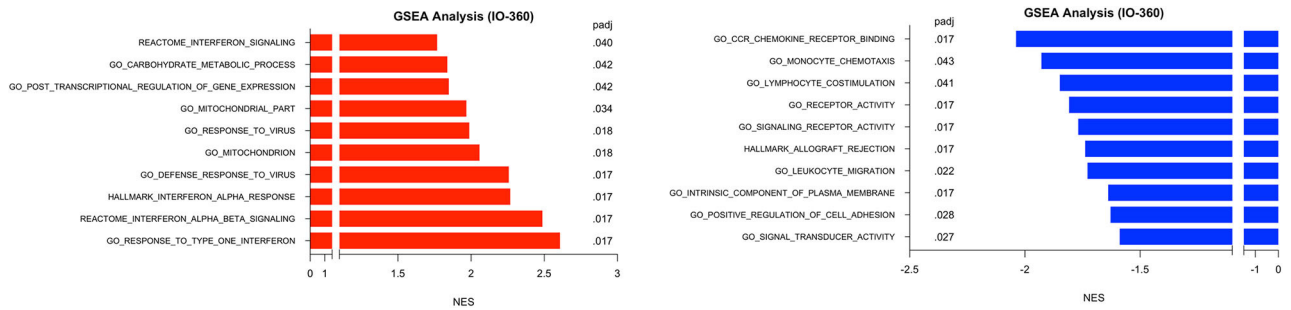

FIGURE 4 | Gene set enrichment analysis (GSEA) for Immune Related Genes. GSEA was performed using pathways derived from gene sets from Molecular Signatures Database (GO, HALLMARK, REACTOME gene sets). Plot above depicts top 10 pathways observed to be at least 1.5 fold increased (black) or 1.5 decreased (red) from surgical samples from MK-2206-treated patients, using untreated patients as a reference baseline which were found to be statistically significant by multiple comparison analysis.

surgical samples by multiple comparisons (all raw $p < 0.001$, adj $p < 0.02$), whereas genes ascribed to monocyte chemotaxis were decreased (raw $p < 0.01$, adj $p = 0.04$) (**Figure 4**) (18). As expected, gene sets highlighting carbohydrate metabolic processing (raw $p < 0.001$, adj $p = 0.04$) were increased in the post-MK-2206 samples.

DISCUSSION

To our knowledge, this is the first study to perform a comprehensive evaluation of the TME in patient breast tumor samples following treatment with an AKT inhibitor. After only two doses, in the window-of-opportunity study, our findings support direct and indirect activity of AKT inhibition on the TME.

Consistent with previous preclinical observations in BC cell lines, and reflecting known direct anti-neoplastic activity of AKT inhibition, we observed greater expression of pro-apoptotic genes and upstream receptor tyrosine kinases including *IGF-1R* and *HER3* following treatment with MK-2206 (19). Additionally, we identified higher levels of *GSK3A* (raw $p = 0.02$), a critical negative regulator of glycogen synthase, in the surgical samples from MK-2206-treated patients as compared to untreated controls, which is consistent with the important role of the PI3K pathway in metabolic regulation (10). These findings provide a transcriptomic basis for the increased serum glucose level ($p = 0.02$), insulin ($p < 0.01$) and C-peptide ($p < 0.01$) levels previously reported in the MK-2206 pre-surgical trial (9).

Notably, our data provides support from a clinical trial that is consistent with pre-clinical findings that that inhibition of the PI3K/AKT pathway are capable of increasing CD8 density in mouse models (13, 20). Therapeutics capable of augmenting CTL density within the TME would be expected to promote a more effective anti-tumor immune response, as high baseline CTL (CD8+) density are associated with chemosensitivity across BC subtypes and improved survival in TNBC and HER2 amplified BC (3, 21). In accordance with the increase in CD8 density by qMIF, we identified a higher expression of single interferon genes, as well as, gene sets related the interferon using the nanoString platform in MK-2206 post-treatment surgical samples. These signatures positively regulate T lymphocyte cytotoxicity and have been found to be upregulated in the context of other locoregional techniques which have demonstrated synergy with immunotherapy (6).

In parallel to our findings regarding CTL activity, we observed decreased expression of myeloid genes, which may contribute to the biologic mechanism underlying the increase in CD8 density and greater expression of cytotoxicity immune signatures seen following MK-2206. In our analysis, Akt inhibition was associated with lower expression levels of both individual myeloid related genes as well as several canonical myeloid gene sets on GSEA. Our observation is consistent with preclinical co-culture experiments with THP-1 cells and MCF7 breast cancer cells which support the PI3K pathway having a critical role in the modulation of macrophage activity in the TME which has in turn been implicated in impaired CTL response and increased metastatic potential (22). The clinical relevance of these findings are supported by clinicopathologic studies in human BC which have demonstrated that increased baseline myeloid cell density as well as expression of myeloid genes, including *CD163*, are associated with worse BC outcomes (22, 23).

STUDY LIMITATIONS AND FUTURE DIRECTIONS

These studies were performed on specimens from a trial that was terminated early due to grade III rash, mucositis, and pruritus, limiting the sample size available for evaluation. Additionally, while we intended to perform transcriptomic analysis on both the pre-treatment and post-treatment tissues specimens, as was done with qMIF, we were only able to perform this analysis on the tissue obtained from surgical resection due to inadequate RNA quantity from biopsy specimens. Despite performing multiplex approaches, B-lymphocyte, natural killer cell, and MDSC activity were underrepresented in our analysis. Preclinical data indicate that these immune subsets likely play an important role in the TME in BC and warrant investigation in further studies (24).

Lastly, equivalent effect on the TME cannot be assumed for agents that target alternative AKT isoforms or other components of the PI3K pathway and may not be generalizable for hormone receptor negative or HER2 amplified BC, as differences in immunobiology exist between BC subtypes (3).

SUMMARY

As preclinical data exist to supports activity of PI3K targeted agents on the immune microenvironment, the goal of this study was to assess the impact of Akt inhibition on the TME of HR+/HER2− BC in samples collected in a pre-surgical clinical trial. By qmIF and targeted genomic expression analysis, we confirmed in human breast cancer specimens the biologic activity of MK-2206, with well-described changes in gene expression of known targets of the PI3K/Akt/mTOR pathway as well as marked indirect immune related effects of Akt inhibition on the TME including an increase in CTL density as well as greater expression of interferon related genes and lower expression of myeloid genes.

In BC, particularly in tumors expressing the estrogen receptor, benefit from immunotherapeutic approaches has been modest and alternative strategies to augment host immune response are needed. Increased expression of interferon signatures is associated with improved relapse-free survival in BC patients, prompting development of agents aimed at specifically increasing CTL infiltration and interferon signaling with efficacy signals observed in other tumor types (25). Our findings support that agents targeting the PI3K pathway lead to a favorable change in the immune microenvironment and provide rationale for combining these agents with immunotherapeutics.

DATA AVAILABILITY STATEMENT

Publicly available datasets were analyzed in this study. This data can be found here: the NCBI Gene Expression Omnibus (GSE150512).

ETHICS STATEMENT

Patient provided written consent to participate in the presurgical study which was approved by the Columbia University Irving Medical Center and Albert Einstein Cancer Center institutional review boards.

AUTHOR CONTRIBUTIONS

DM and RG contributed to study design, performed qMIF and nanostring analyses, final data analysis, preparation of manuscript and provided study supervision. ME performed qMIF and nanostring analyses, final data analysis, preparation of manuscript. SB contributed to final data analysis, preparation of manuscript. TH, QP, and JY contributed to final data analysis. YL performed qMIF and nanostring analyses. HH and HG: reviewed pathology specimens and qMIF images, preparation of manuscript. KC, JS, and DH contributed to study design. EC, YS, and KK contributed to the study design, final data analysis, preparation of manuscript, and provided study supervision. All authors contributed to the article and approved the submitted version.

FUNDING

This work was supported by Women at Risk (KK). This work is also supported by contract N01-CM-62,204 to the New York Cancer Consortium (PI: JS) from the National Institutes of Health. In addition, this publication was supported by the National Center for Advancing Translational Sciences, National Institutes of Health, through Grant Number KL2 TR000081 (EC) and KL2TR001874 (RG). The content is solely the responsibility of the authors and does not necessarily represent the official views of the National Institutes of Health. RG is also supported by Swim Across America. This research was funded in part through the NIH/NCI Cancer Center Support Grant P30CA013696, by virtue of the usage of the Molecular Pathology Shared Resource of the Herbert Irving Comprehensive Cancer Center of Columbia University.

SUPPLEMENTARY MATERIAL

The Supplementary Material for this article can be found online at: https://www.frontiersin.org/articles/10.3389/fonc.2020.00968/full#supplementary-material

Supplementary Table 1 | Treatment and demographic data from MK-2206 and untreated control cohorts.

Supplementary Figure 1 | Change in CTL (C3+CD8+) density between diagnostic biopsies and surgical specimens in MK-2206 treated patients vs. control. M = MK-2206 treated, C = untreated. MK-2206 dose, M1: 200 mg dose, M2: 135 mg, M3: 90 mg, M4: 90 mg, M5: 90 mg. *PI3KCA mutation. **PTEN mutation.

Supplementary Figure 2 | Representative qMIF image of pretreatment and surgical specimen of MK-2206 treated patient. **(A)** qmIF image from pretreatment biopsy of patient selected to receive MK-2206. **(B)** qmIF image of post treatment pathology for same patient. Blue (Dapi/Nuclear), Red (Pancytokeratin), Cyan (CD3+), Magenta (CD8+), Yellow (FOXP3).

Supplementary Figure 3 | qmIF images demonstrating multiplex staining. **(A)** Dapi/Nuclear single stain (blue) **(B)** Dapi + pancytokeratin (red) multiplex image, red dot represents training program for cell phenotype (cell assigned as carcinoma based on pancytokeratin staining and nuclear features) **(C)** Dapi (blue), pancytokeratin (red) and CD3 (cyan) multiplex image **(D)** pancytokeratin (red), CD8 (magenta), and FOXP3 (yellow) multiplex image **(E)** Dapi (blue), pancytokeratin (red), CD4 (orange), CD68 (green) multiplex image.

REFERENCES

1. Loi S, Adams S, Schmid P, Cortés J, Cescon DW, Winer EP, et al. LBA13Relationship between tumor infiltrating lymphocyte (TIL) levels and response to pembrolizumab (pembro) in metastatic triple-negative breast cancer (mTNBC): results from KEYNOTE-086. *Ann Oncol.* (2017) 28:mdx440.005-mdx440.005. doi: 10.1093/annonc/mdx440.005
2. Schmid P, Adams S, Rugo HS, Schneeweiss A, Barrios CH, Iwata H, et al. Atezolizumab and Nab-Paclitaxel in advanced triple-Negative breast cancer. *N Engl J Med.* (2018) 379:2108–21. doi: 10.1056/NEJMoa1809615

3. Denkert C, von Minckwitz G, Darb-Esfahani S, Lederer B, Heppner BI, Weber KE, et al. Tumour-infiltrating lymphocytes and prognosis in different subtypes of breast cancer: a pooled analysis of 3771 patients treated with neoadjuvant therapy. *Lancet Oncol.* (2018) 19:40–50. doi: 10.1016/S1470-2045(17)30904-X
4. Loi S, Drubay D, Adams S, Pruneri G, Francis PA, Lacroix-Triki M, et al. Tumor-Infiltrating lymphocytes and prognosis: a Pooled individual patient analysis of early-Stage triple-Negative breast cancers. *J Clin Oncol.* (2019) 37:559–69. doi: 10.1200/JCO.18.01010
5. Vonderheide RH, LoRusso PM, Khalil M, Gartner EM, Khaira D, Soulieres D, et al. Tremelimumab in combination with exemestane in patients with advanced breast cancer and treatment-associated modulation of inducible costimulator expression on patient t cells. *Clin Cancer Res.* (2010) 16:3485–94. doi: 10.1158/1078-0432.CCR-10-0505
6. McArthur HL, Diab A, Page DB, Yuan J, Solomon SB, Sacchini V, et al. A pilot study of preoperative single-Dose ipilimumab and/or cryoablation in women with early-Stage breast cancer with comprehensive immune profiling. *Clin Cancer Res.* (2016) 22:5729–37. doi: 10.1158/1078-0432.CCR-16-0190
7. Isakoff SJ, Tolaney SM, Tung NM, Adams S, Soliman HH, Brachtel EF, et al. A phase 1b study of safety and immune response to PVX-410 vaccine alone and in combination with durvalumab (MEDI4736) in HLA-A2+ patients following adjuvant therapy for stage 2/3 triple negative breast cancer. *J Clin Oncol.* (2017) 35:TPS1126-TPS1126. doi: 10.1200/JCO.2017.35.15_suppl.TPS1126
8. Nanda R, Liu MC, Yau C, et al. Pembrolizumab plus standard neoadjuvant therapy for high-risk breast cancer (BC): results from I-SPY 2. *J Clin Oncol.* (2017) 35:506. doi: 10.1200/JCO.2017.35.15_suppl.506
9. Kalinsky K, Sparano JA, Zhong X, Andreopoulou E, Taback B, Wiechmann L, et al. Pre-surgical trial of the AKT inhibitor MK-2206 in patients with operable invasive breast cancer: a new york cancer consortium trial. *Clin Transl Oncol.* (2018) 20:1474–83. doi: 10.1007/s12094-018-1888-2
10. Okkenhaug K, Graupera M, Vanhaesebroeck B. Targeting PI3K in cancer: impact on tumor cells, their protective stroma, angiogenesis, and immunotherapy. *Cancer Discov.* (2016) 6:1090–105. doi: 10.1158/2159-8290.CD-16-0716
11. Xue G, Zippelius A, Wicki A, Mandalà M, Tang F, Massi D, et al. Integrated Akt/PKB signaling in immunomodulation and its potential role in cancer immunotherapy. *J Natl Cancer Inst.* (2015) 107:djv171. doi: 10.1093/jnci/djv171
12. Mittendorf EA, Philips AV, Meric-Bernstam F, Qiao N, Wu Y, Harrington S, et al. PD-L1 expression in triple-negative breast cancer. *Cancer Immunol Res.* (2014) 2:361–70. doi: 10.1158/2326-6066.CIR-13-0127
13. Abu-Eid R, Samara RN, Ozbun L, Abdalla MY, Berzofsky JA, Friedman KM, et al. Selective inhibition of regulatory t cells by targeting the PI3K-Akt pathway. *Cancer Immunol Res.* (2014) 2:1080–9. doi: 10.1158/2326-6066.CIR-14-0095
14. Gartrell RD, Marks DK, Hart TD, Li G, Davari DR, Wu A, et al. Quantitative analysis of immune infiltrates in primary melanoma. *Cancer Immunol Res.* (2018) 6:481–93. doi: 10.1158/2326-6066.CIR-17-0360
15. Cesano A, Warren S. Bringing the next generation of immuno-oncology biomarkers to the clinic. *Biomedicines.* (2018) 6:14. doi: 10.3390/biomedicines6010014
16. Du X, Wen J, Wang Y, Karmaus PWF, Khatamian A, Tan H, et al. Hippo/Mst signalling couples metabolic state and immune function of CD8α+ dendritic cells. *Nature.* (2018) 558:141–5. doi: 10.1038/s41586-018-0177-0
17. Burugu S, Asleh-Aburaya K, Nielsen TO. Immune infiltrates in the breast cancer microenvironment: detection, characterization and clinical implication. *Breast Cancer.* (2017) 24:3–15. doi: 10.1007/s12282-016-0698-z
18. Subramanian A, Tamayo P, Mootha VK, Mukherjee S, Ebert BL, Gillette MA, et al. Gene set enrichment analysis: a knowledge-based approach for interpreting genome-wide expression profiles. *Proc Natl Acad Sci U S A.* (2005) 102:15545–50. doi: 10.1073/pnas.0506580102
19. Chandarlapaty S, Sawai A, Scaltriti M, Rodrik-Outmezguine V, Grbovic-Huezo O, et al. AKT inhibition relieves feedback suppression of receptor tyrosine kinase expression and activity. *Cancer Cell.* (2011) 19:58–71. doi: 10.1016/j.ccr.2010.10.031
20. Peng W, Chen JQ, Liu C, Malu S, Creasy C, Tetzlaff MT, et al. Loss of PTEN promotes resistance to t Cell-Mediated immunotherapy. *Cancer Discov.* (2016) 6:202–16. doi: 10.1158/1538-7445.AM2016-4363
21. Ali HR, Provenzano E, Dawson SJ, Blows FM, Liu B, Shah M, et al. Association between CD8+ t-cell infiltration and breast cancer survival in 12,439 patients. *Ann Oncol.* (2014) 25:1536–43. doi: 10.1093/annonc/mdu191
22. Vergadi E, Ieronymaki E, Lyroni K, Vaporidi K, Tsatsanis C. Akt signaling pathway in macrophage activation and M1/M2 polarization. *J Immunol.* (2017) 198:1006–14. doi: 10.4049/jimmunol.1601515
23. Medrek C, Ponten F, Jirstrom K, Leandersson K. The presence of tumor associated macrophages in tumor stroma as a prognostic marker for breast cancer patients. *BMC Cancer.* (2012) 12:306. doi: 10.1186/1471-2407-12-306
24. Brown JR, Wimberly H, Lannin DR, Nixon C, Rimm DL, Bossuyt V. Multiplexed quantitative analysis of CD3, CD8, and CD20 predicts response to neoadjuvant chemotherapy in breast cancer. *Clin Cancer Res.* (2014) 20:5995–6005. doi: 10.1158/1078-0432.CCR-14-1622
25. Ribas A, Dummer R, Puzanov I, VanderWalde A, Andtbacka RHI, Michielin O, et al. Oncolytic virotherapy promotes intratumoral t Cell infiltration and improves anti-PD-1 immunotherapy. *Cell.* (2017) 170:1109–1119.e10. doi: 10.1016/j.cell.2017.08.027

Conflict of Interest: KK has consultancy or advisory positions with bioTheranostics, Lilly, Pfizer, Amgen, Novartis, Eisai, AstraZeneca, Ipsen, Genentech/Roche, Immunomedics, Odonate Therapeutics and immediate family member(s) with stock/ownership interest in Novartis and Array Biofarma. KK has also received fees to speak on behalf of Lilly. JY reports having received consultancy fees from Mount Sinai Health System.

The remaining authors declare that the research was conducted in the absence of any commercial or financial relationships that could be construed as a potential conflict of interest.

frontiers in Oncology

ORIGINAL RESEARCH
published: 19 June 2020
doi: 10.3389/fonc.2020.00805

Evaluation of the Anti-Tumor Activity of the Humanized Monoclonal Antibody NEO-201 in Preclinical Models of Ovarian Cancer

Kristen P. Zeligs[1†], Maria Pia Morelli[1†], Justin M. David[2†], Monica Neuman[1], Lidia Hernandez[1], Stephen Hewitt[1], Michelle Ozaki[1], Akosua Osei-Tutu[1], David Anderson[1], Thorkell Andresson[3], Sudipto Das[3], Justin Lack[4,5], Abdalla Abdelmaksoud[5,6], Massimo Fantini[2], Philip M. Arlen[2], Kwong Y. Tsang[2] and Christina M. Annunziata[1]*

[1] Women's Malignancy Branch, Center for Cancer Research, National Cancer Institute, National Institutes of Health, Bethesda, MD, United States, [2] Precision Biologics, Inc., Bethesda, MD, United States, [3] Protein Characterization Laboratory of the Cancer Research Program (CRTP)/Mass Spectrometry Center, National Institutes of Health, Fredrick, MD, United States, [4] NIAID Collaborative Bioinformatics Resource (NCBR), National Institute of Allergy and Infectious Diseases, National Institutes of Health, Bethesda, MD, United States, [5] Frederick National Laboratory for Cancer Research, Advanced Biomedical Computational Science, Fredrick, MD, United States, [6] Frederick National Laboratory for Cancer Research, CCR Collaborative Bioinformatics Resource, Fredrick, MD, United States

OPEN ACCESS

Edited by:
Niccolò Bolli,
University of Milan, Italy

Reviewed by:
Pierpaolo Correale,
Azienda Ospedaliera 'Bianchi-Melacrino-Morelli', Italy
Maria Shoshan,
Karolinska Institutet (KI), Sweden

***Correspondence:**
Kwong Y. Tsang
al.tsang@precision-biologics.com

[†]These authors have contributed equally to this work

Specialty section:
This article was submitted to Cancer Molecular Targets and Therapeutics, a section of the journal Frontiers in Oncology

Received: *11 December 2019*
Accepted: *23 April 2020*
Published: *19 June 2020*

Citation:
Zeligs KP, Morelli MP, David JM, Neuman M, Hernandez L, Hewitt S, Ozaki M, Osei-Tutu A, Anderson D, Andresson T, Das S, Lack J, Abdelmaksoud A, Fantini M, Arlen PM, Tsang KY and Annunziata CM (2020) Evaluation of the Anti-Tumor Activity of the Humanized Monoclonal Antibody NEO-201 in Preclinical Models of Ovarian Cancer. Front. Oncol. 10:805. doi: 10.3389/fonc.2020.00805

Purpose: Despite high initial response rates with cytoreductive surgery, conventional chemotherapy and the incorporation of biologic agents, ovarian cancer patients often relapse and die from their disease. New approaches are needed to improve patient outcomes. This study was designed to evaluate the antitumor activity of NEO-201 monoclonal antibody (mAb) in preclinical models of ovarian cancer where the NEO-201 target is highly expressed.

Experimental Design: Functional analysis of NEO-201 against tumor cell lines was performed by antibody-dependent cellular cytotoxicity (ADCC) assays. Binding of NEO-201 to tumor tissues and cell lines were determined by immunohistochemistry (IHC) and flow cytometry, respectively. Further characterization of the antigen recognized by NEO-201 was performed by mass spectrometry. Ovarian cancer models were used to evaluate the anti-tumor activity of NEO-201 *in vivo*. NEO-201 at a concentration of 250 g/mouse was injected intraperitoneally (IP) on days 1, 4, and 8. Human PBMCs were injected IP simultaneously as effector cells.

Results: Both IHC and flow cytometry revealed that NEO-201 binds prominently to the colon, pancreatic, and mucinous ovarian cancer tissues and cell lines. Immunoprecipitation of the antigen recognized by NEO-201 was performed in human ovarian, colon, and pancreatic cancer cell lines. From these screening, carcinoembryonic antigen-related cell adhesion molecule 5 (CEACAM5) and CEACAM6 were identified as the most likely targets of NEO-201. Our results confirmed that NEO-201 binds different types of cancers; the binding is highly selective for the tumor cells without cross reactivity with the surrounding healthy tissue. Functional analysis revealed that NEO-201 mediates ADCC killing against human ovarian and colorectal carcinoma cell lines *in vitro*. In addition, NEO-201 inhibited tumor growth in the presence of activated human PBMCs in orthotopic mouse models

of both primary and metastatic ovarian cancer. Importantly, NEO-201 prolonged survival of tumor-bearing mice.

Conclusions: These data suggested that NEO-201 has an antitumor activity against tumor cells expressing its antigen. Targeting an antigen expressed in tumors, but not in normal tissues, allows patient selection for optimal treatment. These findings strongly indicate that NEO-201 warrants clinical testing as both a novel therapeutic and diagnostic agent for treatment of ovarian carcinomas. A first in human clinical trial evaluating NEO-201 in adults with chemo-resistant solid tumors is ongoing at the NIH clinical Center.

Keywords: monoclonal antibody, tumor-associated antigen, antibody-dependent cellular cytotoxicity, natural killer cell, carcinoembryonic antigen-related cell adhesion molecule 5 (CEACAM5), carcinoembryonic antigen-related cell adhesion molecule (CEACAM6)

INTRODUCTION

Ovarian cancer is the most lethal gynecologic malignancy in the United States. Although it accounts for only 3% of cancers among women, it is the fifth most common cause of cancer-related death (1). Most patients are diagnosed when distant metastatic spread is already present. To date, the treatment of primary and recurrent ovarian cancer groups most epithelial ovarian subtypes together, in a common therapeutic approach. Primary mucinous carcinoma of the ovary represents a small subset of epithelial ovarian carcinoma and is histologically, molecularly, and clinically distinct from the other subtypes.

Over the last 10 years, incorporation of precision therapy and immunotherapy has led to important paradigm changes for the treatment of cancer patients. Cancer immunotherapy is aimed to enhance the power of the host immune system for the treatment of malignancy. Recent efforts in cancer therapeutics have focused on the development of immune checkpoint inhibitors, which are FDA approved for the treatment of certain tumor types. To date, this class of drugs in ovarian cancer has shown limited activity when used as monotherapy (2). Ongoing trials are evaluating the activity of PD-1/PD-L1 inhibition in combinations with other therapeutic agents that have shown activity in ovarian cancers such as VEGF and PARP inhibitors (3).

The majority of recent developments in immunotherapy strategies, including immune checkpoint inhibitors (4), vaccines (5), and engineered chimeric T-cell receptors (6), have focused on boosting the adaptive immune system. Additionally, the innate immune response can play an important antitumor role with direct tumoricidal activity, and/or indirect activity through the processing and presenting of tumor antigens to T cells (7). It is well known that monoclonal antibodies (mAbs), such as rituximab and trastuzumab, can mediate antibody-dependent cellular cytotoxicity (ADCC) (8). Natural killer (NK), neutrophils, and other myeloid cells can also kill through ADCC, a process by which engagement of FcγRs results in the release of cytotoxic granules (8). In addition to ADCC, opsonization of tumor cells with antitumor mAbs can lead to macrophages' antibody-dependent phagocytosis (ADPC) and to complement-dependent cytotoxicity (CDC) (9).

NEO-201 is a humanized IgG1 monoclonal antibody (mAb) derived from an immunogenic cancer vaccine. NEO-201 was selected for its tumor specificity and its association with clinical response. It was generated using the Hollinshead allogenic colorectal cancer vaccine platform (10), where tumor-associated antigens (TAA), derived from tumor membrane fractions pooled from colorectal cancer surgical specimens, were screened for delayed-type hypersensitivity and evaluated in clinical trials (11). Those patients who developed a sustained IgG response and a cell-mediated response against the vaccine achieved significant anti-tumor response and increased overall survival (12). NEO-201 binds specifically to a wide range of human cancer cells and tumor tissues, but not with healthy normal tissues. NEO-201 showed to have both ADCC and CDC activity against cancer cell lines *in vitro* (10, 13) and to counteract the growth of human pancreatic xenograft tumors *in vivo* (10). In the present work, we sought to further characterize the antigen recognized by NEO-201, and to demonstrate its efficacy in preclinical ovarian models. We performed mass spectrometry analysis to identify its target antigen. Exome sequencing was conducted to identify mutations shared by cell lines expressing the antigen recognized by NEO-201 and to identify possible effector pathways.

MATERIALS AND METHODS

Drug

NEO-201 humanized monoclonal antibody was generated and provided by Precision Biologics, Bethesda, MD, USA (10).

Cell Lines and Culture

The following human colorectal (CRC), ovarian (OV) and pancreatic (PDAC) cancer cell lines were obtained from the American Type Culture Collection (ATCC) or National Cancer Institute (NCI)-60: LS174T (CRC), SW480 (CRC), Ovcar8 (OV), Ovacar5 (OV), PEO1 (OV), PEO4 (OV), PEO5 (OV), OV90 (OV), ASPC-1 (PDAC), BxPC3 (PDAC), CFPAC-1 (PDAC). Cells were grown in RPMI medium (Corning Life Science, Manassas, VA, USA) supplemented with 10% USA-sourced and heat-inactivated HyClone Fetal Bovine Serum (FBS; GE Healthcare Life Sciences, Issaquah, WA, USA), 1% penicillin/streptomycin (Corning Life Science, Manassas, VA, USA) and maintained at

37°C in incubator under 5% CO_2. Cell lines were authenticated via short tandem repeat at the Frederick National Laboratory.

The highly active natural killer (haNK) cell line was obtained from Nantkwest and cultured with X-VIVO media (Lonza, Basilea, Switzerland) enriched with L-glutamine and 5% heat-inactivated human AB serum (Gemini Bio-Products, West Sacramento, CA, USA) as previously described (14). Cells used for tumor induction were tested by Molecular Testing of Biological Materials (MTBM) as required by the NCI ACUC Committee and confirmed to contain no mouse viruses. Human peripheral blood mononuclear cells (PBMCs) were collected from anonymous healthy donors under protocol 99-CC-0168, approved by the Institutional Review Board of the National Cancer Institute.

Immunoblotting

Cells were seeded in 6-well plates and allowed to grow for 24 h. Protein lysates were prepared in radioimmunoprecipitation assay (RIPA) buffer (Santa Cruz Biotechnology Inc, Dallas, TX, USA) according to manufacturer's protocol. The total protein was determined using the BCA Protein Assay Kit (Thermo Fisher Scientific, Waltham, MA, USA). Twenty-five micrograms of total protein were loaded onto a 4–12% gradient gel, electrophoresed, and transferred to nitrocellulose using the NuPage system (Invitrogen, Thermo Fisher Scientific, Waltham, MA, USA). Membranes were blocked for 1 h in 5% Milk in TBS-Tween blocking buffer and incubated overnight with NEO-201 (1 μg/ml) at 4°C. Following incubation with NEO-201, membranes were washed three times for 10 min in TBS-Tween and then incubated with the appropriate secondary goat anti-human IgG1 Fc-HPR (1:10,000). Membranes were stripped and probed with GAPDH (1:10,000) loading control. Blots were developed using Supersignal Chemiluminescent Substrate system (Thermo Fisher Scientific, Waltham, MA, USA). Immunoblot experiments were done in triplicate.

Immunohistochemistry (IHC)

Formalin-fixed, paraffin-embedded (FFPE) sections of human tumor samples and non-malignant controls were analyzed for NEO-201 target protein expression using immunohistochemistry. Staining was performed manually. Antibody specifications and staining conditions were optimized on control whole colon cancer tissue samples, and negative controls consisted of sections that underwent similar staining procedures with an IgG control antibody of the corresponding isotype. Tissue microarray analysis was performed on 21 colon cancer, 24 lung cancer, 19 breast cancer, 11 lymphoma, 11 melanoma, and 7 glioblastoma multiforme. Tissue microarray of 627 ovarian tumor samples was obtained from Roswell Park Cancer Institute and contained tumor tissues from different subtypes of ovarian cancer, including 446 serous adenocarcinomas, 37 germinal cell tumor, 26 clear cell, 23 endometroid, 22 adenocarcinomas NOS, 22 mucinous adenocarcinoma, 18 sarcomas, 9 transitional cell, 9 carcinoma, 2 signet cell carcinoma, and 13 "other" subtype. Tissues were scored for the expression of the antigen recognized by NEO-201 and percentage of positive tumor tissue. A score of 2+ was given to those tumor tissues with a complete staining of the membrane in more than 10% of the sample analyzed and a score of 1+ to those tumor tissues with a complete staining of the membrane in <10% of the tissue analyzed.

Flow Cytometry

Expression of tumor antigens on tumor cells was analyzed by flow cytometry. Tumor cells (1.0×10^6) were harvested and first incubated with 1 μl per test of LIVE/DEAD Fixable Aqua (Thermo Fisher Scientific, Waltham, MA, USA) in 1× phosphate-buffered saline (PBS) for 30 min at 4°C to accomplish live vs. dead cell discrimination. Cells were then centrifuged, washed twice with cold PBS, and then stained in 1× PBS + 1% BSA (Teknova, Hollister, CA, USA) for 30 min at 4°C with the following anti-human mAbs: Pacific Blue-conjugated or PE-conjugated NEO-201 antibody (BioLegend, San Diego, CA, USA), CEACAM5-FITC (clone C365D3), CEACAM6-PE (clone KOR-SA3544; ThermoFisher Scientific, Waltham, MA, USA). After staining, cells were washed twice with cold PBS and examined using a FACSVerse flow cytometer (BD Biosciences, San Jose, CA, USA). Analysis of cellular fluorescence was performed using BD FACSuite software (BD Biosciences, San Jose, CA, USA). Positivity was determined using fluorescence-minus-one controls.

Proliferation Assay

Antiproliferative effects of NEO-201 were determined using sodium 3,3′-[1(phenylamino)carbonyl]-3,4-tetrazolium]-3is(4-methoxy-6-nitro) benzene sulfonic acid hydrate (XTT) assay as previously described (15). Briefly, cells in logarithmic growth phase were transferred to 96-well flat-bottomed plates with lids. Cell suspensions containing 5×10^3 cells/well were plated and incubated overnight and then treated with different concentrations of NEO-201 for 72 h. After treatment, cell viability was assessed by incubating cultures with 25 μl of XTT freshly mixed with PMS (Sigma), and absorbances were read at a measured timepoint using a Tecan plate reader (Research Triangle Park, NC, USA) as previously described. IC50 was calculated using CompuSyn software. The median dose was obtained from the anti-log of the x-intercept of the median effect plot: log (Fa/Fu) = m*log (D) – m*log (Dm) where Fa is the Fraction affected, Fu is the Fraction unaffected, and m is the slope.

Antibody-Dependent Cellular Cytotoxicity (ADCC) Assay

To evaluate the ADCC activity of NEO-201 against human carcinoma cell lines, both radioactive and non-radioactive ADCC assays were performed. Non-radioactive ADCC assay was performed using a previously described procedure (10) using human cancer cell lines as target cells. Natural killer (NK) cells from normal donor and irradiated haNKs (10 Gy) were used as effector cells. For non-radioactive ADCC assay, target cells were labeled with 10 μM calcein AM cell-permanent dye, for 30 min and then seeded in triplicate at 3.0×10^3 cells/well into black-walled flat-bottomed 96-well plates. Then, human IgG1 isotype control antibody (Thermo Fisher Scientific, Waltham, MA, USA) or NEO-201 antibody was added to target cells at

different concentrations. haNK cells were simultaneously added at specific effector-to-target (E:T) ratios. After 4 h of incubation at 37°C, 1.67 μg/ml of propidium iodide (PI; Thermo Fisher Scientific, Waltham, MA, USA) was added to each well, the plate was imaged using the Celigo Imaging Cytometer (Nexcelom Bioscence LLC, Lawrence, MA, USA), and the numbers of live target cells (calcein AM+/PI–) vs. dead cells (calcein AM+/PI+ or calcein AM–/PI+) were analyzed and recorded by the Celigo Imaging Cytometer analysis software.

For radioactive ADCC assay, chromium release assays were performed using NK cells from human healthy donors. Briefly, NK cells were obtained by negative selection from human healthy donor PBMCs using the EasySep Human NK Cell Isolation Kit (StemCell Technologies, Vancouver, BC, Canada) according to the manufacturer's protocol. Purified NK cells were incubated overnight in RPMI-1640 medium supplemented with L-glutamine, 10% FBS, and antibiotics prior to be used as effector cells in the assay. On the day of the assay, cancer cells were labeled with ^{51}Chromium and then used as target cells in presence of 1 μg/ml of human IgG1 isotype control antibody or NEO-201 antibody at different concentrations. NK cells were added simultaneously at specific effector-to-target (E:T) ratios. Specific lysis was calculated as % specific lysis = 100 – [(average live target cell count for antibody treated samples/average live target count for control samples) Å∼100].

ELISA

Ninety-six-well plates were first coated overnight at 4°C with 100 μl/well of 400 ng/ml recombinant human CEACAM1, 5, 6, and 8 protein (Acro Biosciences) diluted in 0.2 M sodium carbonate–bicarbonate buffer pH 9.4. Plates were washed with 1× Tris-buffered saline (TBS) + 0.05% Tween-20 and then blocked with 200 μl/well of 5% milk in 1× TBS for 1 h at 37°C. Plates were washed, and then 100 μl/well of NEO-201 antibody was added in two-fold serial dilution from 20 ng/ml to 0.156 ng/ml and incubated for 1 h at 37°C. Plates were washed, and 100 μl/well of donkey anti-human IgG antibody peroxidase conjugate (VWR) at a 1:10,000 dilution was added to the plate and incubated for 1 h at 37°C. Plates were washed, and 100 μl/well of tetramethylbenzidine (TMB) substrate solution (VWR) was added and incubated for 10 min at RT in the dark. The reaction was stopped by adding 50 μl/well of 2 N H_2SO_4, and absorption at 450 nm was read using a FLUOstar Omega plate reader (BMG Labtech).

Mass Spectrometry

NEO-201 target antigen identification was performed by mass spectrometry. Briefly, 100 μg of total protein extracted from OV90, CFPAC1, OVCAR8 human cell lines, and protein A beads were incubated with 1 μg of NEO-201 and immunoprecipitated. A dose titration was performed to identify an optimal dose of NEO-201 to immunoprecipitate the proteins for the mass spectrometry analysis. One microgram and 10 ng of NEO-201 were used in the analysis. To identify the proteins bound by NEO-201, those proteins that were common in both OV90 and CFPAC1 were considered as potential targets, and those proteins identified also by the beads and the OVCAR8 were considered as non-specific binding and subtracted from the analysis. PSMs indicate the number of peptides identified of each of those proteins, and the more the number of peptides identified, the more the confidence is in the data.

Plasmid Overexpression and Immunoblot

Overexpression experiments were performed in epithelial human embryonic kidney cell line HEK293T. Expression vectors with the incorporated CEACAM5 or CEACAM6 complementary DNAs were generated using a DHFR mammalian expression vector as the DNA of each plasmid (or empty original vector) was transiently transfected using Lipofectamine 2000 reagent (Invitrogen) into 1 × 10^6 HEK293T cells (80 to 90% confluent) and were seeded on a 6-well plate and cultured for an additional 48–72 h. Then, the cells were harvested and lysed. Whole cell lysates and molecular weight marker standards were applied (50 μg/lane) to polyacrylamide gel and run through electrophoresis, transferred on a nitrocellulose membrane, and subjected to Western blot analysis. Primary antibodies were mouse anti-human CEACAM5 clone CB30 (Cell Signaling Technology, Danvers, MA, USA), mouse anti-human CEACAM6 clone 9A6 (Abcam, Cambridge, UK), and NEO-201.

RNA Interference

Cells were seeded into 6-well plates and transfected with 100 nM of Dharmacon ON-TARGETplus SMARTpool siRNAs specific for CEACAM5, CEACAM6, or a non-targeting control (Horizon Discovery Group, Cambridge, UK) using 4 μl of DharmaFECT 2 transfection reagent (Horizon Discovery Group, Cambridge, UK) per transfection according to the manufacturer's instructions. Cells were incubated for at least 72 h prior to use.

Mutational Analysis

DNA was extracted using the DNAasy Plus mini kit (Qiagen, Valencia, CA, USA) according to the manufacturer's protocol. For whole exome sequencing (WES), DNA libraries were prepared using Agilent SureSelectXT Human All Exon V5 plus UTR target enrichment kit, and samples were pooled and sequenced on an Illumina HiSeq2500 with TruSeq V4 chemistry. Alignment and variant calling was performed using the CCBR Pipeliner (https://github.com/CCBR/Pipeliner) tool on NIH's Biowulf cluster. Reads were trimmed using Trimmomatic v0.33 (16) and mapped to the hs37d5 version of the human reference genome (ftp://ftp.1000genomes.ebi.ac.uk/vol1/ftp/technical/reference/phase2_reference_assembly_sequence/hs37d5.fa.gz) using BWA-mem v07.15. BAM files were processed using Samtools v1.3 (http://www.htslib.org/) (17), and duplicates were marked using Picard v2.1.1 (http://broadinstitute.github.io/picard/). GATK v3.5.0 (18) was used to perform indel realignment and base recalibration. Read- and alignment-level quality control visualization was performed using MultiQC v1.1 (http://multiqc.info/) to aggregate QC metrics from FastQC (http://www.bioinformatics.babraham.ac.uk/projects/fastqc/), FastQ Screen (https://www.bioinformatics.babraham.ac.uk/projects/fastq_screen/), Picard, bamtools (19), stats (http://github.org/pezmaster31/bamtools), and trimmomatic. Variant calling was performed with MuTect2 (20). A panel of normals,

developed from ExAC r0.3.1 (21) and the 1,000 Genomes Project (22), including only variants >0.001 in frequency in the general population was used in cases without a matched germline. Somatic variants with an allele frequency of <0.05 were excluded. Variants were annotated using Oncotator v1.9.1.0 (23) (http://portals.broadinstitute.org/oncotator/).

Assessment of NEO-201 Activity on Tumor Growth and Survival *in vivo*

Primary Ovarian Cancer Model

Female athymic nude mice, 6–8 weeks old, were maintained on a 12-h light/dark cycle, with food and water provided *ad libitum*. Briefly, 2.5×10^5 OV90 cells were injected into the right ovarian bursa, and 5 μl of PBS was injected into the contralateral ovarian bursa. When tumors reached an average of 100–300 mm^3 of volume, mice were randomized into four treatment groups. Animals received treatment with either PBS/IgG as vehicle control, activated PBMCs with IgG, NEO-201 250 μg/mouse, or activated PBMCs with NEO-201. NEO-201 was administered at a dose of 250 μg/mouse IP on days 1, 4, and 8 of treatment, PBS/IgG-control was administered on the same days at a dose of 250 μg/mouse. Before injection, PBMCs were cultured overnight in RPMI media supplemented with IL-2 at 200 U/ml. A total of 500 μl with 8×10^6 PBMCs was inoculated by intraperitoneal (IP) injection into each mouse on days 2, 5, and 9 of treatment. Mice were followed for signs of toxicity, and body weight was measured three times a week. Orthotopic tumor growth was assessed by ultrasound once weekly, and tumor volumes were calculated according to the formula of volume = (length × $width^2$)/0.52. Mice were euthanized 2 weeks after treatment completion.

Metastatic Ovarian Cancer Model

To assess the effect of NEO-201 on survival, 1×10^6 OV90 cells were injected into the peritoneal cavity of each mouse. Tumors were allowed to grow for 2 weeks before mice were randomized into one of the four treatment groups described above. Mice were evaluated biweekly for signs of drug-related toxicity and disease progression based on distress, physical exam changes, and cachexia. Animal care was provided in accordance with the procedures in the Guide for the Care and Use of Laboratory Animals. Experiments were carried out according to a protocol approved by the NCI Animal Care and Use Committee.

Ultrasound Imaging

Mice were anesthetized with isoflurane via nose cone and placed dorsum up on moveable platform with arms and legs taped to the platform. The Vevo-2100 system with a 3D motor and 40-MHz probe was utilized. The platform was angled away from the investigated side. Ultrasound gel was placed over the lateral lumbar area and the motor-operated probe oriented transversely over area. The kidney was located with the ipsilateral ovary often localized at the inferior pole of the kidney, when no xenograft was present. Presence of ovarian artery and vein were confirmed by color Doppler ultrasound. A three-dimensional (3D) image was acquired by computerized 2D images obtained every 50 μm along the axis. Ovaries and ovarian tumor xenografts were analyzed for 3D volume measurement in open mode on Vevo Lab 2.1.0 software.

Statistical Analysis

NEO-201 induced ADCC activity in "*in vitro*" model was evaluated by ordinary one-way ANOVA. Significant differences between the different mice treatment groups were evaluated by Kruskal–Wallis test, using GraphPad Prism 7.0 software (GraphPad Software, La Jolla, CA, USA). Significant differences in survival between the treatment groups were evaluated by Mantel–Cox, using GraphPad Prism 7.0 software. Differences were considered significant when the value of $p < 0.05$.

RESULTS

Expression Profile of NEO-201 Binding in Patient Tumor Tissues and Human Cancer Cell Lines

NEO-201 binding was evaluated by immunohistochemistry (IHC) in patient tissues from 21 colon, 24 lung, 19 breast, and 11 ovarian cancers. Also, we tested the NEO-201 binding in 11 tissues from lymphoma and melanoma, and seven glioblastomas. Respective normal tissues were tested as well (**Figures 1A,B**). All of the tissues from colon cancer patients resulted positive for NEO-201 staining, 84% (20/24) of the lung, 31.6% (6/19) of the breast, and 9% (1/11) of the ovarian cancer patient tissues were positive, while the respective healthy tissues surrounding the tumor were negative for NEO-201 binding. Additionally, no stain was detected in tissues from patients with lymphoma, glioblastoma, and melanoma. We further assessed the degree of NEO-201 binding in the tissues from patients with different ovarian cancer subtypes, using a tissue microarray (TMA) containing 627 ovarian cancer samples including 11 ovarian cancer histological subtype (**Figure 1A**, bottom). Interestingly, mucinous adenocarcinoma showed the highest percentage of positive samples among all the histological subtypes analyzed, with 68.2% positive for NEO-201 staining, and 59% (13/22) had a 2+ score. Serous adenocarcinoma and germinal cell tumors showed 20% (87/446) and 38% (14/37) positive staining, respectively. In order to identify cell line models representative of the human samples, we created a cell pellet array of ovarian and colon cancer cell lines and probed them in the same manner as the patient tissue microarrays (**Figure 1C**). IHC results were verified by flow cytometry except in PEO1 in which staining was discrepant (**Figure 1D**). Ovarian cancer cell line OV90 and colon cancer cell line LS174T showed strong staining with both techniques.

NEO-201 Binds to Carcinoembryonic Antigen-Related Cell Adhesion Molecule (CEACAM) 5 and 6

To identify the specific antigen recognized by NEO-201, protein lysates from OV90 and CFPAC1 were immunoprecipitated with 1 μg/ml or 10 ng/ml of NEO-201 in the presence of protein A beads and run on an acrylamide gel. Beads alone were used as negative control. The blot was probed with NEO-201 to

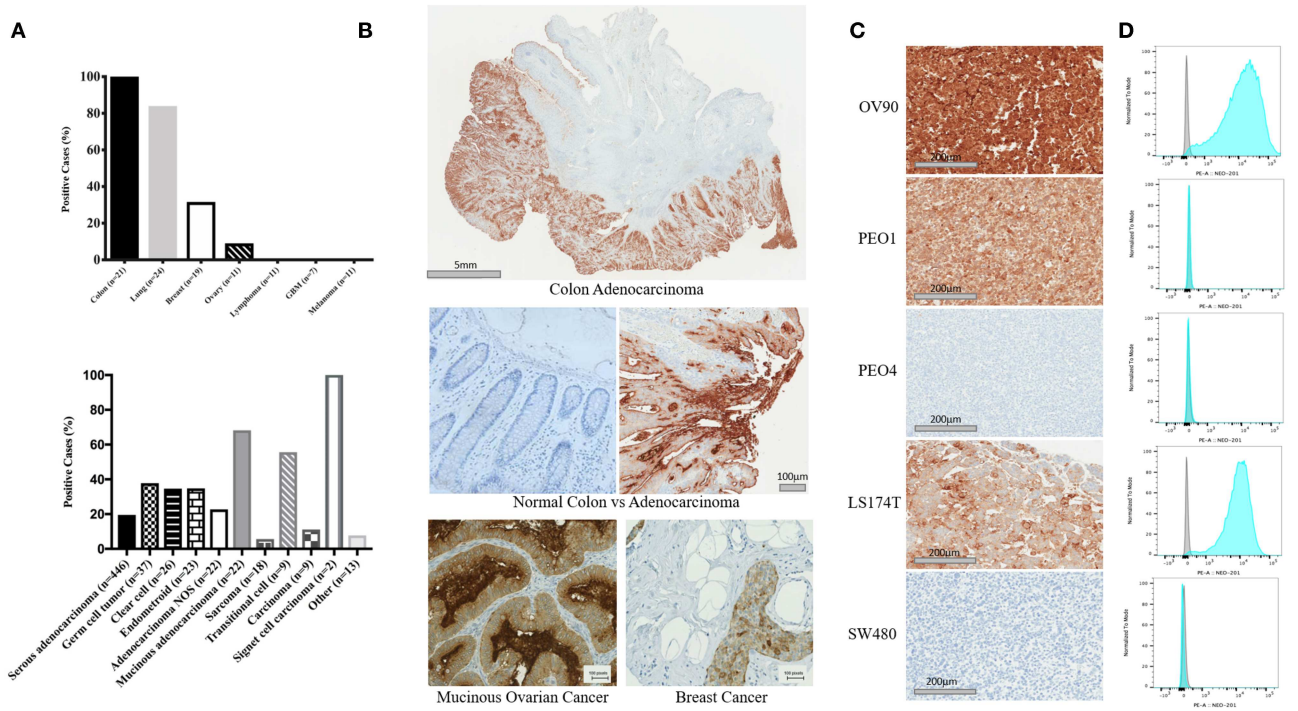

FIGURE 1 | Expression profile of the antigen recognized by NEO-201 in patient tumor tissues and human cancer cell lines. **(A,B)** NEO-201 binding in colon ($n = 21$), lung ($n = 24$), breast ($n = 19$), and ovarian ($n = 11$) cancers, lymphoma ($n = 11$), glioblastoma multiforme ($n = 7$), and melanoma ($n = 11$) was measured by immunohistochemistry (IHC). Additionally, the degree of expression of the antigen recognized by NEO-201 in 627 tissues from more than 10 different ovarian cancer subtypes including serous, germ cell, clear cell, endometroid, mucinous, sarcoma, transitional, and adenocarcinoma NOS, was evaluated by tissue microarray analysis (TMA). Tissues were scored for positive vs. negative expression of the antigen recognized by NEO-201 and for percentage of positive tumor tissue. Those tissues with a complete staining of the membrane in more than 10% of the samples analyzed were given a 2+ score, while those with a complete staining of the membrane in <10% of the tissue analyzed were given a 1+. **(C)** Cell pellet from the ovarian cancer cell lines OV90, PEO1, PEO4, and colorectal cancer cell lines SW480 and LS174T were screened for NEO-201 binding by IHC. **(D)** NEO-201 binding on cancer cell line model was confirmed by FACS analysis. Cells were incubated with NEO-201 PE-conjugated antibody and then analyzed.

confirm the selective isolation of the protein bound by the NEO-201. NEO-201 1 µg showed the best results in terms of protein immunoprecipitation for the proteomic analysis, while 10 ng/ml was not considered sufficient to achieve an adequate result (**Figure 2A**). OVCAR8 cells were used as negative control since they do not express the antigen recognized by NEO-201 (**Figure 2A**). Immunoprecipitated proteins were analyzed by mass spectrometry analysis to identify the antigen recognized by NEO-201. A list of possible antigens was detected comparing the proteins identified in the OV90, CFPAC1, OVCAR8, and protein A beads. Non-specific peptides were eliminated by subtracting those found in the negative control cell line OVCAR8 or in IgG control precipitates, and only the proteins detected in both OV90 and CFPAC1 were considered as relevant. From these screening, the carcinoembryonic antigen-related cell adhesion molecule (CEACAM)5, also known as CEA, and CEACAM 6 were identified as the most likely targets of NEO-201 (**Figure 2A**, bottom).

Dual staining of ASPC-1, BxPC3, CFPAC-1, and LS174T cell lines was performed with NEO-201 and with either anti-CEACAM5 or anti-CEACAM6 antibodies and analyzed by flow cytometry, showing that there is overlap between CEACAM5 or 6 expression with the antigen recognized by NEO-201 (**Figure 2B**). In most cell lines, however, the overlap was incomplete, suggesting that the cells express a normal variant of each CEACAM as well as the cancer-associated variant. By ELISA, NEO-201 antibody bound to both recombinant human CEACAM5 and CEACAM6 but not CEACAM1 or CEACAM8 (**Figure 2C**).

We proceeded to overexpress CEACAM5 and CEACAM6 in HEK293T cells to determine which reacted to NEO-201. HEK293T cell lines are known to have a negative phenotype for NEO-201 binding and do not express CEACAM 5 or 6 at baseline. HEK293T transfected with an empty vector confirmed no expression of either CEACAM5, or CEACAM6, or reaction to NEO-201 immunoblot, and the transfected clones showed a positive expression for either CEACAM 5 or CEACAM6, as intended. By Western blot, NEO-201 reacted with both CEACAM proteins (**Figure 2D**).

Evaluation of the expression of the antigen recognized by NEO-201 in ovarian and colon cancer cell lines by Western blot showed that LS174T colorectal cancer cell line expresses two distinct molecular weights of the antigen recognized by NEO-201, likely representing both CEACAM5 and CEACAM6, consistent with the flow cytometric analysis (**Figure 2E**). Among the ovarian cancer cells, PEO-1 and OV90 expressed only the

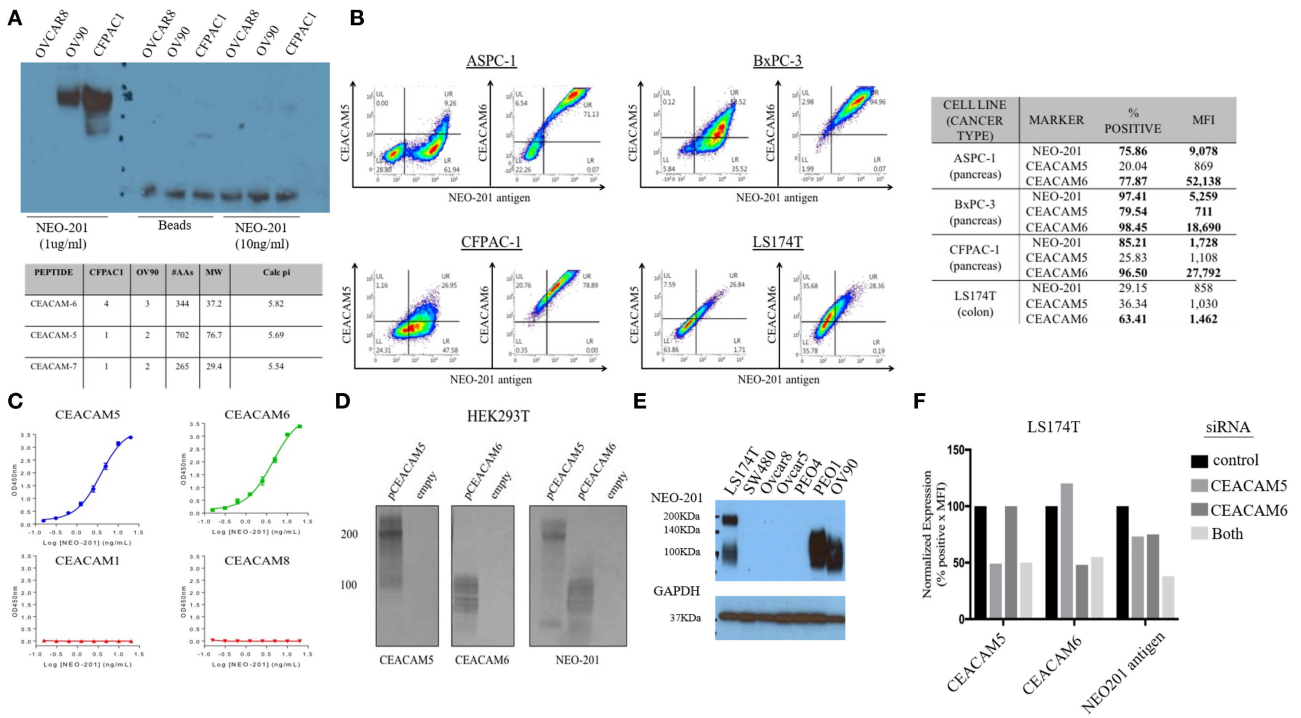

FIGURE 2 | NEO-201 binds to CEACAM 5 and 6. **(A)** To identify the antigen recognized by NEO-201, 100 μg of proteins extracted from OV90, CFPAC1, and OVCAR8 was initially immunoprecipitated with 1 μg, 10 ng of NEO-201 and protein A beads. One microgram of NEO-201 showed the best results in terms of protein isolation and was used to perform intraperitoneal (IP) injection for the protein sample that was then analyzed by mass spectrometry. Peptide suggesting the glycosylated form of CEACAM-5 and−6 was identified as the most likely antigen recognized by NEO-201. **(B)** Flow cytometry analysis of the tumor cell lines ASPC-1, BxPC-3, CFPAC-1, and LS174T was performed to discriminate the native form of CEACAM5 and CEACAM6 from the NEO-201-reactive variant forms of CEACAM5 and CEACAM6. NEO-201 binding on cancer cell line model was assessed using NEO-201 Pacific Blue conjugated antibody. **(C)** NEO-201 binding to different forms of CEACAMs, other than 5 and 6, was measured by ELISA. **(D,F)** To confirm the binding of NEO-201 to CEACAM-5 and−6, CEACAM-negative cells HEK293T were transfected with CEACAM-5 and 6 siRNA. The two proteins, which express a different molecular weight, were equally bound by NEO-201. As proof of concept, CEACAMs and NEO-201-positive cells LS174T were knock-down for CEACAM 5/6 genes, which resulted in an about 25% partial loss of NEO-201 binding when a single gene was knock-down, and a further decreased to about the 50% loss of NEO-201 binding by the combined knockdown of both CEACAMs. **(E)** Western blot confirmed that NEO-201 binds an antigen with two different molecular weights in cell line models.

lower CEACAM6 molecular weight form. SW480, OVCAR5, OVCAR8, and PEO4 were negative. Knockdown of either CEACAM5 or CEACAM6 in LS174T cells showed about 25% partial loss of NEO-201 binding, which was doubled to approximately 50% loss of NEO-201 binding by the combined knockdown of both CEACAMs (**Figure 2F**).

Altogether, these results confirmed that NEO-201 binds different types of cancers. The binding is highly selective for the tumor cells without cross reactivity with the surrounding healthy tissue. Moreover, within cancer tissue origins, the antigen recognized by NEO-201 is differentially expressed between tumor histological and/or molecular subtype. These data suggested that NEO-201-positive tumors express a specific phenotype of a tumor-associated variant of CEACAM 5 (CEA) and 6, which is not expressed in normal tissues.

Mutational Analysis

To investigate the nature of CEACAM 5 (CEA) and 6 variants expressed on tumor cells, we performed whole exome sequencing of OV90 (NEO-201^{pos}), LS174T (NEO-201^{pos}), SW480 (NEO-201^{neg}), and OVCAR8 (NEO-201^{neg}) cell lines. We searched for mutations that were commonly present in both LS174T and OV90 (NEO-201-positive cell lines) but not in SW480 and OVCAR8 (NEO-201 negative). Interestingly, gene analysis failed to show any mutations in the CEACAM family genes. Instead, missense mutations of the zinc-finger protein ZNF141 and major histocompatibility complex HLA-DRB5 genes were detected in both OV90 and LS174T and not in the OVCAR8 or SW480 cell line. Although the role of ZNF141 in cancer is not clear, other zinc finger proteins are known to bind either DNA or RNA and to play a role in gene expression, post-transcriptional modification, and protein trafficking, and may correlate with metastatic process and EMT transformation. HLA-DRB5 is a key component in the antigen presentation process. Mutations in this gene could mediate cancer cell immune escape, but it is currently unclear how it may relate to the expression of the antigen recognized by NEO-201.

NEO-201 Alone Does Not Affect Tumor Cell Viability

To determine the biological significance of NEO-201 reactivity with cell lines, we investigated its effect on viability of OV90 and

LS174T *in vitro*. OV90 cells exposed to increasing concentrations of NEO-201 for 72 h showed no change in viability (data not shown).

NEO-201 Mediates ADCC Killing Against Human Ovarian and Colorectal Carcinoma Cell Lines *in vitro*

To evaluate the ability of NEO-201 to kill tumor cells through NK-mediated ADCC, OV90 or LS174T cells were incubated with either IgG isotype control or NEO-201 at 1 μg/ml, with/without the highly active NK cell line (haNK) for 4 h. Neither NEO-201 nor haNK +IgG isotope control showed any significant effect on cell viability (**Figure 3A**). We evaluated the effect of NEO-201 on NK-mediated ADCC on OV90 and LST174T using effector-to-target (E:T) ratio of 1:1, 10:1, and 20:1. The combination of NEO-201 with haNK showed a statistically significant increase in ADCC in both cell lines at the ratio of 10:1 and 20:1. No significant effect on ADCC was observed at the ratio of 1:1. These data indicate that NEO-201 does not have a direct cytotoxic effect on the tumor cells, suggesting that the NEO-201 targets, CEACAM 5 and 6, have no role in cell proliferation. Instead, these data strongly suggest that the anti-tumor activity of NEO-201 is mediated by the activation of ADCC in both ovarian and colon cancer cells. This is consistent with our previous results confirming the role of NEO-201 in triggering NK-mediated ADCC using anti-CD16 antibody to block NEO-201-induced ADCC (13).

We next screened NK from different donors in order to further optimize the pre-clinical model. A ^{51}Chromium release ADCC assay guided the selection of the NK donor to be used for the animal study (**Figure 3B**). Based on these results, D3 NK was selected to be used in the animal study.

NEO-201 Efficacy in Ovarian Cancer Orthotopic Tumor Model *in vivo*

We designed our mouse model to incorporate the ADCC mechanism of tumor cell killing. Because the NEO-201 antibody is specific to human protein, we are unable to use an immune-competent mouse model of ovarian cancer. We therefore used human xenografts in nude mice and inoculated IL-2-activated human PBMCs at the time of NEO-201 injection. For the first model, mimicking primary ovarian cancer, we inoculated OV90 cells into the bursal sac surrounding the mouse ovary in order to initiate a local orthotopic primary tumor that could be measured over time using ultrasound imaging. In the ovarian bursa model (**Figures 4A,B**), the treatment with NEO-201 or NEO-201 in combination with PBMCs, showed a trend toward tumor control. In a second model, we inoculated the OV90 cells into the peritoneal cavity in order to mimic disseminated ovarian cancer and peritoneal carcinomatosis. We used this model to measure the effect of NEO-201 on overall survival. Mice that received NEO-201 with activated PBMCs experienced the longest survival (**Figure 4C**) ($p < 0.0001$). In this model, NEO-201 alone is also able to improve survival compared to the isotype control treatment. This could be due to direct anti-tumor effects of the antibody in this setting or to the activation of the mouse innate immune system. PBMCs alone had a similar partial effect, likely due to allo-reactivity of the immune cells against a tumor with a different MHC haplotype. The combination of NEO-201 and PBMCs dramatically improved survival over vehicle or either treatment alone. Overall, these mouse models demonstrate *in vivo* activity of NEO-201 against ovarian cancer that specifically expresses the antibody target.

DISCUSSION

Recent efforts in cancer therapeutics have focused on the development of drugs that activate the immune system

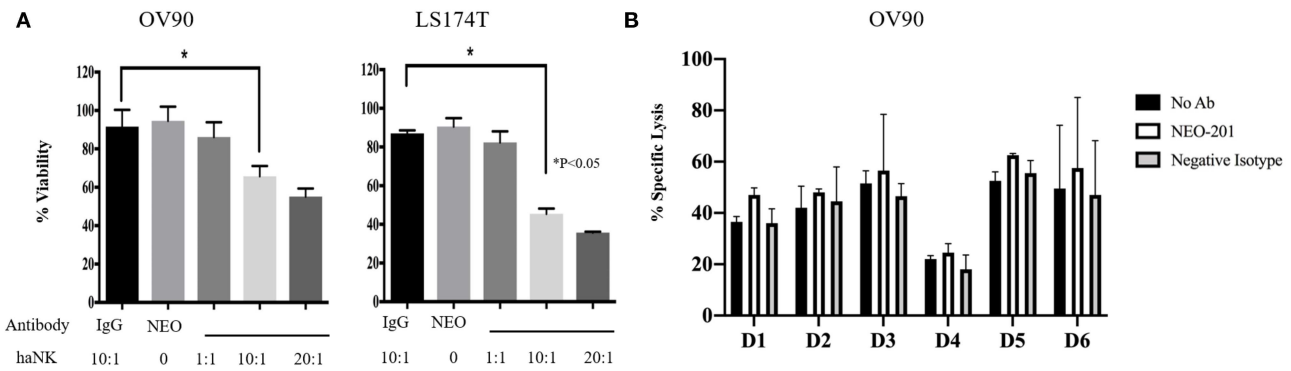

FIGURE 3 | NEO-201 decreases cell viability by activating natural killer (NK)-mediated antibody-dependent cellular cytotoxicity (ADCC) *in vitro*. **(A)** NEO-201-positive OV90 and LS174T cells lines were selected to assess the effect of NEO-201 on NK-mediated ADCC. Cells were incubated with either highly active natural killer (haNK), NEO-201 at a dose of 1 μg/ml, or a combination of NEO-201 with haNK at different effector-to-target (E:T) ratios. ADCC activity was assessed by non-radioactive ADCC assay. Experiment and results from **(A)** were analyzed according to the Celigo program manufacture as described in the Material and Methods section. **(B)** In order to select the best NK human donor to use for *in vivo* experiments, the OV90 cell line was incubated with the NK isolated from the PBMCs from six different donors in the presence of 1 μg/ml of NEO-201. To evaluate specific lysis, NK derived from a selected human donor were activated with IL-2 and used for the experiment in two different effector cells (E):target cells (T) ratios: 50:1 or 100:1. Chromium released assay was used to evaluated specific lysis. Experiments depicted in this figure reflect the mean ± SD of three independent experiments. Ordinary one-way ANOVA was used for statistical analysis. *$P < 0.05$.

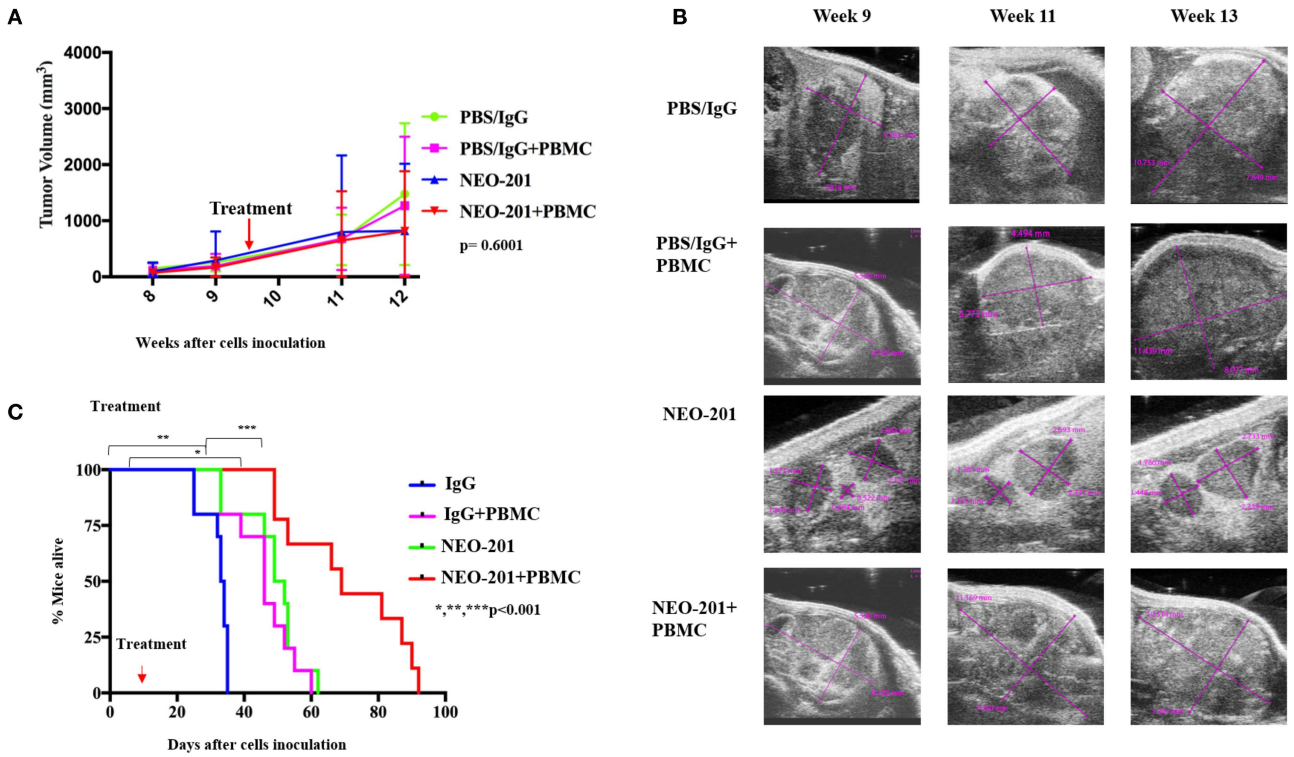

FIGURE 4 | Antiproliferative response to NEO-201 and survival in model of ovarian cancer *in vivo*. **(A)** OV90 cells were injected in the mice ovary bursa and observed for their ability to develop tumors. Tumors were allowed to grow until they reached at least 100 mm^3, about 8 weeks post cell injection. Tumor size was followed by weekly ultrasound. After randomization, each mouse received one cycle of treatment, which consists of two doses of drug on day 1 and day 7 of week 10. Curves represent tumor volume when treated ×3 with either control {phosphate-buffered saline (PBS)/IgG}, PBMCs (8 million cultured in 200 U/ml IL2 overnight), NEO-201 (250 μg), or their combinations. Kruskal–Wallis test was used to evaluate significance ($p = 0.6001$). **(B)** Representative ultrasound images of tumor-bearing mouse ovaries. Purple lines indicate cross sectional measurements from which volume was calculated. **(C)** OV90 cells were injected in the mice peritoneum to reproduce an orthotopic model of peritoneal carcinomatosis from ovarian cancer spreading. Tumors were allowed to grow for 2 weeks before being randomized in the four groups of treatment as described above. Curves represent survival. Significance was evaluated by Mantel–Cox. $^*P < 0.05$, $^{**}P < 0.01$, $^{***}P < 0.001$.

against cancer cells to achieve durable disease control with a physiological strategy and avoiding chemotherapy side effects. The efficacy of immunotherapy has been limited to specific tumor types and correlated with tumor genetic instability due to deficiency of mismatch repair (MMR) and/or the expression of PD-L1 (24). Therefore, there is urgent need for alternative therapeutic approaches to improve immunotherapy efficacy against other cancers. The innate immune system, including monocytes and NK cells, likely works in conjunction with adaptive immunity, to support and sustain anti-tumor activity. Here, we assessed a novel monoclonal antibody for its ability to direct ADCC activity of NK cells against cancer cells expressing an apparent tumor-associated variant of CEACAM-5 and CEACAM-6.

The CEACAMs are a group of cell surface glycoproteins, which are normally expressed on the surface of the epithelial cells, where they regulate tissue architecture and signal transduction (25). They are overexpressed in several tumors where they have been linked to cell migration and metastatic process, and drug resistance (25, 26). Moreover, post-translational modifications occurring during tumorigenesis, such as glycosylation, could result in a different composition of the glycan groups expressed by the CEACAMs (27–29). Colorectal cancers may demonstrate increased expression of mannose, Thomsen–Friendenreich antigen, and sialylation compared to healthy colon tissue (30). Similarly, fucose and mannose can be increased, while N-acetylgalactosamine, N-acetylglucosamine, galactose, branched and bisecting N-glycansin may be lower than normal (31). These modifications could alter cell-to-cell and cell-to-extracellular matrix (ECM) intercellular interaction (32). It is possible that a difference in glycosylation pattern explains the specific binding of NEO-201 to specific tumor-associated CEACAM-5 and CEACAM-6 variants but not to those expressed on healthy tissues as shown by the immunohistochemistry analysis. Interestingly, we also observed that carcinoma cell lines, expressing native forms of CEACAM-5 and CEACAM-6, showed a different profile for expression of the antigen recognized by NEO-201. This data supports the hypothesis that the antigen recognized by NEO-201 is a specific tumor-associated variant of CEACAM-5 and -6.

Mutational analysis was conducted, but no CEACAM gene alteration was found in the cell lines, which had a positive reactivity with NEO-201. Instead, a gene mutation of zinc-finger protein ZNF141 was found (33). The zinc-fingers are a group of protein, which was initially identified as transcription factors, and recent studies showed that this group of protein could be

involved in multiple cellular processes other than gene expression (34). Although ZNF141 expression/role in cancer has not yet been clarified (35), overall zinger-finger proteins have been associated with tissue development abnormalities and epithelial–mesenchymal transformation (36). ZNF141 mutations could be involved into a regulation of the different glycosylation status of CEACAM 5 and 6 that are targeted by NEO-201; however, further studies are needed to better understand the presence and relevance of this mutation in human cancers.

Although NEO-201 showed no direct cytotoxic effect as other mAbs like Trastuzumab (37), Cetuximab (38), or Rituximab (8), it can exert a significant anti-tumor activity not only inducing NK-mediated ADCC but also enhancing direct NK killing against tumor cells. Recently, we showed that NEO-201 mediated enhancement of NK killing against CEACAM5$^+$/NEO-201$^+$ human carcinoma cell lines, demonstrating that the binding between NEO-201 and the tumor variant of CEACAM5 can block the interaction between CEACAM5 on tumor cells and CEACAM1 on NK cells to reverse CEACAM1-dependent inhibition of NK cytotoxicity (39). Similarly, another study demonstrated the ability of an anti-CEACAM5 monoclonal antibody (CC4) to restore NK cytotoxicity in colorectal cancer preclinical models by blocking the CEACAM 5 (CEA)–CEACAM 1 axis (40).

In addition, as previously reported by our group, NEO-201 has antitumor activity *in vitro and vivo*. Our previous work demonstrated that NEO-201 induced cancer cell killing through activation of CDC and ADCC in pancreatic cancer models. *In vivo* NEO-201 reduced the growth of human pancreatic tumor xenografts in mice and demonstrated safety/tolerability in non-human primates with a transient neutropenia lasting ∼8 days as the only adverse effect observed (10). Furthermore, in another study, we have also proved that the stimulation of NK cells with IL-15 superagonist further enhanced the NEO-201-mediated ADCC against cell lines expressing the antibody target *in vitro* (13). Here, we demonstrate the *in vivo* antitumor activity of NEO-201 in a preclinical model of ovarian cancer. The treatment with NEO-201 plus PBMCs dramatically improved survival of mice compared to vehicle or either treatment alone (**Figure 4**), suggesting an *in vivo* activity of NEO-201 against ovarian cancer that specifically expresses the antibody target.

All together, these data suggested that NEO-201 has an antitumor activity and safety profile that we moved forward to clinical validation in a first in human clinical trial that is now ongoing at the NCI (NCT03476681). Targeting an antigen expressed in tumors, but not in normal tissues, allows patient selection for optimal treatment. The antigen recognized by NEO-201, a variant of CEACAM-5 and CEACAM-6, is specific to cancer tissue but expressed across cancer subtypes. Interestingly, it was developed originally using colon cancer tissue, and appears to be expressed predominantly in tumors of gastrointestinal origin or mucinous phenotype. NEO-201, therefore, has both therapeutic and diagnostic potential. Future studies will incorporate companion diagnostics during the course of clinical development in order to identify patient populations who express the antigen recognized by NEO-201 and are most likely to benefit from this potential therapeutic agent targeting tumor-specific variants of CEACAM-5 and CEACAM-6.

DATA AVAILABILITY STATEMENT

The original contributions presented in the study are publicly available. This data can be found here: the NCBI BioProject, ID 625511 (https://www.ncbi.nlm.nih.gov/bioproject/625511).

ETHICS STATEMENT

The studies involving human participants were reviewed and approved by protocol 99-CC-0168, approved by the Institutional Review Board of the National Cancer Institute. The patients/participants provided their written informed consent to participate in this study. The animal study was reviewed and approved by NCI Animal Care and Use Committee.

AUTHOR CONTRIBUTIONS

MM wrote the manuscript and analyzed the data. KZ, JD, MN, LH, MO, DA, SH, AO-T, TA, SD, and MF performed the experiments and analyzed the data. JL and AA analyzed the data. PA, KT, and CA designed the experiments, interpreted the data, edited the manuscript and provided administrative, technical, and material support.

FUNDING

CA received funding from Precision Biologics under a Cooperative Research and Development Agreement with the National Cancer Institute (02992) and the National Cancer Institute Intramural Research Program (ZIA BC 011775).

ACKNOWLEDGMENTS

We thank Dr. Kunle Odunsi for providing ovarian cancer tissue for IHC analysis.

REFERENCES

1. Siegel RL, Miller KD, Jemal A. Cancer statistics, 2015. *CA Cancer J Clin*. (2000) 65:5–29. doi: 10.3322/caac.21254
2. Disis ML, Taylor MH, Kelly K, Beck JT, Gordon M, Moore KM, et al. Efficacy and safety of avelumab for patients with recurrent or refractory ovarian cancer: phase 1b results from the JAVELIN solid tumor trial. *JAMA Oncol*. (2019) 5:393–401. doi: 10.1001/jamaoncol.2018.6258
3. Monk BJ, Minion LE, Coleman RL. Anti-angiogenic agents in ovarian cancer: past, present, and future. *Ann Oncol*. (2016) 27:i33–9. doi: 10.1093/annonc/mdw093
4. Sharpe AH, Pauken KE. The diverse functions of the PD1 inhibitory pathway. *Nat Rev Immunol*. (2018) 18:153–67. doi: 10.1038/nri.2017.108
5. Hu Z, Ott PA, Wu CJ. Towards personalized, tumour-specific, therapeutic vaccines for cancer. *Nat Rev Immunol*. (2018) 18:168–82. doi: 10.1038/nri.2017.131

6. Jackson HJ, Rafiq S, Brentjens RJ. Driving CAR T-cells forward. *Nat Rev Clin Oncol*. (2016) 13:370–83. doi: 10.1038/nrclinonc.2016.36
7. O'Donnell JS, Teng MWL, Smyth MJ. Cancer immunoediting and resistance to T cell-based immunotherapy. *Nat Rev Clin Oncol*. (2019) 16:151–67. doi: 10.1038/s41571-018-0142-8
8. Veeramani S, Wang SY, Dahle C, Blackwell S, Jacobus L, Knutson T, et al. Rituximab infusion induces NK activation in lymphoma patients with the high-affinity CD16 polymorphism. *Blood*. (2011) 118:3347–9. doi: 10.1182/blood-2011-05-351411
9. Rogers LM, Veeramani S, Weiner GJ. Complement in monoclonal antibody therapy of cancer. *Immunol Res*. (2014) 59:203–10. doi: 10.1007/s12026-014-8542-z
10. Fantini M, David JM, Saric O, Dubeykovskiy A, Cui Y, Mavroukakis SA, et al. Preclinical characterization of a novel monoclonal antibody NEO-201 for the treatment of human carcinomas. *Front Immunol*. (2018) 8:1899. doi: 10.3389/fimmu.2017.01899
11. Hollinshead A, Arlen M,Yonemoto R, Cohen M, Tanner K, Kundin WD, et al. Pilot studies using melanoma tumor-associated antigens (TAA) in specific-active immunochemotherapy of malignant melanoma. *Cancer*. (1982) 49:1387–404. doi: 10.1002/1097-0142(19820401)49:7<1387::AID-CNCR2820490715>3.0.CO;2-V
12. Hollinshead A, Elias EG, Arlen M, Buda B, Mosley M, Scherrer J. Specific active immunotherapy in patients with adenocarcinoma of the colon utilizing tumor-associated antigens (TAA). A phase I clinical trial. *Cancer*. (1985) 56:480–9. doi: 10.1002/1097-0142(19850801)56:3<480::AID-CNCR2820560312>3.0.CO;2-2
13. Fantini M, David JM, Wong HC, Annunziata CM, Arlen PM, Tsang KY. An IL-15 superagonist, ALT-803, enhances antibody-dependent cell-mediated cytotoxicity elicited by the monoclonal antibody NEO-201 against human carcinoma cells. *Cancer Biother Radiopharm*. (2019) 34:147–59. doi: 10.1089/cbr.2018.2628
14. Jochems C, Hodge JW, Fantini M, Fujii R, Morillon YM II, Greiner JW, et al. An NK cell line (haNK) expressing high levels of granzyme and engineered to express the high affinity CD16 allele.*Oncotarget*. (2016) 7:86359–73. doi: 10.18632/oncotarget.13411
15. Scudiero DA, Shoemaker RH, Paull KD, Monks A, Tierney S, Nofziger TH, et al. Evaluation of a soluble tetrazolium/formazan assay for cell growth and drug sensitivity in culture using human and other tumor cell lines. *Cancer Res*. (1988) 48:4827–33.
16. Bolger AM, Lohse M, Usadel B. Trimmomatic: a flexible trimmer for Illumina sequence data. *Bioinformatics*. (2014) 30:2114–20. doi: 10.1093/bioinformatics/btu170
17. Li H, Handsaker B, Wysoker A, Fennell T, Ruan J, Homer N, et al. Genome project data processing, the sequence alignment/map format and SAMtools. *Bioinformatics*. (2009) 25:2078–9. doi: 10.1093/bioinformatics/btp352
18. McKenna A, Hanna M, Banks E, Sivachenko A, Cibulskis K, Kernytsky A, et al. The genome analysis toolkit: a MapReduce framework for analyzing next-generation DNA sequencing data. *Genome Res*. (2010) 20:1297–303. doi: 10.1101/gr.107524.110
19. Barnett DW, Garrison EK, Quinlan AR, Stromberg MP, Marth GT. BamTools: a C++ API and toolkit for analyzing and managing BAM files. *Bioinformatics*. (2011) 27:1691–2. doi: 10.1093/bioinformatics/btr174
20. Cibulskis K, Lawrence MS, Carter SL, Sivachenko A, Jaffe D, Sougnez C, et al. Sensitive detection of somatic point mutations in impure and heterogeneous cancer samples. *Nat Biotechnol*. (2013) 31:213–9. doi: 10.1038/nbt.2514
21. Lek M, Karczewski KJ, Minikel EV, Samocha KE, Banks E, Fennell T, et al. Analysis of protein-coding genetic variation in 60,706 humans. *Nature*. (2016) 536:285–91. doi: 10.1038/nature19057
22. The 1000 Genomes Project Consortium. A global reference for human genetic variation. *Nature*. (2015) 526:68–74. doi: 10.1038/nature15393
23. Ramos AH, Lichtenstein L, Gupta M, Lawrence MS, Pugh TJ,Saksena G, et al. Oncotator: cancer variant annotation tool. *Hum Mutat*. (2015) 36:E2423–9. doi: 10.1002/humu.22771
24. Le DT, Durham JN, Smith KN, Wang H, Bartlett BR, Aulakh LK, et al. Mismatch repair deficiency predicts response of solid tumors to PD-1 blockade. *Science*. (2017) 357:409–13. doi: 10.1126/science.aan6733
25. Kuespert K, Pils S, Hauck CR. CEACAMs: their role in physiology and pathophysiology. *Curr Opin Cell Biol*. (2006) 18:565–71. doi: 10.1016/j.ceb.2006.08.008
26. Khairnar V, Duhan V, Patil AM, Zhou F, Bhat H, Thoens C, et al. CEACAM1 promotes CD8(+) T cell responses and improves control of a chronic viral infection. *Nat Commun*. (2018) 9:2561. doi: 10.1038/s41467-018-04832-2
27. Pinho SS, Reis CA. Glycosylation in cancer: mechanisms and clinical implications. *Nat Rev Cancer*. (2015) 15:540–55. doi: 10.1038/nrc3982
28. Sato Y, Tateno H, Adachi J, Okuyama H, Endo H, Tomonaga T, et al. Generation of a monoclonal antibody recognizing the CEACAM glycan structure and inhibiting adhesion using cancer tissue-originated spheroid as an antigen. *Sci Rep*. (2016) 6:24823. doi: 10.1038/srep24823
29. Stowell SR, Ju T, Cummings RD. Protein glycosylation in cancer. *Annu Rev Pathol*. (2015) 10:473–510. doi: 10.1146/annurev-pathol-012414-040438
30. Saeland E, Belo AI, Mongera S, van Die I, Meijer GA, van Kooyk Y. Differential glycosylation of MUC1 and CEACAM5 between normal mucosa and tumour tissue of colon cancer patients. *Int J Cancer*. (2012) 131:117–28. doi: 10.1002/ijc.26354
31. Zhao Q, Zhan T, Deng Z, Li Q, Liu Y, Yang S, et al. Glycan analysis of colorectal cancer samples reveals stage-dependent changes in CEA glycosylation patterns. *Clin Proteomics*. (2018) 15:9. doi: 10.1186/s12014-018-9182-4
32. Zhuo Y, Yang JY, Moremen KW, Prestegard JH. Glycosylation alters dimerization properties of a cell-surface signaling protein, carcinoembryonic antigen-related cell adhesion molecule 1 (CEACAM1). *J Biol Chem*. (2016) 291:20085–95. doi: 10.1074/jbc.M116.740050
33. Munro D, Ghersi D, Singh M. Two critical positions in zinc finger domains are heavily mutated in three human cancer types. *PLoS Comput Biol*. (2018) 14:e1006290. doi: 10.1371/journal.pcbi.1006290
34. Jen J, Wang YC. Zinc finger proteins in cancer progression. *J Biomed Sci*. (2016) 23:53. doi: 10.1186/s12929-016-0269-9
35. Kalsoom UE, Klopocki E, Wasif N, Tariq M, Khan S, Hecht J, et al. Whole exome sequencing identified a novel zinc-finger gene ZNF141 associated with autosomal recessive postaxial polydactyly type A. *J Med Genet*. (2013) 50:47–53. doi: 10.1136/jmedgenet-2012-101219
36. Hajra KM, Chen DY, Fearon ER. The SLUG zinc-finger protein represses E-cadherin in breast cancer. *Cancer Res*. (2002) 62:1613–8.
37. Collins DM, O'Donovan N, McGowan PM, O'Sullivan F, Duffy MJ, Crown J. Trastuzumab induces antibody-dependent cell-mediated cytotoxicity (ADCC) in HER-2-non-amplified breast cancer cell lines. *Ann Oncol*. (2012) 23:1788–95. doi: 10.1093/annonc/mdr484
38. Trotta AM, Ottaiano A, Romano C, Nasti G, Nappi A, De Divitiis C, et al. Prospective evaluation of cetuximab-mediated antibody-dependent cell cytotoxicity in metastatic colorectal cancer patients predicts treatment efficacy. *Cancer Immunol Res*. (2016) 4:366–74. doi: 10.1158/2326-6066.CIR-15-0184
39. Fantini M, David JM, Annunziata CM, Morelli MP, Arlen PM, Tsang KY. The monoclonal antibody NEO-201 enhances NK cell cytotoxicity against tumor cells through blockade of the inhibitory CEACAM5/CEACAM1 immune checkpoint pathway. *Cancer Biother Radiopharm*. (2020) 35:190–8. doi: 10.1089/cbr.2019.3141
40. Zheng C, Feng J, Lu D, Wang P, Xing S, Coll JL. A novel anti-CEACAM5 monoclonal antibody, CC4, suppresses colorectal tumor growth and enhances NK cells-mediated tumor immunity. *PLoS ONE*. (2011) 6:e21146. doi: 10.1371/journal.pone.0021146

Conflict of Interest: JD, MF, KT, and PA conducted this research as employees of Precision Biologics, Inc. PA has ownership interest in Precision Biologics, Inc. CA received research funding from Precision Biologics. Precision Biologics had a role in the study design, data collection and analysis of the *in vitro* experiments; and had a role in the preparation of the manuscript.

The remaining authors declare that the research was conducted in the absence of any commercial or financial relationships that could be construed as a potential conflict of interest.

frontiers in Oncology

ORIGINAL RESEARCH
published: 07 July 2020
doi: 10.3389/fonc.2020.01047

Lanreotide Induces Cytokine Modulation in Intestinal Neuroendocrine Tumors and Overcomes Resistance to Everolimus

Concetta Sciammarella[1,2†], Amalia Luce[1†], Ferdinando Riccardi[3], Carmela Mocerino[3], Roberta Modica[2], Massimiliano Berretta[4], Gabriella Misso[1], Alessia Maria Cossu[5], Annamaria Colao[2], Giovanni Vitale[6,7], Alois Necas[8], Jan Fedacko[9], Marilena Galdiero[10], Pierpaolo Correale[11], Antongiulio Faggiano[12], Michele Caraglia[1,5], Anna Capasso[13*] and Anna Grimaldi[1]*

[1] Department of Precision Medicine, University of Campania "Luigi Vanvitelli", Naples, Italy, [2] Department of Clinical Medicine and Surgery, University "Federico II" of Naples, Naples, Italy, [3] Oncology Unit, AORN Cardarelli, Naples, Italy, [4] Department of Medical Oncology, Centro di Riferimento Oncologico, Istituto Nazionale Tumori CRO, Aviano, Italy, [5] Laboratory of Precision and Molecular Oncology, Institute of Genetic Research, Biogem Scarl, Avellino, Italy, [6] Laboratory of Geriatric and Oncologic Neuroendocrinology Research, Istituto Auxologico Italiano, IRCCS, Milan, Italy, [7] Department of Clinical Sciences and Community Health (DISCCO), University of Milan, Milan, Italy, [8] CEITEC – Central European Institute of Technology, University of Veterinary and Pharmaceutical Sciences Brno, Brno, Czechia, [9] 1st Department of Internal Medicine, Centre of Excellency for Atherosclerosis Research, University of Pavol Jozef Safarik, Košice, Slovakia, [10] Department of Experimental Medicine, University of Campania "Luigi Vanvitelli", Naples, Italy, [11] Medical Oncology Unit, "Bianchi-Melacrino-Morelli" Grand Metropolitan Hospital, Reggio Calabria, Italy, [12] Department of Experimental Medicine, Division of Endocrinology, Sapienza University of Rome, Rome, Italy, [13] Department of Oncology, Livestrong Cancer Institutes, Dell Medical School, The University of Texas, Austin, TX, United States

Somatostatin analogs mantain their major role in the treatment of patients with advanced neuroendocrine tumors (NETs) and have multiple modulatory effects on the immune system. Here, we evaluated the effects of lanreotide treatment on expression of Th1, Th2 cytokine patterns in serum of patients with NETs and in bronchial and pancreatic NET cell lines. Our results showed that lanreotide treatment promoted a Th1 cytotoxic immune-phenotype in patients with NETs originated by intestinal sites. Similar results were obtained also *in vitro* where lanreotide induced expression of Th1 cytokines only in pancreatic and not in bronchial-derived NET cell lines. It seems, therefore, that cytokinomics can represent a useful tool for the identification of tumor biomarkers for the early diagnosis and evaluation of the response to therapy in NET patients. To avoid the drug-resistance induced by everolimus (mTOR inhibitor), we made the pancreatic NET cell line resistant to this drug. After treatment with lanreotide we found that the drug reduced its viability compared to that of sensitive cells. These data may have direct implications in design of future translation combination trial on NET patients.

Keywords: neuroendocrine tumors, cytokines, somatostatin analogs, mTOR–mammalian target of rapamycin, drug-resistance

OPEN ACCESS

Edited by:
Niels Weinhold,
Heidelberg University, Germany

Reviewed by:
Paolo Grieco,
University of Naples Federico II, Italy
Cristina Pérez Ruiz,
University of Navarra, Spain

***Correspondence:**
Michele Caraglia
michele.caraglia@unicampania.it;
michele.caraglia@fastwebnet.it
Anna Capasso
anna.capasso@austin.utexas.edu

[†]These authors have contributed equally to this work

Specialty section:
This article was submitted to Cancer Molecular Targets and Therapeutics, a section of the journal Frontiers in Oncology

Received: *26 January 2020*
Accepted: *27 May 2020*
Published: *07 July 2020*

Citation:
Sciammarella C, Luce A, Riccardi F, Mocerino C, Modica R, Berretta M, Misso G, Cossu AM, Colao A, Vitale G, Necas A, Fedacko J, Galdiero M, Correale P, Faggiano A, Caraglia M, Capasso A and Grimaldi A (2020) Lanreotide Induces Cytokine Modulation in Intestinal Neuroendocrine Tumors and Overcomes Resistance to Everolimus. Front. Oncol. 10:1047. doi: 10.3389/fonc.2020.01047

INTRODUCTION

Neuroendocrine Neoplasms (NENs) are heterogeneous, with increasing incidence in the last decades arising from altered stem cells programmed to evolve in ultimate lineages scattered with secretory granules and the ability to produce hormones (neuropeptidic, neurotransmitter and neuromodulator with endocrine, autocrine and paracrine action) that lead to carcinoid syndrome. Our study was performed on neuroendocrine tumors (NETs) that are differentiated NENs. Although the incidence of NETs is largely underestimated and comprises <2% of gastrointestinal malignancies, their prevalence appears to be greater than that of stomach as well as pancreatic adenocarcinomas (1, 2). Most common NETs occur in the gastro-entero-pancreatic (70%) and respiratory (25%) systems even though they may rise from any tissue and body district, including genitourinary tract, skin (merkelioma), thyroid, adrenal, nervous ganglia etc. (1). Most patients with NETs are diagnosed with advanced diseases and the mortality rate is 50% within five years (3, 4). Their treatment is based upon surgical resection for localized tumors or for NETs with a regional diffusion and, to alleviate the symptoms, in metastatic or high-grade tumors (5, 6). Unfortunately, the symptoms associated with this tumor may be nonspecific or absent. In fact, the diagnosis of NETs is often delayed and becomes necessary to use medical therapy. Being slowly growing tumors, patients are often subjected to long-lasting treatments (6). In the last twenty years, the best therapeutic approaches to these tumors have been based on the use of somatostatin analogs (SSAs) (octreotide, lanreotide) and, later on, mammalian target of rapamycin (mTOR) inhibitors such as everolimus (7, 8) have also shown their efficacy in the treatment of patients with these malignacies. Somatostatin receptor (SSR) subtypes are 5 (SSR 1–5) (9, 10) and somatostatin, binding to its receptors, activate both antisecretory and antiproliferative effects. The antisecretory effects are mainly due to inhibition of exocytosis mainly induced by the decrease of intracellular cAMP and calcium levels. Antiproliferative effects are induced by cell cycle arrest or apoptosis activated by protein tyrosine phosphatases or through the inhibition of the secretion of growth factors (11, 12). The receptors can also form dimers thus having complex effects on the cells through the activation of alternative signal transduction pathways (13). Most of these NETs express SSR, predominantly subtypes 1, 2, and 3 with an inverse correlation with the grade of differentiation of the tumor (14).

Octreotide and lanreotide are the first-generation SSAs and show a high binding affinity to SSR2 and 5, while pasireotide, which is a second-generation SSA, has high affinity for multiple SSRs (SSR5 > SSR2 > SSR3 > SSR1) (15). Lanreotide, in details, is currently approved for treatment of NETs and has a relevant cytostatic and antisecretive effect. Two important phase III trials, PROMID (placebo-controlled, prospective, randomized study in patients with metastatic neuroendocrine midgut tumors) and the CLARINET (controlled study of lanreotide antiproliferative response in neuroendocrine tumors), have been performed on patients with midgut and gastroenteropancreatic NETs, respectively. In the PROMID trial, 85 patients with NET were randomized to receive either octreotide or placebo. Octreotide was associated to a significant longer time to tumor progression compared to the placebo (14.3 months within the octreotide group and 6.0 months in the placebo group) and lower tumor progression rates (16). CLARINET assessed the SSA lanreotide in patients with advanced, G1/G2 differentiated, nonfunctioning, somatostatin receptor-positive NETs and documented disease progression status. In that study, lanreotide was linked to significantly prolonged progression-free survival (PFS) compared to the placebo (estimated rates of PFS at 24 months 65.1% in the lanreotide group and 33.0% in the placebo group) (17). Long-term results from both trials demonstrated the long-lasting control of the disease for octreotide and poor side effects in prolonged treatment for lanreotide (18). On the other hand, mTOR is an intracellular effector involved in cell survival, proliferation and metabolism regulation (19) acting through Thr^{389}phosphorylation of translational regulator, ribosomal protein S6 kinase β-1 (S6K1) and phosphorylation of eukaryotic translation initiation factor 4E-binding protein 1/2 (4eBP1/2), which, respectively, induce mRNA biogenesis and cap-dependent translation, increasing protein synthesis, cell growth and proliferation (19, 20). mTOR expression was observed significantly higher both in primary lesions and in metastases from NETs. This finding is coherent with a driver role of mTOR pathway activation in NET tumorigenesis (21). It is evident that the inhibition of this signaling pathway represents an excellent pharmacological target. Currently, based on the results of several clinical trials, everolimus (a pharmacologically active inhibitors of mTOR) is approved for the treatment of advanced pancreatic, gastrointestinal and lung NETs (22, 23). Moreover, everolimus should be considered a valid therapeutic option for extrapancreatic NETs (24). However, one-third of NET patients show primary insensitivity (primary resistance) to treatment with everolimus, while in others the disease is initially stabilized and then develops resistance (acquired resistance) and disease progression; this could depend on the genetic instability and the heterogeneity of tumor cells (25). Lastly, some indications suggest that combination of mTOR inhibitors with other target-based drugs, including dopamine agonists and SSAs could be a promising strategy in NET treatment (26, 27). Recent studies have highlighted the cell interactions between the tumor and the immune system in the tumor microenvironment; these interactions allow the malignant cells to use the local mechanisms present in the latter, preventing the activation of the functions of the immunological effectors and, thus, protecting the tumor from the attack of the immunological effectors (28). Two mechanisms of immunosuppression have been highlighted: (i) alteration of the genes (oncogenes) of the tumor cells and (ii) adaptive immuno-resistance supported by tumor-specific T cells (28). Several studies performed on somatostatin and its analogs have also shown that tumor cells synthesize cytokines that favor escape from immunosurveillance and may also act as tumor growth factors (29–33).

Somatostatin is a very pleiotropic molecule able to exert different effects on a number of immune cells where different SSRs are expressed. Firstly, somatostatin by itself is able to stimulate the production of Interleukin-1β (IL-1β) and Tumor

Necrosis Factor α (TNFα) (34), two dominant pro-inflammatory cytokines which are critically involved in the activation of both inflammation as well as immune reactions consequent to specific tissue damages. In this light, one of its analogs, octreotide, whose binding activity is limited to SSR2 and 5, seems to be able to inhibit the production of TNFα (31) and to increase the production of Interleukin-10 (IL-10) in patients with autoimmune diseases (32). In another study, octreotide and pasireotide also showed the ability to decrease the production of both Interferon γ (INF-γ) and Interleukin-2 (IL-2) by *in vitro* stimulated T cells (33). All together, these results suggest that the two SSR2 stimulating agents seem to promote the induction of a type 2 helper immunophenotype (Th2) that drives the immune reaction from cell mediated (Th1) toward a humoral response. In this way, it can be hypothesized that SSR agonists may interfere with both tumor microenvironment and immune reaction. On these bases, we believe that cytokinomics can represent a useful tool to study either inflammatory and/or immunological issues in patients with advanced NET under treatment with lanreotide aimed to detect potential biomarkers of response and new therapeutic targets for these patients. Moreover, we have evaluated the effects of lanreotide on Th1 and Th2 functional profile on NET cell lines (typical bronchial NET NCI-H727 and pancreatic NET BON-1) and in patients with advanced NETs by evaluating specific cytokine patterns (IL-2, IL-4, IL-6, IL-10, IFN-γ, and TNFα). By taking in consideration that PI3K/AKT/mTOR inhibitors, like everolimus, are known immunesuppressive drugs used in the prevention of bone marrow transplantation and are currently used in the treatment of not resectable pancreatic NET and bronchial carcinoids, we have also evaluated whether treatment with lanreotide may also be used to revert resistance to everolimus in NET cell lines.

MATERIALS AND METHODS

Cell Cultures

BON-1 cells were a kind gift from University of Turin, San Luigi Hospital, Orbassano. BON-1 cell line is the most widely used *in vitro* GEP-NET cell line model. In fact, this is an easy-to-handle immortalized cell line that allows a high rate of experimental reproducibility. NCI-H727 cells were provided by American Type Culture Collection (ATCC). BON-1 R (everolimus-Resistant) cells were obtained after chronic treatment with everolimus for eight weeks. During treatment, increasing drug concentrations (from 1.25 to 10 μM) were added to the culture medium every 48 h, doubling its concentration every two weeks. All cell lines were confirmed as mycoplasm-free. BON-1 and BON-1 R cell lines were cultured in DMEM-F12 supplemented with FCS (10% v/v), L-glutamine (2 mmol/L), fungizone (0.5 mg/L) and penicillin (1×10^5 u/L). The NCI-H727 cell line was cultured in RPMI-1640 supplemented with FBS (10% v/v), L-glutamine (2 mmol/L), penicillin (1×10^5 u/L) and streptomycin (1×10^5 u/L). Cells were incubated in a humidified incubator containing 95% air and 5% CO_2 with temperature at 37°C.

Compounds

Everolimus was provided from Novartis Pharma Basel, Switzerland. Lanreotide was provided from Sigma-Aldrich (Darmstadt, Germany). Everolimus and lanreotide powders were dissolved in dimethylsulfoxide (DMSO) at a concentration of 1×10^{-3} M and 4.56×10^{-6} M, respectively; stock solutions were stored at −20°C and then diluted in DMSO immediately before use. mTOR, p-mTOR^{Ser2448}, S6K1, p-S6K1^{Thr389}, 4eBP1 and p-4eBP1^{Thr70} antibodies were purchased by Cell Signaling Technology (Beverly, MA, USA); IL-10, IL-6, and TNFα antibodies were supplied from Abcam (Cambridge, UK), while the anti-α-Tubulin antibody from Calbiochem (Jaffrey, NH, USA).

Patient Inclusion Criteria

According to WHO 2010 classification, 30 patients with intestinal (17 cases), bronchial (10 typical carcinoid), and mammary (3 cases) NETs, under treatment with lanreotide were enrolled. However, cytokine analysis was performed on only 10 patients due to the inadequacy of the sample: 6 patients with intestinal, 2 with bronchial (typical carcinoid) and 2 with breast NETs. The following criteria were required for study selection: histologically confirmed, unresectable, measurable, locally advanced, or metastatic NET either with carcinoid syndrome or functionally inactive; disease progression within 6 months of study entry, based on radiographic images according to the Response Evaluation Criteria in Solid Tumors (RECIST 1.1) (35); expression of somatostatin receptors in the tumor, demonstrated by a positive Octreoscan result; adequate cardiac, hematopoietic, hepatic, and renal function; a wash-out time of at least 4 weeks from any previous treatment with antitumor agents (chemotherapy and/or biological therapy) and 3 months from radiotherapy; no previous treatments with SSAs.

Treatment Schedule

Slow-release lanreotide (Ipsen S.p.A, Milan, Italy) was administered in a 90-mg deep sc injection every 28 days. No other anticancer medications were allowed during the course of the study.

Sample Collection

Samples have been collected before treatment with lanreotide started, ten days after the beginning of treatment and then about once a month, for six months, accordingly to clinical practice. The peripheral blood serum of NET patients was centrifuged at 1500 *g* for 10 min; then, it was aliquoted in cryovials and stored at −80°C for the following analyses. All the procedures have been performed with respect to the standard biosecurity and institutional safety measures. Informed consent was obtained from patients to use their samples for research and ethical committee approval was acquired from the Hospital of our University (protocol number 94 of 31st January 2015).

Cytokine Expression by Cytofluorimetric Analysis

Cytofluorimetric analysis was performed using the BD™ Cytometric Bead Array (CBA) Human Th1/Th2 Cytokine kit

TABLE 1 | Clinical characteristics of patients with NETs.

Patient	Age	Gender	Tumor localization	Metastatic sites	Previous medical treatments	OS (months)	PFS (months)	Response to treatment
1	60	M	Intestinal NET	Liver, nodes	None	30	6	SD
2	62	M	Intestinal NET	Liver	None	47+	5	CR
3	71	M	Intestinal NET	Liver, Mesenteric	None	53+	12	PR
4	67	M	Intestinal NET	Liver, nodes	None	50+	13	PR
5	68	M	Intestinal NET	Nodes, liver, heart	None	38	2	PD
6	67	M	Intestinal NET	Nodes, liver	None	40	5	SD
7	71	M	Bronchial NET	Liver, bone, nodes	None	96	7	PD
8	70	M	Bronchial NET	Liver, bone	None	90	6	PD
9	70	F	Mammary NET	Liver, bone	3 Chemotherapy lines	9	3	PD
10	68	F	Mammary NET	Liver, bone	2 Chemotherapy lines	8	2	PD

OS, overall survival; PFS, progression-free survival; SD, stable disease, CR, complete response; PR, partial response; PD, progression disease.

II (BD Biosciences, Franklin Lakes, NJ, USA), according to the protocol by supplier. The kit was used to quantitatively measure INF-γ, TNFα, IL-10, IL-6, IL-4, IL-2 in NET serum samples. The analytical properties of BD™ CBA assay was used to evaluate the relevant protein concentrations (pg/mL) in serum: this assay provides a method to capture by flow cytometry a set of analytes with known size beads. Each captured bead is conjugated with a specific antibody. When the capture beads and detector reagent are incubated with an unknown sample containing recognized analytes, sandwich complexes (capture bead + analyte + detection reagent) are formed. These complexes can be measured using flow cytometry detectable in FL3 channel. Six bead populations with distinct fluorescence intensities have been coated with capture antibodies specific for INF-γ, TNFα, IL-10, IL-6, IL-4, IL-2 proteins. The six bead populations were mixed together and resolved in a red channel. The mix of bead was incubated with phycoerythrin (PE)-conjugated antibodies for different cytokines mixture (resolved in FL2 channel). After that, standard curve (0–5000 pg/mL) and the samples were added to bead mix and 1×10^4 events for each sample were acquired. The analysis was performed by BD Accuri™ C6 flow cytometer (BD, Biosciences, Franklin Lakes, NJ, USA), using FCAP Array™ 3.0.1 software. Each sample was processed in triplicate and the data were expressed as mean ± SD.

MTT Cell Viability Assay

BON-1 and NCI-H727 cells were plated into 96-well plates at a density of 15×10^3 cells/well in 4 replicates. After 24 h, lanreotide was added at increasing concentrations (0.195 to 100 μM). Cells were incubated for 6, 16, and 24 h at 37°C in a humidified atmosphere containing 5% CO_2. After 6, 16, and 24 h of treatment, cells were used for MTT cell viability assay (Sigma-Aldrich). To evaluate the resistance to everolimus, BON-1 R cells were treated with increasing everolimus concentrations (from 0.62 to 10 μM) and at 24, 48, and 72 h was performed MTT cell viability assay. MTT solution (MTT 5 mg/mL in PBS) was added to the cells and then incubated at 37°C for 1 h. The absorbance of the converted dye was measured at a wavelength of 570 nm, using Victor™ X4 Multilabel Plate Reade (PerkinElmer, MA, USA). Percentage of growth was normalized respect to control cells, represented by untreated cells (100% growth). Each experiment was conducted at least three times and the data were expressed as mean ± SD.

Western Blot Analysis

Total proteins were homogenized in lysis buffer (Triton 1%, sodium deoxycholate 0.5%, NaCl 0.1 M, EDTA 1 mM, pH 7.5, Na2HPO4 10 mM, pH 7.4, PMSF 10 mM, benzamidine 25 mM, leupeptin 1 mM, aprotinin 0.025 U/mL). Total proteins (50 μg) were separated using Sodium Dodecyl Sulfate—PolyAcrylamide Gel Electrophoresis (SDS-PAGE) at 10% (TGX Stain-Free, BIORAD, Hercules, CA, USA). Proteins were transferred to Nitrocellulose Blotting Membranes 0.2 μm (Trans-Blot Turbo, Mini, BIORAD, Hercules, CA, USA) using the Trans-Blot Turbo® Transfer System (BIORAD, Hercules, CA, USA). Membranes were blocked with 5% milk in T-TBS (0.05% Tween-20, 200 mM Tris-HCl pH 7.5, 1.5M NaCl) for 1 h at room temperature and then incubated overnight in primary antibodies

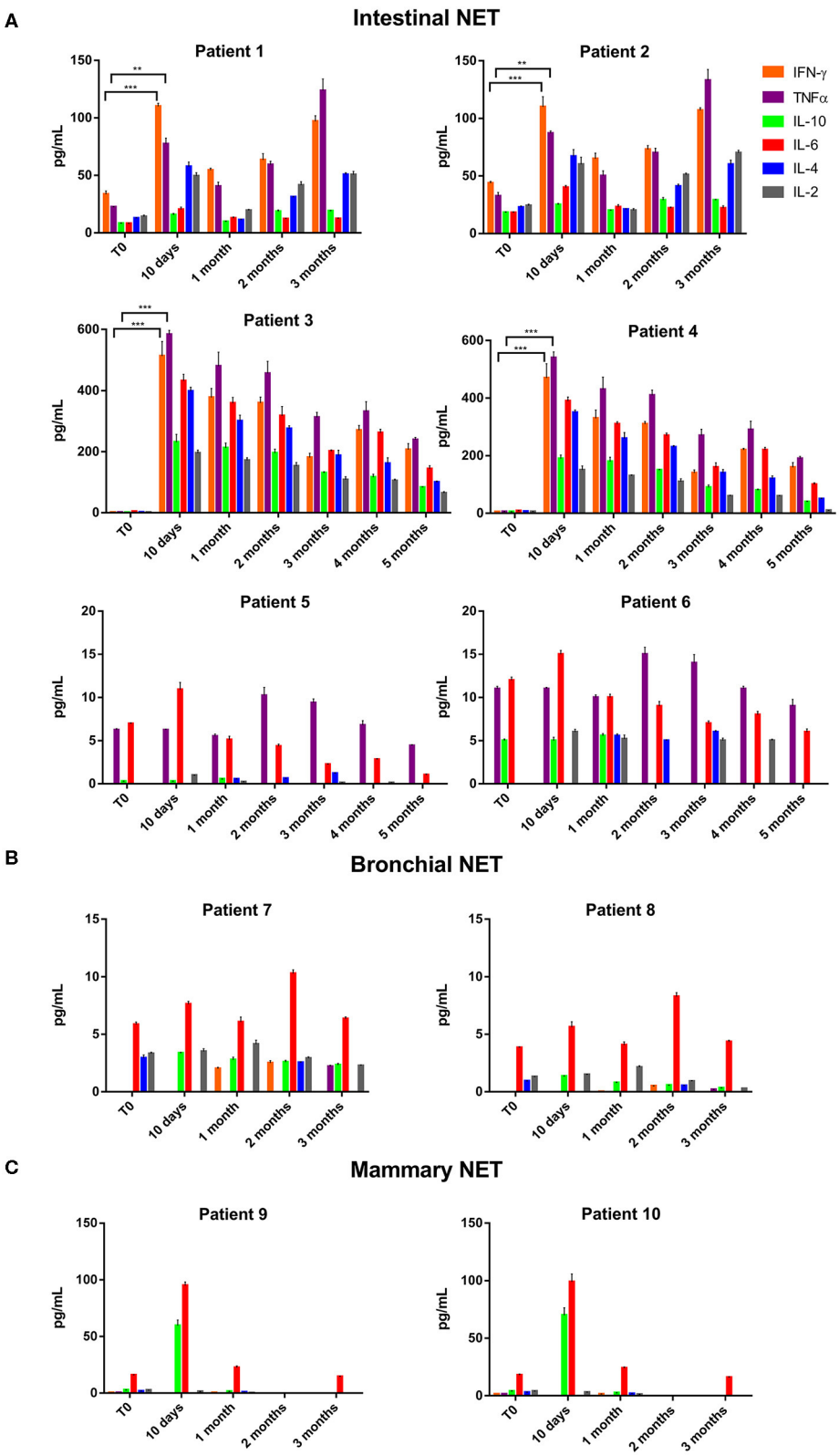

FIGURE 1 | INF-γ, TNFα, IL-10, IL-6, IL-4, and IL-2 expression in serum of patients with: **(A)**, intestinal NET (patient 1-6); **(B)**, bronchial (patients 7 and 8) and **(C)**, mammary NETs (patients 9 and 10) after treatment with lanreotide by cytofluorimetric analysis. Each experiment was repeated three times and the data are representative samples of the total number of patients analyzed and shown as mean ± SD. ** $P \leq 0.01$; *** $P \leq 0.001$.

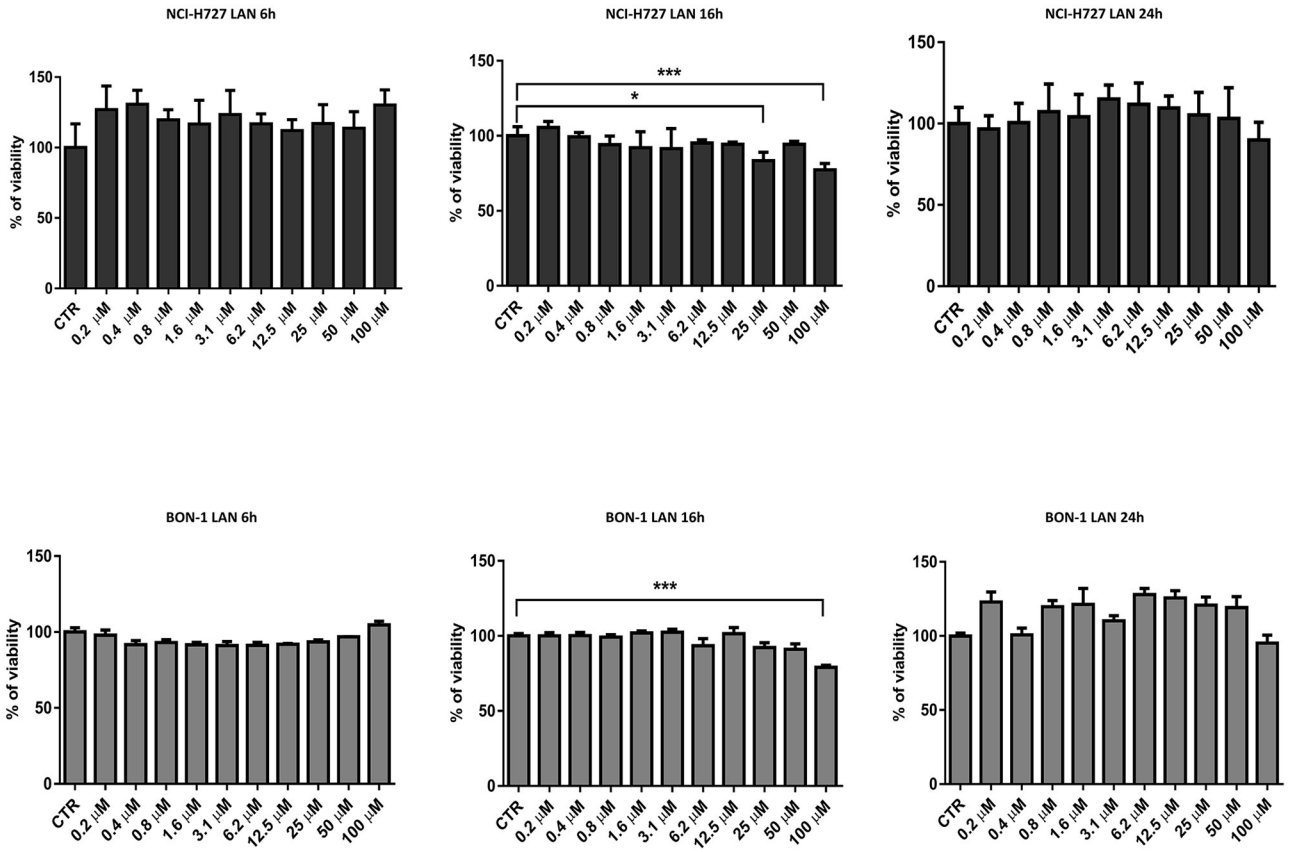

FIGURE 2 | Cell viability evaluated by MTT, after 6, 16 and 24 h of treatment with lanreotide (from 0.195 to 100 μM) in NCI-H727 and BON-1 cell lines. Each experiment was repeated three times and shown as mean ± SD. * $P \leq 0.05$; *** $P \leq 0.001$.

at 4°C. Rabbit monoclonal antibodies for IL-6, TNFα, and mouse monoclonal antibody for IL-10 were used in BON-1 and NCI-H727 cells treated with lanreotide (100 and 200 μM). Rabbit monoclonal antibodies for mTOR, p-mTOR^{Ser2448}, S6K1, 4eBP1, p-4eBP1^{Thr70}, TNFα, and mouse monoclonal antibody for p-S6K1^{Thr389} and IL-10 were used in BON-1 and BON-1 R cells. The nitrocellulose membranes were washed twice with T-TBS and incubated with secondary antibody in the T-TBS/Milk for 1 h at room temperature. Secondary antibodies include IgG directed against the mouse or rabbit determinants of the first antibody and are conjugated to peroxidase. Membranes were revealed through chemiluminescence reaction reagents (relevant Clarity™ Western ECL Blotting Substrate, BIORAD, Hercules, CA, USA). The quantative analysis was performed with the Image Lab 5.2.1 software (ChemiDoc XRS$^+$, BIORAD, Hercules, CA, USA) and the values were normalized on the α-Tubulin expression. Each experiment was conducted three times and the data were expressed as mean ± SD.

Statistical Analyses

Statistical analysis was performed using Graphpad 5 software (Graphpad Software, La Jolla, CA, USA) and the results were considered statistically significant at a level of $P \leq 0.05$. IC_{50} concentrations were calculated by Spline method. Differences between treatment and control cells were analyzed using a one-way ANOVA followed by a multiple comparative test (Newman-Keuls).

RESULTS

Patient Characteristics and Serum Cytokine Determination

We performed a cytofluorimetric analysis aimed to evaluate the parallel expression of IFN-γ, TNFα, IL-10, IL-6, IL-4, IL-2 in the serum of 10 patients (8 males and 2 females, mean age: 67.4 ± 3.7, median age: 68) with intestinal (6 patients), bronchial (typical carcinoid, 2 patients), and breast NETs (2 patients) receiving treatment with lanreotide. The patients enrolled in the study were at least for 1 month without any other specific cancer treatments and all the values were compared to the baseline in absence of lanreotide administration. During the study, 1 complete response (CR) lasting 5 months was recorded in a patient with intestinal NET, 2 partial responses (PRs) lasting 12 and 13 months, respectively, in 2 patients with intestinal NETs and 2 stable diseases (SDs) lasting 6 and 5 months in other 2 patients with intestinal NETs, respectively (**Table 1**).

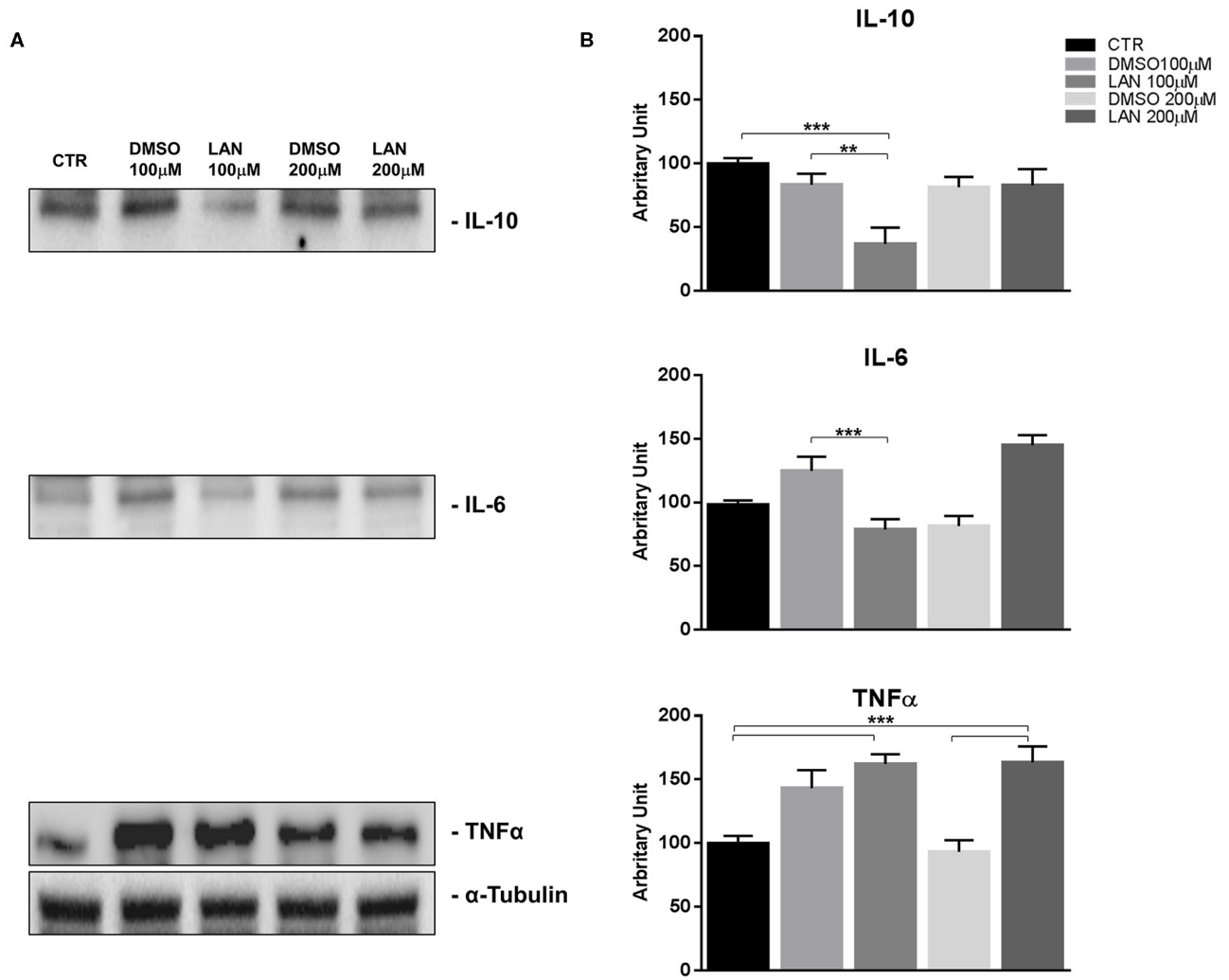

FIGURE 3 | IL-10, IL-6, TNFα expression in BON-1 cell line after treatment with 100 and 200 μM lanreotide. **(A)**, Western blotting analysis of IL-10, IL-6, TNFα. **(B)**, Quantitative analysis reported as arbitrary units showing the variation of IL-10, IL-6, TNFα expression levels compared to a-Tubulin, as housekeeping protein, using Image Lab 5.2.1 ChemiDoc XRS+ (BIORAD). The results are shown as mean ± SD of three independent experiments. ** $P \leq 0.01$; *** $P \leq 0.001$.

A progression disease (PD) was recorded in a patient with intestinal NET, in the 2 patients with bronchial NETs and in the 2 patients with mammary NETs (**Table 1**). All the patients had liver metastases at the beginning of the treatment and only 3 patients are still presently alive: all with intestinal NETs with an overall survival (OS) of 47, 53, and 50 months, respectively (**Table 1**). Only the 2 patients with mammary NETs received previous chemotherapy lines while all the remaining patients did not receive any previous medical and/or radiation treatments.

The data of the analyzed patients show a different trend of serum cytokine concentrations in relation to the primary tumor site. In details, in all the analyzed patients and independently from the tumor site of origin, the levels of IL-6 increased after 10 days of treatment with lanreotide and decreased in the following six months; whereas the levels of IL-2 and IL-10 raised only in some patients. On the contrary, the levels of IL-4 decreased already at 10 days, as compared to baseline untreated control in sera from the patients affected by bronchial NETs. Only in intestinal NETs, IFN-γ and TNFα increased after 10 days of treatment with lanreotide (**Figure 1A**). Therefore, our data suggest that intestinal NETs are characterized by a higher early and more significant Th1 than Th2 response that could be associated to a greater sensitivity to the immune-mediated effects of lanreotide. Interestingly, all the clinical responses were recorded in intestinal NETs with 3 patients still alive after about 50 months from the beginning of the treatment.

On the other hand, IFN-γ and TNFα were not detectable in sera from patients with bronchial and mammary NETs (**Figures 1B,C**). The latter data suggest that bronchial and mammary NETs have an inflammatory and immunological micro-environment poorly

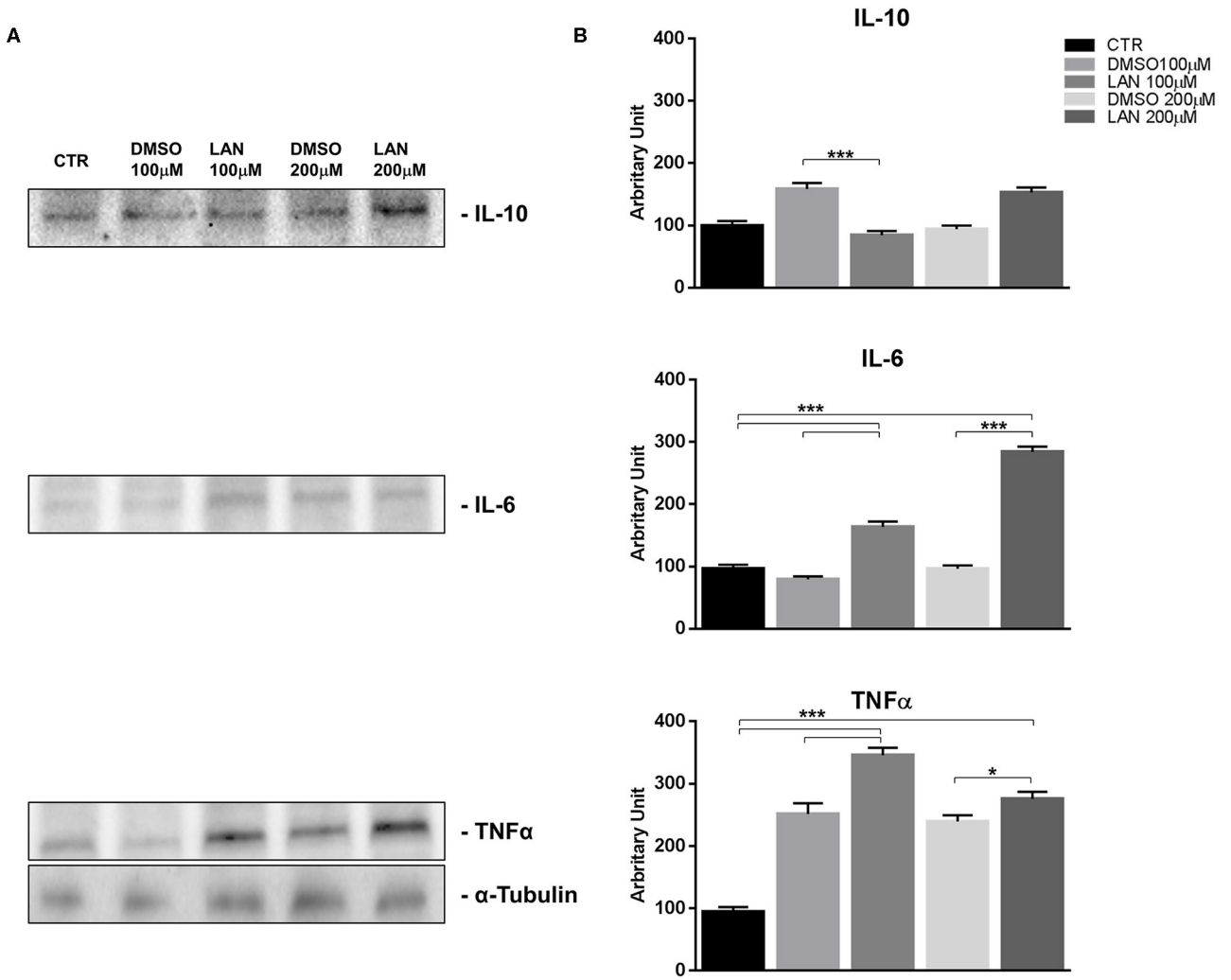

FIGURE 4 | IL-10, IL-6, TNFα expression in NCI-H727 cell line after treatment with 100 and 200 μM lanreotide. **(A)**, Western blotting analysis of IL-10, IL-6, TNFα. **(B)**, Quantitative analysis reported as arbitrary units showing the variation of IL-10, IL-6, TNFα expression levels compared to α-Tubulin, as housekeeping protein, using Image Lab 5.2.1 ChemiDoc XRS+ (BIORAD). The results are shown as mean ± SD of three independent experiments. * $P \leq 0.05$; *** $P \leq 0.001$.

responsive to lanreotide. Interestingly, all these patients experienced a PD with a limited OS in heavily pre-treated mammary NETs.

Lanreotide Effect on Cell Viability in Bronchial and Pancreatic NET Cell Lines

Thereafter, we evaluated the *in vitro* effects of lanreotide on NCI-H727 bronchial and BON-1 pancreatic NET cell lines expressing SSRs. The viability of these cells exposed to escalating lanreotide concentrations [range 0.195–100 μM] was evaluated after 6, 16, and 24 h from the beginning of the exposure to lanreotide with MTT cell viability assay. In both cell lines, lanreotide caused minimal cytostatic effects at 16 h. In particular, NCI-H727 cell line showed a reduction in viability of 17% ($P \leq 0.05$) and 23% ($P \leq 0.001$) when exposed to a lanreotide concentration of 25 and 100 μM, respectively; while BON-1 cell line showed no effect up to 25 μM and 21% ($P \leq 0.001$) reduction in viability at 100 μM (**Figure 2**). The exposure of the two cell lines to lanreotide for more prolonged times (up to 6 days) determined a lost of the growth inhibitory effects (data not shown).

Lanreotide Effects on Inflammatory Cytokine Expression by Bronchial and Pancreatic NET Cell Lines *in vitro*

Considering the difficulty to evaluate the effects of treatment with lanreotide on the cytokine levels in rare tumors, such as NETs, we analyzed the protein expression by Western Blotting on stable and reproducible NET models, NCI-H727 and BON-1 cell lines, exposed for 24 h to lanreotide at the final concentration of 100 and 200 μM, respectively. The cytostatic effect induced by treatment with lanreotide on the cells was very minimal thus,

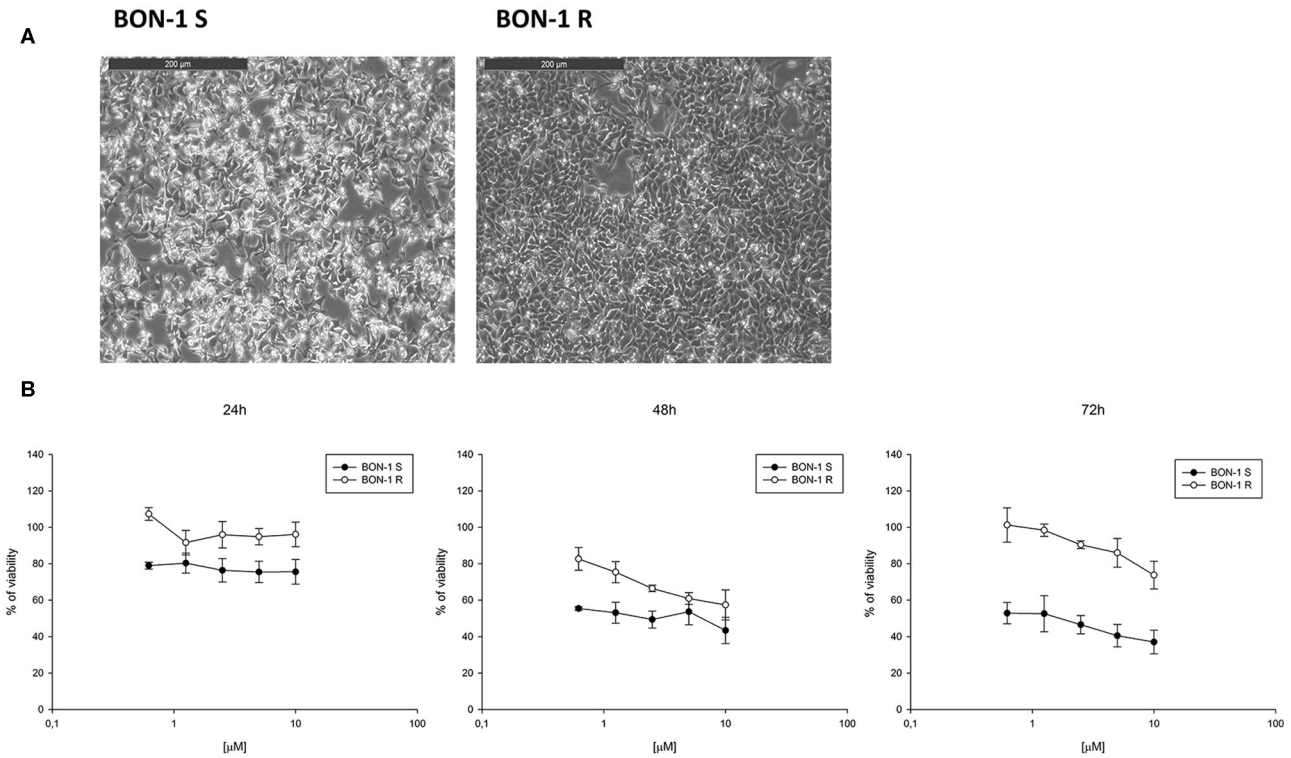

FIGURE 5 | (A), Morphological analysis of BON-1 cell line, sensitive (S) and resistant (R) to everolimus. **(B)**, Cell viability by MTT assay on sensitive and resistant BON-1 cell line after 24, 48, and 72 h of treatment with everolimus (from 0.625 to 10 μM). Each experiment was repeated three times and shown as a mean ± SD.

to evaluate the protein expression of cytokines, we increased the concentration to 200 μM.

Our experiments in BON-1 cells derived from a pancreatic NET revealed significant treatment-related increase in TNFα synthesis paralleled by a significant reduction in IL-6 and IL-10 expression; this cytokine profile reflects the ability of lanreotide to induce a Th1 cytotoxic immune-response (**Figures 3A,B**). On the other hand, exposure of NCI-H727 bronchial NET cell line to lanreotide induced a treatment-related increase of IL-6 and of TNFα expression paralleled by a decrease in the expression of IL-10 (**Figures 4A,B**). The above-mentioned findings were not recorded in tumor cell lines, untreated or exposed to DMSO (100 and 200 μM) used as drug vehicle negative control. Therefore, the effects obtained *in vitro* on the two cell lines were on line with those recorded *ex vivo* on patient sera.

Lanreotide Effects on a Pancreatic NET Cell Line Resistant to Everolimus

In order to evaluate the ability of lanreotide to overcome tumor cell resistance to mTOR inhibitors, we generated an everolimus-resistant BON-1 pancreatic NET cell line. At this purpose, we performed a long lasting (8 weeks) culture of these cells with escalating everolimus concentrations (range 1.25–10 μM). The resistance to everolimus was demonstrated by performing MTT cell viability assay after 24, 48, and 72 h of exposure to everolimus (concentration range: 0.62–10 μM) (**Figure 5B**). Additional experiments were also performed to demonstrate mTOR pathway inactivation in the resistant BON-1 cell line (R) compared to sensitive cells (S) with no other detectable morphological and phenotypic changes (**Figures 5A**, **6A,B**).

Indeed, a significant reduction (from 5 to 2-fold) of mTOR phosphorylation was detected as well as of the activity of its downstream effectors (S6K1 and 4eBP1). Noteworthy, the reduction of molecular target activity is one of the best-known mechanisms of resistance to target-based agents.

Thereafter, we evaluated the antitumor effects of lanreotide on cells resistant to everolimus compared with the sensitive BON-1 parental cells in 24, 48, and 72 h MTT cell viability assays. In these experiments, we found a significant dose-time dependent anti-tumor effect of lanreotide only on the tumor cells resistant to everolimus (**Figure 7**). This antitumor effect of lanreotide was maximal after 72 h of exposure with a 50% proliferative inhibition (IC_{50}) of 25 μM. These data suggest that lanreotide blocks transduction pathways alternative to mTOR in everolimus-resistant tumor cells and sensitizes these cells to the antiproliferative effects induced by chronic exposure to mTOR inhibitors. We have also evaluated the effects of everolimus-induced resistance on the expression of membrane-associated isoform of TNFα and of IL-10 in these cells. We have found an increase of both cytokines in everolimus-resistant cells as compared with sensitive ones (**Figures 6A,B**). The previous data suggest that the resistant phenotype confers an increase of TNFα, a Th1 cytokine making the cells likely more sensitive to the inhibitory activity of lanreotide.

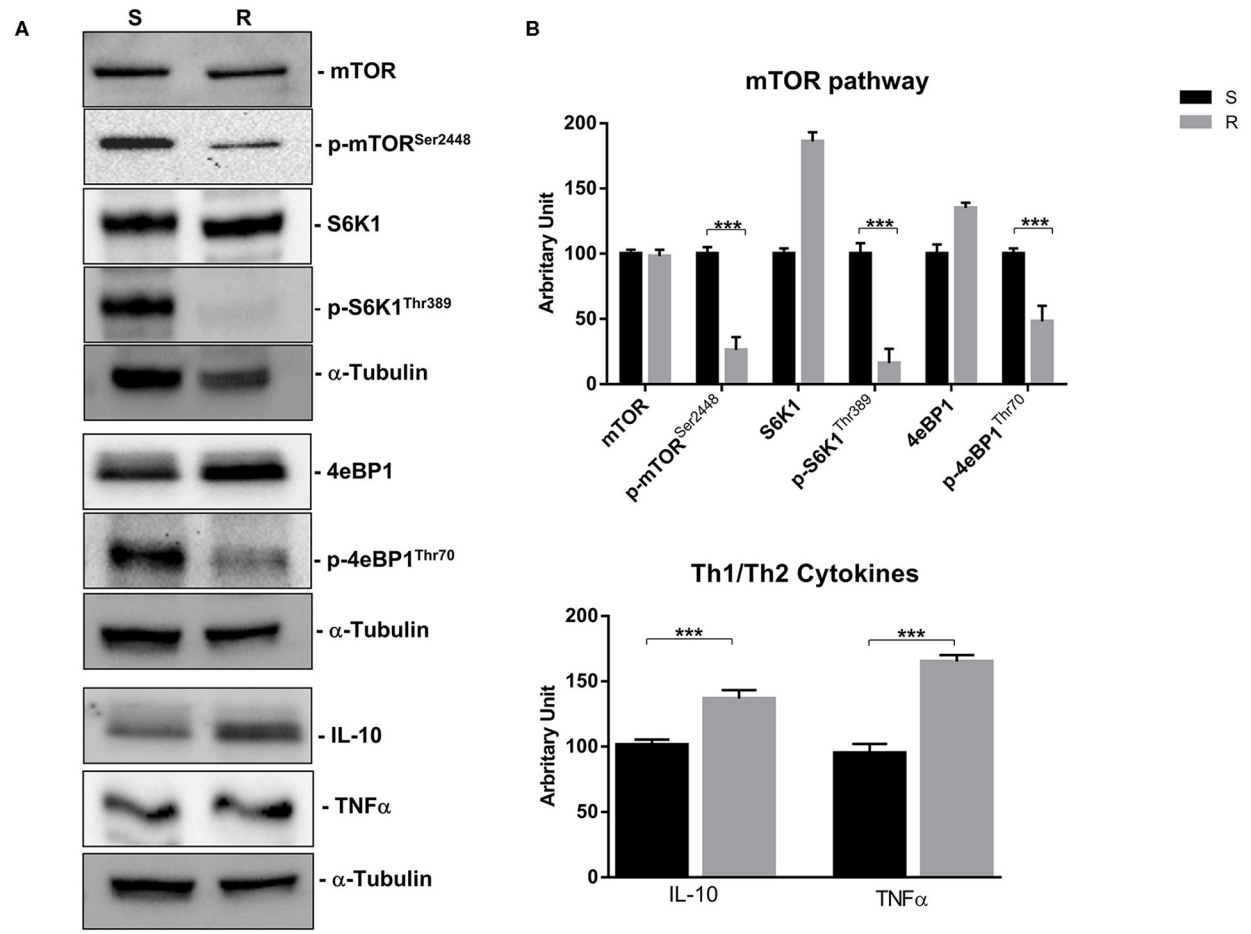

FIGURE 6 | mTOR pathway (mTOR, p-mTOR^{Ser2448}, S6K1, p-S6K1^{Thr389}, 4eBP1, and p-4eBP1^{Thr70}) and Th1 cytokines (IL-10 and TNFα) proteins expression in sensitive and resistant BON-1 cell line. **(A)**, Western blotting analysis of mTOR, p-mTOR^{Ser2448}, S6K1, p-S6K1^{Thr389}, 4eBP1, p-4eBP1^{Thr70}, IL-10, and TNFα. **(B)**, Densitometric analysis of bands showing the variation of the expression levels of the mTOR pathway and Th1/Th2 cytokines compared to α-Tubulin, as housekeeping protein, using Image Lab 5.2.1 ChemiDoc XRS+ (BIORAD). The results are obtained from three independent experiments and plotted as mean ± SD. *** $P \leq 0.001$.

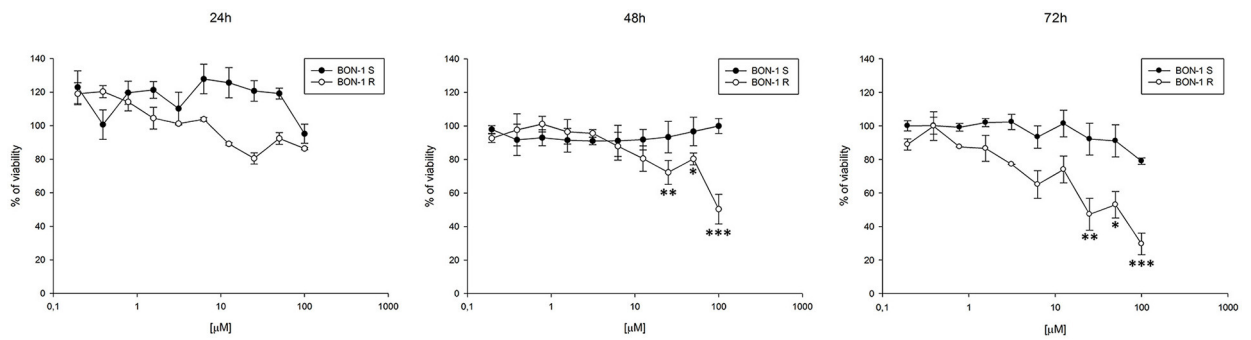

FIGURE 7 | Analysis of cell viability by MTT assay on sensitive (S) and resistant (R) BON-1 cell line after 24, 48, and 72 h of treatment with lanreotide (from 0.195 to 100 μM). Each experiment was repeated three times and shown as mean ± SD. * $P \leq 0.05$; ** $P \leq 0.01$; *** $P \leq 0.001$.

DISCUSSION

Neuroendocrine tumors (NETs) are neoplasms that arise from cells of the so-called "Neuroendocrine Diffuse System" with morphological and functional features similar to neurons, although they are without axons or synapses.

The most relevant therapeutic strategies for this disease consist in the use of molecules able to interfere with the main

pathways involved in the pathogenesis and function of NET cells. These approaches regard the use of SSAs, including octreotide and lanreotide as well as mTOR inhibitors like everolimus.

Several studies have shown that neuroendocrine tumor cells may synthesize cytokines (CKs) (29) that in turn, act as tumor growth factors (i.e., IL-8) and also affect the immunosurveillance efficacy (30). Th1 immunity is gaining an important role in cancer therapy and weak Th1 responses are suggestive of poor treatment response and prognosis (36). This role for Th1 immunity is likely due to the CD4+ T helper cell function in stimulating both innate and adaptive components of immune system in response to tumors through direct cytotoxic tumoricidal activity, modification of antitumor cytokine responses and potentiation of long term immunologic memory (37). In line with other scientific findings, we have recorded that lanreotide treatment is able to restore a Th1 phenotype in patients with intestinal NETs as showed by a significant increase in TNFα and IFN-γ. Additionally, we also showed that all patients continue to produce high levels of Th2 cytokines probably as consequence of a higher representation of lanreotide-resistant cells and previous different treatments. In this light, both IFN-γ and TNFα were not detectable in patients with mammary and bronchial NETs suggesting that other cytokines such as IL-17A as well as IL-8 might be involved in the activation pathways of these tumors or that simply their expression may not be modulated by lanreotide for a different expression of sensitive SSRs. The modulation of IFN-γ production observed in patients with NETs was not tested *in vitro* experiment due to the inability of tumor cells to produce this cytokine. In line with these results, we also found that the exposure to lanreotide is able to upregulate the production of TNFα and downregulate the expression of IL-6 and IL-10 only in the pancreatic-derived cells, while lung NETs showed an opposite profile. On this light, we have previously demonstrated that lanreotide can increase the activity of IL-2-activated peripheral blood mononuclear cells against a cellular model of NET of the thyroid, the medullary thyroid carcinoma (MTC) TT cell line. Moreover, we have showed that a combination schedule based upon the concomitant administration of recombinant IL-2 and lanreotide in a series of 6 patients affected by metastatic MTC was an active and safe treatment (38). Another previous therapeutic approach in this cancer subset was the combination between lanreotide and interferon α (IFNα) that gave some clinical results even if less promising (39). The previous and present data encourage the exploration of new strategies in NET based upon the combined use of immunological checkpoint inhibitors and lanreotide. In this context, everolimus has gained an important role in the treatment guidelines of NET, but one-third of NET patients invariably show primary resistance to everolimus, while the majority of the patients develop acquired resistance and disease progression within 24 months (25). In our study, we have investigated the effects of lanreotide in pancreatic cell lines made resistant to everolimus *in vitro*. We have characterized this cell line for the activity and expression of the mTOR-dependent pathway and we have found, as expected, an increased activity of the targets as an explanation of the resistance. In this experimental model, our data suggest that the parental pancreatic NET cells were highly resistant to the antiproliferative effects induced by lanreotide compared to everolimus resistant derivative cells. The use of lanreotide in this setting could have a new indirect mechanism of action which could overcome the resistance to everolimus. We have also demonstrated an increased expression in everolimus-resistant cell line, as compared to the parental counterpart of TNFα suggesting that a Th1 response could be useful in immunological integrated treatment strategies. IL-10 showed the same expression profile in NET cell line resistant to everolimus compared to sensitive one. In fact, as reported by Stassi et al. the cancer resistance to chemotherapeutic drugs is related to the autocrine production of IL-4 and IL-10 (40).

Experiments are currently in progress to evaluate the cytokine expression modulation in the resistant cells by lanreotide as well as its effects on the expression of the different SSTR subtypes.

Overall our results suggest that lanreotide treatment of intestinal NET tumors promotes the occurrence of a Th1 cytotoxic phenotype, a fact that may represent a solid rationale to combine lanreotide with immune-oncological strategies which include immunodulating cytokines (IL-2, IFNα) or PD-1/PD-L1 inhibitors. Additionally, our *in vitro* results suggest that lanreotide may be considered as an efficient rescue treatment when everolimus resistance occurs in patients with intestinal NETs.

DATA AVAILABILITY STATEMENT

The datasets generated for this study are available on request to the corresponding author.

ETHICS STATEMENT

Written informed consent was obtained from the individuals for the publication of any potentially identifiable images or data included in this article.

AUTHOR CONTRIBUTIONS

CS and AL have contributed equally to this work, prepared the manuscript, and assembled figures. FR, CM, MB, GM, ACo, GV, and PC conceived and designed the experiments. AG performed experiments and analyzed data. RM clinically evaluated patients enrolled for the study. AMC conducted the experiments. AF, AN, JF, MG, MC, and ACa revised the manuscript. All authors contributed to the article and approved the submitted version.

FUNDING

This work has been supported by IPSEN, by the NSP project nos. LO1508 and LO1309, MZ-VES project nos. 16-28637A, 16-2960A, and 17-32285A, by funds institutional research (TA29) of UVPS Brno and by AIRC (IG 2017, code 20711). The funder (IPSEN) was not involved in the study design, collection, analysis, interpretation of data, the writing of this article or the decision to submit it for publication.

REFERENCES

1. Kloppel G. Neuroendocrine neoplasms: dichotomy, origin and classifications. *Visc Med.* (2017) 33:324–30. doi: 10.1159/000481390
2. Fraenkel M, Kim M, Faggiano A, de Herder WW, Valk GD, Knowledge N. Incidence of gastroenteropancreatic neuroendocrine tumours: a systematic review of the literature. *Endocr Relat Cancer.* (2014) 21:R153–63. doi: 10.1530/ERC-13-0125
3. Bhate K, Mok WY, Tran K, Khan S, Al-Nahhas A. Functional assessment in the multimodality imaging of pancreatic neuro-endocrine tumours. *Minerva Endocrinol.* (2010) 35:17–25.
4. Scherubl H, Streller B, Stabenow R, Herbst H, Hopfner M, Schwertner C, et al. Clinically detected gastroenteropancreatic neuroendocrine tumors are on the rise: epidemiological changes in Germany. *World J Gastroenterol.* (2013) 19:9012–9. doi: 10.3748/wjg.v19.i47.9012
5. Plockinger U, Wiedenmann B. Treatment of gastroenteropancreatic neuroendocrine tumors. *Virchows Arch.* (2007) 451 Suppl 1:S71–80. doi: 10.1007/s00428-007-0446-z
6. Faggiano A, Lo Calzo F, Pizza G, Modica R, Colao A. The safety of available treatments options for neuroendocrine tumors. *Expert Opin Drug Saf.* (2017) 16:1149–61. doi: 10.1080/14740338.2017.1354984
7. Arnold R, Trautmann ME, Creutzfeldt W, Benning R, Benning M, Neuhaus C, et al. Somatostatin analogue octreotide and inhibition of tumour growth in metastatic endocrine gastroenteropancreatic tumours. *Gut.* (1996) 38:430–8. doi: 10.1136/gut.38.3.430
8. Zaytseva YY, Valentino JD, Gulhati P, Evers BM. mTOR inhibitors in cancer therapy. *Cancer Lett.* (2012) 319:1–7. doi: 10.1016/j.canlet.2012.01.005
9. Lamberts SW, van der Lely AJ, de Herder WW, Hofland LJ. Octreotide. *N Engl J Med.* (1996) 334:246–54. doi: 10.1056/NEJM199601253340408
10. Patel YC. Somatostatin and its receptor family. *Front Neuroendocrinol.* (1999) 20:157–98. doi: 10.1006/frne.1999.0183
11. Modlin IM, Pavel M, Kidd M, Gustafsson BI. Review article: somatostatin analogues in the treatment of gastroenteropancreatic neuroendocrine (carcinoid) tumours. *Aliment Pharmacol Ther.* (2010) 31:169–88. doi: 10.1111/j.1365-2036.2009.04174.x
12. Rai U, Thrimawithana TR, Valery C, Young SA. Therapeutic uses of somatostatin and its analogues: Current view and potential applications. *Pharmacol Ther.* (2015) 152:98–110. doi: 10.1016/j.pharmthera.2015.05.007
13. Msaouel P, Galanis E, Koutsilieris M. Somatostatin and somatostatin receptors: implications for neoplastic growth and cancer biology. *Expert Opin Investig Drugs.* (2009) 18:1297–316. doi: 10.1517/13543780903176399
14. Hankus J, Tomaszewska R. Neuroendocrine neoplasms and somatostatin receptor subtypes expression. *Nucl Med Rev Cent East Eur.* (2016) 19:111–7. doi: 10.5603/NMR.2016.0022
15. Gatto F, Barbieri F, Arvigo M, Thellung S, Amaru J, Albertelli M, et al. Biological and biochemical basis of the differential efficacy of first and second generation somatostatin receptor ligands in neuroendocrine neoplasms. *Int J Mol Sci.* (2019) 20:16. doi: 10.3390/ijms20163940
16. Rinke A, Muller HH, Schade-Brittinger C, Klose KJ, Barth P, Wied M, et al. Placebo-controlled, double-blind, prospective, randomized study on the effect of octreotide LAR in the control of tumor growth in patients with metastatic neuroendocrine midgut tumors: a report from the PROMID Study Group. *J Clin Oncol.* (2009) 27:4656–63. doi: 10.1200/JCO.2009.22.8510
17. Caplin ME, Pavel M, Cwikla JB, Phan AT, Raderer M, Sedlackova E, et al. Lanreotide in metastatic enteropancreatic neuroendocrine tumors. *N Engl J Med.* (2014) 371:224–33. doi: 10.1056/NEJMoa1316158
18. Stueven AK, Kayser A, Wetz C, Amthauer H, Wree A, Tacke F, et al. Somatostatin analogues in the treatment of neuroendocrine tumors: past, present and future. *Int J Mol Sci.* (2019) 20:12. doi: 10.3390/ijms20123049
19. Laplante M, Sabatini DM. mTOR signaling in growth control and disease. *Cell.* (2012) 149:274–93. doi: 10.1016/j.cell.2012.03.017
20. Huang J, Manning BD. A complex interplay between Akt, TSC2 and the two mTOR complexes. *Biochem Soc Trans.* (2009) 37(Pt 1):217–22. doi: 10.1042/BST0370217
21. Lamberti G, Brighi N, Maggio I, Manuzzi L, Peterle C, Ambrosini V, et al. The role of mtor in neuroendocrine tumors: future cornerstone of a winning strategy? *Int J Mol Sci.* (2018) 19:3. doi: 10.3390/ijms19030747
22. Yao JC, Pavel M, Lombard-Bohas C, Van Cutsem E, Voi M, Brandt U, et al. Everolimus for the treatment of advanced pancreatic neuroendocrine tumors: overall survival and circulating biomarkers from the randomized, phase III RADIANT-3 study. *J Clin Oncol.* (2016) 34:3906–13. doi: 10.1200/JCO.2016.68.0702
23. Gallo M, Malandrino P, Fanciulli G, Rota F, Faggiano A, Colao A, et al. Everolimus as first line therapy for pancreatic neuroendocrine tumours: current knowledge and future perspectives. *J Cancer Res Clin Oncol.* (2017) 143:1209–24. doi: 10.1007/s00432-017-2407-5
24. Faggiano A, Malandrino P, Modica R, Agrimi D, Aversano M, Bassi V, et al. Efficacy and safety of everolimus in extrapancreatic neuroendocrine tumor: a comprehensive review of literature. *Oncologist.* (2016) 21:875–86. doi: 10.1634/theoncologist.2015-0420
25. Gagliano T, Bellio M, Gentilin E, Mole D, Tagliati F, Schiavon M, et al. mTOR, p70S6K, AKT, and ERK1/2 levels predict sensitivity to mTOR and PI3K/mTOR inhibitors in human bronchial carcinoids. *Endocr Relat Cancer.* (2013) 20:463–75. doi: 10.1530/ERC-13-0042
26. Pivonello C, Rousaki P, Negri M, Sarnataro M, Napolitano M, Marino FZ, et al. Effects of the single and combined treatment with dopamine agonist, somatostatin analog and mTOR inhibitors in a human lung carcinoid cell line: an *in vitro* study. *Endocrine.* (2017) 56:603–20. doi: 10.1007/s12020-016-1079-2
27. Ferolla P, Brizzi MP, Meyer T, Mansoor W, Mazieres J, Do Cao C, et al. Efficacy and safety of long-acting pasireotide or everolimus alone or in combination in patients with advanced carcinoids of the lung and thymus (LUNA): an open-label, multicentre, randomised, phase 2 trial. *Lancet Oncol.* (2017) 18:1652–64. doi: 10.1016/S1470-2045(17)30681-2
28. Yaguchi T, Kawakami Y. Cancer-induced heterogeneous immunosuppressive tumor microenvironments and their personalized modulation. *Int Immunol.* (2016) 28:393–9. doi: 10.1093/intimm/dxw030
29. Wojtowicz-Praga S. Reversal of tumor-induced immunosuppression: a new approach to cancer therapy. *J Immunother.* (1997) 20:165–77. doi: 10.1097/00002371-199705000-00001
30. Hofsli E, Thommesen L, Yadetie F, Langaas M, Kusnierczyk W, Falkmer U, et al. Identification of novel growth factor-responsive genes in neuroendocrine gastrointestinal tumour cells. *Br J Cancer.* (2005) 92:1506–16. doi: 10.1038/sj.bjc.6602535
31. Lamrani A, Tulliez M, Chauvelot-Moachon L, Chaussade S, Mauprivez C, Hagnere AM, et al. Effects of octreotide treatment on early TNF-alpha production and localization in experimental chronic colitis. *Aliment Pharmacol Ther.* (1999) 13:583–94. doi: 10.1046/j.1365-2036.1999.00515.x
32. Casnici C, Lattuada D, Franco P, Cattaneo L, Marelli O. Regulation of human peripheral blood lymphocytes IL-10 BY SMS 201-995. *J Neuroimmunol.* (2004) 149:210–6. doi: 10.1016/j.jneuroim.2003.12.020
33. Lattuada D, Casnici C, Crotta K, Mastrotto C, Franco P, Schmid HA, et al. Inhibitory effect of pasireotide and octreotide on lymphocyte activation. *J Neuroimmunol.* (2007) 182:153–9. doi: 10.1016/j.jneuroim.2006.10.007
34. Hayry P, Raisanen A, Ustinov J, Mennander A, Paavonen T. Somatostatin analog lanreotide inhibits myocyte replication and several growth factors in allograft arteriosclerosis. *FASEB J.* (1993) 7:1055–60. doi: 10.1096/fasebj.7.11.8370476
35. Schwartz LH, Litiere S, de Vries E, Ford R, Gwyther S, Mandrekar S, et al. RECIST 1.1-Update and clarification: From the RECIST committee. *Eur J Cancer.* (2016) 62:132–7. doi: 10.1016/j.ejca.2016.03.081
36. Datta J, Fracol M, McMillan MT, Berk E, Xu S, Goodman N, et al. Association of depressed anti-HER2 T-helper type 1 response with recurrence in patients with completely treated her2-positive breast cancer: role for immune monitoring. *JAMA Oncol.* (2016) 2:242–6. doi: 10.1001/jamaoncol.2015.5482

37. Cintolo JA, Datta J, Mathew SJ, Czerniecki BJ. Dendritic cell-based vaccines: barriers and opportunities. *Future Oncol.* (2012) 8:1273–99. doi: 10.2217/fon.12.125
38. Vitale G, Lupoli G, Guarrasi R, Colao A, Dicitore A, Gaudenzi G, et al. Interleukin-2 and lanreotide in the treatment of medullary thyroid cancer: *in vitro* and *in vivo* studies. *J Clin Endocrinol Metab.* (2013) 98:E1567–74. doi: 10.1210/jc.2013-1443
39. Vitale G, Tagliaferri P, Caraglia M, Rampone E, Ciccarelli A, Bianco AR, et al. Slow release lanreotide in combination with interferon-alpha2b in the treatment of symptomatic advanced medullary thyroid carcinoma. *J Clin Endocrinol Metab.* (2000) 85:983–8. doi: 10.1210/jcem.85.3.6435
40. Stassi G, Todaro M, Zerilli M, Ricci-Vitiani L, Di Liberto D, Patti M, et al. Thyroid cancer resistance to chemotherapeutic drugs via autocrine production of interleukin-4 and interleukin-10. *Cancer Res.* (2003) 63:6784–90.

Conflict of Interest: The authors declare that the research was conducted in the absence of any commercial or financial relationships that could be construed as a potential conflict of interest.

The reviewer PG declared a past co-authorship with several of the authors AL, AMC, and MC to the handling editor.

frontiers in Oncology

ORIGINAL RESEARCH
published: 29 September 2020
doi: 10.3389/fonc.2020.565950

Prognostic Value and Potential Immunoregulatory Role of SCARF1 in Hepatocellular Carcinoma

Daniel A. Patten, Alex L. Wilkinson, Joanne M. O'Rourke and Shishir Shetty*

National Institute for Health Research Birmingham Liver Biomedical Research Unit and Centre for Liver and Gastrointestinal Research, Institute of Immunology and Immunotherapy, University of Birmingham, Birmingham, United Kingdom

Scavenger receptor class F member 1 (SCARF1) is thought to play an important role in the selective recruitment of $CD4^+$ T cells to liver sinusoidal endothelial cells during chronic liver disease. However, the contribution of SCARF1 to hepatocellular carcinoma (HCC) is currently unknown. We utilized publically-available RNA-sequencing data from The Cancer Genome Atlas (TGCA) to explore *SCARF1* expression in HCC and correlated it with a number of clinicopathological features. Flow adhesion assays were used to determine the role of SCARF1 in $CD4^+$ T cell subset recruitment. SCARF1 expression was downregulated in HCC tumor tissues, compared to non-tumoral tissues, and loss of *SCARF1* expression was associated with poorly differentiated/aggressive tumors. Additionally, higher *SCARF1* expression in HCC tumor tissues was highly prognostic of better overall, disease-free and progression-free survival. SCARF1 within HCC was largely associated with tumor endothelial cells and adhesion studies suggested that it played a role in the specific recruitment of proinflammatory $CD4^+$ T cells ($CD4^+CD25^-$) to HCC tumor tissues. Endothelial SCARF1 expression in tumor biopsies may provide critical prognostic information. Additionally, SCARF1 may also be a novel endothelial target that could help re-programme the microenvironment of HCC by promoting effector T cell tumor infiltration.

Keywords: scavenger receptor, leukocyte recruitment, tumor endothelial cells, liver cancer, tumor microenviroment

OPEN ACCESS

Edited by:
Niccolò Bolli,
University of Milan, Italy

Reviewed by:
Anetta Härtlova,
University of Gothenburg, Sweden
Edward N. Harris,
University of Nebraska System, United States

****Correspondence:***
Daniel A. Patten
d.a.patten@bham.ac.uk

Specialty section:
This article was submitted to Cancer Molecular Targets and Therapeutics, a section of the journal Frontiers in Oncology

Received: *26 May 2020*
Accepted: *26 August 2020*
Published: *29 September 2020*

Citation:
Patten DA, Wilkinson AL, O'Rourke JM and Shetty S (2020) Prognostic Value and Potential Immunoregulatory Role of SCARF1 in Hepatocellular Carcinoma. Front. Oncol. 10:565950. doi: 10.3389/fonc.2020.565950

INTRODUCTION

Globally, hepatocellular carcinoma (HCC) is the second most common cause of cancer-related deaths and its incidence is predicted to further increase (1). Due to a combination of poor surveillance and lack of conclusive biomarkers (2), a large majority of HCC patients present with advanced disease and, consequently, current interventional therapies can only act to prolong survival by a few months. In more than 90% of cases, HCC occurs on the background of chronic liver disease/cirrhosis and thus provides a paradigm for inflammation-induced cancer (3). It is well-known that tumor-infiltrating lymphocytes (TILs) significantly influence the tumor microenvironment and their phenotype strongly influences prognosis in HCC (4–6); consequently, immunotherapies for the treatment of HCC are receiving increasing attention in the literature (7, 8). Present research is predominantly focussed on the efficacy of checkpoint blockade inhibitors (CIs) to "remove the brake" on the immune system in order to provide an anti-tumoral

immune response; however, recent success of CIs with anti–vascular endothelial growth factor (VEGF) treatment has highlighted the importance of the endothelium in the context of immunotherapy (9). Only a subset of patients with HCC appear to respond to immunotherapy, but selecting which patients will benefit continues to be a challenge and the presence or absence of TILs in HCC is likely to play a significant role in the response to immunotherapy. Despite this, the endothelial pathways and molecules involved in the entry of TILs to HCC tumors are considerably understudied. Lymphocyte recruitment to the liver occurs within the specialized low flow channels of the sinusoids and via a sequential step-wise process known as the "leukocyte adhesion cascade" (10). The leukocyte adhesion cascade is mediated by a number of receptor-ligand interactions between the lymphocytes and liver sinusoidal endothelial cells (LSEC) and previous studies from our lab and others have implicated members of the scavenger receptor super-family in the recruitment of leukocytes to LSEC *in vitro* (11–16). We have also shown that these endothelial-expressed scavenger receptors are present within the sinusoids of HCC tumor tissues (13, 14); however, their role in shaping the tumor microenvironment via the recruitment of TILs has not been studied to date.

Scavenger receptors are a large super-family of proteins which are defined by their ability to bind and endocytose a vast range of endogenous and exogenous ligands, eliciting the "scavenging" of unwanted macromolecules from the bloodstream (17). Functionally, scavenger receptors generally play beneficial roles in tissue homeostasis and protective roles during infection, but have also been implicated in the persistence of inflammatory disorders, including chronic liver diseases (17, 18) and cancers (19). Liver sinusoidal endothelial cells (LSEC) express an array of scavenger receptors at high density, a phenotype which is consistent with their primary biological function of removing gut-derived antigens from the portal blood (10). However, we have also reported that LSEC-expressed scavenger receptors perform an important secondary role in which they mediate the recruitment of leukocytes to the liver (11).

Scavenger receptor class F, member 1 (SCARF1 or SR-F1), also known as scavenger receptor expressed by endothelial cells (SREC)-I, was first identified in cDNA libraries from human umbilical vein endothelial cells (HUVEC) (20). SCARF1 has been shown to bind and internalize modified low density lipoproteins (LDLs), specifically acLDLs (21), and a wide range of other endogenous damage-associated products (22), such as heat-shock proteins (HSPs) (23–25) and apoptotic host cells (26, 27). In addition to a diverse range of endogenous ligands, SCARF1 also binds a wide array of viral (28–30), fungal (31), and bacterial (32–35) antigens. Furthermore, our lab was the first to comprehensively characterize SCARF1 expression in human liver tissues and primary LSEC and we were able to demonstrate that SCARF1 plays a role in the selective recruitment of $CD4^+$ T cells to the sinusoidal endothelium under physiological shear stress (14). In this regard, we hypothesized that SCARF1 actively contributed to the hepatic microenvironment and played an important role in the pathophysiology of chronic inflammatory liver diseases and malignancies (14).

Here, through the utilization of the publically-available TGCA (The Cancer Genome Atlas) RNA-sequencing datasets (http://cancergenome.nih.gov), we describe the differential regulation of scavenger receptors in HCC tumor tissues, compared to non-tumorous control tissues, and specifically focussed on the downregulation of *SCARF1* expression. We corroborated these findings with immunohistochemical staining, which also showed reduced protein expression in HCC tumor tissues, and next explored the relationship of *SCARF1* expression with tumor progression. Consequently, we found an association with loss of *SCARF1* expression with aggressive tumor biology. Following this, we evaluated the prognostic value of *SCARF1* expression in HCC tumors by generating survival curve data, via KM Plotter (http://kmplot.com/analysis/). In support of the pathological findings, high *SCARF1* expression in HCC tumor tissues was found to correlate with a better overall survival, disease-free survival and progression-free survival. Next, via a combination of TGCA data analysis and immunofluorescent staining, we determined that SCARF1 within HCC was largely associated with tumor endothelial cells. Finally, we extended our previous findings with primary human liver endothelial cells by studying subsets of $CD4^+$ T cells. Using flow-based adhesion assays under physiological levels of shear stress our findings suggested that SCARF1 could play a role in the recruitment of proinflammatory $CD4^+$ T cells ($CD4^+CD25^-$), rather than immunosuppressive T cell subsets, to the HCC tissue microenvironment. Our results demonstrate that SCARF1 could be a prognostic biomarker in HCC. Furthermore, SCARF1 expression could potentially be targeted to alter the inflammatory status of the tumor microenvironment, shifting it toward an anti-tumoral immune response and supporting immunotherapy regimes for HCC.

MATERIALS AND METHODS

In silico Data Analysis

Publically-available data from the The Cancer Genome Atlas (TGCA) was utilized throughout this study. To explore scavenger receptor family expression in tumor and relevant non-tumorous tissue controls from the TGCA dataset, the University of California Santa Cruz (UCSC) Xena tool (https://xenabrowser.net/) was used. Correlation of SCARF1 expression with tumor progression/aggression and cell-specific markers was performed via the cBioPortal website (https://www.cbioportal.org/) (accessed 25th Feb 2020). With the use of the publically-accessible tool KM Plotter (http://kmplot.com/analysis/), survival data was generated from the TGCA dataset over a 60-month time period, with the data being split into two groups ("High" and "Low") by the median of SCARF1 expression. Resultant data was exported to Prism® 6 software (GraphPad Software Inc.) and survival curves were produced. The Gene Expression Profiling Interactive Analysis (GEPIA) website (http://gepia.cancer-pku.cn/) was used to generate a list of the top 25 genes regulated in conjunction with SCARF1 in HCC tumor tissues. Level of $CD4^+$ T cell infiltration of HCC tumors

was correlated with SCARF1 expression via the Tumor IMmune Estimation Resource (TIMER; https://cistrome.shinyapps.io/timer/; accessed 12th May 2020).

Human Tissue Samples

All liver tissue samples were collected from patients undergoing transplantation for chronic liver disease or primary hepatocellular carcinoma (HCC) at the University Hospitals Birmingham NHS Foundation Trust, with written informed consent and local ethics committee approval. All experiments were performed in accordance with the regulations and guidelines sanctioned by the West Midlands—South Birmingham Research Ethics Committee, Birmingham, UK (LREC reference 06/Q2702/61 and 04/Q2708/41).

Immunohistochemistry

Immunohistochemical staining was performed on 7 μm thick acetone-fixed cryosections, stored at −20°C. Prior to staining, sections were thawed to room temperature (RT) and hydrated with PBS/0.1% Tween® 20 (PBST) for 5 min. Endogenous peroxidase activity was then blocked with 0.3% hydrogen peroxide in methanol and blocking of non-specific binding was performed by incubation with 2X Casein Solution (Vector Laboratories, Inc.). Sections were incubated with anti-SCARF-1 primary antibody (8 μg/ml; Abcam; ab92308) diluted in PBS for 1 h at RT and then washed twice in PBST for 5 min. Isotype matched controls at appropriate concentrations were performed in all experiments. Subsequently, sections were incubated with the anti-rabbit ImmPRESS™ HRP for 30 min at RT. Excess secondary antibody was washed off with PBST for 5 min (twice) and sections were then incubated with DAB chromogen (Vector Laboratories Inc.) for 2 min; the reaction was stopped with the addition of distilled H_2O. Nuclei were then counterstained with Mayer's Hematoxylin (Pioneer Research Chemicals Ltd.) for 30 s and slides were washed in warm H_2O for 2 min. Sections were subsequently dehydrated in sequential washes of alcohol (3×) and xylene (3×) and mounted using DPX (Phthalate-free) mounting medium (CellPath). Images were taken using an Axio ScanZ1 microscope (ZEISS). Surface area coverage of SCARF1 staining was performed by via threshold analysis using ImageJ software. Five random high-power fields of view were analyzed per section, with the average value taken for each matched pair of tumor and non-tumorous tissues.

Immunofluorescence

For immunofluorescent staining, 7 μm acetone-fixed cryosections were thawed and then blocked for non-specific binding by incubation in PBS with 10% goat serum and casein solution, for 30 min at RT. This was followed by 1 h incubation with primary antibodies for SCARF-1 (8 μg/ml, Abcam ab92308) and CD31 (5 μg/ml, DAKO JC70A). Samples were washed three times in PBS followed by 30 min incubation with Alexa Fluor® conjugated secondary antibodies (1:500 dilution; Thermo Fisher Scientific). Nuclei were stained with 300 nM DAPI (Invitrogen) and slides were subsequently mounted with ProLong™ Gold Antifade Mountant (Invitrogen). Fluorescence images were acquired using a Zeiss 780 Zen confocal fluorescence microscope (ZEISS).

LSEC Isolation and Culture

Liver sinusoidal endothelial cells (LSEC) were isolated from ∼30 g human liver tissue as described previously (36). Briefly, tissues were subjected to enzymatic digestion via collagenase (10 mg/ml collagenase IA; Sigma-Aldrich) and non-parenchymal cells were separated out via density gradient centrifugation on a 33%/77% Percoll (GE Healthcare) gradient at 800 × g for 25 min. The relevant cell layer was then removed, and LSEC were isolated by positive immunomagnetic selection using CD31 antibody-conjugated DynabeadsTM (Invitrogen). LSEC were then seeded in rat tail collagen (1 in 100; Sigma-Aldrich)-coated culture vessels in medium composed of human endothelial serum-free media (SFM; Invitrogen) supplemented with 10% human serum (HD Supplies), 10 ng/ml vascular endothelial growth factor (VEGF; PeproTech), and 10 ng/ml hepatocyte growth factor (HGF; PeproTech). All cells were grown and maintained at 37°C in a humidified incubator with 5% CO_2.

Primary Lymphocyte Isolation

Peripheral blood mononuclear cells (PBMCs) were isolated from whole blood via density gradient centrifugation; briefly, whole blood was layered on Lympholyte®-H (Cedarlane) and centrifuged at 800 × g for 25 min. The PBMC layer was removed and washed in PBS with 2% FCS and 1 mM EDTA (Gibco™ by Thermo Fisher Scientific) and centrifuged at 800 × g for 5 min. A platelet depletion step was then performed by a second wash in PBS with 2% FCS and 1 mM EDTA and centrifugation at 350 × g for 10 min. $CD4^+CD25^+$ T lymphocytes were subsequently isolated from PBMCs by Dynabeads™ Regulatory $CD4^+/CD25^+$ T Cell Kit, and in accordance with manufacturer's instructions. The $CD4^+/CD25^-$ fraction obtained via this isolation protocol was kept and used as an "effector" population in flow-based adhesion assays, as previously described (13).

Flow-Based Adhesion Assays

Flow-based adhesion assays over monolayers of LSEC (13, 37) were used to study lymphocyte recruitment *in vitro*, under conditions of physiological flow. Briefly, approx. 7.5×10^5 LSEC were seeded in rat tail collagen-coated μ-slide VI 0.4 and grown to confluence overnight. Cells were then stimulated with 10 ng/ml TNFα for 24 h to induce endothelial activation. $CD4^+CD25^+$ or $CD4^+CD25^-$ T lymphocytes were isolated (see 'Primary Lymphocyte Isolation' above) and resuspended at a cell density of 1×10^6 cells/ml in a flow medium of Endothelial SFM with 0.1% BSA. Lymphocytes were then perfused over the LSEC at a physiological shear of 0.05 Pa, with each channel of the μ-slide perfused for 5 min. Subsequently, channels were washed though for 3 min with flow media alone, after which video recordings were taken. All flow

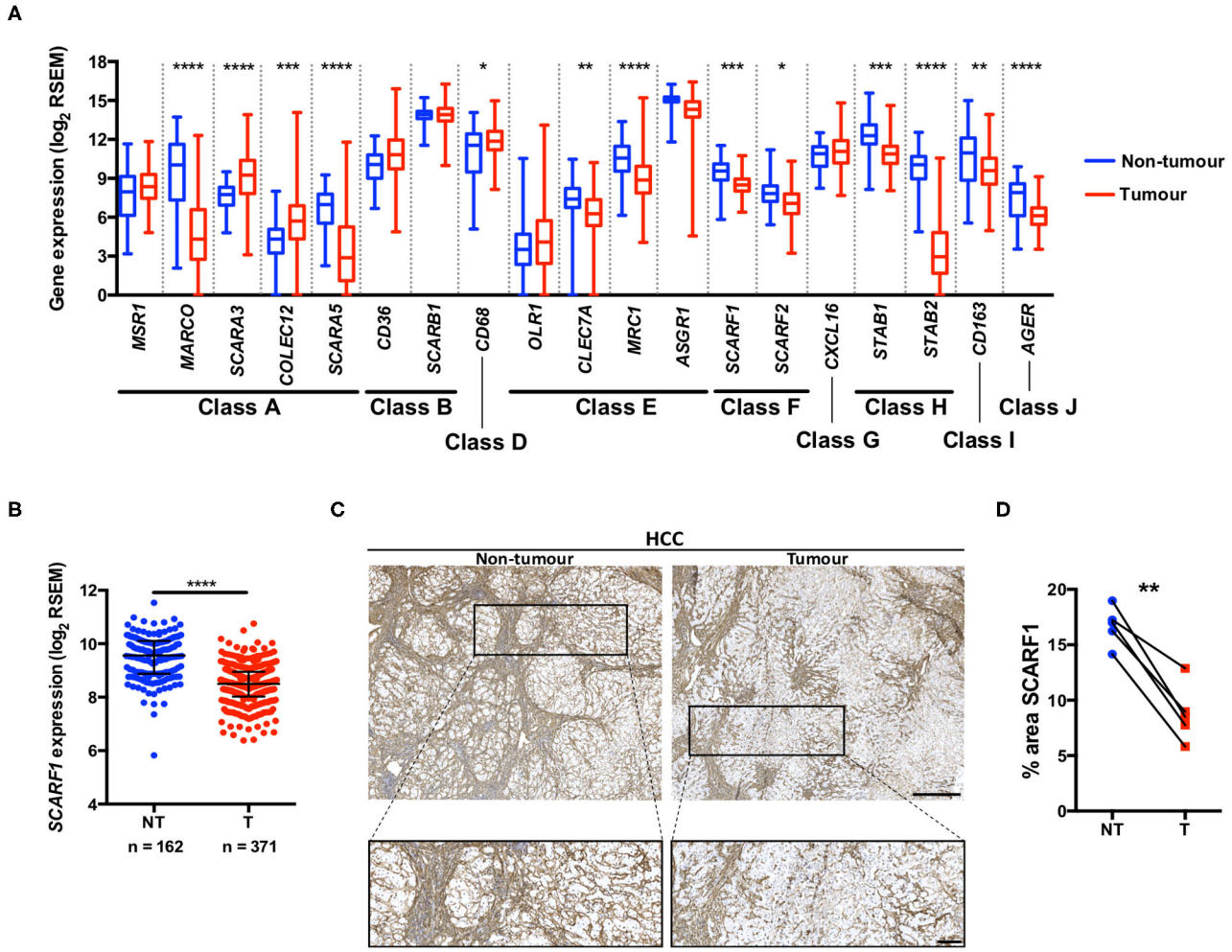

FIGURE 1 | SCARF1 gene and protein expression is downregulated in HCC tumors. **(A)** Regulation of scavenger receptor gene expression in HCC tumors (blue; $n = 371$), compared to non-tumoral tissues (red; $n = 162$). *, **, *** and **** are representative of statistical significance as measured by the Kruskal–Wallis test, where $p \leq 0.05$, $p \leq 0.01$, $p \leq 0.005$, and $p \leq 0.001$, respectively. RSEM = RNA-Seq by Expectation Maximization. **(B)** Comparison of SCARF1 gene expression in non-tumoral (NT) tissues with HCC tumor tissues (T). ****Indicates statistical significance as measured by Mann–Whitney *U*-test, where $p \leq 0.001$ **(C)**. Representative images of SCARF1 immunohistochemical staining (brown) in HCC tumor (Right panels) and matched distal, non-tumorous (Left panels) tissues from the same patient. Scale bar = 400 μm; zoomed image scale bar = 100 μm. **(D)** Surface area quantification of immunohistochemical staining in matched HCC tumor (T) and non-tumorous (NT) tissues was performed by via threshold analysis using ImageJ software. **Indicates statistical significance as measured by a paired *T*-test, where $p \leq 0.01$. $n = 5$, with the average of 5 random high-power fields of view taken per section. Data in **(A,B)** was generated from the TGCA dataset using the University of California Santa Cruz (UCSC) Xena tool (https://xenabrowser.net/).

assays were imaged via phase-contrast microscopy on an Olympus IX50 Inverted Microscope (Olympus) and 12 frames from each channel were analyzed. The number of adherent lymphocytes was firstly counted and then normalized to cells/mm^2/10^6 cells perfused using the following equation: adherent cells/flow rate (0.28 ml/min) × bolus (5 min) × field of view area (0.154 mm^2) × (1/ concentration of lymphocytes 1 × 10^6 cells/ml). The addition of SCARF-1 blocking antibody (10 μg/ml; Abcam; ab92308) or rabbit polyclonal negative control (10 μg/ml; DAKO) was performed immediately preceding each assay and incubated for 30 min (14).

Statistical Analyses

All data were tested for normal distribution by the D'Agostino-Pearson omnibus test. All data were found to be non-parametric and so were expressed as median ± interquartile range (IQR), with the number of experimental repeats (n) specified in each case. For single comparisons, statistical significance was determined by Mann–Whitney *U*-test, whereas evaluation of multiple treatments was performed by Kruskall–Wallis one-way analysis of variance with *post hoc* Dunn's test. Statistical significance of paired data was calculated via a paired *T*-test. A *p*-value of ≤ 0.05 was considered as statistically significant. All statistical analyses

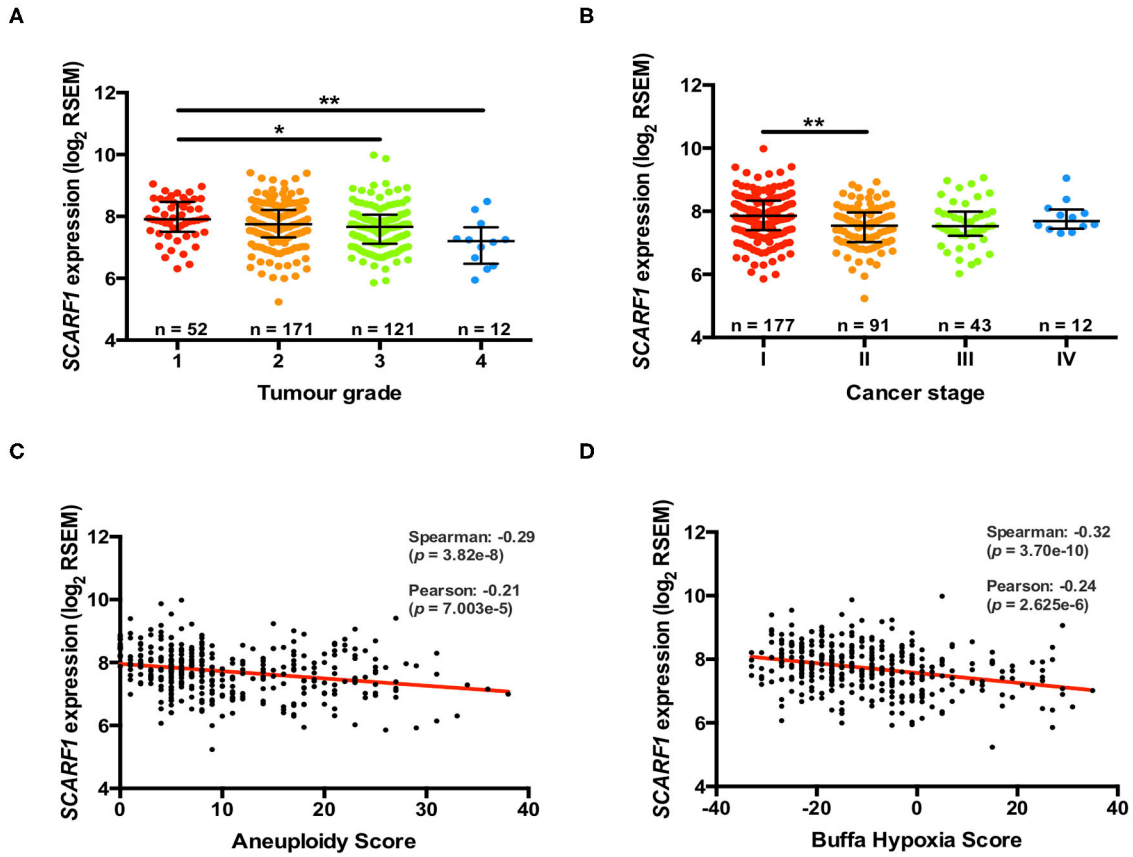

FIGURE 2 | More advanced and aggressive tumors exhibit lower SCARF1 expression. **(A)** SCARF1 expression in HCC tumor tissues of different histological grade. * and ** are representative of statistical significance as measured by the Kruskal–Wallis test, where $p \leq 0.05$ and $p \leq 0.01$, respectively. **(B)** SCARF1 expression in HCC tumor tissues from the four cancer stages. **indicates statistical significance as measured by the Kruskal–Wallis test, where $p \leq 0.01$. SCARF1 expression correlated to tumor aggression parameters **(C)**. Aneuploidy score (n =355) and **(D)** Buffa Hypoxia score (n = 361). Data in this Figure was generated from the TGCA dataset using the cBioPortal website (https://www.cbioportal.org/) (accessed 25th Feb 2020).

were undertaken using Prism® 6 software (GraphPad Software Inc.).

RESULTS

SCARF1 Expression Is Downregulated in HCC Tumors

A number of scavenger receptors have previously been shown to be significantly dysregulated within tumor tissues and have consequently been implicated in the pathophysiology of a wide variety of cancers (19). Here, we explored the mRNA expression of the scavenger receptor super-family in HCC and highlight that a number of members exhibited differential regulation in tumor tissues, compared to non-tumorous control tissues. Interestingly, the majority of scavenger receptors (*MARCO*, *SCARA5*, *CLEC7A*, *MRC1*, *SCARF1*, *SCARF2*, *STAB1*, *STAB2*, *CD163*, *AGER*) demonstrated significantly decreased expression in HCC tumor, compared to non-tumorous liver tissues (**Figure 1A**). However, in contrast, *SCARA3*, *COLEC12*, and *CD68* were all up-regulated (**Figure 1A**) and several others (*MSR1*, *CD36*, *OLR1*, *ASGR1*, and *CXCL16*) did not exhibit any regulation (**Figure 1A**). Of those significantly regulated, we were particularly interested in those previously implicated in leukocyte recruitment to the liver and specifically focussed on SCARF1 in the current study.

Utilizing qPCR analysis, we have previously shown a strong trend for decreased SCARF1 mRNA expression in HCC tumor tissue compared to normal liver tissue (14); here, we corroborated this finding with publically-available RNA-sequencing data from The Cancer Genome Atlas (TGCA). Analysis of the TGCA data showed that *SCARF1* expression is significantly ($p \leq 0.001$) lower in HCC tumor tissues in comparison to non-tumorous tissues (**Figure 1B**). In addition, *SCARF1* expression is also reduced in tumor tissues of other gastrointestinal cancers, namely esophageal carcinoma, stomach adenocarcinoma and colon adenocarcinoma, compared to their respective non-tumorous tissue controls (**Figure S1**). Interestingly, and in contrast to the other cancer types explored here, pancreatic adenocarcinoma tumors showed no dysregulation of *SCARF1* expression

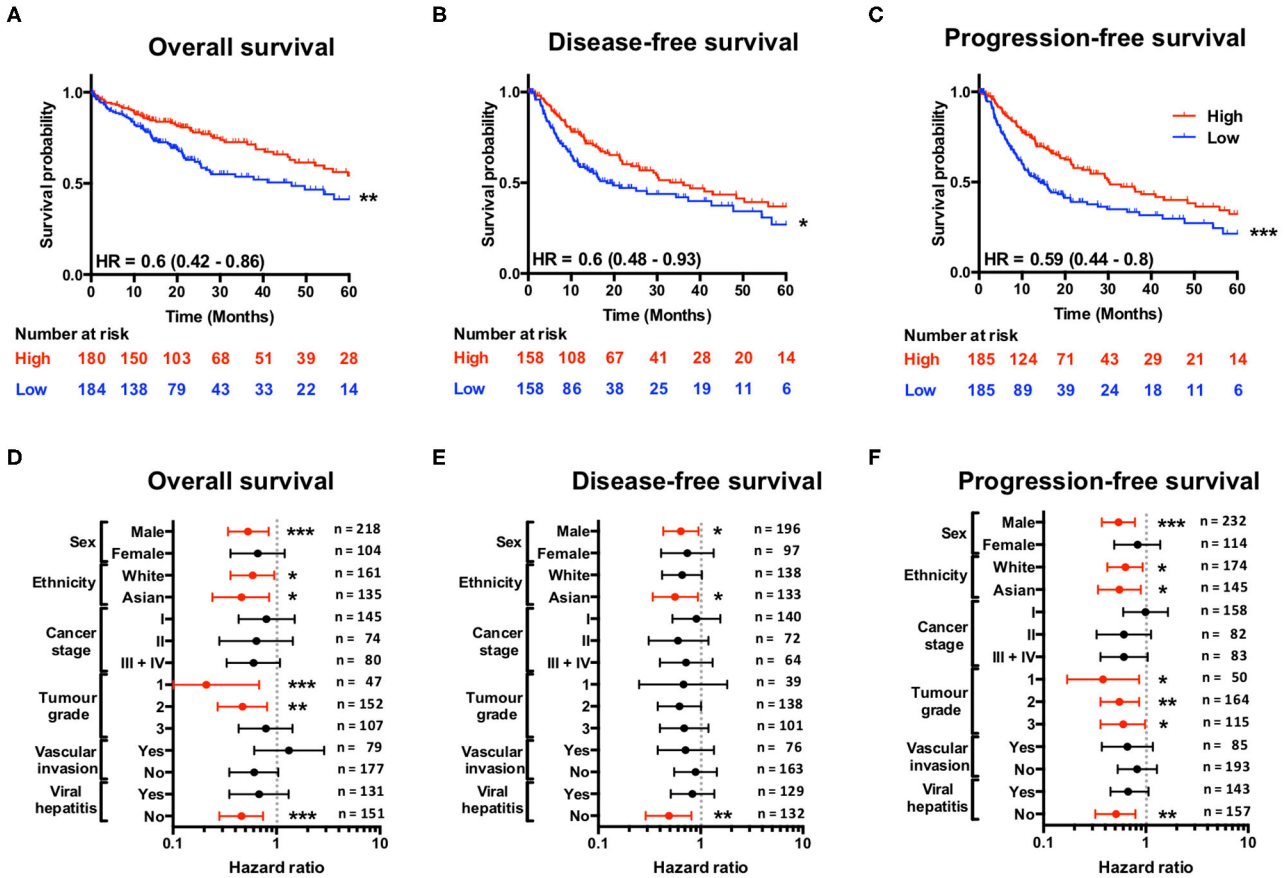

FIGURE 3 | SCARF1 expression is predictive of survival in HCC. **(A)** Overall survival, **(B)** Disease-free survival, and **(C)** Progression-free survival of HCC patients separated into two groups ("High" and "Low" expression) via the median expression of SCARF1. *, ** and *** indicate statistical significance where $p \leq 0.05$, $p \leq 0.01$, or $p \leq 0.005$, respectively. HR = hazard ratio. Forest plots of **(D)** Overall survival, **(E)** Disease-free survival, and **(F)** Progression-free survival in relation to various clinicopathological features of HCC patients. Data is displayed as hazard ratio with 95% confidence intervals. **(D–F)** Red plots highlight clinicopathological parameters in which statistical significance was achieved. *, ** and *** indicate statistical significance where $p \leq 0.05$, $p \leq 0.01$ or $p \leq 0.005$, respectively. Data in this Figure was generated with use of KM Plotter (http://kmplot.com/analysis/).

when compared to non-tumorous tissues (**Figure S1**). Next, we confirmed the downregulation of SCARF1 expression in tumors at the protein level by immunohistochemical staining of HCC tumors and matched distal, non-tumorous tissues (**Figure 1C**). Surface area quantification of SCARF1 staining in matched samples from several patients showed a significant ($p \leq 0.01$) reduction in SCARF1 expression in tumor tissues, when compared to distal, non-tumorous tissues (**Figure 1D**).

Loss of SCARF1 Expression Is Associated With More Advanced and Aggressive Tumors

Previously, we have shown that the level of immunohistochemical staining of SCARF1 in poorly differentiated HCC tumor tissues was greatly reduced when compared with well- and moderately-differentiated tumors (14); here, we aimed to utilize the TGCA dataset to further corroborate those findings. Differentiation status of solid tumors informs their histological grading and, consequently, gives an indication of tumor aggressiveness; therefore, we initially explored the expression of *SCARF1* in HCC tumors of different histological grades. In doing this, we showed significantly reduced levels in Grade 3 ($p \leq 0.05$) and Grade 4 ($p \leq 0.01$) tumors, when compared to Grade 1 tumors (**Figure 2A**). Next, we explored the *SCARF1* expression levels in cases of HCC at different stages of the disease, from early stage disease (Stage I) through to highly developed and metastatic disease (Stage IV). When compared to patients with Stage I disease, cohorts of patients with Stages II, III and IV disease all demonstrated a trend for decreased *SCARF1* expression; however, only the data for the Stage II cohort was calculated to be statistically significant ($p \leq 0.01$) (**Figure 2B**). We further aimed to confirm these findings by correlating *SCARF1* expression with other parameters commonly associated with increased tumor aggressiveness and grade, in particular, we

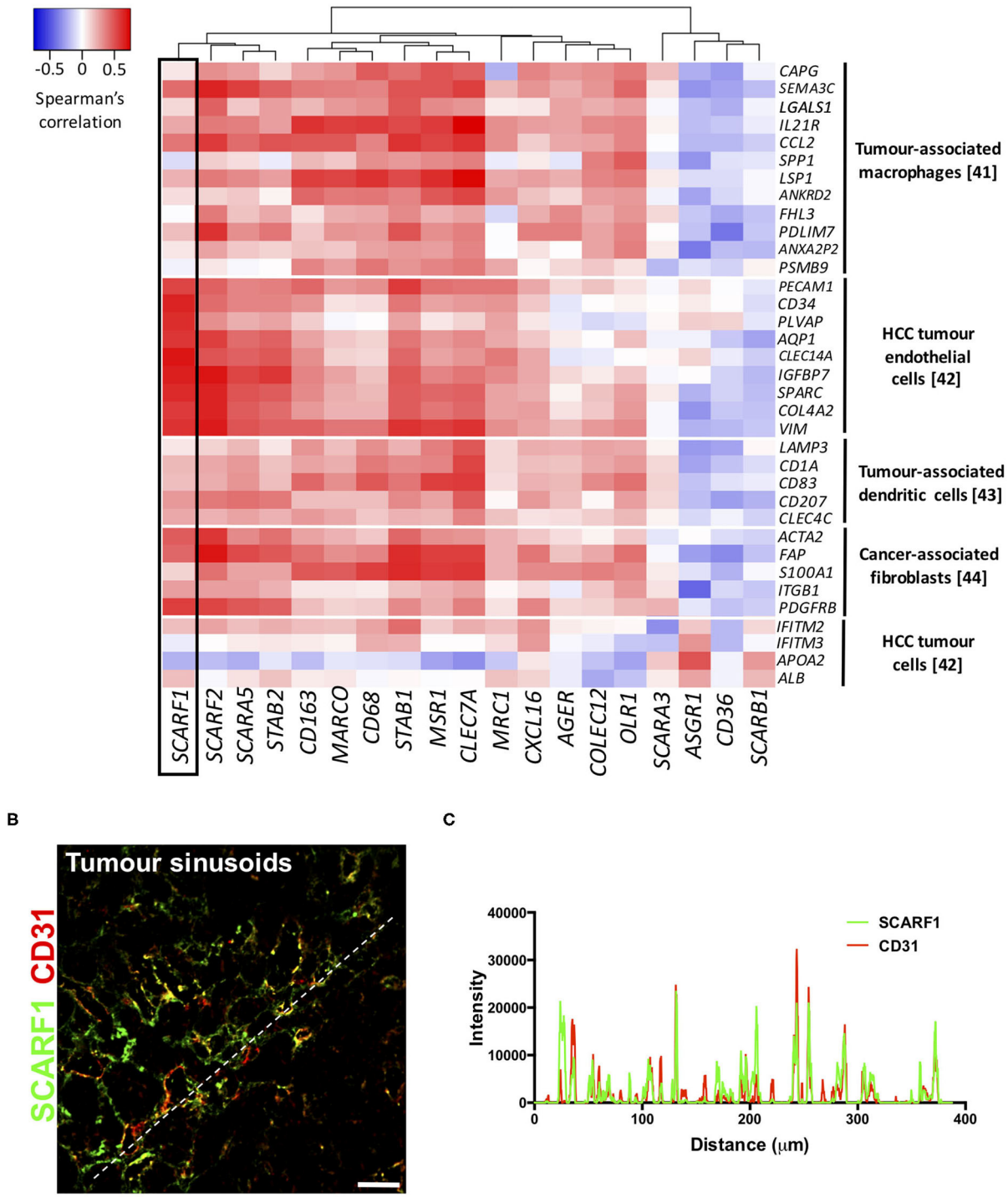

FIGURE 4 | SCARF1 is expressed in HCC tumor endothelial cells. **(A)** Correlation of scavenger receptor gene expression with tumor-associated cell-specific markers. This analysis was performed via the cBioPortal website (https://www.cbioportal.org/) (accessed 10th August 2020). $n = 358$. The heatmap was generated with use of the Heatmapper website (http://www.heatmapper.ca/). The black box highlights the expression profile of *SCARF1*. **(B)** Representative image of dual color immunofluorescent staining of SCARF1 (green) and CD31 (red) within HCC tumor sinusoids. Scale bar = 40 μm. White dashed line delineates site of intensity measurements. **(C)** Intensity measurements of immunofluorescent staining shown in **(B)**.

focussed on Aneuploidy Score (38) and Buffa Hypoxia Score (39). In both instances, *SCARF1* expression demonstrated a moderate negative correlation in HCC tumor tissues (**Figures 2C,D**), thus providing further evidence that a loss of SCARF1 expression is associated with adverse biology and aggressive HCC tumors.

Prognostic Value of *SCARF1* Expression in HCC

Having found that a loss of *SCARF1* expression correlates with more advanced and aggressive tumors, we next sought to investigate its prognostic value in HCC. With regards to overall survival, high expression of *SCARF1* was highly indicative of a better prognosis (HR = 0.60, 95% CI = 0.42–0.86, $p \leq 0.01$; **Figure 3A** and **Figure S2**. Interestingly, with the exception of *ASGR1*, which is expressed in HCC tumor cells and known to prevent metastasis (40), *SCARF1* was the only other scavenger receptor gene which was associated with increased survival in HCC (**Figure S2**). A high expression of *SCARF1* was also associated with a better prognosis when disease-free survival (HR = 0.60, 95% CI = 0.48–0.93, $p \leq 0.05$; **Figure 3B**) and progression-free survival (HR = 0.59, 95% CI = 0.44–0.80, $p \leq 0.01$; **Figure 3C**) were considered. We also assessed the prognostic value of *SCARF1* expression in correlation with a range of clinicopathological features. In male patients, higher *SCARF1* expression was suggestive of better overall survival (HR = 0.53, 95% CI = 0.34–0.84, $p \leq 0.005$; **Figure 3D**), disease-free survival (HR = 0.64, 95% CI = 0.43–0.95, $p \leq 0.05$; **Figure 3E**) and progression-free survival (HR = 0.54, 95% CI = 37–0.78, $p \leq 0.005$; **Figure 3F**), but, surprisingly, showed no prognostic value in female patients (**Figures 3D–F**). In Asian patient cohorts, higher *SCARF1* expression was strongly associated with better overall (HR = 0.46, 95% CI = 0.24–0.85, $p \leq 0.05$; **Figure 3D**), disease-free (HR = 0.56, 95% CI = 0.34–0.94, $p \leq 0.05$; **Figure 3E**) and progression-free (HR = 0.55, 95% CI = 0.34–0.89, $p \leq 0.05$; **Figure 3F**) survival; however, in white patients it was indicative of better overall (HR = 0.59, 95% CI = 0.36–0.95, $p \leq 0.05$; **Figure 3D**) and progression-free survival (HR = 0.63, 95% CI = 0.42–0.93, $p \leq 0.05$; **Figure 3F**), but not disease-free survival (**Figure 3E**). With regards to histological grade of HCC tumors, a higher *SCARF1* expression was strongly associated with better overall survival (HR = 0.21, 95% CI = 0.07–0.68, p ≤ 0.005; **Figure 3D**) and progression-free survival (HR = 0.38, 95% CI = 0.17–0.86, $p \leq 0.05$; **Figure 3F**) in Grade 1 tumors, but held no prognostic value for disease-free survival (**Figure 3E**). High expression of *SCARF1* in Grade 2 HCC tumors was again indicative of improved overall survival (HR = 0.47, 95% CI = 0.27–0.81, $p \leq 0.05$; **Figure 3D**) and progression-free survival (HR = 0.55, 95% CI = 0.34–0.89, $p \leq 0.05$; **Figure 3F**), but showed no effect on disease-free survival (**Figure 3E**). Higher SCARF1 expression in Grade 3 HCC tumors was only associated with better progression-free survival (HR = 0.60, 95% CI = 0.36–0.98, $p \leq 0.05$; **Figure 3F**), but had no prognostic value for overall (**Figure 3D**) or disease-free survival (**Figure 3E**). *SCARF1* expression was, however, highly prognostic of better overall survival (HR = 0.46, 95% CI = 0.28–0.74, $p \leq 0.005$), disease-free survival (HR = 0.49, 95% CI = 0.29–0.81, $p \leq 0.01$) and progression-free survival (HR = 0.51, 95% CI = 0.32–0.79, $p \leq 0.01$) in patients with non-viral HCC, but exhibited no prognostic value in viral HCC patients. Furthermore, expression of *SCARF1* showed no prognostic value with regards to cancer staging or in the presence/absence of vascular invasion (**Figures 3D–F**).

HCC Tumor-Expressed SCARF1 Exhibits a Strong Endothelial Signature

To explore the cell-specific expression of *SCARF1* within HCC tumors, we correlated the gene expression of the scavenger receptor superfamily with a number of gene sets known to be expressed in tumor-associated cell populations (41–44). Interestingly, of the entire scavenger receptor superfamily, *SCARF1* demonstrated the most endothelial-specific signature within HCC tumor tissues, exhibiting low to moderate correlations with the majority of the other cell type gene sets (**Figure 4A**). We next utilized the publically-available tool Gene Expression Profiling Interactive Analysis (GEPIA; http://gepia.cancer-pku.cn/) to generate a list of genes commonly regulated in conjunction with *SCARF1* within HCC tumor tissues (**Table S1**). Out of the top 25 hits, a number of genes were endothelial-specific and we selected some of these to further explore their relationship with *SCARF1* expression. Consequently, all of the endothelial markers selected (*ADGRF5, CD93, FLT4, MMRN2, ESAM, PEAR1, PECAM1, TIE1*, and *CLEC14A*) exhibited a highly significant positive correlation with *SCARF1* expression (**Figure S3**). Next, to corroborate the expression of *SCARF1* in tumor sinusoidal endothelial cells we undertook dual immunofluorescence staining of SCARF1 and CD31, a commonly used tumor endothelial marker known to be expressed in HCC (42, 45). Within HCC tumor tissue, we demonstrated a strong co-localization of SCARF1 and CD31 (**Figures 4B,C**).

SCARF1 Preferentially Supports Adhesion of $CD4^+CD25^-$ "Effector" T Cells to Human Liver Endothelial Cells

Having previously shown that SCARF1 mediates the specific recruitment of $CD4^+$ T cells to LSEC *in vitro*, under conditions of physiological flow (14), we aimed to determine whether it could play a role in the recruitment of TILs to the HCC tumor microenvironment. Firstly, and again utilizing the data available on the cBioPortal website, we correlated the expression of *SCARF1* with *CD4* expression and showed a moderate positive correlation between the two (**Figure 5A**). We next used a publically-available tool, Tumor IMmune Estimation Resource (TIMER; https://cistrome.shinyapps.io/timer/) to correlate *SCARF1* expression with the level of $CD4^+$ T cell infiltration of HCC tumors. Using TIMER, we confirmed that *SCARF1* expression is absent from tumor cells, as indicated by a negative "purity" correlation (−0.295; **Figure 5B**, left panel), and demonstrated a moderate positive correlation with $CD4^+$ T cell infiltration (purity-corrected

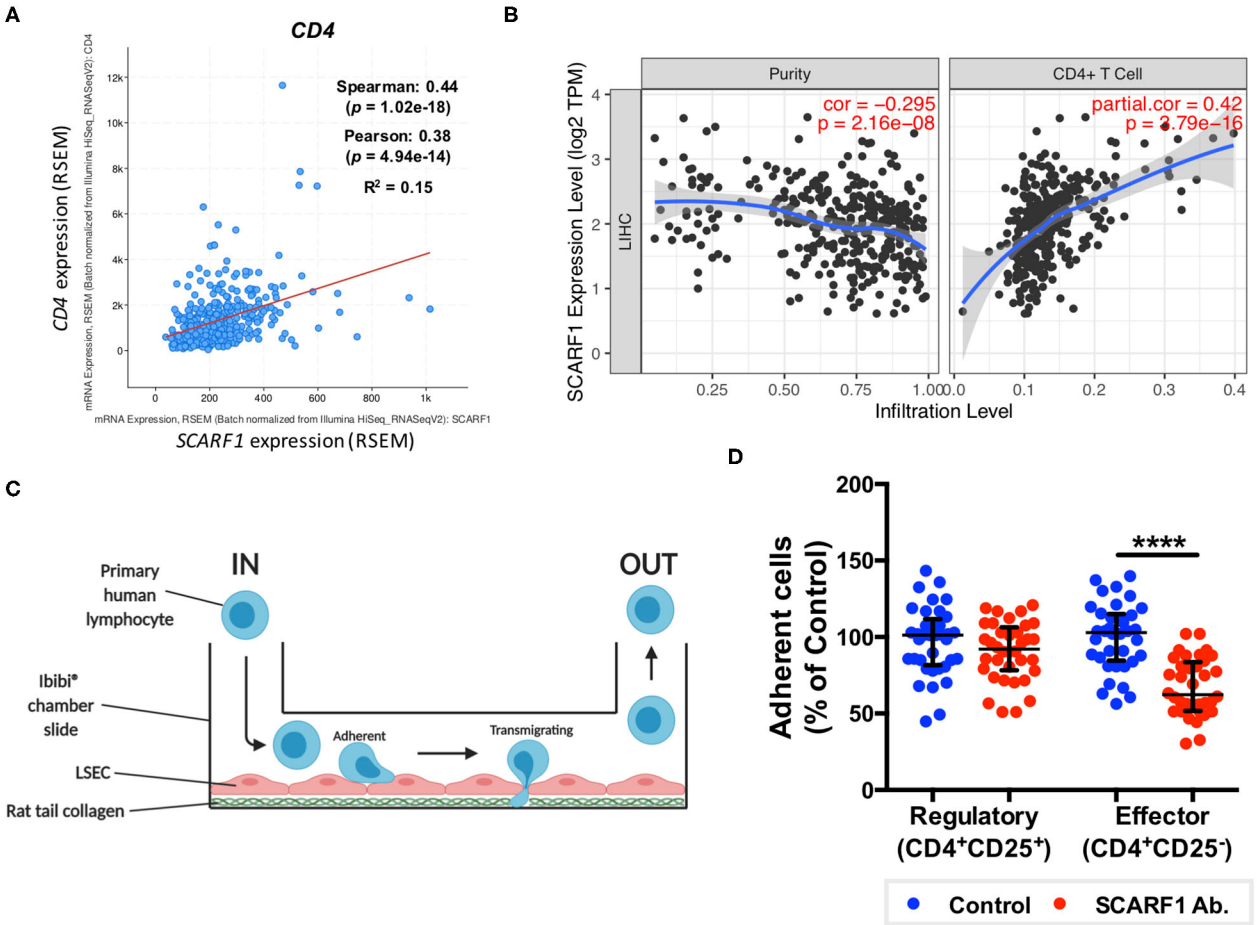

FIGURE 5 | SCARF1 potentially mediates the recruitment of proinflammatory $CD4^+$ T cells to HCC tumors. **(A)** Correlation of SCARF1 expression with CD4 expression in HCC tumor tissues. $n = 358$. **(B)** Correlation of SCARF1 expression with the extent of $CD4^+$ T cell infiltration in HCC tumor tissues. $n = 358$. **(C)** Schematic representation of a flow-based adhesion assay with primary human lymphocytes flowed across primary human LSEC. **(D)** Quantification of percentage of adherent $CD4^+$ T cell subsets [regulatory ($CD4^+CD25^+$) and effector ($CD4^+CD25^-$)] in the presence of SCARF1 blocking antibody or isotype-matched control (Control) antibody. **** indicates statistical significance as measured by a paired *T*-test, where $p \leq 0.001$. $n = 3$ independent experiments with different LSEC and lymphocyte donors, with 12 fields of view taken from each. Data in **(B)** was generated with use of Tumor IMmune Estimation Resource (TIMER; https://cistrome.shinyapps.io/timer/; accessed 12th May 2020). Image in **(C)** created with BioRender.com.

partial Spearman's rho value = 0.420, $p = 3.79e^{-16}$; **Figure 5B**, right panel). The balance of immune subsets within the tumor microenvironment plays a critical role in tumor development and progression, with an immunosuppressive microenvironment promoting immune escape and a poor prognosis (46). To assess if SCARF1 could functionally contribute to the balance of immune effector vs. immunosuppressive subsets within the tumor microenvironment, we studied its role in $CD4^+$ T cell subset recruitment. Using flow-based adhesion assays under conditions of physiological shear stress with primary human LSEC and purified populations of primary human $CD4^+$ T cells (**Figure 5C**), we showed that antibody blockade of SCARF1 on LSEC had a significant (~40%; $p \leq 0.001$) inhibitory effect on the adhesion of proinflammatory ($CD4^+CD25^-$) T cells (effectors), but a negligible (~10%) effect on regulatory ($CD4^+CD25^+$) T cells (T_{regs}) (**Figure 5D**).

DISCUSSION

Hepatocellular carcinoma (HCC) predominantly manifests on a background of cirrhosis and, consequently, in conjunction with the global rise in chronic liver diseases, incidence of HCC is also set to rise. Novel medical therapies are urgently required as patients often present to clinic with advanced tumors without curative options (47). Recently, immunotherapies have provided a number of very promising prospects in the treatment of a wide range of cancers; in particular, checkpoint inhibitors and chimeric antigen receptor (CAR)-T cell therapy have received significant attention. Checkpoint inhibitors aim to

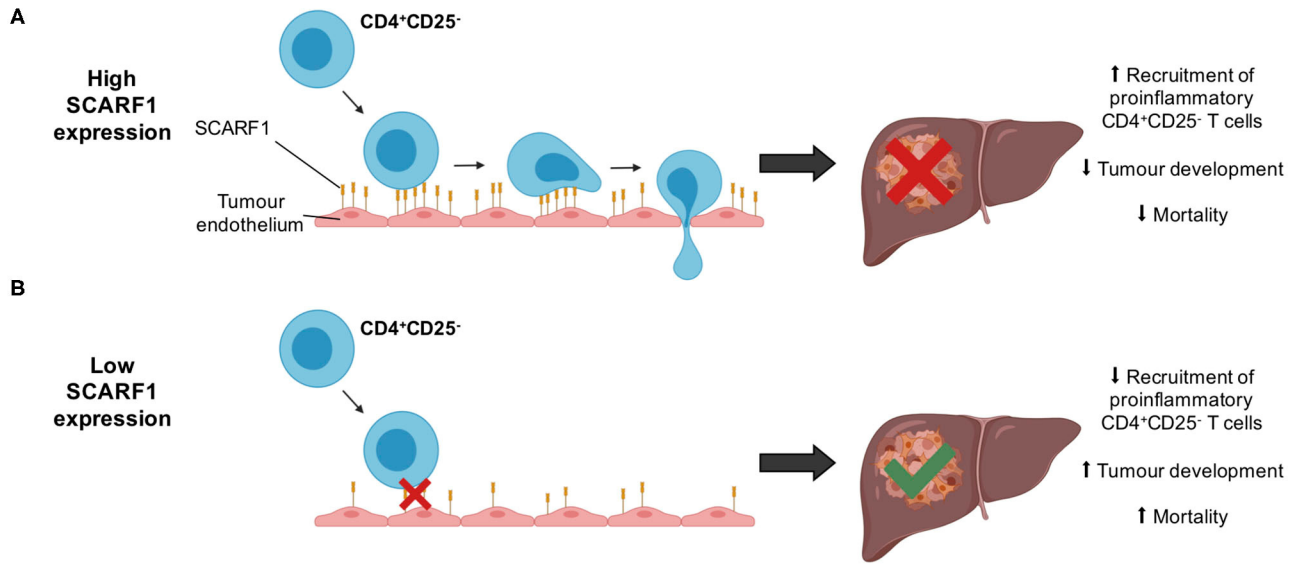

FIGURE 6 | Schematic representation of potential mechanism of action of SCARF1 in HCC tumors. **(A)** In the presence of high expression of SCARF1 in tumor endothelial cells, proinflammatory $CD4^+CD25^-$ T cells are recruited to HCC tumors, resulting in decreased tumor development and, ultimately, decreased mortality. **(B)** In low expression of SCARF1 in tumor endothelial cells, recruitment of $CD4^+CD25^-$ T cells lower, resulting in increased tumor development and mortality. Image created with BioRender.com.

release the "brake" from the immune system, thus allowing a robust anti-tumoral host immune response (48, 49) and CAR-T cells are genetically-engineered T cells specifically designed to recognize tumor antigen-expressing cells and subsequently kill them (50). However, in solid organ tumors, both these approaches are reliant on leukocyte trafficking to the tumor and this remains a significantly under-studied aspect of cancer immunotherapy (51). In the liver, leukocyte trafficking occurs within the microvasculature, known as the hepatic sinusoids. The low shear environment leads to a unique adhesion cascade with the lack of selectin-mediated recruitment and a number of atypical adhesion receptors involved in immune cell recruitment to liver sinusoidal endothelial cells (LSEC). Our previous studies have explored immune cell recruitment in the context of chronic inflammatory liver diseases, with a particular focus on LSEC-expressed scavenger receptors; however, we have also identified members of the scavenger receptor family which are expressed *in vivo* on the endothelium of human HCC, thus suggesting that they may also contribute to immune cell recruitment to the tumor microenvironment (13, 14).

Scavenger receptors represent a major subset of innate pattern recognition receptors able to bind a number of cancer-relevant ligands, such as heat shock proteins (HSPs) (52, 53) and bacterial lipopolysaccharide (LPS) (54–56), and are known to be involved in the pathophysiology of a range of cancers, including HCC (19). Interestingly, the expression of a number of scavenger receptors is often associated with poor prognosis and less favorable clinicopathological features in HCC. For example, increased expression of CD68 and CD163, which is indicative of increased numbers of anti-inflammatory macrophages, is associated with poor overall and disease-free survival (57, 58). In addition, upregulation of the CXCL16-CXCR6 axis was associated with increased invasiveness and recurrence and, as a consequence, was also associated with poorer survival in HCC (59). In contrast to this, we show that higher intratumoral expression of SCARF1 in HCC was associated with less advanced and less aggressive cancers (**Figure 2**). In addition, from a prognostic perspective, higher SCARF1 expression in HCC tumors was highly indicative of better overall, disease-free and progression-free survival (**Figure 3**).

Consistent with our previous findings in normal and chronically diseased liver tissues (14), SCARF1 in HCC tumor tissues exhibited a highly sinusoidal expression pattern (**Figure 1C**) and correlation data from the TGCA dataset further corroborated its largely endothelial expression (**Figure 4A**). A number of the top 25 genes commonly regulated in conjunction with *SCARF1* within HCC tumor tissues were endothelial-specific (**Table S1**) and all demonstrated a strong positive correlation with levels of *SCARF1* expression (**Figure S2**). We were able to confirm protein expression of SCARF1 in tumoral sinusoidal endothelial cells through dual immunofluorescence staining with the common endothelial marker CD31 (**Figure 4B**) and subsequent co-localization of the two proteins (**Figure 4C**). Having previously shown that SCARF1 mediates the specific recruitment of $CD4^+$ T cells to LSEC in inflammatory conditions (14), we next explored whether it could play a role in the recruitment of TILs to the HCC tumor microenvironment. We found that *SCARF1* expression showed a positive correlation with

both *CD4* expression (**Figure 5A**) and the level of $CD4^+$ T cell infiltration of HCC tumors (**Figure 5B**, right panel). Given that a loss of *SCARF1* expression was associated with more advanced and aggressive HCC tumors and that increased expression was highly prognostic of better survival, we hypothesized that SCARF1 could potentially be playing a beneficial role in the pathophysiology of HCC by shaping the immune infiltration of the tumor microenvironment (60). We used primary human LSEC in flow-based adhesion assays with $CD4^+$ T cells subsets and showed that antibody blockade of SCARF1 could indeed significantly inhibit the adhesion of proinflammatory ($CD4^+CD25^-$) T cells (effectors), but had little effect the adhesion of regulatory ($CD4^+CD25^+$) T cells (T_{regs}). This is in direct contrast to our previous work on another endothelial-expressed scavenger receptor, Stabilin-1, which is also present in HCC tumors, but plays a role in the specific recruitment of anti-inflammatory regulatory ($CD4^+CD25^+$) T cells (13).

These findings highlight the potential role of SCARF1 expression as a prognostic biomarker in HCC. Down regulation of *SCARF1* was associated with a poorer outcome and interestingly this may be a relevant to other tumors as we showed that tumors of other gastrointestinal cancers, such as esophageal, gastric and colonic cancers, also significantly down-regulated SCARF1 expression (**Figure S1**). In addition to high *SCARF1* expression correlating with a good outcome, our functional assays also suggest that SCARF1 may have an active anti-tumoral role for by promoting the recruitment of effector $CD4^+$ T cells rather than tumor promoting regulatory T cells (T_{regs}). This is particularly pertinent as previous studies have specifically shown that an increased prevalence of T_{regs} is an independent prognostic factor in HCC; therefore, shifting this balance could have a significant impact on patient outcome (61). In contrast to other GI malignancies, we found that pancreatic adenocarcinoma tumor tissues exhibited comparable SCARF1 expression to non-tumorous tissues (**Figure S1**). This could be due to the fact that pancreatic tumors are inherently and notoriously immunogenically "cold" tumors, due to a combination of low neoantigenic burden, heterogeneous dense stroma and an immunosuppressive tumor microenvironment (62). Therefore, an active downregulation of SCARF1 expression, in order to provide more favorable tumorigenic conditions, may not play a role in the pathogenesis of this tumor.

Whilst immunotherapy has shown exciting results in subgroups of HCC patients, there is limited stratification to support the selection of these subgroups. The correlation of SCARF1 with $CD4^+$ T cell tumor infiltration and its role in recruitment may help in the identification of patients who will respond to immunotherapies. However, further *in vivo* work is now required with SCARF1 knockout models to confirm the extent of its contribution to the HCC immune microenvironment. In addition, the identity of the receptor for SCARF1 present on $CD4^+CD25^-$ lymphocytes remains unknown, thus further studies are also required to identify its ligand. Furthermore, SCARF1 is primarily a scavenger receptor, and so the impact of its presence with regards to its scavenging function also needs to be considered in future studies. SCARF1 has been shown to bind a range of endogenous ligands, such as oxidized lipoproteins (21), heat shock proteins (23–25) and apoptotic cells (26, 27), and regulate LPS responses (35); therefore, all these functions could also potentially influence the tumor microenvironment. For example, the uptake of these factors by SCARF1 could prevent neutrophil and macrophage accumulation in the tumor microenvironment, thus providing an alternative mode-of-action for the anti-tumoral action of SCARF1, as myeloid cell accumulation is often associated with poor prognosis in HCC (63, 64). Nevertheless, our data here show that SCARF1 could potentially support the recruitment of proinflammatory ($CD4^+CD25^-$) T cells to HCC tumors, leading to decreased tumoral progression and, ultimately, a better overall outcome (**Figure 6**). Our findings also suggest that future agonistic agents acting to increase the expression of SCARF1 within tumors could boost the numbers of tumor-infiltrating proinflammatory lymphocytes. Further experimental studies of SCARF1 could therefore lead to novel combination immunotherapeutic strategies in HCC as well as in other gastrointestinal tumors.

DATA AVAILABILITY STATEMENT

The raw data supporting the conclusions of this article will be made available by the authors, without undue reservation.

ETHICS STATEMENT

The studies involving human participants were reviewed and approved by West Midlands–South Birmingham Research Ethics Committee. The patients/participants provided their written informed consent to participate in this study.

AUTHOR CONTRIBUTIONS

DP: conceptualization, formal analysis, and writing–original draft. DP, AW, and JO'R: data curation and investigation. DP and SS: funding acquisition, methodology, and writing–review and editing. All authors contributed to the article and approved the submitted version.

FUNDING

DP and SS are funded by a Medical Research Council Project Grant (MR/R010013/1) and a Rosetrees Trust Research Grant. AW is funded by a Well-come Trust PhD studentship (Mechanisms of Inflammatory Diseases (MIDAS) scheme). JO'R is supported by HUNTER, funded through a partnership between Cancer Research UK, Fondazione AIRC and Fundacion Cientifica de la Asociacion Espanola Contra el Cancer.

ACKNOWLEDGMENTS

We thank Dr. Gary Reynolds for his technical assistance. We also thank the patients and clinical staff from the Queen Elizabeth Hospital, Birmingham, for donation and collection of tissue and blood. This paper presents independent research supported by

the Birmingham NIHR Liver Biomedical Research Unit based at the University Hospitals Birmingham NHS Foundation Trust and the University of Birmingham. The views expressed are those of the authors and not necessarily those of the NHS, the NIHR or the Department of Health.

SUPPLEMENTARY MATERIAL

The Supplementary Material for this article can be found online at: https://www.frontiersin.org/articles/10.3389/fonc.2020.565950/full#supplementary-material

REFERENCES

1. Bertuccio P, Turati F, Carioli G, Rodriguez T, La Vecchia C, Malvezzi M, et al. Global trends and predictions in hepatocellular carcinoma mortality. *J Hepatol.* (2017) 67:302–9. doi: 10.1016/j.jhep.2017.03.011
2. Debes JD, Carrera E, Mattos AZ, Prieto JE, Boonstra, A. Hepatocellular carcinoma, a unique tumor with a lack of biomarkers. *Ann Hepatol.* (2019) 18:786–7. doi: 10.1016/j.aohep.2019.07.009
3. O'Rourke JM, Sagar VM, Shah T, Shetty, S. Carcinogenesis on the background of liver fibrosis: implications for the management of hepatocellular cancer. *World J Gastroenterol.* (2018) 24:4436–47. doi: 10.3748/wjg.v24.i39.4436
4. Zhang JP, Yan J, Xu J, Pang XH, Chen MS, Li L, et al. Increased intratumoral IL-17-producing cells correlate with poor survival in hepatocellular carcinoma patients. *J Hepatol.* (2009) 50:980–9. doi: 10.1016/j.jhep.2008.12.033
5. Yao W, He JC, Yang Y, Wang JM, Qian YW, Yang T, et al. The prognostic value of tumor-infiltrating lymphocytes in hepatocellular carcinoma: a systematic review and meta-analysis. *Sci Rep.* (2017) 7:7525. doi: 10.1038/s41598-017-08128-1
6. Gao Q, Qiu SJ, Fan J, Zhou J, Wang XY, Xiao YS, et al. Intratumoral balance of regulatory and cytotoxic T cells is associated with prognosis of hepatocellular carcinoma after resection. *J Clin Oncol.* (2007) 25:2586–93. doi: 10.1200/JCO.2006.09.4565
7. Greten TF, Sangro, B. Targets for immunotherapy of liver cancer. *J Hepatol.* (2018) 68:157–66. doi: 10.1016/j.jhep.2017.09.007
8. Prieto J, Melero I, Sangro, B. Immunological landscape and immunotherapy of hepatocellular carcinoma. *Nat Rev Gastroenterol Hepatol.* (2015) 12:681–700. doi: 10.1038/nrgastro.2015.173
9. Hilmi M, Neuzillet C, Calderaro J, Lafdil F, Pawlotsky JM, et al. Angiogenesis and immune checkpoint inhibitors as therapies for hepatocellular carcinoma: current knowledge and future research directions. *J Immunother Cancer.* (2019) 7:333. doi: 10.1186/s40425-019-0824-5
10. Shetty S, Lalor PF, Adams, D.H. Liver sinusoidal endothelial cells—gatekeepers of hepatic immunity. *Nat Rev Gastroenterol Hepatol.* (2018) 15:555–67. doi: 10.1038/s41575-018-0020-y
11. Patten DA, Shetty, S. More than just a removal service: scavenger receptors in leukocyte trafficking. *Front Immunol.* (2018) 9:2904. doi: 10.3389/fimmu.2018.02904
12. Patten DA, Wilson GK, Bailey D, Shaw RK, Jalkanen S, Salmi M, et al. Human liver sinusoidal endothelial cells promote intracellular crawling of lymphocytes during recruitment: a new step in migration. *Hepatology.* (2017) 65:294–309. doi: 10.1002/hep.28879
13. Shetty S, Weston CJ, Oo YH, Westerlund N, Stamataki Z, Youster J, et al. Common lymphatic endothelial and vascular endothelial receptor-1 mediates the transmigration of regulatory T cells across human hepatic sinusoidal endothelium. *J Immunol.* (2011) 186:4147–55. doi: 10.4049/jimmunol.1002961
14. Patten DA, Kamarajah SK, Rose JM, Tickle J, Shepherd EL, Adams DH, et al. SCARF-1 promotes adhesion of CD4+ T cells to human hepatic sinusoidal endothelium under conditions of shear stress. *Sci Rep.* (2017) 7:17600. doi: 10.1038/s41598-017-17928-4
15. Jung MY, Park SY, Kim IS. Stabilin-2 is involved in lymphocyte adhesion to the hepatic sinusoidal endothelium via the interaction with αMβ2 integrin. *J Leuk Biol.* (2007) 82:1156–65. doi: 10.1189/jlb.0107052
16. Patten DA, Shetty, S. The role of Stabilin-1 in lymphocyte trafficking and macrophage scavenging in the liver microenvironment. *Biomolecules.* (2019) 9:283. doi: 10.3390/biom9070283
17. Canton J, Neculai D, Grinstein, S. Scavenger receptors in homeostasis and immunity. *Nat Rev Immunol.* (2013) 13:621–34. doi: 10.1038/nri3515
18. Armengol C, Bartoli R, Sanjurjo L, Serra I, Amezaga N, Sala M, et al. Role of scavenger receptors in the pathophysiology of chronic liver diseases. *Crit Rev Immunol.* (2013) 33:57–96. doi: 10.1615/CritRevImmunol.2013006794
19. Yu X, Guo C, Fisher PB, Subjeck JR, Wang XY. Scavenger receptors: emerging roles in cancer biology and immunology. *Adv Cancer Res.* (2015) 128:309–64. doi: 10.1016/bs.acr.2015.04.004
20. Adachi H, Tsujimoto M, Arai H, Inoue, K. Expression cloning of a novel scavenger receptor from human endothelial cells. *J Biol Chem.* (1997) 272:31217–20. doi: 10.1074/jbc.272.50.31217
21. Tamura Y, Osuga JI, Adachi H, Tozawa RI, Takanezawa Y, Ohashi K, et al. Scavenger receptor expressed by endothelial cells I (SREC-I) mediates the uptake of acetylated low density lipoproteins by macrophages stimulated with lipopolysaccharide. *J Biol Chem.* (2004) 279:30938–44. doi: 10.1074/jbc.M313088200
22. Patten DA. SCARF1: a multifaceted, yet largely understudied, scavenger receptor. *Inflam Res.* (2018) 67:627–32. doi: 10.1007/s00011-018-1154-7
23. Murshid A, Gong J, Calderwood SK. Hsp90–peptide complexes stimulate antigen presentation through the class II pathway after binding scavenger receptor SREC-I. *Immunobiology.* (2014) 219:924–31. doi: 10.1016/j.imbio.2014.08.001
24. Facciponte JG, Wang XY, Subjeck JR. Hsp110 and Grp170, members of the Hsp70 superfamily, bind to scavenger receptor-A and scavenger receptor expressed by endothelial cells-I. *Eur J Immunol.* (2007) 37:2268–79. doi: 10.1002/eji.200737127
25. Gong J, Zhu B, Murshid A, Adachi H, Song B, Lee A, et al. T cell activation by heat shock protein 70 vaccine requires TLR signaling and scavenger receptor expressed by endothelial cells-1. *J Immunol.* (2009) 183:3092–98. doi: 10.4049/jimmunol.0901235
26. Ramirez-Ortiz ZG, Pendergraft III WF, Prasad A, Byrne MH, Iram T, Blanchette CJ, et al. The scavenger receptor SCARF1 mediates the clearance of apoptotic cells and prevents autoimmunity. *Nat Immunol.* (2013) 14:917–26. doi: 10.1038/ni.2670
27. Wicker-Planquart C, Dufour S, Tacnet-Delorme P, Bally I, Delneste Y, Frachet P, et al. Molecular and cellular interactions of scavenger receptor SR-F1 with complement C1q provide insights into its role in the clearance of apoptotic cells. *Front Immunol.* (2020) 11:544. doi: 10.3389/fimmu.2020.00544
28. Beauvillain C, Meloni F, Sirard JC, Blanchard S, Jarry U, Scotet M, et al. The scavenger receptors SRA-1 and SREC-I cooperate with TLR2 in the recognition of the hepatitis C virus non-structural protein 3 by dendritic cells. *J Hepatol.* (2010) 52:644–51. doi: 10.1016/j.jhep.2009.11.031
29. Murshid A, Gong J, Ahmad R, Borges TJ, Calderwood SK. Scavenger receptor SREC-I promotes double stranded RNA-mediated TLR3 activation in human monocytes. *Immunobiology.* (2015) 220:823–32. doi: 10.1016/j.imbio.2014.12.011
30. Piccolo P, Vetrini F, Mithbaokar P, Grove NC, Bertin T, Palmer D, et al. SR-A and SREC-I are Kupffer and endothelial cell receptors for helper-dependent adenoviral vectors. *Mol Ther.* (2013) 21:767–74. doi: 10.1038/mt.2012.287
31. Means TK, Mylonakis E, Tampakakis E, Colvin RA, Seung E, Puckett L, et al. Evolutionarily conserved recognition and innate immunity to fungal pathogens by the scavenger receptors SCARF1 and CD36. *J Exp Med.* (2009) 206:637–53. doi: 10.1084/jem.20082109
32. Rechner C, Kühlewein C, Müller A, Schild H, Rudel T. Host glycoprotein Gp96 and scavenger receptor SREC interact with PorB of disseminating Neisseria gonorrhoeae in an epithelial invasion pathway. *Cell Host Microbe.* (2007) 2:393–403. doi: 10.1016/j.chom.2007.11.002
33. Jeannin P, Bottazzi B, Sironi M, Doni A, Rusnati M, Presta M, et al. Complexity and complementarity of outer membrane protein A recognition by cellular and humoral innate immunity receptors. *Immunity.* (2005) 22:551–60. doi: 10.1016/j.immuni.2005.03.008

34. Baur S, Rautenberg M, Faulstich M, Grau T, Severin Y, Unger C, et al. A nasal epithelial receptor for Staphylococcus aureus WTA governs adhesion to epithelial cells and modulates nasal colonization. *PLoS Pathog.* (2014) 10:e1004089. doi: 10.1371/journal.ppat.1004089
35. Murshid A, Gong J, Prince T, Borges TJ, Calderwood SK. Scavenger receptor SREC-I mediated entry of TLR4 into lipid microdomains and triggered inflammatory cytokine release in RAW 264.7 cells upon LPS activation. *PLoS ONE.* (2015) 10:e0122529. doi: 10.1371/journal.pone.0122529
36. Lalor PF, Edwards S, McNab G, Salmi M, Jalkanen S, Adams DH. Vascular adhesion protein-1 mediates adhesion and transmigration of lymphocytes on human hepatic endothelial cells. *J Immunol.* (2002) 169:983–92. doi: 10.4049/jimmunol.169.2.983
37. Shetty S, Weston CJ, Adams DH, Lalor PF. A flow adhesion assay to study leucocyte recruitment to human hepatic sinusoidal endothelium under conditions of shear stress. *JoVE.* (2014) 85:51330. doi: 10.3791/51330
38. Taylor AM, Shih J, Ha G, Gao GF, Zhang X, Berger AC, et al. Genomic and functional approaches to understanding cancer aneuploidy. *Cancer Cell.* (2018) 33:676–89. doi: 10.1016/j.ccell.2018.03.007
39. Buffa F, Harris A, West C, Miller, C. Large meta-analysis of multiple cancers reveals a common, compact and highly prognostic hypoxia metagene. *Br J Cancer.* (2010) 102:428–35. doi: 10.1038/sj.bjc.6605450
40. Gu D, Jin H, Jin G, Wang C, Wang N, Hu F, et al. The asialoglycoprotein receptor suppresses the metastasis of hepatocellular carcinoma via LASS2-mediated inhibition of V-ATPase activity. *Cancer Letters.* (2016) 379:107–16. doi: 10.1016/j.canlet.2016.05.030
41. Cassetta L, Fragkogianni S, Sims AH, Swierczak A, Forrester LM, Zhang H, et al. Human tumor-associated macrophage and monocyte transcriptional landscapes reveal cancer-specific reprogramming, biomarkers, and therapeutic targets. *Cancer Cell.* (2019) 35:588–602. doi: 10.1016/j.ccell.2019.02.009
42. Aizarani N, Saviano A, Mailly L, Durand S, Herman JS, Pessaux P, et al. et al. A human liver cell atlas reveals heterogeneity and epithelial progenitors. *Nature.* (2019) 572:199–204. doi: 10.1038/s41586-019-1373-2
43. Hubert M, Gobbini E, Bendriss-Vermare N, Caux C, Valladeau-Guilemond J. Human tumor-infiltrating dendritic cells: From in situ visualization to high-dimensional analyses. *Cancers.* (2019) 11:1082. doi: 10.3390/cancers11081082
44. Costa A, Kieffer Y, Scholer-Dahirel A, Pelon F, Bourachot B, Cardon M, et al. Fibroblast heterogeneity and immunosuppressive environment in human breast cancer. *Cancer Cell.* (2018) 33:463–79. doi: 10.1016/j.ccell.2018.01.011
45. Qian H, Yang L, Zhao W, Chen, H, He S. A comparison of CD105 and CD31 expression in tumor vessels of hepatocellular carcinoma by tissue microarray and flow cytometry. *Exp Ther Med.* (2018) 16:2881–8. doi: 10.3892/etm.2018.6553
46. Rabinovich GA, Gabrilovich D, Sotomayor EM. Immunosuppressive strategies that are mediated by tumor cells. *Ann Rev Immunol.* (2007) 25:267–96. doi: 10.1146/annurev.immunol.25.022106.141609
47. Than NN, Ghazanfar A, Hodson J, Tehami N, Coldham C, Mergental H, et al. Comparing clinical presentations, treatments and outcomes of hepatocellular carcinoma due to hepatitis C and non-alcoholic fatty liver disease. *QJM.* (2017) 110:73–81. doi: 10.1093/qjmed/hcw151
48. Sharpe AH. Introduction to checkpoint inhibitors and cancer immunotherapy. *Immunol Rev.* (2017) 276:5–8. doi: 10.1111/imr.12531
49. Iwai Y, Hamanishi J, Chamoto K, Honjo, T. Cancer immunotherapies targeting the PD-1 signaling pathway. *J Biomed Sci.* (2017) 24:26. doi: 10.1186/s12929-017-0329-9
50. Jackson HJ, Rafiq S, Brentjens RJ. Driving CAR T-cells forward. *Nat Rev Clin Oncol.* (2016) 13:370–83. doi: 10.1038/nrclinonc.2016.36
51. Georganaki M, van Hooren L, Dimberg, A. Vascular targeting to increase the efficiency of immune checkpoint blockade in cancer. *Front Immunol.* (2018) 9:3081. doi: 10.3389/fimmu.2018.03081
52. Calderwood SK, Gong, J. Heat shock proteins promote cancer: it's a protection racket. *Trends Biochem Sci.* (2016) 41:311–23. doi: 10.1016/j.tibs.2016.01.003
53. Wu J, Liu T, Rios Z, Mei Q, Lin X, Cao, et al. Heat shock proteins and cancer. *Trends Pharmacol Sci.* (2017) 38:226–56. doi: 10.1016/j.tips.2016.11.009
54. Ikebe M, Kitaura Y, Nakamura M, Tanaka H, Yamasaki A, Nagai S, et al. Lipopolysaccharide (LPS) increases the invasive ability of pancreatic cancer cells through the TLR4/MyD88 signaling pathway. *J Surg Oncol.* (2009) 100:725–31. doi: 10.1002/jso.21392
55. Hsu RY, Chan CH, Spicer JD, Rousseau MC, Giannias B, Rousseau S, et al. LPS-induced TLR4 signaling in human colorectal cancer cells increases β1 integrin-mediated cell adhesion and liver metastasis. *Cancer Res.* (2011) 71:1989–98. doi: 10.1158/0008-5472.CAN-10-2833
56. Kisseleva T, Song L, Vorontchikhina M, Feirt N, Kitajewski J, Schindler, et al. NF-κB regulation of endothelial cell function during LPS-induced toxemia and cancer. *J Clin Invest.* (2006) 116:2955–63. doi: 10.1172/JCI27392
57. Kong LQ, Zhu XD, Xu HX, Zhang JB, Lu L, Wang WQ, et al. The clinical significance of the $CD163^+$ and $CD68^+$ macrophages in patients with hepatocellular carcinoma. *PLoS ONE.* (2013) 8:e59771. doi: 10.1371/journal.pone.0059771
58. Yeung OW, Lo CM, Ling CC, Qi X, Geng W, Li CX, et al. Alternatively activated (M2) macrophages promote tumour growth and invasiveness in hepatocellular carcinoma. *J Hepatol.* (2015) 62:607–16. doi: 10.1016/j.jhep.2014.10.029
59. Gao Q, Zhao YJ, Wang XY, Qiu SJ, Shi YH, Sun J, et al. CXCR6 upregulation contributes to a proinflammatory tumor microenvironment that drives metastasis and poor patient outcomes in hepatocellular carcinoma. *Cancer Res.* (2012) 72:3546–56. doi: 10.1158/0008-5472.CAN-11-4032
60. Borst J, Ahrends T, Babała N, Melief CJ, Kastenmüller, W. $CD4^+$ T cell help in cancer immunology and immunotherapy. *Nat Rev Immunol.* (2018) 18:635–47. doi: 10.1038/s41577-018-0044-0
61. Tu JF, Ding YH, Ying XH, Wu FZ, Zhou XM, Zhang DK, et al. Regulatory T cells, especially $ICOS^+$ $FOXP3^+$ regulatory T cells, are increased in the hepatocellular carcinoma microenvironment and predict reduced survival. *Sci Rep.* (2016) 6:35056. doi: 10.1038/srep35056
62. Upadhrasta S, Zheng, L. Strategies in developing immunotherapy for pancreatic cancer: recognizing and correcting multiple immune "defects" in the tumor microenvironment. *J Clin Med.* (2019) 8:1472. doi: 10.3390/jcm8091472
63. Margetts J, Ogle LF, Chan SL, Chan AW, Chan KA, Jamieson D, et al. Neutrophils: driving progression and poor prognosis in hepatocellular carcinoma? *Br J Cancer.* (2018) 118:248–57. doi: 10.1038/bjc.2017.386
64. Yeung OW, Lo CM, Ling CC, Qi X, Geng W, Li CX, et al. Alternatively activated (M2) macrophages promote tumour growth and invasiveness in hepatocellular carcinoma. *J Hepatol.* (2015) 62:607–16. doi: 10.1016/j.jhep.2014.10.029

Conflict of Interest: SS has received a research grant from Faron Pharmaceuticals to design a Phase I/II trial (TIETALC) of the drug "Clevergen" in patients with HCC and also reports consulting for Faron Pharmaceuticals.

The remaining authors declare that the research was conducted in the absence of any commercial or financial relationships that could be construed as a potential conflict of interest.

frontiers in Oncology

ORIGINAL RESEARCH
published: 08 December 2020
doi: 10.3389/fonc.2020.565414

Bioinformatics Analysis of the Prognostic and Biological Significance of ZDHHC-Protein Acyltransferases in Kidney Renal Clear Cell Carcinoma

Zhuang Liu[1†], Chang Liu[2†], Mingming Xiao[1†], Yamei Han[1], Siyue Zhang[1] and Bo Xu[1,3]*

[1] Department of Biochemistry and Molecular Biology, Key Laboratory of Breast Cancer Prevention and Therapy, Ministry of Education, Tianjin Medical University Cancer Institute and Hospital, National Clinical Research Center for Cancer, Key Laboratory of Cancer Prevention and Therapy, Tianjin, Tianjin's Clinical Research Center for Cancer, Tianjin, China, [2] Department of Microbiology, School of Laboratory Medicine, Tianjin Medical University, Tianjin, China, [3] Center for Intelligent Oncology, Chongqing University Cancer Hospital, Chongqing University School of Medicine, Chongqing, China

OPEN ACCESS

Edited by:
Cirino Botta, Cosenza Hospital, Italy

Reviewed by:
Kaisheng Liu, Jinan University, China
Zaixiang Tang, Soochow University Medical College, China

***Correspondence:**
Bo Xu
xubo@tmu.edu.cn

[†]These authors have contributed equally to this work

Specialty section:
This article was submitted to Cancer Molecular Targets and Therapeutics, a section of the journal Frontiers in Oncology

Received: *25 May 2020*
Accepted: *10 November 2020*
Published: *08 December 2020*

Citation:
Liu Z, Liu C, Xiao M, Han Y, Zhang S and Xu B (2020) Bioinformatics Analysis of the Prognostic and Biological Significance of ZDHHC-Protein Acyltransferases in Kidney Renal Clear Cell Carcinoma. Front. Oncol. 10:565414. doi: 10.3389/fonc.2020.565414

ZDHHC-protein acyltransferases (ZDHHCs) are a family of 23 signature Asp-His-His-Cys (DHHC) domain-containing enzymes that mediate palmitoylation by covalent attachment of the 16-carbon fatty acid palmitate to thiol groups of specific cysteine residues in substrate proteins. Emerging evidence has shown abnormal expression of ZDHHCs in a variety of disease states, including cancer. Kidney renal clear cell carcinoma (KIRC) is the eighth most common type of cancer, which accounts for the majority of malignant kidney tumors. However, there are currently no effective therapeutic targets or biomarkers for clinical treatment and prognosis in KIRC. In this study, we first analyzed the expression pattern of the 23 ZDHHCs in KIRC using TCGA and GEPIA database, and found that the expression of ZDHHC2, 3, 6, 14, 15, 21, and 23 was significantly down-regulated whereas the expression of ZDHHC9, 17, 18, 19 and 20 was significantly up-regulated in KIRC patient tissues vs. normal tissues. And the expression of ZDHHC2, 3, 6, 9, 14, 15, and 21 in tumors decreased with the increase of the pathological stage of KIRC patients. Notably, KIRC patients with decreased expression of ZDHHC3, 6, 9, 14, 15, 17, 20, 21, 23 and increased expression of ZDHHC19 were significantly associated with poor prognosis. Further, we found that there was a significant correlation between ZDHHC3, 6, 9, 14, 15, 17, 19, 20, 21, 23 expressions and immune cell infiltration. Besides, high mRNA expression was the most common type of gene alteration and there was a high correlation among the expression of ZDHHC6, 17, 20 and 21. Finally, function prediction indicated that the immune or metabolic disorders or the activation of oncogenic signaling pathways caused by abnormal expression of these ZDHHCs may be important mechanisms of tumor progression and poor prognosis in patients with KIRC.

Our results may provide novel insight for identifying tumor markers or molecular targets for the treatment of KIRC.

Keywords: kidney renal clear cell carcinoma, ZDHHC-protein acyltransferases, prognosis, immune cell infiltration, pathway analysis

INTRODUCTION

Kidney renal clear cell carcinoma (KIRC) is one of the eight most common cancer types, accounting for 70%–80% of renal cell carcinoma (1). Approximately 210,000 new cases are diagnosed worldwide each year (2). Although breakthroughs have been made in the molecular mechanisms and treatment strategies for KIRC in recent years, the prognosis of KIRC patients is still poor, especially for patients with the late clinical stage (3). Studies show that patients with stage I KIRC have a five-year disease-specific survival of about 80%–95%, whereas the five-year disease-specific survival rate of patients with IV KIRC drops sharply to less than 10% (4). Therefore, there is an urgent need to identify promising novel prognostic biomarkers and therapeutic targets, which will help clinicians choose appropriate therapeutic targets and drugs and more accurately predict the long-term prognosis of KIRC patients.

ZDHHC-protein acyltransferases (ZDHHCs) are a family of signature Asp-His-His-Cys (DHHC) domain-containing enzymes that mediate palmitoylation by covalent attachment of the 16-carbon fatty acid palmitate to thiol groups of specific cysteine residues in substrate proteins (5). In humans, the ZDHHC family has been identified to contain 23 members (ZDHHC1-24 skipping ZDHHC10) that play important roles in protein localization, accumulation, secretion, stability, and function (6). Emerging evidence has shown that abnormal expression of ZDHHCs is involved in tumorigenesis and metastasis of various cancers, which seriously affects the treatment and prognosis of cancer patients (7). For example, the low expression of ZDHHC2 in hepatocellular carcinoma was closely related to poor over survival and disease-free survival of patients (8). Elevated expression of ZDHHC3 correlated with enhanced carcinoma growth and diminished patient survival in breast cancer (9). ZDHHC9 inactivation favored NRAS-driven leukemia treatment (10) and enhanced immunotherapy effects for breast cancer (11). Decreasing ZDHHC20 expression increases tumor cell sensitivity to EGFR tyrosine kinase inhibitors (12).

However, the expression pattern, prognostic value, and biological function of ZDHHCs have not been elucidated in KIRC. In this study, we conducted a comprehensive bioinformatics analysis of the expression of ZDHHCs in KIRC. Then, the potential of differentially expressed ZDHHCs to be used as therapeutic targets and prognostic biomarkers was evaluated. Further, function prediction was performed to investigate the potential functions and associated pathways of 10 differentially expressed ZDHHCs. Our study may provide more data to help clinicians choose appropriate therapeutic targets and drugs and more accurately predict the long-term prognosis of KIRC patients.

MATERIALS AND METHODS

Databases and Web Platforms (TCGA, GEPIA, Timer, cBioPortal, STRING, GeneMANIA, GSCALite)

In our study, RNA-Seq data of ZDHHCs in 538 kidney renal clear cell carcinoma (KIRC) tissue samples and 72 normal kidney tissue samples were extracted from The Cancer Genome Atlas (TCGA) database (https://portal.gdc.cancer.gov/) for gene expression analysis and gene set enrichment analysis (GSEA).

GEPIA (Gene Expression Profiling Interactive Analysis, http://gepia.cancer-pku.cn/) was developed at Peking University and is used to analyze differential gene expression, correlation, and patient prognosis based on TCGA and the Genotype-Tissue Expression (GTEx) projects, using a standard processing pipeline (13). In this study, we performed gene expression analysis, pathological stage analysis, prognostic analysis and correlation analysis of ZDHHCs using the "KIRC" dataset in GEPIA. The parameter "Match TCGA normal and GTEx data" was set and Student's t test was used to generate a p value for gene expression analysis. The method for gene expression analysis among different pathological stage is one-way ANOVA, using pathological stage as variable for calculating differential expression. Prognostic analysis was performed using a Kaplan–Meier curve and the group cutoff choice was the median. Pearson correlation coefficient was chosen for gene correlation analysis. The p value cutoff was 0.05.

Timer (https://cistrome.shinyapps.io/timer/) provides a user-friendly web interface for dynamic analysis and visualization associations between immune infiltrates and a wide spectrum of factors including gene expression and clinical outcomes across 23 cancer types from TCGA (14). In this study, we evaluated the correlation between differentially expressed ZDHHCs and the infiltration of immune cells using "Gene module" and the "KIRC" dataset. Spearman correlation coefficient was chosen for this correlation analysis and a value of $P < 0.05$ was considered statistically significant.

STRING (Search Tool for the Retrieval of Interacting Genes/proteins, https://string-db.org/) is designed to collect, score, and integrate all public sources of protein-protein interaction (PPI) information, and further calculations are used to construct PPI networks and predict potential interactions (15). In our research, we constructed a PPI network to explore the interaction among differentially expressed ZDHHCs.

The cBioPortal (http://cbioportal.org) provides a web resource for exploring, visualizing, and analyzing multidimensional cancer genomics data based on TCGA database (16). In this study, the data of ZDHHC genetic alterations were obtained from cBioPortal. 538 KIRC samples were selected (TCGA, firehose legacy) for analysis.

mRNA expression z scores (RNA Seq V2 RSEM) were obtained using a z score threshold of ±2.0 and protein expression z scores (RPPA) were obtained using a z score threshold of ±2.0.

GeneMANIA (http://genemania.org) is a user-friendly web site that can be used to accurately predict the function of the genes submitted and find functionally similar genes using a wealth of genomics and proteomics data (17). In this study, co-expression and interaction analyses of differentially expressed ZDHHCs was performed using GeneMANIA.

GSCALite (http://bioinfo.life.hust.edu.cn/web/GSCALite/) is an available and web-based analysis platform for the gene sets in 32 cancer types from TCGA (18). In this study, GSCALite was used to provide miRNA network analysis of KIRC samples using "TCGA KIRC" dataset.

GSEA Method

GSEA (gene set enrichment analysis) reveals many common biological pathways, and this method derives its power by focusing on groups of genes that share common biological function, chromosomal location, or regulation (19, 20). In this study, GSEA v4.0.3 software was used to identify the potential underlying mechanisms of differentially expressed ZDHHCs on the pathogenesis and prognosis of KIRC (TCGA). The V7.0.Gene set in the gene sets database and 1000 for the number of permutations were selected for each analysis.

Statistical Analysis

SPSS 20.0 (IBM, SPSS Inc., Chicago, IL) software was used to perform the statistical analyses in this study. In **Figure 1A**, if two groups were with normal distribution, then we used the standard Student's test for equal variance or Welch t-test for unequal variance. Otherwise, we used the Mann-Whitney U-test (non-normal distribution). In **Figure 1B**, the paired t-test was used to determine statistical differences between the paired two groups. One-way ANOVA was used to determine gene expression difference among the pathological stage of KIRC patients in GEPIA. Survival curves were generated from Kaplan-Meier Plotter and GEPIA with HR and P-value or Cox P-value using log-rank test. The correlation between gene expression and immune cell infiltration (Timer) was assessed based on statistical significance and Spearman's correlation. A value of $P < 0.05$ was considered statistically significant. For the GSEA method, the nominal p-value (NOM $p < 0.05$) and false discovery rate (FDR $q < 0.25$) were used to determine significantly enriched gene sets.

RESULTS

Expression Pattern of ZDHHCs in KIRC

We first explored the expression pattern of ZDHHCs in KIRC using the TCGA database. As shown in **Figures 1A, B**, by evaluating the expression of ZDHHCs in 538 KIRC patient tissues and 72 normal tissues as well as 72 paired KIRC tissues and corresponding adjacent normal tissues, we found that ZDHHC2, 3, 6, 9, 14, 15, 16, 17, 18, 19, 20, 21, 22, and 23 had consistent and significant expression differences. Next, we used the GEPIA database to verify these ZDHHCs (**Figure 1C**). After further excluding ZDHHC16 and 22 that had no significant difference in expression, we finally determined the expression of ZDHHC2, 3, 6, 14, 15, 21, and 23 was significantly down-regulated whereas the expression of ZDHHC9, 17, 18, 19, and 20 was significantly up-regulated in KIRC patient tissues vs. normal tissues.

Then we further evaluated the expression patterns of these differentially expressed ZDHHCs in the main pathological stages of KIRC patients by generating expression violin plots using GEPIA (**Figures 2A–L**), and found a significant correlation between the expression of ZDHHC2, 3, 6, 9, 14, 15, 21 and the pathological stage of KIRC patients. With the progression of tumors, the expression of ZDHHC2, 3, 6, 9, 14, 15, 21 decreased significantly, indicating that these ZDHHCs played an important role in the progression and tumorigenesis of KIRC.

Prognostic Value of Differentially Expressed ZDHHCs in KIRC

To explore the prognostic value of the ZDHHCs in patients with KIRC, we assessed the impact of differentially expressed ZDHHCs on clinical outcomes including overall survival and disease-free survival using GEPIA. The survival significance map (**Figures 3A** and **4A**) was drawn based on the cox proportional hazard ratio (HR). We found that high expression of ZDHHC3, 6, 9, 14, 15, 20, 21, 23 was significantly favorable whereas high expression of ZDHHC19 was significantly unfavorable for the overall survival of KIRC patients (**Figure 3A**). And high expression of ZDHHC3, 6, 9, 14, 17, 21, 23 was significantly favorable for the disease-free survival of KIRC patients (**Figure 4A**). The Kaplan-Meier plots of these ZDHHCs having significant impacts on the overall survival or disease-free survival of KIRC patients were further presented in **Figures 3** and **4**. We found that KIRC patients with decreased ZDHHC3, 6, 9, 14, 15, 20, 21, 23 expressions and increased ZDHHC19 expression were strongly associated with poor overall survival (**Figures 3B–J**). And KIRC patients with decreased ZDHHC3, 6, 9, 14, 17, 21, 23 expressions were significantly associated with poor disease-free survival (**Figures 4B–H**). In view of the prognostic value of ZDHHC3, 6, 9, 14, 15, 17, 19, 20, 21, and 23, we conducted the following analysis on these 10 differently expressed ZDHHCs.

The Correlation of Immune Cell Infiltration With 10 Differentially Expressed ZDHHCs in KIRC Patient Tissues

Immune cell infiltration is an important determinant of immune response and prognosis in cancer patients, including those with KIRC (21). Thus, we analyzed the correlation between the expression of these 10 differentially expressed ZDHHCs and infiltration of six immune cell types, including B cells, CD8+ T cells, CD4+ T cells, macrophages, neutrophils, and dendritic cells using the Time database (**Figures 5A–J**). Interestingly, the expression of ZDHHC6, 17, 20, 21 was significantly and positively correlated with the infiltration of all the six immune cell types and the expression of ZDHHC3 and 14 was significantly and positively correlated with the infiltration of five immune cell

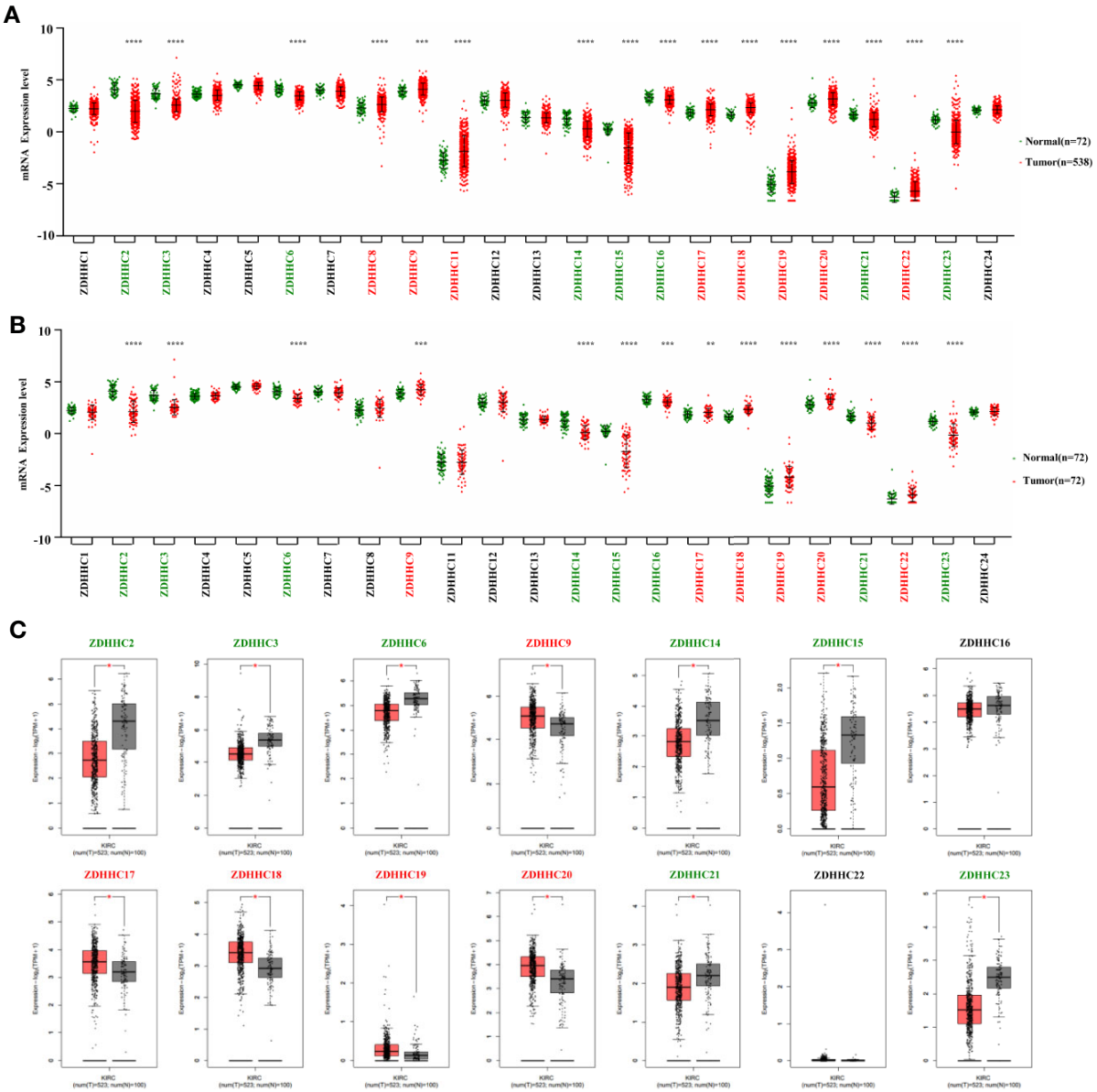

FIGURE 1 | Expression pattern of ZDHHCs in kidney renal clear cell carcinoma (KIRC). **(A)** Expression pattern of ZDHHCs in 538 KIRC patient tissues and 72 normal tissues (TCGA) and statistical differences between two groups were determined by Student's test for equal variance or Welch t-test for unequal variance (normal distribution) and the Mann-Whitney U-test (non-normal distribution). **(B)** Expression pattern of ZDHHCs in 72 paired KIRC tissues and corresponding adjacent normal tissues (TCGA) and statistical differences between two groups were determined using the paired t-test. **(C)** Expression pattern of ZDHHCs in KIRC patients and normal tissues from GEPIA. statistical differences between the two groups were determined by Student's t-test and the p value cutoff was 0.05. The green font represents down-regulation, the red font represents up-regulation, and the black font represents no expression difference. * < 0.05; ** < 0.01; *** < 0.001; **** < 0.0001.

types excluding B cells. Further, ZDHHC9 expression was significantly and positively correlated with the infiltration of B cells, macrophages, neutrophils, and dendritic cells. ZDHHC23 expression was significantly and positively correlated with the infiltration of B cells, macrophages, and neutrophils and negatively correlated with the infiltration of CD8+ T cells. Besides, the expression of ZDHHC15 and 19 was significantly and positively correlated with the infiltration of CD4+ T cells.

Gene Alterations, Expression Correlation, Micro(mi)RNA Networks, Co-Expression, and Interaction Analyses of 10 Differentially Expressed ZDHHCs in KIRC

We then performed a comprehensive analysis of the molecular characteristics of these 10 differentially expressed ZDHHCs in KIRC. The gene alterations for these ZDHHCs in KIRC was analyzed using cBioPortal. A total of 538 KIRC patients (TCGA,

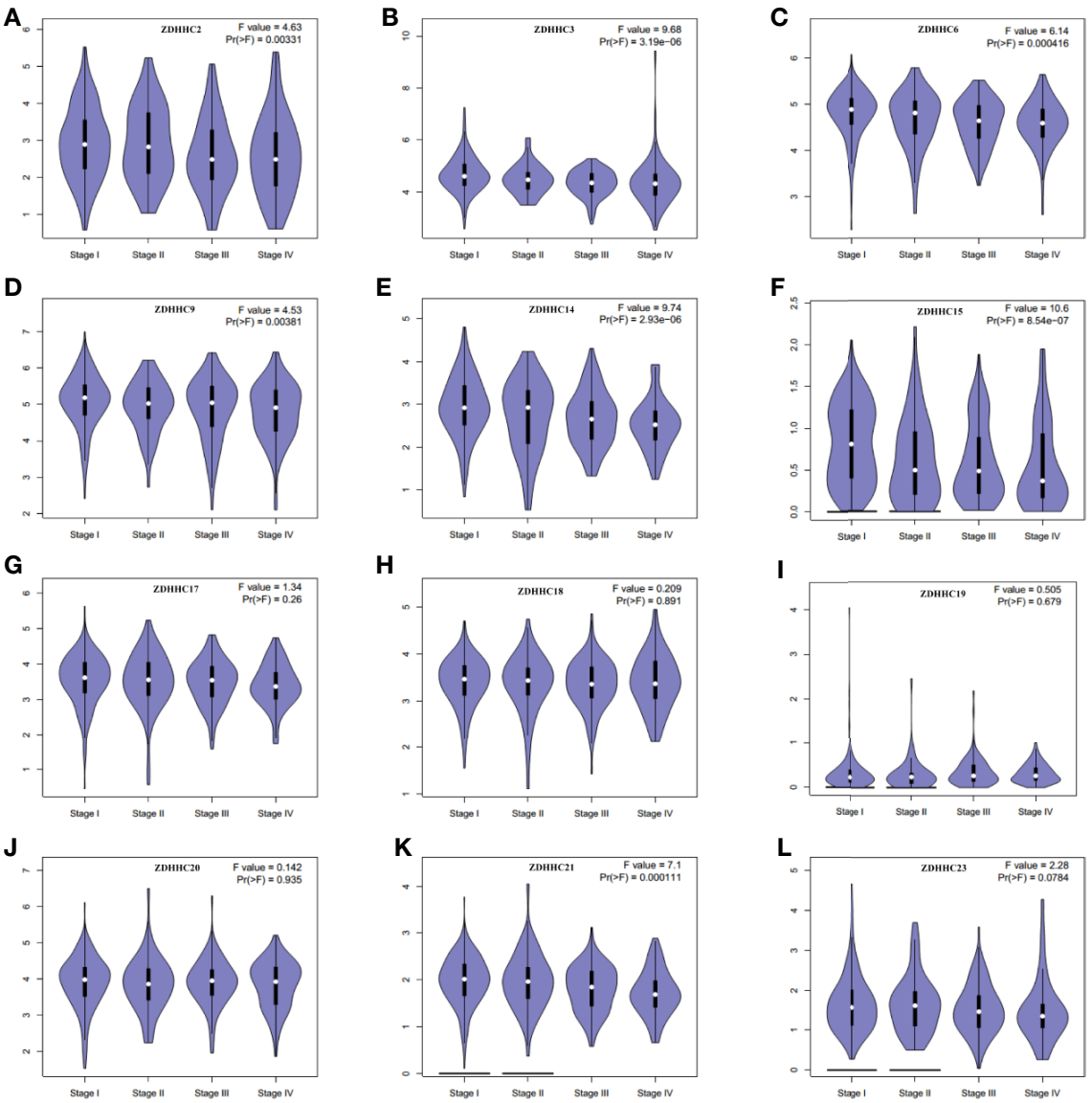

FIGURE 2 | The expression patterns of these differentially expressed ZDHHCs in the main pathological stages of kidney renal clear cell carcinoma (KIRC) patients (GEPIA). The expression patterns of **(A)** ZDHHC2, **(B)** ZDHHC3, **(C)** ZDHHC6, **(D)** ZDHHC9, **(E)** ZDHHC14, **(F)** ZDHHC15, **(G)** ZDHHC17, **(H)** ZDHHC18, **(I)** ZDHHC19, **(J)** ZDHHC20, **(K)** ZDHHC21, **(L)** ZDHHC23 in the main pathological stage of KIRC patients. One-way ANOVA was used to determine gene expression difference among the pathological stage of KIRC patients and a value of $P < 0.05$ was considered statistically significant.

firehose legacy) were selected. The frequency of ZDHHC gene alterations in KIRC, mainly including multiple alterations, mRNA low, mRNA high, deep deletion, amplification, and mutation, varied from 0.2% to 11%, respectively (**Figure 6A**). High mRNA expression was the most common type of gene alteration in these samples and deep deletion was the major type of gene alteration of ZDHHC3 (**Figure 6B**). The missense mutation was identified in ZDHHC6, 9, and 21 (**Figure 6C**). The truncating mutation was found in ZDHHC9 (**Figure 6C**). We next explored the expression correlation among these ZDHHCs and found that there was a high correlation among the expression of ZDHHC6, 17, 20, and 21 and a low to moderate correlation among ZDHHC3, 9, 14, 15, 19, and 23 (**Figure 6D**, **Table S1**). We also analyzed the miRNA network involved with these ZDHHCs using GSCALite. As shown in **Figure 6E**, there were more miRNAs to potentially regulate ZDHHC3, 6, 9, 14, 15, 17, 21, and 23 than ZDHHC19 and 20 (**Figure 6E**, **Table S2**). A protein-protein interaction (PPI) network constructed using the String database indicated that there was little interaction among these ZDHHCs (**Figure S1A**). As expected, co-expression and interaction analyses (**Figure 6F**) from GeneMANIA revealed that the functions of these ZDHHCs were primarily related to protein palmitoylation, protein acylation, lipoprotein biosynthetic and metabolic process.

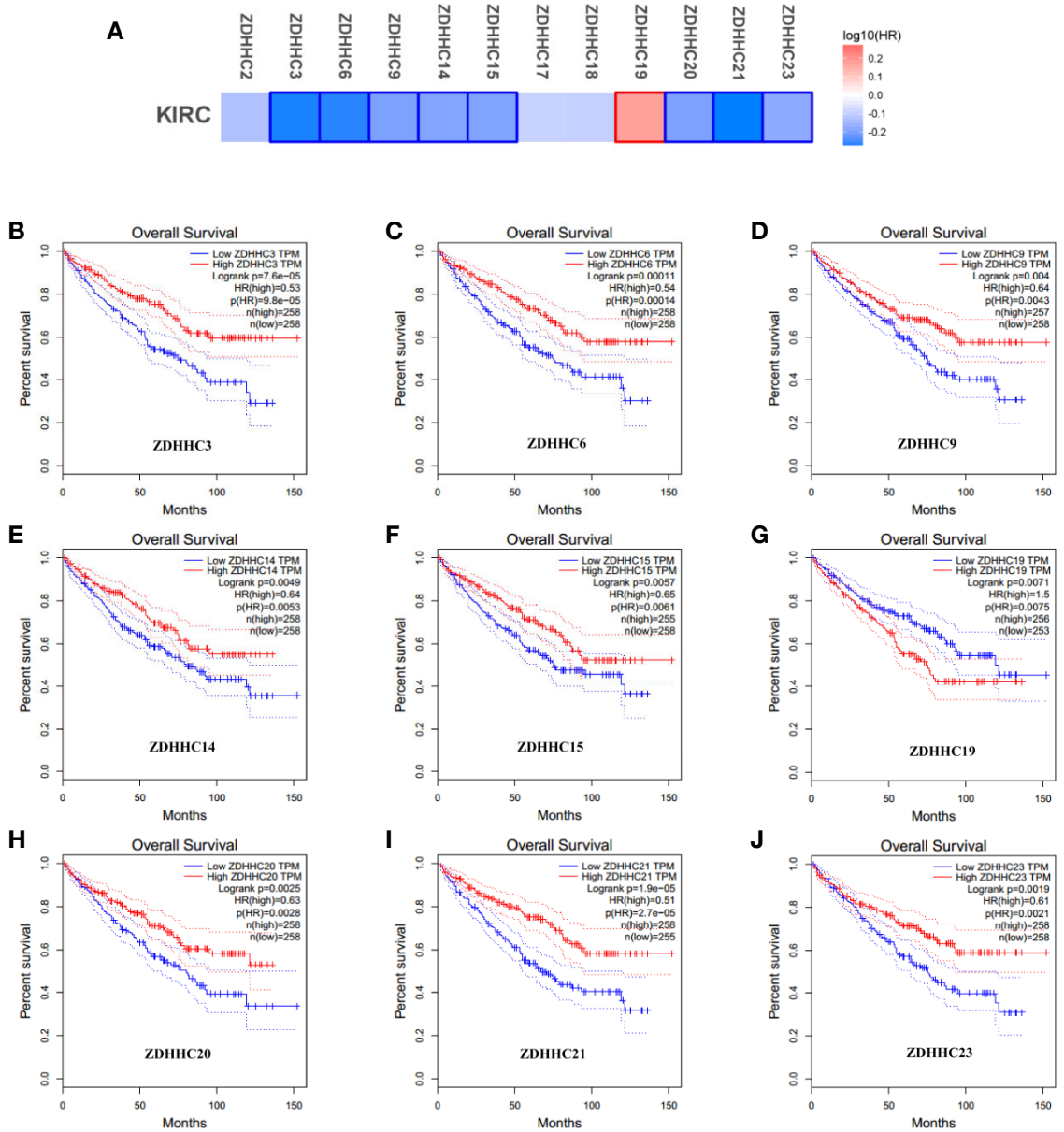

FIGURE 3 | The effect of differentially expressed ZDHHCs on the overall survival of kidney renal clear cell carcinoma (KIRC) patients (GEPIA). **(A)** Survival significance map of differentially expressed ZDHHCs showed the over survival analysis results based on the cox proportional hazard ratio (HR) through GEPIA (the red and blue blocks denoted higher and lower risks, respectively; the rectangles with frames indicated significant unfavorable and favorable results). The overall survival curve of **(B)** ZDHHC3, **(C)** ZDHHC6, **(D)** ZDHHC9, **(E)** ZDHHC14, **(F)** ZDHHC15, **(G)** ZDHHC19, **(H)** ZDHHC20, **(I)** ZDHHC21, **(J)** ZDHHC23 in KIRC. The group cutoff choice for overall survival was the median. A log-rank test was used to estimate the difference in overall survival and a value of $P < 0.05$ was considered statistically significant.

Predicted Functions of 10 Differently Expressed ZDHHCs in KIRC

We further investigated potential mechanisms of these 10 differently expressed ZDHHCs in KIRC by the GSEA method. Pathways with higher frequency enriched in phenotype high of ZDHHC19 and in phenotype low of ZDHHC3, 6, 14, 15, 17, 19, 20, 21, and 23 were shown in the WeiQi diagram (**Figure 7**), indicating that most of these ZDHHCs were closely related to immune-correlated signal pathways. ZDHHC19, 15, 3, 21, 23, 6, 14, and 20 were related to systemic lupus erythematosus. ZDHHC19, 15, 3, 21, 23, and 9 were involved in primary immunodeficiency and natural killer cell-mediated cytotoxicity. ZDHHC19, 15, 3, 21, 9, and 6 were connected with the intestinal immune network for IgA production. ZDHHC19, 15, 3, and 23 were associated with T cell receptor signaling pathway. Moreover, many of these ZDHHCs were closely linked to

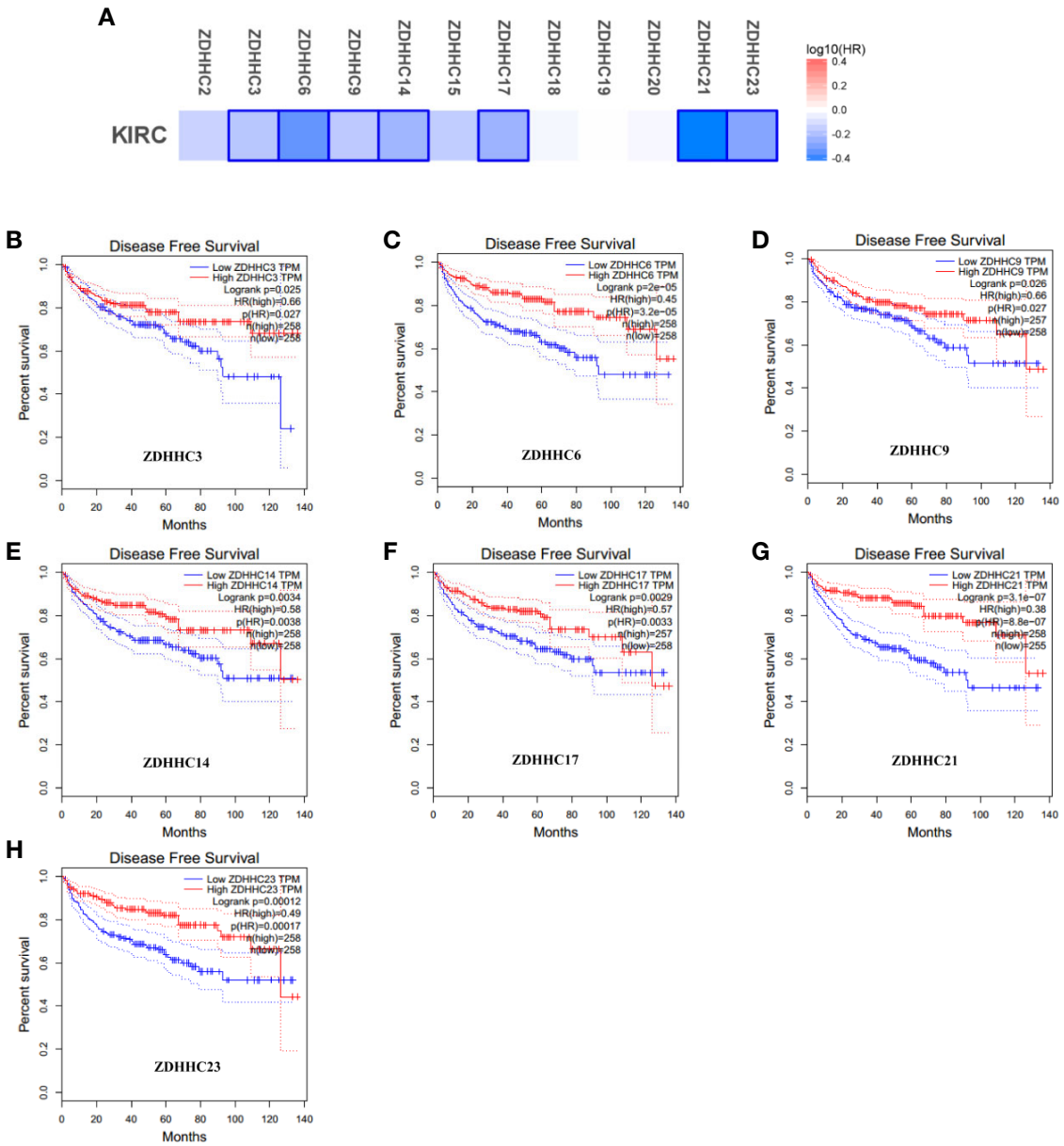

FIGURE 4 | The effect of differentially expressed ZDHHCs on disease-free survival of kidney renal clear cell carcinoma (KIRC) patients (GEPIA). **(A)** Survival significance map of differentially expressed ZDHHCs showed the disease-free survival analysis results based on the cox proportional hazard ratio (HR) through GEPIA (blue blocks denoted higher and lower risks, respectively; the rectangles with frames indicated significant favorable results). The disease-free survival curve of **(B)** ZDHHC3, **(C)** ZDHHC6, **(D)** ZDHHC9, **(E)** ZDHHC14, **(F)** ZDHHC17, **(G)** ZDHHC21, **(H)** ZDHHC23 in KIRC. The group cutoff choice for disease-free survival was the median. A log-rank test was used to estimate the difference in disease-free survival and a value of $P < 0.05$ was considered statistically significant.

metabolism-related signaling pathways. ZDHHC19, 3, 21, 23, 6, 14, 20, and 17 were associated with ribosome pathway. ZDHHC3, 21, 14, 20, and 17 were connected with glycine, serine and threonine metabolism. ZDHHC15, 3, 14, and 17 were associated with porphyrin and chlorophyll metabolism. ZDHHC3, 14, 20, and 17 were related to metabolism of xenobiotics by cytochrome P450. The results of enrichment analysis for these 10 ZDHHCs were shown in **Table S3**, which also showed that oncogenic signaling activation was associated with certain ZDHHCs. For example, the JAK/STAT signaling pathway was enriched in phenotype high of ZDHHC19 and in phenotype low of ZDHHC15 and 23. The Wnt signaling pathway was activated by down-expressed ZDHHC6, 9, and 23. Taken together, these results suggested that the immune or metabolic disorders or the activation of oncogenic signaling pathways caused by abnormal expression of these ZDHHCs

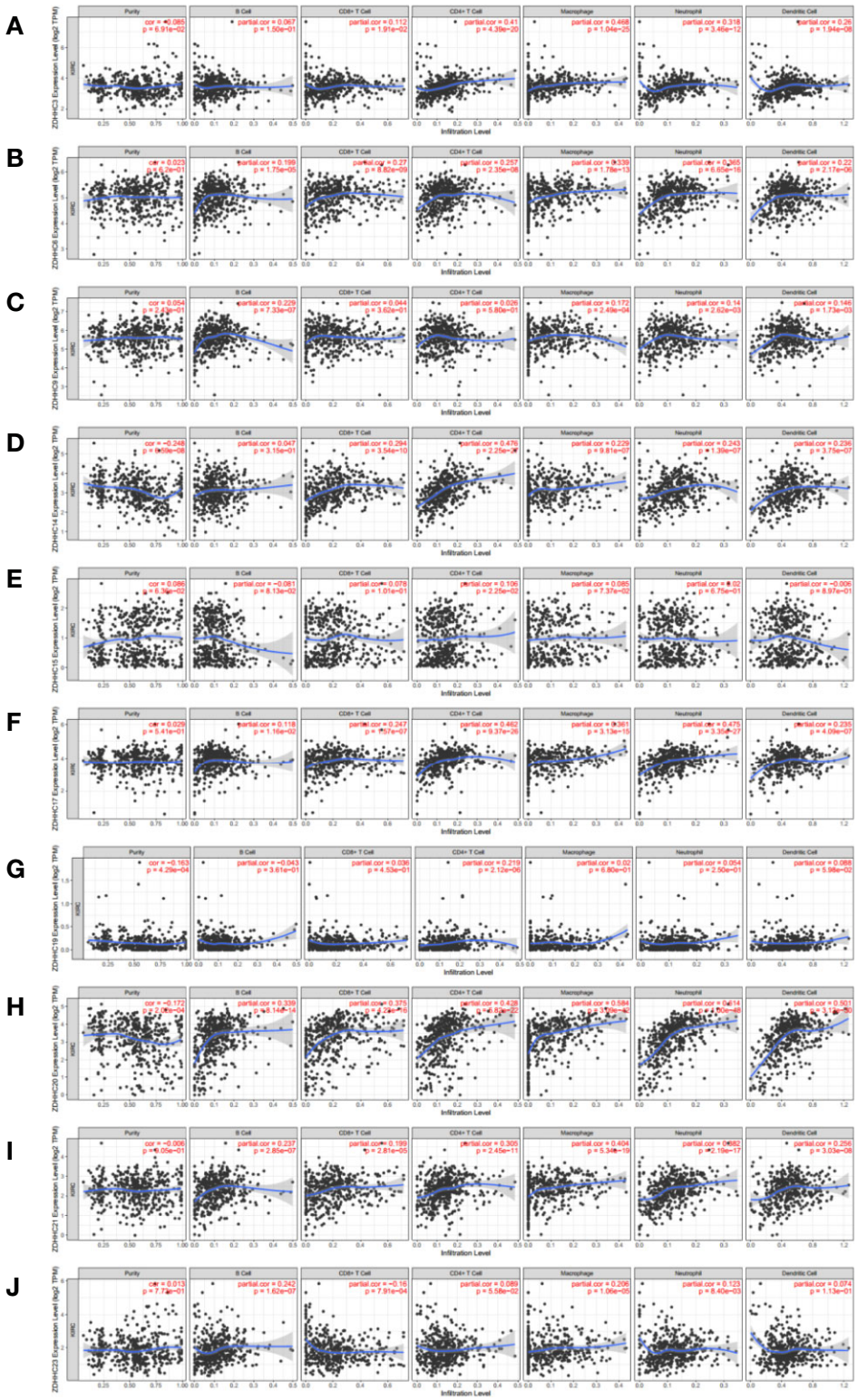

FIGURE 5 | The correlation of immune cell infiltration with 10 differentially expressed ZDHHCs in kidney renal clear cell carcinoma (KIRC) patient tissues (Timer). The correlation between the abundance of immune cells and the expression of **(A)** ZDHHC3, **(B)** ZDHHC6, **(C)** ZDHHC9, **(D)** ZDHHC14, **(E)** ZDHHC15, **(F)** ZDHHC17, **(G)** ZDHHC19, **(H)** ZDHHC20, **(I)** ZDHHC21, **(J)** ZDHHC23 in KIRC. Spearman correlation coefficient was chosen for the correlation analysis and a value of $P < 0.05$ was considered statistically significant.

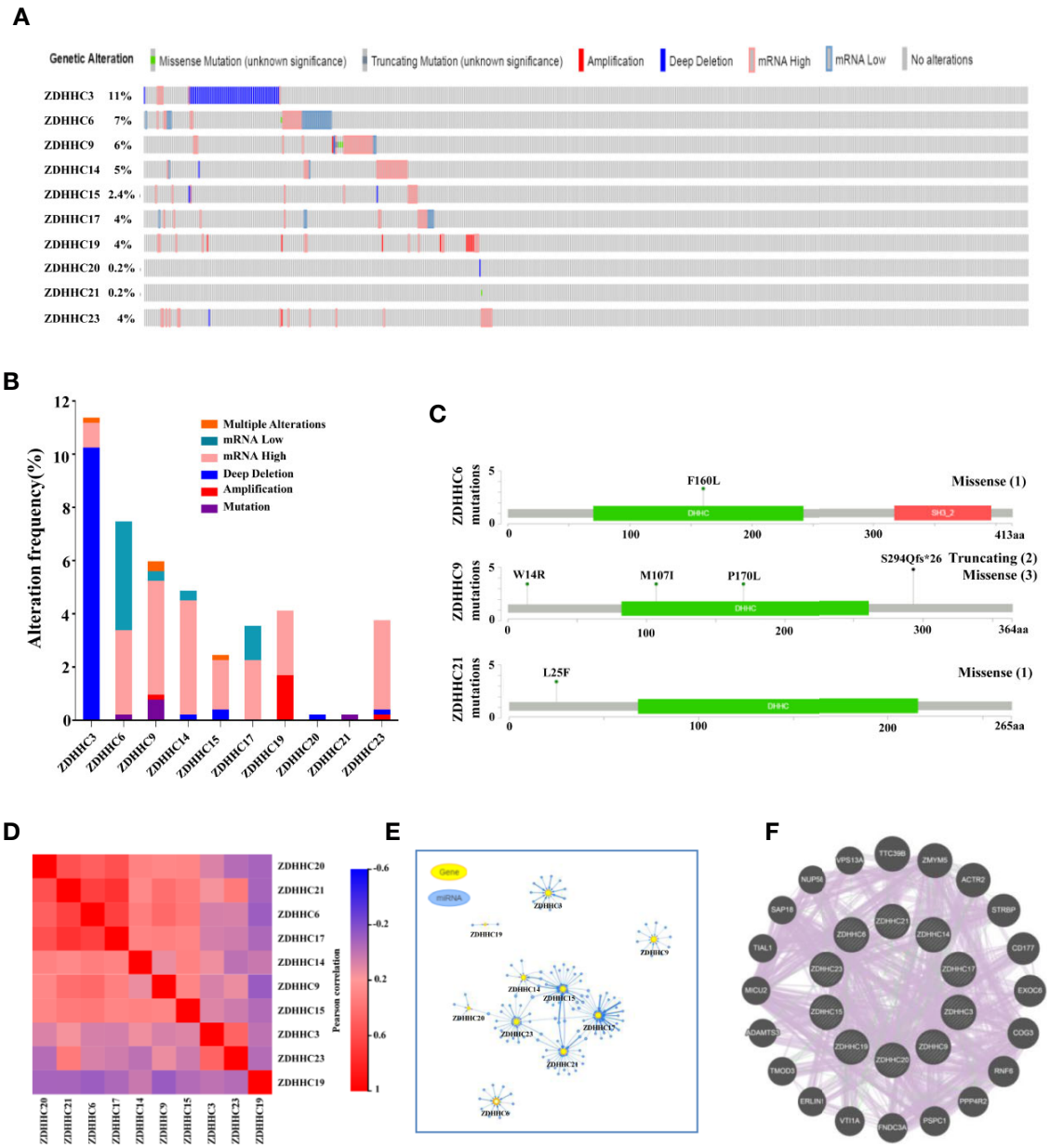

FIGURE 6 | Gene alterations, expression correlation, micro(mi)RNA networks, co-expression and interaction analyses of 10 differentially expressed ZDHHCs in kidney renal clear cell carcinoma (KIRC). **(A, B)** Summary of gene alterations of differentially expressed ZDHHCs in KIRC (cBioPortal). **(C)** The mutations of ZDHHC6, 9, and 21 were plotted (cBioPortal) and (1), (2) and (3) represent the number of mutation sites. **(D)** Correlation heat map of different expressed ZDHHCs in KIRC (GEPIA). **(E)** miRNA network of different expressed ZDHHCs in KIRC (GSCALite). **(F)** Co-expression and interaction analyses of differentially expressed ZDHHCs in KIRC (GeneMANIA). The purple lines represent co-expression, and the green lines represent interaction.

may be important mechanisms of tumor progression and poor prognosis in patients with KIRC.

DISCUSSION

The 23 human ZDHHC family members were firstly identified in 2004 (22). These ZDHHCs have homologous and highly conserved Asp-His-His-Cys (D-H-H-C) tetrapeptide motifs that are directly involved in the palmitoyl transfer reaction (23). However, because of the variable extent of palmitoyl acyltransferase activity and specificity of substrate proteins, all ZDHHCs play an indispensable role in multiple cellular biological processes and signaling pathways (24). Emerging evidence has indicated that ZDHHCs not only regulate normal physiological processes but are also involved in a variety of

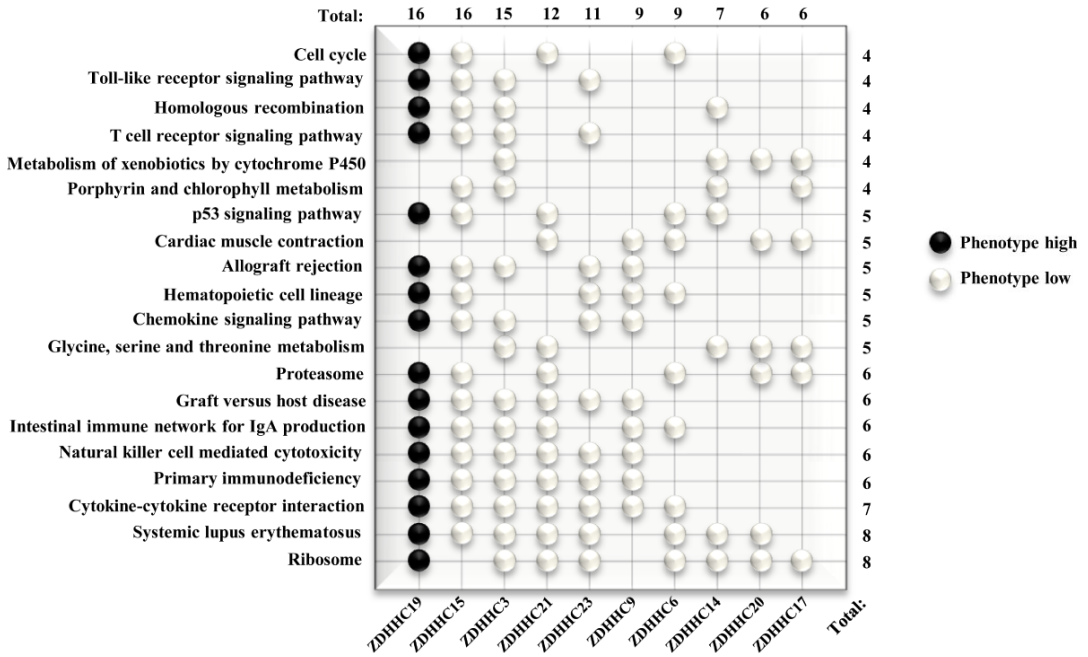

FIGURE 7 | Predicted Functions of 10 differently expressed ZDHHCs in kidney renal clear cell carcinoma (KIRC) by GSEA. Pathway enrichment for differently expressed ZDHHCs in KIRC was shown in the WeiQi diagram. Black stones represent pathways enriched in phenotype high, and white stones represent pathways enriched in phenotype low. The number (right) represents the number of ZDHHCs associated with the enrichment of the pathway and the number (top) represents the number of pathways enriched by the gene. The V7.0.Gene set in the gene sets database and 1000 for the number of permutations were selected for each analysis and all gene sets were significantly enriched at nominal $p < 5\%$ and FDR < 25%.

disease states including cancer (25). Over the past decade, numerous studies showed that these ZDHHCs modulated the function of important oncogenes and tumor suppressors and often displayed altered expression patterns in cancer (6, 26). Their abnormal expression and loss of function affect tumor progression, metastasis, the efficacy of cancer treatment, and patient prognosis (5). Thus, a better understanding of ZDHHCs in KIRC will be necessary for future development of ZDHHCs-based therapy.

In this study, we first evaluated the expression pattern of the 23 ZDHHCs in KIRC based on TCGA and GEPIA database. We found that 12 genes were differentially expressed in KIRC vs. normal tissues (ZDHHC2, 3, 6, 14, 15, 21, and 23 were down-regulated; ZDHHC9, 17, 18, 19, and 20 were up-regulated). We further evaluated the expression patterns of these differentially expressed ZDHHCs in the main pathological stages of KIRC patients and demonstrated that the expression of ZDHHC2, 3, 6, 9, 14, 15, 21 in tumors decreased with the increase of the pathological stage of KIRC patients. These data suggested that these differentially expressed ZDHHCs may play a significant role in the tumorigenesis and progression of KIRC.

To evaluate whether these differentially expressed ZDHHCs can be used as molecular markers to predict the survival of KIRC patients or to guide clinical treatment, we analyzed the impact of differentially expressed ZDHHCs on the prognosis of KIRC patients. Interestingly, we found that 10 of 12 differently expressed ZDHHCs were significantly associated with the prognosis of KIRC patients. In detail, KIRC patients with down-regulation of ZDHHC3, 6, 9, 14, 15, 20, 21, 23, and up-regulation of ZDHHC19 were strongly associated with poor overall survival and KIRC patients with down-regulation of ZDHHC3, 6, 9, 14, 17, 21, and 23 were significantly associated with poor disease-free survival. These results indicated the potential of ZDHHC3, 6, 9, 14, 15, 17, 19, 20, 21, 23 as prognostic markers or molecular targets.

Immune cells that infiltrate tumors form an ecosystem in the tumor microenvironment to regulate cancer progression and are closely associated with clinical outcome in KIRC (27). Tumor immune infiltrating cells mainly include innate immune cells (such as macrophages, neutrophils, and dendritic cells) and adaptive immune cells (T and B lymphocytes). These diverse immune cells communicate directly or indirectly with each other and together control the growth of tumor cells (28). Therefore, tumor-infiltrating immune cells are expected to be effective targets for improving clinical outcomes. In this study, we evaluated the correlation between 10 differentially expressed ZDHHCs and tumor infiltration of six immune cell types, including B cells, CD8+ T cells, CD4+ T cells, macrophages, neutrophils, and dendritic cells, and found a significant correlation between differentially expressed ZDHHCs and the infiltrating immune cells. These results revealed that these 10 ZDHHCs may regulate the immune status of KIRC patients, which may be an important factor affecting tumor progression and patient prognosis.

Tumorigenesis and progression of KIRC are complex and multifaceted, and genetic alterations also play an important role in this process (29). Thus, we evaluated the genetic alterations of these 10 differentially expressed ZDHHCs in KIRC and found that there were frequent genetic alterations in these ZDHHCs and high mRNA expression was the most common type of gene alteration. We also explored the potential expression correlation of these 10 ZDHHCs and found that there was a high correlation among the expression of ZDHHC6, 17, 20, and 21. As expected, co-expression and interaction network analysis showed that the functions of these ZDHHCs were mainly protein palmitoylation and acetylation, etc. In addition, in the past few decades, miRNAs have been shown to affect tumor progression and patient prognosis by inhibiting transcription or degrading mRNAs of target protein (30, 31). The miRNA network indicated that these differentially expressed ZDHHCs were potentially regulated by miRNA.

We then focused on the potential mechanisms of action of these 10 differentially expressed ZDHHCs by GSEA. Consistent with the results of immune cell infiltration (**Figures 5A–L**), most of these ZDHHCs were closely related to immune-correlated signal pathways such as systemic lupus erythematosus, immunodeficiency and natural killer cell mediated cytotoxicity, suggesting that these ZDHHCs may play important regulatory roles in the immune microenvironment of KIRC. Historically, KIRC is one of the few tumors for which immunotherapy is effective (32). And the development and application of immune-related targeted therapy agents have been proven to be feasible and effective for the treatment of KIRC patients (33). However, the genes for the development of targeted approaches to KIRC immunotherapy have not been well identified. In view of the important roles of differentially expressed ZDHHCs on the KIRC immune environment, the development of immunomodulatory therapy targeting ZDHHCs may bring survival benefits to KIRC patients. Previous research has also shown that KIRC is closely related to reprogramming in cellular metabolism and is therefore also described as a "metabolic disease" (34, 35). Changes in metabolic gene expression patterns and abnormalities in metabolic-related pathways such as protein or amino acid metabolism are considered important causes of KIRC metabolic reprogramming, seriously affecting the prognosis of KIRC patients. Thus, targeting metabolic reprogramming in KIRC will also be important in future therapeutic planning. In this study, GSEA analyses also showed that many of these 10 differentially expressed ZDHHCs were closely related to abnormalities in metabolic pathways such as ribosome, amino acid metabolism, porphyrin and chlorophyll metabolism and metabolism of xenobiotics by cytochrome P450, suggesting the important functions of ZDHHCs in cellular metabolism. Besides, we also found that many well-known oncogenic signaling activations including JAK/STAT signaling and Wnt signaling were associated with abnormal expression of certain ZDHHCs. Taken together, the analysis above suggested that these ZDHHCs had potential as therapeutic targets in the clinical treatment of KIRC.

In conclusion, we performed a systematic analysis of ZDHHC expression patterns, prognostic value, immune infiltration, molecular characteristics and signaling pathways involved in KIRC. We hope our results will provide novel insight for identifying tumor markers or molecular targets for the treatment of KIRC. However, further research including *in vivo* and *in vitro* experiments is needed to validate our findings and promote further understanding of the ZDHHCs in KIRC.

DATA AVAILABILITY STATEMENT

Publicly available datasets were analyzed in this study. RNA-Seq data was downloaded from the TCGA database (https://portal.gdc.cancer.gov/) and the data of genetic alterations were obtained from cBioPortal (http://www.cbioportal.org/study/summary?id=kirc_tcga).

AUTHOR CONTRIBUTIONS

ZL and BX developed the idea and designed the research. ZL and MX analyzed the data. ZL and CL drafted the manuscript. YH, YZ, and BX revised the writing. All authors contributed to the article and approved the submitted version.

FUNDING

This work was supported by grants from the National Natural Science Foundation of China [81672743 and 81974464], Shenzhen Basic Research Project (JCYJ20160331114230843), Tianjin Medical University Cancer Institute and Hospital Innovation Fund [1803], and Beijing Tianjin Hebei Basic Research Cooperation Project (Grant No. 19JCZDJC64500(Z)).

SUPPLEMENTARY MATERIAL

The Supplementary Material for this article can be found online at: https://www.frontiersin.org/articles/10.3389/fonc.2020.565414/full#supplementary-material

REFERENCES

1. Moch H. An overview of renal cell cancer: pathology and genetics. *Semin Cancer Biol* (2013) 23:3–9. doi: 10.1016/j.semcancer.2012.06.006
2. Ljungberg B, Bensalah K, Canfield S, Dabestani S, Hofmann F, Hora M, et al. EAU guidelines on renal cell carcinoma: 2014 update. *Eur Urol* (2015) 67:913–24. doi: 10.1016/j.eururo.2015.01.005
3. Gray RE, Harris GT. Renal Cell Carcinoma: Diagnosis and Management. *Am Fam Physician* (2019) 99:179–84.
4. Jonasch E, Gao J, Rathmell WK. Renal cell carcinoma. *Bmj* (2014) 349:g4797. doi: 10.1136/bmj.g4797
5. Fraser NJ, Howie J, Wypijewski KJ, Fuller W. Therapeutic targeting of protein S-acylation for the treatment of disease. *Biochem Soc Trans* (2020) 48:281–90. doi: 10.1042/BST20190707

6. Ko PJ, Dixon SJ. Protein palmitoylation and cancer. *EMBO Rep* (2018) 19 (10). doi: 10.15252/embr.201846666
7. De I, Sadhukhan S. Emerging Roles of DHHC-mediated Protein S-palmitoylation in Physiological and Pathophysiological Context. *Eur J Cell Biol* (2018) 97:319–38. doi: 10.1016/j.ejcb.2018.03.005
8. Li SX, Tang GS, Zhou DX, Pan YF, Tan YX, Zhang J, et al. Prognostic significance of cytoskeleton-associated membrane protein 4 and its palmitoyl acyltransferase DHHC2 in hepatocellular carcinoma. *Cancer* (2014) 120:1520–31. doi: 10.1002/cncr.28593
9. Sharma C, Wang HX, Li Q, Knoblich K, Reisenbichler ES, Richardson AL, et al. Protein Acyltransferase DHHC3 Regulates Breast Tumor Growth, Oxidative Stress, and Senescence. *Cancer Res* (2017) 77:6880–90. doi: 10.1158/0008-5472.CAN-17-1536
10. Liu P, Jiao B, Zhang R, Zhao H, Zhang C, Wu M, et al. Palmitoylacyltransferase Zdhhc9 inactivation mitigates leukemogenic potential of oncogenic Nras. *Leukemia* (2016) 30:1225–8. doi: 10.1038/leu.2015.293
11. Yang Y, Hsu JM, Sun L, Chan LC, Li CW, Hsu JL, et al. Palmitoylation stabilizes PD-L1 to promote breast tumor growth. *Cell Res* (2019) 29:83–6. doi: 10.1038/s41422-018-0124-5
12. Runkle KB, Kharbanda A, Stypulkowski E, Cao XJ, Wang W, Garcia BA, et al. Inhibition of DHHC20-Mediated EGFR Palmitoylation Creates a Dependence on EGFR Signaling. *Mol Cell* (2016) 62:385–96. doi: 10.1016/j.molcel.2016.04.003
13. Tang Z, Li C, Kang B, Gao G, Li C, Zhang Z. GEPIA: a web server for cancer and normal gene expression profiling and interactive analyses. *Nucleic Acids Res* (2017) 45:W98–w102. doi: 10.1093/nar/gkx247
14. Li T, Fan J, Wang B, Traugh N, Chen Q, Liu JS, et al. TIMER: A Web Server for Comprehensive Analysis of Tumor-Infiltrating Immune Cells. *Cancer Res* (2017) 77:e108–10. doi: 10.1158/0008-5472.CAN-17-0307
15. Szklarczyk D, Gable AL, Lyon D, Junge A, Wyder S, Huerta-Cepas J, et al. STRING v11: protein-protein association networks with increased coverage, supporting functional discovery in genome-wide experimental datasets. *Nucleic Acids Res* (2019) 47:D607–d613. doi: 10.1093/nar/gky1131
16. Gao J, Aksoy BA, Dogrusoz U, Dresdner G, Gross B, Sumer SO, et al. Integrative analysis of complex cancer genomics and clinical profiles using the cBioPortal. *Sci Signal* (2013) 6:pl1. doi: 10.1126/scisignal.2004088
17. Franz M, Rodriguez H, Lopes C, Zuberi K, Montojo J, Bader GD, et al. GeneMANIA update 2018. *Nucleic Acids Res* (2018) 46:W60–w64. doi: 10.1093/nar/gky311
18. Liu CJ, Hu FF, Xia MX, Han L, Zhang Q, Guo AY. GSCALite: a web server for gene set cancer analysis. *Bioinformatics* (2018) 34:3771–2. doi: 10.1093/bioinformatics/bty411
19. Subramanian A, Tamayo P, Mootha VK, Mukherjee S, Ebert BL, Gillette MA, et al. Gene set enrichment analysis: a knowledge-based approach for interpreting genome-wide expression profiles. *Proc Natl Acad Sci U S A* (2005) 102:15545–50. doi: 10.1073/pnas.0506580102
20. Mootha VK, Lindgren CM, Eriksson KF, Subramanian A, Sihag S, Lehar J, et al. PGC-1alpha-responsive genes involved in oxidative phosphorylation are coordinately downregulated in human diabetes. *Nat Genet* (2003) 34:267–73. doi: 10.1038/ng1180
21. Ghatalia P, Gordetsky J, Kuo F, Dulaimi E, Cai KQ, Devarajan K, et al. Prognostic impact of immune gene expression signature and tumor infiltrating immune cells in localized clear cell renal cell carcinoma. *J Immunother Cancer* (2019) 7:139. doi: 10.1186/s40425-019-0735-5
22. Fukata M, Fukata Y, Adesnik H, Nicoll RA, Bredt DS. Identification of PSD-95 palmitoylating enzymes. *Neuron* (2004) 44:987–96. doi: 10.1016/j.neuron.2004.12.005
23. Rana MS, Lee CJ, Banerjee A. The molecular mechanism of DHHC protein acyltransferases. *Biochem Soc Trans* (2019) 47:157–67. doi: 10.1042/BST20180429
24. Greaves J, Chamberlain LH. DHHC palmitoyl transferases: substrate interactions and (patho)physiology. *Trends Biochem Sci* (2011) 36:245–53. doi: 10.1016/j.tibs.2011.01.003
25. Resh MD. Palmitoylation of proteins in cancer. *Biochem Soc Trans* (2017) 45:409–16. doi: 10.1042/BST20160233
26. Linder ME, Jennings BC. Mechanism and function of DHHC S-acyltransferases. *Biochem Soc Trans* (2013) 41:29–34. doi: 10.1042/BST20120328
27. Zhang S, Zhang E, Long J, Hu Z, Peng J, Liu L, et al. Immune infiltration in renal cell carcinoma. *Cancer Sci* (2019) 110:1564–72. doi: 10.1111/cas.13996
28. Grivennikov SII, Greten FR, Karin M. Immunity, inflammation, and cancer. *Cell* (2010) 140:883–99. doi: 10.1016/j.cell.2010.01.025
29. Yap NY, Rajandram R, Ng KL, Pailoor J, Fadzli A, Gobe GC. Genetic and Chromosomal Aberrations and Their Clinical Significance in Renal Neoplasms. *BioMed Res Int* (2015) 2015:476508. doi: 10.1155/2015/476508
30. Di Leva G, Garofalo M, Croce CM. MicroRNAs in cancer. *Annu Rev Pathol* (2014) 9:287–314. doi: 10.1146/annurev-pathol-012513-104715
31. Jonas S, Izaurralde E. Towards a molecular understanding of microRNA-mediated gene silencing. *Nat Rev Genet* (2015) 16:421–33. doi: 10.1038/nrg3965
32. Ross K, Jones RJ. Immune checkpoint inhibitors in renal cell carcinoma. *Clin Sci* (2017) 131:2627–42. doi: 10.1042/CS20160894
33. Díaz-Montero CM, Rini BII, Finke JH. The immunology of renal cell carcinoma. *Nat Rev Nephrol* (2020) 16:721–35. doi: 10.1038/s41581-020-0316-3
34. Linehan WM, Srinivasan R, Schmidt LS. The genetic basis of kidney cancer: a metabolic disease. *Nat Rev Urol* (2010) 7:277–85. doi: 10.1038/nrurol.2010.47
35. Linehan WM, Schmidt LS, Crooks DR, Wei D, Srinivasan R, Lang M, et al. The Metabolic Basis of Kidney Cancer. *Cancer Discov* (2019) 9:1006–21. doi: 10.1158/2159-8290.CD-18-1354

Conflict of Interest: The authors declare that the research was conducted in the absence of any commercial or financial relationships that could be construed as a potential conflict of interest.

frontiers in Oncology

REVIEW
published: 15 January 2021
doi: 10.3389/fonc.2020.604084

Driving Immune Responses in the Ovarian Tumor Microenvironment

Franklin Ning, Christopher B. Cole and Christina M. Annunziata *

Translational Genomics Section, Women's Malignancies Branch, National Cancer Institute (NCI), National Institutes of Health (NIH), Bethesda, MD, United States

Ovarian cancer is the leading cause of death among gynecological neoplasms, with an estimated 14,000 deaths in 2019. First-line treatment options center around a taxane and platinum-based chemotherapy regimen. However, many patients often have recurrence due to late stage diagnoses and acquired chemo-resistance. Recent approvals for bevacizumab and poly (ADP-ribose) polymerase inhibitors have improved treatment options but effective treatments are still limited in the recurrent setting. Immunotherapy has seen significant success in hematological and solid malignancies. However, effectiveness has been limited in ovarian cancer. This may be due to a highly immunosuppressive tumor microenvironment and a lack of tumor-specific antigens. Certain immune cell subsets, such as regulatory T cells and tumor-associated macrophages, have been implicated in ovarian cancer. Consequently, therapies augmenting the immune response, such as immune checkpoint inhibitors and dendritic cell vaccines, may be unable to properly enact their effector functions. A better understanding of the various interactions among immune cell subsets in the peritoneal microenvironment is necessary to develop efficacious therapies. This review will discuss various cell subsets in the ovarian tumor microenvironment, current immunotherapy modalities to target or augment these immune subsets, and treatment challenges.

Keywords: ovarian cancer, tumor microenvironment, innate immunity, adaptive immunity, cancer therapeutics

OPEN ACCESS

Edited by:
Marco Rossi,
University of Catanzaro, Italy

Reviewed by:
Victor C. Kok,
Asia University, Taiwan
Alexander Deneka,
Fox Chase Cancer Center, United States

***Correspondence:**
Christina M. Annunziata
annunzic@mail.nih.gov

Specialty section:
This article was submitted to Cancer Molecular Targets and Therapeutics, a section of the journal Frontiers in Oncology

Received: *08 September 2020*
Accepted: *30 November 2020*
Published: *15 January 2021*

Citation:
Ning F, Cole CB and Annunziata CM (2021) Driving Immune Responses in the Ovarian Tumor Microenvironment. Front. Oncol. 10:604084. doi: 10.3389/fonc.2020.604084

INTRODUCTION

Ovarian cancer presents a unique tumor microenvironment (TME) with its predilection to metastasize in the peritoneal cavity and generate malignant ascites. The cancer spreads by direct shedding into the ascites and movement throughout the peritoneal cavity. Common sites of tumor deposits are on the mesenteric and serosal surfaces of the abdominal organs. The immune microenvironment in this location is characterized by interactions among the tumor cells, myeloid and lymphoid immune cells, as well as fibroblasts and adipocytes in the peritoneum that promote tumor growth. Growth factors, such as fibroblast growth factor and vascular endothelial growth factor (VEGF), promote angiogenesis and direct fibroblast differentiation towards cancer-associated fibroblasts that promote metastases (1). Adipocytes in the omentum can also provide energy for tumor growth and metastases (2). Little is known about how these cells interact with immune cells and if they promote immunosuppression. Additional information is therefore needed about cellular interactions and trafficking in the peritoneal TME in order to better develop immunotherapies for ovarian cancer.

Advances in immunotherapy, such as immune checkpoint inhibitors and chimeric antigen-receptor T cells (CAR-T), have demonstrated efficacy in various cancers. However, performance in ovarian cancer patients has remained poor. Multiple studies have demonstrated that the highly immunosuppressive TME and low mutational burden of ovarian cancer is a barrier to effective treatment (3). Inhibitiory cells in the TME, such as regulatory T and B cells, myeloid-derived suppressor cells (MDSCs), and tumor-associated macrophages (TAMs) inevitably contribute to tumor growth through a milieu of inhibitory effects (4–7). In this review, we discuss key subsets of adaptive and innate immunity that play a role in the ovarian TME and current efforts to target or augment these populations (**Figure 1**).

ADAPTIVE IMMUNITY

Tumor-Infiltrating T Lymphocytes

T cells play a significant role in anti-tumor processes by recognizing tumor neoantigens and facilitating and directly inducing apoptosis of tumor cells. $CD3^+$ tumor-infiltrating T lymphocytes (TILs) were shown to be correlated with improved clinical outcome in ovarian cancer (8). Of 186 tumor samples, 102 samples were identified to have $CD3^+$ cells within the tumor and 72 did not have any. Between these two groups, the 5-year overall survival (OS) for patients with TILs was 38% while those without TILs was 4.5%, suggesting a beneficial effect of TILs in women treated with standard chemotherapy. Interestingly, the absence of TILs correlated with increased levels of VEGF.

TILs, $CD3^+$, can be further divided into $CD4^+$ and $CD8^+$ cells. In brief, CD4+ T cells, also known as helper T cells, recognize MHC class II and shape the adaptive immune response while CD8+ T, also known as cytotoxic T cells, recognize MHC class I and mediate direct killing Studies looking at patient survival have shown increased CD8+ T cells within the tumor predict better prognoses (9). An increase in intra-tumoral CD4+ T cells have also shown to be correlated with increased survival (10).

ACT/CAR-T

To boost the tumor-specific T cell response, adoptive cell therapy (ACT) has been used to increase the number of T cells that can recognize a tumor-associated antigen (TAA). ACT requires apheresis of a patient's T cells and expanding them *ex vivo* to suitable levels after stimulation with lysed tumor cells. Recent advances in autologous therapy now include genetically modifying the T-cell receptor (TCR) or generating chimeric antigen receptor T-cells (CAR-T) to engineer a stronger, more precise, immune response to pre-determined tumor neoantigens (11).

Briefly, CAR-T cells are T cells that have been transfected to express a transmembrane protein with 1) a single chain fraction variable, also known as the antigen-recognizing domain, and 2) a TCR zeta chain, allowing for intracellular signaling. Since then, new generations have modified the CAR for improved immune responses. Second generation CAR-Ts added in either CD28 or 4-1BB as a costimulatory gene, third generation CAR-Ts allowed for two downstream signaling domains and the possibility of using OX40, and fourth generation CAR-Ts further improved effector functions by giving the receptor the ability to induce cytokines, such as IL-12 (12).

ACT and CAR-T have shown great promise in hematological tumors. However, they have demonstrated poor efficacy in solid tumors (13, 14). Part of this has been attributed to a lack of tumor specific antigens, a highly immunosuppressive TME, and a lack of persistence in the tumor. Some CAR-Ts that have

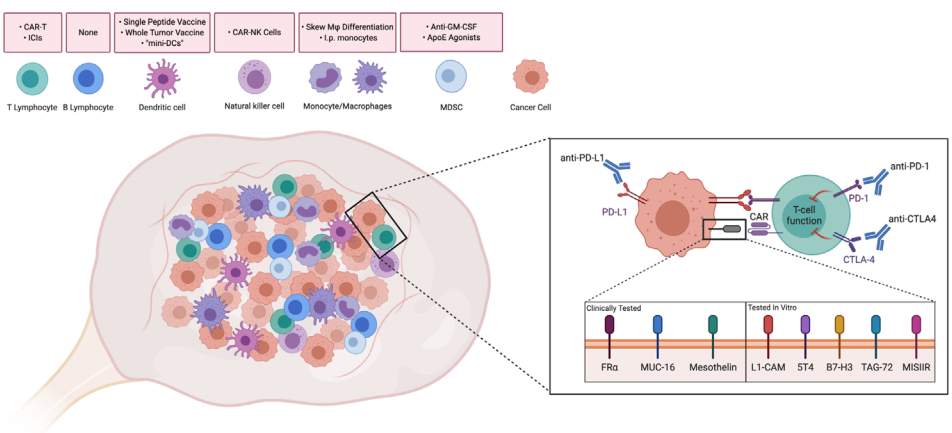

FIGURE 1 | Driving Immune Responses in the Ovarian Tumor Microenvironment. Immune cells are present intratumorally and in the ovarian tumor microenvironment. Strategies discussed throughout the paper have been summarized above the corresponding cell type. Attempts to improve T cell functionality in the ovarian TME include Immune checkpoint inhibitors, such as anti-PD-1, anti-PD-L1, and anti-CTLA4, which have been used in clinical trials to reduce inhibitory signaling. Similarly, T cells with chimeric antigen receptors (CAR-Ts) against folate receptor-alpha (FRα), MUC-16, and mesothelin have been tested in clinical trials in order to recognize tumor-associated antigens. CAR-Ts have been tested *in vitro* against novel antigens. CAR-T: Chimeric antigen receptor T-cell. ICI, Immune checkpoint inhibitor; CAR-NK, Chimeric antigen receptor-Natural Killer cell; Mφ, Macrophage; I.p., Intraperitoneal; GM-CSF, Granulocyte-monocyte colony stimulating factor; ApoE, ApolipoproteinE; MDSC, Myeloid-derived suppressor cell. Created with Biorender.com.

made it to Phase 1 clinical trials for ovarian cancer include those targeting folate receptor, MUC-16, and mesothelin (**Figure 1**). Other examples in pre-clinical testing are also discussed.

Folate Receptor

Folate receptor-α (FRα) is one of a number of high affinity receptors that facilitates the uptake of folate into the cell (15). While it is rarely found in normal tissues, its overexpression has been identified in multiple malignancies, including ovarian cancer (16). When overexpressed in ovarian cancer, FRα has been correlated with a poor response to chemotherapy (17–20). Interestingly, correlation with survival has been inconclusive. Studies on FR overexpression have ranged from negatively prognostic to having no impact on survival to even an improvement in survival (19–22). Additional studies will be needed to determine the prognostic value of FRα.

In the first CAR-T treatment against FR, 14 patients with recurrent epithelial FR^+ ovarian cancer were enrolled. Cohort 1 was given interleukin-2 (IL-2) and generic T cells transfected with a first generation anti-FR CAR while Cohort 2 was given T cells that were endogenously specific to FR (23). Cohort 1 was given 3×10^9 T cells, with possible dose escalation to 1×10^{10} and 3 to 5×10^{10} cells, with a dose of 720,000 IU/kg IL-2 each cycle. Cohort 2 was given 2×10^9 to 4×10^9 T cells. Most common Grade 1-2 drug-related side effects in Cohort 1 were fatigue and nausea compared to erythema at the site of injection for Cohort 2. Cohort 1 also experienced some Grade 3–4 side-effects, such as hypotension and dyspnea, that were attributed to the addition of IL-2. Unfortunately, no reduction in tumor burden or improvement in survival was seen in either cohort. A noted issue was the lack of persistence of these improved autologous T cells in circulation.

As a means of increasing persistence, investigators have added the co-stimulatory molecule CD137, or 4-1BB, to the CAR in order to improve cytokine secretion and the antitumor response *in vivo* (24). Intravenous (i.v.) injection of these CAR-Ts into NSG mice, inoculated subcutaneously with FR^+ SKOV3, showed improved antitumor effects and reduced tumor volume. These T cells also showed improved persistence in circulating blood. Upon waiting 30 days for metastases in their model, only mice treated with the CAR-T cells were devoid of malignant ascites.

Although a thorough discussion is outside the scope of this review, a number of monoclonal antibodies (mAbs) have also been designed to target FR expression in ovarian cancer. In brief, farletuzumab was evaluated in a Phase 3 clinical trial, but did not reach the primary endpoint of PFS. Mirvetuximab soravtansine, an anti-FR coupled to tubulin-targeting agent DM4, was shown to be well-tolerated when given as a monotherapy or with bevacizumab (25–27).

MUC-16

Cancer antigen 125 (CA-125) is cleaved from the cell surface and is commonly used as a circulating serum marker for ovarian cancer relapse. MUC-16 is the remnant of the protein that is retained on the cancer cell membrane after cleavage. It is known that there is some overlap in MUC-16 expression with derivates of the fetal coelomic epithelia, such as the uterus, fallopian tubes, and the trachea (28).

Chekmosova et al. demonstrated that second generation CAR-Ts against MUC-16 were able to lyse $MUC\text{-}16^+$ cells *in vitro* (29). These CAR-T cells were subsequently injected into SCID mice, inoculated i.p. or i.v. with $MUC\text{-}16^+$ OVCAR3, and showed significant survival improvement when compared to untreated mice or those given anti-CD19 CAR-Ts. Later improvement to MUC-16 specific CAR-T cells included the ability to secrete IL-12 and an "elimination" gene to improve immune signaling and minimalize off-target effects (30). This "elimination" gene is a truncated portion of epidermal growth factor receptor (EGFR) that does not signal, but retains the ability to be bound by cetuximab and induce antibody-dependent cellular cytotoxicity or complement-mediated cytotoxicity against cells expressing this chimeric receptor. Mice inoculated i.p. with SKOV3 and treated with this novel CAR-T showed enhanced survival compared to CAR-Ts without the IL-12 domain. Interestingly, i.p. administration was found to be more effective than an i.v. route. A phase 1 clinical trial was proposed to test its efficacy in recurrent platinum-resistant ovarian cancer (31).

Similar to FR, mAbs have also been developed against CA-125. One of the leading antibodies, oregovomab, enhanced anti-cancer activity when given with carboplatin and paclitaxel, although oregovomab did not show clinical efficacy when treating patients with ovarian cancer as a monotherapy (32, 33). The combination significantly improved PFS to 41.8 months, when given front-line, compared to 12.2 months for patients given standard carboplatin-paclitaxel (34). Interestingly, patients who had better survival outcomes had lower levels of HLA-DR-CD14+ MDSCs and a lower neutrophil-and-monocyte to lymphocyte ratio (35).

Mesothelin

Mesothelin is a surface antigen found overexpressed on malignant mesothelioma as well as pancreatic, ovarian, and lung cancers (36). However, it is also found expressed at low levels on other mesothelial surfaces, such as the pleura, pericardium, and peritoneum.

In ovarian cancer, a mesothelin-specific CAR-T was developed using mRNA transfection in order to minimalize off-target toxicity due to CAR-T persistence (37, 38). Five patients with ovarian cancer were inoculated i.v. with second-generation CARs against mesothelin in a phase 1 clinical trial (39). Up to 1 to $3*10^8/m^2$ CAR-T cells were given with or without lymphodepletion by 1.5 g/m^2 cyclophosphamide. Only one patient demonstrated a sizable reduction in tumor burden, but did not qualify as a partial reduction per formal criteria for objective response. This may have been due to a lack of persistence of CAR-Ts by day 28 in most patients and the single-chain variable fraction being murine-based. There were also no significant changes in cytokine levels during the first month post-infusion. The most common low-grade adverse events (AEs) included fatigue, nausea, and emesis, while development of Grade 3 ascites was the most common high-grade AE. A similar Phase 1 trial is evaluating MCY-M11, a mRNA-based

anti-mesothelin therapy, when given intraperitoneally (i.p.) for platinum-resistant OC patients, with or without cyclophosphamide (NCT03608618). Another clinical trial evaluating anti-mesothelin CAR-T cells, but generated using a lentiviral delivery system, is ongoing (NCT03054298).

Recently, Hassan et al. published the first in-human clinical trial evaluating anetumab, an anti-mesothelin mAb in a Phase 1 clinical trial (40). Sixty-four patients were enrolled with ovarian cancer, and of those, they noted 1 CR, 4 PRs, and 29 patients with SD. Interestingly, all patients who responded had high mesothelin expression, defined as ≥60% by immunohistochemistry staining. A Phase 1b clinical trial is currently ongoing (NCT02751918).

Other Tumor-Associated Antigens

Other surface antigens have been identified in pre-clinical studies as possible neoantigens with anti-tumor activity and high specificity for ovarian cancer. Hong et al. showed that L1-CAM was overexpressed in a wide panel of ovarian samples (41). Administration of second-generation anti-L1-CAM CAR-Ts, to NSG mice, inoculated i.p. with SK-OV3, improved median survival time to 104.5 days when compared to mock (50 days) or anti-CD19 CAR-T cells (56.5 days). Similar tissue expression, *in vitro*, and *in vivo* studies can be seen with 5T4, B7-H3, TAG-72, and MISIIR (42–45). Interestingly, Du et al. demonstrated the addition of 4-1BB to the anti-B7-H3 CAR mediated lower expression of PD-1 in transfected $CD8^+$ T cells, possibly enabling them to better enact effector functions. In this pre-clinical study, i.p. administration of CAR-T cells was shown to have improved survival benefit when compared to an i.v. route.

Immune Checkpoint Inhibitors

Other mechanisms of promoting immune cell activity are immune checkpoint inhibitors that target surface proteins such as cytotoxic T-lymphocyte-associated protein 4 (CTLA4), programmed cell death protein 1 (PD-1), and its ligand (PD-L1; **Figure 1**). These proteins normally function to prevent autoimmunity, but their upregulation on a tumor prevents an appropriate immune response. CTLA-4 competes with B7 (CD80) in binding to CD28 on T cells, inducing a suppressive phenotype rather than activating. PD-1 and PD-L1 belong to the CD28 and B7 family of receptors on T cells, respectively, and have been shown to induce a suppressive phenotype in peripheral tissues.

Drugs targeting CTLA-4, such as ipilimumab, have shown great success in other cancers. In unresectable Grade 3 and 4 melanoma, ipilimumab improved 1-year survival from 25% to 46% when used in combination with a gp-100 peptide vaccine, granting it FDA approval in March 2011. In a phase 1 clinical trial with nine Stage IV ovarian cancer patients, three instances of stable disease (SD) were observed (46). Multiple toxicities occurred, including two cases of Grade 3 inflammation in the GI tract, one case of Sweet's syndrome, and multiple dermatological reactions. A phase 2 clinical trial was later done in patients with recurrent platinum-sensitive ovarian cancer (NCT01611558). Patients received 10 mg/kg of ipilimumab once every 3 weeks for four doses then once every 12 weeks. The overall response rate (ORR) was low at 10.3%. 18 patients experienced drug-related severe AEs, the most common being small intestinal obstruction, diarrhea, pneumonitis, and adrenal insufficiency.

Trials combining ipilimumab with other treatment regiments have also been conducted. Recently, Zamarin et al. published a Phase 2 trial comparing nivolumab to nivolumab and ipilimumab for recurrent ovarian cancer. One hundred patients were either given 3 mg/kg nivolumab every 2 weeks or 3 mg/kg nivolumab plus 1 mg/kg ipilimumab every 3 weeks (47). In the nivolumab monotherapy group, 3 complete responses (CRs), 3 partial responses (PRs), and 14 patients with SD were noted compared to the 3 CRs, 16 PRs, and 20 patients with SD in the combination group. Median progression-free survival (PFS) was 2 and 3.9 months while median OS was 21.8 and 28.1 months for the monotherapy and combination therapy, respectively. There were no treatment-related deaths with the most common grade 3 or higher AEs being asymptomatic elevation of pancreatic and liver enzymes, anemia, colitis, and diarrhea. A number of other ongoing trials are evaluating anti-CTLA-4 antibodies in combination with chemotherapy, poly (ADP-ribose) polymerase inhibitors (PARPi), and other immunotherapies (**Table 1**).

Anti-PD-1 therapy has also had some success in treating ovarian cancer. In a phase two trial, 20 patients with platinum-resistant recurrent ovarian cancer were treated with either 1 or 3 mg/kg single-dose nivolumab every 2 weeks for one year (48). In the 1 mg/kg cohort, two patients had a CR and four had SD while in the 3 mg/kg cohort, one patient had a PR while two had SD. Median OS was 20 months and PFS was 3.5 months. Low-grade AEs included mild fever, rash, arthralgia, elevated liver function tests (LFTs), and lymphocytopenia. Two patients experienced Grade 3 disorientation and gait disorder or Grade 3 fever and a deep vein thrombosis, respectively. Notably, two patients developed a PR to maintenance chemotherapy post-treatment with nivolumab (49). An open-label, randomized clinical trial is ongoing in Japan.

One Phase 2 study has been published evaluating the combination of nivolumab and bevacizumab in relapsed ovarian cancer (50). Thirty-eight women with relapsed OC were enrolled and treated with 10 mg/kg bevacizumab and 240 mg nivolumab once every 2 weeks. In platinum-sensitive patients, there were eight PRs and nine patients with SD compared to 3 PRs and 10 patients with SD in the platinum-resistant group. Median PFS was 12.1 months and 7.7 months for platinum-sensitive and -resistant patients, respectively. Grade 3 AEs reported were hypertension, myalgia, arthralgia, and elevations in LFTs and serum amylase. Two patients experienced Grade 4 increases in serum lipase levels as a result of treatment. Like anti-CTLA-4 compounds, several ongoing trials are evaluating combinations of nivolumab with chemotherapy, PARPi, or vaccines (**Table 1**).

Pembrolizumab, another anti-PD-1 agent, has also been evaluated as a single agent. In a phase 1b trial, 26 patients

TABLE 1 | Ongoing clinical trials of immune checkpoint inhibitors in women with ovarian cancer.

Intervention	NCT/Author	Phase	Enrollment	Primary Endpoint
Anti-CTLA4				
Tremelimumab + Olaparib	NCT02571725	1/2	~50 patients with BRCA1/2-mutant ROC	RP2D, ORR
Tremelimumab + Olaparib	NCT04034927	2	~170 RPS OC	
Anti-PD-1				
Nivolumab ± Ipilimumab	NCT03355976	2	~62 patients with ovarian or renal cell carcinoma	ORR
Intraperitoneal Nivolumab ± Ipiliumumab	NCT03508570	1b	~48 patients with recurrent/high-grade gynecologic cancer with peritoneal metastases	RP2D
Nivolumab ± Ipiliumumab + CarboTaxol	NCT03245892	1	~40 patients with High Grade Serous Ovarian, Fallopian Tube, or Primary Peritoneal Cancer	DLT
Nivolumab + Bevacizumab ± Rucaparib	NCT02873962	2	~76 patients with ROC	ORR
Nivolumab + Poly-ICIC (a viral mimic)	NCT04024878	1	~30 patients with OC	Safety and Activity
Nivolumab + WT1 vaccine	NCT02737787	1	~11 patients with ROC	DLT
Durvalumab ± Tremelimumab + CarboTaxol	NCT03249142	1/2	~40 patients with Ovarian, Fallopian Tube or Primary Peritoneal Adenocarcinoma	DLT
Durvalumab + Tremelimumab + CarboTaxol	NCT03899610	2	~24 patients with treatment-naïve clinical stage IIIC/IV ovarian cancer	PFS
Sequential vs. combination Durvalumab + Tremelimumab	NCT03026062	2	~100 patients with RPR OC	irPFS
Olaparib + Tremelimumab + Durvalumab	NCT02953457	1/2	~36 patients BRCA1/2-mutant ROC	DLT and PFS
Anti-PD-L1				
Avelumab ± PLD	NCT02580058	3	566 patients with RPR OC	OS and PFS

RP2D, Recommended phase 2 dose; ORR, Overall response rate; RPS, recurrent platinum-sensitive; OC, ovarian cancer; PFS, Progression free survival; DLT, dose-limiting toxicity; irPFS, immune-related progression free survival; CarboTaxol, carboplatin and paclitaxel; ROC, recurrent ovarian cancer; PLD, pegylated liposomal doxorubicin; OS, overall survival.

with advanced metastatic ovarian cancer received 10 mg/kg every 2 weeks for up to two years (51). ORR was documented at 11.5%, with one CR and two PRs, and seven patients experienced SD. Median PFS was 1.9 months while OS was 13.8 months. Drug-related AEs occurred in 19 patients with one patient experiencing Grade 3 increases in transaminase levels. Eight immune-related AEs occurred where the only Grade 3 AE was pancreatitis. Later, Keynote-100 looked at pembrolizumab in 396 patients with advanced recurrent ovarian cancer. Two cohorts were formed based on prior lines of treatment (52). Cohort A (285 patients) had one to three lines of prior treatment while cohort B (91 patients) had four to six. Patients received 200 mg IV every 3 weeks. ORR in cohorts A and B was 7.4% and 9.9%, respectively. Median PFS was 2.1 months for both cohorts while median OS was not reached in cohort A and 17.6 months in cohort B. The most common low-grade treatment-related AE was fatigue while the most common immune-related AE was hypothyroidism. The most common Grade 3 immune-related AEs were skin reactions and colitis. More severely, two patient deaths were attributed to treatment, one due to hyperaldosteronism and the other to Stevens-Johnson syndrome. These recurring AEs led to the need for early recognition and treatment to prevent devastating complications from immune checkpoint inhibitor therapy (53).

Recently, a single-arm phase I/II trial evaluated niraparib in combination with pembrolizumab in patients with recurrent platinum-resistant OC (54). 62 patients with OC were enrolled between Phase I and II. ORR was 18% with 3 CRs and 8 confirmed PRs. Another 28 patients were noted to have SD. Median PFS was 3.4 months. Most common low-grade AEs were fatigue, nausea, anemia, and constipation while high-grade AEs were noted to be anemia and thrombocytopenia. Extensive ongoing work is exploring combination therapies with pembrolizumab.

Durvalumab, another anti-PD-1 compound, has been tested in combination with PARPi in both Phase I and II trials. In a Phase 1 trial, seven patients with ovarian cancer, along with one endometrial and triple negative breast cancer, were treated with olaparib and cediranib, a VEGFR1-3 inhibitor (55). ORR was 44% with four partial responses and three patients with SD. Most common low-grade AEs were fatigue, nausea, and increased LFTs. Five patients experienced grade 3 hematological AEs, three with lymphopenia and two with anemia). In a subsequent Phase 2, 35 OC patients were enrolled in a single-center study (56). ORR was noted to be 14% with five patients achieving a partial response while 20 patients had SD. Overall, median PFS was noted to be 3.9 months. Like the Phase 1, hematologic toxicity, mainly anemia, was the most common high-grade AE, affecting eleven patients. The study also found significant increases in VEGFR3 were correlated with worse PFS. Of note, when evaluating durvalumab and olaparib in PARPi-naïve patients with platinum-sensitive and mutated BRCA in a Phase II trial, a 63% RR was noted, with six patients achieving a CR and fourteen achieving PRs (57). The most common grade three or higher AEs were anemia, increased lipase and amylase, and neutropenia.

Avelumab, an anti-PD-L1 therapy, though not directly inhibiting the suppression of T cells, plays a role in preventing

the inactivation of T cells. In a phase 1b trial, 125 ovarian cancer patients with Stage III or IV disease received 10 mg/kg avelumab every 2 weeks (58). Confirmed objective response was seen in only twelve patients with one CR and eleven PRs. Median OS was 11.2 months. The most common treatment-related AEs were fatigue, diarrhea, and nausea while the most common high-grade was an increase in lipase-levels. Low grade immune-related AEs mainly were hypothyroidism while three patients separately experienced high-grade colitis, type 2 diabetes, or myositis. Ongoing clinical trials are evaluating avelumab with chemotherapy and PARPi (**Table 1**).

Regulatory T Cells

Discovered in 1995, Tregs were originally shown to be involved in immune homeostasis, preventing an over-activation of the immune system towards self (59). They have been characterized to express CD4, CD25, and, most notably, FoxP3 (4). Tregs enact their function by suppressing activation of immune cells, inducing cell death of effector cells, and secreting anti-inflammatory cytokines, such as TGF-beta and IL-10 (60). Since their discovery, Tregs have been shown to be involved in a number of disease processes, including cancer.

In ovarian cancer, Tregs have been shown to be an indicator of poor prognosis. Curiel et al. showed that in 104 patients, increased numbers of intratumoral Tregs predicted poor survival (61). Absolute Treg counts may overlook certain cellular interactions, because in a study of 117 patients, intraepithelial Treg counts did not correlate with a significant difference in survival (9). Instead, increased ratios of $CD8^+$ T cells to $CD4^+CD25^+FoxP3^+$ T cells were shown to significantly associate with improved survival. Later studies also showed that a high $CD8^+$/Treg ratio as well as $CD4^+$/Treg ratio were associated with better survival outcomes (62).

Treg function can also be influenced by the ovarian TME. TAMs and tumor cells have been shown to increase levels of CCL22, which aid in Treg recruitment to the ovarian TME (61). In a set of 75 ovarian cancer patients, CCL22 levels were shown to be elevated in the peritoneal fluid, possibly contributing to Treg recruitment and cancer progression (63). Tregs have also been shown to be highly activated when found intratumorally in ovarian cancer. $CD45RA^-FoxP3^{hi}$ effector Tregs expressed significantly higher levels of 4-1BB, ICOS, OX40, and CTLA4 compared to $CD45RA^-FoxP3^{lo}$ effector T cells (64). Tregs expressing high PD-1 and 4-1BB were subsequently both more responsive to stimulation by anti-CD3/anti-CD28 and were able to better suppress T cells *in vitro*.

One method of reducing Treg effector functions is to directly deplete Tregs. Low-dose cyclophosphamide has been tested for use in conjunction with cancer vaccines due to its ability to deplete FoxP3 Tregs (65). However, Tregs treated with low-dose cyclophosphamide were unable to suppress the proliferation of CD4+ and CD8+ T cells *in vitro*. When tested in ovarian cancer, a combination therapy of low-dose cyclophosphamide with a p53-SLP vaccine did not directly suppress either Treg counts or functionality (66). However, overall T cell counts were higher and persisted longer in the combination group when compared to vaccination alone. Similarly, a phase 1/2 clinical trial found a single i.v. dose of cyclophosphamide had no effect on circulating Tregs (67).

Regulatory B Cells

In ovarian cancer, there is evidence infiltrating B cells can be either good or bad prognostic indicators. Milne et al. found that intraepithelial CD20+ B cells, when present in patients optimally debulked from high-grade serous OC, positively correlated with disease-specific survival (68). Patients who had residual disease or another histological subtype, however, did not demonstrate any significant survival benefit with infiltrating CD20+ B cells. In a follow-up study, tumor-infiltrating CD20+ cells were found to have responded to antigen, having undergone class switching, somatic hypermutation, and clonal expansion (69). These CD20 + B cells, when found co-localized with CD8+ T cells in tumor, also correlated with improved patient survival compared to tumor-infiltrating T cells alone. In an independent study, Santoiemma et al. also found tumor-infiltrating CD20+ B cells to positively correlate with OS (70). Later, these $CD20^+$ B cells, in addition to $CD138^+$ plasma cells and $CD4^+$ TILs, were found to co-localize with $CD8^+$ T cells in tertiary lymphoid structures and indicate better prognosis (71). Interestingly, Kroeger et al. also found tumor-infiltrating plasma cells, in high-grade serous ovarian cancer, to express IgG and CXCR3, the latter being normally expressed under immuno-stimulatory environments (72).

Contrary to this finding, Lundgren et al. found CD138+ plasma cells to positively correlate with tumor grade and negatively with OS (73). Furthermore, they found CD20+ B cells only correlated with tumor grade and had no significant correlation with survival. Other studies have also shown infiltrating B cells to be detrimental. Yang et al. showed that high levels of CD19+ B cells in the omentum correlated with poor survival (74). Ultimately, additional phenotype characterization of tumor-infiltrating B cells needs to be completed to determine their impact in the TME and patient outcomes.

Recently, a subset of B cells known as B regulatory cells has been found in ovarian cancer patients (75). More specifically, $IL\text{-}10^+$ B cells were increased in ascites compared to peripheral blood. These B cells were inversely correlated with the number of $CD8^+$ T cells in ascites and positively correlated with $FoxP3^+CD4^+$ T cells. *Ex vivo* studies showed these B cells were capable of suppressing IFN gamma secretion by T cells even under stimulation by anti-CD28. Finally, accumulation of these cells in the ascites correlated with more late-stage and aggressive disease. In models of spontaneous ovarian cancer, increased CD25+ pre-B-like cells were found intratumorally (76). These pre-B-like cells were shown in breast cancer models to develop into tBregs ($CD19+ CD25^{Hi}CD69^{Hi}$) and promote metastases. There are no modalities currently available that specifically target Bregs. Additional research is necessary to determine which markers best define this subset and how they function in ovarian cancer.

INNATE IMMUNITY

Despite recent advances in the use of checkpoint inhibitors and augmenting the T cell response, attempts at augmenting adaptive immunity have been unsuccessful in treating ovarian cancer patients. Recent efforts have shifted to include exploiting the innate immune response (77). Myeloid cells of the innate immune system, such as monocytes, classical macrophages, natural killer cells, and dendritic cells, all play key roles in promoting an effective adaptive response; the lack of accounting for these interactions may be where current immunotherapies fall short. Alternatively, cell types such as TAMs and MDSCs induce a highly immuno-suppressive TME and may be targets of future therapeutic strategies (6, 7).

Dendritic Cells

As the main mediator of responses between the innate and adaptive immune response, conventional human DCs (cDCs, CD141+, or CD1c+), are critical for the adaptive response by up-taking antigen and skewing helper T cell differentiation (78). However, cancer cells subvert proper antigen presentation by down-regulating MHC, reducing TAAs on their surface, and can be suppressed by numerous cytokines (79). DCs can also induce T cell suppression themselves through PD-1 and CD277 in the ovarian cancer TME (80, 81). Human plasmacytoid dendritic cells (pDCs, CD303+) increase immunosuppression in the ovarian cancer TME through upregulation of Tregs (82, 83). Furthermore, tumor-associated pDCs have been correlated with poor prognosis and early relapse for ovarian cancer patients, possibly due to their influence on CD4+ T cells to produce increased IL-10 (84).

Multiple clinical trials have looked at the benefit of utilizing DCs, obtained through leukapheresis or derived from monocytes, that are pulsed with specific antigens as immunotherapy. In one trial, autologous DCs were pulsed with Her2/neu, human telomerase reverse transcriptase, and pan-DR epitope with or without a single-dose of cyclophosphamide. Five of eleven patients had no evidence of disease at the time of publication with only one patient dying of disease within 36 months after the initial vaccination (67). No grade 3 or 4 treatment-related AEs were reported. Two studies introduced IL-2 in conjunction with DC treatment. Rahma et al. evaluated the optimal mechanism of peptide delivery to DCs, with 6 OC patients receiving DCs pulsed *ex vivo* with wild-type p53 peptide 264-272 (85). PFS and median OS was found to be 8.7 and 29.6 months, respectively, comparable to those patients receiving subcutaneous injections of solely peptide. Notably, all Grade 3 or 4 AEs occurred during cycles of IL-2 administration—the most common being fatigue, lymphopenia, and elevated liver enzymes. IL-2 administration also led to increases in Tregs. In another study by Baek et al., 10 patients with minimal residual disease were treated with DCs pulsed with keyhole limpet haemocyanin (KLH) and IL-2 (86). KLH has previously been used as a surrogate marker for DC vaccination. Three patients underwent complete remission with the most common AEs being flu-like symptoms, attributed to IL-2 administration. Contrastingly, this study found treatment decreased CD4 +CD25+ T cells, albeit they did not characterize FoxP3 expression. A recent Phase I/II study enrolled three ovarian cancer patients and treated them with DCs pulsed with Wilms' tumor protein 1 (87). One patient reached SD by RECIST criteria while the other two had progressive disease. No Grade 3 or greater AEs were reported.

Alternatively, DCs could be pulsed with whole tumor lysate as a means of eliciting a response to a variety of neoantigens as opposed to a single one. In a phase I study with six ovarian cancer patients, autologous DCs were pulsed with autologous tumor lysate and (KLH) (84). No grade 2 or higher AEs reported. Most common Grade 1 AEs included pain, fatigue, nausea, and abdominal pain. In another clinical study, 25 immunotherapy-naïve OC patients were treated with either a) intranodal injections of DCs pulsed with oxidized whole tumor lysate, b) whole-tumor lysate pulsed DCs with bevacizumab or c) the prior combination with cyclophosphamide (88). No toxicities greater than Grade 2 were reported due to the treatment. The most common Grade 1 AEs overall were pain, fatigue, nausea and abdominal pain. There were two PRs and thirteen patients had SD. Of note, patients without intratumoral T cells reactive for autologous tumor had poorer outcomes, again suggesting the success of DC vaccinations relies on the ability to generate a specific T cell response. Interestingly, the addition of cyclophosphamide improved both immune response, as measured by IFN-gamma release, and ultimately patient survival.

But despite some success of these DC vaccines, limitations include the ability to generate a consistent immuno-stimulatory effect and the difficulty of vaccine production (89). In an attempt to generate a more efficient T-cell response in a preclinical setting, Mirandola et al. treated DCs infected with a recombinant adeno-associated virus (rAAV) containing cancer/testis antigen mSP17 with a p38 MAPK inhibitor (90). A p38 inhibitor was used due to previous studies showing its use improving monocyte-derived DC survival and decreasing Treg production (91, 92). Murine DCs were infected with rAAV-mSP17 and treated with a p38 MAPK inhibitor. Survival analyses showed that when C57BL/6 mice, injected i.p. with 1×10^6 ID8 cells, were treated with DCs plus p38 inhibitor, 95% of mice survived up to 300 days, as compared to those receiving solely DCs surviving up to 98 days. Furthermore, the addition of p38 inhibitor increased lymphocyte trafficking to the tumor. When using human DCs, the addition of p38 inhibitor significantly decreased PD-L1 expression, reversing one contributor to the highly immunosuppressive TME. In a separate attempt to alternatively produce DCs for use in OC patients, Cheng et al. developed "mini DCs" through the use of cell membrane coating nanotechnology, i.e., fusing cell membranes onto synthetic polymer cores (93). To traffic tumor antigens to the membrane prior to fusion, ID8 murine cells were lysed and pulsed onto bone marrow-derived DCs. Additionally, IL-2 was loaded into the nanoparticle prior to emulsion. Mice inoculated with ID8 cells

subcutaneously showed significant growth reduction when treated with the mini DCs compared to normal DCs and empty nanoparticles. Increased CD8+ T cell infiltration and decreased Tregs were also observed intratumorally in the mini DC treated mice. When evaluating the effect of mini DCs on metastases, mice injected i.p. with ID8 cells and treated with mini DCs had significantly fewer nodules on the peritoneal wall when compared to vehicle or those treated with normal DCs. No changes in body weight or liver and kidney functions were observed in mice treated with mini DCs, indicating good biocompatibility.

Natural Killer Cells

Natural killer cells, CD56+, have become increasingly popular as an immunotherapy due to their ability to kill without prior sensitization to antigen. Instead, they integrate activating and inhibitory receptors in order to mediate their cytotoxic effect. Receptors, such as killer cell immunoglobulin-like receptors (KIRs) and NKG2A-C that recognize MHC and NKG2D that recognize stress molecules, cooperate to sense "missing self," "induced self," or "altered self (94)." Similar to T cells, these cells are able to kill by perforin-granzyme and also by FAS and TRAIL-mediated mechanisms (95). In OC, NK cells have been reported to both be positively and negatively prognostic. One study evaluated the prognostic value of intra-tumoral NK cells in 82 patients with mixed histologies (96). Researchers found patients with only intra-epithelial infiltration of NK cells had an increased OS (106 months) compared to those with only intra-stromal infiltration (58 months); no difference was seen in PFS between these two groups. However, tumor infiltration of CD56+ NK cells did not correlate with prognosis. Additionally, this study evaluated the presence of ULBP2 and MICA/B on patient outcomes—both activating ligands of NKG2D thought of commonly to mark cells for elimination. Interestingly, high levels of ULBP2 on tumor samples was found to indicate a poor prognosis for cancer patients, while MICA/B did not correlate with prognosis. This may be due to high levels of ULBP2 inhibiting proper T cell functioning. Samples from 283 patients with high-grade serous carcinoma were evaluated by immunohistochemistry for NK cell infiltration (97). Median OS in patients with high levels of CD57+ NK cells (≥10 cells/mm^2) was improved, compared to patients with low levels (<10 cells/mm^2), 45 vs. 29 months, respectively. Interestingly, higher CD56+ NK cells:lymphocyte fraction in ascites was associated with both a better PFS and OS in 20 OC patients (98). It was noted though that by selecting for patients that had enough ascites, patients with poor prognosis were inadvertently selected. Further studies will be needed to evaluate the importance of intra-tumoral NK cells.

There are multiple clinical trials in progress evaluating the benefits of augmenting NK cell number and function. One Phase I trial is evaluating IP FATE-NK100, a donor-derived NK product compromised from terminally differentiated cells, with IL-2, as a means of promoting NK survival, and lymphodepletion by cyclophosphamide and fludarabine (CyFlu) in women with recurrent OC (NCT03213964). Another Phase I trial is evaluating i.p. NK cells, instead generated from CD34 hematopoietic stem cells in umbilical cord blood, in twelve recurrent OC patients with lymphodepletion by CyFlu (NCT03539406). In an attempt to boost the body's own NK cells, one Phase II trial is evaluating the use of i.p. as well as subcutaneous (s.q.) IL-15Ra super-agonist, ALT-803, after first-line chemotherapy (NCT03054909). It was previously shown that in OC, ascites-derived NK cells and healthy donor NK cells improved their reactivity when stimulated with IL-15 or ALT-803 (98). One published Phase II study evaluated i.v. NK cells, treated *ex vivo* with IL-2, given post-lymphodepletion by CyFlu in 14 ovarian cancer patients (99). Five patients also received total body irradiation to deplete lymphocytes and allow for NK expansion. Despite four patients reaching PRs and eight having SD, one patient developed a grade 5 toxicity due to tumor lysis syndrome. Other severe AEs, such as passenger lymphocyte syndrome and neutropenia, were attributed to the irradiation.

CARs have been also added to NK cells, as well as NKT cells (CD3+CD56+), in an attempt to utilize these cells. Briefly, NKT cells carry characteristics of both NK and T cells, enabling them to enact cytotoxic killing without prior activation. Utilizing a CAR against FR, Zuo and colleagues showed NKTs with improved cytotoxicity towards FR^+ PEO1 cells *in vitro* when compared to CAR-Ts by transfecting NKT cells with CARs carrying both the CD28 and 4-1BB co-stimulatory signaling domain, (100). However, the NKT cells performed worse than CAR-T cells in nude mice inoculated subcutaneously with PEO1 cells. NK cells, specifically NK-92, were also used as a surrogate for a third-generation anti-FR CAR (101). Similarly, these NK cells demonstrated cytotoxic effects against SKOV3 *in vitro* and in B-NDG mice inoculated i.p. with SKOV3. One clinical trial utilizing anti-mesothelin NK cells, obtained from peripheral blood mononuclear cells, has been proposed (NCT03692637).

Changes in synthesis methods and receptor signaling may also be beneficial to the success of CAR-NKs. Li et al. created anti-mesothelin CAR-NKs, with additional NKG2D and 2B4 domains, from induced pluripotent stem cells (iPSCs) (102). Advantages to using iPSC include better clonal manipulation of the end product and increased speed of production. In a xenograft model injected i.p. with A1847 cells, treatment with their CAR-NK, along with IL-2 and IL-15, significantly reduced tumor burden and, ultimately, improved survival. When directly compared to a CAR-T with the same receptor, but with 4-1BB and CD28 signaling motifs instead, mice treated with the CAR-NK had less weight loss and pathogenic damage in organs such as the liver and kidney. Furthermore, those treated with CAR-NK also had improved survival when directly compared to those given CAR-T cells. Another group has created a CAR-NKs against glypican-3 (GPC3), with CD28 and 4-1BB signaling motifs, also from iPSCs derived immune cells (103). In NSG mice inoculated i.p. with KOC7c, a GPC3-expressing ovarian cancer cell line, a statistically significant difference in survival was seen when compared to PBS. Klapdor et al. has also developed dual-CAR-NKs, using NK-92, against CD24 and mesothelin with CD28 and 4-1BB signaling motifs (104). CD24 was chosen as a target due to its presence on

cancer stem cells and lack thereof on normal tissues; mesothelin has been previously discussed. In A2780 and HEK293T cells previously transfected with CD24, mesothelin, or both, the dual-CAR was able to target both mesothelin-positive cells and CD24-positive cells.

Monocytes and Macrophages

Monocytes can be classified into three subsets based on CD14 and CD16 expression: classical monocytes (CD14+CD16−), intermediate monocytes (CD14+CD16+), and non-classical monocytes (CD14-CD16+). Upon inflammation, monocytes traffic to the tissue and differentiate on a spectrum ranging from classically activated macrophages, or M1-like, to alternatively activated macrophages, or M2-like. A holistic review on M1 vs. M2 macrophage differentiation is more thoroughly reviewed in (105). In brief, M1-like macrophages, induced by IFN-γ and TNF-α, secrete inflammatory cytokines, such as IL-6 and IL-12, while M2-like macrophages are induced by TGF-β and IL-4/13 and secrete anti-inflammatory cytokines and recruiting Tregs (106). Cancer cells themselves are able to induce a shift towards an M2 phenotype through the secretion of signaling molecules. In OC specifically, CSCs were shown to increase levels of CCL2, COX-2 and PGE-2 as well as activate the PPARγ pathway, all of which correlated with increased polarization towards M2 macrophages (107, 108). Unsurprisingly, a high M1/M2 ratio has been correlated with improved survival in OC patients (109). A meta-analysis also indicated the presence of CD163+ TAMs was correlated with poor prognosis (110). A decreased lymphocyte-to-monocyte ratio (LMR) also indicated both poor overall and PFS in retrospective reviews (111–114).

In order to bolster immunity against cancer, the goal would be to decrease M2-like macrophages and/or increase their M1-like counterparts. Pre-clinical studies have attempted to decrease the prominence of M2 macrophages in the OC TME by interfering with the number of TAMs. Trabectedin, an inhibitor of DNA repair and transcription, was found to activate caspase-8 in monocytes through TRAIL-R1/2, leading to decreases in TAMs (115). Paclitaxel, a microtubule inhibitor currently in use to treat ovarian cancer, was recently found to shift M2 macrophages towards M1 in a TLR4-dependent fashion (116).

In OC, the addition of IFN-α/γ to monocytes was hypothesized to maintain the M1-like phenotype when used as an anti-cancer therapy. Importantly, this combination was shown to significantly reduce tumor burden and improve survival in BALB/c mice inoculated subcutaneously with OVCAR-3 (117). Mice treated with the combination of IFNs and monocytes survived to 170 days when compared to 87 and 81 days for IFNs or monocytes alone, respectively. Intra-tumoral macrophages were identified by CD31 and CD68 staining. Further immunofluorescence (IF) characterization showed that the cells expressed M1 markers IL12, CXCL10 and NOS2, but decreased M2 markers IL-10 and arginase, indicating that the IFN-treated monocytes retained differentiation towards an M1-like phenotype. Extrapolating these findings to other ovarian cancer cell lines, Johnson et al. reinforced the ability of monocytes and IFNs to kill tumor cells synergistically, although sensitivity varied between lines (118). A Phase 1 clinical trial was created to evaluate the intraperitoneal administration of autologous monocytes treated *ex vivo* with pegylated inteferon α-2b and interferon γ-1b (119). Preliminary results showed a well-tolerated treatment with two PRs and four patients with SD (120).

Myeloid-Derived Suppressor Cell

Compared to the veteran immunosuppressive Tregs (discovered in 1969), myeloid derived suppressor cells (MDSCs) are a relatively "young" subset (121). Poorly-differentiated myeloid cells with the capacity to suppress T cell activation were reported in the 1970s (122), but the term "MDSC" was not coined until 2007 (123), and many questions relating to the origin, classification, and behavior of MDSCs remain unresolved (124).

A comprehensive review of the current understanding of MDSCs have been presented previously (7, 125). Briefly, MDSCs are myeloid derived cells which develop in bone marrow, traffic through peripheral blood to the tumor, and increase during tumor development in response to chemotactic and growth factor signals released by the tumor itself such as G-CSF, GM-CSF, VEGF, and IFN-γ (126, 127). MDSCs are functionally characterized by the ability to suppress T cell activation *ex vivo* (122), and to suppress the ability of immune cells in the TME to mount an antitumor response *in vivo* by mechanisms which are incompletely characterized, but include direct suppression of cytotoxic T cells and NK cells via PDL1/2, promotion of Treg expansion by TGF-beta, CD40L, and Il-10, and promotion of M2-like/TAM development (128). MDSCs can be identified by their expression of specific markers, allowing division into monocytic and granulocytic subtypes according to consensus guidelines, although these classification schemes remain in flux (125). In mice, monocytic MDSCs are defined as $CD11b^{+}$ $Ly6C^{high}$ $Ly6G^{-}$ while granulocytic MDSCs are $CD11b^{+}$ $Ly6C^{low}$ $Ly6G^{+}$. In humans, monocytic MDSCs are $HLA\text{-}DR^{-}CD11b^{+}CD33^{+}CD14^{+}$ while granulocytic MDSCs are $HLA\text{-}DR\text{-}CD11b^{+}CD33^{+}CD15^{+}$.

The clinical relevance of MDSCs as drivers of ovarian cancer pathogenesis has been demonstrated by correlative studies in humans associating MDSC frequency and phenotype with worse prognosis as well as by experimental manipulations in mice, in which direct ablation of MDSCs can impede tumor development. In patient series, higher MDSC frequency in tumor biopsy (129), in peripheral blood (130), or in ascites (131) correlated with decreased OS or relapse free survival, as did high MDSC-to-dendritic cell ratio in peripheral blood (132). Syngeneic mouse model studies have demonstrated that MDSCs accumulate during the course of tumor development (133) and that ablation of MDSC by clodronate liposomes led to increased survival. Depletion of MDSC by anti-Gr1 antibodies also inhibited tumor growth in mouse and depletion of MDSC led to increased mouse survival whereas adoptive transfer of MDSC from one tumor-bearing mouse to another improved tumor growth (134, 135). Similarly, depletion of MDSCs by anti-GM-CSF therapy reversed anti-VEGF therapy resistance, reducing intra-tumoral MDSCs and increasing $CD8^{+}$ TILs (136).

MDSCs have the capacity to develop into immunosuppressive M2-like macrophages, but they can also differentiate into non-immunosuppressive cell types such as conventional M1 macrophages and dendritic cells. Agents such as all-trans-retinoic acid (ATRA) and epigenetic modifiers such as histone-deacetylase inhibitors (HDACi) have been demonstrated to induce differentiation of MDSC (resulting in functional depletion) in preclinical studies. In ovarian cancer, the phase II trial of histone deacetylase inhibitor entinostat in combination with checkpoint inhibitor avelumab failed to demonstrate an advantage over avelumab alone (137). Differentiation vs depletion of MDSC by the hypomethylating agent azacytidine has been reported in mouse (138). Of note, azacytidine has also been reported to sensitize platinum resistant ovarian cancer cells to platinum by mechanisms that are not entirely understood (139), which has been the inspiration for other trials. Decitabine has been pursued as a platinum sensitizer and reported as having disease activity by CA-125 reduction but not by reduction in tumor size, i.e., RECIST criteria (140). A phase 1 trial of azacytidine and valproic acid, another HDACi, in combination with carboplatin in patients with platinum-refractory solid tumors was reported in abstract form as displaying disease activity but with a very high (78%) rate of grade 3–4 toxicity (141).

Blocking of MDSC migration to tumor might be achieved by a variety of manipulations, including blocking of cytokines such as VEGF, G-CSF, GM-CSF, and M-CSF, as discussed above. VEGF inhibition by bevacizumab already has an established role in treatment of ovarian cancer, with approvals in both the first-line and later-line settings. Interestingly, mouse data in bevacizumab-resistant tumors demonstrated that MDSCs recruited by GM-CSF, produced by the tumor drove immunosuppression which was reversible by blockade of GM-CSF production (136). In the clinic, early phase I/II experimental approaches are focusing on blocking the receptors on MDSCs which mediate response to the above cytokines, namely CXCR2 (NCT02370238 and NCT02499328), CCR5 (NCT01736813), and CSF1R (NCT01349036). In addition, a phase 1 combination trial of the anti-CSF1R antibody cabiralizumab plus nivolumab (NCT02526017) including ovarian cancer patients is underway.

Finally, inhibition of MDSC function has been hampered to some extent by an incomplete understanding of the complex mechanisms by which MDSCs downregulate antitumor immunity. Depletion of L-arginine in the TME via expression of arginase-1 and inducible nitric oxide synthase (NOS-1) is thought to directly inhibit T cell function and result in cell cycle arrest (142). Disruption of this process may be achieved *in vitro* by inhibiting upstream inflammatory cyclooxygenase-2 (COX-2), prostaglandin E2 (PGE2) or phosphodiesterase-5 (PDE-5) signaling (143). Similarly, use of PDE-5 inhibitors such as sildenafil and tadalafil, which are already FDA approved for non-cancer indications, is being tested in combination trials in a variety of solid tumors. A phase I study of the anti-VEGFR2 molecule regorafenib and sildenafil in multiple solid tumors was reported, with evidence of disease activity including two ovarian cancer patients who achieved SD for >24 weeks (144).

CHALLENGES AND FUTURE DIRECTIONS

Ovarian cancer remains a lethal disease due to late-stage diagnoses and a lack of suitable treatment options in the recurrent setting. Despite recent advances in PARPi and anti-VEGF treatment modalities, a better understanding of the immune cell subsets and their interactions in the peritoneal TME may bring forth novel targeted therapies and additional combination therapies. Herein, we discussed key subsets of the many immune cells that play a role in the immuno-suppressive and tumor-promoting microenvironment of ovarian cancer, and recent attempts to therapeutically employ both adaptive (**Table 2**) and innate (**Table 3**) immunity. Tumor-specific lymphocytes have been found in ovarian cancer, and have been associated with better prognoses, but anti-inflammatory cytokines produced by Tregs and other cells may overwhelm their effector functions. Depleting Tregs by cyclophosphamide has not been shown to directly affect Treg counts, but may promote overall T cell count. Reducing counts of other immunosuppressive cells, mainly those of innate immunity, may be significant in future treatments. MDSCs or M2-like macrophages may be important target populations.

A lack of tumor associated antigens and proper stimulation may also hinder a targeted immune response. A main problem seen in CAR-T therapies included a lack of persistence within circulation and poor penetrance into the peritoneal TME. Therapies such as checkpoint inhibitors and CAR-T cells may have demonstrated poor efficacy due to cellular interactions between adaptive and innate immunity that are yet to be fully characterized. Bregs are one class of cells that have yet to be fully understood. MDSCs have also been shown to play a significant role in decreasing immune function in the TME by secreting cytokines and directly inhibiting adaptive immune cells, but need further characterization.

Augmenting the innate immune response may be a mechanism by which to improve the anti-tumor response. Multiple groups have evaluated DCs as ways to augment a tumor-specific T cell response. Trials evaluating various peptides and whole tumor lysate have shown varied results though, but with minimal AEs. Future studies evaluating additional mechanisms of sustaining DC activation as well as possible bio-nanotechnology to replace synthesis of DCs will be critical in developing this option. Another possible mechanism is to use NK or NKT cells as an effector cell because they do not require additional activation. These cells have demonstrated the capacity to be transfected with CARs and clinical trials are currently underway. Similarly, efforts to utilize monocytes as effector cells are underway. Targeting of MDSCs is an exciting avenue for ovarian cancer therapy, with the multiple agents and combinations discussed above being tested, and many others with promising preclinical data. However, there are outstanding questions which need to be addressed in order for these approaches to be maximally beneficial. One invaluable is given the rapidly increasing number of available therapeutic combinations, how do we rationally choose which combinations to test in our patients? Ultimately, further understanding of the

TABLE 2 | Published clinical trials of immunotherapies modulating adaptive immunity of ovarian cancer patients.

Intervention	NCT/Author	Phase	Enrollment	Primary Endpoint	PFS	OS	ORR
CAR-T							
Anti-Folate Receptor	Kershaw et al.	1	14 recurrent FR^+ OC	Safety and Activity	–	–	*
Anti-Mesothelin	Beatty et al.	1	5 OC	Safety and Activity	–	–	0/5
Anti-CTLA4							
Ipilimumab	Hodi et al.	1	9 Stage 4 OC	Safety and Activity	–	–	0/9
	NCT01611558	2	40 RPS OC	DrAEs	–	–	4/39 (10.3%)
Nivolumab**+**Ipilimumab	Zamarin et al. NCT02498600	2	100 recurrent OC	ORR	3.9 months	28.1 months	16/51 (31.4%)
Anti-PD-1							
Nivolumab	Hamanishi et al.	2	20 RPR OC	Safety and Activity	3.5 months	20.0 months	3/20 (15%)
Nivolumab + Bevacizumab	Liu et al.	2	38 recurrent OC	ORR	12.1 months in RPS 7.7 months in RPR	–	8/20 (40%) in RPS 3/18 (16.7%) in RPR
Pembrolizumab	Varga et al.	1b	26 PD-$L1^+$ OC	ORR	1.9 months	13.8 months	3/26 (11.5%)
Pembrolizumab	Matulonis et al.	2	Cohort A: 285 recurrent OC Cohort B: 91 recurrent OC	ORR	Cohort A: 2.1 months Cohort B: 2.1 months	Cohort A: - Cohort B: 17.6 months	Cohort A: 7.4% Cohort B: 9.9%
Pembrolizumab + Niraparib	Konstantinopoulos et al.	1/2	Phase 1: 9 RPR OC Phase 2: 53 RPR OC	Phase 1: Safety and RP2D Phase 2: ORR	3.4 months	–	Integrated: 18%
Durvalumab + Olaparib + Cediranib	Zimmer et al.	1	7 recurrent OC 1 peritoneal cancer 1 endomterial 1 TNBC	RP2D	–	–	4/9 (44%)
Durvalumab + Olaparib	Lampert et al.	2	35 recurrent OC	ORR	3.9 months	–	5/35 (14%)
Durvalumab + Olaparib	Drew et al.	2	32 $BRCA^{mut}$, RPS OC	ORR	–	–	20/32 (63%)
Anti-PD-L1							
Avelumab	Disis et al. NCT01772004	1b	125 recurrent OC	ORR	2.6 months	11.2 months	12/125 (9.6%)

*-Not reported; *No patients responded to treatment; RPR, recurrent platinum-sensitive; RPR, recurrent platinum-resistant; RP2D, Recommended phase 2 dose; TNBC, Triple-negative breast cancer; ORR, Overall response rate.*

TABLE 3 | Published clinical trials of immunotherapies modulating innate immunity in ovarian cancer patients.

Intervention	NCT/Author	Phase	Enrollment	Primary Endpoint	PFS	OS	ORR
Dendritic Cell Vaccines (peptide target)							
(Her2/neu + hTRT + PADRE) +/- cyclophosphamide	Chu et al.	1/2	14 OC in first or second remission	Safety and Activity	–	–	–
(WT p53 peptide) + IL-12	Rahma et al.	2	21 recurrent OC	Activity	8.7 months	29.6 months	–
(KLH) + IL-2	Baek et al.	1/2	10 with MRD	Safety and Activity	–	65.0 months	3/10 (30%)
(WT1)	Zhang et al.	1/2	3 OC	DrAE	–	–	0/3 (0%)
(Autologous tumor lysate) + KLH	Hernando et al.	1	6 progressive or recurrent OC	Safety and Activity	–	–	0/6 (0%)
(Autologous tumor lysate) +/- bevacizumab +/-cyclophosphamide	Tanyi et al.	1?	25 immunotherapy-naïve recurrent OC	Safety and Activity	–	–	2/25 (8%)
Natural Killer Cells							
NK Cells + IL-2 + CyFlu	Geller et al.	2	14 OC	Activity	–	–	4/14 (28.5%)
Monocytes							
Monocytes + IFNα/γ	Cole et al.	1	11 recurrent OC	Safety and Activity	–	–	2/11 (18.1%)

-Not reported; RPR, recurrent platinum-sensitive; RPR, recurrent platinum-resistant; RP2D, Recommended phase 2 dose; ORR, Overall response rate; KLH, Keyhole limpet haemocyanin; hTRT, human telomerase reverse transcriptase; PADRE, pan-DR epitope; WT-1, Wilms' tumor protein 1; CyFlu, Cyclophosphamide + Fludarabine; SQ, subcutaneous; MRD, minimal residual disease.

interactions amongst tumor and immune cells in the unique peritoneal microenvironment will allow us to better develop optimal targeted therapies for the treatment of ovarian cancer.

AUTHOR CONTRIBUTIONS

FN: conceived and designed the manuscript, performed the research, and wrote the manuscript. CC: wrote the manuscript and edited the manuscript. CA: conceived and designed the manuscript and edited the manuscript. All authors contributed to the article and approved the submitted version.

FUNDING

Intramural Research Program, National Cancer Institute (CMA, BC011775).

REFERENCES

1. Nwani NG, Sima LE, Nieves-Neira W, Matei D. Targeting the microenvironment in high grade serous ovarian cancer. *Cancers* (2018) 10(8):1–22. doi: 10.3390/cancers10080266
2. Nieman KM, Kenny HA, Penicka CV, Ladanyi A, Buell-Gutbrod R, Zillhardt MR, et al. Adipocytes promote ovarian cancer metastasis and provide energy for rapid tumor growth. *Nat Med* (2011) 17:1498–503. doi: 10.1038/nm.2492
3. Hamanishi J, Mandai M, Konishi I. Immune checkpoint inhibition in ovarian cancer. *Int Immunol* (2016) 28:339–48. doi: 10.1093/intimm/dxw020
4. Sakaguchi S, Mikami N, Wing JB, Tanaka A, Ichiyama K, Ohkura N. Annual Review of Immunology Regulatory T Cells and Human Disease. *Annu Rev* (2020) 38:541–66. doi: 10.1146/annurev-immunol-042718
5. Rosser EC, Mauri C. Regulatory B Cells: Origin, Phenotype, and Function. *Immunity* (2015) 42:607–12. doi: 10.1016/j.immuni.2015.04.005
6. Noy R, Pollard JW. Tumor-Associated Macrophages: From Mechanisms to Therapy. *Immunity* (2014) 41:49–61. doi: 10.1016/j.immuni.2014.06.010
7. Ostrand-Rosenberg S, Fenselau C. Myeloid-Derived Suppressor Cells: Immune-Suppressive Cells That Impair Antitumor Immunity and Are Sculpted by Their Environment. *J Immunol* (2018) 200:422–31. doi: 10.4049/jimmunol.1701019
8. Zhang L, Conejo-Garcia JR, Gimotty PA, Massobrio M, Regnani G, Makrigiannakis A, et al. Intratumoral T Cells, Recurrence, and Survival in Epithelial Ovarian Cancer. *N Eng J Med* (2003) 348:203–13. doi: 10.1056/NEJMoa020177
9. Sato E, Olson SH, Ahn J, Bundy B, Nishikawa H, Qian F, et al. Intraepithelial CD8 tumor-infiltrating lymphocytes and a high CD8 regulatory T cell ratio are associated with favorable prognosis in ovarian cancer. *PNAS* (2005) 102(51):18538–43. doi: 10.1073/pnas.0509182102
10. Pinto MP, Balmaceda C, Bravo ML, Kato S, Villarroel A, Owen GI, et al. Patient inflammatory status and CD4+/CD8+ intraepithelial tumor lymphocyte infiltration are predictors of outcomes in high-grade serous ovarian cancer. *Gynecol Oncol* (2018) 151:10–7. doi: 10.1016/j.ygyno.2018.07.025
11. Li D, Li X, Zhou WL, Huang Y, Liang X, Jiang L, et al. Genetically engineered t cells for cancer immunotherapy. *Signal Transduct Target Ther* (2019) 4:1–17. doi: 10.1038/s41392-019-0070-9
12. van Schandevyl S, Kerre T. Chimeric antigen receptor T-cell therapy: design improvements and therapeutic strategies in cancer treatment. *Acta Clin Belgica: Int J Clin Lab Med* (2020) 75:26–32. doi: 10.1080/17843286.2018.1545373
13. Martinez M, Moon EK. CAR T cells for solid tumors: New strategies for finding, infiltrating, and surviving in the tumor microenvironment. *Front Immunol* (2019) 10:128. doi: 10.3389/fimmu.2019.00128
14. Wagner J, Wickman E, DeRenzo C, Gottschalk S. CAR T Cell Therapy for Solid Tumors: Bright Future or Dark Reality? *Mol Ther* (2020) 28:2320–39. doi: 10.1016/j.ymthe.2020.09.015
15. Scaranti M, Cojocaru E, Banerjee S, Banerji U. Exploiting the folate receptor α in oncology. *Nat Rev Clin Oncol* (2020) 17:349–59. doi: 10.1038/s41571-020-0339-5
16. Lu Y, Low PS. Immunotherapy of folate receptor-expressing tumors: Review of recent advances and future prospects. *J Controlled Release (Elsevier)* (2003) 91(1-2):17–29. doi: 10.1016/S0168-3659(03)00215-3
17. Siu MKY, Kong DSH, Chan HY, Wong ESY, Ip PPC, Jiang LL, et al. Paradoxical Impact of Two Folate Receptors, FRα and RFC, in Ovarian Cancer: Effect on Cell Proliferation, Invasion and Clinical Outcome. *PLoS One* (2012) 7(11):e47201. doi: 10.1371/journal.pone.0047201
18. Chen YL, Chang MC, Huang CY, Chiang YC, Lin HW, Chen CA, et al. Serous ovarian carcinoma patients with high alpha-folate receptor had reducing survival and cytotoxic chemo-response. *Mol Oncol* (2012) 6:360–9. doi: 10.1016/j.molonc.2011.11.010
19. Chen J, Li L. Aberrant expression of folate metabolism enzymes and its diagnosis and survival prediction in Ovarian Carcinoma. *Anal Cell Pathol* (2019) 2019:1–9. doi: 10.1155/2019/1438628
20. Toffoli G, Russo A, Gallo A, Cernigoi C, Miotti S, Sorio R, et al. *Expression Of Folate Binding Protein As A Prognostic Factor For Response To Platinum-Containing Chemotherapy And Survival In Human Ovarian Cancer*. Wiley-Liss, Inc (1998).
21. Notaro S, Reimer D, Fiegl H, Schmid G, Wiedemair A, Rössler J, et al. Evaluation of folate receptor 1 (FOLR1) mRNA expression, its specific promoter methylation and global DNA hypomethylation in type I and type II ovarian cancers. *BMC Cancer* (2016) 16:1–13. doi: 10.1186/s12885-016-2637-y
22. Köbel M, Madore J, Ramus SJ, Clarke BA, Pharoah PDP, Deen S, et al. Evidence for a time-dependent association between FOLR1 expression and survival from ovarian carcinoma: Implications for clinical testing. An Ovarian Tumour Tissue Analysis consortium study. *Br J Cancer* (2014) 111:2297–307. doi: 10.1038/bjc.2014.567
23. Kershaw MH, Westwood JA, Parker LL, Wang G, Eshhar Z, Mavroukakis SA, et al. A phase I study on adoptive immunotherapy using gene-modified T cells for ovarian cancer. *Clin Cancer Res* (2006) 12:6106–15. doi: 10.1158/1078-0432.CCR-06-1183
24. Song DG, Ye Q, Carpenito C, Poussin M, Wang LP, Ji C, et al. In vivo persistence, tumor localization, and antitumor activity of CAR-engineered T cells is enhanced by costimulatory signaling through CD137 (4-1BB). *Cancer Res* (2011) 71:4617–27. doi: 10.1158/0008-5472.CAN-11-0422
25. Vergote I, Armstrong D, Scambia G, Teneriello M, Sehouli J, Schweizer C, et al. A randomized, double-blind, placebo-controlled, phase 3 study to assess efficacy and safety of weekly farletuzumab in combination with carboplatin and taxane in patients with ovarian cancer in first platinum-sensitive relapse. *J Clin Oncol* (2016) 34:2271–8. doi: 10.1200/JCO.2015.63.2596
26. Moore KN, Martin LP, O'Malley DM, Matulonis UA, Konner JA, Perez RP, et al. Safety and activity of mirvetuximab soravtansine (IMGN853), a folate receptor alpha-targeting antibody-drug conjugate, in platinum-resistant ovarian, fallopian tube, or primary peritoneal cancer: A phase i expansion study. *J Clin Oncol* (2017) 35:1112–8. doi: 10.1200/JCO.2016.69.9538
27. O'Malley DM, Matulonis UA, Birrer MJ, Castro CM, Gilbert L, Vergote I, et al. Phase Ib study of mirvetuximab soravtansine, a folate receptor alpha (FRα)-targeting antibody-drug conjugate (ADC), in combination with bevacizumab in patients with platinum-resistant ovarian cancer. *Gynecol Oncol* (2020) 157:379–85. doi: 10.1016/j.ygyno.2020.01.037
28. Wang Y, Cheon DJ, Lu Z, Cunningham SL, Chen CM, Luo RZ, et al. MUC16 expression during embryogenesis, in adult tissues, and ovarian cancer in the mouse. *Differentiation* (2008) 76:1081–92. doi: 10.1111/j.1432-0436.2008.00295.x

29. Chekmasova AA, Rao TD, Nikhamin Y, Park KJ, Levine DA, Spriggs DR, et al. Successful eradication of established peritoneal ovarian tumors in SCID-Beige mice following adoptive transfer of T cells genetically targeted to the MUC16 antigen. *Clin Cancer Res* (2010) 16:3594–606. doi: 10.1158/1078-0432.CCR-10-0192
30. Koneru M, Purdon TJ, Spriggs D, Koneru S, Brentjens RJ. IL-12 secreting tumor-targeted chimeric antigen receptor T cells eradicate ovarian tumors in vivo. *OncoImmunology* (2015) 4:1–11. doi: 10.4161/2162402X.2014.994446
31. Koneru M, O'Cearbhaill R, Pendharkar S, Spriggs DR, Brentjens RJ. A phase I clinical trial of adoptive T cell therapy using IL-12 secreting MUC-16ecto directed chimeric antigen receptors for recurrent ovarian cancer. *J Trans Med* (2015) 13:1–11. doi: 10.1186/s12967-015-0460-x
32. Berek JS, Taylor PT, Gordon A, Cunningham MJ, Finkler N, Orr J, et al. Randomized, placebo-controlled study of oregovomab for consolidation of clinical remission in patients with advanced ovarian cancer. *J Clin Oncol* (2004) 22:3507–16. doi: 10.1200/JCO.2004.09.016
33. Braly P, Nicodemus CF, Chu C, Collins Y, Edwards R, Alan Gordon J, et al. The Immune Adjuvant Properties of Front-line Carboplatin-Paclitaxel: A Randomized Phase 2 Study of Alternative Schedules of Intravenous Oregovomab Chemoimmunotherapy in Advanced Ovarian Cancer. *J Immunother* (2008) 32(1):54–65. doi: 10.1097/CJI.0b013e31818b3dad
34. Brewer M, Angioli R, Scambia G, Lorusso D, Terranova C, Panici PB, et al. Front-line chemo-immunotherapy with carboplatin-paclitaxel using oregovomab indirect immunization in advanced ovarian cancer: A randomized phase II study. *Gynecol Oncol* (2020) 156:523–9. doi: 10.1016/j.ygyno.2019.12.024
35. Battaglia A, Buzzonetti A, Fossati M, Scambia G, Fattorossi A, Madiyalakan MR, et al. Translational immune correlates of indirect antibody immunization in a randomized phase II study using scheduled combination therapy with carboplatin/paclitaxel plus oregovomab in ovarian cancer patients. *Cancer Immunol Immunother* (2020) 69:383–97. doi: 10.1007/s00262-019-02456-z
36. Argani P, Iacobuzio-Donahue C, Ryu B, Rosty C, Goggins M, Wilentz RE, et al. Mesothelin Is Overexpressed in the Vast Majority of Ductal Adenocarcinomas of the Pancreas: Identification of a New Pancreatic Cancer Marker by Serial Analysis of Gene Expression (SAGE) 1. *Clin Cancer Res* (2001) 7:3862–8.
37. Carpenito C, Milone MC, Hassan R, Simonet JC, Lakhal M, Suhoski MM, et al. Control of large, established tumor xenografts with genetically retargeted human T cells containing CD28 and CD137 domains. *PNAS* (2009) 106(9):3360–5. doi: 10.1073/pnas.0813101106
38. Beatty GL, Haas AR, Maus MV, Torigian DA, Soulen MC, Plesa G, et al. Mesothelin-specific chimeric antigen receptor mRNA-engineered T cells induce anti-tumor activity in solid malignancies. *Cancer Immunol Res* (2014) 2:112–20. doi: 10.1158/2326-6066.CIR-13-0170
39. Haas AR, Tanyi JL, O'Hara MH, Gladney WL, Lacey SF, Torigian DA, et al. Phase I Study of Lentiviral-Transduced Chimeric Antigen Receptor-Modified T Cells Recognizing Mesothelin in Advanced Solid Cancers. *Mol Ther* (2019) 27:1919–29. doi: 10.1016/j.ymthe.2019.07.015
40. Hassan R, Blumenschein GR, Moore KN, Santin AD, Kindler HL, Nemunaitis JJ, et al. First-in-Human, Multicenter, Phase I Dose-Escalation and Expansion Study of Anti-Mesothelin Antibody-Drug Conjugate Anetumab Ravtansine in Advanced or Metastatic Solid Tumors. *J Clin Oncol* (2020) 38:1824–35. doi: 10.1200/JCO.19
41. Hong H, Brown CE, Ostberg JR, Priceman SJ, Chang WC, Weng L, et al. L1 cell adhesion molecule-specific chimeric antigen receptor-redirected Human T cells exhibit specific and efficient antitumor activity against human ovarian cancer in mice. *PLoS One* (2016) 11(1):e0146885. doi: 10.1371/journal.pone.0146885
42. Owens GL, Sheard VE, Kalaitsidou M, Blount D, Lad Y, Cheadle EJ, et al. Preclinical Assessment of CAR T-Cell Therapy Targeting the Tumor Antigen 5T4 in Ovarian Cancer. *J Immunother* (2017) 41(3):130–40. doi: 10.1097/CJI.0000000000000203
43. Murad JP, Kozlowska AK, Lee HJ, Ramamurthy M, Chang WC, Yazaki P, et al. Effective targeting of TAG72+peritoneal ovarian tumors via regional delivery of CAR-engineered T cells. *Front Immunol* (2018) 9:2268. doi: 10.3389/fimmu.2018.02268
44. Du H, Hirabayashi K, Ahn S, Kren NP, Montgomery SA, Wang X, et al. Antitumor Responses in the Absence of Toxicity in Solid Tumors by Targeting B7-H3 via Chimeric Antigen Receptor T Cells. *Cancer Cell* (2019) 35:221–37.e8. doi: 10.1016/j.ccell.2019.01.002
45. Rodriguez-Garcia A, Sharma P, Poussin M, Boesteanu AC, Minutolo NG, Gitto SB, et al. CAR T Cells Targeting MISIIR for the Treatment of Ovarian Cancer and Other Gynecologic Malignancies. *Mol Ther* (2020) 28:548–60. doi: 10.1016/j.ymthe.2019.11.028
46. Hodi FS, Butler M, Oble DA, Seiden MV, Haluska FG, Kruse A, et al. Immunologic and clinical effects of antibody blockade of cytotoxic T lymphocyte-associated antigen 4 in previously vaccinated cancer patients. *PNAS* (2008) 105(8):3005–10. doi: 10.1073/pnas.0712237105
47. Zamarin D, Burger RA, Sill MW, Powell DJ Jr, Lankes HA, Feldman MD, et al. Randomized Phase II Trial of Nivolumab Versus Nivolumab and Ipilimumab for Recurrent or Persistent Ovarian Cancer: An NRG Oncology Study. *J Clin Oncol* (2020) 38(16):1814–23. doi: 10.1200/JCO.19.02059
48. Hamanishi J, Mandai M, Ikeda T, Minami M, Kawaguchi A, Murayama T, et al. Safety and antitumor activity of Anti-PD-1 antibody, nivolumab, in patients with platinum-resistant ovarian cancer. *J Clin Oncol* (2015) 33:4015–22. doi: 10.1200/JCO.2015.62.3397
49. Inayama Y, Hamanishi J, Matsumura N, Murakami R, Abiko K, Yamaguchi K, et al. Antitumor Effect of Nivolumab on Subsequent Chemotherapy for Platinum-Resistant Ovarian Cancer. *Oncol* (2018) 23:1382–4. doi: 10.1634/theoncologist.2018-0167
50. Liu JF, Herold C, Gray KP, Penson RT, Horowitz N, Konstantinopoulos PA, et al. Assessment of Combined Nivolumab and Bevacizumab in Relapsed Ovarian Cancer: A Phase 2 Clinical Trial. *JAMA Oncol* (2019) 5:1731–8. doi: 10.1001/jamaoncol.2019.3343
51. Varga A, Piha-Paul S, Ott PA, Mehnert JM, Berton-Rigaud D, Morosky A, et al. Pembrolizumab in patients with programmed death ligand 1–positive advanced ovarian cancer: Analysis of KEYNOTE-028. *Gynecol Oncol* (2019) 152:243–50. doi: 10.1016/j.ygyno.2018.11.017
52. Matulonis UA, Shapira-Frommer R, Santin AD, Lisyanskaya AS, Pignata S, Vergote I, et al. Antitumor activity and safety of pembrolizumab in patients with advanced recurrent ovarian cancer: results from the phase II KEYNOTE-100 study. *Ann Oncol* (2019) 30:1080–7. doi: 10.1093/annonc/mdz135
53. Gutierrez C, McEvoy C, Munshi L, Stephens RS, Detsky ME, Nates JL, et al. Critical Care Management of Toxicities Associated With Targeted Agents and Immunotherapies for Cancer. *Crit Care Med* (2019) 48(1):10–21. doi: 10.1097/CCM.0000000000004087
54. Konstantinopoulos PA, Waggoner S, Vidal GA, Mita M, Moroney JW, Holloway R, et al. Single-Arm Phases 1 and 2 Trial of Niraparib in Combination with Pembrolizumab in Patients with Recurrent Platinum-Resistant Ovarian Carcinoma. *JAMA Oncol* (2019) 5:1141–9. doi: 10.1001/jamaoncol.2019.1048
55. Zimmer AS, Nichols E, Cimino-Mathews A, Peer C, Cao L, Lee MJ, et al. A phase i study of the PD-L1 inhibitor, durvalumab, in combination with a PARP inhibitor, olaparib, and a VEGFR1-3 inhibitor, cediranib, in recurrent women's cancers with biomarker analyses. *J Immunother Cancer* (2019) 7:1–8. doi: 10.1186/s40425-019-0680-3
56. Lampert EJ, Zimmer AS, Padget MR, Cimino-Mathews A, Nair JR, Liu Y, et al. Combination of PARP inhibitor olaparib, and PD-L1 inhibitor durvalumab, in recurrent ovarian cancer: a proof-of-concept phase 2 study. *Clin Cancer Res* (2020) 26:4268–4279. doi: 10.1158/1078-0432.ccr-20-0056. clincanres.0056.2020.
57. Drew Y, de Jonge M, Hong SH, Park YH, Wolfer A, Brown J, et al. An open-label, phase II basket study of olaparib and durvalumab (MEDIOLA): Results in germline BRCA-mutated (gBRCAm) platinum-sensitive relapsed (PSR) ovarian cancer (OC). *Gynecol Oncol* (2018) 149:246–7. doi: 10.1016/j.ygyno.2018.04.555
58. Disis ML, Taylor MH, Kelly K, Beck JT, Gordon M, Moore KM, et al. Efficacy and Safety of Avelumab for Patients with Recurrent or Refractory Ovarian Cancer: Phase 1b Results from the JAVELIN Solid Tumor Trial. *JAMA Oncol* (2019) 5:393–401. doi: 10.1001/jamaoncol.2018.6258
59. Sakaguchi S, Sakaguchi N, Asano M, Itoh M, Toda M. autoimmune diseases. mechanism of self-tolerance causes various alpha-chains (CD25). Breakdown of a single activated T cells expressing IL-2 receptor Immunologic self-tolerance maintained by. *J Immunol* (1995) 155 (3):1151–64. http://www.jimmunol.org/content/155/3/1151.

60. Ou Y, Cannon MJ, Nakagawa M. Regulatory T Cells in Gynecologic Cancer. *MOJ Immunology* (2018) 6(2):34–42. doi: 10.15406/moji.2018.06.00189
61. Curiel TJ, Coukos G, Zou L, Alvarez X, Cheng P, Mottram P, et al. Specific recruitment of regulatory T cells in ovarian carcinoma fosters immune privilege and predicts reduced survival. *Nat Med* (2004) 10:942–9. doi: 10.1038/nm1093
62. Knutson KL, Maurer MJ, Preston CC, Moysich KB, Goergen K, Hawthorne KM, et al. Regulatory T cells, inherited variation, and clinical outcome in epithelial ovarian cancer. *Cancer Immunol Immunother* (2015) 64:1495–504. doi: 10.1007/s00262-015-1753-x
63. Wertel I, Surówka J, Polak G, Barczyński B, Bednarek W, Jakubowicz-Gil J, et al. Macrophage-derived chemokine CCL22 and regulatory T cells in ovarian cancer patients. *Tumor Biol* (2015) 36:4811–7. doi: 10.1007/s13277-015-3133-8
64. Toker A, Nguyen LT, Stone SC, Cindy Yang SY, Katz SR, Shaw PA, et al. Regulatory T cells in ovarian cancer are characterized by a highly activated phenotype distinct from that in melanoma. *Clin Cancer Res* (2018) 24:5685–96. doi: 10.1158/1078-0432.CCR-18-0554
65. Lutsiak MEC, Semnani RT, de Pascalis R, Kashmiri SVS, Schlom J, Sabzevari H. Inhibition of CD4+25+ T regulatory cell function implicated in enhanced immune response by low-dose cyclophosphamide. *Blood* (2005) 105:2862–8. doi: 10.1182/blood-2004-06-2410
66. Vermeij R, Leffers N, Hoogeboom BN, Hamming ILE, Wolf R, Reyners AKL, et al. Potentiation of a p53-SLP vaccine by cyclophosphamide in ovarian cancer: A single-arm phase II study. *Int J Cancer* (2012) 131:e670–80. doi: 10.1002/ijc.27388
67. Chu CS, Boyer J, Schullery DS, Gimotty PA, Gamerman V, Bender J, et al. Phase I/II randomized trial of dendritic cell vaccination with or without cyclophosphamide for consolidation therapy of advanced ovarian cancer in first or second remission. *Cancer Immunol Immunother* (2012) 61:629–41. doi: 10.1007/s00262-011-1081-8
68. Milne K, Köbel M, Kalloger SE, Barnes RO, Gao D, Gilks CB, et al. Systematic analysis of immune infiltrates in high-grade serous ovarian cancer reveals CD20, FoxP3 and TIA-1 as positive prognostic factors. *PLoS One* (2009) 4(7):1–14. doi: 10.1371/journal.pone.0006412
69. Nielsen JS, Sahota RA, Milne K, Kost SE, Nesslinger NJ, Watson PH, et al. CD20+ tumor-infiltrating lymphocytes have an atypical CD27 - memory phenotype and together with CD8+ T cells promote favorable prognosis in ovarian cancer. *Clin Cancer Res* (2012) 18:3281–92. doi: 10.1158/1078-0432.CCR-12-0234
70. Santoiemma PP, Reyes C, Wang LP, McLane MW, Feldman MD, Tanyi JL, et al. Systematic evaluation of multiple immune markers reveals prognostic factors in ovarian cancer. *Gynecol Oncol* (2016) 143:120–7. doi: 10.1016/j.ygyno.2016.07.105
71. Kroeger DR, Milne K, Nelson BH. Tumor-infiltrating plasma cells are associated with tertiary lymphoid structures, cytolytic T-cell responses, and superior prognosis in ovarian cancer. *Clin Cancer Res* (2016) 22:3005–15. doi: 10.1158/1078-0432.CCR-15-2762
72. Schwartz M, Zhang Y, Rosenblatt JD. B cell regulation of the anti-tumor response and role in carcinogenesis. *J Immunother Cancer* (2016) 4:1–15. doi: 10.1186/s40425-016-0145-x
73. Lundgren S, Berntsson J, Nodin B, Micke P, Jirström K. Prognostic impact of tumour-associated B cells and plasma cells in epithelial ovarian cancer. *J Ovarian Res* (2016) 9:1–9. doi: 10.1186/s13048-016-0232-0
74. Yang C, Lee H, Jove V, Deng J, Zhang W, Liu X, et al. Prognostic Significance of B-Cells and pSTAT3 in Patients with Ovarian Cancer. *PLoS One* (2013) 8 (1):1–6. doi: 10.1371/journal.pone.0054029
75. Wei X, Jin Y, Tian Y, Zhang H, Wu J, Lu W, et al. Regulatory B cells contribute to the impaired antitumor immunity in ovarian cancer patients. *Tumor Biol* (2016) 37:6581–8. doi: 10.1007/s13277-015-4538-0
76. Ragonnaud E, Moritoh K, Bodogai M, Gusev F, Garaud S, Chen C, et al. Tumor-Derived Thymic Stromal Lymphopoietin Expands Bone Marrow B-cell Precursors in Circulation to Support Metastasis. *Cancer Res* (2019) 79:5826–38. doi: 10.1158/0008-5472.CAN-19-1058
77. Demaria O, Cornen S, Daëron M, Morel Y, Medzhitov R, Vivier E. Harnessing innate immunity in cancer therapy. *Nature* (2019) 574:45–56. doi: 10.1038/s41586-019-1593-5
78. Eisenbarth SC. Dendritic cell subsets in T cell programming: location dictates function. *Nat Rev Immunol* (2019) 19:89–103. doi: 10.1038/s41577-018-0088-1
79. Wculek SK, Cueto FJ, Mujal AM, Melero I, Krummel MF, Sancho D. Dendritic cells in cancer immunology and immunotherapy. *Nat Rev Immunol* (2020) 20:7–24. doi: 10.1038/s41577-019-0210-z
80. Cubillos-Ruiz JR, Martinez D, Scarlett UK, Rutkowski MR, Nesbeth YC, Camposeco-Jacobs AL, et al. cd277 is a Negative Co-stimulatory Molecule Universally Expressed by Ovarian Cancer Microenvironmental Cells. *Oncotarget* (2010) 1(5):329–38. doi: 10.18632/oncotarget.165
81. Krempski J, Karyampudi L, Behrens MD, Erskine CL, Hartmann L, Dong H, et al. Tumor-Infiltrating Programmed Death Receptor-1 + Dendritic Cells Mediate Immune Suppression in Ovarian Cancer. *J Immunol* (2011) 186:6905–13. doi: 10.4049/jimmunol.1100274
82. Labidi-Galy SI, Sisirak V, Meeus P, Gobert M, Treilleux I, Bajard A, et al. Quantitative and functional alterations of plasmacytoid dendritic cells contribute to immune tolerance in ovarian cancer. *Cancer Res* (2011) 71:5423–34. doi: 10.1158/0008-5472.CAN-11-0367
83. Labidi-Galy SI, Treilleux I, Goddard-Leon S, Combes JD, Blay JY, Ray-Coquard I, et al. Plasmacytoid dendritic cells infiltrating ovarian cancer are associated with poor prognosis. *OncoImmunology* (2012) 1:380–2. doi: 10.4161/onci.18801
84. Hernando J, Park TW, Kübler K, Offergeld R, Schlebusch H, Bauknecht T. Vaccination with autologous tumour antigen-pulsed dendritic cells in advanced gynaecological malignancies: Clinical and immunological evaluation of a phase I trial. *Cancer Immunol Immunother* (2002) 51:45–52. doi: 10.1007/s00262-001-0255-1
85. Rahma OE, Ashtar E, Czystowska M, Szajnik ME, Wieckowski E, Bernstein S, et al. A gynecologic oncology group phase II trial of two p53 peptide vaccine approaches: Subcutaneous injection and intravenous pulsed dendritic cells in high recurrence risk ovarian cancer patients. *Cancer Immunol Immunother* (2012) 61:373–84. doi: 10.1007/s00262-011-1100-9
86. Baek S, Kim YM, Kim SB, Kim CS, Kwon SW, Kim YM, et al. Therapeutic DC vaccination with IL-2 as a consolidation therapy for ovarian cancer patients: A phase I/II trial. *Cell Mol Immunol* (2015) 12:87–95. doi: 10.1038/cmi.2014.40
87. Zhang W, Lu X, Cui P, Piao C, Xiao M, Liu X, et al. Phase I/II clinical trial of a Wilms' tumor 1-targeted dendritic cell vaccination-based immunotherapy in patients with advanced cancer. *Cancer Immunol Immunother* (2019) 68:121–30. doi: 10.1007/s00262-018-2257-2
88. Tanyi JL, Bobisse S, Ophir E, Tuyaerts S, Roberti A, Genolet R, et al. Personalized cancer vaccine effectively mobilizes antitumor T cell immunity in ovarian cancer. *Sci Transl Med* (2018) 10(436):Eaao5931. doi: 10.1126/scitranslmed.aao5931
89. Perez CR, de Palma M. Engineering dendritic cell vaccines to improve cancer immunotherapy. *Nat Commun* (2019) 10:1–10. doi: 10.1038/s41467-019-13368-y
90. Mirandola L, Chiriva-Internati M, Bresalier R, Piccotti L, Grizzi F, Marincola FM. A novel method for efficient generation of antigen-specific effector T-cells using dendritic cells transduced with recombinant adeno-associated virus and p38 kinase blockade. *J Trans Med* (2019) 17:1–9. doi: 10.1186/s12967-019-02163-4
91. Xie J, Qian J, Yang J, Wang S, Freeman ME, Yi Q. Critical roles of Raf/MEK/ERK and PI3K/AKT signaling and inactivation of p38 MAP kinase in the differentiation and survival of monocyte-derived immature dendritic cells. *Exp Hematol* (2005) 33:564–72. doi: 10.1016/j.exphem.2005.03.001
92. Jarnicki AG, Conroy H, Brereton C, Donnelly G, Toomey D, Walsh K, et al. Attenuating Regulatory T Cell Induction by TLR Agonists through Inhibition of p38 MAPK Signaling in Dendritic Cells Enhances Their Efficacy as Vaccine Adjuvants and Cancer Immunotherapeutics 1. *J Immunol* (2008) 180(6):3797–806. doi: 10.4049/jimmunol.180.6.3797
93. Cheng S, Xu C, Jin Y, Li Y, Zhong C, Ma J, et al. Artificial Mini Dendritic Cells Boost T Cell–Based Immunotherapy for Ovarian Cancer. *Adv Sci* (2020) 7:1–14. doi: 10.1002/advs.201903301
94. Long EO, Rajagopalan S. Stress signals activate natural killer cells. *J Exp Med* (2002) 196:1399–402. doi: 10.1084/jem.20021747
95. Zamai L, Ahmad M, Bennett IM, Azzoni L, Alnemri ES, Perussia B. Natural Killer (NK) Cell-mediated Cytotoxicity: Differential Use of TRAIL and Fas Ligand by Immature and Mature Primary Human NK Cells. *J Exp Med* (1998) 188:2375–80. doi: 10.1084/jem.188.12.2375

96. Li K, Mandai M, Hamanishi J, Matsumura N, Suzuki A, Yagi H, et al. Clinical significance of the NKG2D ligands, MICA/B and ULBP2 in ovarian cancer: High expression of ULBP2 is an indicator of poor prognosis. *Cancer Immunol Immunother* (2009) 58:641–52. doi: 10.1007/s00262-008-0585-3
97. Henriksen JR, Donskov F, Waldstrøm M, Jakobsen A, Hjortkjaer M, Petersen CB, et al. Favorable prognostic impact of Natural Killer cells and T cells in high-grade serous ovarian carcinoma. *Acta Oncol* (2020) 59:652–9. doi: 10.1080/0284186X.2019.1711173
98. Hoogstad-Van Evert JS, Maas RJ, van der Meer J, Cany J, van der Steen S, Jansen JH, et al. Peritoneal NK cells are responsive to IL-15 and percentages are correlated with outcome in advanced ovarian cancer patients. *Oncotarget* (2018) 9(78):34810–20. doi: 10.18632/oncotarget.26199
99. Geller MA, Cooley S, Judson PL, Ghebre R, Carson LF, Argenta PA, et al. A phase II study of allogeneic natural killer cell therapy to treat patients with recurrent ovarian and breast cancer. *Cytotherapy* (2011) 13:98–107. doi: 10.3109/14653249.2010.515582
100. Zuo S, Wen Y, Panha H, Dai G, Wang L, Ren X, et al. Modification of cytokine-induced killer cells with folate receptor alpha (FRα)-specific chimeric antigen receptors enhances their antitumor immunity toward FRα-positive ovarian cancers. *Mol Immunol* (2017) 85:293–304. doi: 10.1016/j.molimm.2017.03.017
101. Ao X, Yang Y, Li W, Tan Y, Guo W, Ao L, et al. Anti-αFR CAR-engineered NK-92 Cells Display Potent Cytotoxicity Against αFR-positive Ovarian Cancer. *J Immunother* (2019) 42(8):284–96. doi: 10.1097/CJI.0000000000000286
102. Li Y, Hermanson DL, Moriarity BS, Kaufman DS. Human iPSC-Derived Natural Killer Cells Engineered with Chimeric Antigen Receptors Enhance Anti-tumor Activity. *Cell Stem Cell* (2018) 23:181–92. doi: 10.1016/j.stem.2018.06.002
103. Ueda T, Kumagai A, Iriguchi S, Yasui Y, Miyasaka T, Nakagoshi K, et al. Non–clinical efficacy, safety and stable clinical cell processing of induced pluripotent stem cell-derived anti–glypican-3 chimeric antigen receptor-expressing natural killer/innate lymphoid cells. *Cancer Sci* (2020) 111:1478–90. doi: 10.1111/cas.14374
104. Klapdor R, Wang S, Morgan M, Dörk T, Hacker U, Hillemanns P, et al. Characterization of a novel third-generation anti-CD24-CAR against ovarian cancer. *Int J Mol Sci* (2019) 20(3):1–15. doi: 10.3390/ijms20030660
105. Lewis CE, Pollard JW. Distinct role of macrophages in different tumor microenvironments. *Cancer Res* (2006) 66:605–12. doi: 10.1158/0008-5472.CAN-05-4005
106. Mantovani A, Sozzani S, Locati M, Allavena P, Sica A. Macrophage polarization: tumor-associated macrophages as a paradigm for polarized M2 mononuclear phagocytes. *Trends Immunol* (2002) 23(11):549–55. doi: 10.1016/S1471-4906(02)02302-5
107. Zhang Q, Cai DJ, Li B. Ovarian cancer stem-like cells elicit the polarization of M2 macrophages. *Mol Med Rep* (2015) 11:4685–93. doi: 10.3892/mmr.2015.3323
108. Deng X, Zhang P, Liang T, Deng S, Chen X, Zhu L. Ovarian cancer stem cells induce the M2 polarization of macrophages through the PPARγ and NF-κB pathways. *Int J Mol Med* (2015) 36(8):449–54. doi: 10.3892/ijmm.2015.2230
109. Zhang M, He Y, Sun X, Li Q, Wang W, Zhao A, et al. A high M1/M2 ratio of tumor-associated macrophages is associated with extended survival in ovarian cancer patients. *J Ovarian Res* (2014) 7:1–16. doi: 10.1186/1757-2215-7-19
110. Yuan X, Zhang J, Li D, Mao Y, Mo F, Du W, et al. Prognostic significance of tumor-associated macrophages in ovarian cancer: A meta-analysis. *Gynecol Oncol* (2017) 147:181–7. doi: 10.1016/j.ygyno.2017.07.007
111. Lu C, Zhou L, Ouyang J, Yang H, Ding J. Prognostic value of lymphocyte-to-monocyte ratio in ovarian cancer: A meta-analysis. *Med (U S)* (2019) 98(24):1–8. doi: 10.1097/MD.0000000000015876
112. Gong J, Jiang H, Shu C, Hu MQ, Huang Y, Liu Q, et al. Prognostic value of lymphocyte-to-monocyte ratio in ovarian cancer: A meta-analysis. *J Ovarian Res* (2019) 12:1–7. doi: 10.1186/s13048-019-0527-z
113. Cao Y, Ni X, Wang Y, Wang L, Yuan K, Gan G, et al. Clinical and prognostic significance of combined plasma fibrinogen concentrations and the monocyte-to-lymphocyte ratio in patients with ovarian cancer. *Ann Trans Med* (2019) 7:242. doi: 10.21037/atm.2019.04.78
114. Cai L, Song Y, Zhao X. Prognostic significance of lymphocyte monocyte ratio in patients with ovarian cancer. *Medicine* (2020) 99:e19638. doi: 10.1097/md.0000000000019638
115. Germano G, Frapolli R, Belgiovine C, Anselmo A, Pesce S, Liguori M, et al. Role of Macrophage Targeting in the Antitumor Activity of Trabectedin. *Cancer Cell* (2013) 23:249–62. doi: 10.1016/j.ccr.2013.01.008
116. Wanderley CW, Colón DF, Luiz JPM, Oliveira FF, Viacava PR, Leite CA, et al. Paclitaxel reduces tumor growth by reprogramming tumor-associated macrophages to an M1 profile in a TLR4-dependent manner. *Cancer Res* (2018) 78:5891–900. doi: 10.1158/0008-5472.CAN-17-3480
117. Nakashima H, Miyake K, Clark CR, Bekisz J, Finbloom J, Husain SR, et al. Potent antitumor effects of combination therapy with IFNs and monocytes in mouse models of established human ovarian and melanoma tumors. *Cancer Immunol Immunother* (2012) 61:1081–92. doi: 10.1007/s00262-011-1152-x
118. Johnson CL, Green DS, Zoon KC. Human monocytes in the presence of interferons alpha2a and gamma are potent killers of serous ovarian cancer cell lines in combination with paclitaxel and carboplatin. *J Interferon Cytokine Res* (2015) 35:55–62. doi: 10.1089/jir.2014.0057
119. Green DS, Nunes AT, David-Ocampo V, Ekwede IB, Houston ND, Highfill SL, et al. A Phase 1 trial of autologous monocytes stimulated ex vivo with Sylatron ® (Peginterferon alfa-2b) and Actimmune ® (Interferon gamma-1b) for intra-peritoneal administration in recurrent ovarian cancer. *J Trans Med* (2018) 16:1–9. doi: 10.1186/s12967-018-1569-5
120. Cole CB, Annunziata CM. First-in-human phase I study of intraperitoneally administered interferon-activated autologous monocytes in platinum-resistant or refractory ovarian cancer. *J Clin Oncol* (2020) 38:1. doi: 10.1200/JCO.2020.38.5_suppl.1
121. Talmadge JE, Gabrilovich DI. History of myeloid-derived suppressor cells. *Nat Rev Cancer* (2013) 13:739–52. doi: 10.1038/nrc3581
122. Bennett JA, Rao VS, Mitchell MS. Systemic bacillus Calmette-Guerin (BCG) activates natural suppressor cells (in vitro immunization/cell-mediated immunity/suppression of immunization by non-T cells). *PNAS* (1978) 75(10):5142–4. doi: 10.1073/pnas.75.10.5142
123. Gabrilovich DI, Bronte V, Chen SH, Colombo MP, Ochoa A, Ostrand-Rosenberg S, et al. The terminology issue for myeloid-derived suppressor cells [1]. *Cancer Res* (2007) 67:425. doi: 10.1158/0008-5472.CAN-06-3037
124. Veglia F, Perego M, Gabrilovich D. Myeloid-derived suppressor cells coming of age review-article. *Nat Immunol* (2018) 19:108–19. doi: 10.1038/s41590-017-0022-x
125. Bronte V, Brandau S, Chen SH, Colombo MP, Frey AB, Greten TF, et al. Recommendations for myeloid-derived suppressor cell nomenclature and characterization standards. *Nat Commun* (2016) 7:1–10. doi: 10.1038/ncomms12150
126. Duwe~ AK, Singhal SK. The lmmunoregulatory Role of Bone Marrow I. Suppression of the Induction of Antibody Responses to T-Dependent and T-Independent Antigens by Cells in the Bone Marrow'. *Cell Immunol* (1979) 43:362–71. doi: 10.1016/0008-8749(79)90180-1
127. Young M, Young M, Wright M. Stimulation of immune-suppressive bone-marrow cells by colony-stimulating factors. *Exp Hematol* (1990) 18:806–11.
128. Kumar V, Patel S, Tcyganov E, Gabrilovich DI. The Nature of Myeloid-Derived Suppressor Cells in the Tumor Microenvironment. *Trends Immunol* (2016) 37:208–20. doi: 10.1016/j.it.2016.01.004
129. Cui TX, Kryczek I, Zhao L, Zhao E, Kuick R, Roh MH, et al. Myeloid-derived suppressor cells enhance stemness of cancer cells by inducing microRNA101 and suppressing the corepressor CTBP2. *Immunity* (2013) 39:611–21. doi: 10.1016/j.immuni.2013.08.025
130. Okła K, Czerwonka A, Wawruszak A, Bobiński M, Bilska M, Tarkowski R, et al. Clinical relevance and immunosuppressive pattern of circulating and infiltrating subsets of myeloid-derived suppressor cells (MDSCs) in epithelial ovarian cancer. *Front Immunol* (2019) 10:691. doi: 10.3389/fimmu.2019.00691
131. Wu L, Deng Z, Peng Y, Han L, Liu J, Wang L, et al. Ascites-derived IL-6 and IL-10 synergistically expand CD14 + HLA-DR-/low myeloid-derived suppressor cells in ovarian cancer patients. *Oncotarget* (2017) 8(44):76483–856. doi: 10.18632/oncotarget.20164
132. Santegoets SJAM, de Groot AF, Dijkgraaf EM, Simões AMC, van der Noord VE, van Ham JJ, et al. The blood mMDSC to DC ratio is a sensitive and easy to assess independent predictive factor for epithelial ovarian cancer survival. *OncoImmunology* (2018) 7:E1465166. doi: 10.1080/2162402X.2018.1465166

133. Baert T, Vankerckhoven A, Riva M, van Hoylandt A, Thirion G, Holger G, et al. Myeloid derived suppressor cells: Key drivers of immunosuppression in ovarian cancer. *Front Immunol* (2019) 10:1273. doi: 10.3389/fimmu.2019.01273
134. Horikawa N, Abiko K, Matsumura N, Hamanishi J, Baba T, Yamaguchi K, et al. Expression of vascular endothelial growth factor in ovarian cancer inhibits tumor immunity through the accumulation of myeloid-derived suppressor cells. *Clin Cancer Res* (2017) 23:587–99. doi: 10.1158/1078-0432.CCR-16-0387
135. Rattan R, Dar S, Rasool N, Ali-Fehmi R, Giri S, Munkarah AR. Depletion of immunosuppressive myeloid-derived suppressor cells impedes ovarian cancer growth. *Gynecol Oncol* (2017) 145:213–4. doi: 10.1016/j.ygyno.2017.03.491
136. Horikawa N, Abiko K, Matsumura N, Baba T, Hamanishi J, Yamaguchi K, et al. Anti-VEGF therapy resistance in ovarian cancer is caused by GM-CSF-induced myeloid-derived suppressor cell recruitment. *Br J Cancer* (2020) 122:778–88. doi: 10.1038/s41416-019-0725-x
137. ENCORE 603. A Phase II Randomized Study of Avelumab Plus Entinostat vs Avelumab Plus Placebo in Patients With Advanced and Recurrent Epithelial Ovarian Cancer. *JCO* (2019) 376(15 Supplemental):5511–5511. doi: 10.1200/JCO.2019.37.15_suppl.5511
138. Mikyšková R, Indrová M, Vlková V, Bieblová J, Šímová J, Paračková Z, et al. DNA demethylating agent 5-azacytidine inhibits myeloid-derived suppressor cells induced by tumor growth and cyclophosphamide treatment. *J Leukocyte Biol* (2014) 95:743–53. doi: 10.1189/jlb.0813435
139. Li Y, Hu W, Shen DY, Kavanagh JJ, Fu S. Azacitidine enhances sensitivity of platinum-resistant ovarian cancer cells to carboplatin through induction of apoptosis. *Am J Obstet Gynecol* (2009) 200:177.e1–9. doi: 10.1016/j.ajog.2008.08.030
140. Fang F, Balch C, Schilder J, Zhang S, Shen C, Li L, et al. Abstract #3593: Clinical and pharmacodynamic activity of decitabine in vivo for patients with recurrent, platinum-resistant, epithelial ovarian cancer. *Cancer Res* (2009) 69:3593.
141. Bustinza-Linares E, Falchook GS, Fu S, Naing A, Hong DS, Hu W, et al. Phase I trial of sequential azacitidine and valproic acid plus carboplatin in the treatment of patients with advanced malignancies. *J Clin Oncol* (2010) 28:2595. doi: 10.1200/jco.2010.28.15_suppl.2595
142. Nagaraj S, Gupta K, Pisarev V, Kinarsky L, Sherman S, Kang L, et al. Altered recognition of antigen is a mechanism of CD8+ T cell tolerance in cancer. *Nat Med* (2007) 13:828–35. doi: 10.1038/nm1609
143. Zeng X, Yi S. Cyclooxygenase Inhibitors in Epithelial Ovarian Cancer Treatment. *Int J Gynecol Cancer* (2018) 28:1085–9. doi: 10.1097/IGC.0000000000001269
144. Poklepovic AS, Gordon SW, McGuire WP, Thacker LR, Deng X, Tombes MB, et al. Phase I study of regorafenib and sildenafil in advanced solid tumors. *J Clin Oncol* (2020) 38:3593. doi: 10.1200/JCO.2020.38.15_suppl.3593

Conflict of Interest: The authors declare that the research was conducted in the absence of any commercial or financial relationships that could be construed as a potential conflict of interest.

frontiers in Oncology

ORIGINAL RESEARCH
published: 02 February 2021
doi: 10.3389/fonc.2020.571524

Identification of Key Gene Signatures Associated With Bone Metastasis in Castration-Resistant Prostate Cancer Using Co-Expression Analysis

Zhongxiang Yu[1†], *Hanlin Zou*[2†], *Huihao Wang*[3], *Qi Li*[4*] and *Dong Yu*[5*]

[1] Department of Orthopaedics, Shuguang Hospital Affiliated to Shanghai Traditional Chinese Medical University, Shanghai, China, [2] Department of Orthopedics, Putuo Hospital Affiliated to Shanghai Traditional Chinese Medical University, Shanghai, China, [3] Shi's Center of Orthopedics and Traumatology, Shuguang Hospital Affiliated to Shanghai Traditional Chinese Medical University, Shanghai, China, [4] Department of Oncology, Shuguang Hospital Affiliated to Shanghai Traditional Chinese Medical University, Shanghai, China, [5] Center for Translational Medicine, Second Military Medical University, Shanghai, China

About 80–90% of castration-resistant prostate cancer (CRPC) patients would develop bone metastasis. However, the molecular mechanisms of bone metastasis are still not clear. This study aimed to detect the differences between the tumor and normal samples in bone after metastatic colonization. Four transcriptional datasets (GSE32269, GSE101607, GSE29650, and GSE74685) were obtained from the GEO database. 1983 differentially expressed genes (DEGs) were first identified between tumor and normal marrow samples in GSE32269. Most of the top 10 up-regulated DEGs are related with prostate cancer, and the top 10 down-regulated DEGs are mainly related with bone development. Seven co-expression modules were then detected based on the 1469 DEGs shared by the four datasets. Three of them were found highly preserved among the four datasets. Enrichment analysis showed that the three modules were respectively enriched in Cell adhesion molecules (CAMs), Leukocyte transendothelial migration and cell cycle, which might play significantly important roles in the tumor development in bone marrow. Ten, 17, and 99 hub genes for each module were then identified. And four genes (C3AR1, IL10RA, LY86, and MS4A6A) were detect to be tightly related to progression of bone metastatic CRPC. ROC curve was plotted and AUC was calculated to distinguish tumor and normal bone marrow samples as well as bone and non-bone metastatic CRPCs. The present study identified key genes and modules involved in bone metastatic CRPCs, which may provide new insights and biomarkers for understanding of the molecular mechanisms of bone metastatic CRPC.

Keywords: bone metastatic CRPC, differentially expressed genes, weighted gene co-expression network analysis, module, hub genes

OPEN ACCESS

Edited by:
Giuseppe Giaccone, Cornell University, United States

Reviewed by:
Paul B. Fisher, Virginia Commonwealth University, United States
Marco Rossi, University of Catanzaro, Italy

***Correspondence:**
Dong Yu
yudong615@126.com
Qi Li
lzwf@hotmail.com

†These authors have contributed equally to this work

Specialty section:
This article was submitted to Cancer Molecular Targets and Therapeutics, a section of the journal Frontiers in Oncology

Received: *11 June 2020*
Accepted: *14 December 2020*
Published: *02 February 2021*

Citation:
Yu Z, Zou H, Wang H, Li Q and Yu D (2021) Identification of Key Gene Signatures Associated With Bone Metastatic Samples in Castration-Resistant Prostate Cancer Using Co-Expression Analysis. Front. Oncol. 10:571524. doi: 10.3389/fonc.2020.571524

INTRODUCTION

Prostate cancer (PCa) is one of the most common cancers and the tenth most common cause of cancers related mortality in men in China (1). The rankings rise first in men in the developed countries (2). Castration-resistant prostate cancer (CRPC) is an advanced form of prostate cancer by disease progression following surgical or pharmaceutical castration. This process is not inevitable, which is usually companied by poor prognosis and reduced survival time. To be known, CRPC patients are also at high risk of developing metastases. The common sites are bone, lymph nodes, liver, lungs and brain. Bone is the most prominent site for metastases. About 80–90% of CRPC patients develop bone metastases (3). Bone metastases could lead to the disorder of bone metabolism and induce skeletal related events (SREs), such as pathological fracture, spinal cord compression and hypercalcemia, which not only reduce survival time and life quality, but also increase burden of treatment (4).

However, the molecular mechanisms of bone metastases are still not clear. A widely accepted mechanism is the 'seed and soil hypothesis', which describes an interaction between circulating tumor cell and microenvironment of bone tissue (5). The communication between bone and cancer cells is believed to be critical for the development and progression of bone metastases (6, 7). Most of researches focus on dissecting the process of initiation to development of distant metastasis, such as cancer cells migrating through the endothelial cells to gain access to systemic circulation *via* the tortuous and leaky tumor vasculature and cell signaling aberrations (8, 9). A set of marked differences were identified between metastases and primary tumors and the subgroups of bone metastasis were also detected by transcriptome or proteome analysis (10–12). In addition, David A. Quigley et al. explore the genomic hallmarks and structural variation in metastatic PC, including bone metastatic CRPCs (13). However, these researches do not pay more attention on the state of tumor cells after metastatic colonization and also do not explore the differences between the tumor cells and normal cells in bone. This study aimed to identify the differences between tumor and normal bone marrow samples through differential expression analysis and weighted gene co-expression analysis. The identified key genes and modules will provide new insights for understanding of the molecular mechanisms and clinical treatment for bone metastatic CRPC.

METHODS

Data Collection and Preprocessing

Four expression profile datasets containing CRPC bone metastasis were downloaded from the GEO database (https://www.ncbi.nlm.nih.gov/geo). Dataset GSE32269 was chosen for further analysis with 29 CRPC bone metastatic marrow samples and four normal bone marrow samples, which was used for bone cancer significantly expressed genes selection and correlated modules detection. The other three datasets GSE101607, GSE29650, and GSE74685 were kept with only CRPC bone metastatic samples, which was used to validate and screen the truly significant and preserved bone cancer related modules. Detailed information of datasets was shown in **Table 1**.

Before the analysis, all the raw data were reprocessed. Probes were mapped to the gene symbols. Empty probes and probes mapping to multiple genes were both discarded according to each annotation platform. If there were multiple probes that mapped to the same gene symbol, their mean values were considered as the gene expression value. The reprocessed data was normalized by the limma (linear models for microarray data) package in R (14).

Identification of Differentially Expressed Genes

The eBayes analysis was used to detect the differentially expressed genes (DEGs) between metastatic bone marrow samples and normal marrow samples in GSE32269 using limma package (14). The adjusted P-value <0.05 and |log-fold change|>1 were set as the threshold for DEGs screening.

Enrichment Analysis

R package clusterProfiler (15) was used for the Enrichment analysis. False discovery rate (FDR) < 0.05 was set as the threshold for the identification of significant GO-Enrichment terms and Pathway-Enrichment terms.

WGCNA Analysis

The co-expression network analysis was performed using weighted gene co-expression network analysis (WGCNA) (16). First, the soft threshold for network construction was selected, which is the lowest power for which the scale-free topology fit index curve flattens out upon reaching a high value. Second, the function blockwiseModules was used for one-step network construction and module detection. The module eigengene (ME) of each module and the correlation between MEs was then calculated. Thirdly, module preservation was calculated between GSE32269 and the other three datasets using the function modulePreservation (17). The comparability of two datasets is assessed by correlating measures of average gene expression and overall connectivity of two datasets. The higher the correlations of these properties, the better chance you will have of finding similarities between the two datasets at subsequent stages of analysis. Fourthly, the key node (hub gene) was determined by high intramodule connectivity of genes. The cut-off criteria was set |cor.geneModuleMembership| > 0.8. According to the intramodule connectivity, the detected hub genes were visualized using VisANT software (18). Finally, the study (19) containing mRNA and clinical data of 444 metastatic CRPC samples was used to validate the hub genes and subjected to survival analysis. The database GEPIA2 containing TCGA datasets (20) and the database Oncomine containing cancer microarray datasets (21) were used to validate the expression levels of hub genes.

Abbreviations: CRPC, Castration-Resistant Prostate Cancer; DEG, Differentially Expressed Gene, WGCNA, Weighted Gene Correlation Network Analysis; ME, module eigengene.

TABLE 1 | Datasets of gene expression profiles.

GEO accession	Platform	Probe number	Total sample number	CRPC bone metastasis sample number	Normal bone sample number
GSE32269	GPL96	22283	55	29	4
GSE101607	GPL10558	48107	60	40	0
GSE29650	GPL6947	49576	30	30	0
GSE74685	GPL15659	38695	149	20	0

RESULTS

DEG Identification for CRPC Bone Metastatic Patients

In order to detect the transcriptomic differences between CRPC bone metastatic marrow samples and normal marrow samples, the dataset GSE32269 with 29 CRPC bone metastatic marrow samples and four normal bone marrow samples was selected and downloaded from GEO databases. DEGs were identified using the limma package. 1983 DEGs were screened with the threshold of |logFC|>1 and p.adjust<0.05, as shown in >>**Figure 1A**, which contains 825 up-regulated genes and 1158 down-regulated genes for bone metastatic marrow samples (see **Supplementary Table 1**). The top 10 significantly expressed genes are KLK3, KRT18,

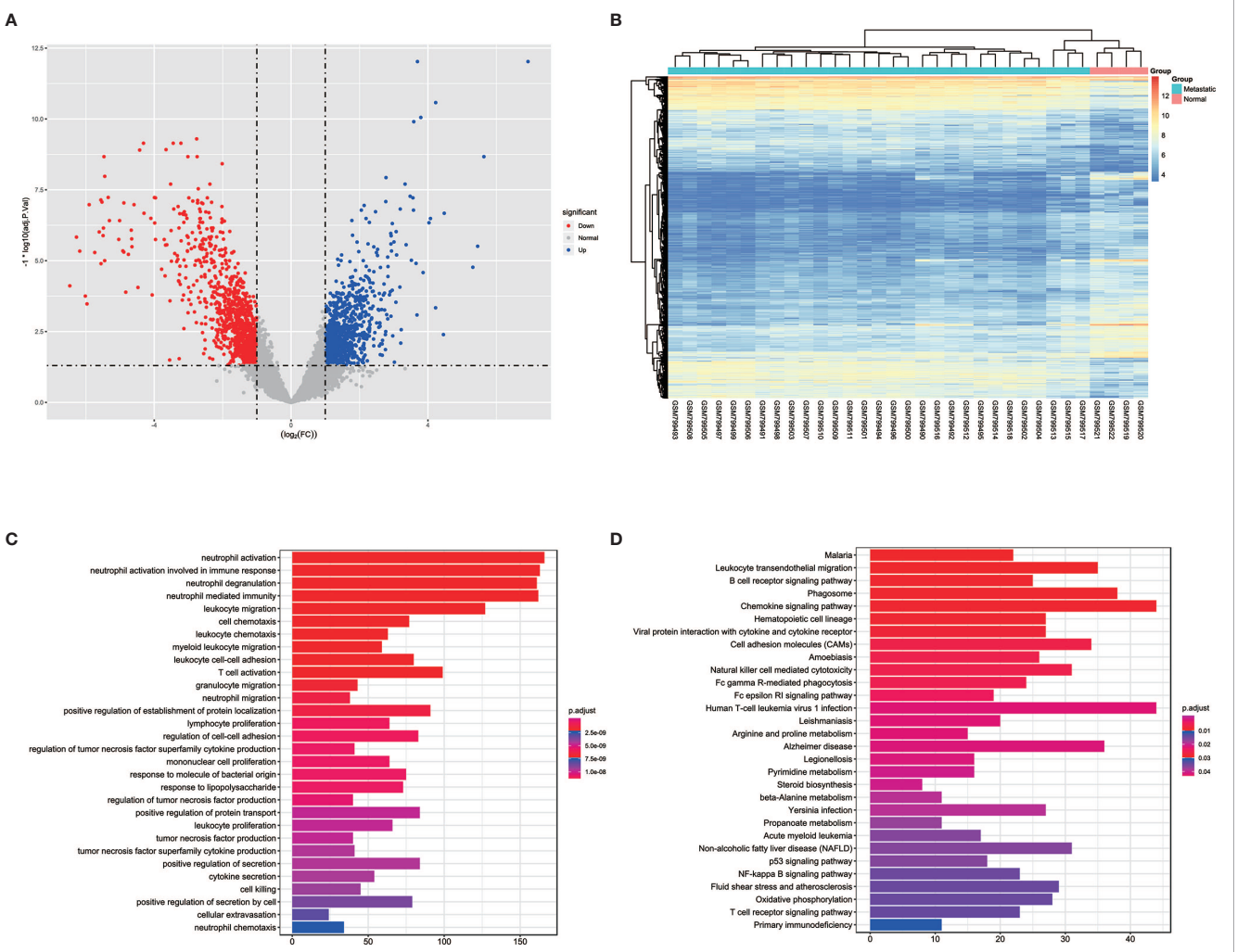

FIGURE 1 | The volcano, heatmap, GO and KEGG enrichment results of differentially expressed genes (DEGs) between tumor and normal cells in bone. **(A)** The volcano plot for DEGs. Grey dots represent genes which are not differentially expressed, red dots represent the upregulated genes, and the blue dots represent the downregulated genes. **(B)** The heatmap for DEGs. **(C)** The annotation of gene ontology function of DEGs using GO enrichment analysis. **(D)** The annotation of pathway function of DEGs using KEGG enrichment analysis.

EFNA1, SLC396A, NKX3-1, PGLYRP1, MGAM, RHD, GFI1, FAR2, of which the first five are up-regulated and the following five are down-regulated. The expression profiles of these DEGs were showed as a heatmap in **Figure 1B**. Enrichment analysis was further conducted. The result was shown in **Figures 1C, D**. The most enriched GO terms are neutrophil and leukocyte-associated terms. The top5 pathway terms are Malaria, Leukocyte transendothelial migration, B cell receptor signaling pathway, phagosome and chemokine signaling pathway.

WGCNA Analysis

Since the four datasets come from different platforms, we should ensure that the four datasets are comparable. First, we need to limit the analysis to genes that expressed among the datasets. The intersection was taken among the DEGs of GSE32269 and the genes of other three datasets. 1469 genes were selected, and the corresponding expression profiles of these genes in four datasets were then prepared. Second, the comparability of GSE32269 and other dataset was assessed by measuring the average gene expression and overall connectivity between two datasets (**Figure 2**). It's clear to see that the correlations are positive and the p-value are significant in all cases, which suggests that the datasets are comparable.

Prior to gene co-expression network detection, the analysis of network topology for various soft-thresholding powers was performed to obtain relative balanced scale independence and mean connectivity. As shown in **Figure 3A**, power seven was the lowest power for which the scale-free topology fit index reaches 0.85. Based on this power, seven modules were generated as shown in **Figure 3B**. The largest module was the turquoise module, which contained 585 genes, the smallest module was the black module containing 49 genes. Averagely, each module contained 183 genes.

Enrichment analysis was further performed to detect biological significance of each module as listed in **Supplementary Table 2**. In the top 5 terms of each module,

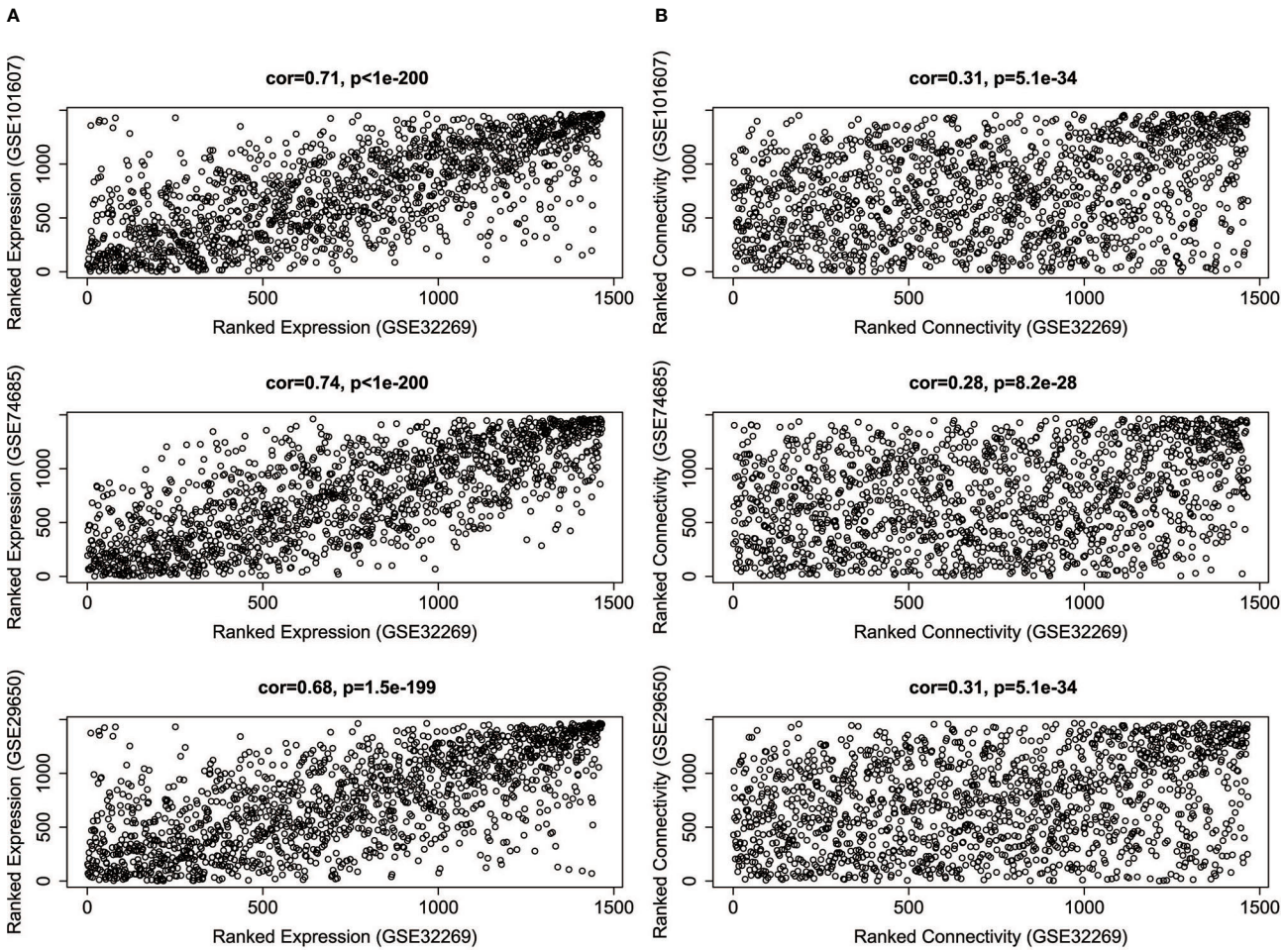

FIGURE 2 | The correlations of average gene expression **(A)** and overall connectivity **(B)** between GSE32269 and other three datasets (GSE101607, GSE74685, GSE29650).

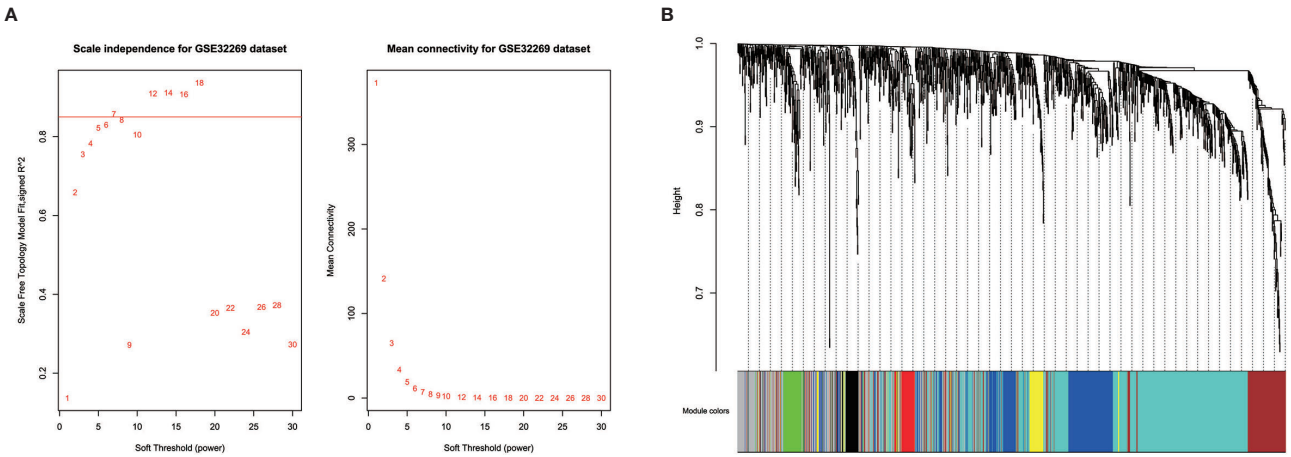

FIGURE 3 | Identification of modules in the dataset GSE32269. **(A)** Network topology of different soft-thresholding powers. The left panel displays the influence of soft-thresholding power (x-axis) on scale-free fit index (y-axis). The right panel shows the influence of soft-thresholding power (x-axis) on the mean connectivity (degree, y-axis). **(B)** Clustering dendrogram showing eight modules that contain a group of highly connected genes. Each designated color represents a certain gene module.

Yellow, Turquoise and Brown module were mainly enriched in neutrophil-associated GO terms, which were all related with leukocyte mediated immunity. Red module had no significantly enriched pathways. Yellow and brown module shared an enriched pathway term, named Osteoclast differentiation, which is related with bone development. It's worth noting that turquoise enriched pathways contain a set of signaling pathways, such as B cell receptor signaling pathway, chemokine signaling pathway, NF-kappa B signaling pathway, Fc epsilon RI signaling pathway and hematopoietic cell lineage. These are reported to be related with tumorigenesis. In the yellow module enriched pathways, Cell adhesion molecules are related with cancer invasion and metastasis. The green module is enriched with cell cycle-associated pathways.

Module Validation Among the Other Three Datasets

In order to detect whether these modules are preserved between the other three datasets, module preservation statistics were calculated using the function modulePreservation. The preservation Z-summaries was showed in **Figure 4**. We set the threshold Z>10 to screen the highly preserved modules. 3, 4, and 5 modules are separately found to be preserved in the dataset GSE29650, GSE74685 and GSE101607. And three modules (green, yellow, and turquoise) are shared and highly preserved in the three datasets, which were chosen for subsequent analysis.

Identification and Validation of Hub Genes

10, 17 and 99 hub genes were separately identified in the three preserved modules (Green, Yellow, Turquoise). The corresponding networks of hub genes were showed in **Figure 5**. The study containing mRNA data followed clinical information of 160 bone metastatic CRPC samples and 284 non-bone metastatic CRPC samples were subjected to survival analysis and regression analysis. Four hub genes (C3AR1, IL10RA, LY86, and MS4A6A) were identified to significantly associated with the overall survival (**Figure 6**). The patients with lower expression of the genes had a longer survival. However, the four genes have significantly higher expression level in bone compared to other non-bone metastatic tissues as showed in **Figure 7**. In CRPC patients with metastases, the bone metastases have the worst median progression to non-bone tissues metastases (22).

In addition, ROC curve analysis was implemented to evaluate the capacity of the hub genes to distinguish bone and non-bone metastatic tissues. AUC values for the four genes were greater than 0.6 (**Figure 8**).

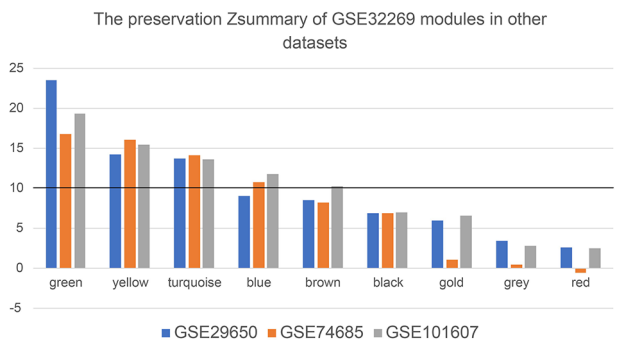

FIGURE 4 | The preservation Zsummary values of eight GSE32269 modules in other datasets (GSE29650, GSE74685 and GSE101607). The black horizontal line is the threshold to define the highly preserved modules among the four datasets.

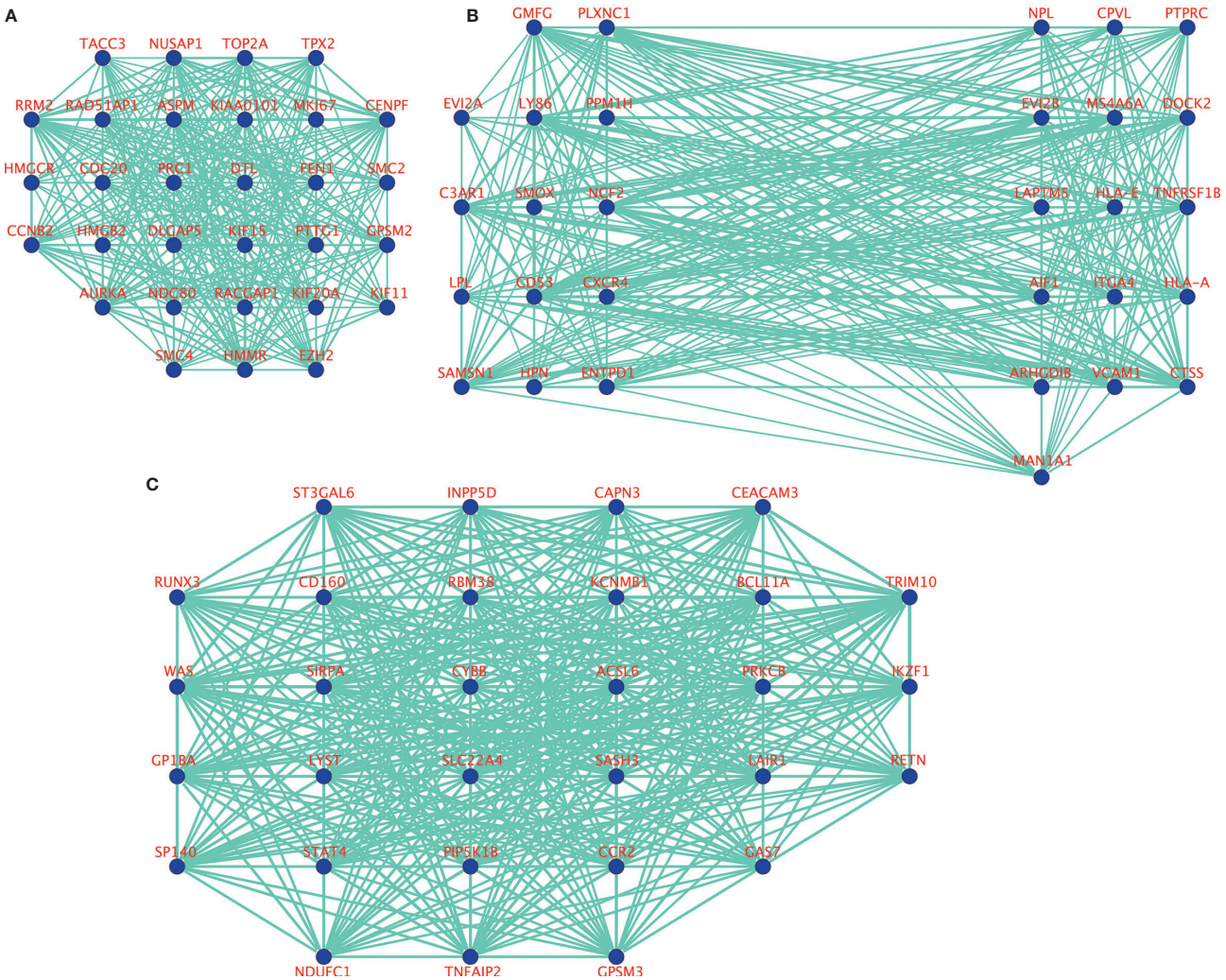

FIGURE 5 | The visualization of hub genes in green module **(A)**, yellow module **(B)**, and turquoise module **(C)**.

DISCUSSION

Development of bone metastases is a key and usual event in the progression of CRPC, which could lead to disorders of bone metabolism and skeletal related events. The median survival form men with bone metastases CRPC is approximately 1.5–2 years. The purpose of this study was to dissect the expression profile differences between the established metastatic tumor and normal bone marrow samples and then identified some key gene signatures and modules based on co-expression network analysis. These results will be helpful to deeply understand the molecular mechanisms of bone metastases and also provide candidate biomarkers for the prognosis prediction of bone metastatic CRPC patients.

The screened DEGs are found to be mainly related with prostate cancer and bone development. For example, among the top 10 up-regulated genes, KLK3 and KLK2, are highly enriched in prostate cancer, which are taken as effective biomarkers for diagnose and prognostic monitoring of prostate cancer (23). GOLM1 (24), FOLH1B (25), STEAP1 (26) and PLPP1 (27) are also identified as a candidate biomarker for prostate cancer. AGR2 expresses strongly in prostate tissue and show increased expression in prostate cancer (28). In a word, the up-regulated genes are mainly related with the tumorigenesis of prostate cancer. As for the top10 down-regulated genes, all of them are identified to be overexpressed in whole blood according to GTEx (29) and take part in embryonic development of blood and bone according to LifeMap Discovery (30). Therefore, the down-regulation of these genes would have effects on the function of bone or bone marrow, which might be genetic causes of SKE. These results indicated that the colonization in bone of metastatic CRPC cells not only keep the expression features of prostate cancer, but also induce new expression variations associated with bone. In another way, these results suggest the

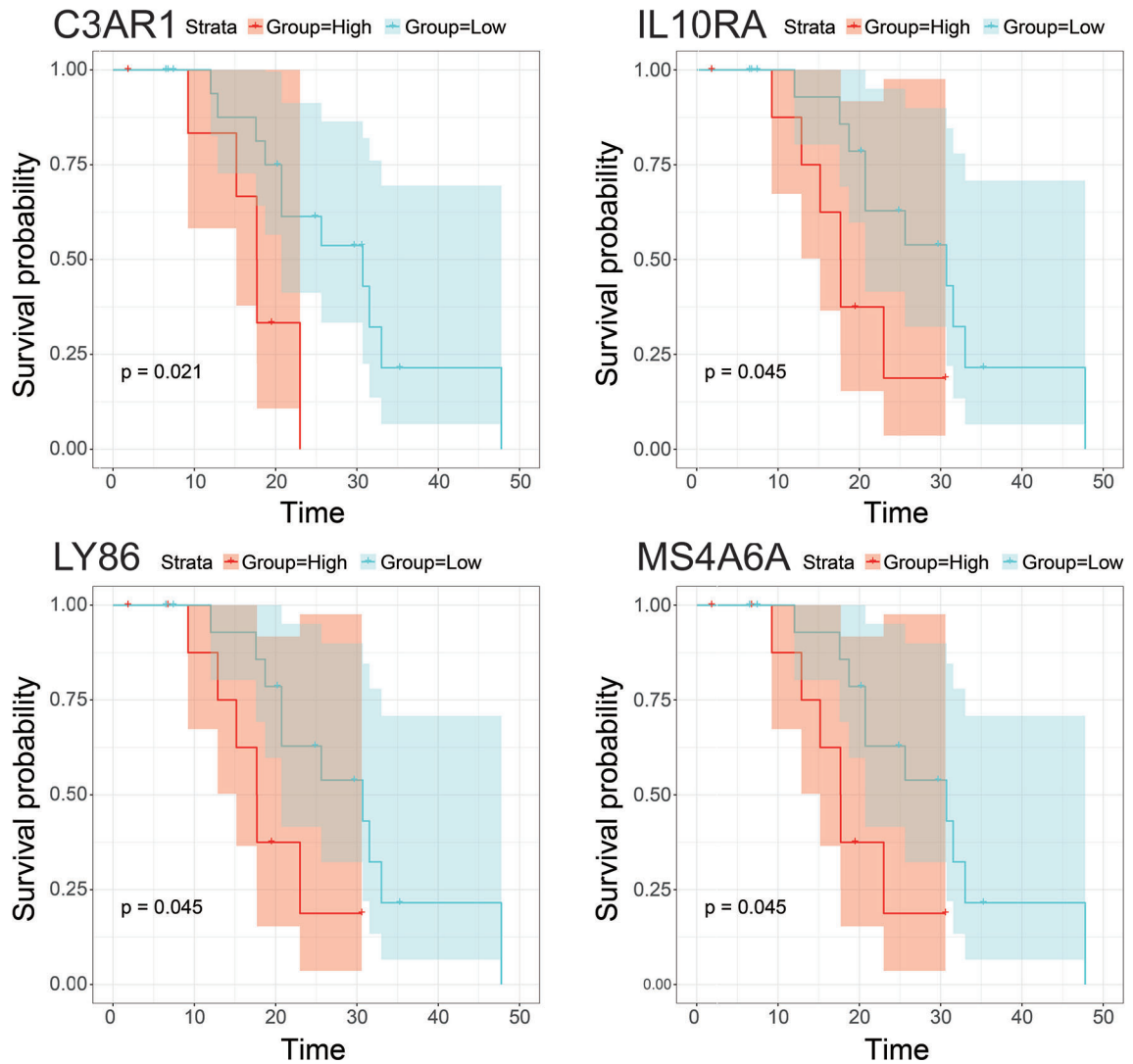

FIGURE 6 | Survival analysis of hub gens with statistical significance (pvalue<0.05) in the dataset derived from Abida W's study. Orange lines represent high expression of the hub genes and blue lines represent low expression.

tissue specificity of DEGs, and the reliability of our results. Therefore, it is important to further dissect the expression differences between the established tumor and the normal bone marrow samples.

After a series of bioinformatic analysis, four hub genes identified from the three highly preserved co-expression modules among the four datasets were found to be tightly associated with overall survival in bone metastases CRPC patients. At present, there are no direct evidences to verify the functions of the four genes in prostate cancer or bone metastatic CRPC, but a set of researches showed that these genes were involved in the tumorigenesis and tumor proliferation in other cancers. It was shown that C3AR1 was significantly correlated with the overall survival In glioblastoma, which showed a longer survival time in the patients with lower expression of C3AR1 (31). In a recent study, over-expression of C3AR1 was proved to promotes HL-60 cell migration and invasion *in vitro* experiment (32). In other words, down-expression might decrease the migration and invasion capacities of tumor cells. Moreover, C3a, which binds to an orphan G protein-coupled receptor encoded by C3AR1, was reported as an immune regulator in the tumor microenvironment and act as insidious propagators of tumor growth and progression (33). In this respect, the down-regulation of C3AR1 might inhibit the process of tumor growth and progression. Therefore, these may be the reasons why the patients with lower expression of C3AR1 had good prognosis. IL10RA encodes a receptor for interleukin 10, which can inhibit the synthesis of proinflammatory cytokines. In colorectal cancer,

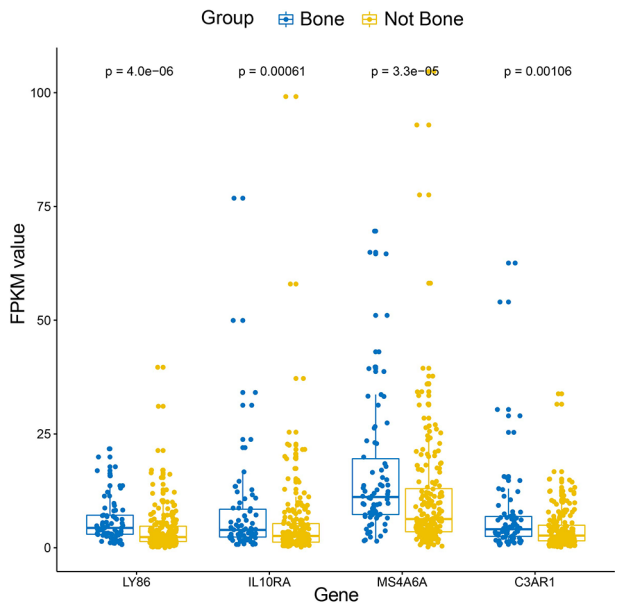

FIGURE 7 | Box-plot of expression values (FPKM) of the four hub genes between bone and non-bone tissues in the metastatic CRPC patients derived from Abida W's study.

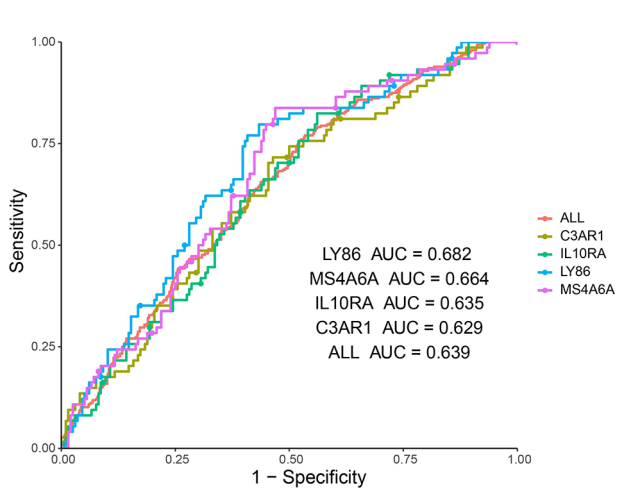

FIGURE 8 | ROC analysis of four hub genes in the dataset derived from Abida W's study. Receiver operating characteristic (ROC) curves and area under the curve (AUC) statistics is to evaluate the capacity of distinguishing bone and non-bone metastatic tissues in the metastatic CRPC patients.

the expression of IL10RA is found to be higher in healthy tissue than in the CRC tissue and showed association with the proliferation index, confirming the importance of IL10RA in the pathogenesis of CRC (34). However, increased level of IL10RA in the study population was not linked with overall survival time. In diffuse large B-cell lymphoma, IL10 receptor is highly expressed and predicts worse survival (35). Functional experiment showed that IL10 receptor plays an important role in IL10-JAK-STAT signaling pathway. Blocking IL10R would interrupt the IL10 autostimulatory loop and lead to cell death through cell cycle arrest and introduction of apoptosis. LY86 encodes the lymphocyte antigen 86, which may cooperate with CD180 and TLR4 to mediate the innate immune response to bacterial lipopolysaccharide (LPS) and cytokine production. LY86 was identified as a novel biomarker for the prediction of osteosarcoma prognosis and therapeutic targets (36). Moreover, healthy hematopoietic stem progenitor cells (HSPCs) can be transformed genetically by leukemia macrovesicles to over express LSC specific genes, which contains LY86, LRG1 and PDE9A and so on (37). These suggests that LY86 might play an important role in the transformation of localized normal bone marrow cells to cancer cells. MS4A6A encodes a member of the membrane-spanning 4A gene family, which display unique expression patterns among hematopoietic cells and nonlymphoid tissues. GWAS researches showed that MS4A6A is associated with heel bone mineral density and Alzheimer's disease (38). MS4A6A was reported to be highly expressed in putative Tumor-associated macrophages (TAMs) populations. Previous reports suggest that TAMs may show an immunosuppressive M2 signature, which promotes tumorigenesis by suppressing immune surveillance and inducing angiogenesis, rather that the activating M1-type signature (39). In addition, a recent study found that high expression of MS4A6A was associated with poor progression-free survival of ovarian cancer (40), which is consistent with the result of this study. Therefore, this gene might take an important role in the colonization of metastatic cancer cells in bone marrow and tumorigenesis of localized bone marrow cells. In above-mentioned studies, high expression of the four genes are all significantly associated with poor prognosis, which is consistent with the performances. These will serve as important references to explore the molecular mechanisms of the genes on bone metastatic CRPC.

In our results, the four genes were all down-regulated in tumor bone marrow samples compared to the normal samples, which was different from the performances in other tumors described above, However, the four genes present consistency trends as this study in the lung squamous cell carcinoma according to TCGA datasets (20). Some of the four genes were also lowly expressed in ACC, COAD or DLBC (**Figure 9**). We also made a search of the four genes in Oncomine database (21) with parameters (Analysis Type: Differential analysis, Cancer vs. Normal analysis, Prostate cancer vs. Normal analysis; Data Type: mRNA). The results showed that these genes have no differences in expression between tumor and normal samples in most of prostate cancer datasets as listed in the **Figure 10**, which is consistent with the result in the TCGA prostate cancer dataset.

At present, a growing number of researches focus on the communication between tumor cells and bone stroma (41). Existing discoveries show that a vicious cycle of molecular crosstalk between tumor cells and the bone metastatic niche often take place in osteolytic bone metastasis (42). Targeting the bone metastatic niche is also evolving into a promising avenue for the prevention of bone metastatic relapse, therapeutic resistance, and other aspects of cancer progression (43–45).

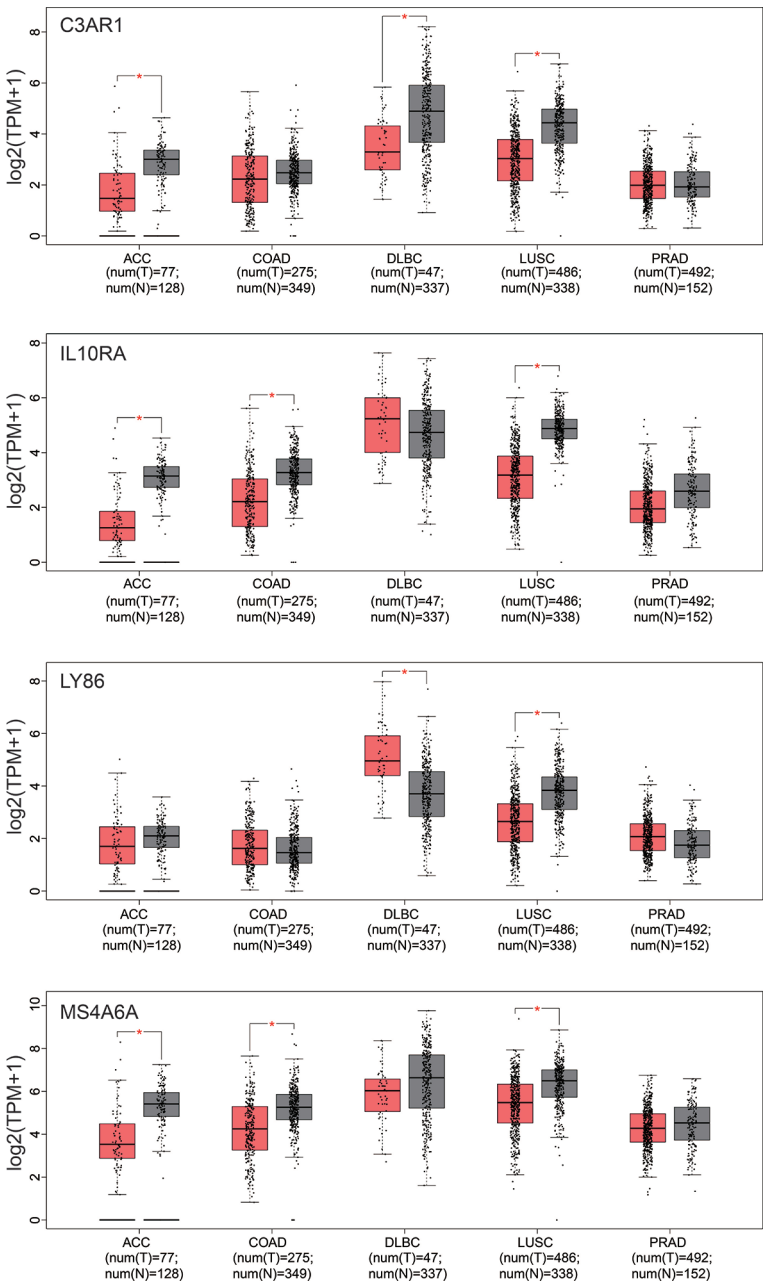

FIGURE 9 | Box-plot of expression values (TMP) of the four hub genes between tumor and normal samples derived from the TCGA datasets. ACC, Adrenocortical carcinoma; COAD, Colon adenocarcinoma; DLBC, Lymphoid Neoplasm Diffuse Large B-cell Lymphoma; LUSC, Lung squamous cell carcinoma; PRAD, Prostate adenocarcinoma. Differential analysis between tumor and normal group was conducted using one-way ANOVA method. *pvalue < 0.05.

Therefore, it is meaningful and important to dissect the differences between tumor cells and bone metastatic niche at different level, including transcriptome, which will be essential to explore the molecular mechanisms or interaction underlying the bone metastases and new clinical practice. Based on this consideration, this study has creatively used public data to dissect the expression differences between established tumor and normal bone marrow samples derived CRPCs. The first screened DEGs were involved in prostate cancer and bone development. And the followed illustrated four hub genes are not only associated with overall survival of bone metastatic CRPC samples, but also be capable of distinguishing bone metastases and non-bone metastases. These findings would greatly provide new insights and biomarkers for understanding of the molecular mechanisms and clinical treatment for bone metastatic CRPC.

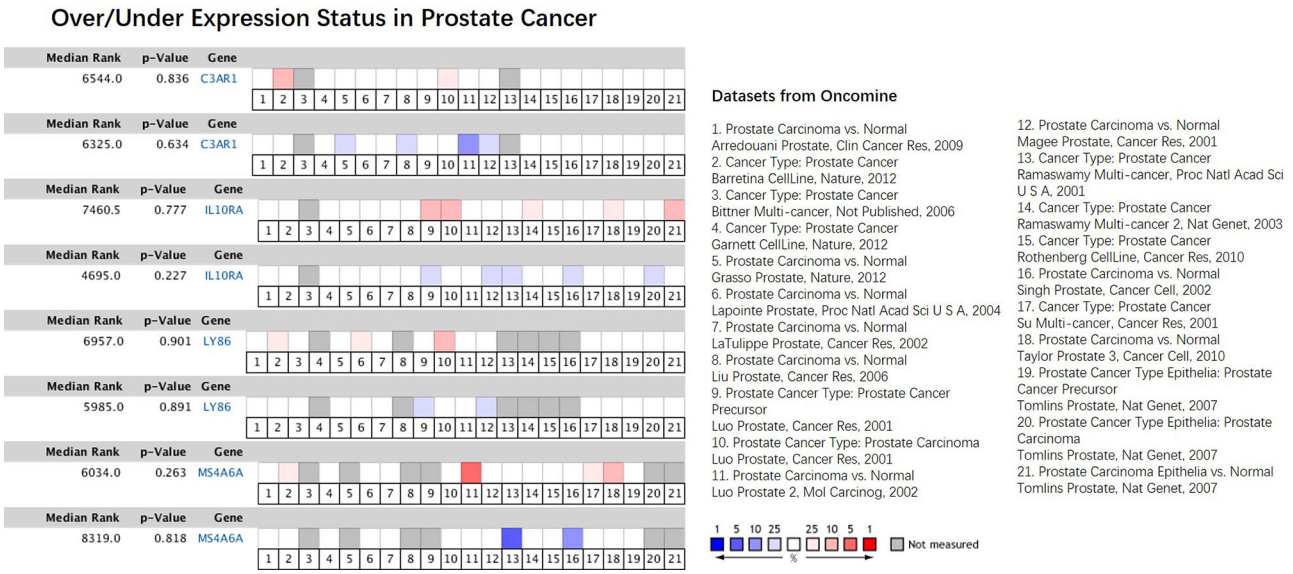

FIGURE 10 | Comparison of the four hub genes across 21 analyses of prostate cancer datasets. The colored box denotes the gene's percentile rank for that analyses. The more saturated the color, the higher the percentile rank. Red denotes over-expression; blue denotes under-expression. The datasets were listed on the right.

DATA AVAILABILITY STATEMENT

Publicly available datasets were analyzed in this study, these can be found in here: the NCBI Gene Expression Omnibus (GSE32269, GSE101607, GSE29650 and GSE74685).

AUTHOR CONTRIBUTIONS

ZY and DY designed the study and drafted the manuscript. ZY, HZ, and HW performed all the data analysis. HW helped the preparation of figures and tables. QL and DY contributed to the writing of the manuscript. All authors contributed to the article and approved the submitted version.

FUNDING

This work was supported by Shanghai University of Traditional Chinese Medicine research grants (18LK038). The funders had no role in study design, data collection and analysis, decision to publish, or preparation of the manuscript.

ACKNOWLEDGMENTS

This manuscript has been released as a pre-print at Research Square (46).

SUPPLEMENTARY MATERIAL

The Supplementary Material for this article can be found online at: https://www.frontiersin.org/articles/10.3389/fonc.2020.571524/full#supplementary-material

Supplementary Table 1 | All the differentially expressed genes between metastatic tumor and normal bone marrow samples in GSE32269.

Supplementary Table 2 | GO and KEGG enrichment analysis results for each module.

REFERENCES

1. Chen W, Zheng R, Baade PD, Zhang S, Zeng H, Bray F, et al. Cancer statistics in China, 2015. *CA Cancer J Clin* (2016) 66:115–32. doi: 10.3322/caac.21338
2. Siegel RL, Miller KD, Jemal A. Cancer statistics, 2016. *CA Cancer J Clin* (2016) 66:7–30. doi: 10.3322/caac.21332
3. Wirth M, Tammela T, Cicalese V, Gomez Veiga F, Delaere K, Miller K, et al. Prevention of bone metastases in patients with high-risk nonmetastatic prostate cancer treated with zoledronic acid: efficacy and safety results of the Zometa European Study (ZEUS). *Eur Urol* (2015) 67:482–91. doi: 10.1016/j.eururo.2014.02.014
4. Sathiakumar N, Delzell E, Morrisey MA, Falkson C, Yong M, Chia V, et al. Mortality following bone metastasis and skeletal-related events among men with prostate cancer: a population-based analysis of US Medicare beneficiaries, 1999-2006. *Prostate Cancer Prostatic Dis* (2011) 14:177–83. doi: 10.1038/pcan.2011.7

5. Pedersen EA, Shiozawa Y, Pienta KJ, Taichman RS. The prostate cancer bone marrow niche: more than just 'fertile soil'. *Asian J Androl Asian J Androl* (2012) 14:423–7. doi: 10.1038/aja.2011.164
6. Hiraga T. Bone metastasis: Interaction between cancer cells and bone microenvironment. *J Oral Biosci* (2019) 61:95–8. doi: 10.1016/j.job.2019.02.002
7. Zheng Y, Zhou H, Dunstan CR, Sutherland RL, Seibel MJ. The role of the bone microenvironment in skeletal metastasis. *J Bone Oncol* (2013) 2:47–57. doi: 10.1016/j.jbo.2012.11.002
8. Wan LL, Pantel K, Kang YB. Tumor metastasis: moving new biological insights into the clinic. *Nat Med Nat Med* (2013) 19:1450–64. doi: 10.1038/nm.3391
9. Weis SM, Cheresh DA. Tumor angiogenesis: molecular pathways and therapeutic targets. *Nat Med Nat Med* (2011) 17:1359–70. doi: 10.1038/nm.2537
10. Ylitalo EB, Thysell E, Jernberg E, Lundholm M, Crnalic S, Egevad L, et al. Subgroups of Castration-resistant Prostate Cancer Bone Metastases Defined Through an Inverse Relationship Between Androgen Receptor Activity and Immune Response. *Eur Urol* (2017) 71:776–87. doi: 10.1016/j.eururo.2016.07.033
11. Iglesias-Gato D, Thysell E, Tyanova S, Crnalic S, Santos A, Lima TS, et al. The Proteome of Prostate Cancer Bone Metastasis Reveals Heterogeneity with Prognostic Implications. *Clin Cancer Res Clin Cancer Res* (2018) 24:5433–44. doi: 10.1158/1078-0432.CCR-18-1229
12. Djusberg E, Jernberg E, Thysell E, Golovleva I, Lundberg P, Crnalic S, et al. High levels of the AR-V7 Splice Variant and Co-Amplification of the Golgi Protein Coding YIPF6 in AR Amplified Prostate Cancer Bone Metastases. *Prostate* (2017) 77:625–38. doi: 10.1002/pros.23307
13. Quigley DA, Dang HX, Zhao SG, Lloyd P, Aggarwal R, Alumkal JJ, et al. Genomic Hallmarks and Structural Variation in Metastatic Prostate Cancer. *Cell* (2018) 175:889. doi: 10.1016/j.cell.2018.10.019
14. Ritchie ME, Phipson B, Wu D, Hu Y, Law CW, Shi W, et al. limma powers differential expression analyses for RNA-sequencing and microarray studies. *Nucleic Acids Res* (2015) 43:e47. doi: 10.1093/nar/gkv007
15. Yu G, Wang LG, Han Y, He QY. clusterProfiler: an R package for comparing biological themes among gene clusters. *OMICS* (2012) 16:284–7. doi: 10.1089/omi.2011.0118
16. Langfelder P, Horvath S. WGCNA: an R package for weighted correlation network analysis. *BMC Bioinf* (2008) 9:559. doi: 10.1186/1471-2105-9-559
17. Langfelder P, Luo R, Oldham MC, Horvath S. Is my network module preserved and reproducible? *PloS Comput Biol* (2011) 7:e1001057. doi: 10.1371/journal.pcbi.1001057
18. Hu ZJ, Chang YC, Wang Y, Huang CL, Liu Y, Tian F, et al. VisANT 4.0: Integrative network platform to connect genes, drugs, diseases and therapies. *Nucleic Acids Res Nucleic Acids Res* (2013) 41:W225–31. doi: 10.1093/nar/gkt401
19. Abida W, Cyrta J, Heller G, Prandi D, Armenia J, Coleman I, et al. Genomic correlates of clinical outcome in advanced prostate cancer. *Proc Natl Acad Sci U.S.A.* (2019) 116:11428–36. doi: 10.1073/pnas.1902651116
20. Tang Z, Kang B, Li C, Chen T, Zhang Z. GEPIA2: an enhanced web server for large-scale expression profiling and interactive analysis. *Nucleic Acids Res* (2019) 47:W556–60. doi: 10.1093/nar/gkz430
21. Rhodes DR, Yu J, Shanker K, Deshpande N, Varambally R, Ghosh D, et al. ONCOMINE: a cancer microarray database and integrated data-mining platform. *Neoplasia* (2004) 6:1–6. doi: 10.1016/s1476-5586(04)80047-2
22. Koo KC, Park SU, Kim KH, Rha KH, Hong SJ, Yang SC, et al. Prognostic Impacts of Metastatic Site and Pain on Progression to Castrate Resistance and Mortality in Patients with Metastatic Prostate Cancer. *Yonsei Med J* (2015) 56:1206–12. doi: 10.3349/ymj.2015.56.5.1206
23. Fagerberg L, Hallström BM, Oksvold P, Kampf C, Djureinovic D, Odeberg J, et al. Analysis of the human tissue-specific expression by genome-wide integration of transcriptomics and antibody-based proteomics. *Mol Cell Proteomics* (2014) 13:397–406. doi: 10.1074/mcp.M113.035600
24. Varambally S, Laxman B, Mehra R, Cao Q, Dhanasekaran SM, Tomlins SA, et al. Golgi protein GOLM1 is a tissue and urine biomarker of prostate cancer. *Neoplasia* (2008) 10:1285–94. doi: 10.1593/neo.08922
25. Zhang Z, Wu H, Zhou H, Gu Y, Bai Y, Yu S, et al. Identification of potential key genes and high-frequency mutant genes in prostate cancer by using RNA-Seq data. *Oncol Lett* (2018) 15:4550–6. doi: 10.3892/ol.2018.7846
26. Gomes IM, Arinto P, Lopes C, Santos CR, Maia CJ. STEAP1 is overexpressed in prostate cancer and prostatic intraepithelial neoplasia lesions, and it is positively associated with Gleason score. *Urol Oncol* (2014) 32:53 e23–9. doi: 10.1016/j.urolonc.2013.08.028
27. Uhlen M, Zhang C, Lee S, Sjostedt E, Fagerberg L, Bidkhori G, et al. A pathology atlas of the human cancer transcriptome. *Science* (2017) 357(6352). doi: 10.1126/science.aan2507
28. Maresh EL, Mah V, Alavi M, Horvath S, Bagryanova L, Liebeskind ES, et al. Differential expression of anterior gradient gene AGR2 in prostate cancer. *BMC Cancer* (2010) 10:680. doi: 10.1186/1471-2407-10-680
29. Consortium GT. The Genotype-Tissue Expression (GTEx) project. *Nat Genet* (2013) 45:580–5. doi: 10.1038/ng.2653
30. Edgar R, Mazor Y, Rinon A, Blumenthal J, Golan Y, Buzhor E, et al. LifeMap Discovery: the embryonic development, stem cells, and regenerative medicine research portal. *PloS One* (2013) 8:e66629. doi: 10.1371/journal.pone.0066629
31. Di J, Li S, Li D, Xue H, Yang D, Liu Y. Mining TCGA database for genes of prognostic value in glioblastoma microenvironment. *Aging (Albany NY)* (2018) 10:592–605. doi: 10.18632/aging.101415
32. Yan Q, Li Z, Cen J-N, Chen S-N, Pan J, Hu S-Y. Over-expression of C3AR1 Promotes HL-60 Cell Migration and Invasion. *Zhongguo Shi Yan Xue Ye Xue Za Zhi* (2017) 25:1–7. doi: 10.7534/j.issn.1009-2137.2017.01.001
33. Sayegh ET, Bloch O, Parsa AT. Complement anaphylatoxins as immune regulators in cancer. *Cancer Med* (2014) 3:747–58. doi: 10.1002/cam4.241
34. Zadka Ł, Kulus MJ, Kurnol K, Piotrowska A, Glatzel-Plucińska N, Jurek T, et al. The expression of IL10RA in colorectal cancer and its correlation with the proliferation index and the clinical stage of the disease. *Cytokine* (2018) 110:116–25. doi: 10.1016/j.cyto.2018.04.030
35. Béguelin W, Sawh S, Chambwe N, Chan FC, Jiang Y, Choo J-W, et al. IL10 receptor is a novel therapeutic target in DLBCLs. *Leukemia* (2015) 29:1684–94. doi: 10.1038/leu.2015.57
36. Shi Y, He R, Zhuang Z, Ren J, Wang Z, Liu Y, et al. A risk signature-based on metastasis-associated genes to predict survival of patients with osteosarcoma. *J Cell Biochem* (2020) 121:3479–90. doi: 10.1002/jcb.29622
37. Razmkhah F, Ghasemi S, Soleimani M, Amini Kafi-Abad S. LY86, LRG1 and PDE9A genes overexpression in umbilical cord blood hematopoietic stem progenitor cells by acute myeloid leukemia (M3) microvesicles. *Exp Hematol Oncol* (2019) 8:23. doi: 10.1186/s40164-019-0147-8
38. Ma J, Zhang W, Tan L, Wang H-F, Wan Y, Sun F-R, et al. MS4A6A genotypes are associated with the atrophy rates of Alzheimer's disease related brain structures. *Oncotarget* (2016) 7:58779–88. doi: 10.18632/oncotarget.9563
39. Martinez FO, Gordon S, Locati M, Mantovani A. Transcriptional profiling of the human monocyte-to-macrophage differentiation and polarization: new molecules and patterns of gene expression. *J Immunol* (2006) 177:7303–11. doi: 10.4049/jimmunol.177.10.7303
40. Pan X, Chen Y, Gao S. Four genes relevant to pathological grade and prognosis in ovarian cancer. *Cancer Biomark* (2020) 29:169–78. doi: 10.3233/CBM-191162
41. Ren G, Esposito M, Kang Y. Bone metastasis and the metastatic niche. *J Mol Med* (2015) 93:1203–12. doi: 10.1007/s00109-015-1329-4
42. Ell B, Kang Y. SnapShot: Bone Metastasis. *Cell* (2012) 151:690–690.e1. doi: 10.1016/j.cell.2012.10.005
43. Boyerinas B, Zafrir M, Yesilkanal AE, Price TT, Hyjek EM, Sipkins DA. Adhesion to osteopontin in the bone marrow niche regulates lymphoblastic leukemia cell dormancy. *Blood Blood* (2013) 121:4821–31. doi: 10.1182/blood-2012-12-475483
44. Sison EA, McIntyre E, Magoon D, Brown P. Dynamic chemotherapy-induced upregulation of CXCR4 expression: a mechanism of therapeutic resistance in pediatric AML. *Mol Cancer Res* (2013) 11:1004–16. doi: 10.1158/1541-7786.MCR-13-0114
45. Park SI, Liao J, Berry JE, Li X, Koh AJ, Michalski ME, et al. Cyclophosphamide creates a receptive microenvironment for prostate cancer skeletal metastasis. *Cancer Res Cancer Res* (2012) 72:2522–32. doi: 10.1158/0008-5472.CAN-11-2928
46. Yu Z, Zou H, Wang H, Li Q, Yu D. Candidate biomarkers and gene modules investigation for bone tumor samples derived from castration-resistant

prostate cancer bone metastasis patients using WGCNA. (2019). doi: 10.21203/rs.2.17291/v1

Conflict of Interest: The authors declare that the research was conducted in the absence of any commercial or financial relationships that could be construed as a potential conflict of interest.

frontiers in Oncology

ORIGINAL RESEARCH
published: 04 March 2021
doi: 10.3389/fonc.2021.620674

Identification and Validation of a Stromal EMT Related LncRNA Signature as a Potential Marker to Predict Bladder Cancer Outcome

*YiHeng Du[1], Bo Wang[1], Xiang Jiang[2], Jin Cao[2], Jiang Yu[1], Yi Wang[1], XiZhi Wang[1] and HaiTao Liu[3]**

[1] Department of Urology, Suzhou Kowloon Hospital, Shanghai Jiaotong University School of Medicine, Suzhou, China,
[2] Department of Pathology, Suzhou Kowloon Hospital, Shanghai Jiaotong University School of Medicine, Suzhou, China,
[3] Department of Urology, Shanghai General Hospital, Shanghai Jiaotong University School of Medicine, Shanghai, China

OPEN ACCESS

Edited by:
Marco Rossi,
University of Catanzaro, Italy

Reviewed by:
Lasse Dahl Ejby Jensen,
Linköping University, Sweden
Luis E. Arias-Romero,
National Autonomous University of Mexico, Mexico

***Correspondence:**
HaiTao Liu
haitao.liu@shgh.cn

Specialty section:
This article was submitted to Cancer Molecular Targets and Therapeutics, a section of the journal Frontiers in Oncology

Received: *23 October 2020*
Accepted: *25 January 2021*
Published: *04 March 2021*

Citation:
Du Y, Wang B, Jiang X, Cao J, Yu J, Wang Y, Wang X and Liu H (2021) Identification and Validation of a Stromal EMT Related LncRNA Signature as a Potential Marker to Predict Bladder Cancer Outcome. Front. Oncol. 11:620674. doi: 10.3389/fonc.2021.620674

Bladder cancer (BLCA) has become one of the most common malignant tumors in the genitourinary system. BLCA is one of the tumors considered suitable for immunotherapy because of the large proportion of immune cells in TME. Epithelial to mesenchymal transition (EMT) is closely related to tumor immunity through its crosstalk with immune cells. A recent study validated that EMT-related genes were mainly expressed by stromal cells and could influence immunotherapy responsiveness. Stromal EMT-related gene signature was also demonstrated to affect the prognosis of multiple tumors, including BLCA. To further explore the prognostic roles of stromal components, we performed a comprehensive analysis of LncRNAs closely associated with stromal EMT-related genes in the TCGA BLCA cohort. We identified a signature including five stromal EMT gene-related LncRNAs that showed significant prognostic value for BLCA patients. By the CIBERSORT and MCP-COUNTER algorithm, we found the signature was markedly correlated with infiltrated immune cells and stromal components of the tumor microenvironment, which may further influence patient's responsiveness to immune checkpoint blockade therapy. Through immunohistochemical analysis, we confirmed the correlation of the signature with macrophages M2 and CAFs. Meanwhile, key genes related to these LncRNAs, including VIM, MMP2, were also differentially expressed in the stromal components concerning the signature. Our research confirmed the prognostic and immune-associated role of stromal EMT-related LncRNAs. Meantime, we further confirmed that EMT-related genes were mainly expressed in stromal components. Targeting these LncRNAs as well as their related stromal EMT genes may provide potential therapeutic targets for BLCA immunotherapy and precision medicine.

Keywords: bladder cancer, epithelial to mesenchymal transition, long non-coding RNAs, tumor microenvironment, immunosuppression

INTRODUCTION

Bladder cancer (BLCA) has become one of the most common malignant tumors in the genitourinary system (1). Transitional cell carcinoma is the most common pathological type of BLCA. According to the invasion depth, BLCA can be divided into non-muscle invasive(NMIBC) and muscle invasive bladder cancer (MIBC).NMIBC can be treated by transurethral resection of bladder tumor (TURBT) and has a favorable prognosis but still faces recurrence risk. MIBC is poorly treated clinically and often with radical surgery supplemented by postoperative chemotherapy and radiotherapy (2). The 5-year survival rate of MIBC patients is only 50% (3). Due to the rapid development of immunotherapy, immune checkpoint inhibitors for advanced BLCA have recently received significant attention. However, the responsiveness to existing immune checkpoint inhibitors is limited among BLCA patients, partly due to a complex heterogeneous tumor microenvironment (TME). Further study of TME is of great importance for BLCA immunotherapy.

TME is a complex and integrated system mainly composed of stromal cells and infiltrated immune cells. Emerging evidence suggests that the stromal components can shape antitumor immunity and affect immunotherapy responsiveness, thus promoting tumors' malignant development (4). The TME is particularly important in BLCA because of the overwhelming evidence that BLCA represents a growing number of solid tumors characterized by a significant number of stromal and immune cells in the TME (5, 6). The heterogeneity of TME in BLCA is closely related to patients' different response rates to immunotherapy, in which expression of stromal epithelial to mesenchymal transition (EMT) related genes plays a vital role (7).

EMT has been defined as a dynamical process with intermediate states (8). A complicated regulatory network is engaged in EMT's dynamic procedure at different levels, which further remodels the tumor extracellular matrix and promotes tumor metastasis. Although EMT is a biological process unique to tumor cells and has been studied extensively *in vitro* and in model organisms, evidence for this phenomenon in human tumors has been limited (9). In contrast, accumulating evidence showed that the up-regulation of EMT-related genes in bulk tumors was driven by expression changes in fibroblasts rather than in epithelial tumor cells (10). For example, Li et al. demonstrated that EMT-related genes were up-regulated only in a subpopulation of cancer-associated fibroblasts (CAFs) through single-cell RNA sequencing (11). A recent study also indicated that stromal EMT-related gene expression might alter T-cell infiltration level, which might eventually impact the responsiveness to immune therapy and patient's survival (7). These findings illuminated intertwined and complicated crosstalks between the stromal components and the EMT process in the development of cancer immune evasion, making the stromal components promising therapeutic targets for cancer immunotherapy.

LncRNAs are novel, potential therapeutic targets and biomarkers for cancer treatments (12). Moreover, researchers have demonstrated that LncRNAs obtain more specificity on indicating actual tumor condition than other types of markers (13). Previous studies have already discussed the prognostic value of stromal EMT-related genes in BLCA (7, 14), but the roles of stromal EMT-associated LncRNAs (sEMTLncs) have rarely been reported. Therefore, we carried out this present study to explore the function of sEMTLncs and seek their potential application for predicting BLCA outcome. We constructed a stromal EMT-related LncRNA prognostic signature (sEMTLS) in the present study, which showed good predictive accuracy for BLCA outcome. By adopting the CIBERSORT and MCP-COUNTER algorithm, we further found the sEMTLS was significantly associated with the levels of CAFs and tumor infiltrated immune cells (TIICs). Through immunohistochemical validation of the expressions of ACTA2, CD206, and these sEMTLnc-targeted EMT genes, we found that with the different expression levels of these sEMTLncs, these genes were also differentially expressed in the stromal components. These results shed light on the dual regulatory effect of sEMTLncs on both stromal and immune components in BLCA and laterally confirmed the EMT-related genes' expression was indeed in tumor stromal but not in epithelial tumor cells. Moreover, the ImmuneCell AI database (15) predicted that the expression of these sEMTLncs might also affect BLCA patients' responsiveness to immune checkpoint blockade (ICB) treatment. Targeting these sEMTLncs as well as their related stromal EMT genes may provide potential therapeutic targets for BLCA immunotherapy and precision medicine.

METHODS AND MATERIALS

Raw Data Acquisition

430 samples of transcriptome profiling data, including 19 normal samples, 411 tumor samples, and the corresponding clinical data of 405 bladder transitional cell papilloma and carcinoma patients were downloaded from the TCGA database (https://portal.gdc.cancer.gov/). Finally, 403 BLCA patients were selected and randomly arranged into training (n = 203) and testing groups (n = 200) for further study. Patients' baseline information was listed in **Table 1**.

Stromal Scoring and Differential Expressed Genes (DEGs) Screening

R language version 4.0.2 loaded with ESTIMATE package was used to calculate the scores of the immune and stromal component in TME for each sample of BLCA patients. After estimation, stromal score, immune score, and estimate score were obtained, representing the abundance of stromal, immune components, and the total. Then, samples were categorized into high and low-stromal score groups based on all samples' median stromal score. Package limma was applied to perform differential analysis of the gene expression; DEGs were screened by comparing the gene expressions in samples between high and the low stromal score groups. DEGs with fold change more than 1 after transformation of log2 and FDR <0.01 were considered significant.

sEMTLnc Acquisition

The Molecular Signatures Database v7.2 (hallmark_epithelial_mesenchymal_transition M5930, http://www.broadinstitute.org/

TABLE 1 | Clinical characteristic of patients in training, testing and entire groups.

characteristic		Entire group (N = 403)	Training group (N = 203)	Testing group (N = 200)
age	≤65	159 (39.5%)	82(40.4%)	77(38.5%)
	>65	244 (60.5%)	121(59.6%)	123(61.5%)
gender	male	298 (73.9%)	145(71.4%)	153(76.5%)
	female	105 (26.1%)	58(28.6%)	47(23.5%)
grade	low	20 (5.0%)	10(5.0%)	10(5%)
	high	380 (95.0%)	191(95.0%)	189(95%)
stage	stages I–II	130 (32.4%)	72(35.8%)	58(29.0%)
	stage III	138 (34.4%)	64(31.8%)	74(37.0%)
	stage IV	133 (33.2%)	65(32.4%)	68(34.0%)
T	T1–T2	122 (32.9%)	68(36.6%)	54(29.2%)
	T3–T4	249 (67.1%)	118(63.4%)	131(70.8%)
N	N0	234 (64.6%)	118(64.8%)	116(64.4%)
	N1	46 (12.7%)	25(13.7%)	21(11.7%)
	N2	75 (20.7%)	38(20.9%)	37(20.6%)
	N3	7 (2.0%)	1(0.6%)	6(3.3%)
M	M0	193(94.6%)	103(94.5%)	90(94.7%)
	M1	11(5.4%)	6(5.5%)	5(5.3%)

gsea/msigdb/index.jsp) was used to provide 200 EMT-related genes. By Pearson correlation analysis, we defined LncRNAs co-expressed with EMT-associated genes as EMTLnc, with |R| >0.4 and P <0.001. sEMTLncs were further defined as EMTLnc that significantly affected the stromal score, obtained by taking the intersection of stromal DEGs and EMTLnc. Similarly, immune-related LncRNAs (ImmLncs) were obtained through co-expression analysis with genes in immune-related genesets (Immune system process M13664, Immune response M19817, The Molecular Signatures Database v7.2, http://www.broadinstitute.org/gsea/msigdb/index.jsp). ImmLncs were used to check the involvement of sEMTLnc in the immune process.

sEMTLnc Signatures

sEMTLncs affecting the survival of BLCA were selected by univariate COX analysis using R software survival packages (P < 0.01). Lasso and multivariate cox regression were further used to construct the sEMTLS. Hazard ratio (HR) was used to classify sEMTLnc into the protective (HR < 1) and deleterious (HR > 1) portion (**Table 2**). Patients were classified into high- and low-risk groups based on the medium riskscore of the signature. The riskscore was calculated by the formula as followed:

$$riskscore = \sum_{i=1}^{n} Coef(i) * (expression\ of\ sEMTLnc(i))$$

*Coef: coefficient of the multi-Cox regression

Survival Analysis

R language v4.0.2 with package survival and survminer were used for survival analysis. Kaplan–Meier survival analysis was used for analyzing the survival difference between different groups. P-value of the log-rank test less than 0.05 were considered significant.

Time and Multi-ROC Curves

ROC curves analyzed the predictive accuracy of the signature on BLCA overall survival at 1, 3 and 5 years. Package timeROC of R language v4.0.2 was used for plotting timeROC curves. Independent risk analysis of different clinical characteristics, including age, gender, stage, T classification, and risk score on predicting 1-year overall survival, was conducted by Package survivalROC (**Table 3**).

Principal Component Analysis (PCA) and Nomogram Construction

PCA was used to cluster the samples based on the expression of sEMTLnc. A 3D scatterplot visualized patients' distribution. Nomogram was constructed by including the expression level of the sEMTLnc in the signature. A calibration plot was used to explore the calibration and discrimination of the nomogram.

GO, KEGG, and GSEA Enrichment Analysis

DEGs between the high- and low-risk groups of sEMTLS were used for GO and KEGG enrichment analysis. The

TABLE 2 | EMT-related LncRNAs identified from Cox regression analysis.

Symbol	Description	Multi-Cox regression	Uni-Cox regression			
		coefficient	HR	HR.95L	HR.95H	P-value
AL583785.1		0.056	1.079	1.027	1.133	0.002
TMEM51-AS1	TMEM51 antisense RNA 1	–0.353	0.709	0.555	0.906	0.006
AC073534.1		–0.793	0.400	0.211	0.762	0.005
LINC01711	long intergenic non-protein coding RNA 1711	0.062	1.101	1.046	1.159	<0.001
LINC02446	long intergenic non-protein coding RNA 2446	–0.567	0.684	0.515	0.909	0.009

TABLE 3 | Independent analysis by univariate and multivariate Cox regression of training, testing, and entire groups.

Uni-Cox regression					multi-Cox regression				
Training group									
Variables	HR	HR.95L	HR.95H	P-value	Variables	HR	HR.95L	HR.95H	P-value
Age	2.344	1.358	4.045	0.002	Age	2.266	1.293	3.972	0.004
Gender	0.863	0.530	1.406	0.555	Gender	0.935	0.564	1.549	0.794
Stage	1.953	1.441	2.645	<0.001	Stage	1.623	1.130	2.332	0.009
T	1.911	1.363	2.678	<0.001	T	1.495	0.973	2.298	0.067
RiskScore	1.141	1.093	1.191	<0.001	RiskScore	1.124	1.075	1.175	<0.001
Testing group									
Variables	HR	HR.95L	HR.95H	P-value	Variables	HR	HR.95L	HR.95H	P-value
Age	1.649	0.984	2.763	0.058	Age	1.791	1.042	3.077	0.035
Gender	0.789	0.457	1.361	0.394	Gender	0.624	0.354	1.099	0.103
Stage	1.936	1.371	2.733	<0.001	Stage	1.775	1.192	2.644	0.005
T	1.710	1.183	2.471	0.004	T	1.210	0.783	1.871	0.391
RiskScore	1.397	1.202	1.624	<0.001	RiskScore	1.325	1.127	1.558	0.001
Entire group									
Variables	HR	HR.95L	HR.95H	P-value	Variables	HR	HR.95L	HR.95H	P-value
Age	1.960	1.348	2.850	<0.001	Age	1.919	1.315	2.799	0.001
Gender	0.840	0.586	1.204	0.343	Gender	0.780	0.540	1.125	0.183
Stage	1.943	1.546	2.442	<0.001	Stage	1.745	1.338	2.277	<0.001
T	1.774	1.387	2.269	<0.001	T	1.292	0.957	1.744	0.094
RiskScore	1.157	1.115	1.200	<0.001	RiskScore	1.137	1.094	1.182	<0.001

Hallmark_Epithelial_Mesenchymal_Transition gene set was used for GESA between the low-risk and high-risk group, which was performed using the GSEA software (version 4.1.0) obtained from the Broad Institute. NOM p <0.05 and False Discovery Rate (FDR) q <0.05 were considered to be significant.

Calculation of TIIC Levels and CAFs Abundance

The CIBERSORT algorithm was used for calculating the levels of 22 different types of TIICs in all tumor samples; Samples with a p-value less than 0.05 were selected for the following analysis. The MCP-COUNTER algorithm (16, 17), provided by TIMER 2.0 (http://timer.cistrome.org/) (18), was applied for calculating the abundance of TME components, including endothelial cells and CAFs.

ICB Treatment Reactiveness Predicting

Immune cell abundance identifier (Immune cell AI, http://bioinfo.life.hust.edu.cn/ImmuCellAI) was applied to estimate the difference of immune cell infiltration in low- and high-risk groups. Patients' response to ICB therapy was then predicted based on the estimation of immune cell infiltration levels.

Real-Time Quantitative PCR

According to the manufacturer's instructions, we used triazole (Invitrogen) to extract total RNA from all recruited BLCA samples. cDNA Synthesis Kit (Osaka, Japan of TaKaRa) combining with RNA (1 μg) was utilized to reverse-transcribed cDNA. The quantitative polymerase chain reaction (qPCR), using the SYBR-Green method (TaKaRa), was performed on an ABI 7500 real-time PCR system (Applied Biosystems). The relative expression level of each lncRNA was calculated by the $2^{-\Delta\Delta Ct}$ method after normalizing to β-actin level. The forward and reverse primer sequences are shown in **Table 4**.

Immunohistochemistry Analysis

The gene expression in tumor tissues was detected using the BenchMark GX automatic multifunctional immunohistochemical staining system (Roche, Switzerland) with OptiView DAB Detection Kit (Ventana, USA) according to the manufacturer's instructions. The staining's straightforward procedures were listed as follows: deparaffinization and epitope retrieval in cell conditioner for 90 min. Short (8 min), mild (30 min), and standard (60 min) cell conditioning was performed after epitope retrieval. Primary antibodies were then incubated with the section for 32 min followed by biotinylated anti-IgG antibody and streptavidin–

TABLE 4 | The primer sequences of sEMTLnc.

AC073534.1	Forward(5′–3′)	TCACCTCAGCCAGCAGAAAC
	Reverse(5′–3′)	GGTGTTGACCATCTGTGGACT
TMEM51-AS1	Forward(5′–3′)	CAACAAGACCGAGCCAGGAG
	Reverse(5′–3′)	GCCCCGTCAGTGACTCATAG
AL583785.1	Forward(5′–3′)	GTGGTGCTTTTGCCTACTTGG
	Reverse(5′–3′)	TGGGCATACATCTTGAAGGGT
LINC02446	Forward(5′–3′)	AGCGGAGTGCAAAATGAAGTG
	Reverse(5′–3′)	CAATCCCACACAGGGTGTCC
LINC01711	Forward(5′–3′)	CTGGTCTGGAGCCGTTTCTC
	Reverse(5′–3′)	ATCCATCCTTGACCCTCGGA
β-actin	Forward(5′–3′)	AAACGTGCTGCTGACCGAG
	Reverse(5′–3′)	TAGCACAGCCTGGATAGCAAC

biotinylated-complex horseradish peroxidase. Hematoxylin was used for counterstaining and Bluing Reagent for post counterstaining. Details of the analyzed genes were listed in **Table 5**.

Statistics Analysis

Correlation of sEMTLS with infiltrated immune cells was analyzed with Pearson correlation test; p <0.01 was considered significant. Kaplan–Meier curve with log-rank test was used to evaluate the OS between different groups. The Wilcoxon test examined the differences for variables of two groups. Kruskal test estimated statistical significance for variables of more than two groups. Univariate and multivariate Cox regression analyses were displayed to verify the independent prognostic factors for BLCA. Fisher exact test was used to calculate the difference of ICB response between high- and low-risk groups. Two-sided P-value <0.05 was considered significant. R language v4.0.2 was used for all statistical analyses.

RESULTS

72 sEMTLnc Were Identified for Signature Construction

After we scored the stromal components by the ESTIMATE algorithm, DEGs between low and high stromal score groups were screened. 2,693 DEGs were identified. The top 50 of both up- and down-regulated genes with the most significant fold changes were represented by the heatmap (**Figure 1A**). The distribution of all DEGs on the two dimensions of -log10(FDR) and logFC was depicted in the volcano plot (**Figure 1B**). 421 EMTLncs were enrolled by co-expression with EMT-related genes. 82 sEMTLncs were selected after the intersection of the EMTLnc with the DEGs (**Figure 1C**). After the intersection with ImmLnc, 72 out of 82 sEMTLncs were confirmed to be highly co-expressed with genes related to the immune process, which further demonstrated the close relationships between EMT and the immune process. These 72 sEMTLncs were chosen for the construction of sEMTLnc signature.

sEMTLS Efficiently Predicted the Clinical Outcome of BLCA Patients in the TCGA Cohort

403 TCGA BLCA patients were randomly assigned to the training (203 patients) and the testing (200 patients) groups (**Table 1**). Five sEMTLncs were included in the signature, namely AL583785.1, TMEM51-AS1, AC073534.1, LINC01711, and LINC02446 (**Table 2**). A forest plot illustrated the corresponding HRs and 95% CIs for each sEMTLnc (**Figure 2A**). Patients were classified into a high-risk group and a low-risk group based on the training group's median risk score. Patients' overall survival (OS) in the high-risk group was significantly shorter than that in the low-risk group ($p < 0.001$). Time ROC curve showed good predictive accuracy with AUC of 0.777, 0.776, and 0.799 for predicting 1, 3 and 5 years' OS. Subsequently, we validated the sEMTLS in testing and the entire groups. Statistically, significant OS differences were observed between the high- and low-risk groups in the testing ($p < 0.001$) and the entire group ($p < 0.001$). AUC of time ROC curves in the testing and the entire group were 0.667, 0.666, 0.663, and 0.709, 0.719, 0.740 for predicting 1, 3, and 5 years' OS, respectively (**Figure 2B**).

The Risk Score of sEMTLS Could Essentially Predict the Clinical Status of BLCA Patients

Based on our signature, the mortality risk of patients in each group climbed with the risk score increased. The expression levels of AL583785.1 and LINC01711 were elevated, while TMEM51-AS1, AC073534.1, and LINC02446 expressed decreasingly as risk score increased (**Figure 3A**). Combined with other clinical and demographic characteristics of BLCA patients, the risk score was identified by multivariate cox regression analysis to be an independent prognostic factor for BLCA patients, with a hazard ratio of 1.124(1.075–1.175), 1.325 (1.127–1.558), 1.137(1.094–1.182) in training, testing and entire group respectively (**Figure 3B**). The ROC curve validated the prognostic accuracy of the risk score. The AUC of the risk score was higher than any other clinical and demographic characteristics in each group, which further suggested the risk score could be an independent prognostic factor (**Table 3**). To further validate the prognostic value and explore the broad applicability of sEMTLS, we analyzed the relationships between sEMTLS with different clinical features, including patient age, tumor grade, staging, and TNM classification in the entire group. The risk score was found significantly related to all of these clinical features confirming the significant association of sEMTLS with the progression of BLCA (**Figures 4A–F**). Last, we constructed a nomogram of sEMTLS to predict patient survival (**Figure 4G**). The calibration curve indicated that

TABLE 5 | Genes used in immunohistochemical analysis.

Primary antibody	Description	Role of gene	Manufacturer	Catalog	Dilution
ACTA2	Actin Alpha 2, smooth muscle	a marker of CAFs	Abcam	ab7817	1:100
CD206	Mannose receptor C-type 1	a marker of Macrophages M2	Abcam	ab252921	1:4000
MMP-2	Matrix metallopeptidase 2	Key sEMTLnc-related gene	Abcam	ab97779	1:200
VIM	Vimentin	Key sEMTLnc-related gene	Abcam	ab92547	1:200
CALU	Calumenin	Key sEMTLnc-related gene	Abcam	ab137019	1:250

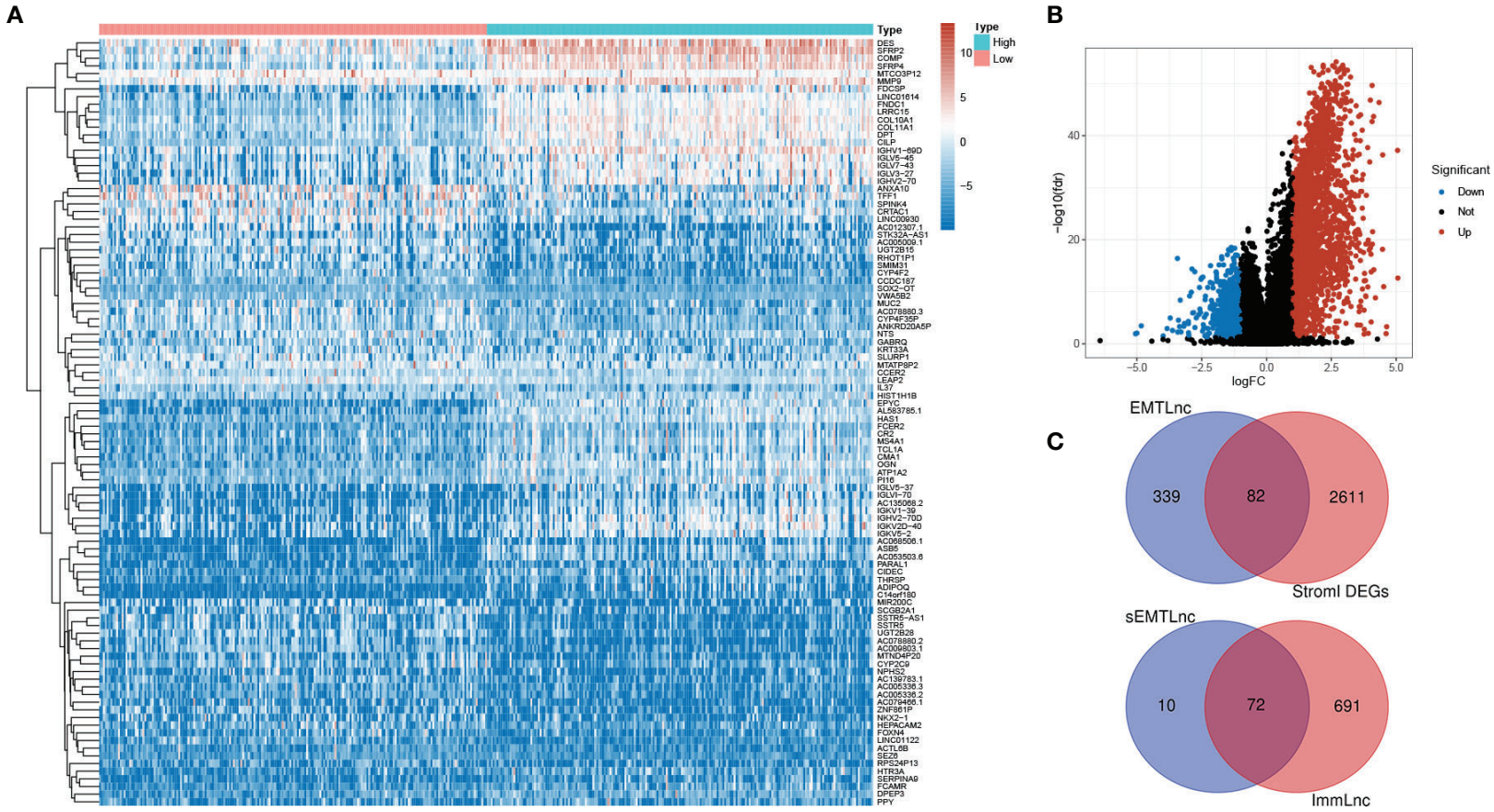

FIGURE 1 | Screening for sEMTLnc. **(A)** The top 50 of both up- and down-regulated stromal DEGs with the most significant differences were represented by the heatmap. **(B)** The distribution of all DEGs on the two dimensions of -log (FDR) and logFC was depicted in the volcano plot. **(C)** The intersection of stromal DEGs and EMTLnc identified 82 sEMTLncs, 72 out of 82 sEMTLncs were involved in the immune process.

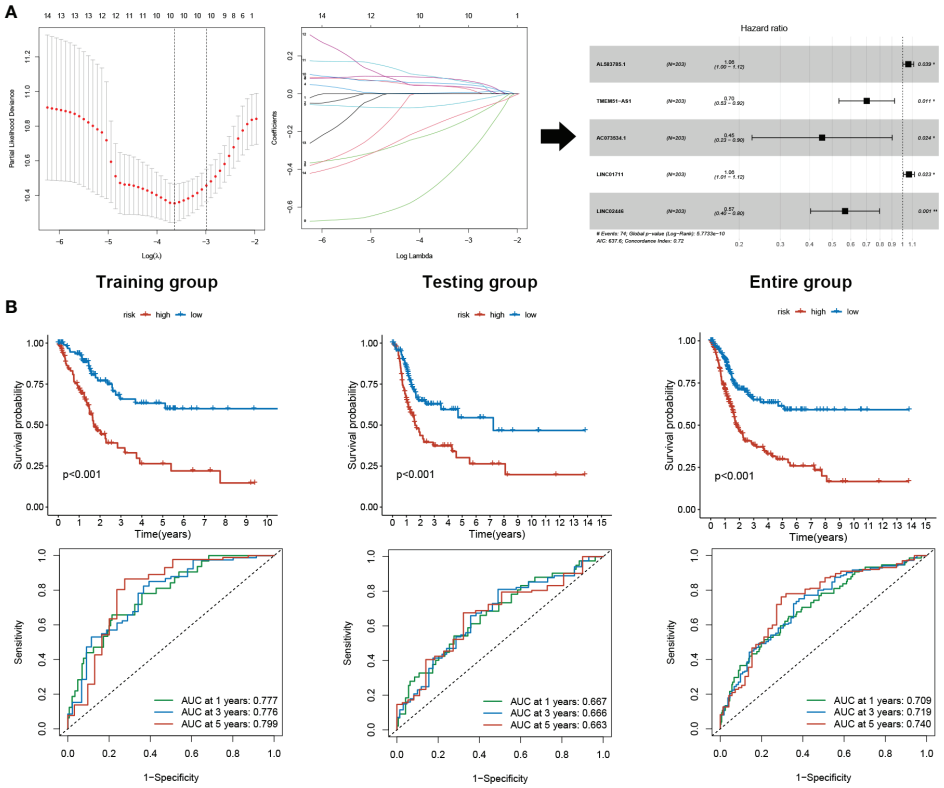

FIGURE 2 | sEMTLS construction and prognostic value validation. **(A)** sEMTLS were constructed by uni-cox regression, lasso regression, and multi-cox regression, which included three protective and two hazardous sEMTLnc. **(B)** Kaplan–Meier survival analysis suggested a lower OS in high-risk groups. ROC curve showed good accuracy of the sEMTLS in predicting 1, 3 and 5 years patients' OS.

sEMTLS had a high consistency with the actual 3-year survival (**Figure 4H**).

PCA and Functional Analysis Between High- and Low-Risk Groups of sEMTLS

Based on the expressions of sEMTLnc recruited in the sEMTLS, we employed the principal component analysis (PCA) to provide an overview of different distribution patterns between the low-risk group and the high-risk group. Results indicated a relatively scattered distribution of patients in testing and the entire groups, but with a small overlap in the training group (**Figures 5A–C**). GO and KEGG analysis of DEGs between high and low-risk groups of the entire group were enriched in terms related to extracellular matrix remodeling, including extracellular matrix organization, extracellular matrix structural constituent, and ECM-receptor interaction (**Figure 5D**). GSEA further proved the functional annotation, with the more EMT-related activity in the high-risk group (**Figure 5E**).

Close Relationships Were Found Between sEMTLS and TIICs

Utilizing the CIBERSORT algorithm, we obtained an estimation of the abundances of 22 TIICs. The infiltration proportion of the immune cells in each sample was shown in the barplot (**Figure 6A**). Among all the TIICs, Macrophages M0 and M2 were positively correlated to the risk score while T cell CD8+ and T cell CD4 memory activated exhibited negative correlations (**Figure 6B**). Further, elevated levels of Macrophages M0, M2, and decreased levels of T cell CD8+ and T cell CD4 memory activated were found in the high-risk group when compared with the low-risk group (**Figure 6C**). Combined with the survival time and survival state, all these four TIICs showed significant relations with the OS of BLCA patients, with Macrophages M0, M2 being detrimental factors and T cell CD8+, T cell CD4 memory activated being protective factors (**Figure 6D**). The above results highlighted the association between sEMTLS and TIICs, indicating the immune-modulating role of the sEMTLnc.

Correlation of sEMTLS With CAFs and Its Predicting Value to the Responsiveness of ICB Treatment

MCP-COUNTER algorithms calculated CAFs abundance in patients of the TCGA BLCA cohort. The relative abundance of CAFs was represented in the heatmap (**Figure 7A**). After comparing the TME components calculated by MCP-COUNTER between high- and low-risk groups, T cells CD8+ were further

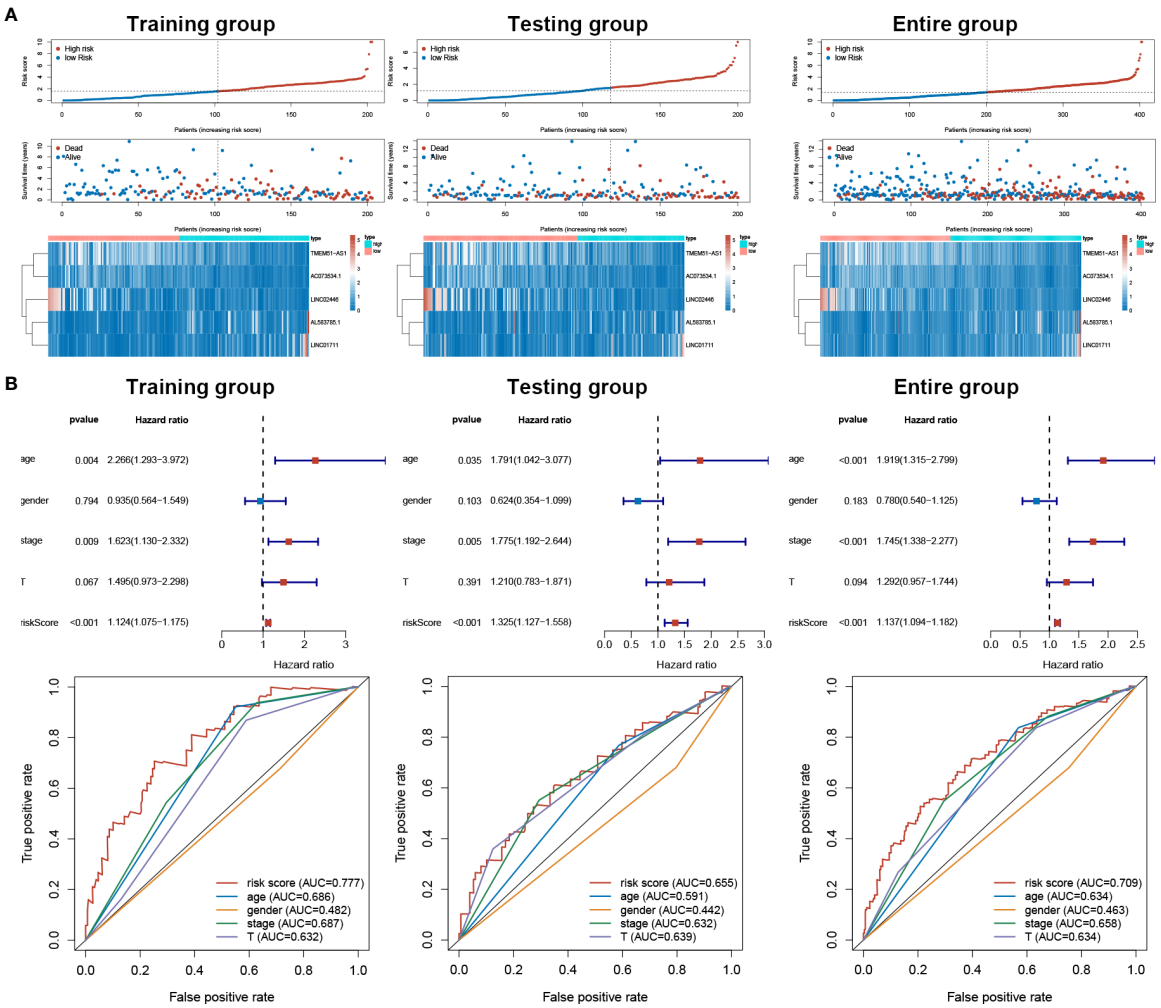

FIGURE 3 | sEMTLS correlated with mortality risk and could be used as an independent prognostic factor for BLCA. **(A)** Patients' mortality status and sEMTlnc expression in each patient were plotted according to the ordered risk score of sEMTLS. **(B)** Multivariate and ROC curves confirmed sEMTLS as an independent prognostic factor for BLCA.

confirmed to be reduced in the high-risk group, while CAFs abundance was significantly higher in the high-risk group than in the low-risk group (**Figure 7B**). The risk score was further validated positively correlated with CAFs abundance and the stromal score (**Figure 7C**). Using the immune cell AI database, We found significantly lower ICB treatment responsiveness in high-risk groups than the low-risk group (p=0.040). The risk scores between responders and non-responders also differed with relative higher risk scores in non-responders (p = 0.014) (**Figure 7D**).

Validation of the Association Between sEMTLS and TME Components in a Clinical Cohort

A clinical BLCA cohort of 16 patients with different stages was established to validate the correlation between sEMTLS, sEMTLnc targeted key genes, TIICs and CAFs. In our study, a total of five molecules were used for further research, of which CD206 and ACTA2 were used to represent the relative expression of macrophage M2 and CAFs, while three key lncRNA-targeted genes, VIM, CALU and MMP2, were used to detect expression in patients at different risks. The above five molecules in the TCGA cohort were significantly differentially expressed between the high- and low-risk groups (**Figure 8A**). Relative expressions of the five sEMTLnc were analyzed by real-time quantitative PCR. The risk score of each patient was calculated according to the formula. A close relation of sEMTLnc with the clinical stage was found and shown in the barplot (**Figure 8B**). Expression of CD206 was found in areas where ACTA2 was expressed in high risk patients (**Figure 8C**). We further compared the expression of CD206, ACTA2, VIM, CALU and MMP2 between patients with low and high risk scores (**Figures 8D–H**). The results confirmed an elevated

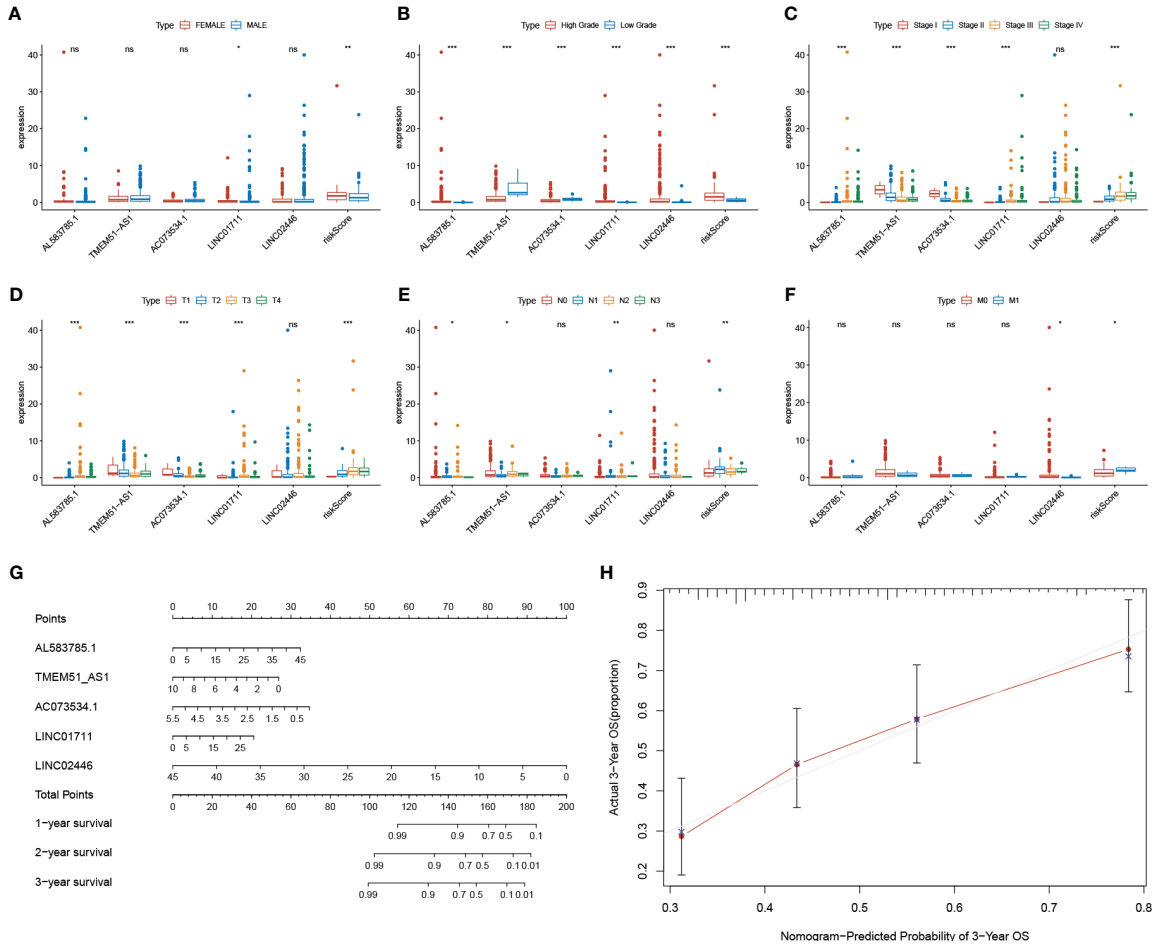

FIGURE 4 | Relationships between sEMTLS and clinical features of BLCA patients and nomogram of sEMTLS. **(A–F)** sEMTLS was significantly related to clinical features, including gender, grade, staging and TNM classification. **(G, H)** Nomogram of sEMTLS showed high consistency with the actual 3-year survival.

expression of all the five genes in high risk group patients. Furthermore, the expressions of ACTA2, VIM, and MMP2, which are markers of CAFs, were mainly found in the stromal area. These results demonstrated the relationship between CAFs and macrophages M2 and highlighted the association of sEMTLS with CAFs and macrophages M2 in BLCA patients. Our immunohistochemical results also revealed that in addition to CAFs, vascular smooth muscle cells also expressed EMT-related genes, which confirmed and complemented the previous findings of Li et al.

DISCUSSION

BLCA is one of the tumors considered suitable for immunotherapy because of the large proportion of immune cells in TME. Recent advances in treatment indeed demonstrated immune checkpoint blockers on T cells result in significantly improved survival in BLCA (19). However, challenges remain since there are still many BLCA patients who showed low responsiveness to ICB therapy. Over the past decade, EMT has been considered as a pivotal regulator in metastatic progression (20) and therapy resistance (21), including chemo- (22), radio- (23), and targeted therapy resistance. Under the current understanding, the EMT process is profound for regulating immune cells in TME, including CD8+ T cells and macrophages M2 (24). Evidence is now accumulating that such crosstalks might be a critical mechanism in promoting cancer immune escape (25). Recent studies have identified EMT as a dynamic process with an intermediate status, making the EMT process a promising target for therapeutic intervention (26), which may further promote immunotherapy efficacy in low responsive cancer patients (27).

The TME has been characterized as inflammatory and immunosuppressive (28, 29). It owned a variety types of immune and stromal cells. Among the immune cells, macrophages are highly plastic and crucial to the EMT process (30). Previous studies have confirmed that M2 macrophages secrete a series of cytokines that promote EMT and cancer progression *via* multiple signaling pathways, including ZEB1

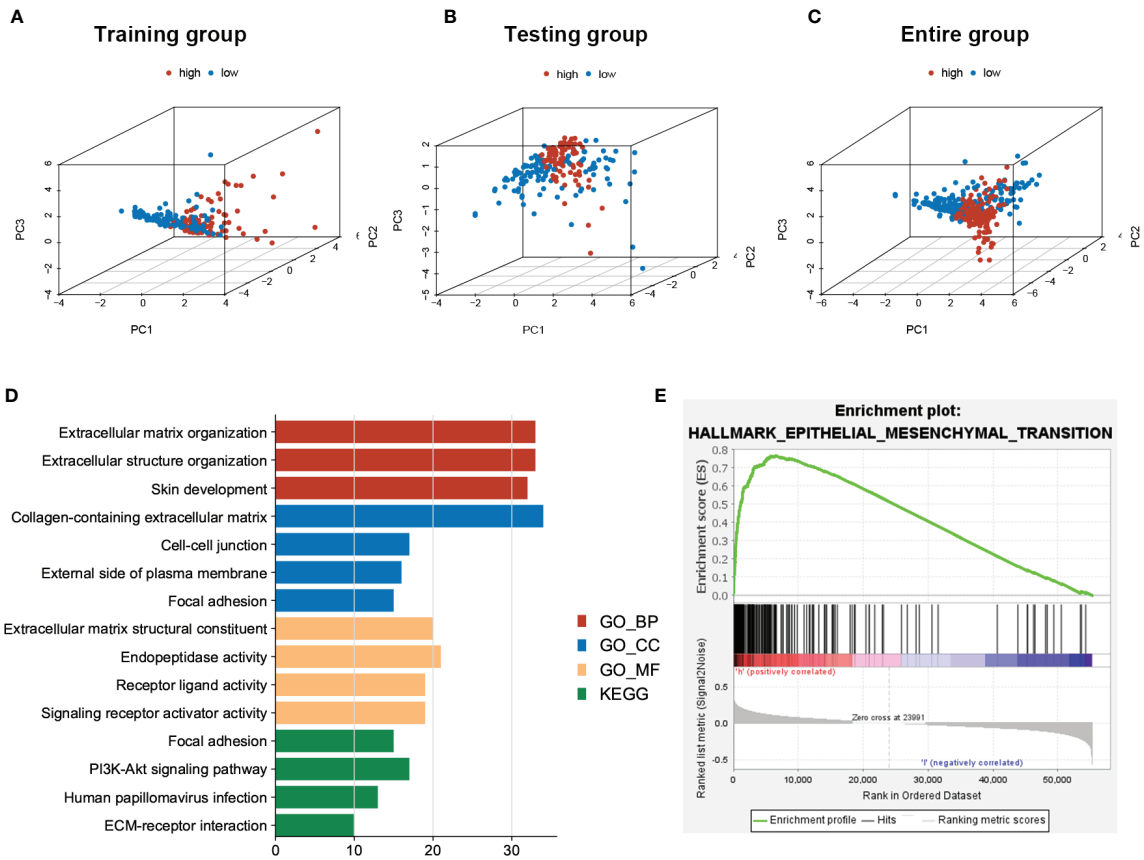

FIGURE 5 | PCA of patients' distribution and functional analysis between low- and high-risk patients in the entire group. **(A–C)** PCA showed a scattered distribution of patients in testing and the entire groups, while a small portion of overlap was observed in the testing group. **(D)** DEGs between high and low-risk groups majorly enriched in EMT related functions and pathways. **(E)** GSEA confirmed a high EMT activity in high-risk groups.

(31), SNAL1 (32), VIM (33), and TWIST1 (34). Stromal cells dominated by CAFs also participate in the EMT process. One previous study demonstrated that CAFs could increase the expressions of EMT-related genes and differentiated the recruited monocytes into M2 macrophages, further exerting their immunosuppressive roles targeting CD8+ T cells (35). These results are consistent with our finding in this study that macrophage M2 and CAFs are co-expressed in the stromal compartment. Given all the above evidence, we clearly noticed the association between TME components and the EMT process.

Although EMT is a biological process unique to tumor cells has been studied extensively *in vitro* and in model organisms, evidence for this phenomenon in human tumors has been limited (11). A recent study indicated that stromal components of BLCA comprise a key source of EMT-related gene expression. Expression of these stromal genes correlated with T-cell infiltration and impacted response to immune checkpoint blockade, further influencing BLCA patients' survival (7). In the present study, we found that the expression of sEMTLnc may also affect the infiltration of T-cells and macrophages M2. Immunohistochemical results of these lncRNA-targeted EMT genes also validated that EMT genes were mainly expressed in stromal components. Whereas, questions may raise that since EMT is a unique process of the tumor cells, why EMT related genes were mainly expressed in stromal components but not in tumor cells themselves. Available evidence suggests that the EMT process may not only act in the epithelial tumor cells but also involve intertwined and complex crosstalks between stromal components and tumor cells. Based on the fact that EMT-related genes are only expressed in a subpopulation of CAFs, CAFs have been suggested to even arise from tumor cells undergoing EMT (7). It is difficult to explain these mechanisms by bulk RNA sequencing. Further research is still needed to validate the exact mechanisms between stromal EMT-related gene expression and tumor cells' EMT process. Perhaps applying single-cell sequencing to explore these EMT-associated genes' cellular origin could be useful in explaining this intricate process.

On the other hand, LncRNAs are novel, potential therapeutic targets and biomarkers for cancer treatments (12). Moreover, researchers have demonstrated that LncRNAs obtain more specificity on indicating actual tumor condition than other types of markers (13). Previous research indicated that stromal EMT-related genes could provide a predictive role in tumor patients'

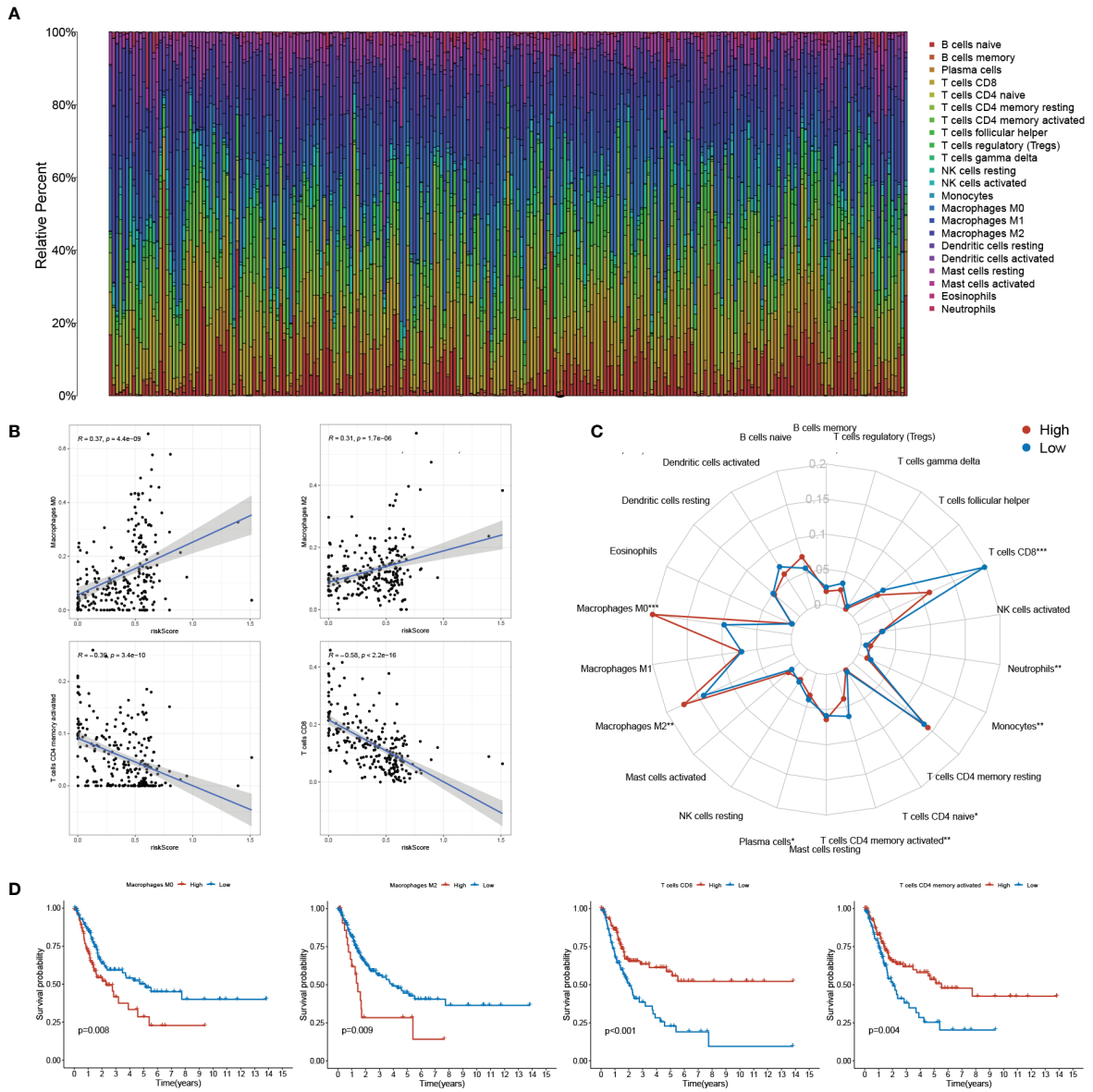

FIGURE 6 | sEMTLS is correlated with TIICs levels, including macrophages and CD8+ T cells. **(A)** The percentage of 22 TIICs in each patient of the entire group was shown in the barplot. **(B, C)** sEMTLS positively related to Macrophages M0 and M2, while negative relationships were observed between sEMTLS and CD8+ T cells and T cell CD4 memory activated. **(D)** All of the four sEMTLS related TIICs affected the OS of BLCA patients. Macrophages M0 and M2 served as detrimental factors, while T cell CD8+ and T cell CD4 memory as protective factors.

prognosis and affect response to ICB therapy in BLCA patients. Could sEMTLnc play a similar role? From the present results, we confirmed the prognostic value of sEMTLnc in BLCA patients. The sEMTLS could be an independent risk factor to patients' OS. Close correlations between sEMTLS, macrophage M2 and CAFs were also found, suggesting that the combined expression of sEMTLnc was associated with the abundance of macrophages and CAFs. Also, there was a negative correlation between sEMTLS and CD8+ T cells and a significant difference in ICB treatment responsiveness between high and low-risk groups. These results suggested that sEMTLnc, like stromal EMT-related genes, had a significant influence on the immunotherapeutic response and may ultimately affect the prognosis of BLCA.

Using a clinical validation cohort, we further confirmed the relationship between CAFs, macrophage M2 and the sEMTLnc. The key genes related to the sEMTlnc, including VIM, MMP2, and CALU, also expressed differently concerning the risk score. VIM and MMP2 are also markers of CAFs, which promote cancer progression and metastasis (36, 37). Simultaneously, CALU was demonstrated to express significantly higher levels

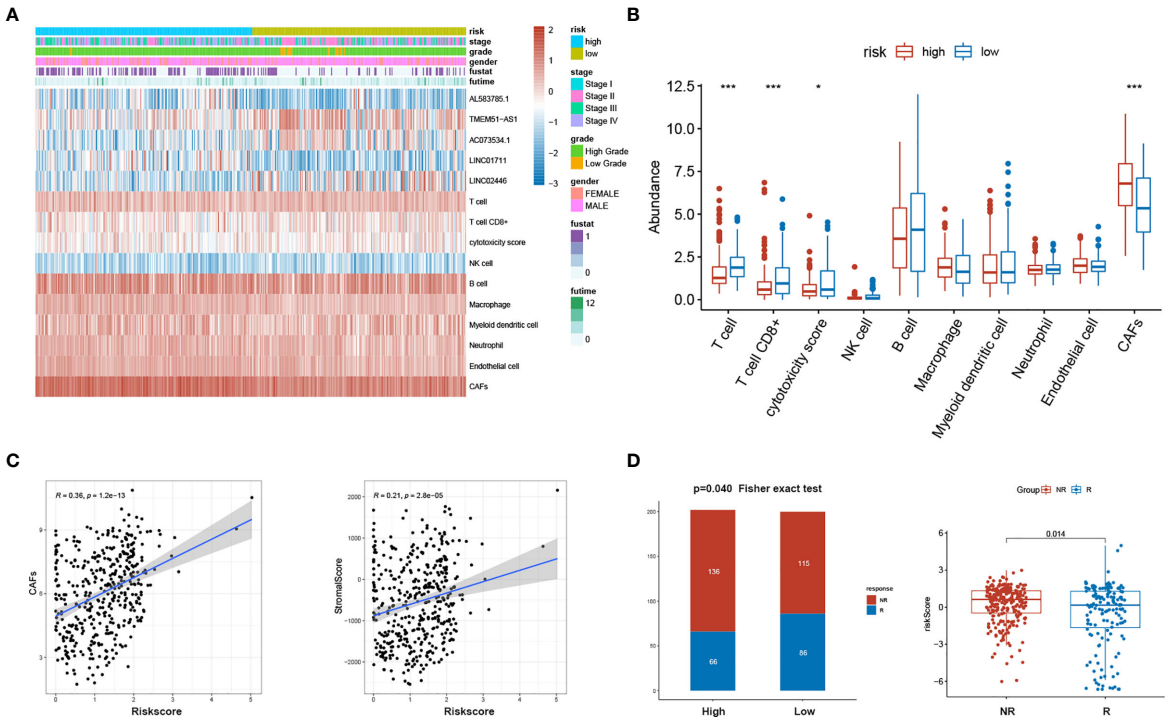

FIGURE 7 | sEMTLS was related to the stromal components and ICB responsiveness. **(A)** Expression of sEMTLnc and TME cells calculated by MCP-COUNTER in each patient was shown in the heatmap. **(B)** Significant lower CD8+ T cells and higher CAFs abundance were observed in the high-risk group. **(C)** The risk score of sEMTLS was positively related to CAFs abundance and the stromal score. **(D)** Patients in the high-risk group earned a lower responsiveness rate to ICB therapy. Risk scores are lower in patients who respond to ICB therapy than those who do not respond.

in the metastatic cancer tissues (38). Through our immunohistochemical results, we could see that markers such as ACTA2, VIM, and MMP2 were mostly differentially expressed in the stromal area, including CAFs and vascular smooth muscle cells, but not in the tumor cells between the different risk score groups. These results are consistent with the previous literature (7, 11), while the detection of expression of key genes targeted by these sEMTlnc in vascular smooth muscle cells also suggested that these EMTlnc may be involved in the formation of tumor neovascularization (39). Taken together, we suggest that these sEMTlnc play a key role in TME remodeling and regulation of TIICs, including T cells and macrophages. The expression of sEMTlnc may ultimately influence immune responsiveness and overall survival of BLCA patients. Further studies on sEMTLnc may provide potential therapeutic targets for BLCA immunotherapy and precision medicine.

However, limitations still existed since our results were mainly based on the bioinformatics analysis. Although highly correlated with EMT-related genes, critical questions still existed: Do sEMTLnc expression indeed reflect the biological process of EMT, How do sEMTLnc expression alter T-cells and macrophages M2 infiltration, why sEMTLnc can impact outcomes and affect the responsiveness to ICB treatment in BLCA patients. Simultaneously, It is not sufficient to study sEMTLnc-associated TIICs only by bulk RNA sequencing data based on bioinformatics algorithms, which may lead to different results between different algorithms. The exact association between sEMTLnc, CAFs, macrophages, and T cells still needs to be verified by a series of *in vitro* and *in vivo* experiments, including single-cell RNA sequencing. Besides, due to the limited number of cases in the clinical cohort we included, we still need a larger external clinical cohort to validate the relative expressions of the sEMTLnc and the predictive value of the signature.

CONCLUSION

In the present study, we constructed a prognostic signature containing five sEMTLnc, which predicted BLCA patients' prognosis. Further study on the signature confirmed its significant correlation with the abundance of CAFs, macrophages M2 and CD8+ T cells. Similar to the literature reporting that stromal EMT gene expression affects BLCA prognosis and immunotherapy responsiveness, the combined expression of stromal EMT-related lncRNAs may also affect BLCA outcome and immunotherapy responsiveness. Through immunohistochemical analysis, we laterally verified that EMT-related genes are mainly expressed in the stromal components,

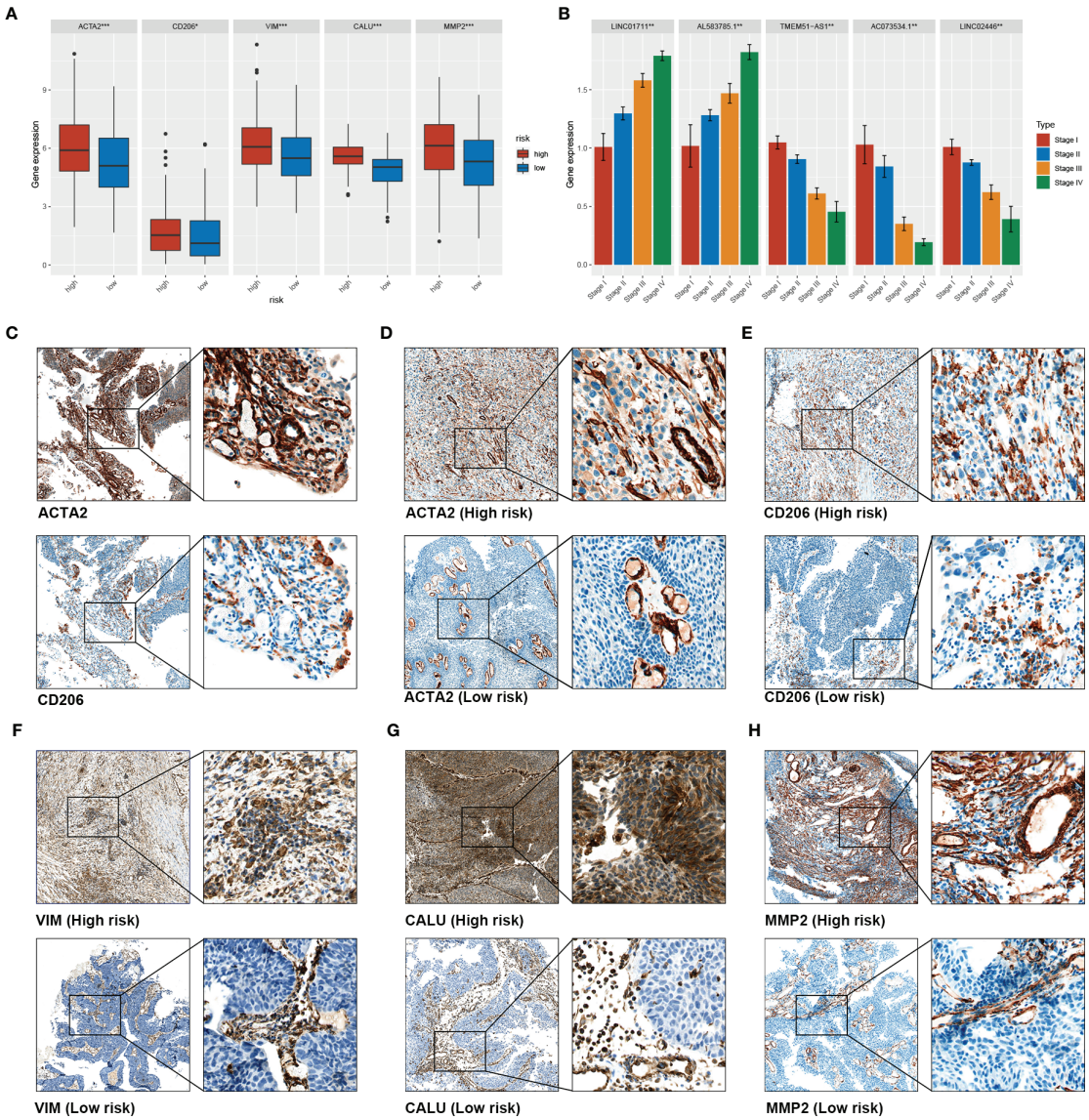

FIGURE 8 | Validation of the association between sEMTLS and TME Components in our clinical cohort. **(A)** the expression level of ACTA2, CD206, VIM, MMP2, and CALU in the high- and low-risk group of the TCGA cohort. **(B)** PCR analysis confirmed that sEMTLncs were differentially expressed between different stages in our clinical validation cohort **(C)**. Co-expression of CD206 and ACTA2 was found in high-risk patients, confirming the association between macrophages M2 and CAFs **(D)** to **(H)**. The expression levels of ACTA2, CD206, VIM, CALU and MMP2 in the high-risk patients were significantly higher than those in the low-risk patients.

including CAFs and vascular smooth muscle cells. The crosstalk between tumor stroma and tumor cell's EMT process is intricate and requires in-depth study. Further study of stromal EMT-related lncRNAs and their targeted genes will help provide possible new targets for BLCA precision therapy and immunotherapy.

DATA AVAILABILITY STATEMENT

The datasets presented in this study can be found in online repositories. The names of the repository/repositories and accession number(s) can be found in the article/supplementary material.

ETHICS STATEMENT

The studies involving human participants were reviewed and approved by Medical Ethics Committee of Shanghai General Hospital. The patients/participants provided their written informed consent to participate in this study.

AUTHOR CONTRIBUTIONS

YD and BW had an equal contribution to this manuscript. HL designed the whole study. YD and BW participated in the

bioinformatics and statistical analysis, XJ and JC did the immunohistochemistry analysis. YD performed real-time PCR analysis. YW and JY made the manuscript and figure editing. XW and HL revised the manuscript. All authors contributed to the article and approved the submitted version.

FUNDING

This study was funded by the National Natural Science Foundation of China (Grant number: 81972371) and Basic Research on medical and health Application of Suzhou Municipal Science and Technology Bureau (Grant number: SYSD2020076).

REFERENCES

1. Siegel RL, Miller KD, Jemal A. Cancer Statistics, 2017. *CA Cancer J Clin* (2017) 67(1):7–30. doi: 10.3322/caac.21387
2. Kamat AM, Hahn NM, Efstathiou JA, Lerner SP, Malmstrom PU, Choi W, et al. Bladder cancer. *Lancet* (2016) 388(10061):2796–810. doi: 10.1016/S0140-6736(16)30512-8
3. Babjuk M, Bohle A, Burger M, Capoun O, Cohen D, Comperat EM, et al. EAU Guidelines on Non-Muscle-invasive Urothelial Carcinoma of the Bladder: Update 2016. *Eur Urol* (2017) 71(3):447–61. doi: 10.1016/j.eururo.2016.05.041
4. Ngambenjawong C, Gustafson HH, Pun SH. Progress in tumor-associated macrophage (TAM)-targeted therapeutics. *Adv Drug Deliv Rev* (2017) 114:206–21. doi: 10.1016/j.addr.2017.04.010
5. Michaud DS. Chronic inflammation and bladder cancer. *Urol Oncol* (2007) 25 (3):260–8. doi: 10.1016/j.urolonc.2006.10.002
6. Volkmer JP, Sahoo D, Chin RK, Ho PL, Tang C, Kurtova AV, et al. Three differentiation states risk-stratify bladder cancer into distinct subtypes. *Proc Natl Acad Sci U S A* (2012) 109(6):2078–83. doi: 10.1073/pnas.1120605109
7. Wang L, Saci A, Szabo PM, Chasalow SD, Castillo-Martin M, Domingo-Domenech J, et al. EMT- and stroma-related gene expression and resistance to PD-1 blockade in urothelial cancer. *Nat Commun* (2018) 9(1):3503. doi: 10.1038/s41467-018-05992-x
8. Gupta PB, Pastushenko I, Skibinski A, Blanpain C, Kuperwasser C. Phenotypic Plasticity: Driver of Cancer Initiation, Progression, and Therapy Resistance. *Cell Stem Cell* (2019) 24(1):65–78. doi: 10.1016/j.stem.2018.11.011
9. Fischer KR, Durrans A, Lee S, Sheng J, Li F, Wong ST, et al. Epithelial-to-mesenchymal transition is not required for lung metastasis but contributes to chemoresistance. *Nature* (2015) 527(7579):472–6. doi: 10.1038/nature15748
10. Peng YX, Yu B, Qin H, Xue L, Liang YJ, Quan ZX. EMT-related gene expression is positively correlated with immunity and may be derived from stromal cells in osteosarcoma. *PeerJ* (2020) 8:e8489. doi: 10.7717/peerj.8489
11. Li H, Courtois ET, Sengupta D, Tan Y, Chen KH, Goh JJL, et al. Reference component analysis of single-cell transcriptomes elucidates cellular heterogeneity in human colorectal tumors. *Nat Genet* (2017) 49(5):708–18. doi: 10.1038/s41588-018-0299-1
12. Schmitt AM, Chang HY. Long Non-coding RNAs in Cancer Pathways. *Cancer Cell* (2016) 29(4):452–63. doi: 10.1016/j.ccell.2016.03.010
13. Qu L, Wang ZL, Chen Q, Li YM, He HW, Hsieh JJ, et al. Prognostic Value of a Long Non-coding RNA Signature in Localized Clear Cell Renal Cell Carcinoma. *Eur Urol* (2018) 74(6):756–63. doi: 10.1016/j.eururo.2018.07.032
14. Cao R, Yuan L, Ma B, Wang G, Qiu W, Tian Y. An EMT-related gene signature for the prognosis of human bladder cancer. *J Cell Mol Med* (2020) 24 (1):605–17. doi: 10.1111/jcmm.14767
15. Miao YR, Zhang Q, Lei Q, Luo M, Xie GY, Wang H, et al. ImmuCellAI: A Unique Method for Comprehensive T-Cell Subsets Abundance Prediction and its Application in Cancer Immunotherapy. *Adv Sci (Weinh)* (2020) 7 (7):1902880. doi: 10.1002/advs.201902880
16. Sturm G, Finotello F, Petitprez F, Zhang JD, Baumbach J, Fridman WH, et al. Comprehensive evaluation of transcriptome-based cell-type quantification methods for immuno-oncology. *Bioinformatics* (2019) 35(14):i436–i45. doi: 10.1093/bioinformatics/btz363
17. Becht E, Giraldo NA, Lacroix L, Buttard B, Elarouci N, Petitprez F, et al. Estimating the population abundance of tissue-infiltrating immune and stromal cell populations using gene expression. *Genome Biol* (2016) 17 (1):218. doi: 10.1186/s13059-016-1070-5
18. Li T, Fu J, Zeng Z, Cohen D, Li J, Chen Q, et al. TIMER2.0 for analysis of tumor-infiltrating immune cells. *Nucleic Acids Res* (2020) 48(W1):W509–W14. doi: 10.1093/nar/gkaa407
19. Rouanne M, Roumiguie M, Houede N, Masson-Lecomte A, Colin P, Pignot G, et al. development of immunotherapy in bladder cancer: present and future on targeting PD(L)1 and CTLA-4 pathways. *World J Urol* (2018) 36(11):1727–40. doi: 10.1007/s00345-018-2332-5
20. Singh M, Yelle N, Venugopal C, Singh SK. EMT: Mechanisms and therapeutic implications. *Pharmacol Ther* (2018) 182:80–94. doi: 10.1016/j.pharmthera.2017.08.009
21. Shibue T, Weinberg RA. EMT, CSCs, and drug resistance: the mechanistic link and clinical implications. *Nat Rev Clin Oncol* (2017) 14(10):611–29. doi: 10.1038/nrclinonc.2017.44
22. Zheng X, Carstens JL, Kim J, Scheible M, Kaye J, Sugimoto H, et al. Epithelial-to-mesenchymal transition is dispensable for metastasis but induces chemoresistance in pancreatic cancer. *Nature* (2015) 527(7579):525–30. doi: 10.1038/nature16064
23. Shao M, Bi T, Ding W, Yu C, Jiang C, Yang H, et al. OCT4 Potentiates Radio-Resistance and Migration Activity of Rectal Cancer Cells by Improving Epithelial-Mesenchymal Transition in a ZEB1 Dependent Manner. *BioMed Res Int* (2018) 2018:3424956. doi: 10.1155/2018/3424956
24. Zhang Q, Zhang Y, Chen Y, Qian J, Zhang X, Yu K. A Novel mTORC1/2 Inhibitor (MTI-31) Inhibits Tumor Growth, Epithelial-Mesenchymal Transition, Metastases, and Improves Antitumor Immunity in Preclinical Models of Lung Cancer. *Clin Cancer Res* (2019) 25(12):3630–42. doi: 10.1158/1078-0432.CCR-18-2548
25. Terry S, Savagner P, Ortiz-Cuaran S, Mahjoubi L, Saintigny P, Thiery JP, et al. New insights into the role of EMT in tumor immune escape. *Mol Oncol* (2017) 11(7):824–46. doi: 10.1002/1878-0261.12093
26. Marzagalli M, Raimondi M, Fontana F, Montagnani Marelli M, Moretti RM, Limonta P. Cellular and molecular biology of cancer stem cells in melanoma: Possible therapeutic implications. *Semin Cancer Biol* (2019) 59:221–35. doi: 10.1016/j.semcancer.2019.06.019
27. Dong P, Xiong Y, Yue J, Hanley SJB, Watari H. Tumor-Intrinsic PD-L1 Signaling in Cancer Initiation, Development and Treatment: Beyond Immune Evasion. *Front Oncol* (2018) 8:386. doi: 10.3389/fonc.2018.00386
28. Zhan HX, Zhou B, Cheng YG, Xu JW, Wang L, Zhang GY, et al. crosstalk between stromal cells and cancer cells in pancreatic cancer: New insights into stromal biology. *Cancer Lett* (2017) 392:83–93. doi: 10.1016/j.canlet.2017.01.041
29. Najafi M, Goradel NH, Farhood B, Salehi E, Solhjoo S, Toolee H, et al. Tumor microenvironment: Interactions and therapy. *J Cell Physiol* (2019) 234 (5):5700–21. doi: 10.1002/jcp.27425
30. Thomas D, Apovian C. Macrophage functions in lean and obese adipose tissue. *Metabolism* (2017) 72:120–43. doi: 10.1016/j.metabol.2017.04.005
31. Cortes M, Sanchez-Moral L, de Barrios O, Fernandez-Acenero MJ, Martinez-Campanario MC, Esteve-Codina A, et al. Tumor-associated macrophages (TAMs) depend on ZEB1 for their cancer-promoting roles. *EMBO J* (2017) 36 (22):3336–55. doi: 10.15252/embj.201797345
32. Brenot A, Knolhoff BL, DeNardo DG, Longmore GD. SNAIL1 action in tumor cells influences macrophage polarization and metastasis in breast cancer through altered GM-CSF secretion. *Oncogenesis* (2018) 7(3):32. doi: 10.1038/s41389-018-0042-x
33. Yu MB, Guerra J, Firek A, Langridge WHR. Extracellular vimentin modulates human dendritic cell activation. *Mol Immunol* (2018) 104:37–46. doi: 10.1016/j.molimm.2018.09.017
34. Wang J, Wang X, Wang Y, Li S, Wang X. Kruppel like factor 6 splice variant 1 (KLF6-SV1) overexpression recruits macrophages to participate in lung cancer metastasis by up-regulating TWIST1. *Cancer Biol Ther* (2019) 20 (5):680–91. doi: 10.1080/15384047.2018.1550570
35. Gok Yavuz B, Gunaydin G, Gedik ME, Kosemehmetoglu K, Karakoc D, Ozgur F, et al. Cancer associated fibroblasts sculpt tumour microenvironment by

recruiting monocytes and inducing immunosuppressive PD-1(+) TAMs. *Sci Rep* (2019) 9(1):3172. doi: 10.1038/s41598-019-39553-z
36. Costa VL, Henrique R, Danielsen SA, Duarte-Pereira S, Eknaes M, Skotheim RI, et al. Three epigenetic biomarkers, GDF15, TMEFF2, and VIM, accurately predict bladder cancer from DNA-based analyses of urine samples. *Clin Cancer Res* (2010) 16(23):5842–51. doi: 10.1158/1078-0432.CCR-10-1312
37. Winerdal ME, Krantz D, Hartana CA, Zirakzadeh AA, Linton L, Bergman EA, et al. Urinary Bladder Cancer Tregs Suppress MMP2 and Potentially Regulate Invasiveness. *Cancer Immunol Res* (2018) 6(5):528–38. doi: 10.1158/2326-6066.CIR-17-0466
38. Nagano K, Imai S, Zhao X, Yamashita T, Yoshioka Y, Abe Y, et al. Identification and evaluation of metastasis-related proteins, oxysterol binding protein-like 5 and calumenin, in lung tumors. *Int J Oncol* (2015) 47 (1):195–203. doi: 10.3892/ijo.2015.3000
39. Thaker PH, Han LY, Kamat AA, Arevalo JM, Takahashi R, Lu C, et al. Chronic stress promotes tumor growth and angiogenesis in a mouse model of ovarian carcinoma. *Nat Med* (2006) 12(8):939–44. doi: 10.1038/nm1447

Conflict of Interest: The authors declare that the research was conducted in the absence of any commercial or financial relationships that could be construed as a potential conflict of interest.

frontiers in Oncology

ORIGINAL RESEARCH
published: 15 March 2021
doi: 10.3389/fonc.2021.621278

Subgroup-Independent Mapping of Renal Cell Carcinoma—Machine Learning Reveals Prognostic Mitochondrial Gene Signature Beyond Histopathologic Boundaries

André Marquardt[1,2,3], Antonio Giovanni Solimando[4,5]*, Alexander Kerscher[1], Max Bittrich[6], Charis Kalogirou[7], Hubert Kübler[7], Andreas Rosenwald[2], Ralf Bargou[1], Philip Kollmannsberger[8], Bastian Schilling[9], Svenja Meierjohann[2,3] and Markus Krebs[1,7]*

[1] Comprehensive Cancer Center Mainfranken, University Hospital Würzburg, Würzburg, Germany, [2] Institute of Pathology, University of Würzburg, Würzburg, Germany, [3] Interdisciplinary Center for Clinical Research, University Hospital Würzburg, Würzburg, Germany, [4] Guido Baccelli Unit of Internal Medicine, Department of Biomedical Sciences and Human Oncology, School of Medicine, Aldo Moro University of Bari, Bari, Italy, [5] IRCCS Istituto Tumori "Giovanni Paolo II" of Bari, Bari, Italy, [6] Department of Internal Medicine II, University Hospital Würzburg, Würzburg, Germany, [7] Department of Urology and Pediatric Urology, University Hospital Würzburg, Würzburg, Germany, [8] Center for Computational and Theoretical Biology, University of Würzburg, Würzburg, Germany, [9] Department of Dermatology, University Hospital Würzburg, Würzburg, Germany

OPEN ACCESS

Edited by:
Cirino Botta,
Cosenza Hospital, Italy

Reviewed by:
Helge Taubert,
University Hospital Erlangen, Germany
Raffaele Ratta,
Hôpital Foch, France

***Correspondence:**
André Marquardt
marquardt_a@ukw.de
Antonio Giovanni Solimando
antonio.solimando@uniba.it

Specialty section:
This article was submitted to Cancer Molecular Targets and Therapeutics, a section of the journal Frontiers in Oncology

Received: 25 October 2020
Accepted: 15 February 2021
Published: 15 March 2021

Citation:
Marquardt A, Solimando AG, Kerscher A, Bittrich M, Kalogirou C, Kübler H, Rosenwald A, Bargou R, Kollmannsberger P, Schilling B, Meierjohann S and Krebs M (2021) Subgroup-Independent Mapping of Renal Cell Carcinoma—Machine Learning Reveals Prognostic Mitochondrial Gene Signature Beyond Histopathologic Boundaries. Front. Oncol. 11:621278. doi: 10.3389/fonc.2021.621278

Background: Renal cell carcinoma (RCC) is divided into three major histopathologic groups—clear cell (ccRCC), papillary (pRCC) and chromophobe RCC (chRCC). We performed a comprehensive re-analysis of publicly available RCC datasets from the TCGA (The Cancer Genome Atlas) database, thereby combining samples from all three subgroups, for an exploratory transcriptome profiling of RCC subgroups.

Materials and Methods: We used FPKM (fragments per kilobase per million) files derived from the ccRCC, pRCC and chRCC cohorts of the TCGA database, representing transcriptomic data of 891 patients. Using principal component analysis, we visualized datasets as t-SNE plot for cluster detection. Clusters were characterized by machine learning, resulting gene signatures were validated by correlation analyses in the TCGA dataset and three external datasets (ICGC RECA-EU, CPTAC-3-Kidney, and GSE157256).

Results: Many RCC samples co-clustered according to histopathology. However, a substantial number of samples clustered independently from histopathologic origin (*mixed subgroup*)—demonstrating divergence between histopathology and transcriptomic data. Further analyses of *mixed subgroup* via machine learning revealed a predominant mitochondrial gene signature—a trait previously known for chRCC—across all histopathologic subgroups. Additionally, ccRCC samples from *mixed subgroup* presented an inverse correlation of mitochondrial and angiogenesis-related genes in the TCGA and in three external validation cohorts. Moreover, *mixed subgroup* affiliation was associated with a highly significant shorter overall survival for patients with ccRCC—and a highly significant longer overall survival for chRCC patients.

Conclusions: Pan-RCC clustering according to RNA-sequencing data revealed a distinct histology-independent subgroup characterized by strengthened mitochondrial and weakened angiogenesis-related gene signatures. Moreover, affiliation to *mixed subgroup* went along with a significantly shorter overall survival for ccRCC and a longer overall survival for chRCC patients. Further research could offer a therapy stratification by specifically addressing the mitochondrial metabolism of such tumors and its microenvironment.

Keywords: kidney cancer, pan-RCC, machine learning, mitochondrial DNA, mtDNA, mTOR

INTRODUCTION

Basic and clinical research in renal cell carcinoma (RCC) mainly focuses on established histopathologic subgroups, specifically clear cell (ccRCC), papillary (pRCC) and chromophobe RCC (chRCC). Accordingly, histopathology is of crucial relevance for determining treatment strategies including drug sequencing in RCC patients, especially in a metastasized situation. As reflected in the WHO classification for renal neoplasms (1), dividing RCC in three distinct (sub-)entities does not completely mirror tumor biology and its complexity. Instead, sub-categories such as clear cell papillary RCC (2) were introduced, indicating substantial greyscales between classical histopathologic subgroups.

By performing transcriptomic analyses, researchers have identified characteristic signatures of ccRCC, pRCC, and chRCC—thereby supporting established histopathologic classification (3–5). Although comprehensive pan-RCC analyses have been performed previously, the boundaries of histopathologic origin usually were not scrutinized (6, 7).

Using principal component analysis (PCA) with subsequent machine learning (ML) algorithms, we mapped 891 RCC specimen irrespective of histopathologic boundaries. Following this comprehensive pan-RCC approach allowed us to identify novel RCC subgroups with a prognostic impact for cancer patients and provide first functional insight.

MATERIALS AND METHODS

Data Acquisition

This work mainly based on data provided by The Cancer Genome Atlas (TCGA) consortium. Utilized entities were ccRCC (KIRC cohort, $n = 538$ tumor samples), chRCC (KICH cohort, $n = 65$ samples) and pRCC (KIRP cohort, $n = 288$ samples) downloaded from the GDC portal (https://portal.gdc.cancer.gov). For evaluation, we used data provided by the ICGC (international network of cancer genome projects) (8), specifically the RECA-EU data set, comprising of $n = 91$ ccRCC samples (https://dcc.icgc.org/projects/RECA-EU) with available RNA-sequencing data. Additionally, we used ccRCC samples from the CPTAC-3-Kidney cohort ($n = 101$) as further external validation (https://portal.gdc.cancer.gov/projects/CPTAC-3) (9). Regarding RCC caused by hereditary leiomyomatosis (hlRCC)—also known as fumarate hydratase (FH)-deficient RCC—we further examined the smaller GSE157256 cohort (10) as another source for evaluation ($n = 26$) (https://www.ncbi.nlm.nih.gov/geo/query/acc.cgi?acc=GSE157256). For all mentioned datasets, we used unprocessed FPKM or RSEM (GSE157256) values as provided.

Bioinformatical Analyses

The presented work was implemented in a Jupyter Notebook environment (version 7.5.0)—which is available upon request—using the Python version 3.6.9, SciPy version 1.3.0 (11) and scikit-learn version 0.22.1 (12).

t-SNE Plotting

Our project was based on the 2D representation of high-dimensional data with subsequent cluster analysis using ML. For plotting unprocessed FPKM data in 2D, we performed a PCA with 50 components—using PCA of the sklearn.decomposition module—and used the results as input for t-SNE plotting (sklearn.manifold module) (13). For calculating and plotting in 2D, we used a random initiation with a learning rate of 300 and a perplexity of 27 with 10.000 iterations. For reproducibility, we used the random state 0 (n_components=2, init='random', perplexity=27, n_iter=10,000, learning_rate=300, random_state=0). Additionally, cluster annotation and t-SNE coordinates for each TCGA sample from all RCC subgroups are shown in **Supplementary Table 1**.

Random Forest Learning

After manual annotation, we used these clusters for subsequent learning steps. For this, we applied a model utilizing Random Forest (RF) Classifier (RandomForestClassifier of the sklearn.ensemble module). For training our model, we used a 70/30 split, letting the model learn on 70% of the data and evaluating it on the remaining 30%, with 1,000 trees in the forest (n_estimators=1,000), leaving out the pRCC samples not clustering in one of the three annotated clusters or the *mixed subgroup*. For further investigation, we trained 20 models and used the one with the highest test accuracy for subsequent feature analysis. For this purpose, we assigned the according "feature values," implying the importance of each feature, to each feature, representing the Ensembl gene IDs. We identified the top 200 genes with the strongest influence on our model, which distinguished our manually annotated clusters with the highest accuracy. These top 200 genes of our best performing model overlapped in 92 genes with the mean of the other 19 trained models, outperforming them in test accuracy—with 92.06%

compared to the mean of 83.42% (min. 79.37%, max. 86.11%). A 10-fold-crossvalidation of the data yielded a mean accuracy of 84.52% (+/- 9.16%).

Plots and Statistical Analysis

Correlation and scatter plots were generated using matplotlib. Indicated Pearson Rs were calculated using the according module from scipy.stats. For subsequent survival analysis of patient survival, Kaplan Meier (KM) plots were generated using the lifelines module (version 0.23.1) with the KaplanMeierFitter (14).

If not stated otherwise, statistical tests were performed using Kruskal-Wallis-Test—using scipy.stats module including indicated significances, for which we used the statannot module for python (version 0.2.3; https://github.com/webermarcolivier/statannot). For the analysis of further interactions and relations between the identified 200 genes with the highest influence on the learned model, we used a Network generated by StringDB (15). The coloring of the nodes was done directly by StringDB for selected gene-sets stated as significant.

For validation purposes of relevant pathways and genes previously identified by mRNA expression patterns, we used the level four protein expression levels provided by The Cancer Proteome Atlas (16) (TCPA—https://tcpaportal.org/tcpa/) for the three investigated cohorts.

RESULTS

Clustering 891 RCC Samples Independently From Histopathologic Origin

For PCA, we used the RNAseq data of all registered RCC specimen ($n = 891$) within the TCGA database, irrespective of their histopathologic origin. We combined all tumor specimen in a t-SNE-plot in order to illustrate familiarities and discordances between samples based upon unprocessed FPKM values. **Figure 1A** represents the t-SNE plot, with ccRCC, pRCC and chRCC samples marked in red, green and blue, respectively. Of note, most tumor samples clustered to RCC subgroups, thereby confirming the familiarity and the validity of histopathologic classification. **Figure 1B** represents the schematic distribution of clusters identified within the t-SNE-plot. Interestingly, pRCC samples did not cluster in a single subgroup, but instead in three distinct subgroups (cluster I-III), whereas ccRCC specimen built another cluster (IV). However, apart from most samples clustering according to histopathology, we identified a distinct cluster containing a mixture of ccRCC, pRCC and chRCC samples (**Figure 1B**; cluster V). We named this accumulation *mixed subgroup*. As depicted in **Figure 1C**, we manually split and defined the novel clusters for further ML-based analyses. Aside from three distinct pRCC clusters, which surely merit future investigation, we were mainly interested in this *mixed subgroup*—containing 19% of ccRCC, 36.8% of pRCC and 81.5% of chRCC samples (**Figure 1D**). Of note, our clustering approach revealed no clear separation between type 1 and type 2 pRCC (**Supplementary Figure 1**).

Clinical Characterization of Patient Samples From *Mixed Subgroup*

We next examined the clinical characteristics of RCC patient samples depending on their affiliation to the *mixed subgroup* (**Table 1**). Comparing ccRCC samples inside and outside the *mixed subgroup*, we found no significant differences in age, gender, tumor stage, tumor extension (T classification), lymphonodal invasion (*N* classification) or metastasis (M classification). In contrast, tumor grading was significantly different ($p = 0.014$). For pRCC, *mixed subgroup* patients were significantly older (65.1 ± 10.9 vs. 59.6 ± 12.1 years; $p = 0.0002$) than patients with pRCC not belonging to this cluster. Moreover, the proportion of male patients was significantly higher in the *mixed subgroup* ($p = 0.001$). In contrast to the age distribution in patients with pRCC, chRCC samples from the *mixed subgroup* were significantly younger (49.6 ± 13.2 vs. 61.9 ± 12.9 years; $p = 0.012$). In addition, the lymphonodal status differed significantly between the two subgroups ($p = 0.005$).

ML-Based Functional Characterization of Patient Samples Affiliated to *Mixed Subgroup*

To learn more about functional traits and characteristic differences of the clusters, we applied further ML based on the visual separation (**Figure 1C**). Therefore, we determined the top 200 genes best classifying the novel clusters. As shown in **Figure 2**, we depicted these genes in a StringDB gene network to uncover relevant signaling pathways. We found a substantial accumulation of mitochondrial genes—with String DB identifying "oxidative phosphorylation" (GO:0006119) and "respiratory electron transport chain" (GO:0022904) as highly overrepresented pathways in our analysis. Additionally, "blood vessel development" (GO:0001568) and "blood vessel morphogenesis" (GO:0048514) were also highly overrepresented.

Moreover, mtDNA genes represented all of the top 10 classifier genes in our RF calculation—as shown in **Table 2**. In conclusion, we found mitochondrial and angiogenesis-related gene signatures to be most predictive within our clustering approach.

Mitochondrial and Angiogenesis-Related Genes Inside and Outside *Mixed Subgroup*

Alterations and overexpression of mtDNA have been described as characteristic traits of chRCC (5, 17, 18)—and more than 80% of the chRCC samples in our analysis were located in the *mixed subgroup* (see **Figure 1D**). Due to this relative overrepresentation of chRCC in this cluster, we first checked whether our RF analysis was biased by a high proportion of chRCC samples. For this reason, we compared unprocessed FPKM values of mitochondrial genes for ccRCC, pRCC, and chRCC samples depending on the affiliation to the *mixed subgroup*. We found a highly significant overexpression of mitochondrial genes for chRCC samples inside compared to samples outside the *mixed subgroup*.

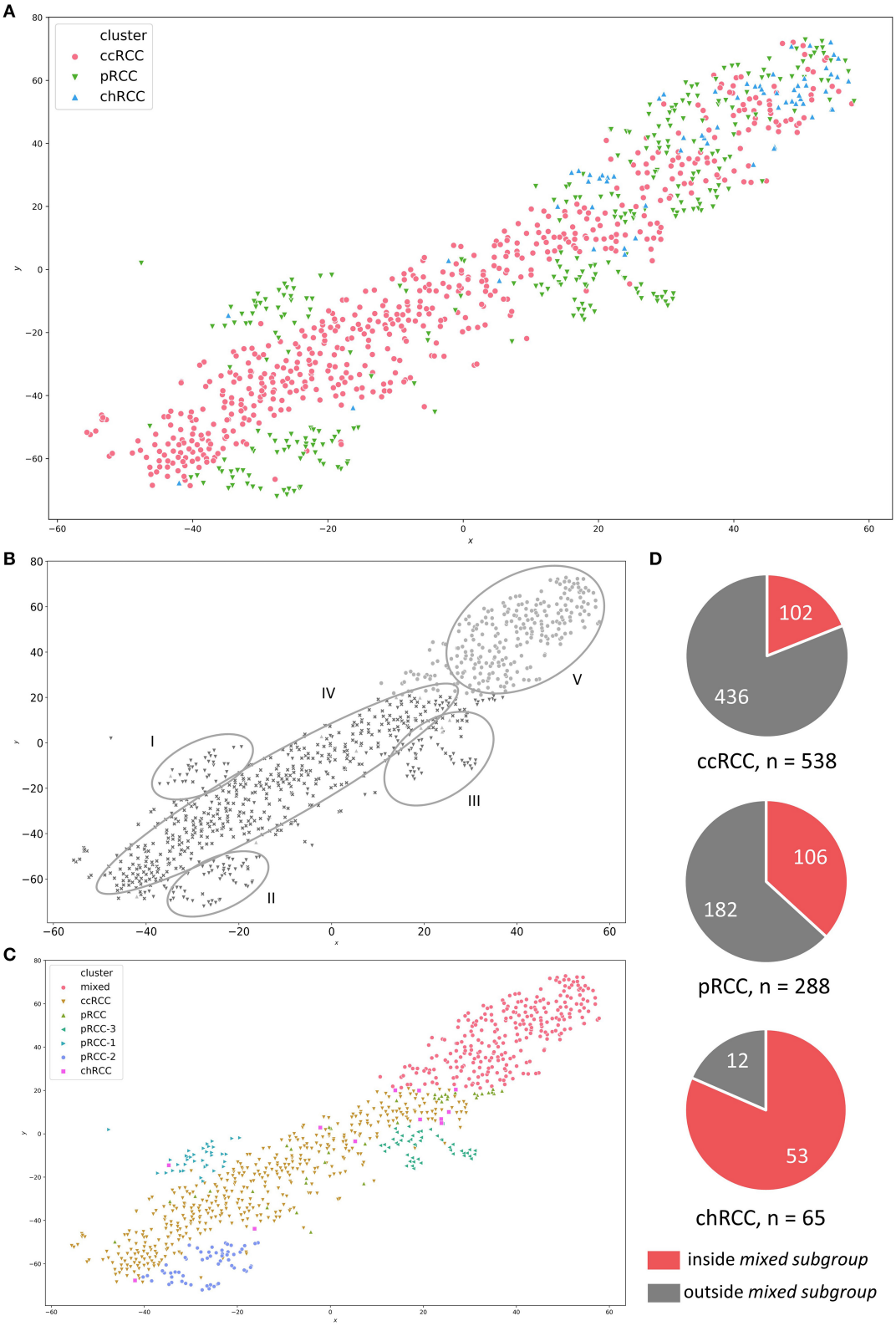

FIGURE 1 | (A) t-SNE-plot for RNA-sequencing data from ccRCC (red), pRCC (green) and chRCC (blue) specimen within the TCGA database. **(B)** Visually identified clusters—I to III: distinct pRCC subgroups; IV: ccRCC samples; V: mixed subgroup containing ccRCC, pRCC and chRCC tumors. **(C)** Manually defined clusters based on visual separation. **(D)** Pie charts illustrating absolute numbers and proportions of RCC samples inside/outside the mixed subgroup for each RCC subgroup.

TABLE 1 | Clinical characteristics of RCC patients inside and outside the mixed subgroup.

		ccRCC non-mixed	ccRCC mixed	*p*	pRCC non-mixed	pRCC mixed	*p*	chRCC non-mixed	chRCC mixed	*p*
		***n* = 428**	***n* = 102**		***n* = 182**	***n* = 105**		***n* = 12**	***n* = 53**	
Age	mean	60.2 ± 2.2	62.0 ± 11.8	0.196	59.6 ± 12.1	65.1 ± 10.9	**0.00021**	61.9 ± 12.9	49.6 ± 13.2	**0.012**
Gender	m	273 (63.79%)	71 (69.61%)	0.269	123 (67.58%)	89 (84.76%)	**0.001**	10 (83.33%)	29 (54.72%)	0.07
	f	155 (36.21%)	31 (30.39%)		59 (32.42%)	16 (15.24%)		2 (16.67%)	24 (45.28%)	
Tumor stage	I	223 (52.47%)	42 (64.29%)	0.166	108 (64,70%)	64 (38,32%)	0.419	2 (16.67%)	18 (33.96%)	0.1
	II	43 (10.12%)	14 (8.33%)		16 (9,60%)	4 (2,40%)		5 (41.67%)	20 (37.74%)	
	III	90 (21.18%)	33 (19.64%)		34 (20,30%)	16 (9,58%)		1 (8.33%)	13 (24.53%)	
	IV	69 (16.23%)	13 (7.74%)		9 (5,40%)	6 (3,60%)		4 (33.33%)	2 (3.77%)	
T	T1	228 (53.27%)	43 (42.57%)	0.092	119 (64.67%)	74 (70.48%)	0.463	2 (16.67%)	18 (33.962%)	0.14
	T2	53 (12.38%)	16 (15.84%)		22 (11.96%)	10 (9.52%)		5 (41.67%)	20 (37.74%)	
	T3	137 (32.00%)	41 (40.59%)		39 (21.20%)	20 (19.05%)		3 (25%)	15 (28.30%)	
	T4	10 (2.33%)	1 (0.99%)		4 (2.17%)	1 (0.95%)		2 (16.66%)	0 (0%)	
N	N0	192 (93.66%)	47 (94%)	0.929	29 (59.18%)	20 (71.43%)	0.21	4 (57.14%)	35 (94.60%)	**0.005**
	N1	13 (6.34%)	3 (6%)		16 (32.66%)	8 (28.57%)		2 (28.57%)	1 (2.7%)	
	N2	0 (0%)	0 (0%)		4 (8.16%)	0 (0%)		1 (14.29%)	1 (2.7%)	
M	M0	19 (90.48%)	3 (75%)	0.392	60 (63.16%)	35 (89.74%)	0.654	4 (80%)	3 (75%)	0.866
	M1	2 (9.52%)	1 (25%)		35 (36.84%)	4 (10.26%)		1 (20%)	1 (25%)	
Grading	G1	13 (3.06%)	13 (11.93%)	**0.014**						
	G2	195 (45.88%)	32 (29.36%)							
	G3	158 (37.18%)	48 (44.04%)							
	G4	59 (13.88%)	16 (14.67%)							

Except for age (mean ± standard deviation), all characteristics were presented as absolute values. p-values highlighted as bold were significant for $p < 0.05$.

However, alterations in mtDNA expression were not limited to chRCC. Instead, *mixed subgroup* samples from pRCC as well as ccRCC exhibited a highly significant mtDNA overexpression. **Figures 3A,B** illustrate unprocessed FPKM values for candidate genes MT-CO2 (**Figure 3A**) and MT-CO3 (**Figure 3B**).

For angiogenesis-related genes such as FLT1 (**Figure 3C**) and KDR (**Figure 3D**), we discovered significantly lower expression levels within ccRCC samples from *mixed subgroup*. Additionally, we discovered significant expression differences for genes displayed in **Table 2**, regardless of the underlying histopathologic entity, when compared to normal tissue samples (**Supplementary Figures 2–7**). Regarding expression of mitochondrial and angiogenesis-related genes in ccRCC, we found negative Pearson R correlations in the TCGA dataset (**Figure 4A**) as well as all three RCC validation cohorts (**Figures 4B–D**). In line with a weaker angiogenesis signature, ccRCC and pRCC samples from *mixed subgroup* displayed significantly lower levels of c-MET (**Supplementary Figure 8**).

Summing up the results, mtDNA and angiogenesis signatures proved to be predictive not only for our pan-RCC clustering approach—but also specifically for ccRCC samples. Moreover, expression levels of mitochondrial and angiogenesis-associated genes were negatively correlated in four independent RCC cohorts.

Impact of *Mixed Subgroup* Affiliation on Patient Survival

After characterizing *mixed subgroup* samples from a clinical and a functional perspective, we next investigated whether an affiliation to this cluster impacted patient prognosis. Strikingly, survival analysis revealed a significantly worse prognosis ($p = 0.005$) for ccRCC patients from the TCGA database belonging to the *mixed subgroup* (**Figure 5A**). For chRCC patients (**Figure 5B**), cluster affiliation had the opposite effect—with significantly higher survival rates ($p = 0.003$) for patients inside the *mixed subgroup*. In contrast, there was no significant survival difference for patients with pRCC (**Figure 5C**).

Given that clinical characteristics such as tumor stage and TNM classification did not differ significantly for patients with ccRCC (**Table 1**), we reasoned that the survival impact could partially be due to an inadequate therapy stratification. Using *The Cancer Proteome Atlas* (TCPA) (16, 19), we therefore analyzed the protein expression of *bona fide* gene candidates related to mTOR and PI3K/Akt signaling, angiogenesis and immune signaling (**Figure 5D**). Regarding ccRCC as well as pRCC samples, we found a significant downregulation of VEGFR2 and HIF1A protein expression in *mixed subgroup* samples. For both subgroups, this downregulation of angiogenesis-related genes was accompanied by a significant upregulation of PD-L1 expression. Moreover, protein expression of TSC1 and PTEN

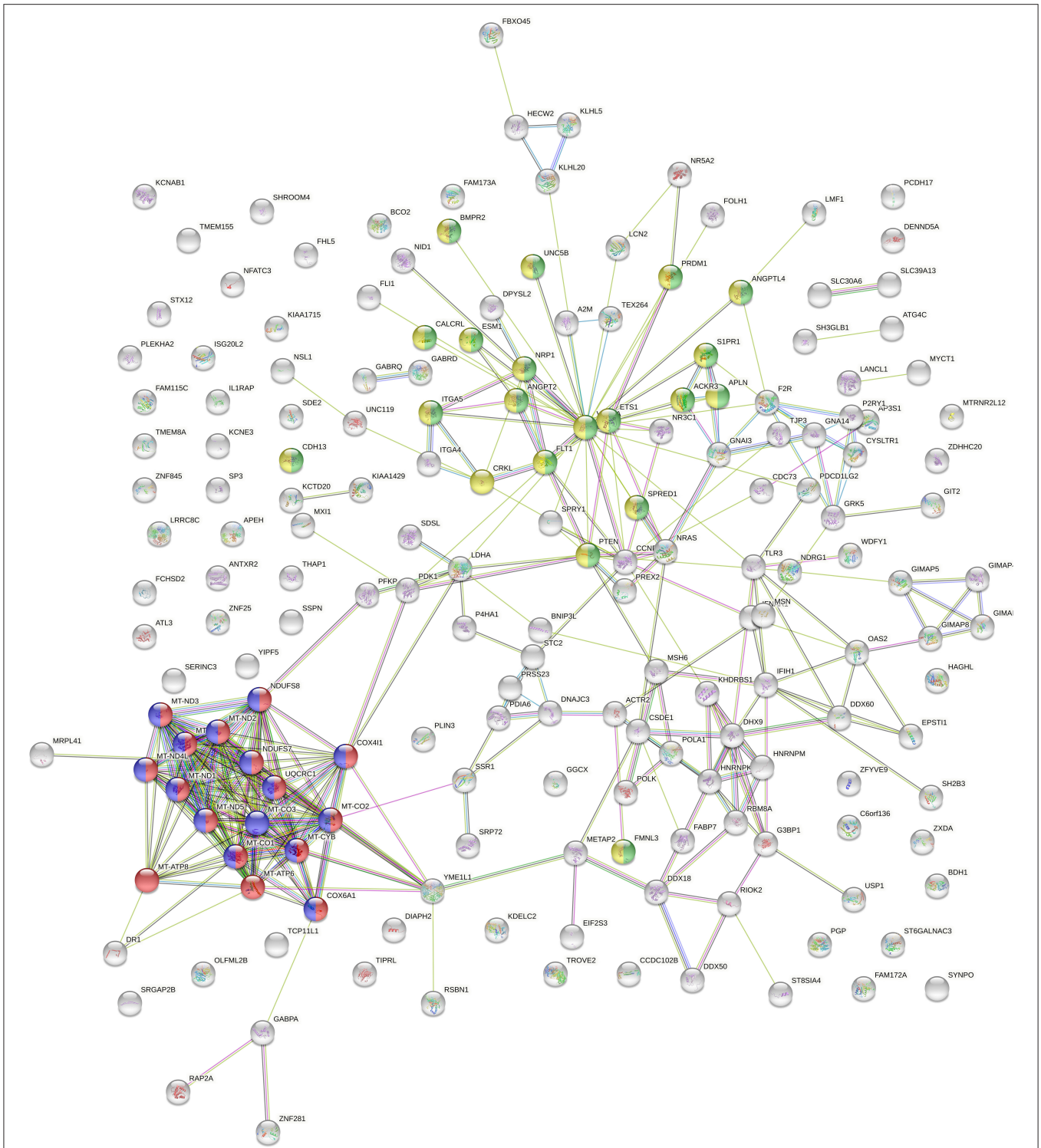

FIGURE 2 | StringDB network of the top 200 genes identified as relevant classifiers for RCC sample clusters from **Figure 1C**. Genes affiliated with oxidative phosphorylation and respiratory electron transport chain are marked in red and blue, genes related to blood vessel morphogenesis and blood vessel development are marked in green and yellow.

was downregulated in *mixed subgroup* samples. While pRCC samples from our novel cluster exhibited a significant mTOR downregulation, the slight increase in mTOR protein expression of ccRCC samples from *mixed subgroup* was not significant. Potentially due to lower sample numbers, TCPA analysis revealed no significant expression differences for chRCC specimen.

TABLE 2 | Gene families significantly overrepresented in the top 200 cluster classifying genes from Random Forest (RF) analysis.

Mitochondrial Genes			Angiogenesis-related Genes		
HGNC Symbol	**Ensembl gene ID**	**RF-Feature Position**	**HGNC Symbol**	**Ensembl gene ID**	**RF-Feature Position**
MT-CYB	ENSG00000198727	1	ETS1	ENSG00000134954	13
MT-ND4	ENSG00000198886	2	ANGPT2	ENSG00000091879	33
MT-CO1	ENSG00000198804	3	APLN	ENSG00000171388	37
MT-CO3	ENSG00000198938	4	FLT1	ENSG00000102755	38
MT-CO2	ENSG00000198712	5	CRKL	ENSG00000099942	46
MT-ND4L	ENSG00000212907	6	ITGA5	ENSG00000161638	54
MT-ATP6	ENSG00000198899	7	NRP1	ENSG00000099250	56
MT-RNR1	ENSG00000211459	8	PRDM1	ENSG00000057657	93
MTATP6P1	ENSG00000248527	9	PTEN	ENSG00000171862	109
MT-ND1	ENSG00000198888	10	VEGFA	ENSG00000112715	112
MT-ND2	ENSG00000198763	20	ACKR3	ENSG00000144476	114
MT-ND3	ENSG00000198840	24	CDH13	ENSG00000140945	146
MT-RNR2	ENSG00000210082	25	BMPR2	ENSG00000204217	148
			CALCRL	ENSG00000064989	177
			ESM1	ENSG00000164283	191

For each gene, HGNC symbol, Ensembl gene IDs, and the position in our calculation is shown.

In summary, we found a highly significant and clinically relevant influence of *mixed subgroup* affiliation in RCC patients from the TCGA database—with a better prognosis for chRCC and a worse overall survival for ccRCC patients.

DISCUSSION

Classifying cancer tissue into three histopathologic subgroups—clear cell, papillary and chromophobe—critically determines treatment strategies and prognosis of RCC patients. However, growing evidence highlights that this classification is not absolute nor distinct. Instead, the WHO system of renal cell tumors from 2016 contained several additional subgroups, such as succinate dehydrogenase-deficient renal carcinoma and clear cell papillary RCC (1). Previous functional analyses on RCC mainly focused on isolated gene signatures, which were characteristic and prognostic for single histopathologic subgroups (4, 5, 20, 21)—e.g., ClearCode34 (22) for determining the individual risk of recurrence in localized ccRCC. Moreover, researchers aimed to identify biomarkers and gene networks predictive of future therapy response—especially for angiogenesis inhibition, tyrosine kinase inhibition (TKI) and immune checkpoint blockade (23–27). Interestingly, a recent study was able to discriminate ccRCC and pRCC samples originating from proximal tubules of the nephron from chRCC specimen originating from distal tubules based on the metabolic and lipidomic profile of the samples (28).

Pan-RCC Clustering Identifies Subgroup Beyond Established Histopathologic Classification

While most studies focused on gene signatures within given histopathologic boundaries, we aimed to challenge the absoluteness and robustness of RCC subgroup classification. In our pan-RCC approach, we performed a clustering for all RCC specimen from the TCGA database. Of note, a substantial number of RCC samples clustered independently from histopathologic origin. We called this cluster *mixed subgroup*. Conferring samples inside and outside the *mixed subgroup*, ccRCC patients exhibited no significant differences regarding age, gender, tumor stage and TNM classification. In contrast, grading of tumor samples appeared significantly different, partially due to a higher proportion of G1 tumors in the *mixed subgroup*. pRCC patients from this cluster were significantly older than the remainder of the group. Moreover, the proportion of male patients was higher inside the *mixed subgroup*. All other clinical characteristics did not differ significantly. Patients with chRCC within the cluster were significantly younger and had a higher proportion of N0 patients.

ML Reveals Mitochondrial Genes as Most Influential for Pan-RCC Clustering

For further functional characterization, we applied RF learning in order to identify gene signatures most predictive for the novel clusters. This ML approach revealed mitochondrial genes to be most influential for the basic clustering, followed by genes related to angiogenesis. As mtDNA overexpression is a reported feature of chRCC (5, 17, 18), we had to rule out a systematic bias caused by the high proportion of chRCC samples within the *mixed subgroup*. Therefore, we analyzed mtDNA expression in all RCC subgroups depending on subgroup affiliation. Of note, ccRCC, pRCC, and chRCC specimen belonging to the *mixed subgroup* all displayed significantly higher levels of mtDNA expression compared to the counterparts outside this cluster. In ccRCC, this mtDNA upregulation went along with a downregulation of angiogenesis-related genes. Taking these results together led

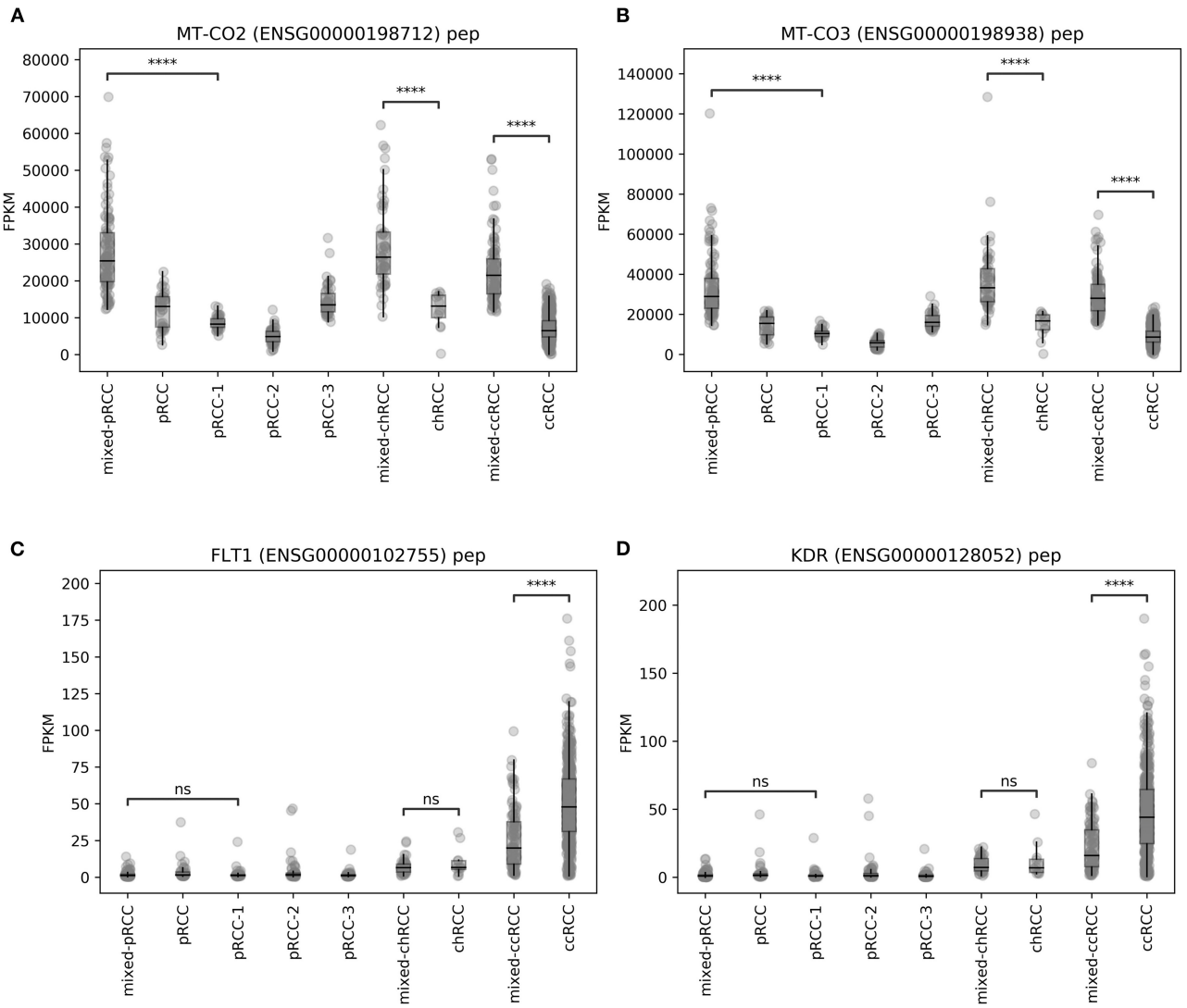

FIGURE 3 | Unprocessed FPKM values of exemplary candidate genes–**(A,B)** MT-CO2 and MT-CO3, **(C,D)** FLT1 and KDR. ns, not significant, ****$p < 0.0001$.

to significantly negative correlations between mitochondrial and angiogenesis signatures—not only in ccRCC samples from TCGA but also in the RECA-EU and CPTAC-3-Kidney cohorts taken as external validation. Moreover, comparable results from the GSE157256 cohort representing fumarate hydratase-deficient RCC could imply a general underlying mechanism beyond RCC subgroups.

A pan-RCC subgroup characterized by a prominent mtDNA signature appeared surprising at first sight. Although aberration in mitochondrial signaling is known across RCC subgroups, these deviations are not considered being unidirectional toward an upregulation of mitochondrial transcripts and mitochondrial mass (29). While mtDNA aberrations and overexpression are mainly regarded as a characteristic trait of chRCC tissue (5, 17, 18), downregulation of mitochondrial enzymes with increasing tumor stages and decreased oxidative capacity were previously reported for ccRCC (30–32). However, growing evidence indicates that mtDNA can also have oncogenic functions, thereby appearing as a potential (co-)target in future cancer therapies (33). Specifically, researchers showed that tumor cells lacking mtDNA could not metastasize *in vivo*—after restoration of mtDNA levels, cancer cells regained this ability (34). In line with these findings, Schöpf et al. demonstrated the importance of oxidative phosphorylation in high-grade prostate cancer by describing a high-risk subgroup characterized by a distinct mitochondrial signature (35). Given the established role of angiogenesis and angiogenesis-related genes such as VEGFR2 in high-risk prostate cancer (36, 37), further examining the interaction of mitochondrial and angiogenesis pathways in prostate cancer could prove beneficial.

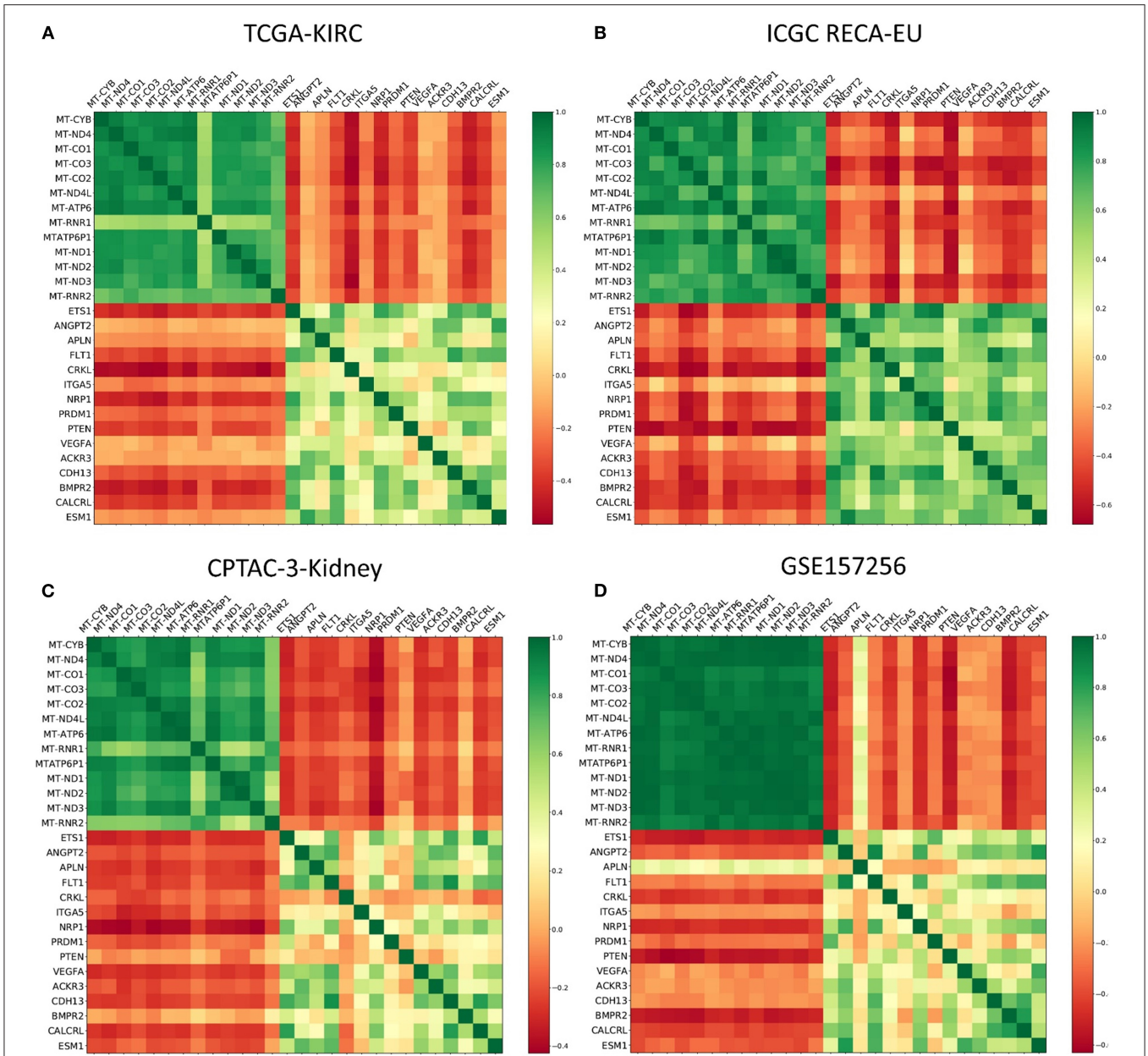

FIGURE 4 | Color-coded presentation of the Pearson R correlation matrix of mitochondrial genes and angiogenesis-associated genes for ccRCC samples from the **(A)** TCGA, **(B)** the ICGC RECA-EU, and **(C)** the CPTAC-3-Kidney cohort as well as **(D)** Fumarate hydratase-deficient RCC samples contained within the GSE157256 cohort.

Assessing Prognosis and Therapeutic Windows for *Mixed Subgroup* Patients

Importantly, ccRCC patients inside the *mixed subgroup* suffered from significantly worse overall survival. This result was even more surprising given the non-significant differences in TNM stage between both subgroups. For pRCC patients, we did not find significant survival differences regarding *mixed subgroup* affiliation. However, we identified three distinct pRCC clusters. This result surely merits further investigation regarding functions and prognosis of each pRCC cluster. In contrast, patients with chRCC belonging to the *mixed subgroup* exhibited a significantly longer overall survival. In summary, survival data from ccRCC and chRCC patients underline the role of the *mixed subgroup* as a novel prognostic RCC cluster identified by our comprehensive clustering approach. Regarding the striking survival impact in ccRCC combined with non-differing clinical characteristics, it was tempting to assume that diverging outcomes were at least partially treatment-related.

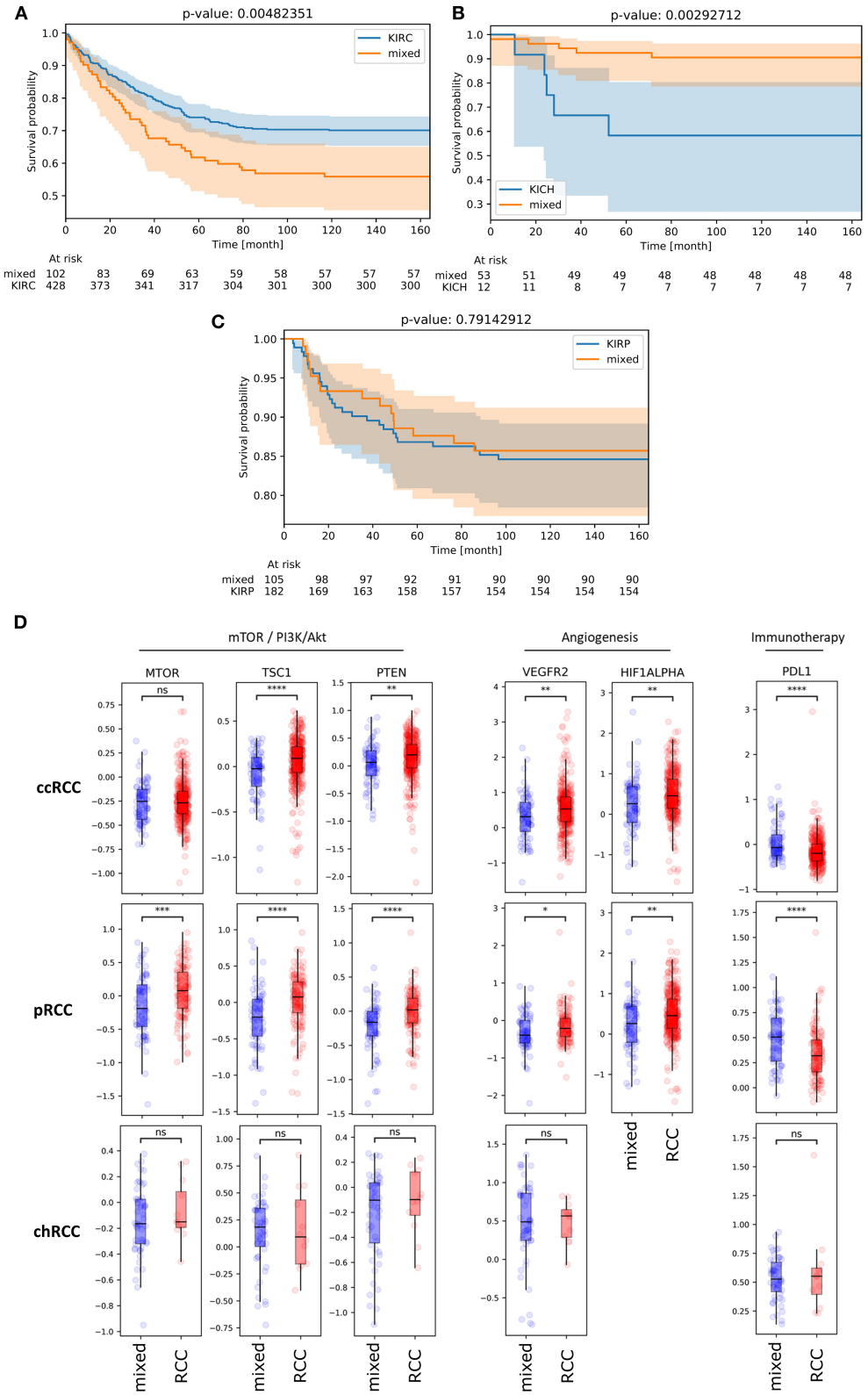

FIGURE 5 | (A,B) KM plots illustrating overall survival of patients with ccRCC **(A)**, chRCC **(B)** and pRCC **(C)** from TCGA database depending on mixed subgroup affiliation. **(D)** Protein expression levels of *bona fide* candidate genes from mTOR-associated, angiogenesis-related and immune-related signaling for ccRCC, pRCC and chRCC samples inside (blue) and outside (red) the mixed subgroup (TCPA database). ns, not significant. $^{*}p < 0.05$, $^{**}p < 0.01$, $^{***}p < 0.001$, $^{****}p < 0.0001$.

First, addressing mtDNA overexpression appears as an attractive therapeutic approach, as compounds such as the anthelmintic drug atovaquone (38) and the antibiotic tigecycline (39) were shown to chemo-sensitize RCC. Moreover, our results could explain the beneficial effect of additional Metformin intake during treatment of metastatic RCC, as this biguanide works as a mitochondrial inhibitor (40–42). Above all, mTOR inhibitors—which already have the approval for treating RCC—appear as promising candidates for *mixed subgroup* RCC patients. mTOR signaling is tightly linked to mitochondrial function (43, 44). Recently, a mitochondrial complex I inhibitor (IACS-010759) targeting oxidative phosphorylation in cancer cells showed efficacy in brain cancer and leukemia models (45).

Given the downregulation of angiogenesis-related gene signatures in ccRCC patients from the *mixed subgroup*, inhibition of angiogenesis and TKI do not appear as attractive first-line approaches for these patients. Indeed, the predominant use of TKI within the historical RCC cohort from the TCGA database may partially explain the striking survival differences observed in this analysis. Supporting our findings from RNA-sequencing, protein levels of VEGFR2 and HIF2A were lowered in the *mixed subgroup* for ccRCC as well as pRCC patients. Regarding the downregulation of c-MET in ccRCC and pRCC samples from the *mixed subgroup*, treatment with MET (co-)inhibitors such as Cabozantinib (46) does not appear promising, either.

Further research could clarify whether immune checkpoint inhibition constitutes a viable treatment strategy in our new cluster. At first sight, highly significant protein overexpression of PD-L1 in ccRCC and pRCC patients from the *mixed subgroup* makes it an attractive therapeutic target. However, unlike in entities as melanoma and non-small cell lung cancer (47), it is still unclear whether PD-L1 overexpression in RCC results in better response to immunotherapy (48). Completely in line with our findings, several clinical trials already stated that PD-L1 overexpression marked a RCC high-risk cohort (48, 49).

Our study has some limitations regarding its methodology and its retrospective nature. We are aware that manual cluster annotation approaches naturally contain immanent biases. Moreover, our findings derive from the re-analysis of historic cohorts and require further—ideally prospective—validation in future studies. Essentially, we identified a high-risk ccRCC subgroup best described by a mitochondrial signature and a downregulation of angiogenesis-related genes, which was not exclusive to one RCC subgroup. Although preliminary, these results could contribute to an individual risk classifier based on transcriptomic data from patients' samples and help establishing personalized medicine in RCC.

DATA AVAILABILITY STATEMENT

Publicly available datasets were analyzed in this study. This data can be found here: https://portal.gdc.cancer.gov/projects https://dcc.icgc.org/projects/RECA-EU https://www.ncbi.nlm.nih.gov/geo/query/acc.cgi?acc=GSE157256 https://portal.gdc.cancer.gov/projects/CPTAC-3.

AUTHOR CONTRIBUTIONS

AM, AGS, BS, SM, MK: conceptualization. AM, PK: methodology. AM, AGS, AK, MB, MK: writing – draft preparation. AM, AGS, MB, CK, HK, AR, RB, PK, BS, SM, MK: writing – review and editing. HK, AR, RB, BS, SM: supervision/funding/infrastructure. All authors contributed to the article and approved the submitted version.

FUNDING

AM was funded by a grant of the Central Unit for Precision Oncology (Z-14, Interdisciplinary Center for Clinical Research, University Hospital Würzburg, Germany). Additionally, this project was supported in part by the Apulian Regional Project Medicina di Precisione to AGS. Moreover, MK was funded by a personal grant from Else-Kröner-Foundation (Else Kröner Integrative Clinician Scientist College for Translational Immunology, University Hospital Würzburg, Germany). This publication was supported by the Open Access Publication Fund of the University of Würzburg.

ACKNOWLEDGMENTS

The results shown here are based upon data generated by the TCGA Research Network: https://www.cancer.gov/tcga.

SUPPLEMENTARY MATERIAL

The Supplementary Material for this article can be found online at: https://www.frontiersin.org/articles/10.3389/fonc.2021.621278/full#supplementary-material

Supplementary Figure 1 | Isolated illustration of pRCC samples from the pan-RCC clustering approach based on t-SNE plotting—with known affiliation to clinically established type 1 and type 2 pRCC subtypes. RCC, renal cell carcinoma; pRCC, papillary renal cell carcinoma.

Supplementary Figure 2 | Expression comparison between clear cell renal cell carcinomas outside (ccRCC) and inside (mixed) the *mixed subgroup* and respective normal tissue samples for mitochondrial genes identified by machine learning. ns, not significant. $*p < 0.05$, $**p < 0.01$, $***p < 0.001$, $****p < 0.0001$.

Supplementary Figure 3 | Expression comparison between clear cell renal cell carcinomas outside (ccRCC) and inside (mixed) the *mixed subgroup* and respective normal tissue samples for angiogenesis genes identified by machine learning. ns, not significant. $*p < 0.05$, $**p < 0.01$, $***p < 0.001$, $****p < 0.0001$.

Supplementary Figure 4 | Expression comparison between the identified papillary renal cell carcinoma cluster outside (pRCC 1 to 3) and inside (mixed) the *mixed subgroup* and respective normal tissue samples for mitochondrial genes identified by machine learning. ns, not significant. $*p < 0.05$, $**p < 0.01$, $***p < 0.001$, $****p < 0.0001$.

Supplementary Figure 5 | Expression comparison between the identified papillary renal cell carcinoma cluster outside (pRCC 1 to 3) and inside (mixed) the *mixed subgroup* and respective normal tissue samples for angiogenesis genes identified by machine learning. ns, not significant. $*p < 0.05$, $**p < 0.01$, $***p < 0.001$, $****p < 0.0001$.

Supplementary Figure 6 | Expression comparison between chromophobe renal cell carcinomas outside (chRCC) and inside (mixed) the *mixed subgroup* and

respective normal tissue samples for mitochondrial genes identified by machine learning. ns, not significant. *$p < 0.05$, **$p < 0.01$, ***$p < 0.001$, ****$p < 0.0001$.

Supplementary Figure 7 | Expression comparison between chromophobe renal cell carcinomas outside (chRCC) and inside (mixed) of *mixed subgroup* and respective normal tissue samples for angiogenesis genes identified by machine learning. ns, not significant. *$p < 0.05$, **$p < 0.01$, ***$p < 0.001$, ****$p < 0.0001$.

Supplementary Figure 8 | Unprocessed FPKM values for c-MET within manually annotated clusters across RCC subgroups. ns, not significant. **$p < 0.01$, ****$p < 0.0001$.

Supplementary Table 1 | Coordinates within the t-SNE-plot and subsequent attributed cluster affiliation for all RCC samples from the TCGA database included in our analysis. RCC, renal cell carcinoma.

REFERENCES

1. Moch H, Cubilla AL, Humphrey PA, Reuter VE, Ulbright TM. The 2016 WHO classification of tumours of the urinary system and male genital organs—part a: renal, penile, and testicular tumours. *Eur Urol.* (2016) 70:93–105. doi: 10.1016/j.eururo.2016.02.029
2. Zhou H, Zheng S, Truong LD, Ro JY, Ayala AG, Shen SS. Clear cell papillary renal cell carcinoma is the fourth most common histologic type of renal cell carcinoma in 290 consecutive nephrectomies for renal cell carcinoma. *Hum Pathol.* (2014) 45:59–64. doi: 10.1016/j.humpath.2013.08.004
3. The cancer genome atlas research network comprehensive molecular characterization of clear cell renal cell carcinoma. *Nature.* (2013) 499:43–49. doi: 10.1038/nature12222
4. The cancer genome atlas research network comprehensive molecular characterization of papillary renal-cell carcinoma. *N Engl J Med.* (2016) 374:135–45. doi: 10.1056/NEJMoa1505917
5. Davis CF, Ricketts CJ, Wang M, Yang L, Cherniack AD, Shen H, et al. The somatic genomic landscape of chromophobe renal cell carcinoma. *Cancer Cell.* (2014) 26:319–30. doi: 10.1016/j.ccr.2014.07.014
6. Jia K, Wu Y, Huang J, Wu H. Survival-associated alternative splicing events in pan-renal cell carcinoma. *Front Oncol.* (2019) 9:1317. doi: 10.3389/fonc.2019.01317
7. Chen F, Zhang Y, Senbabaoglu Y, Ciriello G, Yang L, Reznik E, et al. Multilevel genomics-based taxonomy of renal cell carcinoma. *Cell Rep.* (2016) 14:2476–89. doi: 10.1016/j.celrep.2016.02.024
8. The international cancer genome consortium international network of cancer genome projects. *Nature.* (2010) 464:993–8. doi: 10.1038/nature08987
9. Clark DJ, Dhanasekaran SM, Petralia F, Pan J, Song X, Hu Y, et al. Integrated proteogenomic characterization of clear cell renal cell carcinoma. *Cell.* (2019) 179:964–83.e31. doi: 10.1016/j.cell.2019.10.007
10. Crooks DR, Maio N, Lang M, Ricketts CJ, Vocke CD, Gurram S, et al. Mitochondrial DNA alterations underlie an irreversible shift to aerobic glycolysis in fumarate hydratase–deficient renal cancer. *Sci Signal.* (2021) 14:eabc4436. doi: 10.1126/scisignal.abc4436
11. SciPy 1.0 Contributors, Virtanen P, Gommers R, Oliphant TE, Haberland M, Reddy T, et al. SciPy 1.0: fundamental algorithms for scientific computing in python. *Nat Methods.* (2020) 17:261–72. doi: 10.1038/s41592-019-0686-2
12. Pedregosa F, Varoquaux G, Gramfort A, Michel V, Thirion B, Grisel O, et al. Scikit-learn: machine learning in Python. *J Mach Learn Res.* (2011) 12:2825–30.
13. van der Maaten LJP, Hinton GE. Visualizing data using t-SNE. *J Mach Learn Res.* (2008) 9:2579–605.
14. Davidson-Pilon C, Kalderstam J, Zivich P, Kuhn B, Fiore-Gartland A, Moneda L, et al. *CamDavidsonPilon/lifelines: v0.23.1.* Zenodo (2019). doi: 10.5281/zenodo.3555617
15. Szklarczyk D, Gable AL, Lyon D, Junge A, Wyder S, Huerta-Cepas J, et al. STRING V11: protein–protein association networks with increased coverage, supporting functional discovery in genome-wide experimental datasets. *Nucleic Acids Res.* (2019) 47:D607–13. doi: 10.1093/nar/gky1131
16. Li J, Lu Y, Akbani R, Ju Z, Roebuck PL, Liu W, et al. TCPA: a resource for cancer functional proteomics data. *Nat Methods.* (2013) 10:1046–7. doi: 10.1038/nmeth.2650
17. Kovacs A, Storkel S, Thoenes W, Kovacs G. Mitochondrial and chromosomal DNA alterations in human chromophobe renal cell carcinomas. *J Pathol.* (1992) 167:273–7. doi: 10.1002/path.1711670303
18. Nagy A, Wilhelm M, Sükösd F, Ljungberg B, Kovacs G. Somatic mitochondrial DNA mutations in human chromophobe renal cell carcinomas. *Genes Chromosomes Cancer.* (2002) 35:256–60. doi: 10.1002/gcc.10118
19. Li J, Akbani R, Zhao W, Lu Y, Weinstein JN, Mills GB, et al. Explore, visualize, and analyze functional cancer proteomic data using the cancer proteome atlas. *Cancer Res.* (2017) 77:e51–4. doi: 10.1158/0008-5472.CAN-17-0369
20. Ricketts CJ, De Cubas AA, Fan H, Smith CC, Lang M, Reznik E, et al. The cancer genome atlas comprehensive molecular characterization of renal cell carcinoma. *Cell Rep.* (2018) 23:313–26.e5. doi: 10.1016/j.celrep.2018.03.075
21. Hsieh JJ, Le V, Cao D, Cheng EH, Creighton CJ. Genomic classifications of renal cell carcinoma: a critical step towards the future application of personalized kidney cancer care with pan-omics precision: categorical classification of renal cell carcinoma by integrated-omics. *J Pathol.* (2018) 244:525–37. doi: 10.1002/path.5022
22. Brooks SA, Brannon AR, Parker JS, Fisher JC, Sen O, Kattan MW, et al. ClearCode34: a prognostic risk predictor for localized clear cell renal cell carcinoma. *Eur Urol.* (2014) 66:77–84. doi: 10.1016/j.eururo.2014.02.035
23. Argentiero A, Solimando AG, Krebs M, Leone P, Susca N, Brunetti O, et al. Anti-angiogenesis and immunotherapy: novel paradigms to envision tailored approaches in renal cell-carcinoma. *JCM.* (2020) 9:1594. doi: 10.3390/jcm9051594
24. Smith CC, Beckermann KE, Bortone DS, De Cubas AA, Bixby LM, Lee SJ, et al. Endogenous retroviral signatures predict immunotherapy response in clear cell renal cell carcinoma. *J Clin Invest.* (2018) 128:4804–20. doi: 10.1172/JCI121476
25. Miao D, Margolis CA, Gao W, Voss MH, Li W, Martini DJ, et al. Genomic correlates of response to immune checkpoint therapies in clear cell renal cell carcinoma. *Science.* (2018) 359:801–6. doi: 10.1126/science.aan5951
26. D'Costa NM, Cina D, Shrestha R, Bell RH, Lin Y-Y, Asghari H, et al. Identification of gene signature for treatment response to guide precision oncology in clear-cell renal cell carcinoma. *Sci Rep.* (2020) 10:2026. doi: 10.1038/s41598-020-58804-y
27. Hakimi AA, Voss MH, Kuo F, Sanchez A, Liu M, Nixon BG, et al. Transcriptomic profiling of the tumor microenvironment reveals distinct subgroups of clear cell renal cell cancer: data from a randomized phase III trial. *Cancer Discov.* (2019) 9:510–25. doi: 10.1158/2159-8290.CD-18-0957
28. Schaeffeler E, Büttner F, Reustle A, Klumpp V, Winter S, Rausch S, et al. Metabolic and lipidomic reprogramming in renal cell carcinoma subtypes reflects regions of tumor origin. *Eur Urol Focus.* (2019) 5:608–18. doi: 10.1016/j.euf.2018.01.016
29. DiNatale RG, Sanchez A, Hakimi AA, Reznik E. Metabolomics informs common patterns of molecular dysfunction across histologies of renal cell carcinoma. *Urol Oncol.* (2020) 38:755–62. doi: 10.1016/j.urolonc.2019.04.028
30. Simonnet H. Low mitochondrial respiratory chain content correlates with tumor aggressiveness in renal cell carcinoma. *Carcinogenesis.* (2002) 23:759–68. doi: 10.1093/carcin/23.5.759
31. Brüggemann M, Gromes A, Poss M, Schmidt D, Klümper N, Tolkach Y, et al. Systematic analysis of the expression of the mitochondrial ATP synthase (complex V) subunits in clear cell renal cell carcinoma. *Transl Oncol.* (2017) 10:661–8. doi: 10.1016/j.tranon.2017.06.002
32. Ellinger J, Poss M, Brüggemann M, Gromes A, Schmidt D, Ellinger N, et al. Systematic expression analysis of mitochondrial complex I identifies NDUFS1 as a biomarker in clear-cell renal-cell carcinoma. *Clin Genitourin Cancer.* (2017) 15:e551–62. doi: 10.1016/j.clgc.2016.11.010
33. Gammage PA, Frezza C. Mitochondrial DNA: the overlooked oncogenome? *BMC Biol.* (2019) 17:53. doi: 10.1186/s12915-019-0668-y
34. Tan AS, Baty JW, Dong L-F, Bezawork-Geleta A, Endaya B, Goodwin J, et al. Mitochondrial genome acquisition restores respiratory function and tumorigenic potential of cancer cells without mitochondrial DNA. *Cell Metab.* (2015) 21:81–94. doi: 10.1016/j.cmet.2014.12.003

35. Schöpf B, Weissensteiner H, Schäfer G, Fazzini F, Charoentong P, Naschberger A, et al. OXPHOS remodeling in high-grade prostate cancer involves MtDNA mutations and increased succinate oxidation. *Nat Commun.* (2020) 11:1487. doi: 10.1038/s41467-020-15237-5
36. Huss WJ, Hanrahan CF, Barrios RJ, Simons JW, Greenberg NM. Angiogenesis and prostate cancer: identification of a molecular progression switch. *Cancer Res.* (2001) 61:2736–43.
37. Krebs M, Solimando AG, Kalogirou C, Marquardt A, Frank T, Sokolakis I, et al. MiR-221-3p regulates VEGFR2 expression in high-risk prostate cancer and represents an escape mechanism from sunitinib in vitro. *JCM.* (2020) 9:670. doi: 10.3390/jcm9030670
38. Chen D, Sun X, Zhang X, Cao J. Targeting mitochondria by anthelmintic drug atovaquone sensitizes renal cell carcinoma to chemotherapy and immunotherapy. *J Biochem Mol Toxicol.* (2018) 32:e22195. doi: 10.1002/jbt.22195
39. Wang B, Ao J, Yu D, Rao T, Ruan Y, Yao X. Inhibition of mitochondrial translation effectively sensitizes renal cell carcinoma to chemotherapy. *Biochem Biophys Res Commun.* (2017) 490:767–73. doi: 10.1016/j.bbrc.2017.06.115
40. Hamieh L, McKay RR, Lin X, Moreira RB, Simantov R, Choueiri TK. Effect of metformin use on survival outcomes in patients with metastatic renal cell carcinoma. *Clin Genitourin Cancer.* (2017) 15:221–9. doi: 10.1016/j.clgc.2016.06.017
41. Tseng C-H. Use of metformin and risk of kidney cancer in patients with type 2 diabetes. *Eur J Cancer.* (2016) 52:19–25. doi: 10.1016/j.ejca.2015.09.027
42. Keizman D, Ish-Shalom M, Sella A, Gottfried M, Maimon N, Peer A, et al. Metformin use and outcome of sunitinib treatment in patients with diabetes and metastatic renal cell carcinoma. *Clin Genitourin Cancer.* (2016) 14:420–5. doi: 10.1016/j.clgc.2016.04.012
43. Cunningham JT, Rodgers JT, Arlow DH, Vazquez F, Mootha VK, Puigserver P. MTOR controls mitochondrial oxidative function through a YY1–PGC-1α transcriptional complex. *Nature.* (2007) 450:736–40. doi: 10.1038/nature06322
44. Ramanathan A, Schreiber SL. Direct control of mitochondrial function by MTOR. *PNAS.* (2009) 106:22229–32. doi: 10.1073/pnas.0912074106
45. Molina JR, Sun Y, Protopopova M, Gera S, Bandi M, Bristow C, et al. An inhibitor of oxidative phosphorylation exploits cancer vulnerability. *Nat Med.* (2018) 24:1036–46. doi: 10.1038/s41591-018-0052-4
46. Yakes FM, Chen J, Tan J, Yamaguchi K, Shi Y, Yu P, et al. Cabozantinib (XL184), a novel MET and VEGFR2 inhibitor, simultaneously suppresses metastasis, angiogenesis, and tumor growth. *Mol Cancer Ther.* (2011) 10:2298–308. doi: 10.1158/1535-7163.MCT-11-0264
47. Patel SP, Kurzrock R. PD-L1 expression as a predictive biomarker in cancer immunotherapy. *Mol Cancer Ther.* (2015) 14:847–56. doi: 10.1158/1535-7163.MCT-14-0983
48. Lopez-Beltran A, Henriques V, Cimadamore A, Santoni M, Cheng L, Gevaert T, et al. The identification of immunological biomarkers in kidney cancers. *Front Oncol.* (2018) 8:456. doi: 10.3389/fonc.2018.00456
49. Flaifel A, Xie W, Braun DA, Ficial M, Bakouny Z, Nassar AH, et al. PD-L1 expression and clinical outcomes to cabozantinib, everolimus, and sunitinib in patients with metastatic renal cell carcinoma: analysis of the randomized clinical trials METEOR and CABOSUN. *Clin Cancer Res.* (2019) 25:6080–8. doi: 10.1158/1078-0432.CCR-19-1135

Conflict of Interest: The authors declare that the research was conducted in the absence of any commercial or financial relationships that could be construed as a potential conflict of interest.

frontiers in Oncology

ORIGINAL RESEARCH
published: 31 March 2021
doi: 10.3389/fonc.2021.637023

CXCL5 Has Potential to Be a Marker for Hepatocellular Carcinoma Prognosis and Was Correlating With Immune Infiltrates

*Yuan Nie, Mei-chun Jiang, Cong Liu, Qi Liu and Xuan Zhu**

Department of Gastroenterology, The First Affiliated Hospital of Nanchang University, Nanchang, China

Backgrounds: Tumor microenvironment (TME) plays a crucial role in the initiation and progression of Hepatocellular Carcinoma (HCC), especially immune infiltrates. However, there is still a challenge in understanding the modulation of the immune and stromal components in TME, especially TME related genes.

Methods: The proportion of tumor-infiltrating immune cells (TICs) and the immune and stromal scores in 374 HCC patients from The Cancer Genome Atlas (TCGA) database were determined using CIBERSORT and ESTIMATE computational methods. The final screened genes were confirmed by the PPI network and univariate Cox regression of the differentially expressed genes based on different immune or stromal scores. The correlation between the expression levels of the final gene interactions and the clinical characteristics was based on TCGA database and local hospital data. Gene set enrichment analysis (GSEA) and the effect of CXCL5 expression on TICs were conducted.

Results: There were correlations between the expression of CXCL5 and survival of HCC patients and TMN classification both in TCGA database and local hospital data. The immune-related activities were enriched in the high-expression group; however, the metabolic pathways were enriched in the low-expression group. The result of CIBERSORT analyzing had indicated that CXCL5 expression were correlated with the proportion of NK cells activated, macrophages M0, Mast cells resting, Neutrophils.

Conclusions: CXCL5 was a potential prognostic marker for HCC and provides clues regarding immune infiltrates, which offers extra insight for therapeutics of HCC, however, more independent cohorts and functional experiments of CXCL5 are warranted.

Keywords: CXCL5, hepatocellular carcinoma, tumor microenvironment, immune infiltration, prognosis

OPEN ACCESS

Edited by:
Cirino Botta, Cosenza Hospital, Italy

Reviewed by:
Shaolai Zhou, Fudan University, China
Antonio Giovanni Solimando, University of Bari Aldo Moro, Italy

***Correspondence:**
Xuan Zhu
jyyfyzx@163.com

Specialty section:
This article was submitted to Cancer Molecular Targets and Therapeutics, a section of the journal Frontiers in Oncology

Received: *02 December 2020*
Accepted: *01 March 2021*
Published: *31 March 2021*

Citation:
Nie Y, Jiang M-c, Liu C, Liu Q and Zhu X (2021) CXCL5 Has Potential to Be a Marker for Hepatocellular Carcinoma Prognosis and Was Correlating With Immune Infiltrates. Front. Oncol. 11:637023. doi: 10.3389/fonc.2021.637023

INTRODUCTION

Liver cancer is a typical inflammation driven tumor and often develops from chronic hepatitis and cirrhosis (1). Hepatocellular carcinoma (HCC) accounts for 75–85% of primary liver cancers, ranking sixth among the most common cancers in the world, and fourth among cancer-related deaths. Eighty-five percent of all HCC patients occurs in poor or developing countries, especially in

East Asia and Africa (2). The main treatment methods include surgery, liver transplantation, local ablation, molecular targeted therapy, and systemic chemotherapy, had limitation on the improvement of patient's survival and imposes a heavy burden on health-care costs. It is urgently needed to explore the carcinogenesis and therapeutics of HCC (3).

Increasing evidence demonstrated the importance of the tumor microenvironment (TME) in the tumor development, especially in HCC (4). As an inflammatory tumor, the immunosuppressive microenvironment of HCC can promote immune tolerance through a variety of mechanisms. Immunotherapy that activates tumor specific immune response brings new hope for the treatment of HCC. The microenvironment of HCC is mainly composed of tumor associated macrophages, tumor associated neutrophils and myeloid-derived suppressor cells (MDSCs), tumor associated fibroblasts, tumor infiltrating lymphocytes and other cellular components, as well as extracellular matrix, cytokines, and other non-cellular components. Previous studies showed that the tumor-infiltrating immune cells (TICs) in TME plays an important role in development of HCC and served as a predicting parameter for prognosis. For example, Kupffer cells play an important role in inhibitory microenvironment by producing anti-inflammatory molecules such as TGF -β, IL-10, and prostaglandin E2 (PGE2) (5). Interferon-γ (IFN-γ) derived from Natural killer (NK) cells promotes HCC through the epithelial cell adhesion Molecule-Epithelial-to-Mesenchymal Transition (EMT) axis in Hepatitis B virus (HBV) transgenic mice. A previous study had indicated that neutrophil to lymphocyte ratio and platelet to lymphocyte ratio as prognostic predictors for HCC with various treatments (6). Immune tolerance is one of the main causes of the adverse consequences of high mortality, poor therapeutic effect, and poor prognosis of HCC (7). Immune cells in tumor microenvironment together with cancer cells and extracellular matrix, thus inhibiting the antitumor activity of immune cells and playing an important role in promoting of HCC. Therefore, the analysis of TICs of HCC is helpful to study the pathogenesis of HCC.

Transcriptome-sequencing patterns followed by functional genomics analysis have shed light on the roles of different types of cells during TME modulation. In this paper, we calculated the ratio of tic and immune/stromal components of HCC patients in The Cancer Genome Atlas (TCGA) database by using ESTIMATE and CIBERSORT, and determined that C-X-C Motif Chemokine Ligand 5 (CXCL5) is a predictive biomarker. CXCL5, also known as human epithelial neutrophil activating peptide (ENA 78), is a member of angiogenic CXC chemokine. CXCL5 is secreted by epithelial cells, endothelial cells, immune cells, etc. and recognized and combined with the G protein coupled receptor CXCR2 (8). It can recognize and bind to CXCR2, and perform many cellular functions including adhesion, invasion, and diffusion through autocrine or non-autocrine pathways, thus affecting the growth, proliferation, metastasis, and invasion of tumors. CXCL5 is secreted not only by neutrophils, monocytes, and megaphone immune cells, but also by non-immune cells such as epithelial cells, endothelial cells, and fibroblasts. As an inflammatory mediator, CXCL5 has a strong chemotactic effect on neutrophils and can activate neutrophils, suggesting that CXCL5 might play a role in TME (9). Hence, we examined the differentially expressed genes (DEGs) generated by comparison between immune components and stromal components in HCC samples and revealed that the CXCL5 might be a potential indicator for the alteration of TME status in HCC.

MATERIALS AND METHODS

Raw Data

Transcriptome RNA-seq data of 424 HCC samples (normal samples, 50 cases; tumor samples, 374 cases) and the corresponding clinical data were downloaded from TCGA database (https://portal.gdc.cancer.gov/). At the same time, the blood sample of HCC patients in hospital were collected in this study. Refusal to give consent, cerebrovascular disease, cardiovascular disease, hematologic disorders, renal failure, combined other cancer, and correspond treatment were exclusion criteria. The study protocol was approved by the institutional ethics committee of First Affiliated Hospital of Nanchang University (No. 2017-0106). Written informed consent was obtained from all the study participants.

Bioinformatics Analysis

The ratio of immune-stromal component in TME was calculated by Using the Feat estimation algorithm in R language version 3.5.1, which expressed in three scoring forms: Immune Score, Stromal Score, and ESTIMATE Score. According the median of the Immune score, Stromal Score, and ESTIMATE Score, tumor samples were labeled as high or low. The differential expression genes (DEGs) was generated by comparing high score samples with low score samples in package limma. DEGs with fold change larger than 1 after transformation of $\log_2$(high-score group/low-score group) and false discovery rate (FDR) < 0.05 were considered significant.

GO and KEGG enrichment analyses were performed by packages clusterProfiler, enrichplot, and ggplot2 of R language. Only terms with both P value and q-value < 0.05 were considered significantly enriched. PPI network was constructed by STRING database, followed by reconstruction with Cystoscope of version 3.6.1. Nodes with confidence of interactive relationship larger than 0.95 were used for building network.

Hallmark and C7 gene sets v 6.2 collections were downloaded from Molecular Signatures Database as the target sets with which GSEA performed using the software GESA 3.0. The whole transcriptome of all tumor samples was used for GSEA, and only gene sets with NOM p < 0.05 and

FDR q < 0.05 were considered as significant. CIBERSORT computational method was applied for estimating the TIC abundance profile in all tumor samples, and only tumor samples with P < 0.05 were selected for the following analysis.

Definitions

Patients with chronic HBV infection were confirmed by the detection of Hepatitis B surface antigen (HBsAg) positivity for more than 6 months. The liver cirrhosis was diagnosed by the presence of ascites, hepatic encephalopathy (HE), Hepatorenal syndrome (HRS), and/or variceal bleeding at the time of the study. The diagnosis of HCC and TMN classification was mainly based on pathological and clinical characteristics.

ELISA and Real-Time Quantitative PCR

Peripheral venous blood was collected through the elbow vein, centrifuged at 3,000 r/min for 10 min, and the supernatant was stored in −80°C refrigerator. Serum CXCL5 level was determined by the standard photometric method using the ELISA kit (R&D company, USA). For real-time PCR analysis, PCR was performed with a reaction mixture containing cDNA template, primers, and TB Green™ Fast qPCR Mix (TaKaRa) in a Step One Plus Real-Time PCR System (Thermo Fisher Scientific).

The primers of CXCL5 were 5'-CCGCTGCTGTGTTG AGAG-3' and 5'-TCTGCTGAAGACTGGGAAAC-3'.

Statistical Analysis

Statistical analyses were performed using SPSS software version 16.0 (SPSS Inc., Chicago, IL, USA) and R 3.62. Continuous and categorical variables were initially described as median [interquartile range (IQR)] and frequency [percentage (%)]. Univariate Cox regression was used to completed by package survival of R language and the top 18 genes ordered by p value from small to large in univariate Cox were shown in the plot. Survival analysis was completed by the survival and survminer package of R language. Kaplan–Meier (K-M) method was used to plot the survival curve, and log rank as the statistical significance test. Heatmaps of DEGs were produced by package heatmap of R language. $P < 0.05$ was considered significant.

RESULTS

Analysis process of this study was shown in **Figure 1**. The transcriptome RNA-seq data of 424 cases were downloaded from TCGA database followed by calculating with CIBERSORT and ESTIMATE algorithms. Protein-protein interaction (PPI) network was constructed by using DEGs shared by Immune score and Stromal score, and Univariate Cox regression analysis was conducted. Intersection analysis was performed using the core nodes in PPI network and the top significant factors obtained from the analysis of univariate Cox regression. We focused on CXCL5 for the subsequent series of analysis, including survival and clinicopathological characteristics correlation analysis, Cox regression, GSEA, and correlation with TICs.

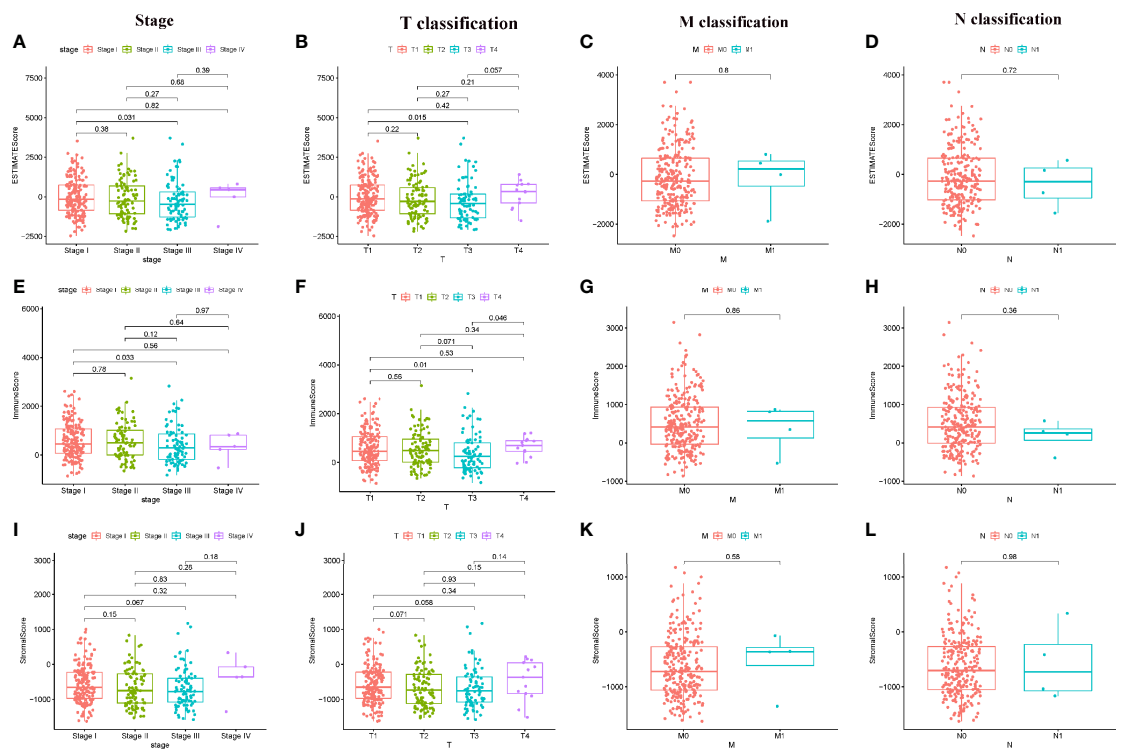

FIGURE 1 | Correlation of ESTIMATE Score, Immune Score, and Stromal Score with clinical characteristics. **(A–D)** Distribution of ESTIMATE Score in different stage and TMN classification; **(E–H)** Distribution of Immune Score in different stage and TMN classification; **(I–L)** Distribution of Stromal Score in different stage and TMN classification.

Scores Were Associated With the Clinical Characteristics of HCC Patients

In order to determine the relationship between Immune score, Stromal score, ESTIMATE Score with clinical characteristics, the clinical information of HCC patients from TCGA were collected. The analyzing result were shown in **Figure 1**. The ESTIMATE Score of stage III is significantly lower than that of stage I ($P = 0.031$); the ESTIMATE Score of T3 classification of TMN stages is significantly lower than that of T1 classification ($P = 0.015$). The Immune Score of stage III is significantly lower than that of stage I ($P = 0.033$); the Immune Score of T3 classification of TMN stages is significantly lower than that of T1 classification ($P = 0.010$). There are no significant different in comparing of Stromal score ($P > 0.05$). These results suggested that TME was associated with the progress of HCC, especially immune related tumor microenvironment.

DEGs Between Lower Immune Score, Stromal Score and Higher Immune Score, Stromal Score

In order to determine the different of gene expression, the gene expression of high and low score samples were compared and analyzed. As shown in **Figure 2**, Compared to the median, the total 1,422 DEGs were obtained from Stromal Score (samples with high score *vs.* low score). Similarly, 1,122 DEGs were obtained from Immune Score. The intersection analysis displayed by Venn plot showed a total of 802 up-regulated genes sharing by high score both in Immune Score and Stromal Score and 28 down-regulated genes sharing by low score as well.

Enrichment Analysis of GO and KEGG

As shown in **Figure 3**, the results of gene ontology (GO) enrichment analysis indicated that the DEGs almost mapped to the immune-related GO terms, such as T cell activation, regulation of lymphocyte activation (**Figures 3A, C**). The Kyoto Encyclopedia of Genes and Genomes (KEGG) enrichment analysis also displayed the enrichment of T cell activation, regulation of lymphocyte activation (**Figures 3B, D**). Therefore, the overall function of DEGs seems to map to immune related activities, which indicates that the involvement of immune factors is a major feature of TME in HCC.

Intersection Analysis of PPI Network and Univariate COX Regression

In order to further explore the underlying mechanism, PPI network based on String database by using the Cytoscape software was conducted. The interactions are shown in **Figure 4A**, and the bar plots were represented for the top 30 genes ranked by the number of nodes (**Figure 4B**). Univariate Cox regression analysis was used to determine the significant factors affecting the survival of HCC patients (**Figure 4C**). And then, the intersection analysis between the leading nodes in PPI network and the top 16 factors ranked by the p-value of univariate Cox regression was carried out, and only one factor, CXCL5, was overlapping from the above analyses (**Figure 4D**).

The Correlation of CXCL5 With Clinical Characteristics of HCC Patients in TCGA

In comparing of CXCL5 gene expression, the CXCL5 expression of normal patients was significantly lower than that of HCC patients (**Figure 5A**). According the gene expression of CXCL5, all HCC samples were grouped into high-expression group and low-expression group. The survival analysis that HCC patients with lower expression had longer survival than that of higher expression (**Figure 5C**). In the paring analysis, the expression of CXCL5 in the tumor samples was significantly lower than that in the normal samples (**Figure 5B**). The above results clearly indicated that the expression of CXCL5 in TME was positive correlation with the prognosis of HCC patient, especially in stage and T classification (**Figures 5D–G**).

The Correlation of CXCL5 With Clinical Characteristics of HCC Patients in This Hospital

There were 65 patients with Chronic HBV infection, 62 patients with liver cirrhosis, 52 patients with HCC of this hospital in this study. The relative mRNA expression of CXCL5 of HCC patients

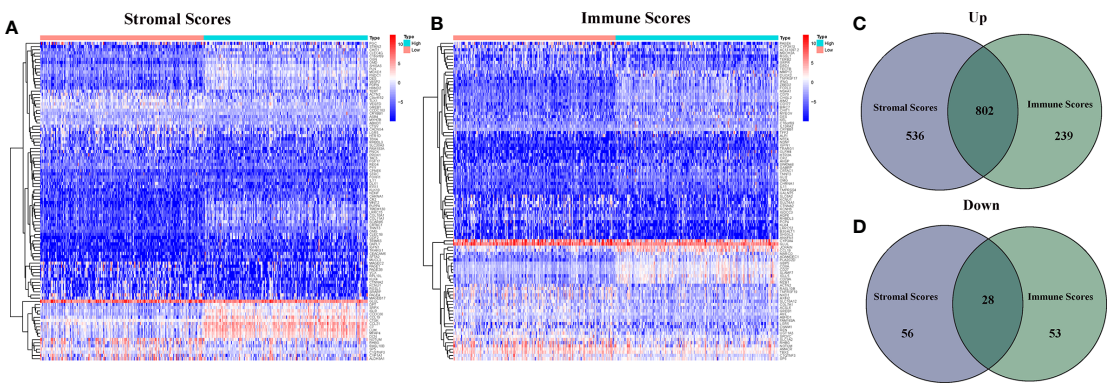

FIGURE 2 | Heatmaps and Venn plots for DEGs. **(A)** Heatmap for DEGs generated by comparison of the high score group *vs* the low score group in Stromal Score; **(B)** Heatmap for DEGs generated by comparison of the high score group *vs* the low score group in Immune Score; **(C, D)** Venn plots showing common up-regulated and down-regulated DEGs shared by Immune Score and Stromal Score.

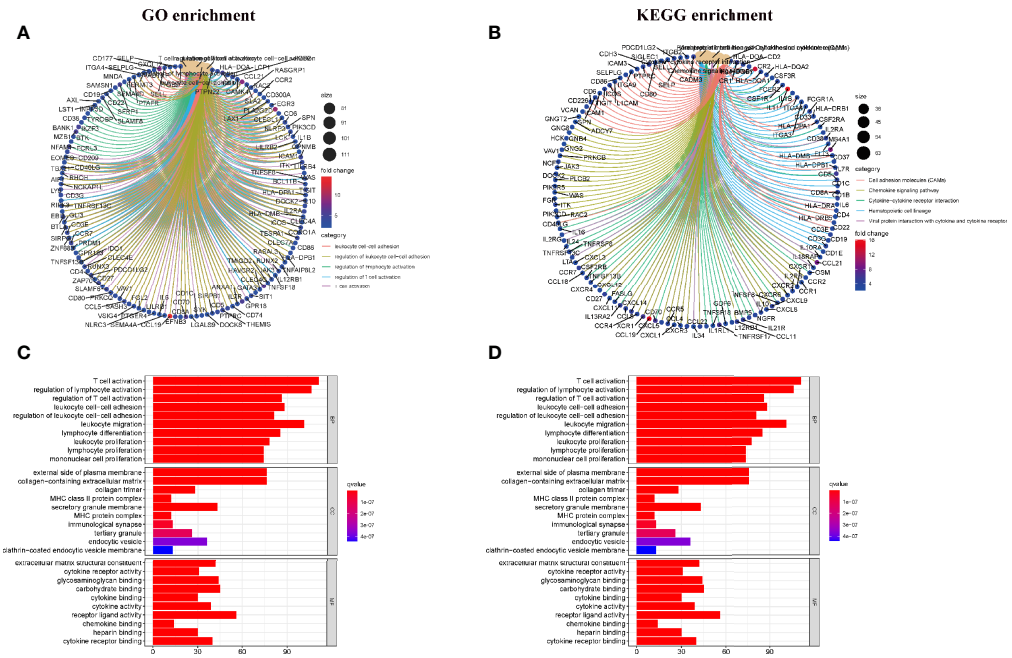

FIGURE 3 | Enrichment analysis of GO and KEGG for DEGs. **(A, C)** GO enrichment analysis for 830 DEGs; **(B, D)** KEGG enrichment analysis for 830 DEGs.

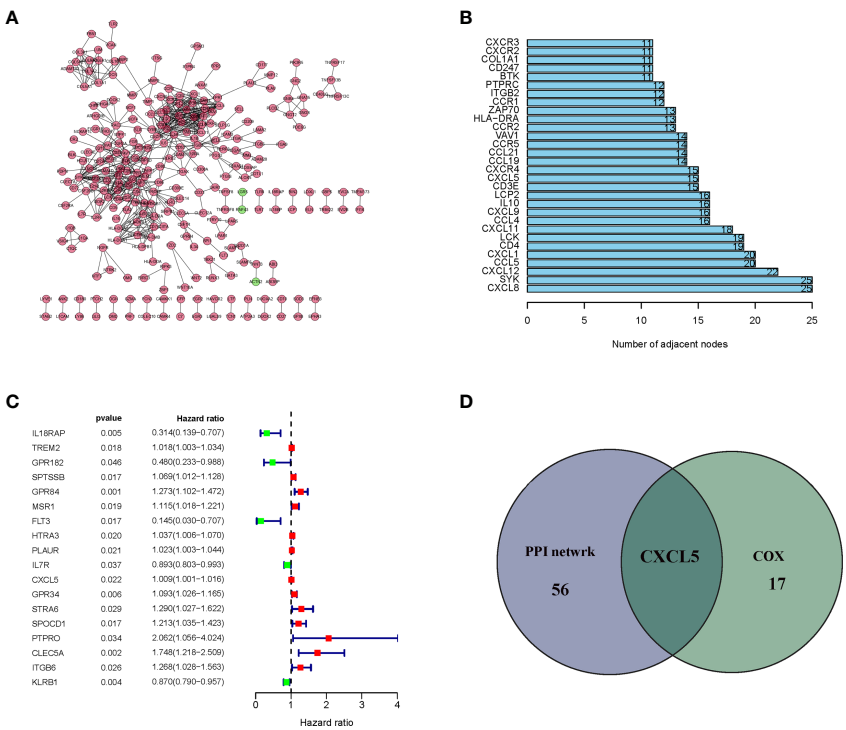

FIGURE 4 | Protein–protein interaction network and univariate cox. **(A)** Interaction network constructed with the nodes with interaction confidence value > 0.95; **(B)** The top 30 genes ordered by the number of nodes; **(C)** Univariate cox regression analysis with 830 DEGs, listing the top significant factors with P < 0.005; **(D)** Venn plot showing the common factors shared by leading 30 nodes in PPI and top significant factors in univariate cox.

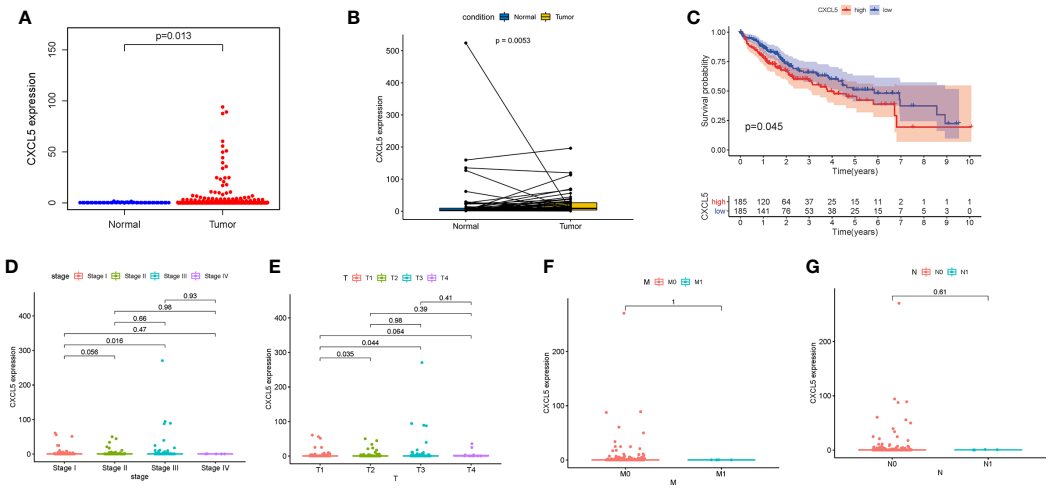

FIGURE 5 | The differentiated expression of CXCL5 and correlation with survival and clinical characteristics. **(A)** Differentiated expression of CXCL5 in the normal and tumor sample; **(B)** Paired differentiation analysis for expression of CXCL5 in the normal and tumor sample deriving from the same one patient; **(C)** Survival analysis for HCC patients with different CXCL5 expression; **(D–G)** The correlation of CXCL5 expression with clinical characteristics.

were higher than patients with liver cirrhosis, patients with Chronic HBV infection (**Figure 6A**), also the ELISA detected results of CXCL5 of HCC patients were higher than patients with liver cirrhosis, patients with Chronic HBV infection (**Figure 6B**). In 52 HCC patients, the relative mRNA expression of CXCL5 also is positive correction with the TMN classification (**Figures 6C–F**). Also, the same result of serum CXCL5 by ELISA was shown in **Figures 6G–J**.

CXCL5 May Be a Potential Indicator of TME Modulation

Comparing with the median level of CXCL5 expression, GESA of CXCL5 in high- and low-expression groups was completed. As shown in **Figure 7A**, the genes in CXCL5 high-expression group were mainly enriched in immune-related activities, such as cell cycle, chemokine signaling, NOD like receptor. As shown in **Figure 7B**, the genes in CXCL5 high-expression group were mainly enriched in metabolism pathways, such as drug metabolism cytochrome, metabolism of xenobiotics. It is suggested that CXCL5 may be a potential indicator of TME status.

Correlation of CXCL5 With the Proportion of TICs

In order to further confirm the correlation between CXCL5 expression and immune microenvironment, the proportion of tumor-infiltrating immune subsets was analyzed using CIBERSORT algorithm, and 21 kinds of immune cell profiles in HCC patients were completed (**Figures 8A, B**). The results showed that the NK cells activated, Mast cells resting of high-expression group of CXCL5 is significantly higher than that of low-expression group of CXCL5 (P = 0.041; P = 0.003); the macrophages M0 of high-expression group of CXCL5 is significantly lower than that of low-expression group of CXCL5 (P = 0.012) (**Figure 8C**). Also, there are significant correlation between CXCL5 expression and the proportion of NK cells activated, macrophages M0, Mast cells resting, Neutrophils ($r = -0.31$, $P = 0.017$; $r = 0.37$, $P = 0.0041$; $r = -0.39$, $P = 0.0025$; $r = 0.35$, $P = 0.0077$). These results further support the effect of CXCL5 expression on the immune activity of TME.

DISCUSSION

In the current study, we attempted to identify TME related genes that affect survival and TMN classification of HCC patients from TCGA database. Firstly, based on the DEGs between lower immune score, stromal score and higher immune score, stromal score, TME related genes was collected. Then, CXCL5 was identified to be involved by intersection analysis of PPI network and univariate cox regression. The gene expression of CXCL5 was significant correction with TMN classification and survival by TCGA database and local hospital data. Finally, CXCL5 might be an indicator of TME status in HCC patients.

TME plays a key role in tumorigenesis and development. As a congenital condition, TME promotes the occurrence and development of tumors (10). It is of great clinical significance to explore potential therapeutic targets based on TME remodeling and promote the transformation of TME from tumor friendly to tumor suppressor (11). A large number of studies have clarified the importance of TME in HCC. As expected, our transcriptome analysis of HCC data from TCGA database showed that the proportion of immune and stromal in TME was significantly correlated with HCC progression (such as invasion and metastasis) (**Figure 2**). These results highlight the value of TME in the development of HCC and provide a new perspective for the development of more effective treatment strategy. HCC as a typical inflammation-related tumor.

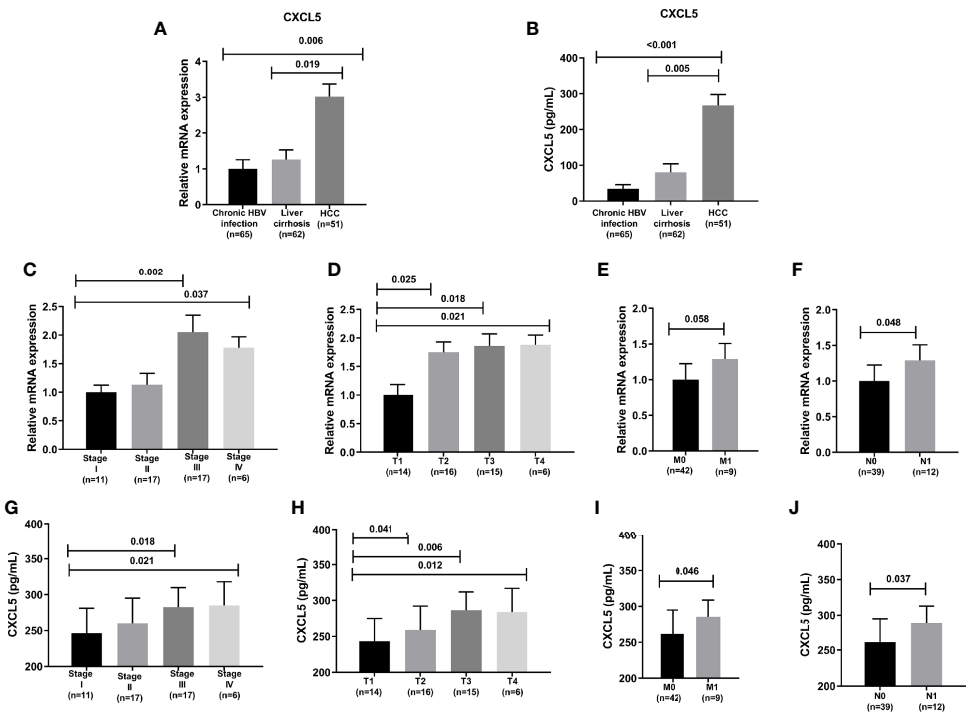

FIGURE 6 | The CXCL5 level and correlation with clinical characteristics. **(A)** The relative mRNA expression of CXCL5 in chronic HBV infection, liver cirrhosis, HCC; **(B)** The CXCL5 level by ELISA in chronic HBV infection, liver cirrhosis, HCC; **(C–F)** The correlation of CXCL5 mRNA expression with clinical characteristics; **(G–J)** The correlation of CXCL5 level by ELISA with clinical characteristics.

The microenvironment of liver cancer is mainly composed of tumor associated macrophages, tumor associated neutrophils, myeloid-derived suppressor cells (MDSCs), tumor associated fibroblasts, tumor infiltrating lymphocytes and dendritic cells (DCs), as well as non-cellular components such as extracellular matrix and cytokines (4). A study had indicated that the increase of $CD4^+CD25^+$ Treg cells in TME was related to tumor size, and these $CD4^+CD25^+$ Treg inhibited the immune response of DCs in HCC. NK cells are anti-tumor immune cells that play an indispensable role in tumor immune surveillance and tumor cell eradication. However, NK cell function is usually inhibited in tumor. miR-561-5p with high expression in HCC directly target to reduce the expression of CXCL3, reduce the infiltration of $CXCR3^+$ NK cell subtypes in TME, promote the survival of cancer cells, and promote lung metastasis (12). Circ HURF derived from hepatoma cell exosomes can inhibit NK cell function, promote immune escape and resist PD-1 immunotherapy resistance through miR-449c-5p/TIM3 pathways. More evidence had indicated that macrophages promote tumor progression and metastasis (13). Osteopontin can stimulate macrophages to secrete colony stimulating factor (CSF1) through PI3K-Akt-p65 pathway, and then promote macrophage polarization by CSF1/CSF 1R pathway, up-regulate the expression of PD-L1 in HCC, create an inhibitory immune microenvironment, and induce immune escape of HCC. Also, the active mediator secreted by Mast cells in hepatocellular carcinoma tissue can make hepatic sinusoidal endothelial cells capillary, resulting in thickening of the basement membrane, and then forming new capillaries to increase the blood supply of tumor tissue, thereby promoting the proliferation and invasion of cancer cells (14).

The type, location, and density of immune cell infiltration in different tumor areas (i.e., tumor center and invasive margin) are evaluated respectively, which is called "immune score." The immune score can not only reveal the immune microenvironment where the tumor is located, but also independently predict the overall survival and relapse-free survival of the patient. It is considered to be a better predictor of clinical outcome than the standard TNM staging (15, 16). Immune score has a good predictive value for the survival of patients with colon cancer (17), but the immune score about HCC were limited. According to the immune score, especially based on the distribution pattern of $CD3^+$T and $CD8^+$T lymphocytes, immune tumors are divided into three types: Immune-inflamed tumor; immune-excluded tumor; immune-desert tumor (18). Immuno-inflammatory tumors are in an activated or semi-activated state. Checkpoints inhibitors, such as programmed death receptor-1 (PD-1), programmed death receptor ligand-1 (PD-L1), are likely to exert anti-tumor effects in this immunophenotype; the immune-excluded tumor shows that there are a large number of immune cells around the tumor cells, but the immune cells cannot penetrate into the core of the tumor cells and are restricted to the peripheral matrix of the tumor cells. Due to the interaction and influence of many factors in the tumor cell matrix, it is difficult for checkpoints

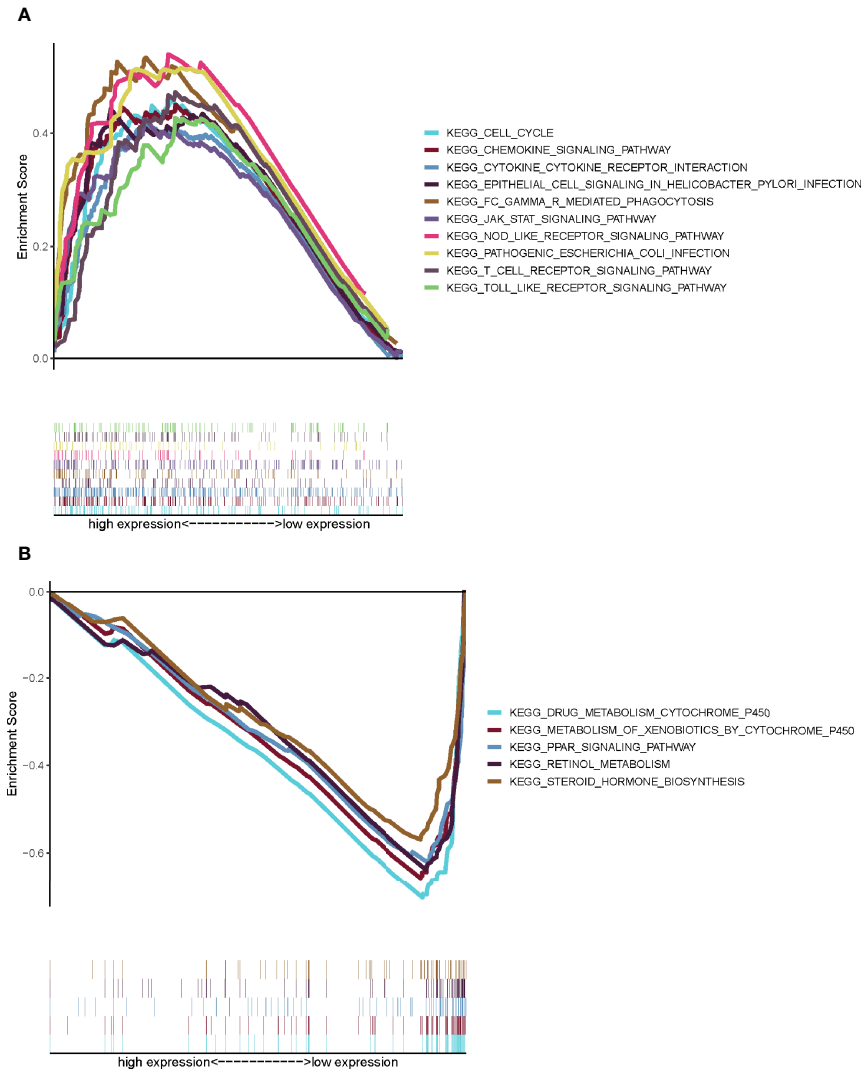

FIGURE 7 | GSEA for samples with high CXCL5 expression and low expression. **(A)** GSEA for samples with high CXCL5 expression; **(B)** GSEA for samples with low CXCL5 expression.

inhibitors to exert anti-tumor effects in this phenotype. After PD-1/PD-L1 inhibitor treatment, peripheral matrix-associated T cells have proliferation and activation, but there is no infiltration, and the clinical response is uncertain. Therefore, how to improve T cell migration is the rate-limiting step for this phenotype; Immune-desert tumor is characterized by the lack of T cells in the inner and outer matrix of tumor cells. PD-1/PD-L1 inhibitors have no any effect on this phenotype. How to induce more tumor-specific T cells is the Phenotypic restriction steps (19, 20).

Immune checkpoint inhibitor (ICI) is one of the most rapidly developed immunotherapies strategies of HCC in recent years. ICI can block tumor-induced immunosuppression, thereby enhancing the anti-tumor immune response. Immune checkpoint are inhibitory tumor immune receptors, which are located on the surface of activated T cells. After the immune checkpoint is combined with the tumor surface antigen, it can inhibit tumor immune response and promote tumor immune escape. And ICI mainly reactivate tumor-specific T cells and exert anti-tumor effects by inhibiting checkpoint-mediated signal transduction (21). ICI targets mainly include PD-1, PD-L1, and cytotoxic T lymphocyte antigen-4 (CTLA-4) (22). However, thorny issues such as super progress and immune tolerance also appear in the course of immunotherapy. Indeed, a lot of combinatory approaches are under investigation, including the combination of different ICI, the addition of ICI after resection or during loco-regional therapy, combination of anti-angiogenic drugs or molecular targeted drugs. Compared with single-agent therapy, ICI combination therapy also reflects better clinical efficacy and good safety (23). The emergence of ICI has brought new research directions to researchers, and we look forward to better development of immune checkpoint inhibitors in the future.

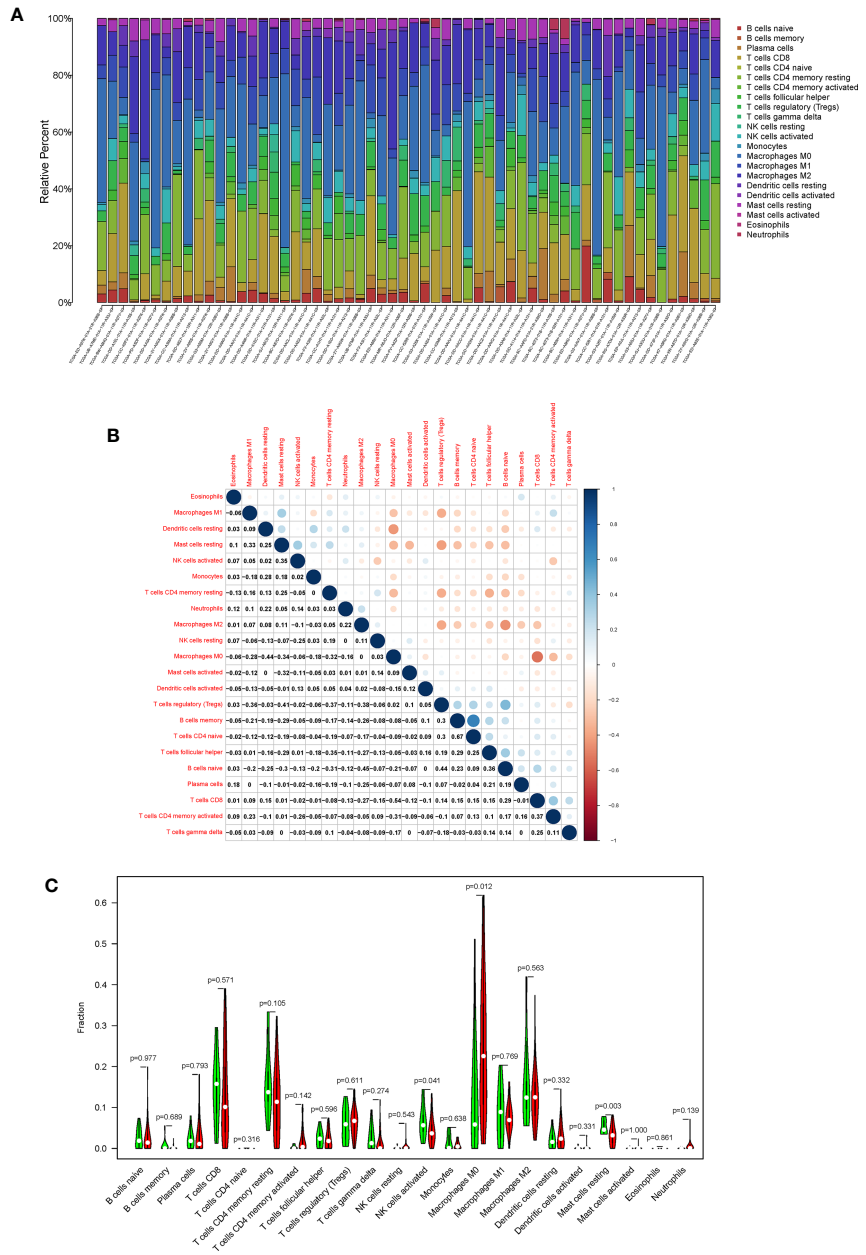

FIGURE 8 | TIC profile in tumor samples and correlation analysis. **(A)** Barplot showing the proportion of 21 kinds of TICs in HCC tumor samples; **(B)** Heatmap showing the correlation between 21 kinds of TICs and numeric; **(C)** Violin plot showed the ratio differentiation of 21 kinds of immune cells between HCC samples with high CXCL5 expression and low CXCL5 expression.

There are many reports on the mechanism of CXCL5 promoting cancer progression. The combination of CXCL5 and CXCR2 exerts a strong granulocyte chemotaxis and angiogenesis effect, and CXCL5/CXCR2 axis plays an important role in mediating the infiltration and metastasis of malignant tumors (8). Recently, the CXCL5/CXCR2 axis is sufficient to promote breast cancer colonization during bone metastasis (24). CXCL5 activated the PI3K-Akt and ERK1/2 signaling pathways in HCC cells and promoted proliferation, migration, and invasion (25). The expression level of CXCR2 in HCC was significantly higher than normal liver tissues, and the expression levels of CXCR2 mRNA and protein were associated with intrahepatic metastasis, portal vein tumor thrombus, and poor differentiation (26). A longitudinal study has indicated that the chronically increasing trend of CXCL5 were associated with the promotion of the progression of NAFLD to HCC in males (27). Xu's study had shown that overexpression of CXCL5 in HCC cells has higher metastatic potential, which also demonstrated that CXCL5/CXCR2 and ERK1/2 highway may play

an important role in the migration of HCC (28). Based on ONCOMINE, GEPIA, and cBioPortal databases, the expression levels of CXCL5 were correlated with different tumor stages and high transcriptional levels of CXCL5 may exhibit poorer overall survival in patients with HCC (29). Previous study had indicated that EGF/EGFR signaling pathway plays an important role in the production of CXCL5 in HCC, and then activates downstream signaling pathways, thus mediating inflammatory microenvironment, as well as cell proliferation, apoptosis, and metastasis, revealing the signaling pathway of CXCL5 in HCC. In this study, the expression of CXCL5 was correlated with the TMN stage of HCC and was verified in our hospital (30). By analyzing the correlation of CXCL5 with the proportion of TICs, there are significant correlation between CXCL5 expression and the proportion of NK cells activated, macrophages M0, mast cells resting, neutrophils. It was well-known that CXCL5 was crucial for the function activation of different cells, especially neutrophil. Up to now, there are many reports about the mechanism of CXCL5 promoting tumor progression. CXCL5 can also activate protein kinase B (PKB) and activator of transcription (STAT) signaling pathways and promote tumor angiogenesis (31). Also, CXCL5 promotes tumor angiogenesis, and new blood vessels act as tumor metastasis channels; CXCL5/CXCR2 can release matrix metalloproteinase-9 (MMP-9), destroys endothelial cells and matrix barrier, and promotes tumor metastasis (32). Recent reports have shown that Retinoic acid receptor-related orphan receptor (ROR)-α inhibits the proliferation, invasion, and migration of HCC MHCC97H *via* down-regulation of CXCL5 (33).

This study has several limitations. Firstly, although it has been verified by patients in our hospital, the main research of this study is bioinformatics analysis based on TCGA database, and functional experiments are necessary to reveal the predictive mechanisms of CXCL5. Secondly, confounding effects of treatment factors are different to control because of the lack of treatment information. considering that the main causes of HCC in different countries are different, proving our signature in more independent cohorts is necessary to expand our model to other populations, especially in patients with advanced stage of HCC (34).

In conclusion, we determined the TME-related genes in HCC using ESTIMATE algorithm in TCGA database. CXCL5 was a potential prognostic factor for HCC patients by intersection analysis of PPI network and univariate cox regression. Then, the expression of CXCL5 was significant corrected with TMN classification both in TCGA database and verification data. More interestingly, CXCL5 might be an indicator for the conversion of TME status from immune-dominant to metabolic-dominant. There was significant correction between CXCL5 expression and the proportion of NK cells activated, macrophages M0, Mast cells resting, Neutrophils. Our signature might reflect CXCL5 has potential to be a marker for HCC prognosis and correlating with immune infiltrates. However, validation of the signature in more independent cohorts from different country and functional experiments of the predictive genes are warranted.

DATA AVAILABILITY STATEMENT

The datasets presented in this study can be found in online repositories. The names of the repository/repositories and accession number(s) can be found below: https://portal.gdc.cancer.gov/.

ETHICS STATEMENT

The studies involving human participants were reviewed and approved by the First Affiliated Hospital of Nanchang University (No. 2017-0106). Written informed consent was obtained from all participants. The patients/participants provided their written informed consent to participate in this study.

AUTHOR CONTRIBUTIONS

YN: study concept, design, and data analyzing. M-CJ and CL: experimental operation. QL: data collection. XZ: obtained funding and critically revised the manuscript. All authors contributed to the article and approved the submitted version.

FUNDING

This study was supported by the National Natural Science Foundation of China (grant number: 81960120), "Gan-Po Talent 555" Project of Jiangxi Province [GCZ (2012)-1], and the Postgraduate Innovation Special Foundation of Jiangxi Province (YC2020-B046).

REFERENCES

1. Forner A, Reig M, Bruix J. Hepatocellular carcinoma. *Lancet* (2018) 391 (10127):1301–14. doi: 10.1016/S0140-6736(18)30010-2
2. Bray F, Ferlay J, Soerjomataram I, Siegel RL, Torre LA, Jemal A, et al. Global cancer statistics 2018: GLOBOCAN estimates of incidence and mortality worldwide for 36 cancers in 185 countries. *CA Cancer J Clin* (2018) 68 (6):394–424. doi: 10.3322/caac.21492
3. Heimbach JK, Kulik LM, Finn RS, Sirlin CB, Abecassis MM, Roberts LR, et al. AASLD guidelines for the treatment of hepatocellular carcinoma. *Hepatology* (2018) 67(1):358–80. doi: 10.1002/hep.29086
4. Lu C, Rong D, Zhang B, Zheng W, Wang X, Chen Z, et al. Current perspectives on the immunosuppressive tumor microenvironment in hepatocellular carcinoma: challenges and opportunities. *Mol Cancer* (2019) 18(1):130. doi: 10.1186/s12943-019-1047-6
5. Thomson AW, Knolle PA. Antigen-presenting cell function in the tolerogenic liver environment. *Nat Rev Immunol* (2010) 10(11):753–66. doi: 10.1038/nri2858
6. Zheng J, Cai J, Li H, Zeng K, He L, Fu H, et al. Neutrophil to Lymphocyte Ratio and Platelet to Lymphocyte Ratio as Prognostic Predictors for Hepatocellular Carcinoma Patients with Various Treatments: a Meta-Analysis and Systematic Review. *Cell Physiol Biochem* (2017) 44(3):967–81. doi: 10.1159/000485396

7. Hato T, Goyal L, Greten TF, Duda DG, Zhu AX. Immune checkpoint blockade in hepatocellular carcinoma: current progress and future directions. *Hepatology* (2014) 60(5):1776–82. doi: 10.1002/hep.27246
8. Zhang W, Wang H, Sun M, Deng X, Wu X, Ma Y, et al. CXCL5/CXCR2 axis in tumor microenvironment as potential diagnostic biomarker and therapeutic target. *Cancer Commun (Lond)* (2020) 40(2-3):69–80. doi: 10.1002/cac2.12010
9. Mao Z, Zhang J, Shi Y, Li W, Shi H, Ji R, et al. CXCL5 promotes gastric cancer metastasis by inducing epithelial-mesenchymal transition and activating neutrophils. *Oncogenesis* (2020) 9(7):63. doi: 10.1038/s41389-020-00249-z
10. Hegde PS, Chen DS. Top 10 Challenges in Cancer Immunotherapy. *Immunity* (2020) 52(1):17–35. doi: 10.1016/j.immuni.2019.12.011
11. Craig AJ, von Felden J, Garcia-Lezana T, Sarcognato S, Villanueva A. Tumour evolution in hepatocellular carcinoma. *Nat Rev Gastroenterol Hepatol* (2020) 17(3):139–52. doi: 10.1038/s41575-019-0229-4
12. Chen EB, Zhou ZJ, Xiao K, Zhu GQ, Yang Y, Wang B, et al. The miR-561-5p/CX3CL1 Signaling Axis Regulates Pulmonary Metastasis in Hepatocellular Carcinoma Involving CX3CR1(+) Natural Killer Cells Infiltration. *Theranostics* (2019) 9(16):4779–94. doi: 10.7150/thno.32543
13. Neophytou CM, Pierides C, Christodoulou MI, Costeas P, Kyriakou TC, Papageorgis P. The Role of Tumor-Associated Myeloid Cells in Modulating Cancer Therapy. *Front Oncol* (2020) 10:899. doi: 10.3389/fonc.2020.00899
14. Peng SH, Deng H, Yang JF, Xie PP, Li C, Li H, et al. Significance and relationship between infiltrating inflammatory cell and tumor angiogenesis in hepatocellular carcinoma tissues. *World J Gastroenterol* (2005) 11(41):6521–4. doi: 10.3748/wjg.v11.i41.6521
15. Anitei MG, Zeitoun G, Mlecnik B, Marliot F, Haicheur N, Todosi AM, et al. Prognostic and predictive values of the immunoscore in patients with rectal cancer. *Clin Cancer Res* (2014) 20(7):1891–9. doi: 10.1158/1078-0432.CCR-13-2830
16. Galon J, Mlecnik B, Bindea G, Angell HK, Berger A, Lagorce C, et al. Towards the introduction of the 'Immunoscore' in the classification of malignant tumours. *J Pathol* (2014) 232(2):199–209. doi: 10.1002/path.4287
17. Pages F, Mlecnik B, Marliot F, Bindea G, Ou FS, Bifulco C, et al. International validation of the consensus Immunoscore for the classification of colon cancer: a prognostic and accuracy study. *Lancet* (2018) 391(10135):2128–39. doi: 10.1016/S0140-6736(18)30789-X
18. Gabrielson A, Wu Y, Wang H, Jiang J, Kallakury B, Gatalica Z, et al. Intratumoral CD3 and CD8 T-cell Densities Associated with Relapse-Free Survival in HCC. *Cancer Immunol Res* (2016) 4(5):419–30. doi: 10.1158/2326-6066.CIR-15-0110
19. Chen DS, Mellman I. Elements of cancer immunity and the cancer-immune set point. *Nature* (2017) 541(7637):321–30. doi: 10.1038/nature21349
20. Kim JM, Chen DS. Immune escape to PD-L1/PD-1 blockade: seven steps to success (or failure). *Ann Oncol* (2016) 27(8):1492–504. doi: 10.1093/annonc/mdw217
21. Xie Y, Xiang Y, Sheng J, Zhang D, Yao X, Yang Y, et al. Immunotherapy for Hepatocellular Carcinoma: Current Advances and Future Expectations. *J Immunol Res* (2018) 2018:8740976. doi: 10.1155/2018/8740976
22. Tsuchiya N, Sawada Y, Endo I, Uemura Y, Nakatsura T. Potentiality of immunotherapy against hepatocellular carcinoma. *World J Gastroenterol* (2015) 21(36):10314–26. doi: 10.3748/wjg.v21.i36.10314
23. Liu L, Qin S, Zhang Y. The Evolving Landscape of Checkpoint Inhibitor Combination Therapy in the Treatment of Advanced Hepatocellular Carcinoma. *Target Oncol* (2021) 16(2):153–63. doi: 10.1007/s11523-020-00787-x
24. Romero-Moreno R, Curtis KJ, Coughlin TR, Miranda-Vergara MC, Dutta S, Natarajan A, et al. The CXCL5/CXCR2 axis is sufficient to promote breast cancer colonization during bone metastasis. *Nat Commun* (2019) 10(1):4404. doi: 10.1038/s41467-019-12108-6
25. Zhou SL, Dai Z, Zhou ZJ, Wang XY, Yang GH, Wang Z, et al. Overexpression of CXCL5 mediates neutrophil infiltration and indicates poor prognosis for hepatocellular carcinoma. *Hepatology* (2012) 56(6):2242–54. doi: 10.1002/hep.25907
26. Liu Z, Yang L, Xu J, Zhang X, Wang B. Enhanced expression and clinical significance of chemokine receptor CXCR2 in hepatocellular carcinoma. *J Surg Res* (2011) 166(2):241–6. doi: 10.1016/j.jss.2009.07.014
27. Mirshahi F, Aqbi HF, Cresswell K, Saneshaw M, Coleman C, Jacobs T, et al. Longitudinal studies can identify distinct inflammatory cytokines associated with the inhibition or progression of liver cancer. *Liver Int* (2020) 40(2):468–72. doi: 10.1111/liv.14323
28. Xu X, Huang P, Yang B, Wang X, Xia J. Roles of CXCL5 on migration and invasion of liver cancer cells. *J Transl Med* (2014) 12:193–203. doi: 10.1186/1479-5876-12-193
29. Wang YH, Huang JH, Tian ZF, Zhou YF, Yang J. The role of CXC cytokines as biomarkers and potential targets in hepatocellular carcinoma. *Math Biosci Eng* (2019) 17(2):1381–95. doi: 10.3934/mbe.2020070
30. Huang P, Xu X, Wang L, Zhu B, Wang X, Xia J. The role of EGF-EGFR signalling pathway in hepatocellular carcinoma inflammatory microenvironment. *J Cell Mol Med* (2014) 18(2):218–30. doi: 10.1111/jcmm.12153
31. Li A, King J, Moro A, Sugi MD, Dawson DW, Kaplan J, et al. Overexpression of CXCL5 is associated with poor survival in patients with pancreatic cancer. *Am J Pathol* (2011) 178(3):1340–9. doi: 10.1016/j.ajpath.2010.11.058
32. Mierke CT, Zitterbart DP, Kollmannsberger P, Raupach C, Schlotzer-Schrehardt U, Goecke TW, et al. Breakdown of the endothelial barrier function in tumor cell transmigration. *Biophys J* (2008) 94(7):2832–46. doi: 10.1529/biophysj.107.113613
33. Liu G, Yang ZF, Zhou PY, Zhou C, Guan RY, Sun BY, et al. ROR- α-1 inhibits the proliferation, invasion, and migration of hepatocellular carcinoma MHCC97H via downregulation of chemokine CXCL5. *Cytokine* (2020) 129:155004. doi: 10.1016/j.cyto.2020.155004
34. Singal AG, Lampertico P, Nahon P. Epidemiology and surveillance for hepatocellular carcinoma: New trends. *J Hepatol* (2020) 72(2):250–61. doi: 10.1016/j.jhep.2019.08.025

Conflict of Interest: The authors declare that the research was conducted in the absence of any commercial or financial relationships that could be construed as a potential conflict of interest.

frontiers in Oncology

ORIGINAL RESEARCH
published: 07 May 2021
doi: 10.3389/fonc.2021.571476

Beta-Elemene Reduces the Malignancy of Non-Small Cell Lung Cancer by Enhancing *C3orf21* Expression

Hu Cai[1], *Lili Ren*[1], *Ying Wang*[2] *and Yongjun Zhang*[1]*

[1] Department of Integration of Traditional Chinese and Western Medicine, Cancer Hospital of the University of Chinese Academy of Sciences (Zhejiang Cancer Hospital), Institute of Basic Medicine and Cancer (IBMC), Chinese Academy of Sciences, Hangzhou, China, [2] Department of Gynecological Oncology, Cancer Hospital of the University of Chinese Academy of Sciences (Zhejiang Cancer Hospital), Institute of Basic Medicine and Cancer (IBMC), Chinese Academy of Sciences, Hangzhou, China

Background: Beta-elemene has potent anti-tumor effect, but its anti-tumor mechanism remains unclear. Chromosome 3 open reading frame 21 (C3orf21) acts as a tumor suppressor. This study tested whether the anti-tumor effect of beta-elemene was associated with modulating C3orf21 expression in non-small cell lung cancer (NSCLC).

Materials and Methods: The impact of beta-elemene on C3orf21 expression in NSCLC cells was quantified. The stable C3orf21 silencing A549 and over-expressing PC-9 cells were established and their effects on the beta-elemene-attenuated proliferation, wound healing and invasion of NSCLC cells as well as the expression of key regulators and signal events were determined.

Results: Beta-elemene significantly up-regulated C3orf21 expression in NSCLC cells. Beta-elemene treatment significantly attenuated the proliferation, wound healing and invasion of NSCLC cells, which were significantly mitigated by C3orf21 silencing, but enhanced by C3orf21 over-expression. Similar patterns of beta-elemene-modulated cyclinD1, c-Myc, COX2, MMP2, MMP9, VEGF, PTEN and Notch1 expression were detected in NSCLC cells.

Conclusions: Such data indicated that beta-elemene treatment attenuated the malignancy of NSCLC cells by up-regulating C3orf21 expression. Our findings may provide new mechanisms underlying the pharmacological action of beta-elemene.

Keywords: elemene injection, C3orf21, non-small cell lung cancer, malignancy, mechanisms

OPEN ACCESS

Edited by:
Niels Weinhold,
Heidelberg University, Germany

Reviewed by:
Basappa Basappa,
Bangalore University, India
Xinbing Sui,
Hangzhou Normal University, China

***Correspondence:**
Yongjun Zhang
zhangyj@zjcc.org.cn

Specialty section:
This article was submitted to Cancer Molecular Targets and Therapeutics, a section of the journal Frontiers in Oncology

Received: *10 June 2020*
Accepted: *09 April 2021*
Published: *07 May 2021*

Citation:
Cai H, Ren L, Wang Y and Zhang Y (2021) Beta-Elemene Reduces the Malignancy of Non-Small Cell Lung Cancer by Enhancing C3orf21 Expression. Front. Oncol. 11:571476. doi: 10.3389/fonc.2021.571476

INTRODUCTION

Non-small cell lung cancer (NSCLC) is the most prevalent malignant lung tumors with high cancer-related mortality worldwide (1, 2). At present, the major treatments for NSCLC are surgical resection, target therapies and chemotherapy. Although these therapeutic strategies for NSCLC have greatly prolonged the survival of patients, many NSCLC patients commonly develop resistance to

target therapies (3). This, together with the fact that many NSCLC patients are diagnosed at advanced stages, leads to a low rate of five-year survival (4). Hence, discovery of new therapeutic reagents and their acting mechanisms will be of high significance in management of NSCLC patients.

Beta-elemene, a natural lipid-soluble plant drug, can be extracted from traditional Chinese medicine *Rhizoma zedoariaem* (5, 6). Previous studies have shown that beta-elemene has potent anti-tumor activity in several types of malignant tumors (7–10). More importantly, beta-elemene is relatively safe and has been widely used as an effective anticancer drug in humans (6, 11). Recent studies have shown that beta-elemene can reduce the malignancy of NSCLC cells by inhibiting their proliferation, migration and invasion (5, 8). Furthermore, beta-elemene can sensitize glioblastoma multiforme cells to gefitinib (12) and synergistically enhances its therapeutic effect on inhibiting stemness and progression of lung cancer by down-regulating EZH2 expression (13). However, the exact molecular mechanisms underlying the therapeutic action of beta-elemene remain largely indistinct, which may be an important obstacle for improving and refining the clinical application of beta-elemene.

Our previous study has indicated that chromosome 3 open reading frame 21 (C3orf21) can regulate the development of lung adenocarcinoma (14, 15). In this study, we tested the hypothesis that beta-elemene could modulate C3orf21 expression to attenuate the malignancy of NSCLC cells. The results indicated that beta-elemene treatment reduced the proliferation, wound healing and invasion of NSCLC cells by increasing C3orf21 expression. Such findings may provide new pharmacological evidence to explain why beta-elemene inhibits the malignancy of NSCLC.

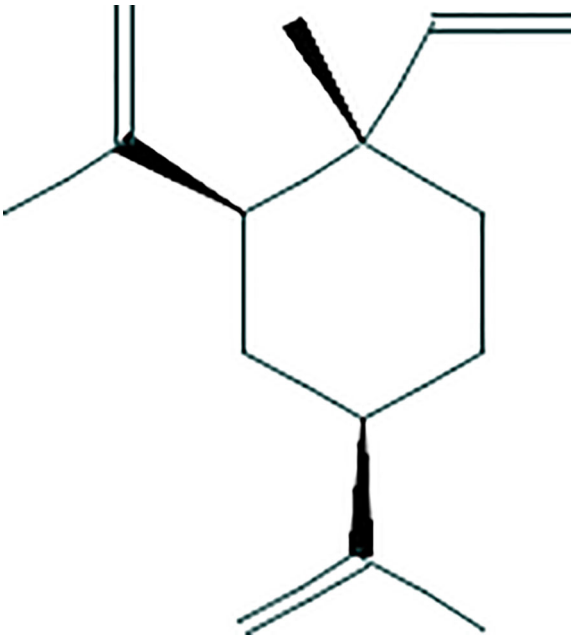

FIGURE 1 | The structure of beta-elemene.

MATERIALS AND METHODS

Beta-Elemene

Beta-elemene [1-methyl-1-vinyl-2,4-diisopropenyl-cyclohexane, C15H24, molecular weight of 204.35, **Figure 1** (16)] is a sesquiterpene compound extracted from the dried rhizome of *Rhizoma curcumae*. The beta-elemene injection (xx% of beta-elemene, National Medical Product Administration approval Number: Chinese medicine H10960114) was produced by Dalian Huali Jingang Pharmaceutical (Dalian, China).

Bioinformatic Analysis of Beta-Elemene-Associated Genes and Proteins

We searched the potential targets of beta-elemene using the BATMAN-TCM (http://bionet.ncpsb.org/batman-tcm/) database and STITCH (http://http://stitch.embl.de) database to predict the beta-elemene-associated genes and proteins. The BATMAN-TCM is an online bioinformatics analysis tool specially designed for studying the molecular mechanisms of traditional Chinese medicine, and is based on traditional Chinese medicine ingredients' target prediction (17). The STITCH also is online Search Tool for Interacting Chemicals, which integrates these disparate data sources for 430,000 chemicals into a single, easy-to-use resource. The user can get a quick overview of the potential effects of the chemical on its interaction partners by STITCH database (18).

Cells

We obtained human NSCLC A549, PC-9, NCI-H1975, MSTO-211H and NCI-H226 cells from Shanghai Institutes for Biological Sciences of Chinese Academy of Sciences. We identified them by STR. We grew them in RMPI1640 medium (Invitrogen) containing 10% fetal bovine serum (FBS, Gibco) in at 37°C 5% CO_2. We treated the cells with, or without, the indicated concentrations of beta-elemene (Dalian Huali Jingang Pharmaceutical, Dalian, China) for varying time periods.

Lentivirus Transduction

We cloned the DNA fragments for the expression of control and specific shRNAs (**Table 1**, Sangon Biotech, Shanghai, China) or the cDNA for C3orf21 expression into pLKO-ZSG-Puro, together with pCMV△R8.92 and pVSVG-I, to generate different types of lentiviruses in 293T cells. Subsequently, we transduced A549 cells with control or lentivirus for the expression of C3orf21-specific shRNA (Addgene) at multiplicity of infection of 4 in the presence of 8 mg/ml hexadimethrine bromide (Sigma). Similarly, we transduced PC-9 cells with control or lentivirus for the over-expression of C3orf21. Three days later, we treated the cells with puromycin (500 ng/ml) or blasticidin (10 mg/ml) to generate shCon, sh-C3orf21 stably silencing A549 and control, C3orf21

TABLE 1 | The sequences of primers and their applications.

Primer	Sequences (5'-3')	Application
C3rof21- F	ATGTTGCTGTGCTGACGGATA	qRT-PCR
C3rof21- R	GGAGTCACTGTAGTAGGTTCCC	qRT-PCR
C3rof21-F		Overexpression
C3rof21-R		Overexpression
shC3orf21		Knockdown
cyclinD1-F	TCTGTTCCTCGCAGACCTCCAGCA	qRT-PCR
cyclinD1-R	CCGTCCATGCGGAAGATC	qRT-PCR
cMyc-F	CAGCTGCTTAGACGCTGGATT	qRT-PCR
cMyc-R	GTAGAAATACGGCTGCACCGA	qRT-PCR
COX2-F	AGATCATCTCTGCCTGAGTATCTT	qRT-PCR
COX2-R	TTCAAATGAGATTGTGGGAAAATTGCT	qRT-PCR
MMP-2-F	GGCCCTGTCACTCCTGAGAT	qRT-PCR
MMP-2-R	GGCATCCAGGTTATCGGGGA	qRT-PCR
MMP-9-F	AGGCCTCTACAGAGTCTTTG	qRT-PCR
MMP-9-R	CAGTCCAACAAGAAAGGACG	qRT-PCR
VEGF-F	GAAGTGGTGAAGTTCATGGATGTC	qRT-PCR
VEGF-R	CGATCGTTCTGTATCAGTCTTTCC	qRT-PCR
PTEN-F	CCGTTACCTGTGTGTGGTGATATC	qRT-PCR
PTEN-R	GAATGTATTTACCCAAAAGTGAAACATT	qRT-PCR
GAPDH-assay-F	CGGATTTGGTCGTATTG	qRT-PCR
GAPDH-assay-R	GAAGATGGTGATGGGATT	qRT-PCR

over-expressing PC-9 cells, respectively. We tested the efficacy of C3orf21 silencing or over-expression by fluorescent microscopy and Western blot assays.

Quantitative Real-Time-PCR (qRT-PCR)

We extracted total RNA from the different groups of cells using TRIzol (Invitrogen) and after qualification and quantification using an Agilent Bioanalyzer 2100 (Agilent Technologies), we reversely transcribed RNA samples into cDNAs using an iScript cDNA Synthesis Kit (BIO-RAD). Subsequently, we quantified the relative levels of mRNA transcripts by qRT-PCR using SYBR Premix ExTaqTM II kit (TaKaRa) and specific primers (**Table 1**). We performed RT-PCR in triplicate at 94°C for 10 s, and 40 cycles of 94°C for 5 s, 52°C for 30 s, 72°C for 15 s. We analyzed the data using the $2^{-\Delta\Delta Ct}$ method.

CCK-8 Cell Assay

We determined the impact of beta-elemene on the proliferation of NSCLC cells by CCK-8 assay (Beyotime Shanghai China). Briefly, the cells ($2–3.5 \times 10^3$/well) from each group were grown in 96-well plates and treated in triplicate with beta-elemene at different concentrations for 24 h. Their proliferation was quantified with 10 μl/well of CCK-8 at 450 nm.

Wound Healing Assay

The different groups of cells (2×10^5 cells/well) were cultured in 6-well plate up to 80–90% confluence. The cell monolayer was wounded with a sterile micropipet tip and treated with, or without, the indicated doses of beta-elemene in serum-free medium. The monolayer of cells was photoimaged before and 24 h after beta-elemene treatment under an Olympus CKX-41 inverted microscope. The migrated areas of cancer cells were measured by Image J software.

Transwell Invasion Assay

We examined whether beta-elemene could modulate NSCLC cell invasion by transwell invasion assay using the BioCoat Matrigel Invasion Chamber (Corning), according to the manufacturer's recommended instructions. In brief, the different groups of cells (4×10^3 cells/well) were cultured in triplicate in the upper chamber that had been coated with Matrigel (REF 3422, Corning). The bottom chambers were filled with 10% FBS medium. After 48-h culture, the invaded cells on the bottom surface of the upper chamber membranes were fixed and stained with crystal violet, followed by photoimaged. The invaded cells in five fields of each membrane were counted.

Western Blot

We quantified the relative levels of interested proteins to the control GAPDH by Western blot. Briefly, we harvested each group of cells and lysed them in cell lysis buffer (Beyotime) containing a cocktail of protease inhibitors (Rocha). After qualification and quantification, we analyzed the cell lysates (30 μg/lane) by SDS-PAGE, and transferred to polyvinyl dene fluoride membranes (Millipore). After blocked, we incubated the membranes with anti-C3orf21 (20913-1-AP, Proteintech), anti-Notch1 (68309T), anti-GAPDH (2118S, Cell Signaling Technology) and detected the bound antibodies with HRP-conjugated second antibodies, followed visualizing using the enhanced chemiluminescence (Pierce, Rockford, USA). We quantified the data using Image J.

Statistical Analysis

Data are present as mean ± SD. The difference between two groups was analyzed by Student's T test, and the difference among multiple groups was analyzed by Two-way ANOVA using the GraphPad Prism 5.0 software. Statistical significance was defined when a P-value of ≤0.05.

RESULTS

Bioinformatic Analysis of Beta-Elemene Targeting Genes and Proteins

To search the potential genes and proteins associated with beta-elememe, we performed bioinformatics analysis using beta-elemene (6918391, PubChem CID) as a key word to search the BATMAN-TCM database. With a cutoff score ≥5, we obtained 522 genes associated with beta-elemene (**Figure 2**). To further search the beta-elemene-associated proteins, we used the STITCH database and found that fifty proteins were associated with beta-elemene, including XXYLT1, Notch and others (**Figure 3**).

Beta-Elemene Enhances C3orf21 Expression in NSCLC Cells

C3orf21 has shown to act as a tumor suppressor of several types of malignant tumors. To understand the antitumor effect of beta-elemene, we tested whether beta-elemene treatment could

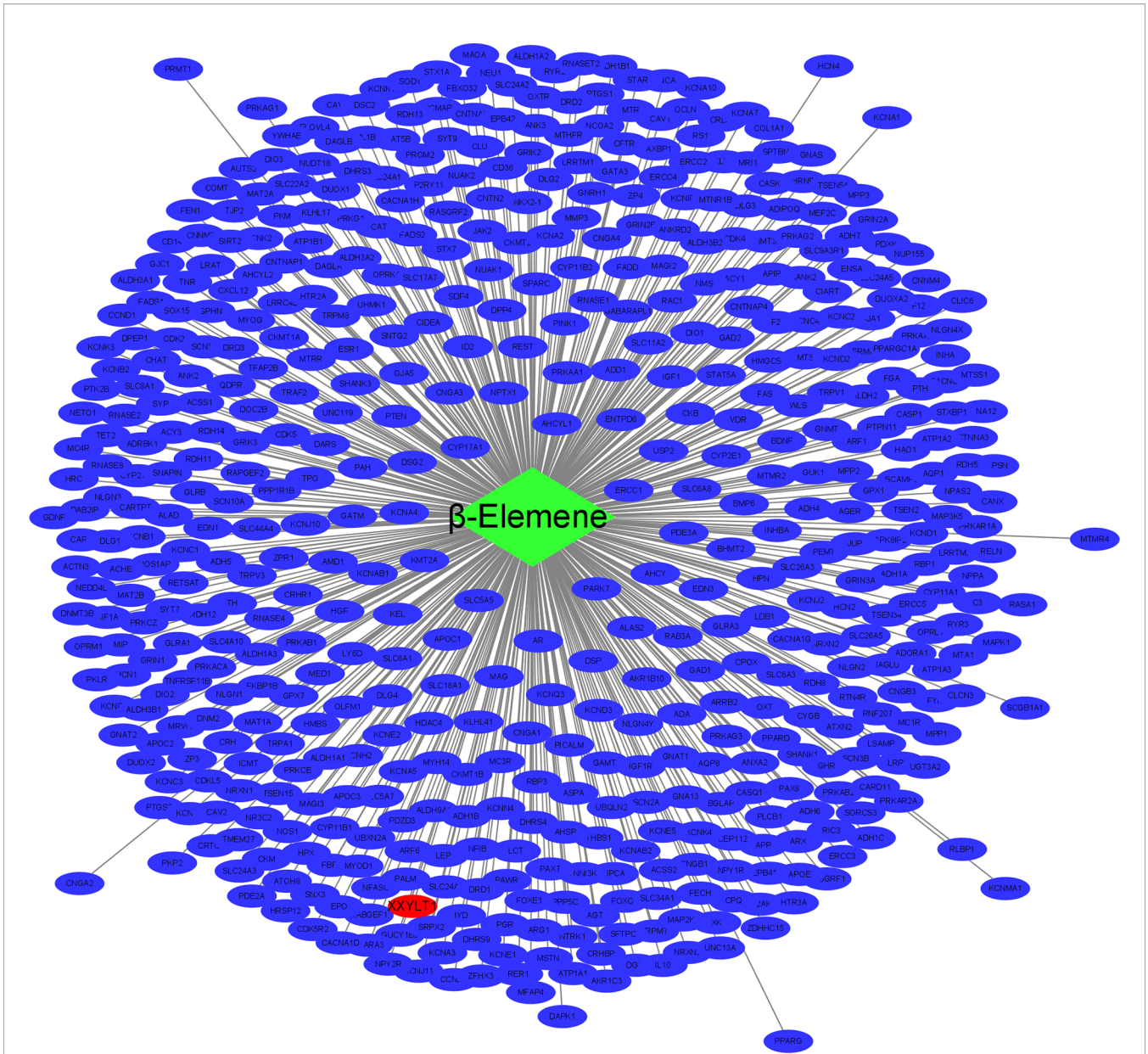

FIGURE 2 | The network of beta-elemene with the potential targeted genes. green rhombus represents beta-elemene; blue ellipse represent the targeted genes of beta-elemene; red ellipse represent the XXYLT1.

modulate C3orf21 expression in several NSCLC cell lines. Western blot analysis indicated that C3orf21 expression varied in the different NSCLC cell lines (**Figure 4A**) and treatment with beta-elemene (10 μg/ml) for 24 h significantly up-regulated C3orf21 expression in these NSCLC cells ($p < 0.05$—$p < 0.001$, **Figure 4B**). Given that A549 cells expressed relatively higher levels of C3orf21 while PC-9 expressed lower levels of C3orf21, we generated C3orf21 stably silenced A549 and C3orf21 over-expressed PC-9 cells (**Figures 4C, D**) and these cell lines were valuable for determining the role of altered C3orf21 expression in regulating the beta-elemene-mediated anti-NSCLC effects.

Beta-Elemene Inhibits the Proliferation of NSCLC Cells, Dependent on C3orf21 Expression

To investigate how altered C3orf21 expression modulated the anti-NSCLC effect of beta-elemene, we first tested the impact of beta-elemene on A549 and PC-9 cell viability by CCK-8 assays. We found that treatment with beta-elemene significantly decreased A549 and PC-9 cell viability in a dose-dependent manner (**Figures 5A, B**). Furthermore, C3orf21 silencing dramatically mitigated the inhibitory effects of beta-elemene on the proliferation of A549 cells while C3orf21 over-expression

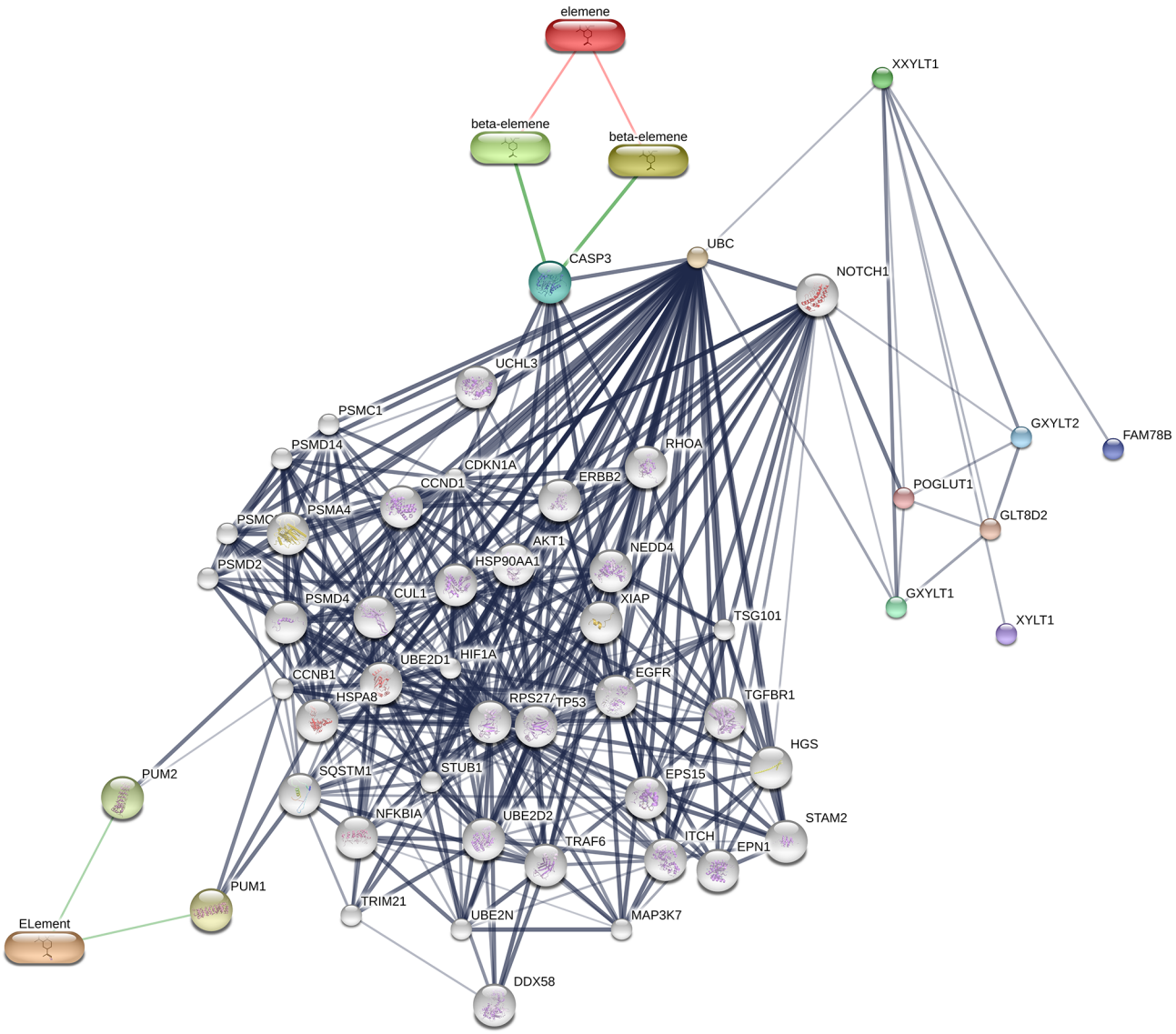

FIGURE 3 | A network of beta-elemene with the potential interacted proteins. Gray lines indicate protein-protein interactions; Green lines indicate compound–protein interactions.

remarkably enhanced its inhibitory effects on the proliferation of PC-9 cells (**Figures 5C, D**). These data indicated that beta-elemene attenuated the proliferation of NSCLC cells, which was regulated by C3orf21 expression.

Beta-Elemene Attenuates the Wound Healing of NSCLC Cells Dependent on C3orf21 Expression

To further explore how beta-elemene modulated the malignancy of NSCLC cells, we tested whether altered C3orf21 expression could change the effect of beta-elemene on the wound healing of shNC-A549, sh-C3orf21-A549, control-PC-9 and C3orf21-PC-9 cells. While C3orf21 silencing significantly increased the wound healing of shNC-A549 cells treatment with beta-elemene significantly decreased their wound healing and the inhibitory effects tended to be dose-dependent (**Figure 6A**). Similarly, beta-elemene treatment also significantly attenuated the wound healing of C3orf21-silenced A549 cells, but the wound healing effects in the C3orf21-silenced A549 cells were significantly stronger relative to their corresponding shNC-A549 cells. Furthermore, beta-elemene treatment also significantly minimized the wound healing of control-PC-9 cells and further decreased it in the C3orf21-over-expressed PC-9 cells (**Figure 6B**). A similar pattern of beta-elemene treatment on the invasion of shNC-A549, sh-C3orf21-A549, control-PC-9 and C3orf21-PC-9 cells was observed by transwell invasion assays (**Figures 6C, D**). Collectively, C3orf21 silencing mitigated the

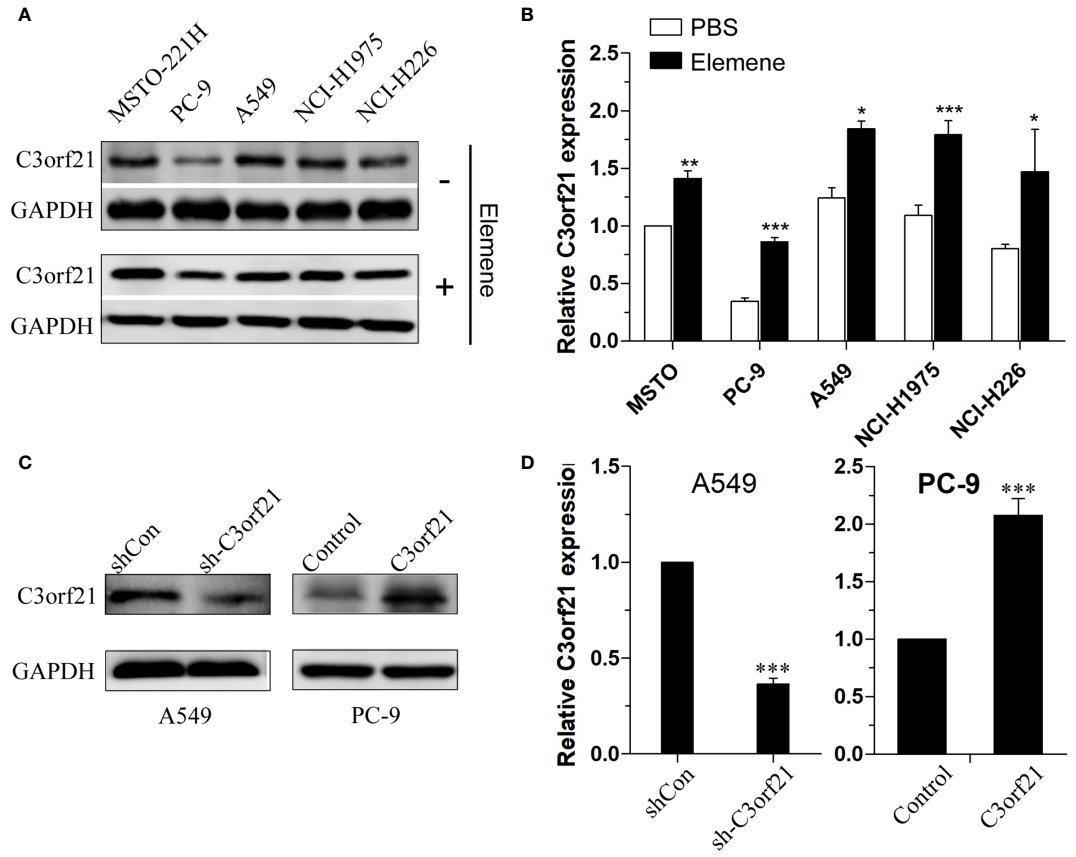

FIGURE 4 | C3orf21 expression in NSCLC cells. **(A)** Western blot analysis of the relative levels of C3orf21 expression in the indicated NSCLC cells. **(B)** Beta-elemene enhances C3orf21 expression in NSCLC cells. **(C, D)** Generation of C3orf21 stable silencing A549 cells and C3orf21 stable over-expressing PC-9 cells. Data are representative images or expressed as the mean ± SD of each group from three biological experiments. *P < 0.05, **P < 0.01 and ***P < 0.001 vs. the control.

inhibition of beta-elemene on the wound healing and invasion of NSCLC while C3orf21 over-expression enhanced its inhibitory effects in NSCLC cells.

Beta-Elemene Modulates the Expression of Several Regulators and Signal Events in NSCLC Cells, Dependent on C3orf21 Expression

To further understand the pharmacological action of beta-elemene in attenuating the malignancy of NSCLC cells, we examined how beta-elemene treatment could modulate the levels of Cyclin D1, c-Myc, COX2, MMP2, MMP9, VEGF and PTEN as well as Notch1 mRNA transcripts and protein expression in different groups of NSCLC cells. As shown in **Figure 7**, C3orf21 silencing significantly increased the relative levels of cyclin D1, c-Myc, Cox2, MMP2, MMP9, VEGF, but decreased PTEN mRNA transcripts in A549 cells. Conversely, C3orf21 over-expression had opposite effects on their expression in PC-9 cells, relative to their controls. Treatment with beta-elemene significantly decreased Cyclin D1, c-Myc, COX2, MMP2, MMP9, PTEN, but increased VEGF mRNA transcripts in both control and C3orf21-silenced A549 cells, relative to that of untreated cells. In addition, beta-elemene treatment also deceased Cyclin D1, c-Myc, COX2, MMP2, MMP9 and VEGF, but increased PTEN mRNA transcripts in both control and C3orf21-over-expressed PC-9 cells, compared with that in their untreated cells. Western blot analysis indicated that C3orf21 silencing up-regulated Notch1 expression in A549 cells while C3orf21 over-expression down-regulated Notch1 expression in PC-9 cells (**Figure 8**). Treatment with beta-elemene significantly reduced Notch1 expression in all groups of cells, particularly in the C3orf21-over-expressed PC-9 cells. Together, such data indicated that beta-elemene treatment modulated the expression of several key regulators and signal events in NSCLC cells, dependent on C3orf21 expression.

DISCUSSION

NSCLC is the most prevalent malignancy, and current treatments for NSCLC include surgical resection, target therapies and chemotherapy, which have side effects. Hence, discovery of new safe and therapeutic reagents is urgently needed. Previous studies have shown that beta-elemene has

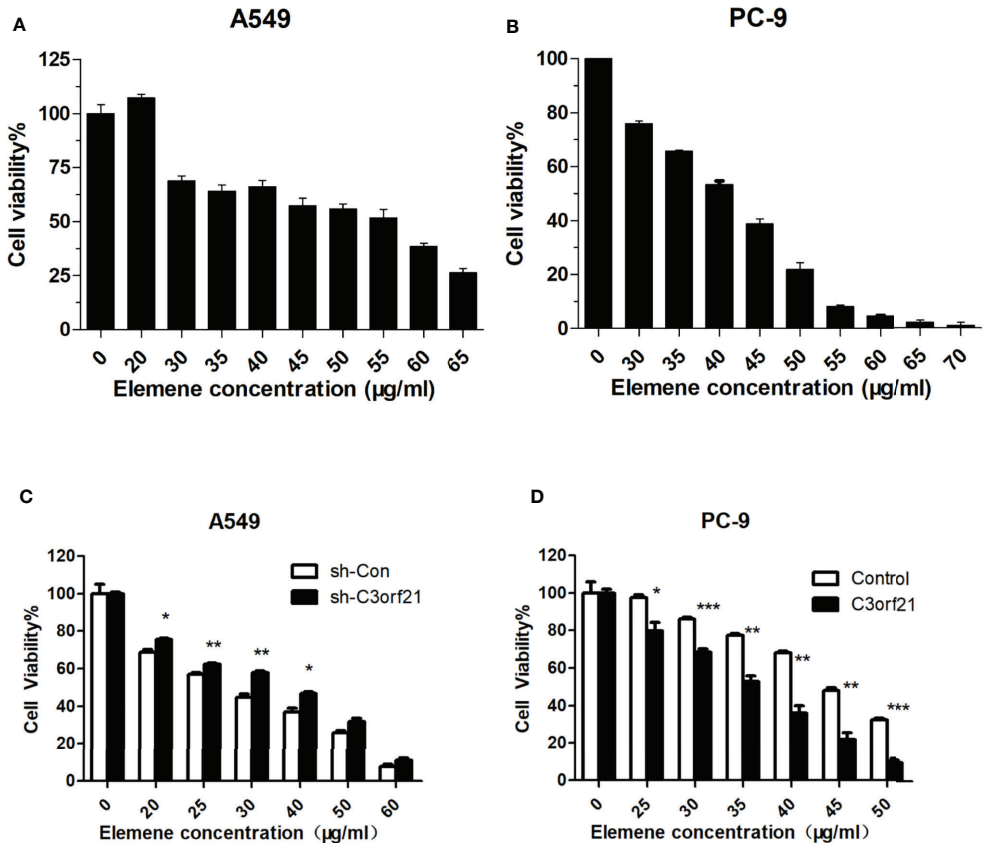

FIGURE 5 | Beta-elemene inhibits the proliferation of NSCLC cells. A549, PC-9, A549-shNC and A549-shC3orf21 cells were treated with, or without, the indicated concentrations of beta-elemene for 24 h and the cell proliferation was determined by CCK-8 assays. Data are expressed as the mean ± SD of each dose group from three biological experiments. **(A, B)** The proliferation of A549 cells. **(B)** The proliferation of PC-9 cells. **(C)** The proliferation of A549-shNC and A549-shC3orf21 cells. **(D)** The proliferation of PC-9-NC and PC-9-C3orf21 over-expression. *P < 0.05, **P < 0.01 and ***P < 0.001 vs. the control.

potent antitumor activity and can minimize the drug resistance of some types of tumor cells (19–21). In this study, we found that beta-elemene significantly enhanced C3orf21 expression in NSCLC cells. Beta-elemene treatment dramatically decreased the proliferation, would healing and invasion of NSCLC cells, which were mitigated by C3orf21 silencing, but enhanced by C3orf21 over-expression in vitro. The significantly decreased proliferation, wound healing and invasion of NSCLC cells indicated that beta-elemene remarkably attenuated the malignancy of NSCLC cells by up-regulating C3orf21 expression. Such novel findings extended previous observations and support the notion that C3orf21 acts as a tumor suppressor in inhibiting the development and progression of malignant tumors. Moreover, C3orf21 over-expression further enhanced the therapeutic effect of beta-elemene, which suggests that C3orf21 may be a new therapeutic target for intervention of NSCLC.

To understand the pharmacological action of beta-elemene, we tested whether beta-elemene treatment could modulate the expression of key regulators for cell behaviors and signal events in NSCLC cells. We found that C3orf21 silencing remarkably increased the relative levels of Cyclin D1, c-Myc, Cox2, MMP2, MMP9, VEGF, besides Notch1, but decreased PTEN expression while C3orf21 over-expression displayed opposite effects in NSCLC cells. Such results extended previous observations that C3orf21 inhibits the Notch signaling (22). It is well known that Cyclin D1, c-Myc and Cox2 can promote the proliferation of tumor cells (23) while PTEN can suppress the PI3K/AKT/mTOR signaling (24). Furthermore, VEGF is an important angiogenic factor and MMP2/9 are crucial for tumor cell motility (25). In addition, decreased levels of C3orf21 expression is related to a poor prognosis in patients with lung cancer (26). Functionally, C3orf21 can prolong the O-linked xylose-glucose (14). The inhibitory effect of C3orf21 on the Notch signaling is likely associated with the differential O-linked glycosylation of its extracellular domain (NECD) (27, 28). More importantly, we found that beta-elemene treatment significantly decreased cyclin D1, c-Myc, Cox2, MMP2/9 expression, which were attenuated by C3orf21 silencing and enhanced by C3orf21 over-expression in NSCLC cells. Interestingly, beta-elemene treatment significantly increased VEGF expression, but decreased PTEN expression in C3orf21-sielnced A549 cells. The same treatment had opposite effects on the VEGF and PTEN expression in the C3orf21-over-expressed PC-9 cells. It is possible that C3orf21 may through the similar mechanisms, regulate the expression of other

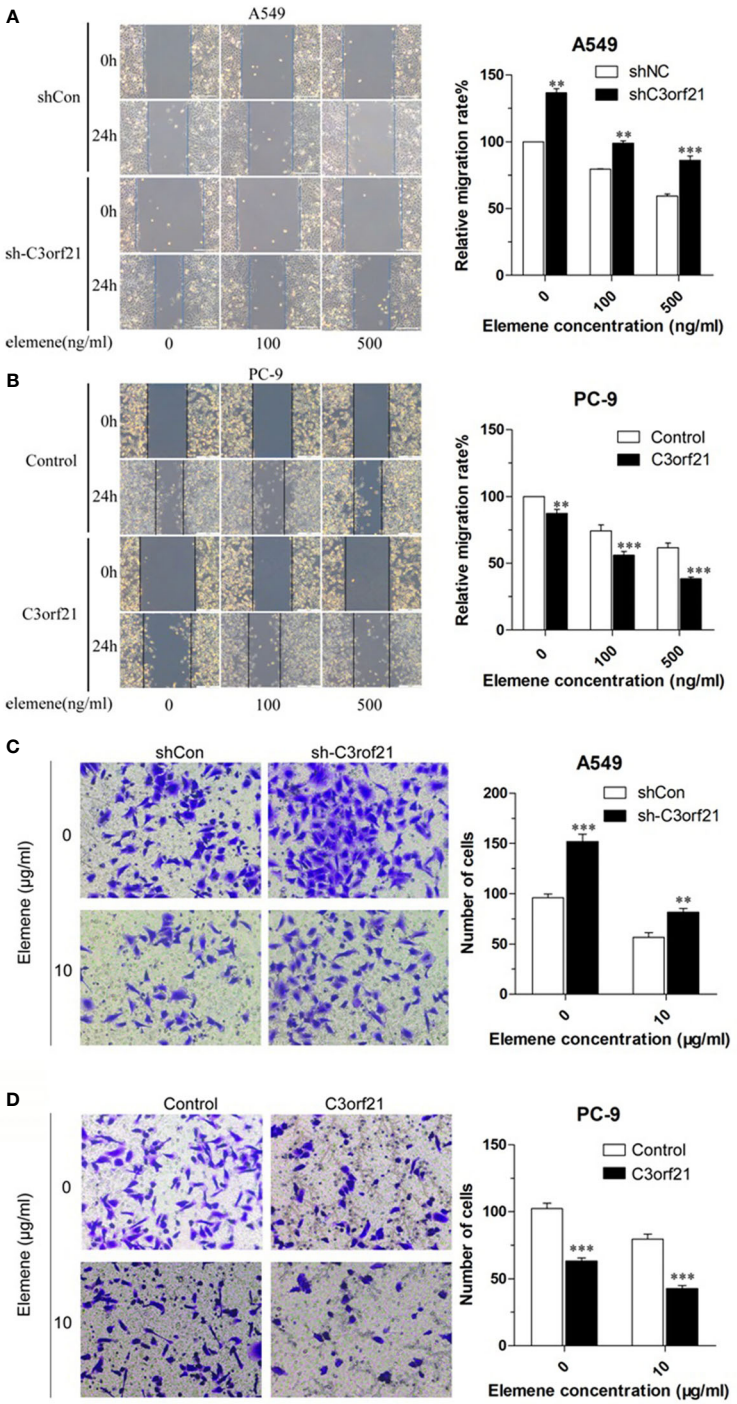

FIGURE 6 | Beta-elemene attenuates the wound healing and invasion of NSCLC cells. **(A)** The wound healing of A549 cells. **(B)** The wound healing of PC-9 cells. **(C)** The invasion of A549 cells. **(D)** The invasion of PC-9 cells. Data are representative images or expressed as the mean ± SD of each group from three biological experiments. **P < 0.01 and ***P < 0.001 vs. the control.

molecules tested. We are interested in further investigating how C3orf21 regulates the expression and functions of these regulators and signaling during the development and progression of NSCLC.

Collectively, our results revealed that beta-elemene treatment dramatically enhanced C3orf21 expression in NSCLC cells. Beta-elemene treatment significantly reduced the malignancy of NSCLC cells, which were attenuated by C3orf21 silencing, but

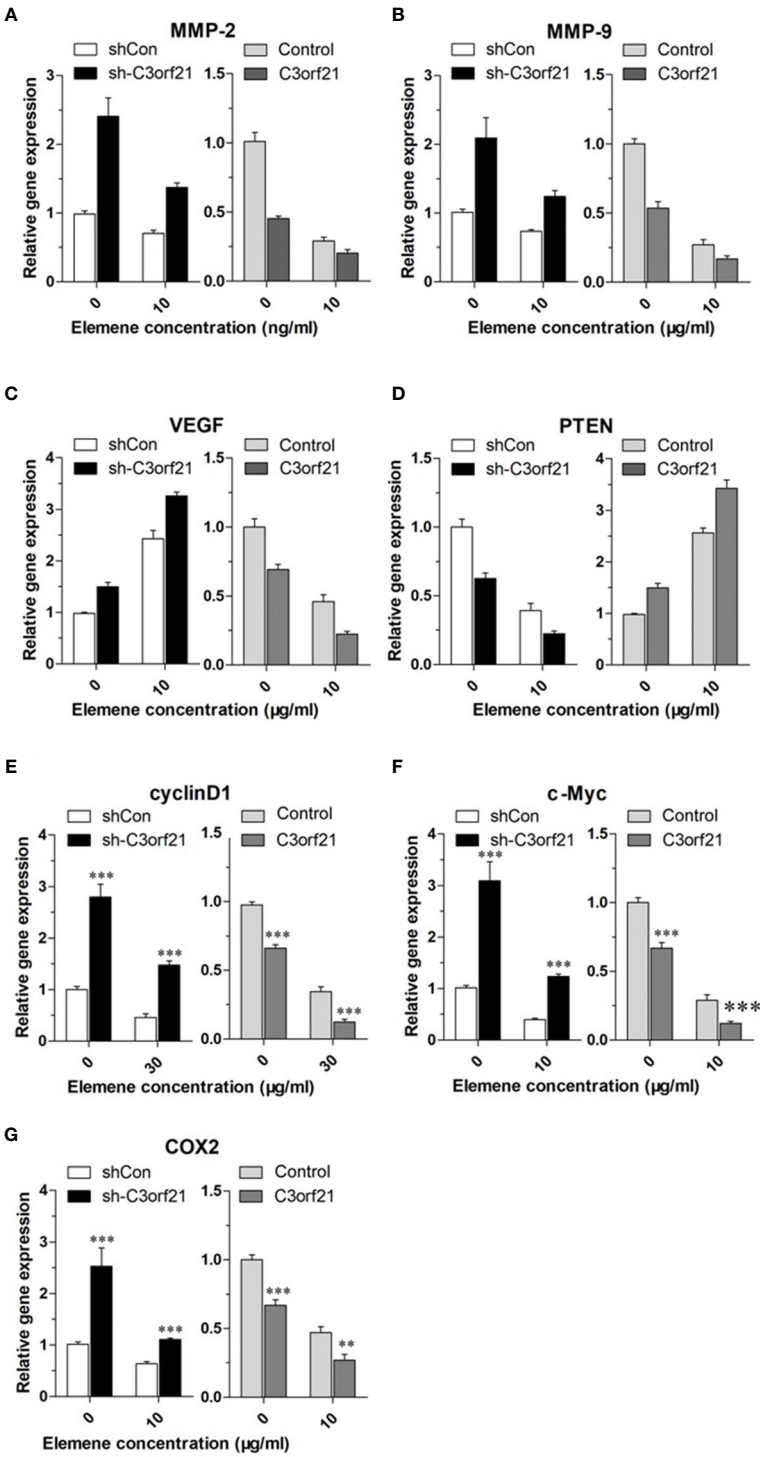

FIGURE 7 | Beta-elemene modulates the expression of several regulators and signal events in NSCLC cells, dependent on C3orf21 expression. The indicated NSCLC cells were treated with, or without, beta-elemene for 24 h and the relative levels of MMP-2 **(A)**, MMP-9 **(B)**, VEGF **(C)**, PTEN **(D)** Cyclin **(E)**, C-Myc **(F)**, and COX2 **(G)** in the indicated NSCLC cells were quantified by RT-PCR. Data are present as mean ± SD of each group from at least three biological experiments. **P < 0.01 and ***P < 0.001 vs. the control.

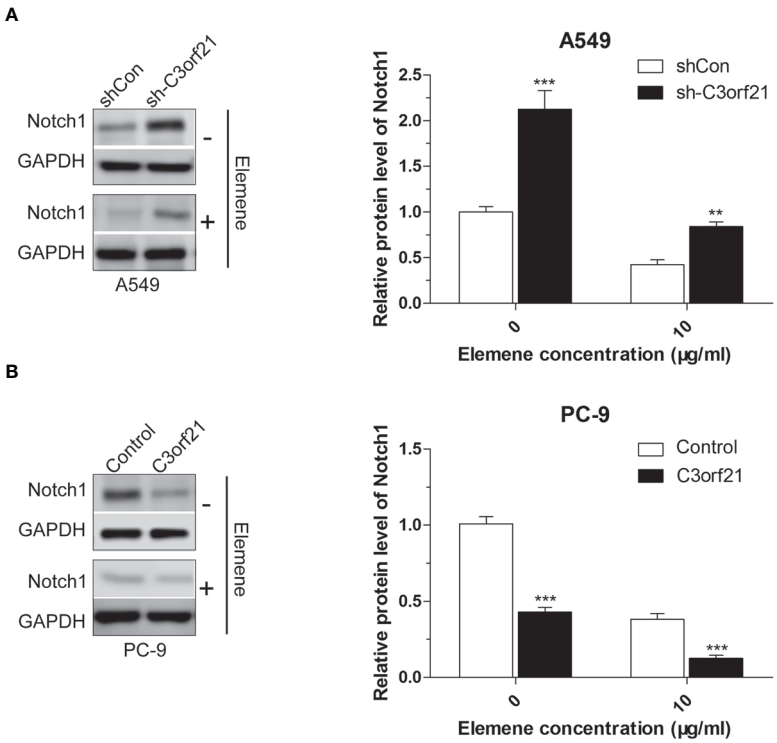

FIGURE 8 | Beta-elemene decreases C3orf21 protein expression in NSCLC cells. The indicated NSCLC cells were treated with, or without, beta-elemene for 24 and their relative levels of Notch1 protein expression **(A, B)** were quantified by Western blot. Data are representative images or present as mean ± SD of each group from at least three biological experiments. **P < 0.01 and ***P < 0.001 vs. the control.

enhanced by C3orf21 over-expression. Similarly, we found that beta-elemene treatment significantly altered the expression of key regulators of malignant behaviors and signal events, which were modulated by altered C3orf21 expression in NSCLC cells. Thus, our findings may provide new insights into the pharmacological action of beta-elemene in inhibiting the development and progression of NSCLC.

DATA AVAILABILITY STATEMENT

The raw data supporting the conclusions of this article will be made available by the authors, without undue reservation.

AUTHOR CONTRIBUTIONS

HC and YZ were responsible for study design, performing experiments, statistical analysis, and manuscript writing. LR and YW collected the data and wrote the manuscript. All authors contributed to the article and approved the submitted version.

FUNDING

This study was supported by grants from the Zhejiang Provincial Medical and Health Scientific and Technical Foundation (No.2017171306, 2018KY296 and 2020KY470).

REFERENCES

1. Ferlay J, Soerjomataram I, Dikshit R, Eser S, Mathers C, Rebelo M, et al. Cancer Incidence and Mortality Worldwide: Sources, Methods and Major Patterns in GLOBOCAN 2012. *Int J Cancer* (2015) 136:E359–86. doi: 10.1002/ijc.29210
2. Sullivan I, Planchard D. ALK Inhibitors in non-Small Cell Lung Cancer: The Latest Evidence and Developments. *Ther Adv Med Oncol* (2016) 8:32–47. doi: 10.1177/1758834015617355
3. Hsu YL, Kuo PL, Lin CC. Proliferative Inhibition, Cell-Cycle Dysregulation, and Induction of Apoptosis by Ursolic Acid in Human non-Small Cell Lung Cancer A549 Cells. *Life Sci* (2004) 75:2303–16. doi: 10.1016/j.lfs.2004.04.027
4. Luque M, Díez FJ, Disdier C. Optimal Sequence of Tests for the Mediastinal Staging of non-Small Cell Lung Cancer. *BMC Med Inform Decis Mak* (2016) 16:9. doi: 10.1186/s12911-016-0246-y
5. Zhao S, Wu J, Zheng F, Tang Q, Yang L, Li L, et al. Beta- Beta-Elemene Inhibited Expression of DNA Methyltransferase 1 Through Activation of ERK1/2 and AMPKalpha Signalling Pathways in Human Lung Cancer Cells: The Role of Sp1. *J Cell Mol Med* (2015) 19:630–41. doi: 10.1111/jcmm.12476
6. Yu X, Xu M, Li N, Li Z, Li H, Shao S, et al. Beta- Beta-Elemene Inhibits Tumor-Promoting Effect of M2 Macrophages in Lung Cancer. *Biochem Biophys Res Commun* (2017) 490:514–20. doi: 10.1016/j.bbrc.2017.06

7. Dai ZJ, Tang W, Lu WF, Gao J, Kang HF, Ma XB, et al. Antiproliferative and Apoptotic Effects of Beta- Beta-Elemene on Human Hepatoma HepG2 Cells. *Cancer Cell Int* (2013) 13:27. doi: 10.1186/1475-2867-13-27
8. Zhang H, Xu F, Xie T, Jin H, Shi L. Beta- Beta-Elemene Induces Glioma Cell Apoptosis by Downregulating Survivin and its Interaction With Hepatitis B X-Interacting Protein. *Oncol Rep* (2012) 28:2083–90. doi: 10.3892/or.2012.2022
9. Guan C, Liu W, Yue Y, Jin H, Wang X, Wang XJ. Inhibitory Effect of Beta-Beta-Elemene on Human Breast Cancer Cells. *Int J Clin Exp Pathol* (2014) 7:3948–56.
10. Hong L, Zeng Y, Yang D. Inhibitory Effect of Beta- Beta-Elemene on Human Airway Granulation Tissue In Vivo and In Vitro. *Respiration* (2016) 92:329–38. doi: 10.1159/000448554
11. Tan W, Lu J, Huang M, Li Y, Chen M, Wu G, et al. Anti-Cancer Natural Products Isolated From Chinese Medicinal Herbs. *Chin Med* (2011) 6:27. doi: 10.1186/1749-8546-6-27
12. Mu L, Wang T, Chen Y, Tang X, Yuan Y, Zhao Y. Beta- Beta-Elemene Enhances the Efficacy of Gefitinib on Glioblastoma Multiforme Cells Through the Inhibition of the EGFR Signaling Pathway. *Int J Oncol* (2016) 49:1427–36. doi: 10.3892/ijo.2016.3626
13. Cheng H, Ge X, Zhuo S, Gao Y, Zhu B, Zhang J, et al. Beta- Beta-Elemene Synergizes With Gefitinib to Inhibit Stem-Like Phenotypes and Progression of Lung Cancer Via Down-Regulating Ezh2. *Front Pharmacol* (2018) 9:1413. doi: 10.3389/fphar.2018.01413
14. Sethi MK, Buettner FF, Krylov VB, Takeuchi H, Nifantiev NE, Haltiwanger RS, et al. Identification of Glycosyltransferase 8 Family Members as Xylosyltransferases Acting on O-glucosylated Notch Epidermal Growth Factor Repeats. *J Biol Chem* (2010) 285:1582–6. doi: 10.1074/jbc.C109.065409
15. Yang L, Wang Y, Fang M, Deng D, Zhang Y. C3orf21 Ablation Promotes the Proliferation of Lung Adenocarcinoma, and its Mutation At the rs2131877 Locus may Serve as a Susceptibility Marker. *Oncotarget* (2017) 8:33422–31. doi: 10.18632/oncotarget.16798
16. PubChem [Internet]. Bethesda (MD): National Library of Medicine (US), National Center for Biotechnology Information; (2004-. *PubChem Compound Summary for CID 6918391, beta-Elemene*; [cited 2021 Apr. 30]. Available from: https://pubchem.ncbi.nlm.nih.gov/compound/beta-Elemene.
17. Liu Z, Guo F, Wang Y, Li C, Zhang X, Li H, et al. Batman-Tcm: A Bioinformatics Analysis Tool for Molecular mechANism of Traditional Chinese Medicine. *Sci Rep* (2016) 6:21146. doi: 10.1038/srep21146
18. Szklarczyk D, Santos A, von Mering C, Jensen LJ, Bork P, Kuhn M. STITCH 5: Augmenting Protein-Chemical Interaction Networks With Tissue and Affinity Data. *Nucleic Acids Res* (2016) 4(D1):D380–4. doi: 10.1093/nar/gkv1277
19. Yao C, Jiang J, Tu Y, Ye S, Du H, Zhang Y. Beta-Elemene Reverses the Drug Resistance of A549/DDP Lung Cancer Cells by Activating Intracellular Redox System, Decreasing Mitochondrial Membrane Potential and P-glycoprotein Expression, and Inducing Apoptosis. *Thorac Cancer* (2014) 5:304–12. doi: 10.1111/1759-7714.12093
20. Yao CC, Tu YR, Jiang J, Ye SF, Du HX, Zhang Y. Beta- Beta-Elemene Reverses the Drug Resistance of Lung Cancer A549/DDP Cells Via the Mitochondrial Apoptosis Pathway. *Oncol Rep* (2014) 31:2131–8. doi: 10.3892/or.2014.3083
21. Lin L, Li L, Chen X, Zeng B, Lin T. Preliminary Evaluation of the Potential Role of Beta- Beta-Elemene in Reversing Erlotinib-Resistant Human NSCLC A549/ER Cells. *Oncol Lett* (2018) 16:3380–8. doi: 10.3892/ol.2018.8980
22. Yuan X, Wu H, Han N, Xu H, Chu Q, Yu S, et al. Notch Signaling and EMT in non-Small Cell Lung Cancer: Biological Significance and Therapeutic Application. *J Hematol Oncol* (2014) 7:87. doi: 10.1186/s13045-014-0087-z
23. Lin X, Tan S, Fu L, Dong Q. Bcat1 Overexpression Promotes Proliferation, Invasion, and Wnt Signaling in Non-Small Cell Lung Cancers. *Onco Targets Ther* (2020) 13:3583–94. doi: 10.2147/OTT.S237306
24. Zhang Y, Kwok-Shing Ng P, Kucherlapati M, Chen F, Liu Y, Tsang YH, et al. A Pan-Cancer Proteogenomic Atlas of PI3K/AKT/mTOR Pathway Alterations. *Cancer Cell* (2017) 31:1–13. doi: 10.1016/j.ccell.2017.04.013
25. Thaker PH, Han LY, Kamat AA. Chronic Stress Promotes Tumor Growth and Angiogenesis in a Mouse Model of Ovarian Carcinoma. *Nat Med* (2006) 12:939–44. doi: 10.1038/nm1447
26. Donnem T, Andersen S, Al-Shibli K, Al-Saad S, Busund LT, Bremnes RM. Prognostic Impact of Notch Ligands and Receptors in Nonsmall Cell Lung Cancer: Coexpression of Notch-1 and Vascular Endothelial Growth Factor-a Predicts Poor Survival. *Cancer* (2010) 116:5676–85. doi: 10.1002/cncr.25551
27. Takeuchi H, Haltiwanger RS. Significance of Glycosylation in Notch Signaling. *Biochem Biophys Res Commun* (2014) 453:235–42. doi: 10.1016/j.bbrc.2014.05.115
28. Yu H, Takeuchi M, LeBarron J, Kantharia J, London E, Bakker H, et al. Notch-Modifying Xylosyltransferase Structures Support an SNi-like Retaining Mechanism. *Nat Chem Biol* (2015) 11:847–54. doi: 10.1038/nchembio.1927

Conflict of Interest: The authors declare that the research was conducted in the absence of any commercial or financial relationships that could be construed as a potential conflict of interest.

frontiers in Oncology

ORIGINAL RESEARCH
published: 11 June 2021
doi: 10.3389/fonc.2021.632352

Long Distance From Microvessel to Cancer Cell Predicts Poor Prognosis in Non-Small Cell Lung Cancer Patients

Haiying Ding[1†], Jiao Sun[1†], Yu Song[1], Wenxiu Xin[1], Junfeng Zhu[1], Like Zhong[1], Yinbo Chen[2], Yiwen Zhang[3], Yinghui Tong[1] and Luo Fang[1*]*

[1] Department of Pharmacy, The Cancer Hospital of the University of Chinese Academy of Sciences (Zhejiang Cancer Hospital), Institute of Basic Medicine and Cancer (IBMC), Chinese Academy of Sciences, Hangzhou, China, [2] Department of Colorectal Cancer, The Cancer Hospital of the University of Chinese Academy of Sciences (Zhejiang Cancer Hospital), Institute of Basic Medicine and Cancer (IBMC), Chinese Academy of Sciences, Hangzhou, China, [3] Department of Pharmacy, Zhejiang Provincial People's Hospital, People's Hospital of Hangzhou Medical College, Hangzhou, China

OPEN ACCESS

Edited by:
Marco Rossi,
University of Catanzaro, Italy

Reviewed by:
Mikhail Durymanov,
Moscow Institute of Physics and Technology, Russia
Barbara Muz,
Washington University in St. Louis, United States

***Correspondence:**
Luo Fang
fangluo@zjcc.org.cn
Yinghui Tong
tongyh@zjcc.org.cn

[†]These authors have contributed equally to this work

Specialty section:
This article was submitted to Cancer Molecular Targets and Therapeutics, a section of the journal Frontiers in Oncology

Received: *23 November 2020*
Accepted: *19 April 2021*
Published: *11 June 2021*

Citation:
Ding H, Sun J, Song Y, Xin W, Zhu J, Zhong L, Chen Y, Zhang Y, Tong Y and Fang L (2021) Long Distance From Microvessel to Cancer Cell Predicts Poor Prognosis in Non-Small Cell Lung Cancer Patients. Front. Oncol. 11:632352. doi: 10.3389/fonc.2021.632352

Background: Blood supply, which is crucial for nutrition and drug delivery, was determined by microvessel density as well as the diffusion distance between vessels and cancer cells. Therefore, we evaluated the distance from microvessels to cancer cells (D_{mvcc}) and its role in the prognosis of non-small cell lung cancer (NSCLC) patients.

Methods: Patients with primary NSCLC were retrospectively analyzed. The tumor samples were immunochemically stained with CD31 to visualize the microvessels. The D_{mvcc} was defined as the mean distance from each microvessel to its nearest cancer cell in the "hot-spot" of an individual patient. The patients were stratified into short- and long-distance groups using five strategies, including dichotomy by the median value, optimal cutoff, trichotomy, quartation and per-10 μm increase. The correlation between the D_{mvcc} and survival was evaluated by using univariate and multivariate analyses with various D_{mvcc} strategies.

Results: In total, 100 patients were analyzed. The median value of D_{mvcc} was 13.1 μm (ranged, 1.6 to 269.7 μm; mean value, 24.4 ± 33.5 μm). The optimal cutoff value of D_{mvcc} for predicting survival outcome was 20 μm. D_{mvcc} was significantly related to overall survival (OS) with all the five categories ($p = 0.001–0.000004$) and progression-free survival (PFS) categorized by optimal cutoff value ($p = 0.024$), trichotomy ($p = 0.041$) and per-10 μm increase ($p = 0.040$) after adjusting for other factors. Patients with longer D_{mvcc} (≥20 μm) were observed to have poor survival outcomes (OS: HR = 13.5, 95CI: 4.42–41.18, $p = 0.000005$; PFS: 3.26, 95CI: 1.56–6.81, $p = 0.002$). A high D_{mvcc} per-10 μm was associated with a significantly increased risk of cancer-related death and progression by 98% ($p = 0.0001$) and 30% ($p = 0.044$), respectively.

Conclusion: The NSCLC tissues had varying distances from microvessels to cancer cells, and long distances were strongly associated with poor survival.

Keywords: non-small cell lung cancer, prognosis marker, distance from microvessel to cancer cell, progression free survival, overall survival

INTRODUCTION

Lung cancer is common and has high incidence and mortality globally (1). Non-small cell lung cancer (NSCLC) accounts for 80–90% of all lung cancers. Angiogenesis contributes to lung cancer development by supplying oxygen and nutrients and driving growth and metastasis (2). Accordingly, numerous factors related to angiogenesis-related molecules and morphological parameters have been exploited as potential prognostic factors for NSCLC. The prominent examples of architectural factors are microvessel area (MVA) and microvessel density (MVD). These two quantitative markers of the microvessels in tumor tissues have been the focus of research (3–5). However, their role in survival prediction remains controversial (6–9). One explanation for this discrepancy is that several vessels were separated from cancer cells by intratumoral stroma. Therefore, cancer cells may not receive adequate oxygen and nutrients if they lie too far from vessels, even when vascularization is dense (10–12).

In several solid tumors, the stroma is desmoplastic and filled with a thick extracellular matrix, including collagen, fibronectin, and laminins (9, 13). The stroma separates cancer cells from the vasculature (14–16). Before diffusion into cancer cells, oxygen, nutrition, and antitumor drugs should cross the stiff stroma and overcome the hamper by increasing interstitial fluid pressure and lengthening transport distance (9, 17, 18). The inadequate supply of oxygen and antineoplastic agents may induce hypoxia and chemoresistance, ultimately driving tumor progression (19–22). Therefore, we hypothesized that the distance between nutrition and drug transport is a promising factor for predicting the prognosis of NSCLC. However, the diffusion distance in tumor tissues has not been measured, and its correlation with survival outcomes also needs to be evaluated. In the present study, we measured the distance between microvessels and cancer cells (D_{mvcc}) and evaluated its role in predicting the prognosis of patients with NSCLC.

MATERIALS AND METHODS

Patients and Samples

This retrospective study reviewed NSCLC patients treated at the Zhejiang Cancer Hospital (Hangzhou, China) from July 2011 to October 2012. The patients included (1) were histologically diagnosed with primary NSCLC, (2) underwent surgical resection as primary treatment, (3) had available biopsied tissue of the primary lesion collected before chemotherapy, and had their full information, including clinicopathologic characteristics and survival outcomes, available. The data on the follow-up was updated on July 20th, 2016. Thoracic and abdominal CT, abdominal ultrasonography, MRI, and chest radiography were used to monitor tumor recurrence. Tumor tissues were obtained from the tissue bank of the Zhejiang Cancer Hospital. This study was approved by the Ethics Committee of Zhejiang Cancer Hospital (No. IRB-2017-67), and it adhered to the ethical principles of the Declaration of Helsinki. Written informed consent was obtained from all the patients.

Immunohistochemical Staining

One specimen of resected lung cancer tumor tissue from each individual was collected. Microvessels were detected by immunohistochemical (IHC) staining of vascular endothelial cells for the CD31 antigen (Ca# 13063, Wuhan Goodbio Technology Co., Ltd) of vascular endothelial cells. In brief, sections of paraffin-embedded tumor tissues (5 μm thick) were de-paraffinized and rehydrated. The deparaffinized sections were incubated with the primary antibody (rabbit polyclonal antibody, Proteintech, Rosemont, USA) at a dilution of 1:300 overnight at 4°C after pretreatment with Dako EnVisionTM FLEX Target Retrieval Solution (high pH, pH 9.0, Ca# K5007, Dako) at 95°C for 20 min for antigen retrieval. The sections were stained with secondary antibodies for 30 min at room temperature. Next, the color was developed with 3,3'-diaminobenzidine in Tris–HCl (50 mmol/L, pH 7.5) containing 0.005% hydrogen peroxide, followed by counterstaining with hematoxylin.

Measurement of D_{mvcc}

D_{mvcc} was defined as the distance from each microvessel to its nearest neighbor cancer cell.

Microvessels and "Hot Spot"

The image analysis procedure is illustrated in **Figure S1**. Microvessels were identified based on specific architectures; the lumen lined by endothelial cells was positively visualized with anti-CD31 staining. Microvessels in the tumor tissue were observed with a fluorescence microscope (Nikon Eclipse TI-SR) equipped with a Nikon DS-U3 digital camera controller. After an overview of the section, the field with the highest density of microvessels was selected as the "hot-spot" field of each section according to a previously reported method (23).

Distance Measure

The distances between each tumor microvessel and its near cancer cells were dependently measured at 200× magnification by two experienced investigators using the Image J software (Wayne Rasband, National Institute of Health, USA), and the shortest distance was identified as the D_{mvcc} of individual tumor vessel. Subsequently, the mean D_{mvcc} of all vessels in the "hot spot" field of individual patients was calculated as the patient's D_{mvcc}.

Statistical Analyses

Statistical analysis was performed using SPSS Statistics (Version 23.0, IBM Inc., New York, USA), R Studio software (Version 0.99.486, R Studio, Inc.), and Prism 7 (GraphPad Software Inc., La Jolla, CA, USA). Where appropriate, linear regression analysis (Pearson correlation coefficient), analysis of variance (ANOVA), and Student's t-tests were used. Overall survival (OS) and progression-free survival (PFS) were defined as the interval between the first diagnosis and death or the first evidence of disease progression, respectively. The Kaplan–Meier method was used for the univariate analysis of OS and PFS, and they were compared using the log-rank test. The discriminative performance of the prognostic survival model was evaluated using the concordance index (C-index). To determine the optimal cutoff value of D_{mvcc} for OS and PFS prediction,

values from 2–50 μm (step size = 1 μm) were taken as 49 potential cutoff values. The patients were stratified into the long or short D_{mvcc} group according to one of the 49 cutoff values, and the HRs of OS and PFS were calculated using the log-rank test. The cutoff value with the most significant correlation between OS and PFS was defined as the optimal cutoff value. The correlation between D_{mvcc} and survival outcome (OS or PFS) was examined using various categorical strategies of D_{mvcc}: (1) dichotomy by median value; (2) dichotomy by optimal cutoff; (3) trichotomy: bottom tertile, middle tertile, and top tertile; (4) quartation: 1st, 2nd, 3rd, and 4th quartile; (5) per-10 μm increase: 0–10 μm, 10–20 μm, 20–30 μm, 30–40 μm, 40–50 μm. A stepwise multivariate Cox proportional hazards regression was performed to further test for the independence of D_{mvcc} measurements from potential prognostic variables (such as age, sex, smoking history, tumor histology, tumor differentiation, disease stage, or chemotherapy). A series of predetermined subgroup analyses was conducted to evaluate the prognostic value of D_{mvcc} in sub-populations with various clinical pathologies, including age, sex, smoking history, tumor histology, age, disease stage, tumor differentiation, or chemotherapy. All tests were two-sided, and statistical differences were considered significant at $p < 0.05$.

RESULTS

Patients

A total of 100 patients (74 men) with 54 adenocarcinomas and 43 squamous cell carcinomas were included. The age of the patients ranged from 40 to 79 years, with a median age of 59 years. The TNM stage was I/II and III/IV in 71 and 29 subjects, respectively. A total of 1, 47, and 49% of the patients had well-, moderately, and poorly differentiated tumors, respectively. During the follow-up period (median, 51.1m; range, 45.5 to 60.0m), 29 patients died (29%) and 44 experienced recurrence (recurrence outcome was unavailable for eight subjects). Of the 81 patients who received chemotherapy, 83% received single-line platinum-based regimens: GP regimen (45 patients, gemcitabine plus cisplatin), DP regimen (nine patients, docetaxel and cisplatin), GC regimen (four patients, gemcitabine plus cisplatin), NP regimen (four patients, vinorelbine plus cisplatin), and PC regimen (five patients, paclitaxel plus carboplatin).

D_{mvcc}

The microvessels were visualized by IHC staining of the CD31 antigen. As shown in **Figure 1A**, the microvessel was surrounded by tumor stroma and away from the cancer cells. A total of 32–569 vessels (mean: 112 ± 77; median: 91) per patient were investigated. The individual D_{mvcc} ranged from 1.61 to 269.70 μm (mean value of 24.37 μm ± 33.45 μm and 1st, 2nd, and 3rd quartile values of 7.34, 13.15, and 30.76 μm). Most of the patients (93 of 100) had a mean D_{mvcc} of less than 50 μm. In all the participants, we recorded a significant correlation between D_{mvcc} and the pathological type ($r = 0.202$, $p = 0.044$), and a longer D_{mvcc} was observed in the tissues of squamous carcinoma than in those of adenocarcinoma (33.7 μm ± 44.6 μm *vs.* 17.2 μm ± 19.6 μm, **Figure 1B**). However, no significant correlations with the other traits were detected.

Correlation of D_{mvcc} and Survival Outcome

Of the 49 candidate cutoff values (from 2 to 50 μm, step = 1 μm), 41 (83.7%, 7 μm, and 9–48 μm), and seven (14.3%, 16–21 μm, and 24 μm) played significant roles in predicting OS and PFS, respectively (**Figure 2A**). A D_{mvcc} of 20 μm was defined as the optimal cutoff value for both OS (HR = 7.36, 95CI = 2.92–18.58, $p = 0.00002$) and PFS (HR = 1.95, 95CI = 1.09–3.48, $p = 0.00006$) (**Figure 2B**).

To determine the prognostic role of D_{mvcc}, five sets of categorical continuous D_{mvcc}, such as median-value dichotomy, optimal cutoff value dichotomy, tertiles, quartile, and per-10-μm increase, were tested. Poor survival outcomes (both OS and PFS) were noted in patients with long D_{mvcc} than in those with short D_{mvcc} based on any of the five stratification conditions (OS: HR = 1.93–7.36, $p = 0.001$–0.00004; PFS: HR = 1.23–1.95, $p = 0.041$–0.024) (**Table 1**). In analyses based on adjustments for age, sex, smoking history, pathology, differentiation, stage, and chemotherapy, the long D_{mvcc} predicted poor survival with median HRs of 1.98–13.50 for OS and 1.30–3.26 for PFS based on various categorical strategies (**Figure 3**). After progressive adjustment for various risk factors, D_{mvcc} remained significantly associated with NSCLC-related death or progression. For a per-10 μm increase in D_{mvcc}, the HRs for NSCLC-related death and progression were 1.98 (95CI: −1.40–2.79) and 1.30 (95CI: −1.01–1.69) in the final multivariable model (**Figure 3**). The median PFS was significantly shortened from 35.1 months (95%CI: 22–1-48.1 months) for short D_{mvcc} (<20 μm) patients to 15.1 months (95% CI: 8.6–21.6 months) for long D_{mvcc} (≥20 μm) patients ($p = 0.024$, **Figure 2B**). As disclosed in the predetermined subgroup analysis, D_{mvcc} was a promising prognostic marker of OS for older ages (age ≥60 years), younger ages (age <60 years), male sex, squamous carcinoma, adenocarcinoma, poor tumor differentiation, advanced stage, early stage, smoking or prior smoking, and prior chemotherapy, as well as a promising prognostic marker of PFS in patients who are male, have squamous carcinoma, are current or former smokers, and have had chemotherapy (**Figure S2**).

Long D_{mvcc} Independently Indicated Poor Prognosis

Several multivariate analyses (**Table 2**) of features, including sex, smoking history, tumor histology, age, disease stage, tumor differentiation, D_{mvcc}, and chemotherapy, were performed with five multivariable models based on different stratified strategies of D_{mvcc}. D_{mvcc} was found to be an independent predictor of tumor-related death ($p = 0.001$–0.000005) or progression ($p = 0.044$–0.002) in all five models. The model based on the 10-μm-stratified D_{mvcc} was disclosed as the optimal model for survival prognosis, with the highest c-index values of 0.830 and 0.771 for OS (HR = 1.98, 95CI: 1.40–2.79, $p = 0.0001$) and PFS (HR = 1.30, 95CI: 1.01–1.69, p = 0.044), respectively. In addition, an advanced stage was suggested as another independent

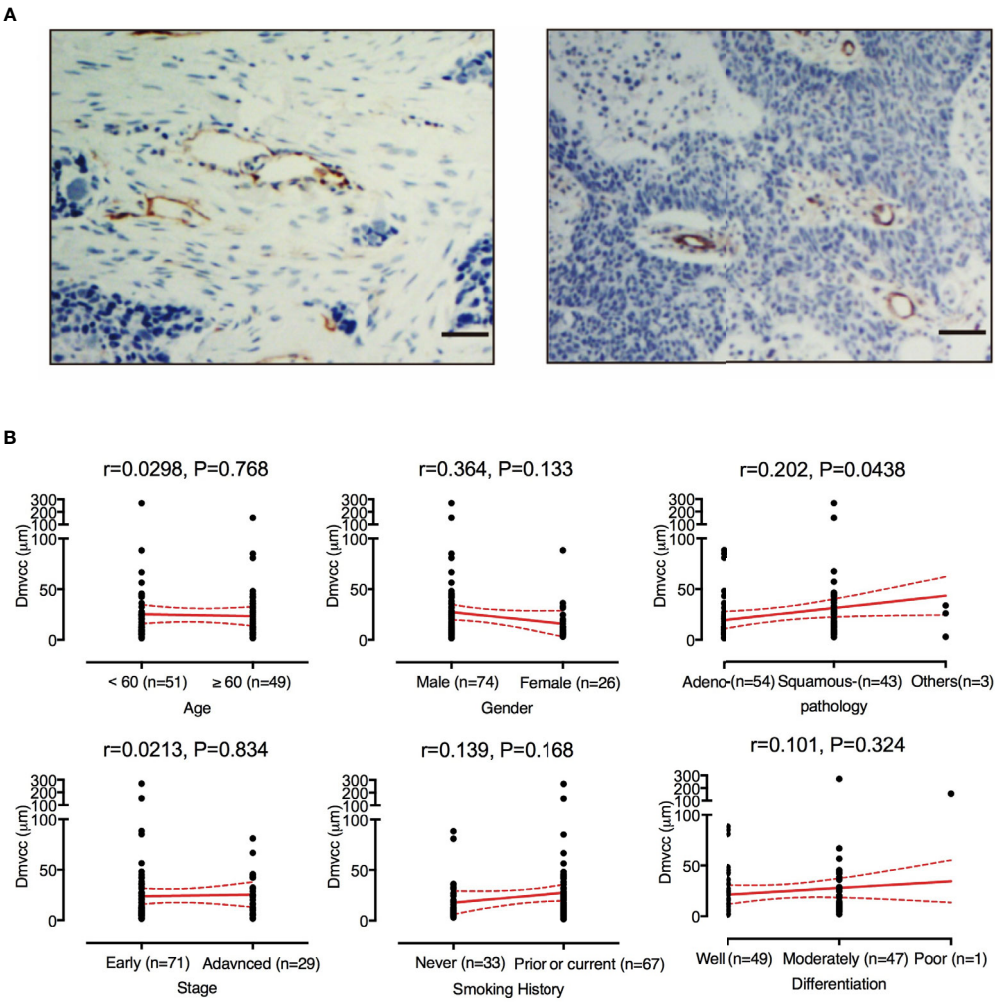

FIGURE 1 | Evaluation of D_{mvcc} in NSCLC tissue sections. **(A)** Immunostaining of endothelial cells for CD31 (brown) with long D_{mvcc} (left panel) and short D_{mvcc} (right panel) in NSCLC tissue sections. Bar: 50 μm, **(B)** Correlates of D_{mvcc} associated with age, gender, smoking history, tumor histology, tumor differentiation, stage, and chemotherapy regimens. The mean value (red full-line) and its 95%CI (red dotted line) are shown.

prognostic factor of OS (HR = 2.51–3.33, p = 0.027-0.008), but it showed no significant correlation with PFS (**Table 2**).

DISCUSSION

Due to the role of the extracellular matrix in NSLC development, subjects with rich stroma were investigated for poor survival (24). Poor survival can be attributed to various profiles of stroma or alterations of rich stroma, such as the proportion of stroma, fibrosis extent (25), impaired vascularization (26, 27), and immune infiltration of the peritumoral stroma (28) and the evidence related to the aforementioned contributors has been explored. For instance, squamous cell carcinoma of patients with fibrous stroma demonstrated a more invasive phenotype and was associated with a significantly poor prognosis (25). However, the impact of the elongated distance of diffusion on survival outcomes has not been focused on. Therefore, the correlation between perfusion distance and patient survival was evaluated in the present study. As expected, a long D_{mvcc} was predictive of poor survival. This suggests that the long distances from vessels to cancer cells partly affected patient survival.

A short diffusion distance between cancer cells and microvessels is crucial for efficient nutrient supply. Enlarged perfusion paths may induce an insufficient supply of oxygen, nutrition, and anti-tumor drugs, ultimately improving tumor growth (29, 30). However, the diffusion distance in the tumor tissues of patients and their correlation with survival outcomes have seldom been reported. Therefore, in the present study, we developed a method to evaluate the distance of nutrient diffusion and examine its role in prognostic prediction. Because the concept of the "distance between cancer cells and vessels" is seldom reported, no definition and measurement methodology can be

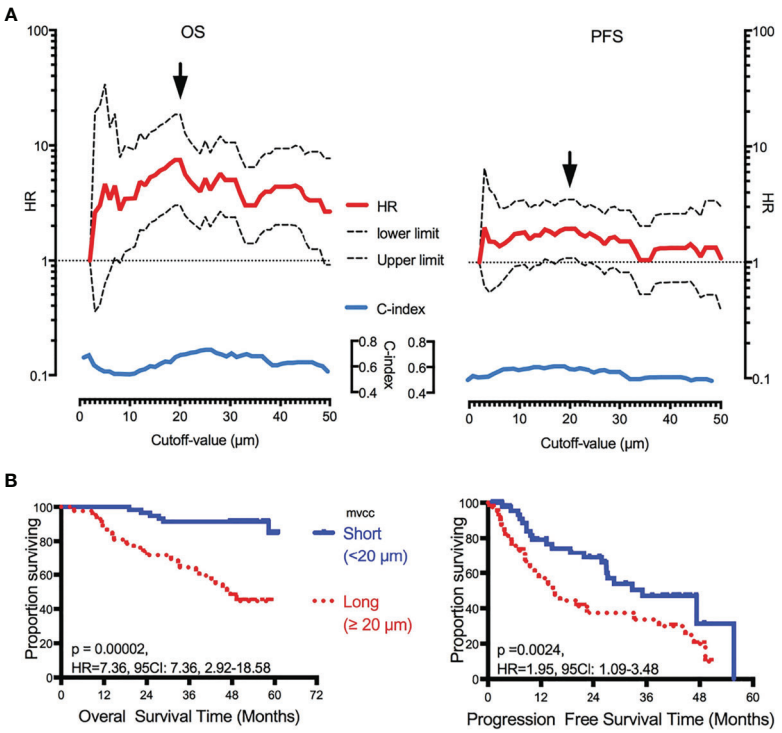

FIGURE 2 | Correlation of D_{mvcc} and survival outcome. **(A)** Significant test: the hazard ratios (HRs, red full-line, long- *vs* short-D_{mvcc}) of OS (right panel) and PFS (left panel) for various cutoff values of D_{mvcc} (from 2 to 50 μm at a step of 1 μm, bottom of the figures) were demonstrated with its upper limit (upper dotted-line) and lower limit (lower dotted-line) of 95% CI. Additionally, the c-index values were displayed as blue full-line. The optimal cutoff-value was demonstrated by a solid arrow. **(B)** Prognostic significance of D_{mvcc} in NSCLC patients. Kaplan–Meier survival curves show OS (left panels) and PFS (right panels) for patients presenting a long (full line) or short (dotted line) D_{mvcc} dichotomized by the optimal cutoff-value (20 μm, **B**).

TABLE 1 | Association of D_{mvcc} with survival outcome using various categorical strategies.

Categorical D_{mvcc}	OS			PFS		
	HR, 95CI	P-value	C-index	HR, 95CI	P-value	C-index
Dichotomy by median value (13 μm)*	4.51, 1.83–11.12	0.001	0.67	1.72, 0.95–3.09	0.072	0.59
Dichotomy by optimal cutoff (20 μm)*	7.36, 2.92–18.58	0.00002	0.74	1.95, 1.09–3.48	0.024	0.61
Trichotomy	2.84, 1.64–4.91	0.0002	0.72	1.44, 1.02–2.04	0.041	0.61
Bottom tertile	1			1		
Middle tertile	1.59, 0.47–5.44	0.459		1.45, 0.68–3.10	0.334	
Top tertile	6.32, 2.13–18.78	0.0009		2.07, 1.03–4.18	0.042	
Quartation	2.30, 1.54–3.46	0.00006	0.74	1.27, 0.99–1.63	0.060	0.61
1st quartile	1			1		
2nd quartile	0.93, 0.19–4.65	0.932		0.91, 0.36–2.25	0.830	
3rd quartile	2.91, 0.77–10.98	0.115		1.85, 0.83–4.15	0.134	
4th quartile	7.95, 2.28–27.74	0.001		1.81, 0.83–3.95	0.137	
Per-10 μm increase	1.93, 1.46–2.56	0.000004	0.76	1.23, 1.01–1.51	0.040	0.63
0–10 μm	1			1		
10–20 μm	0.73, 0.13–3.99	0.715		1.25, 0.52–3.01	0.624	
20–30 μm	4.86, 1.46–16.18	0.010		2.24, 0.998–5.02	0.051	
30–40 μm	7.12, 1.76–28.82	0.006		2.53, 0.80–8.04	0.114	
40–50 μm	10.69, 3.08–37.15	0.0002		2.00, 0.80–5.03	0.140	

**The lower as 1.*

used. We defined D_{mvcc} as the distance between each microvessel and its nearest cancer cell for the following two reasons. First, the vessel was the center of the blood perfusion area; thus, the distance was measured based on each vessel; moreover, the nearest distance was easy to measure instead of the median or farthest distance. As we disclosed, the mean D_{mvcc} value of most patients ranged from 2 to 50 μm, and the mean D_{mvcc} in half of the patients was <13 μm. It was really interested that longer D_{mvcc}

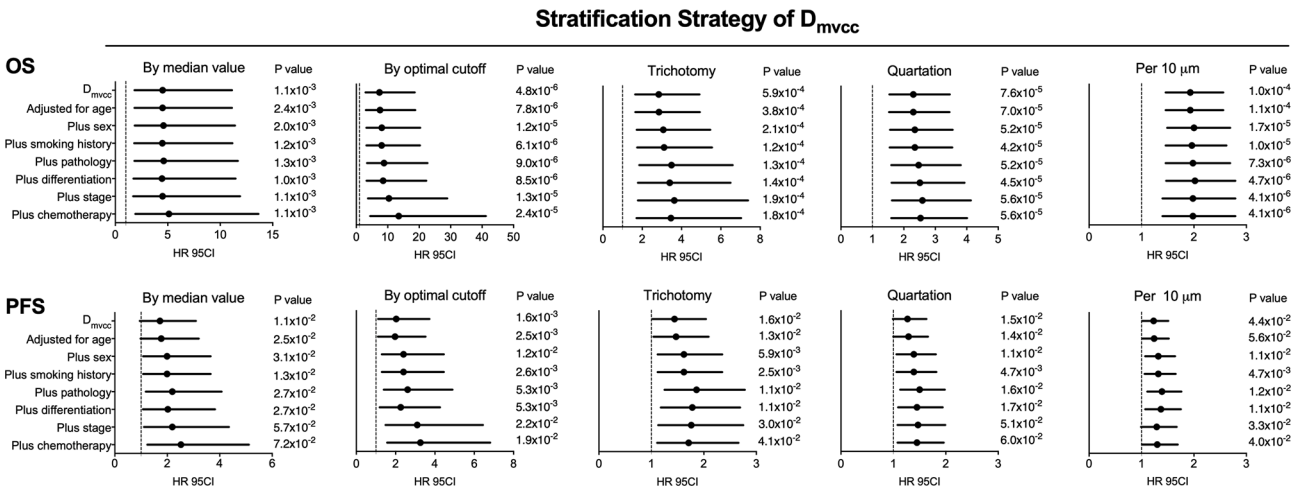

FIGURE 3 | Adjusted correlation of D_{mvcc} and survival outcome. The hazard ratios (HRs) of OS (upper panel) and PFS (lower panel) for various categorical strategies of D_{mvcc}: (1) dichotomy by median value; (2) dichotomy by optimal cutoff; (3) trichotomy: bottom tertile, middle tertile, and top tertile; (4) quartation: 1st, 2nd, 3rd, and 4th quartiles; (5) per-10 μm increase: 0–10, 10–20, 20–30, 30–40, and 40–50 μm after successively adjusting by age, sex, smoking history, tumor histology, tumor differentiation, disease stage, and chemotherapy.

was found in the tissues of squamous carcinoma than adenocarcinoma. It may be attributed to distinct tumor-accociated fibroblasts (TAFs), the cell built extra-cellular matrix, between squamous carcinoma and adenocarcinom. It was reported that TAFs in squamous carcinoma exhibited higher levels of matrix rigidity related factors, such as FAK, β1 expression, and ERK1/2 than TAFs in adenocarcinom. Matrix stiffening induced a larger TAF accumulation in squamous carcinoma compared with adenocarcinom. Therefore, a larger proportion of matrix caused longer distance were observed in squamous carcinoma (31).

The optimal cutoff value of D_{mvcc} was determined by a test that included 49 candidate values (2–50 μm, step = 1 μm). As a result, 20 μm was determined to be the optimal cutoff value. There were 58 patients with short D_{mvcc} (<20 μm) and 42 patients with long D_{mvcc} (≥20 μm). Five categorical strategies, such as per-10μm increase, quartation, trichotomy, dichotomy by median value (13 μm), and dichotomy by optimal cutoff (20 μm), were used to evaluate the role of the D_{mvcc} in survival prediction. A long D_{mvcc} significantly predicted shorter OS of patients based on all five categorical strategies. A significantly shorter PFS was observed in patients with long D_{mvcc} than in those with short D_{mvcc} (<20 μm, or per-10 μm decreased). As disclosed, the risks of cancer-related death and progression were increased by 93% (HR = 1.93, 95CI: 1.46–2.56, $p = 0.000004$) and 23% (HR = 1.23, 95CI: 1.01–1.51, $p = 0.040$), respectively, per 10 μm increase in D_{mvcc}. Moreover, D_{mvcc} and stage were also proven to be independent prognostic factors based on five multivariate analysis models. The models that were based on D_{mvcc} dichotomized by the optimal value (c-index: 0.827 of OS and 0.772 of PFS) and every 10 μm increase (c-index: 0.830 of OS and 0.771 of PFS), respectively, were recommended as the best two prognostic prediction models.

These results can be attributed to the impaired distribution of oxygen, nutrition, and anticancer drugs hampered by prolonged drug penetration from blood vessels to cancer cells. In tumor tissue, microvessels are separated from cancer cells by abnormally dense stroma, which consists of high levels of collagenous fibers and stabilized polysaccharide networks (hyaluronate and proteoglycans) (20). Above all, a long D_{mvcc} indicates poor blood-supply efficiency. The diffusion of oxygen was inversely proportional to the square value of the perfusion distance *in silicon* (32). *In vivo*, at a distance of 50 μm from the vessel, the oxygen partial pressure (pO_2) was decreased by approximately 40 and 50% in xenografts of breast cancer and NSCLC cancer (33, 34). In addition, pO_2 decreased by 100% at a distance of 70 μm from the vessels in breast cancer xenografts (35). The diffusion of glucose also decreased by approximately 40% at a diffusion distance of 100 μm (33). The hypoxic microenvironment is widely accepted as a driver of tumor growth and the cause of therapy resistance (36–39).

The mobility of drugs in penetrating the extracellular matrix is also limited by cell–cell adhesion, high interstitial fluid pressure, lack of convection, drug metabolism, and binding (9, 40). Recent data suggest that inefficient delivery of antineoplastic drugs in the tumor environment is a novel and important contributor to chemoresistance (19, 20, 41–43). A prolonged distance from blood vessels to cancer cells is a significantly difficult route for antitumor agent delivery. This led to a steep decrease in the drug concentration around cancer cells. As reported, the intensity of doxorubicin decreased to half from the nearest blood vessel at a distance of 40–50 μm (44). The incomplete intratumoral distribution of gemcitabine and fluorouracil, which induced the reverse impact of the antitumor effect, has been addressed *in vivo* (21, 45). Our study showed a significant association between a long D_{mvcc} and poor survival outcomes of chemotherapy in

TABLE 2 | Independent prognostic factors of NSCLC patients based on various multivariate analysis models.

Factors	Model 1 (dichotomy by median value)			Model 2 (dichotomy by optimal value)			Model 3 (Trichotomy)			Model 4 (Quartation)			Model 5 (Per 10 μm increase)		
	HR (95CI)	P value	C-index	HR (95CI)	P value	C-index	HR (95CI)	P value	C-index	HR (95CI)	P value	C-index	HR (95CI)	P value	C-index
OS															
D_{mvcc}	5.11 (1.91–13.64)	0.001	0.790	13.5 (4.42–41.18)	0.000005	0.827	3.46 (1.71–7.03)	0.0006	0.792	2.53 (1.60–4.01)	0.0001	0.812	1.98 (1.40–2.79)	0.0001	0.830
Age	1.34 (0.62–2.93)	0.459		2.45 (1.00–6.02)	0.050		1.67 (0.72–3.90)	0.235		1.67 (0.73–3.78)	0.222		2.05 (0.77–5.42)	0.148	
Gender	2.64 (0.31–22.47)	0.375		7.32 (0.76–70.55)	0.085		4.89 (0.54–44.08)	0.157		4.08 (0.46–36.03)	0.206		–	0.935	
Smoking History	2.53 (0.31–20.61)	0.384		3.68 (0.44–30.6)	0.229		4.43 (0.54–36.73)	0.168		3.91 (0.47–32.31)	0.206		–	0.937	
Pathology	0.45 (0.16–1.23)	0.121		0.33 (0.11–1.02)	0.055		0.43 (0.15–1.23)	0.114		0.41 (0.14–1.18)	0.098		0.51 (0.17–1.58)	0.243	
Differentiation	1.06 (0.47–2.39)	0.887		1.08 (0.46–2.56)	0.856		0.96 (0.43–2.15)	0.912		0.99 (0.43–2.27)	0.980		1.16 (0.46–2.92)	0.756	
TNM Stage	2.51 (1.11–5.68)	0.027		3.33 (1.38–8.04)	0.008		2.92 (1.24–6.85)	0.014		2.85 (1.23–6.57)	0.014		3.32 (1.27–8.67)	0.014	
Chemotherapy	3.64 (0.72–18.54)	0.120		4.93 (0.84–28.93)	0.077		1.76 (0.35–8.96)	0.495		2.30 (0.45–11.75)	0.312		1.90 (0.34–10.51)	0.462	
PFS															
D_{mvcc}	2.52 (1.24–5.11)	0.011	0.763	3.26 (1.56–6.81)	0.002	0.772	1.71 (1.11–2.66)	0.016	0.763	1.45 (1.08–1.96)	0.015	0.762	1.30 (1.01–1.69)	0.044	0.771
Age	0.82 (0.43–1.56)	0.540		1.09 (0.54–2.19)	0.815		0.86 (0.44–1.70)	0.672		0.87 (0.45–1.70)	0.691		0.97 (0.48–1.97)	0.934	
Gender	2.75 (0.75–10.13)	0.127		3.95 (1.01–15.47)	0.049		2.83 (0.76–10.60)	0.121		2.80 (0.75–10.48)	0.126		3.11 (0.67–14.45)	0.147	
Smoking History	1.72 (0.48–6.20)	0.410		1.78 (0.49–6.44)	0.376		2.16 (0.59–7.84)	0.243		1.90 (0.52–6.87)	0.329		1.91 (0.41–8.84)	0.407	
Pathology	0.39 (0.16–1.00)	0.050		0.44 (0.18–1.10)	0.078		0.39 (0.15–1.01)	0.052		0.40 (0.15–1.02)	0.054		0.45 (0.17–1.22)	0.118	
Differentiation	0.60 (0.30–1.18)	0.139		0.59 (0.30–1.16)	0.126		0.57 (0.29–1.12)	0.102		0.58 (0.29–1.14)	0.116		0.60 (0.29–1.23)	0.162	
Stage	2.86 (1.48–5.51)	0.002		3.56 (1.76–7.20)	0.000		2.82 (1.45–5.49)	0.002		2.92 (1.50–5.65)	0.002		2.96 (1.44–6.06)	0.003	
Chemotherapy	2.78 (0.92–8.43)	0.070		2.48 (0.84–7.32)	0.100		2.00 (0.68–5.85)	0.206		2.10 (0.72–6.13)	0.174		2.06 (0.69–6.20)	0.197	

patients with NSCLC. It has been suggested that D_{mvcc} is a surrogate biomarker for the prediction of survival outcomes in NSCLC patients.

There are several limitations to the present study that should be addressed. First, perfusion distance was the only contributor to poor outcomes; other factors, such as fibrosis extent and impaired microvessel pattern, should be evaluated. Moreover, only intratumor vessels in the field of "hot spots" were limited to capacity. This may have led to sampling bias. As a novel characteristic of the perfusion system, the definition and measurement of D_{mvcc} need to be validated. At last, it was expected that short distance between cancer and blood vessels, would facilitate cancer cells accessing to vessels and improve the chance of metastasis and cause worse patience survival. However, the correlation between D_{mvcc} and metastatic tumor was not estimated in the present study.

In conclusion, the present study proves that a long distance from an intratumor microvessel to cancer cells is an independent predictive factor of poor survival outcomes in NSCLC patients. It provides clinical insights into the chemoresistance caused by the long penetration distance-induced impaired accumulation of antineoplastic agents in tumors.

DATA AVAILABILITY STATEMENT

The original contributions presented in the study are included in the article/**Supplementary Material**. Further inquiries can be directed to the corresponding authors.

ETHICS STATEMENT

The studies involving human participants were reviewed and approved by the Ethics Committee of Zhejiang Cancer Hospital. The patients/participants provided their written informed consent to participate in this study. Written informed consent was obtained from the individual(s) for the publication of any potentially identifiable images or data included in this article.

AUTHOR CONTRIBUTIONS

HD, LF, and YT contributed to the conception and design of the study. JS, WX and LZ carried out the experiments. JS, YT, YC, and JZ revised the manuscript. YC, YS, YZ and LZ contributed to data collection and analysis. All authors contributed to the article and approved the submitted version.

FUNDING

This work was supported by the National Natural Science Foundation of China (81773819, 81973396 and 82003851), Natural Science Foundation of Zhejiang Province (No: Q17H300007), Natural Science Foundation of Zhejiang Province (LY19H160006), Science and Technology in Zhejiang Province Chinese Medicine Program (No: 2015ZA036, and 2019KY473), Scientific Research key program of Health Bureau of Zhejiang Province (WKJ-ZJ-1504), Medical Science Research Foundation of Zhejiang Province (No: 2015ZDA006), Zhejiang Provincial Program for 151 Talents (LF), and Zhejiang Cancer Hospital Program for the Cultivation of 1022 Talents (LF).

ACKNOWLEDGMENTS

The authors thank Ying He for assistance in preparation of the article.

SUPPLEMENTARY MATERIAL

The Supplementary Material for this article can be found online at: https://www.frontiersin.org/articles/10.3389/fonc.2021.632352/full#supplementary-material

REFERENCES

1. NSCLC Meta-Analysis Collaborative Group. Preoperative Chemotherapy for Non-Small-Cell Lung Cancer: A Systematic Review and Meta-Analysis of Individual Participant Data. *Lancet* (2014) 383(9928):1561–71. doi: 10.1016/S0140-6736(13)62159-5
2. Carmeliet P. Angiogenesis in Life, Disease and Medicine. *Nature* (2005) 438 (7070):932–6. doi: 10.1038/nature04478
3. Bais C, Mueller B, Brady MF, Mannel RS, Burger RA, Wei W, et al. Tumor Microvessel Density as a Potential Predictive Marker for Bevacizumab Benefit: GOG-0218 Biomarker Analyses. *J Natl Cancer Inst* (2017) 109(11): djx066. doi: 10.1093/jnci/djx066
4. Wang Q, Xiang Q, Yu L, Hu T, Chen Y, Wang J, et al. Changes in Tumor-Infiltrating Lymphocytes and Vascular Normalization in Breast Cancer Patients After Neoadjuvant Chemotherapy and Their Correlations With Dfs. *Front Oncol* (2019) 9:1545. doi: 10.3389/fonc.2019.01545
5. Zhang T, Nie J, Liu X, Han Z, Ding N, Gai K, et al. Correlation Analysis Among the Level of IL-35, Microvessel Density, Lymphatic Vessel Density, and Prognosis in Non-Small Cell Lung Cancer. *Clin Trans Sci* (2020) 14 (1):389–94. doi: 10.1111/cts.12891
6. Dong Y, Ma G, Liu Y, Lu S, Liu L. Prognostic Value of Microvessel Density in Head and Neck Squamous Cell Carcinoma: A Meta-Analysis. *Dis Markers* (2020) 2020:8842795. doi: 10.1155/2020/8842795
7. Fang L, He Y, Liu Y, Ding H, Tong Y, Hu L, et al. Adjustment of Microvessel Area by Stromal Area to Improve Survival Prediction in Non-Small Cell Lung Cancer. *J Cancer* (2019) 10(15):3397–406. doi: 10.7150/jca.31231
8. Ntellas P, Dadouli K, Perivoliotis K, Sogka E, Pentheroudakis G, Ioannou M, et al. Microvessel Density and Impact of Angiogenesis on Survival of Resected Pancreatic Cancer Patients: A Systematic Review and Meta-Analysis. *Pancreas* (2019) 48(2):233–41. doi: 10.1097/mpa.0000000000001237
9. Khawar IA, Kim JH, Kuh HJ. Improving Drug Delivery to Solid Tumors: Priming the Tumor Microenvironment. *J Controlled Release* (2015) 201:78–89. doi: 10.1016/j.jconrel.2014.12.018
10. Vaupel P, Mayer A, Briest S, Hockel M. Hypoxia in Breast Cancer: Role of Blood Flow, Oxygen Diffusion Distances, and Anemia in the Development of Oxygen Depletion. *Adv Exp Med Biol* (2005) 566:333–42. doi: 10.1007/0-387-26206-7_44
11. Menon C, Fraker DL. Tumor Oxygenation Status as a Prognostic Marker. *Cancer Lett* (2005) 221(2):225–35. doi: 10.1016/j.canlet.2004.06.029
12. Meert AP, Paesmans M, Martin B, Delmotte P, Berghmans T, Verdebout JM, et al. The Role of Microvessel Density on the Survival of Patients With Lung Cancer: A Systematic Review of the Literature With Meta-Analysis. *Br J Cancer* (2002) 87(7):694–701. doi: 10.1038/sj.bjc.6600551
13. Haider T, Sandha KK, Soni V, Gupta PN. Recent Advances in Tumor Microenvironment Associated Therapeutic Strategies and Evaluation Models. *Mater Sci Eng C Mater Biol Appl* (2020) 116:111229. doi: 10.1016/j.msec.2020.111229
14. Ariffin AB, Forde PF, Jahangeer S, Soden DM, Hinchion J. Releasing Pressure in Tumors: What Do We Know So Far and Where Do We Go From Here? A Review. *Cancer Res* (2014) 74(10):2655–62. doi: 10.1158/0008-5472.can-13-3696
15. Stylianopoulos T, Martin JD, Snuderl M, Mpekris F, Jain SR, Jain RK. Coevolution of Solid Stress and Interstitial Fluid Pressure in Tumors During Progression: Implications for Vascular Collapse. *Cancer Res* (2013) 73(13):3833–41. doi: 10.1158/0008-5472.can-12-4521
16. Valkenburg KC, de Groot AE, Pienta KJ. Targeting the Tumour Stroma to Improve Cancer Therapy. *Nat Rev Clin Oncol* (2018) 15(6):366–81. doi: 10.1038/s41571-018-0007-1
17. Böckelmann LC, Schumacher U. Targeting Tumor Interstitial Fluid Pressure: Will It Yield Novel Successful Therapies for Solid Tumors? *Expert Opin Ther Targets* (2019) 23(12):1005–14. doi: 10.1080/14728222.2019.1702974
18. Gao H. Shaping Tumor Microenvironment for Improving Nanoparticle Delivery. *Curr Drug Metab* (2016) 17(8):731–6. doi: 10.2174/1389200217666160630203600
19. Li YH, Wang J, Wientjes MG, Au JLS. Delivery of Nanomedicines to Extracellular and Intracellular Compartments of a Solid Tumor. *Adv Drug Deliv Rev* (2012) 64(1):29–39. doi: 10.1016/j.addr.2011.04.006
20. Miao L, Lin CM, Huang L. Stromal Barriers and Strategies for the Delivery of Nanomedicine to Desmoplastic Tumors. *J Controlled Release* (2015) 219:192–204. doi: 10.1016/j.jconrel.2015.08.017
21. Olive KP, Jacobetz MA, Davidson CJ, Gopinathan A, McIntyre D, Honess D, et al. Inhibition of Hedgehog Signaling Enhances Delivery of Chemotherapy in a Mouse Model of Pancreatic Cancer. *Science (New York NY)* (2009) 324 (5933):1457–61. doi: 10.1126/science.1171362
22. Rankin EB, Giaccia AJ. Hypoxic Control of Metastasis. *Science (New York NY)* (2016) 352(6282):175–80. doi: 10.1126/science.aaf4405
23. Weidner N, Semple JP, Welch WR, Folkman J. Tumor Angiogenesis and Metastasis–Correlation in Invasive Breast Carcinoma. *N Engl J Med* (1991) 324(1):1–8. doi: 10.1056/nejm199101033240101
24. Zhang T, Xu J, Shen H, Dong W, Ni Y, Du J. Tumor-Stroma Ratio Is an Independent Predictor for Survival in NSCLC. *Int J Clin Exp Pathol* (2015) 8 (9):11348–55.
25. Takahashi Y, Ishii G, Taira T, Fujii S, Yanagi S, Hishida T, et al. Fibrous Stroma Is Associated With Poorer Prognosis in Lung Squamous Cell Carcinoma Patients. *J Thorac Oncol* (2011) 6(9):1460–7. doi: 10.1097/JTO.0b013e318229189d
26. Tong YH, He Y, Hu LY, Liu YJ, Zheng XW, Sun J, et al. Elevated Proportion of Collapsed Microvessels Indicate Poor Survival Outcome in Patients With

Non-Small Cell Lung Cancer. *Tumori* (2019) 105(6):494–500. doi: 10.1177/0300891619871103
27. Fang L, He Y, Tong Y, Hu L, Xin W, Liu Y, et al. Flattened Microvessel Independently Predicts Poor Prognosis of Patients With Non-Small Cell Lung Cancer. *Oncotarget* (2017) 8(18):30092–9. doi: 10.18632/oncotarget.15617
28. Jackute J, Zemaitis M, Pranys D, Sitkauskiene B, Miliauskas S, Vaitkiene S, et al. Distribution of M1 and M2 Macrophages in Tumor Islets and Stroma in Relation to Prognosis of Non-Small Cell Lung Cancer. *BMC Immunol* (2018) 19(1):3. doi: 10.1186/s12865-018-0241-4
29. Vaupel P, Harrison L. Tumor Hypoxia: Causative Factors, Compensatory Mechanisms, and Cellular Response. *Oncol* (2004) 9(Suppl 5):4–9. doi: 10.1634/theoncologist.9-90005-4
30. Miranda-Galvis M, Teng Y. Targeting Hypoxia-Driven Metabolic Reprogramming to Constrain Tumor Progression and Metastasis. *Int J Mol Sci* (2020) 21(15):5487. doi: 10.3390/ijms21155487
31. Puig M, Lugo R, Gabasa M, Giménez A, Velásquez A, Galgoczy R, et al. Matrix Stiffening and β1 Integrin Drive Subtype-Specific Fibroblast Accumulation in Lung Cancer. *Mol Cancer Res MCR* (2015) 13(1):161–73. doi: 10.1158/1541-7786.Mcr-14-0155
32. Thomlinson RH, Gray LH. The Histological Structure of Some Human Lung Cancers and the Possible Implications for Radiotherapy. *Br J Cancer* (1955) 9 (4):539–49. doi: 10.1038/bjc.1955.55
33. Vaupel P. Oxygenation of Human Tumors. *Strahlenther Onkol* (1990) 166 (6):377–86.
34. Swinson DE, Jones JL, Richardson D, Wykoff C, Turley H, Pastorek J, et al. Carbonic Anhydrase IX Expression, a Novel Surrogate Marker of Tumor Hypoxia, Is Associated With a Poor Prognosis in Non-Small-Cell Lung Cancer. *J Clin Oncol* (2003) 21(3):473–82. doi: 10.1200/JCO.2003.11.132
35. Dewhirst MW. Concepts of Oxygen Transport At the Microcirculatory Level. *Semin Radiat Oncol* (1998) 8(3):143–50. doi: 10.1016/S1053-4296(98)80040-4
36. Salem A, Asselin MC, Reymen B, Jackson A, Lambin P, West CML, et al. Targeting Hypoxia to Improve Non-Small Cell Lung Cancer Outcome. *J Natl Cancer Inst* (2018) 110(1):14–30. doi: 10.1093/jnci/djx160
37. Gillies RJ, Schornack PA, Secomb TW, Raghunand N. Causes and Effects of Heterogeneous Perfusion in Tumors. *Neoplasia* (1999) 1(3):197–207. doi: 10.1038/sj.neo.7900037
38. Brustugun OT. Hypoxia as a Cause of Treatment Failure in Non-Small Cell Carcinoma of the Lung. *Semin Radiat Oncol* (2015) 25(2):87–92. doi: 10.1016/j.semradonc.2014.11.006
39. Krishnamachary B, Mironchik Y, Jacob D, Goggins E, Kakkad S, Ofori F, et al. Hypoxia Theranostics of a Human Prostate Cancer Xenograft and the Resulting Effects on the Tumor Microenvironment. *Neoplasia (New York NY)* (2020) 22(12):679–88. doi: 10.1016/j.neo.2020.10.001
40. Gouarderes S, Mingotaud AF, Vicendo P, Gibot L. Vascular and Extracellular Matrix Remodeling by Physical Approaches to Improve Drug Delivery At the Tumor Site. *Expert Opin Drug Deliv* (2020) 17(12):1703–26. doi: 10.1080/17425247.2020.1814735
41. Alfarouk KO, Stock CM, Taylor S, Walsh M, Muddathir AK, Verduzco D, et al. Resistance to Cancer Chemotherapy: Failure in Drug Response From ADME to P-Gp. *Cancer Cell Int* (2015) 15:ARTN 71. doi: 10.1186/s12935-015-0221-1
42. Tredan O, Galmarini CM, Patel K, Tannock IF. Drug Resistance and the Solid Tumor Microenvironment. *J Natl Cancer Inst* (2007) 99(19):1441–54. doi: 10.1093/jnci/djm135
43. Li M, Zhang F, Su Y, Zhou J, Wang W. Nanoparticles Designed to Regulate Tumor Microenvironment for Cancer Therapy. *Life Sci* (2018) 201:37–44. doi: 10.1016/j.lfs.2018.03.044
44. Tan Q, Saggar JK, Yu M, Wang M, Tannock IF. Mechanisms of Drug Resistance Related to the Microenvironment of Solid Tumors and Possible Strategies to Inhibit Them. *Cancer J* (2015) 21(4):254–62. doi: 10.1097/Ppo.0000000000000131
45. Chauhan VP, Martin JD, Liu H, Lacorre DA, Jain SR, Kozin SV, et al. Angiotensin Inhibition Enhances Drug Delivery and Potentiates Chemotherapy by Decompressing Tumour Blood Vessels. *Nat Commun* (2013) 4:2516. doi: 10.1038/ncomms3516

Conflict of Interest: The authors declare that the research was conducted in the absence of any commercial or financial relationships that could be construed as a potential conflict of interest.

Advantages of publishing in Frontiers

OPEN ACCESS
Articles are free to read for greatest visibility and readership

FAST PUBLICATION
Around 90 days from submission to decision

HIGH QUALITY PEER-REVIEW
Rigorous, collaborative, and constructive peer-review

TRANSPARENT PEER-REVIEW
Editors and reviewers acknowledged by name on published articles

Frontiers
Avenue du Tribunal-Fédéral 34
1005 Lausanne | Switzerland

Visit us: www.frontiersin.org
Contact us: frontiersin.org/about/contact

REPRODUCIBILITY OF RESEARCH
Support open data and methods to enhance research reproducibility

DIGITAL PUBLISHING
Articles designed for optimal readership across devices

FOLLOW US
@frontiersin

IMPACT METRICS
Advanced article metrics track visibility across digital media

EXTENSIVE PROMOTION
Marketing and promotion of impactful research

LOOP RESEARCH NETWORK
Our network increases your article's readership